THE JOURNAL
OF
CHEMICAL PHYSICS

VOLUME 33, NUMBER 3 SEPTEMBER, 1960

Dielectric Relaxation of Isoamyl Bromide*

SIVERT H. GLARUM†

Metcalf Research Laboratories, Brown University, Providence, Rhode Island

(Received March 9, 1960)

The complex dielectric constant of isoamyl bromide has been measured at 1, 3, and 9 kMc between −75° and 25°C. Complex plane plots indicate an asymmetric, skewed-arc distribution of relaxation times, with the shape of the distribution function not being appreciably temperature dependent. A defect diffusion model is proposed to explain the dielectric behavior of this system. This model implies that the relaxation of a molecule is more probable immediately after one of its neighbors has relaxed than at an arbitrary time. A distribution of relaxation times is derived which, under the appropriate conditions, closely resembles that of the empirical skewed-arc function.

I. INTRODUCTION

THE dielectric properties of the alkyl halides are of considerable theoretical interest as, unlike alcohols and other hydrogen-bonded media, these substances show no appreciable degree of intermolecular association. From a dielectric viewpoint, therefore, they might be supposed to constitute reasonably simple systems suitable for studies of the liquid state.

Denney has investigated the dielectric relaxation of several supercooled, branched alkyl halides (isobutyl chloride, isobutyl bromide, and isoamyl bromide).[1] He found that the frequency dependence of the complex dielectric constant ϵ^* was accurately described by the empirical skewed-arc expression

$$(\epsilon^*-\epsilon_\infty)/(\epsilon_0-\epsilon_\infty)=1/(1+i\omega\tau_0)^\beta, \qquad (1)$$

the parameters β and τ_0 characterizing the relaxation process, and ϵ_0 and ϵ_∞ being, respectively, the static and high-frequency dielectric constants.[2] Formally this process may be described in terms of a continuous distribution of relaxation frequencies (reciprocal relaxation times), and the logarithmic distribution function for such frequencies may be shown to be

$$F(\alpha)=(\sin\beta\pi/\pi)\,(\alpha-\alpha_0)^{-\beta}, \quad \alpha>\alpha_0,$$
$$=0, \quad \alpha<\alpha_0, \qquad (2)$$

where $\alpha_0=1/\tau_0$.

The appearance of this asymmetric distribution in the supercooled alkyl halides was originally surprising, for previously, similar behavior had been encountered only with supercooled polyhydroxy compounds.[2,3] More recent work has revealed a similar dielectric behavior in supercooled isomeric mixtures of tolyl xylyl sulfone, pentachlorobiphenyl, and hexachlorobiphenyl, and consequently it appears that the skewed-arc function is not specifically a characteristic of associated liquids.[4]

Smyth and co-workers have investigated the dielectric relaxation of isobutyl bromide between 1° and 55°C, reporting no evidence for any appreciable distribution of relaxation times.[5] In view of their results, it would appear that the parameter β occurring in the skewed-arc expression varies from a low-temperature value of 0.5 to nearly unity at room temperature. No studies of dielectric relaxation have heretofore been made over the intermediate temperature range, the experimental frequencies required falling in the microwave region. It was therefore decided to undertake a

* This research was supported in part by the U. S. Air Force through the Air Force Office of Scientific Research of the Air Research and Development Command.

† Present address: Bell Telephone Laboratories, Inc., Murray Hill, New Jersey.

[1] D. J. Denney, J. Chem. Phys. **27**, 259 (1957).

[2] D. W. Davidson and R. H. Cole, J. Chem. Phys. **19**, 1484 (1951).

[3] N. Koizumi and T. Hanai, J. Phys. Chem. **60**, 1496 (1956).

[4] J. W. Winslow, R. J. Good, and P. E. Berghausen, J. Chem. Phys. **27**, 309 (1957).

[5] C. P. Smyth *et al.*, J. Am. Chem. Soc. **70**, 4093–4111 (1948); J. Chem. Phys. **20**, 1121 (1952).

Copyright © 1960 by the American Institute of Physics

TABLE I. Complex dielectric constants of isoamyl bromide.

T(°C)	ϵ_0	ϵ_∞	ϵ^* 1 kMc	3 kMc	9 kMc
25	6.04	2.30	6.00–0.35i	5.81–0.90i	4.63–1.63i
0	6.64	2.34	6.49–0.61i	6.10–1.35i	4.30–1.79i
−25	7.24	2.38	7.00–0.97i	6.05–1.88i	3.74–1.76i
−50	8.00	2.45	7.25–1.68i	5.36–2.28i	3.13–1.46i
−75	9.03	2.52	6.58–2.71i	4.18–2.10i	2.92–1.01i

series of such measurements in order to determine more completely the influence of temperature upon the relaxation process, and thereby possibly obtain an insight into the origins of the hitherto unexplained skewed-arc function. Isoamyl bromide was selected for this study as, of the compounds investigated by Denney, it has the longest relaxation time, and its relaxation parameters could consequently be more accurately determined.

II. EXPERIMENTAL PROCEDURE

A. Purification of Isoamyl Bromide

Isoamyl bromide obtained from Eastman Organic Chemicals was used as starting material. The sample was dried over anhydrous calcium chloride and distilled at 1 atm using a Vigreaux column. The portion collected had a boiling range of 0.3°, and its refractive index, corrected to 15°C, was 1.4437, in satisfactory agreement with the value of 1.4433 cited by Timmermans.[6] The static dielectric constant measured at 0°C was found to be 6.62, a value somewhat smaller than that of 6.74 reported by Denney, but greater than that of 6.52 estimated from data of Baker and Smyth.[7,8]

B. Microwave Measurements

Measurements of the complex dielectric constant of isoamyl bromide were made at 1, 3, and 9 kMc using a microwave bridge described in an earlier paper.[9] Several modifications of the original apparatus were required for its use at low temperatures. The Teflon piece filling the primary line was removed and a 0.003-in. thick Mylar window was inserted at the input of the dielectric cell. Through the use of an air-filled primary line the cutoff frequency for the propagation of the coaxial TE_{11} mode was raised, and the frequency range of the apparatus was extended to 9 kMc. No significant window effects were noted, provided the window was present while the bridge was aligned and calibrated. In addition, the coupler-cell input distance was lengthened to 22.5 cm to minimize the effects of heat flow from the coupler into the cell. The actual frequencies used were 0.996, 2.99, and 8.97 kMc.

Corrections were required to take into account thermal contractions of the dielectric cell and the primary line. If neglected, these changes would have led to appreciable errors, particularly at 9 kMc.

The measuring procedure adopted involved determining the bridge balance position at room temperature, and then quickly cooling the cell to dry-ice temperatures. A series of measurements was made, and the bath was allowed to warm up at its normal rate (1° per 5 min). Readings were taken every 2½° at 3 kMc and every 5° at 9 kMc. At 1 kMc bridge sensitivity was comparatively low, and therefore measurements were made only at 25° intervals between −75° and 25°C.

At higher temperatures bath warming was aided by an electric immersion heater. There was no indication that the rates of heating used were too rapid for, when the heater was shut off and the bath remained at essentially a constant temperature, no detectable variation in bridge balance was noticed. After the apparatus had returned to room temperature it was usually found that the original bridge balance position was observed. In those cases where this was not true, window leakage had taken place. The ability to reproduce this setting was therefore taken as a partial indication of a successful run.

C. Temperature Measurements

All temperatures were measured using a calibrated alcohol thermometer located in the cooling bath near the cell input. At −75°C the temperature inside the cell varied less than 0.5° from its mean value over the full length of the cell, and differed by less than 1° from the temperature of the surrounding bath. The subsequent neglect of this difference should have introduced, at most, a systematic error of the order of 1° in our measurements.

III. RESULTS

Values for the complex dielectric constant of isoamyl bromide between −75° and 25°C are listed in Table I together with values for ϵ_0 and ϵ_∞ based on data furnished by Denney.[7] Measurements of ϵ_0 over a more limited temperature range indicated that the static dielectric constant of our sample was 1½% lower than that of Denney's and consequently his results were reduced by this amount to bring them into better agreement with our own. The values of ϵ_∞ listed in Table I were obtained from a linear $1/T$ extrapolation of Denney's results. Although the procedure of extrapolating data obtained between 120° and 140°K up to room temperature is a hazardous one, the values found are reasonable ones.

In Fig. 1 a reduced complex plane plot has been made using all the data listed in Table I. Surprisingly, all the points fall reasonably close to a single curve. As this

[6] J. Timmermans, *Physico-chemical Constants of Pure Organic Compounds* (Elsevier Publishing Company, Inc., New York, 1950).
[7] D. J. Denney (private communication, 1959).
[8] W. O. Baker and C. P. Smyth, J. Am. Chem. Soc. **61**, 2063 (1939).
[9] S. H. Glarum, Rev. Sci. Instr. **29**, 1016 (1958).

curve lies well within the semicircle corresponding to a single relaxation time, a distribution of relaxation times is apparent. The fact that the maximum of this curve does not appear to be appreciably temperature dependent suggests that the width of the distribution function varies only slightly with temperature over the range studied.

The low-frequency portion of this plot is quite accurately described by a semicircle, all points lying well outside a circular-arc locus. This section of the complex plane plot closely resembles a skewed arc, and the skewed arc for $\beta=0.7$ has been drawn in Fig. 1. The high-frequency behavior of the complex dielectric constant, on the other hand, appears to be somewhat better described by a circular arc. It should be noted, however, that those points which differ most from a a skewed arc were obtained at 9 kMc at low temperatures, and are those points subject to the greatest experimental inaccuracies. If the measured values of ϵ' at 9 kMc were increased 5–10%, then all the points in Fig. 1 would fall satisfactorily on the skewed-arc locus. This difference corresponds to an error of 0.005 to 0.010 in. in determining the correct length of the dielectric cell for bridge balance, and could have possibly been due to unequal thermal contractions of the inner and outer conductors in the primary line.

Several attempts were made to calculate relaxation times assuming a skewed-arc function for the complex dielectric constant. Below 0°C relaxation times calculated from the 9-kMc data were inconsistent with those found from the 1- and 3-kMc data. Alternatively, relaxation times were estimated assuming a circular-arc function. The values so found were more consistent with the complex dielectric constants measured at all three frequencies and are listed in Table II. These times are approximately 10% smaller than the best values of $\beta\tau_0$ obtained by assuming a skewed-arc function. A rate plot of $\ln\tau_0$ vs $1/T$ was found to be linear over the temperature interval studied, with a slope corresponding to an apparent activation energy of 2.1$_8$ kcal/mole.

It therefore appears that, barring a most unusual temperature dependence for ϵ_∞, an appreciable distribution of relaxation times exists in isoamyl bromide over the temperature range studied. As far as may be ascertained, this distribution is asymmetric and not greatly temperature dependent, resembling a skewed-arc distribution with $\beta\simeq 0.7$.

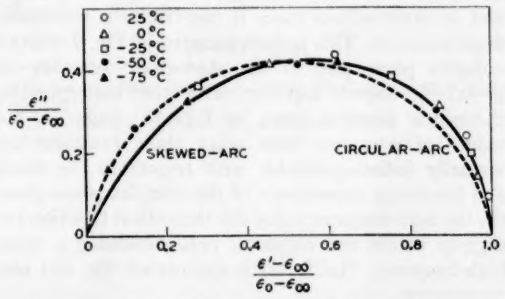

FIG. 1. Reduced complex plane plots for isoamyl bromide.

TABLE II. Estimated relaxation times for isoamyl bromide.

T(°C)	$\tau_0\times10^{11}$ (sec^{-1})
25	1.30
0	1.90
−25	3.05
−50	5.5
−75	11.4

IV. DISCUSSION

A. Defect Diffusion Model

No satisfactory explanation has yet been proposed for the skewed-arc dielectric behavior of isoamyl bromide. It might be supposed that in such a case where a distribution of relaxation times is observed one is merely dealing with a superposition of processes characterized by single relaxation times, i.e., distributions of rotational diffusion constants or of potential-barrier rate constants. This interpretation, however, is difficult to reconcile with the shape and temperature dependence of the skewed-arc distribution function.[3] Moreover, the simplicity and frequent occurrence of this function suggest that a more fundamental explanation exists.

Consequently, let us suppose that skewed-arc behavior is not due to any distribution of molecular parameters, but arises from a cooperative relaxation process. By this we mean that molecules do not relax independently of one another, and that the motion of a particular molecule depends to some degree on that of its neighbors. The origin of this interaction need not be dipolar in nature, for Denney has shown that even in dilute solutions of alkyl halides skewed-arc behavior persists.[10] To take into account such an interaction we have proposed a defect diffusion model for dielectric relaxation.

For mathematical convenience let us consider a one-dimensional system of equivalent polar molecules. Each dipole will be supposed to reorient itself in some manner leading to a single relaxation time. Let us further assume, however, that a number of defects are present as points in our one-dimensional system, and that the motion of these points can be described by a diffusion equation. For simplicity we shall suppose that when a defect reaches a dipole the latter relaxes completely and instantly. Then the molecular relaxation function is given by the expression

$$\phi(t)=\exp(-\alpha_0 t)[1-P(t)],$$

where α_0 is the relaxation frequency (reciprocal relaxation time) of a dipole in a defect-free region, and $P(t)$

[10] D. J. Denney, J. Chem. Phys. **30**, 1019 (1959).

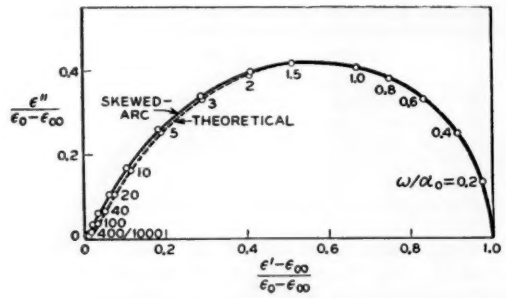

FIG. 2. Comparison of the skewed-arc and theoretical functions.

is the probability that a defect has reached an arbitrary dipole by time t. Differentiation yields

$$-\dot{\phi}(t)=\alpha_0\phi(t)+\exp(-\alpha_0 t)\dot{P}(t), \tag{3}$$

$\dot{P}(t)$ being the probability that a defect arrives at a molecule for the first time at time t. Now let us further restrict our model to take into account only the nearest defect at time $t=0$, and let us suppose that this defect is then a distance l removed from a given molecule. The problem of finding when this defect first reaches the molecule is equivalent to the problem of the absorbing wall discussed by Chandrasekhar, and using his results we find for $\dot{P}(t, l)$[11]

$$\dot{P}(t, l)=[l/(4\pi D)^{\frac{1}{2}}]t^{-\frac{3}{2}}\exp(-l^2/4Dt),$$

where D is the diffusion coefficient of the defect. If we now assume a random distribution of defects throughout our system, the probability that the nearest defect is between l and $l+\Delta l$ is $(1/l_0)\exp(-l/l_0)\Delta l$, l_0 being the average value of l, and $1/(2l_0)$ being the number of defects per unit length. Thus, averaging over all possible values of l,

$$\dot{P}(t)=(D/l_0^2)^{\frac{1}{2}}\times\{[1/(\pi t)^{\frac{1}{2}}]-(D/l_0^2)^{\frac{1}{2}}\exp(Dt/l_0^2)\operatorname{erfc}(Dt/l_0^2)^{\frac{1}{2}}\}.$$

Substitution of this expression in Eq. (3) yields

$$-\dot{\phi}(t)=\alpha_0\phi(t)+\exp(-\alpha_0 t)\,(D/l_0^2)^{\frac{1}{2}}\times\{[1/(\pi t)^{\frac{1}{2}}]-(D/l_0^2)^{\frac{1}{2}}\exp(Dt/l_0^2)\operatorname{erfc}(Dt/l_0^2)^{\frac{1}{2}}\}, \tag{4}$$

and upon taking the inverse Laplace transform of this equation we find that the distribution function for relaxation frequencies is

$$F(\alpha)=\pi^{-1}\frac{(D/l_0^2)^{\frac{1}{2}}}{(\alpha-\alpha_0)^{\frac{1}{2}}}\frac{\alpha}{\alpha-\alpha_0+D/l_0^2}, \qquad \alpha>\alpha_0,$$
$$=0, \qquad \alpha<\alpha_0.$$

[11] S. Chandrasekhar, Revs. Modern Phys. **15**, 1 (1943).

This function may be written more simply in terms of the reduced parameters a and a_0 given by

$$a=\alpha l_0^2/D$$
$$a_0=\alpha_0 l_0^2/D,$$

for then

$$F(a)=\pi^{-1}[1/(a-a_0)^{\frac{1}{2}}][a/(a-a_0+1)], \qquad a>a_0,$$
$$=0, \qquad a<a_0, \tag{5}$$

and the shape of the distribution function is determined solely by a_0.

This quantity may be viewed as the ratio of two relaxation times. One is a rotational relaxation time, defined as $1/\alpha_0$, and corresponds to the cutoff point of the distribution function. The other is a diffusional relaxation time, defined as l_0^2/D, and is a measure of the time required for a defect to move a distance l_0.

Three particular cases are of interest, $a_0\gg1$, $a_0=1$, and $a_0=0$. For these the distribution functions correspond to, respectively, a single relaxation time, a skewed-arc distribution with $\beta=0.5$, and a circular-arc distribution with $\alpha=0.5$ (α refers here to the shape parameter of the circular-arc function).[12] For values of a_0 greater than unity the distribution function given by Eq. (5) resembles a skewed-arc function, and a useful connection between a_0 and β may be found by taking the Laplace transform of Eq. (4). Performing this operation and neglecting minor differences between the macroscopic and microscopic distribution functions, we obtain

$$\mathfrak{L}[-\dot{\phi}(t)]=\frac{1}{1+i\omega/\alpha_0}+\left\{\frac{i\omega/\alpha_0}{1+i\omega/\alpha_0}[1+(a_0)^{\frac{1}{2}}(1+i\omega/\alpha_0)^{\frac{1}{2}}]^{-1}\right\}$$
$$=(\epsilon^*-\epsilon_\infty)/(\epsilon_0-\epsilon_\infty), \tag{6}$$

which expression is to be compared with $(1+i\omega/\alpha_0)^{-\beta}$. Expanding each of these functions to linear terms in $i\omega/\alpha_0$ and equating the results yields

$$\beta=(a_0)^{\frac{1}{2}}/[1+(a_0)^{\frac{1}{2}}]. \tag{7}$$

In the two limits $a_0=1$ and $a_0\gg1$ this equation is exact, and in intermediate cases it constitutes a reasonable approximation. This is demonstrated in Fig. 2 where a complex plane plot of the skewed-arc function for $\beta=0.7$ is shown together with the corresponding theoretical function given by Eqs. (6) and (7). For values of ω/α_0 less than unity these functions are virtually indistinguishable with respect to the shape and frequency dependence of the complex plane plots. On the high-frequency side the theoretical function lies slightly within the empirical one, possessing a small high-frequency "tail" which approaches the real axis

[12] K. S. Cole and R. H. Cole, J. Chem. Phys. **9**, 341 (1941).

at a 45° angle. Very precise measurements would be needed to differentiate between these functions, especially if the high-frequency tail were dismissed as a secondary dispersion.

In view of the limitations of our model it is surprising that our results correspond so closely with observed dielectric behavior. The point which we wish to stress, however, does not concern the quantitative accuracy of our results, but rather that, starting from a simple molecular-relaxation process involving no distribution of microscopic parameters, it has been possible to find distributions of relaxation times which are either symmetric ($a_0=0$) or asymmetric ($a_0\neq 0$) in nature. The origin of these distributions lies in our supposition of a diffusion process as a time-dependent mechanism for relaxation, for such a process is not exponential in time and cannot be characterized by a single relaxation time.

B. An Interpretation of the Defect Model

In the defect diffusion model just discussed little was said as to the physical nature of defects. This is because the model basically describes a system in which the reorientation of a molecule is far more likely immediately after one of its neighbors has relaxed than it is at an arbitrary time. It has not been necessary to postulate explicitly the manner in which this cooperative effect occurs, and the latter may in fact differ from system to system.

The simplest interpretation of a relaxation defect is a hole, for when such a defect reaches a molecule, the increased volume available should allow reorientation to occur more quickly than it would otherwise. Although quite naive, it will be instructive to investigate this particular kind of defect in more detail.

Assuming the validity of the Debye expression for the rotational relaxation time, then

$$\alpha_0=kT/4\pi\eta r^3,$$

η being the viscosity and r the molecular radius.[13] Consequently the temperature dependence of α_0, the cutoff frequency of the relaxation spectrum, should closely parallel that of $1/\eta$. This has been borne out by Denney's studies of the alkyl halides.[14] For a particle of radius r the Stokes-Einstein equation gives for the diffusion coefficient

$$D=kT/6\pi\eta r.$$

In general, however, a hole will be able to diffuse more quickly through a medium than a particle, and Frenkel has derived the relationship

$$D_{\text{hole}}=[(n/V)/(n'/V)]D,$$

for the diffusion coefficient of a hole, n/V being the number of molecules per unit volume, and n'/V being the number of holes per unit volume.[15] The parameter $1/(2l_0)$ is the number of defects per unit length in our one-dimensional system and we shall therefore make the approximation that $2l_0$ equals $(V/n')^{\frac{1}{3}}$. Thus, assuming the hole to be of molecular dimensions, we find that

$$a_0=\tfrac{3}{8}(v/r^3)r(n'/V)^{\frac{1}{3}}, \tag{8}$$

v being the apparent volume per molecule (V/n). This result indicates that a_0 should vary with temperature as the cube root of the defect concentration. A rate plot of $\ln a_0$ vs $1/T$ based on Denney's and our data was found to be linear within the limits of experimental error, with a slope corresponding to an apparent energy for defect formation of 1.7_5 kcal/mole.

When a_0 is close to unity, as is frequently the case, Eq. (8) implies that the distance to the nearest defect is of the same magnitude as the size of a hole or molecule. Under such circumstances it is doubtful whether the above analysis is useful. However, it is possible that Eq. (8) may be numerically in error because of its oversimplified derivation.

At high temperatures, moreover, our model may be inadequate because of the assumption of instant relaxation upon the arrival of a defect. If the defect concentration becomes appreciable, then virtually all molecules will relax at once *via* the defect mechanism. To avoid such a consequence it is necessary to introduce into the model a finite time for relaxation after the arrival of a defect. Presumably then the form of the distribution function would depend upon the ratio of this time to the diffusional relaxation time, and the longer time would correspond to the rate-determining step for dielectric relaxation.

V. ACKNOWLEDGMENTS

The author wishes to thank Professor Robert H. Cole for many helpful discussions concerning this work. He also gratefully acknowledges fellowship grants from the Bell Telephone Laboratories, Inc.

[13] P. Debye, *Polar Molecules* (Dover Publications, Inc., New York, 1945).
[14] D. J. Denney, J. Chem. Phys. **30**, 159 (1959).
[15] J. Frenkel, *Kinetic Theory of Liquids* (Oxford University Press, New York, 1946), p. 29.

Proton-Magnetic-Resonance Study of Barium Bromide Monohydrate*

J. W. McGrath and A. A. Silvidi

Department of Physics, Kent State University, Kent, Ohio

(Received April 4, 1960)

The proton-magnetic-resonance doublets were obtained for rotation of the crystal around its c axis. From these data, the proton-proton separation was computed to be 1.56±0.02 A. The hydrated water molecule was found to lie in one orientation whose proton-proton axis makes direction angles of $\alpha_0=89\pm1°$, $\beta_0=1\pm1°$, and $\gamma_0=90\pm6°$, measured from the positive a, b, and c crystallographic axes, respectively. This orientation fits well into the crystal structure and indicates that the complex, Br_I- -H—O—H- -Br_{II}, exists.

Line widths range from 6.5 to 4.2 gauss and show a correlation with T_1 as a function of orientation. Observation was necessarily made with some saturation.

A new effect, an asymmetry of line areas in the doublets, was observed for narrow ranges near two crystal orientations. The two orientations were symmetrically close to that for which the proton-proton line was parallel to the external magnetic field. It may be due to crossing of the barium quadrupole resonance frequencies over the magnetic-resonance frequencies of the protons.

INTRODUCTION

PAKE[1] was the first person to study proton positions in solids by the nuclear-magnetic-resonance technique. There is a dipole-dipole interaction between the two protons in hydrated water that causes each proton to experience a magnetic field that has two symmetric values on either side of that of the external magnetic field. This causes the resonance line to be split symmetrically into two components. The separation between the two resonance lines is given by

$$\Delta H=2\alpha[3\cos^2(\phi+\phi_0)\cos^2\delta-1]. \quad (1)$$

Here $2\alpha=3\mu/r^3$ in which μ is the proton magnetic moment and r is the proton-proton separation. ϕ is the angle between the external field, H_0, and a reference axis attached to the crystal that is in the plane of crystal rotation. ϕ_0 is the angle between the projection of the $p-p$ line (let $p-p$ mean proton-proton) onto the plane of rotation and the reference axis in the crystal, and δ is the angle between the $p-p$ line and the plane of rotation. Measuring ΔH for several ϕ's allows one to compute r, ϕ_0, and δ. Knowledge of ϕ_0 and δ permits one to compute direction angles for the $p-p$ line within the crystal.

We have measured the positions of the protons in barium bromide monohydrate as part of our general study[2-6] of the structure of the water molecule in hydrated compounds.

EXPERIMENT

We used a slightly modified Pound-Watkins NMR spectrometer with a Varian 6-in. magnet. Parameters were $Rf=27.00$ Mc, $H_0=6341$ gauss, modulation amplitude=0.75 gauss, modulation frequency= 280 cps, time constant=20 sec, and sweep speed=0.0202 gauss/sec.

The barium bromide crystal had a volume of about 2 cc and it was at room temperature. The crystal was grown slowly from saturated solution by evaporation at room temperature. Measurements of the angles between crystalline faces and of density showed that the crystal was the monohydrate.[7]

Two derivative curves were obtained for each crystal orientation while successively sweeping the field in opposite directions. Since the curves were symmetric for all orientations except two, the two sides of the two curves for each orientation except two were averaged to improve the signal-to-noise ratio. These averaged derivative curves were integrated numerically and the ΔH's were obtained from the integrated resonance curves.

At two values of ϕ the resonance spectrum showed a new effect in that the two resonance lines were not of equal areas. Therefore, special derivative curves were obtained also for five orientations closely clustered in each of these two regions. Because of the asymmetry in size, the derivatives for the "high-H_0-side" lines were averaged and the derivatives of the "low-H_0-side" lines were averaged for each orientation. Thus the asymmetry in area was maintained.

Since there was considerable saturation, the rf unit of the Pound-Watkins spectrometer was operated at the lowest rf level for which it was stable.

The rf head was simply the coil of the oscillator tank circuit. The crystal was glued to the supporting Teflon rod by a small drop of Pliobond. This adhesive and the

* This research was partially supported by the U. S. Air Force through the Air Force Office of Scientific Research of the Air Research and Development Command.

[1] G. E. Pake, J. Chem. Phys. **16**, 327 (1948).

[2] J. W. McGrath, A. A. Silvidi, and J. C. Carroll, Bull. Am. Phys. Soc. Ser. II, **3**, 349 (1958).

[3] A. A. Silvidi and J. W. McGrath, J. Chem. Phys. **30**, 1028 (1959).

[4] J. W. McGrath, A. A. Silvidi and J. C. Carroll, J. Chem. Phys. **31**, 1444 (1959).

[5] A. A. Silvidi and J. W. McGrath, Bull. Am. Phys. Soc. Ser. II, **4**, 471 (1959).

[6] A. A. Silvidi and J. W. McGrath, J. Chem. Phys. **32**, 924 (1960).

[7] B. K. Vainstein and Z. G. Pinsker, Zhur. Fiz. Khim. **24**, 432 (1950).

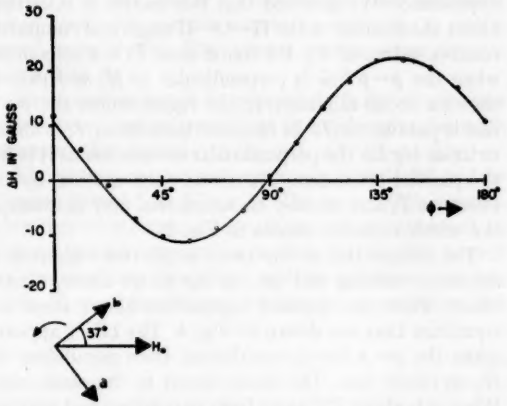

FIG. 1. Pake curve for barium bromide monohydrate. Circles represent experimental values. The solid line is a graph of $\Delta H = 11.16\,[3\cos^2(\phi+36°)-1]$. The c axis was the axis of rotation. The initial crystal orientation is shown in the lower left-hand corner.

trapped free water in the crystal gave a narrow proton signal at a ΔH of zero. This signal was easily deleted from the derivative curves before integration.

Relative resonance line areas were obtained for all crystal orientations by integrating the resonance lines. Line widths were also measured.

Rough measurements of T_1, the spin-lattice relaxation time, were made for several lines by quickly moving H_0 into a position for maximum resonance derivative and then observing the decay of the signal while H_0 remained constant.

RESULTS

The Pake curve for ΔH is shown in Fig. 1. The value of δ is $0\pm6°$ and that of ϕ_0 is $36\pm1°$. The value of 2α was determined by a least-squares deviation method for six trial values of 2α. The best value of 2α (11.16 gauss) resulted in a value of r, the $p-p$ separation, of 1.56 ± 0.02 A.

Since the crystal is orthorhombic with mutually perpendicular crystallographic axes, the direction angles of the $p-p$ line were easily determined from the values of δ and ϕ_0. They are $\alpha_0=89\pm1°$, $\beta_0=1\pm1°$, $\gamma_0=90\pm6°$. These angles are measured away from the positive crystallographic axes, a, b, and c, respectively.

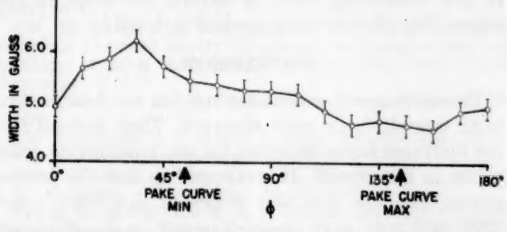

FIG. 2. Resonance line widths. The ordinate values are full line widths at half-height. The circles are average values of adjacent trios of line widths.

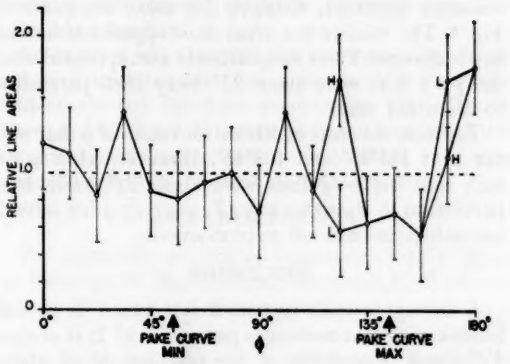

FIG. 3. Circles represent relative resonance line areas with respect to their average for all ϕ's. For the two orientations for which the pair of lines were obviously of different areas, the relative areas for each are shown. L refers to the line on the low-H_0 side while H refers to the line on the high-H_0 side.

The line widths for this crystal are unusually wide[8] owing primarily to saturation. Since line widths here appeared to depend on orientation, we measured them and they are shown in Fig. 2. This variation in line width did not appear to indicate a pair of unresolved doublets.

For most crystal orientations the lines in the doublets were of equal area. However, the line doublets were not of equal area at two values of ϕ. This is shown in Fig. 3. We repeated the observation of the resonance lines at and near the two values of ϕ where this unusual phe-

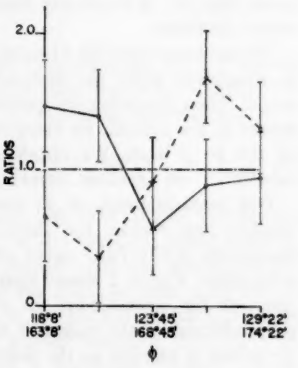

FIG. 4. Circles represent relative resonance line areas with respect to the averages for the five orientations. The ratios are the ratios of low-H_0-side areas to high-H_0-side areas. The solid line represents results for values of ϕ near 123°45′; the dashed line represents results for values of ϕ near 168°45′. The fact that the ratio for the 168°45′ case here is less than one whereas it was greater than one in Fig. 3 may be explained by our having removed the crystal from the rf coil and reinserted it between the two tests with resulting small discrepancy in angle.

[8] Our measured full line widths in gauss at half-height for single crystals are $CaSO_4 \cdot 2H_2O$ (3.2), $K(H_4B_8O_{10}) \cdot 2H_2O$ (3.6), $Li_2SO_4 \cdot H_2O$ (3.7), $K_2HgCl_4 \cdot H_2O$ (1.7), $K_2SnCl_4 \cdot H_2O$ (1.4), $Ba(ClO_3)_2 \cdot H_2O$ (1.9), $K_2CuCl_4 \cdot 2H_2O$ (3.2), $(NH_4)_2CuCl_4 \cdot 2H_2O$ (3.4), $BaCl_2 \cdot 2H_2O$ (2.5). The first three were measured with one gauss modulation amplitude. For the rest the amplitude was 0.75 gauss.

nomenon appeared. Relative line areas are shown in Fig. 4. The relative line areas show opposite inversions as ϕ is changed. These inequalities in area appeared when the $p-p$ lines were about 22° away from parallelism to H_0 either way.

T_1 was of the order of 100 sec for values of ϕ that were not near 123°45′ and 168°45′. However, when ϕ was such that the $p-p$ lines were about 22° away from parallelism to H_0, either way, T_1 was only a few seconds and saturation was not so pronounced.

DISCUSSION

A barium bromide monohydrate crystal is orthorhombic with four molecules per unit cell.[7] It is of class V_h^{16}-*Pmcn*. Knowledge of the positions of all atoms except hydrogen allows one to compute the direction angles of the $p-p$ line if one assumes that the hydrogen atoms bond the bromine atoms to neighboring oxygen atoms. This computation has given consistent results for the nine other crystals[8] that we have measured so there is no doubt that hydrogen-bond formation determines the orientation of the water molecule.

The interatomic distances from oxygen atoms to neighboring bromine atoms, I and II (in the notation of Vainstein and Pinsker[7]), are 3.57 and 3.40 A, respectively. These O—Br distances are not too large for hydrogen-bond formation since the ionic radius sum[9] for O—Br is 3.35 A. Further, we found evidence of hydrogen bonding in barium chloride dihydrate,[6] for which the O—Cl ionic radius sum was 3.21 A and the experimental bond distances were 3.20 and 3.57 A.

The H—O—H angle was computed from the crystallographic data to be 91°37′. If the O—H distances are nearly the normal 1 A, then a $p-p$ separation of 1.56 A indicates an H—O—H angle of about 103°. This suggests that the H bonds are bent, a circumstance often noted elsewhere.

We assumed that the bisector of the H—O—H angle is coincident wirh the bisector of the Br_I—O—Br_{II} angle. Then, knowing the positions of the latter three atoms in the crystal, we computed the direction angles of the $p-p$ lines. We obtained $\alpha_0=90°$, $\beta_0=0°$, and $\gamma_0=91°23'$, in excellent agreement with NMR results.

Our measurements of T_1 tend to indicate that the smaller line widths for those orientations near the maximum of the Pake curve are due to relatively less saturation. Figure 2 shows that line widths tend to be greatest for orientations for which the $p-p$ line is perpendicular to the magnetic field and least where the $p-p$ line is parallel to the field. That this may be expected is suggested by Bloembergen's theoretical treatment[10] of spin-lattice relaxation in hydrated crystals. He derived expressions for T_1 [his Eqs. (30)–(32)] that apply when the $p-p$ line undergoes hindered rotation about one axis. Then T_1 shows an orientation dependence. We assumed that this motion is occurring about the bisector of the H—O—H angle and computed relative values of T_1. We found that T_1 is a maximum when the $p-p$ line is perpendicular to H_0 and that it shows a broad minimum in the region where the $p-p$ line is parallel to H_0. In fact, the theoretical T_1 is about twice as big for the perpendicular orientation as it is for the parallel orietation. Therefore, such motion, by its effect on T_1 and thereby on saturation, may be causing the width variation shown in Fig. 2.

The inequalities of line areas in the two regions of ϕ are most striking and are, so far as we know, a new effect. There are marked regularities about these inequalities that are shown in Fig. 4. The effect appears when the $p-p$ line is equidistant from parallelism to H_0 on either side. The ratios invert in the same way. When ϕ is about 22° away from parallelism and moving toward parallelism the low-H_0-side line is first larger and then smaller than the high-H_0-side line. When ϕ is about 22° beyond parallelism and moving away from parallelism the low-H_0-side is first smaller and then larger than the high-H_0-side line. Elegant symmetry is shown in this effect.

Bloembergen[11] has suggested that this effect probably is due to a crossing of the quadrupole-resonance frequencies of the barium (or bromine) nuclei and the magnetic-resonance frequencies of the protons. The barium nuclei then exchange energy with nearby protons by the spin exchange produced by the barium-proton magnetic dipole-dipole interaction. The result is that T_1 for protons is much decreased so that the proton-resonance line is not so saturated and is bigger. This effect would be sharply orientation dependent. Woessner and Gutowsky[12] have found such sharp reductions in T_1 for protons in solid chlorobenzenes.

That this unequal area effect has not been noted before in hydrates is not surprising since several unusual conditions must be satisfied. They are (1) T_1 for the proton is long so that the proton resonance is partially saturated; (2) the interacting nucleus has a short T_1; (3), the interacting nucleus has a quadrupole coupling constant so that the quadrupole transitions occur at the same frequencies as the magnetic-resonance transitions of the protons. Even with these conditions in existence, the effect might be missed since it occurs over very narrow orientation ranges. Further discussion of this interesting effect is outside the scope of this paper. The effect is being studied in detail by us.

CONCLUSION

Proton-magnetic-resonance spectra for barium bromide monohydrate were observed. They showed that the hydrated water molecule has one equilibrium orientation in the crystal. It is oriented so that the proton-proton line has direction angles of $\alpha_0=89\pm1°$, $\beta_0=$

L. Pauling, *Nature of the Chemical Bond* (Cornell University Press, Ithaca, New York, 1940), p. 346.

[10] N. Bloembergen, Phys. Rev. **104**, 1542 (1956).

[11] N. Bloembergen (private communication).

[12] D. E. Woessner and H. S. Gutowsky, J. Chem. Phys. **29**, 804 (1958).

$1\pm1°$, and $\gamma_0=90\pm6°$. These angles are measured away from the positive crystallographic *a*, *b*, and *c* axes, respectively. The proton-proton separation is 1.56 ± 0.02 A.

The water molecule is oriented so that its hydrogen atoms bond the oxygen atom to neighboring bromine atoms in this manner: $Br_I - - H - O - H - - Br_{II}$.

The resonance lines were unusually broad with widths ranging from 6.5 to 4.2 gauss. The large width is probably due to saturation. Saturation effects appeared to depend on the orientation of the crystal with respect to the magnetic field. Line widths correlated roughly with T_1 as a function of orientation as suggested by Bloembergen's theory[10] for hydrated water molecules in hindered rotation.

A new effect was observed. For two narrow regions of crystal orientation the line areas in the resonance doublet showed line-area asymmetry. The effect is shown in Figs. 3 and 4. It may be due to crossing of the barium quadrupole-resonance frequencies over the magnetic-resonance frequencies of the protons.

ACKNOWLEDGMENTS

We appreciate perceptive suggestions kindly given by Professor N. Bloembergen. We thank K. Wylie for help in obtaining and reducing data.

THE JOURNAL OF CHEMICAL PHYSICS VOLUME 33, NUMBER 3 SEPTEMBER, 1960

Charge Transfer Reactions Producing Intrinsic Chemical Change: Methyl, Methylene, and Hydrogen Radicals Produced from Argon and Methane Reactions

C. E. MELTON

Chemistry Division, Oak Ridge National Laboratory, Oak Ridge, Tennessee*

(Received April 4, 1960)

Charge transfer reactions producing intrinsic chemical changes in the neutral molecule have been proven by mass spectrometric techniques. The charge transfer reaction

$$Ar^+ + CH_4 \rightarrow Ar + CH_3^+ + H$$

producing an intrinsic chemical change in CH_4 was found to be more probable by a factor of five than the simple charge transfer reaction

$$Ar^+ + CH_4 \rightarrow Ar + CH_4^+.$$

Charge transfer reactions in mixtures of Ar and CH_4 and Kr+CH_4 were studied over the pressure range of 0.1–0.5 mm of Hg in the ionization chamber. Reactions were elucidated by catalytic and negative ion studies as well as by the usual pressure and appearance potential techniques. In the Kr+CH_4 mixture, the reaction

$$Kr^+ + CH_4 \rightarrow Kr + CH_3^+ + H$$

producing the charged radical CH_3^+ was found to have a high probability. Absolute values for rate constants and cross sections are given for all of the charge transfer reactions observed in the Ar+CH_4 mixture. Products from these elementary charge transfer reactions are correlated to previously reported radiolytic, α ionization (W value), and hydride ion transfer studies.

INTRODUCTION

WHILE a considerable amount of experimental[1–4] and theoretical[4–10] work has been done on charge transfer reactions, little effort appears to have been directed toward determining the nature of the reactant ions and product species (ions, radicals, etc.). Consider a charge transfer reaction between a low-energy (0–0.2 ev) atomic ion and a polyatomic molecule, e.g.,

$$A^+ + RM \rightarrow A + [RM]^* \qquad (1)$$

where A^+ is any atomic ion, RM is any polyatomic molecule, and $[RM]^*$ is the product (ions, radicals, etc.). A simple charge transfer reaction would produce one product, the parent ion RM^+ perhaps in an excited state. However, there is the possibility that the activated species $[RM]^*$ would dissociate into (R^+, M, etc.), thus introducing a chemical change. Charge transfer reactions producing inherent chemical changes would greatly complicate the establishment of detailed mechanisms in the radiation chemistry of gases, since these reactions would give rise to ions, radicals, and intermediate products.

It is known that traces of impurities in many of the noble gases increase the number of ions produced by

* Operated for the U. S. Atomic Energy Commission by Union Carbide Corporation.

[1] C. E. Melton and G. F. Wells, J. Chem. Phys. **27**, 1132 (1957).

[2] V. Čermák and Z. Herman, Czechoslov. Chem. Commun. **25**, 1210 (1960).

[3] W. H. Hamill and Nico A. I. M. Boelrijk, presented at American Chemical Society Symposium on Nonanalytical Applications of Mass Spectrometry, Atlantic City, New Jersey, September 16, 1959.

[4] P. S. Rudolph and C. E. Melton, J. Chem. Phys. **32**, 586 (1960).

[5] M. Burton and J. L. Magee, J. Phys. Chem. **56**, 842 (1952).

[6] R. S. Mulliken, J. Am. Chem. Soc. **74**, 811 (1952).

[7] R. S. Mulliken, J. Phys. Chem. **56**, 801 (1952).

[8] J. L. Magee, J. Phys. Chem. **56**, 555 (1952).

[9] H. S. W. Massey and E. H. S. Burhop, *Electronic and Ionic Impact Phenomena* (Oxford University Press, New York, 1952).

[10] S. C. Lind and D. C. Bardwell, Science **62**, 422, 593 (1925); **63**, 310 (1926); J. Am. Chem. Soc. **48**, 575 (1926).

alpha particles in these gases.[11,12] This increase in ionization by impurities has been attributed to a discharge of the metastable state of the noble gas (X, e.g., He*) by an impurity (Y, e.g., Ar) which has an ionization potential less than or equal to the metastable level, e.g.,

$$He^* + Ar \rightarrow He + Ar^+ + e^-. \quad (2)$$

This explanation becomes untenable, however, for increased ionization produced by impurities which have an ionization potential higher than that of the metastable level such as have been observed in argon mixtures.[13,14] On the other hand, charge transfer from the noble gas to the impurity producing inherent chemical changes could explain these results very nicely since new products would be formed. Some of these products would have ionization potentials less than that of the metastable levels.

A perusal of the A.P.I. tables[15] of mass spectral data shows that ionization by electron impact of polyatomic molecules is usually accompanied by dissociation or chemical change producing many species, including both ions and radicals. Studies of ionization by α particles[16] and collision-induced dissociation[17,18] suggest that the ionization-dissociation of a molecule is an intrinsic property of the molecule and not a function of the mode of excitation. Hence, the nature of the products from RM produced by charge transfer, reaction (1), should be qualitatively in agreement with those from RM produced by electron impact, if a comparison is made between systems where dissociation of the complex $[RM]^*$ is energetically possible.

Argon was selected to furnish the atomic ion A to react with CH_4 (RM) in this study because chemical changes are likely for this system, since dissociation of the complex species $[CH_4]^*$ is energetically possible. Also, a comparison of the product with those previously reported[15,17] would appear worthwhile. This mixture was also selected because our previous α ionization studies[14] showed that the admixing of 5% of CH_4 to Ar increased the total ionization of 2%. This system is not complicated by ionization of CH_4 from argon metastables, reaction (2), since this reaction is not energetically possible, being endothermic by 1.5 ev. Products, in particular radicals and negative ions, which would give illuminating information to previous ionization and radiolysis studies were explicitly considered and the results are discussed in terms of radiation chemistry, excitation energy, W values,[14] and hydride ion transfer.

EXPERIMENTAL

Descriptions of the research mass spectrometer, experimental procedure, and necessary calibration have been given in detail elsewhere.[1,16,19] Therefore, only a very brief description of the method will be given here.

The gas to be investigated is contained at high pressure, 10–20 cm, in a three-liter expansion volume which is connected to the ionization chamber by a gold foil molecular leak 0.001 in. in diam. Gas flowing through the gold leak passes into the ionization chamber and is ionized by electron bombardment. In this study, the electron energy and intensity could be controlled to produce primary ions from either CH_4 alone or from both Ar and CH_4. Primary ions thus produced could react in the ionization chamber while at low energy (0–0.2 ev). Reaction mechanisms were deduced by the usual methods[20] of studying the intensities of primary and secondary ions as a function of both electron energy and pressure. Proposed reaction mechanisms were further substantiated by catalytic[21] and negative ion studies. Polymeric ions[22] resulting from ion-molecule reactions[22] not involving charge transfer, although observed, are not reported in this study.

Methane (The Matheson Company, Inc., C.P. 99.0+%) and Argon (National Cylinder Gas, 99.9%) were used without further purification.

RESULTS AND DISCUSSION

Striking differences were observed in the ion patterns from CH_4 in pure CH_4 and in a mixture of one CH_4 to 10 Ar, as shown in Fig. 1. The indicated electron energy was reduced to 20 ev for these data to eliminate interference from multiply charged ions. The CH_4 pressure, the intensity, and energy of the ionizing electrons are identical in both determinations, yet the relative intensity of CH_3^+ and CH_2^+ is much higher in the mixture. These data clearly indicate that the enhancement of the relative intensities of both CH_2^+ and CH_3^+ was consummated by the admixing of Ar to the system. The question then arises as to the mechanism for formation of these charged radicals. One possibility which will be shown to be untenable would be a reaction between argon in a metastable state, Ar*, and CH_4 to produce free radicals, e.g.,

$$Ar^* + CH_4 \rightarrow Ar + CH_3 + H$$
$$\rightarrow Ar + CH_2 + H_2.$$

[11] W. P. Jesse, H. Forstat, and J. Saduskis, Phys. Rev. **88**, 417 (1952).
[12] T. E. Bortner and G. S. Hurst, Phys. Rev. **90**, 160 (1953).
[13] J. Sharpe, Proc. Phys. Soc. (London) **A65**, 859 (1952).
[14] C. E. Melton, G. S. Hurst, and T. E. Bortner, Phys. Rev. **96**, 643 (1954).
[15] Catalog of Mass Spectral Data, API Research Project 44, Carnegie Institute of Technology, Pittsburgh, Pennsylvania.
[16] C. E. Melton and P. S. Rudolph, J. Chem. Phys. **30**, 847 (1959).
[17] C. E. Melton and H. M. Rosenstock, J. Chem. Phys. **26**, 314 (1957).
[18] E. Lindholm, Arkiv Fysik **8**, 435 (1954).
[19] G. F. Wells and C. E. Melton, Rev. Sci. Instr. **28**, 1065 (1957).
[20] T. W. Martin and C. E. Melton, J. Chem. Phys. **32**, 700 (1960).
[21] C. E. Melton (to be published).
[22] C. E. Melton and Gus A. Ropp, J. Am. Chem. Soc. **80**, 5573 (1958); P. S. Rudolph and C. E. Melton, J. Phys. Chem. **63**, 915 (1959).

The resultant free radicals would be subsequently ionized by Ar* or by the electron beam.

This possible mechanism was investigated by three independent techniques.

Technique 1 consists of determining the appearance potentials for CH_3^+, CH_2^+, CH_4^+, and Ar^+. Results from these determinations are given in Fig. 2. The data show that Ar* is not a precursor for these ions since they are not detected at the excitation energy of the metastable state of Ar* which is 11.5 ev. These data show that CH_4^+ is not a precursor for CH_3^+ and CH_2^+ by an ion-molecule reaction because of their higher

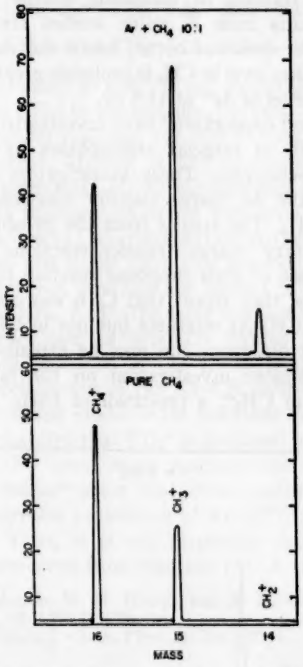

FIG. 1. Relative intensities of ions from CH_4 produced by (a) charge transfer from Ar^+, upper portion, and (b) 20-ev ionizing electrons, lower portion.

appearance potential. Thus, the only other possible reactant is Ar^+.

Technique 2 involves determining the percent of negative ions from CH_4 and from a mixture of CH_4 and Ar for the same partial pressure of CH_4. Data from this study are given in Table I. Although the absolute intensity of all the negative ions is greatly increased in the mixture, the percents of the individual species do not change. The increase in absolute intensity is explained on the basis of ionization by secondary electrons produced in the formation of Ar^+. If large quantities of $\cdot CH_3$ and $\cdot CH_2$ were formed in the mixture, a subsequent ionization of these radicals would increase the percents of CH_3^- and CH_2^-. Since this was not observed, these data indicate that CH_3^+ and

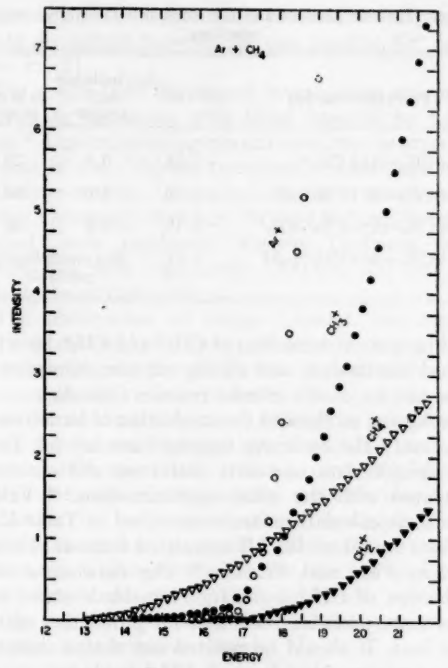

FIG. 2. Appearance potential data for a 10 Ar:1 CH_4 mixture. The energy scale was not calibrated and represents indicated energy.

CH_2^+ are not produced from free radicals. The data from this technique are also consistent with a mechanism involving Ar^+.

Technique 3 involves a study of the relative intensity of CH_3^+ and CH_2^+ as a function of temperature and in the presence of a catalyst. Ion patterns were determined in the mixture while operating a Pt catalyst at 1000°C in the ionization chamber. Under these conditions, free radicals would react very rapidly,[23] and the relative intensities of CH_3^+ and CH_2^+ should be less than that of CH_4^+, mass 16, if they were produced from radicals. However, this was not the case. CH_3^+ was the most intense ion beam observed from CH_4 at both 23° and 1000°C. Thus, the three independent techniques

TABLE I. Negative ions from methane and methane+argon.

Ion	% distribution of negative ions from CH_4[a]	% distribution of negative ions from CH_4+Ar[b]	Intensity CH_4[a]	Ions/sec CH_4+Ar[b]
C^-	47	46	1739	6298
CH^-	40	41	1480	5613
CH_3^-	12	12	444	1643

[a] CH_4 pressure = 1×10^{-5} mm.
[b] Ar pressure = 0.5 mm; CH_4 pressure = 1×10^{-5} mm.

[23] E. W. R. Steacie, *Atomic and Free Radical Reactions* (Reinhold Publishing Corporation, New York, 1954), p. 839 ff.

TABLE II. Cross sections and rate constants for charge transfer reactions.

Probable Reaction	ΔH (ev)	(cc/molecule sec) $K\times10^{9}$	σ_2 in cm^2 $\times10^{-16}$
$Ar^+ + CH_4 \rightarrow Ar + CH_4^+$	−2.78	0.3	20
$Ar^+ + CH_4 \rightarrow Ar + CH_3^+ + H$	−1.36	1.6	104
$Ar^+ + CH_4 \rightarrow Ar + CH_2^+ + H_2$	−0.16	0.3	20
$Ar^+ + CH_4 \rightarrow Ar + CH_2^+ + 2H$	4.34	Not energetically probable	

tend to rule out formation of CH_3^+ and CH_2^+ by a free radical mechanism, and clearly support formation of these ions by charge transfer reaction from Ar^+.

On having established the mechanism of formation of CH_3^+ and CH_2^+ by charge transfer from Ar^+ (cf. Table II), specific rate constants and cross sections were calculated with the usual approximations.[1,20] Values from these calculations are summarized in Table II in addition to values for ΔH calculated from data tabulated in Field and Franklin.[24] The data show that production of CH_3^+ by charge transfer is about five times more probable than that for production of the other ions. It should be pointed out that a material balance requires that for each CH_3^+ produced, an $\cdot H$ radical is produced. Also, CH_2^+ is always formed by the loss of H_2 rather than $2\cdot H$ because of the energetics shown. It might be observed that a hydride ion transfer[25] from CH_4 to Ar^+ could explain the production of CH_3^+. However, to explain the production of CH_3^+ by hydride ion transfer would require postulating the unlikely compound ArH. Charge transfer and hydride ion transfer are indistinguishable in most systems when the reaction results in the loss of one hydrogen from the neutral molecule, e.g.,

$$A^+ + MH \rightarrow A + M^+ + H.$$

On the other hand, hydride ion transfer will not explain the production of CH_2^+ since Ar^+ will not accept either H_2^- or $2H^-$.

If one compares the patterns of ions resulting from charge transfer from Ar^+ to CH_4 to those produced in CH_4 by other modes of ionization,[15,17] marked differences are found. This departure from the normal mode of dissociation for CH_4 is significant in that results from some previous studies of $Ar:CH_4$ mixtures can be readily explained. For example, the 2% decrease in the W value by admixing of 5% of CH_4 in Ar[14] can now be explained on the basis of the CH_2^+ and CH_3^+. CH_2^+ and CH_3^+ are known to react with CH_4 to form polymeric ions such as $C_2H_5^+$, which when neutralized dissociate and become C_2H_4, etc. In addition, CH_2^+ and CH_3^+ when neutralized become $\cdot CH_2$ and $\cdot CH_3$. Subsequent reactions of these radicals are known[23] to produce C_2H_6 and other hydrocarbons which have a lower ionization potential than that of Ar* and would consequently be ionized by Ar*.

A transfer of excitation energy from Ar* to the first excitation level of CH_4, whose configuration is

$$(1S)^2(2S)^2(2p)^5(3sa_1),$$

may or may not be possible. On using the estimated value of 9.9 ev,[26] a transfer of excitation energy would be possible. However, using the calculated value of 18.9 ev,[27] transfer of excitation energy would not occur. Results from W value studies are suggestive that transfer does not occur, hence the value for the first excitation level in CH_4 is probably greater than the excitation level of Ar* at 11.5 ev.

Hamill and co-workers[28] have investigated the radiolysis of CH_4 in rare-gas atmospheres by employing different techniques. These investigators found evidence for the Ar charge transfer reaction producing CH_3^+ in CH_4. The results from the present study of the elementary charge transfer reactions appear to simplify some of their proposed reaction mechanisms. For example, they report that C_2H_4 was observed as a product in CH_4–Ar mixtures but not in CH_4–Kr mixtures. Their difference can now be explained by data from the present investigation on the basis of the production of CH_2^+, a precursor of C_2H_4, by Ar and

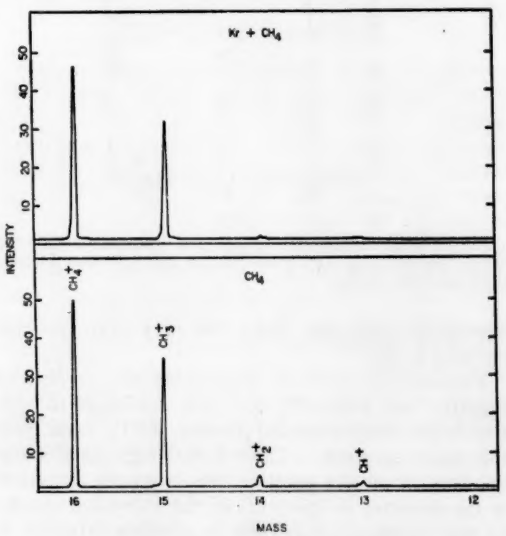

FIG. 3. Relative intensities of ions from CH_4 produced by (a) charge transfer from Kr^+, upper portion and (b) 25-ev ionizing electrons, lower portion.

[24] F. H. Field and J. L. Franklin, *Electron Impact Phenomena* (Academic Press, Inc., New York, 1957), p. 243 ff.
[25] F. W. Lampe, F. H. Field, and J. L. Franklin, J. Am. Chem. Soc. **80**, 5587 (1958).
[26] R. S. Mulliken, J. Chem. Phys. **3**, 517 (1935).
[27] K. Funabashi and J. L. Magee, J. Chem. Phys. **26**, 407 (1957).
[28] G. G. Meisels, W. H. Hamill, and R. R. Williams, Jr., J. Chem. Phys. **25**, 790 (1956).

not by Kr. The Kr charge transfer reaction

$$Kr^+ + CH_4 \rightarrow Kr + CH_2^+ + H_2 \qquad (3)$$

is endothermic by 1.6 ev and hence not probable. Experimentally, CH_2^+ was not observed in significant quantities in a CH_4–Kr mixture, as shown in Fig. 3. The partial pressure of CH_4 was identical in both cases, but the absolute intensity of both CH_3^+ and CH_4^+ was found to be much higher in the mixtures because of the following reactions:

$$Kr^+ + CH_4 \rightarrow Kr + CH_4^+ \qquad \Delta H = -0.9 \text{ ev} \qquad (4)$$

$$Kr^+(^2P_{\frac{1}{2}}) + CH_4 \rightarrow Kr + CH_3^+ + H \qquad \Delta H = 0.4 \text{ ev}$$

$$Kr^+(^2P_{\frac{3}{2}}) + CH_4 \rightarrow Kr + CH_3^+ + H \qquad \Delta H = -0.3 \text{ ev}. \qquad (5)$$

Since the intensity of CH_4^+ is not significantly greater than that of CH_3^+ in the mixture, the cross section and rate constant for reactions (4) and (5) are not significantly different. Meisels, *et al.*[28] concluded that the CH_4–Ar mixture and CH_4–Kr mixture must obey different reaction mechanisms under radiolysis principally because reaction (5) was ruled out on energetic grounds. Results from this study[8] show that reaction (5) is very probable and that products are formed in mixtures of CH_4–Ar and CH_4–Kr by the same reaction mechanisms with the exception of products formed from CH_2^+ which is not produced in the Kr system. In a subsequent investigation of the Kr–CH_4 system, Meisels, *et al.*[29] also found evidence for reactions (4) and (5). Meisels[30] suggested that CH_3^+ is produced by a reaction with $Kr^+(^2P_{\frac{1}{2}})$ ions. Mass spectrometric appearance potential studies[31] show that 20-ev ionizing electrons produce a greater population of $Kr^+(^2P_{\frac{1}{2}})$ ions than of $Kr^+(^2P_{\frac{3}{2}})$. Thus, it is not surprising that the CH_3^+ radical is observed from reaction (5). A study of this reaction by accurate appearance potential techniques[31,32] would distinguish between the two possible Kr^+ reactants in (5).

The results from the present investigation are qualitatively in agreement with those reported by Lindholm.[33] A quantitative agreement would not be expected because of the different experimental conditions used in the two studies. For example, in the present investigation, low-energy (0–0.2 ev) Ar^+ and Kr^+ ions, possibly excited, were employed, whereas Lindholm bombarded CH_4 with high-energy (500 ev) Kr^+ and Ar^+ ions in the ground state.

The observation of charge transfer resulting in intrinsic chemical changes in the neutral may in some instances simplify the elucidation of detailed reaction mechanisms in radiolytic studies. However, in most cases the results will be more difficult to interpret because reactions of this type provide another source of reactants. Charge transfer reactions producing inherent chemical changes in the neutral molecule may be as important in radiation chemistry as simple charge transfer reactions. In systems where charge transfer reactions are energetically possible, but are apparently quite improbable (e.g., C_2H_2 and C_2H_4 systems),[4] charge transfer producing chemical change may explain the seemingly negative results.

ACKNOWLEDGMENT

The author wishes to thank Russell Baldock, P. S. Rudolph, E. H. Taylor, and G. F. Wells for helpful discussions pertaining to this study. Thanks also go to Professor P. H. Emmett of Johns Hopkins for valuable criticisms and suggestions concerning this manuscript.

[28] G. G. Meisels, W. H. Hamill, and R. R. Williams, Jr., J. Phys. Chem. **61**, 1456 (1957).
[29] G. G. Meisels, J. Chem. Phys. **31**, 284 (1959).
[31] R. E. Fox, W. M. Hickam, T. Kjeldaas, Jr., and M. Grove, Phys. Rev. **84**, 859 (1951); R. E. Fox, W. M. Hickam, and T. Kjeldaas, *ibid.* **89**, 555 (1953).
[32] H. Hurzeler, M. G. Inghram, and J. D. Morrison, J. Chem. Phys. **28**, 76 (1958).
[33] E. Lindholm, Z. Naturforch. **9A**, 535 (1954).

THE JOURNAL OF CHEMICAL PHYSICS VOLUME 33, NUMBER 3 SEPTEMBER, 1960

Diffusion in a Linear Lattice*

IGOR W. PLESNER

Institute of Physical Chemistry, University of Copenhagen, Denmark

(Received April 1, 1960)

Diffusion in crystals by a vacancy mechanism is described by a model consisting of an isotope and a vacancy imbedded in a linear lattice of harmonic oscillators. Assuming a 6–12 potential between defects and lattice atoms, the anharmonic interaction is explicitly calculated. The usual approximation of assuming this interaction to depend linearly on the frequency is shown to be valid as long as the Debye approximation for the frequency spectrum is applicable.

The lattice with defects is analyzed using the formalism developed by Brout and Prigogine. In order to solve the equations, the concept of localized modes is introduced. The localized mode is approximated by the oscillation of the defect (isotope) in the lattice. The justification for this is investigated by a method due to Montroll and Potts.

The diffusion constant is calculated and shown to depend on the fourth power of the defect frequency. This is in agreement with an earlier result by Klemens, but deviates appreciably from the usual first power dependence.

I. INTRODUCTION

IN theories of diffusion, it is customary to calculate the rate at which a particle escapes a potential minimum. However, no account is taken of the interaction between the particle and its surroundings that actually causes the particle to "jump."

It is of interest, therefore, to calculate a diffusion coefficient, where we do not neglect the interaction terms in the Hamiltonian of the system.

A formalism well suited for this purpose is the time-dependent perturbation method recently developed by Brout and Prigogine[1] for solving the Liouville equation in phase space. They show how an equation describing a "diffusion in phase space" can be obtained on the basis of the reversible laws of mechanics.

The present paper consists of three main parts. In order to solve the "diffusion equation" in phase space, a quantity describing the irreversible interaction is needed. This quantity can be obtained when a particular interaction potential is introduced. Section II of this paper is concerned with this problem, as well as the solution in detail of the diffusion equation for the density in phase space for a system consisting of a particle immersed in a "thermostat" of harmonic oscillators. However, in solving this equation (this has been done generally by Bak[2]), it is necessary to introduce a factorization of the density function, i.e., we introduce the concept of "localized modes." The justification for this, as well as for the use of the harmonic frequency for this "disturbed" mode, is investigated by the method of Montroll and Potts[3] in Sec. IV, while Sec. III is a brief survey of the necessary formalism from their paper.

Section V concludes the paper with summary and discussion of the results obtained by this method. It is concluded that one can by this treatment describe a vacancy mechanism for diffusion. Because of the approximations it is necessary to make, our results should apply only to isotope diffusion, where the diffusing mass is only slightly different from the lattice atoms.

The model used here is the very simple one of an isotope imbedded in a linear lattice of harmonic oscillators. There is no reason to believe that the introduction of a three-dimensional lattice would alter the results in principle, whereas the mathematics would become considerably more complicated.

II

(a) As a model we take a string of oscillators of which one has a mass different from that of the others. This (isotopic) atom is oscillating around its equilibrium position under the influence of the field from the rest of the lattice. Only nearest-neighbor interactions are considered, and we calculate the harmonic interaction as the second derivative of the assumed potential. For the potential between two particles, we use a 6–12 potential (see the following), in which the characteristic parameters ϵ^* and r^* are the depth and position of the potential minimum, respectively. However, the (defect) particle is also influenced by anharmonic forces from the surroundings. Because of these forces which we can calculate from the potential, the particle will have a tendency to "escape" from its position in the lattice. This can be accomplished if the neighboring lattice position is vacant. This process of jumping into a vacancy, i.e., of surmounting an energy barrier between two potential minima, is characterized by a "mean time of stay," i.e., a rate constant. On having found this, we use the ordinary random-walk expression for the diffusion coefficient:

$$D=\tfrac{1}{2}a^2k,$$

where a is the jump length, i.e., the lattice constant, to calculate D.

* The work reported in this paper was carried out under contract with the U. S. Air Force, Air Research and Development Command, European Office.

[1] R. Brout and I. Prigogine, Physica **22**, 621 (1956).

[2] Thor A. Bak, *Contributions to the Theory of Chemical Kinetics* (John Wiley & Sons, Inc., New York, 1959); T. A. Bak, M. Goche, and F. Henin, Mol. Phys. **2**, 181 (1959).

[3] E. W. Montroll and R. B. Potts, Phys. Rev. **100**, 525 (1955).

Instead of actually considering a vacancy in the lattice, we adopt the suggestion of Montroll and Potts[3] and characterize a hole by a larger than normal spring constant. This corresponds to a relative attraction to the hole of the adjacent particles, which is not unreasonable, since there is nothing in a hole to yield a repulsive force. It has been shown[3] that such a lattice with one (or more) defects will develop "localized modes" around the defect(s). In the present formalism, this fact is necessary in order to calculate the aforementioned rate constant k.

Thus, the model for vacancy diffusion with which we shall be concerned here is simply a particle with its two nearest neighbors, one of which is a vacancy, immersed in a "thermostat" of harmonic oscillators. The anharmonic interactions that induce the particle to diffuse are explicitly calculated and used for the determination of the rate constant for the escape of the particle from its potential minimum.

(*b*) We consider a linear chain of atoms in a lattice. For the potential between two atoms a distance r apart, we take the 6–12 potential

$$U=-\epsilon^*\left[2\left(\frac{r^*}{r}\right)^6-\left(\frac{r^*}{r}\right)^{12}\right] \qquad \text{(II.1)}$$

where ϵ^* and r^* are characteristic parameters. In the calculations we take account of nearest neighbor interactions only.

Let one of the lattice atoms have a mass m different from that of the others. This corresponds to an isotope imbedded in the lattice. We assume that there are only harmonic interactions between the lattice particles, whereas the defect in addition to a harmonic interaction with its neighbors is also influenced by an anharmonic force due to the fact that not only the defect, but also its neighbors are displaced from their equilibrium positions in the lattice.

The Hamiltonian for the total system of lattice and defect is

$$H=\sum_k \omega_k J_k+(p^2/2m)+\tfrac{1}{2}\gamma r^2+\lambda V(r), \qquad \text{(II.2)}$$

where ω_k is the frequency of the mode with wave vector k; J_k the action variable for the kth mode; p, momentum of defect; m, mass of defect; $\gamma=(\partial^2 U/\partial r^2)_{r=a}$, a=lattice spacing; r=displacement of defect from lattice equilibrium position; and $V(r)$ perturbing (anharmonic) potential.

For $V(r)$, we use

$$V(r)=\sum_n W(|\,\mathbf{r}-\mathbf{a}_n\,|)\,u_n$$

$$=\sum_f V_f q_f e^{ifr},$$

with

$$V_f=\sum_n W(|\,r-a_n\,|)\,\exp[-if(r-a_n)]. \qquad \text{(II.3)}$$

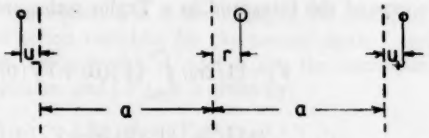

FIG. 1.

Here r is the position vector of the defect, a_n the position vector of the nth lattice point. q_f is the normal coordinate for the fth normal mode. $W(r-a_n)$ is the nonharmonic force from the nth particle on the defect and is given by

$$W(r-a_n)=(\partial U/\partial u_n)_{u_{n=0}}. \qquad \text{(II.4)}$$

The quantity of interest in this framework, i.e., the quantity that determined the irreversible behavior of the system (see the following) is

$$|\,V_f\,|^2/\omega_f^2.$$

Hence, we need to find V_f. The general theory assumes this to be independent of r, the position of the defect. Here we shall use an average value of V_f, where the average is taken over all possible positions of the defect.

For a harmonic potential the connection between the position r and the angle variable α is given by

$$r=(2H_0/\gamma)^{\frac{1}{2}}\sin\alpha\equiv r_0\sin\alpha, \qquad \text{(II.5)}$$

where γ is the above-mentioned force constant and

$$H_0=(p^2/2m)+\tfrac{1}{2}\gamma r^2$$

is the unperturbed Hamiltonian for the defect, r being its displacement from its equilibrium position.

Let us consider the defect and its two nearest neighbors. From Fig. 1 it is clear that we have

$$|\,r-a_+\,|=a-r+u_+$$

$$|\,r-a_-\,|=a+r-u_-.$$

On using Eqs. (1), (3), and (4), we obtain for V_f

$$V_f=C_0\left\{\frac{\exp[if(a-r)]}{(a-r)^7}\left[1-\frac{r^{*6}}{(a-r)^6}\right]\right.$$

$$\left.-\frac{\exp[-if(a+r)]}{(a+r)^7}\left[1-\frac{r^{*6}}{(a+r)^6}\right]\right\} \qquad \text{(II.6)}$$

with

$$C_0=12\epsilon^* r^{*6}.$$

When the angle variable takes on values from $-\frac{1}{2}\pi$ to $+\frac{1}{2}\pi$, r varies from $-r_0$ to $+r_0$. This is the range in which the particle actually moves. The quantity we wish to find is then

$$\bar{V}_f=(1/2r_0)\int_{-r_0}^{r_0} V_f(r)\,dr. \qquad \text{(II.7)}$$

We expand the integrand in a Taylor series around $r=0$ (primes indicate differentiation with respect to r):

$$V_f=(1/2r_0)\int_{-r_0}^{r_0}\{V_f(0)+V_f'(0)r+(1/2!)V_f''(0)r^2+\cdots\}dr$$

$$=(1/2r_0)\{V_f(0)2r_0+V_f'(0)[\tfrac{1}{2}r_0^2-\tfrac{1}{2}r_0^2]+(1/2!)V_f''(2r_0^3/3)+\cdots\}$$

$$=V_f(0)+\tfrac{1}{6}V_f''(0)r_0^2+\cdots. \tag{II.8}$$

The second derivative is found in a straightforward manner, and putting $r=0$, we obtain

$$V_f''(0)=C_0\{\{(56/a^9)-(182r^{*6}/a^{15})-f^2[(1/a^7)-(r^{*6}/a^{13})]\}2i\sin fa-4i[(7/a^8)-(13r^{*6}/a^{14})]f\cos fa\}. \tag{II.9}$$

For $V(0)$, we obtain

$$V(0)=C_0[(1/a^7)-(r^{*6}/a^{13})]2i\sin fa. \tag{II.10}$$

Hence, we have

$$\tilde{V}_f=C_0\{[(1/a^7)-(r^{*6}/a^{13})]2i\sin fa+\{[(56/a^9)-(182r^{*6}/a^{15})]\tfrac{1}{3}i\sin fa-[(1/a^7)-(r^{*6}/a^{13})]\tfrac{1}{3}if^2\sin fa$$
$$-[(7/a^8)-(13r^{*6}/a^{14})](2i/3)f\cos fa\}r_0^2+\cdots\}. \tag{II.11}$$

Here, as in the following, we retain only r_0^2. On writing V_0 for the term not containing r_0, and V_1 for the coefficient of r_0^2, we have

$$\tilde{V}_f=V_0+V_1r_0^2$$
$$|\tilde{V}_f|^2=|V_0|^2+2|V_0V_1|r_0^2[+0(r_0^4)]. \tag{II.12}$$

In order to simplify the expression somewhat, let us put

$$a/r^*=1+\delta$$

and neglect all terms of order δ^2 or higher.

For V_0, we then have

$$V_0=12\epsilon^*r^{*6}(2i/a^7)[1-(r^{*6}/a^6)]\sin fa$$
$$=24\epsilon^*i[1/(1+\delta)^6](1/a)[1-[1/(1+\delta)^6]\sin fa$$
$$\simeq 24i\epsilon^*(1-6\delta)6\delta(\sin fa/a)$$
$$\simeq 144i\epsilon^*\delta(\sin fa/a). \tag{II.13}$$

V_1 becomes

$$V_1=4i\epsilon^*r^{*6}\{(14/a^9)\{4-[13/(1+\delta)^6]\}\sin fa$$
$$-(1/a^7)\{1-[1/(1+\delta)^6]f^2\sin fa$$
$$-(2/a^8)\{7-[13/(1+\delta)^6]\}f\cos fa$$
$$\simeq 4i\epsilon^*(1-6\delta)(1/a^8)\{14\sin fa[78\delta-6]$$
$$-6\delta(af)^2\sin fa-2af\cos fa[78\delta-6]\}. \tag{II.14}$$

In this expression, we put

$$\sin fa\simeq fa\cos fa,$$

which is valid for small f, and we obtain

$$V_1=(4i\epsilon^*/a^8)\sin fa\{[936-6(af)^2]\delta-114+(756-72)\delta\}\simeq(4i\epsilon^*/a^8)\sin fa[1620\delta-114]. \tag{II.15}$$

On inserting these expressions in Eq. (II.12), we obtain

$$|\tilde{V}_f|^2=144^2\epsilon^{*2}(\delta^2/a^2)\sin^2fa+\frac{8\cdot144\epsilon^{*2}\sin fa}{a^4}(1620\delta+114)r_0^2$$
$$=144\epsilon^{*2}(\sin^2fa/a^2)\{144\delta^2+(8\delta/a^2)r_0^2[1620\delta-144]\}$$
$$=144^2\epsilon^{*2}(\sin^2fa/a^2)\delta^2\{1+(r_0^2/a^2)[90-(19/3\delta)]\}$$
$$\simeq 144^2\epsilon^{*2}(\delta^2/a^2)\sin^2fa\{1-(19/3\delta)(r_0^2/a^2)\}. \tag{II.16}$$

For a linear chain with nearest-neighbor interactions only, we have

$$\omega_f=\omega_0\sin(fa/2),$$

and hence

$$\frac{|\tilde{V}_f|^2}{\omega_f^2}=\frac{144^2\epsilon^{*2}(\delta^2/a^2)\sin^2fa\{1-(19/3\delta)(r_0^2/a^2)\}}{\omega_0^2\sin^2(fa/2)}. \tag{II.17}$$

In the general theory, this quantity is considered to be independent of f, and we see that this is so only for small f, for which we have

$$\sin fa \simeq fa,$$

i.e., we can use a Debye frequency spectrum

$$\omega_f = cf$$

where c is the velocity of sound in the lattice.

In this approximation, we then have

$$|\tilde{V}_f|^2/\omega_f^2 = 4\cdot 144^2(\epsilon^{*2}/\omega_0^2)(\delta^2/a^2)\{1-(19/3\delta)(r_0^2/a^2)\}$$

$$= (144^2\epsilon^{*2}\delta^2/c^2)\{1-(19/3\delta)(r_0^2/a^2)\}$$

$$= \beta_1 - \beta_2 r_0^2 \qquad \text{(II.18)}$$

$$\beta_1 = 144^2\epsilon^{*2}\delta^2/c^2 \qquad \text{(II.19)}$$

$$\beta_2 = 144^2\epsilon^{*2}19\delta/3c^2a^2. \qquad \text{(II.20)}$$

The equation we wish to solve for the density in action space is[2]

$$\frac{\partial\rho}{\partial t} = \pi\lambda^2\frac{L}{2\pi}\sum_\nu\int d\omega_f\frac{\partial f}{\partial\omega_f}\left\{\left(\frac{\partial}{\partial J_f}+\nu\frac{\partial}{\partial J}\right)|V_{\nu,f}|^2\right.$$

$$\times\delta(\nu\omega+\omega_f)\left(\frac{\partial}{\partial J_f}+\nu\frac{\partial}{\partial J}\right)+\left(\frac{\partial}{\partial J_f}-\nu\frac{\partial}{\partial J}\right)|V_{\nu,f}|^2$$

$$\left.\times\delta(\nu\omega-\omega_f)\left(\frac{\partial}{\partial J_f}-\nu\frac{\partial}{\partial J}\right)\right\}\rho. \qquad \text{(II.21)}$$

In this equation L is the length of the chain, J_f and J are action variables for the normal mode f and the defect, respectively, ω_f and ω are the corresponding frequencies, and $|V_{\nu,f}|^2$ is given by

$$|V_{\nu,f}|^2 = |V_f|^2\,|q_f|^2 J_\nu^2(fr_0),$$

where q_f is the normal coordinate for the phonon with wave number f, and $J_\nu(fr_0)$ is the νth Bessel function. $\delta(x)$ is the Dirac δ function. This equation is obtained by the application of the double limiting procedure, described by Brout and Prigogine,[1] to the Liouville equation.

In order to solve this equation for the problem we consider, we assume that the lattice is in equilibrium with a Boltzmann distribution, and hence we write for ρ

$$\rho = \exp[-(kT)^{-1}\sum_f\omega_f J_f]\cdot\phi(J,t). \qquad \text{(II.22)}$$

$\phi(J,t)$ is then a probability density in action space for the defect. This involves an assumption of "localized modes." We consider the justification of this procedure in Sec. IV. We also use a Debye spectrum for the frequencies:

$$\omega_f = cf,$$

and hence

$$\partial f/\partial\omega_f = 1/c.$$

With the frequencies independent of the action variables, Eq. (II.21) becomes

$$\exp[-(kT)^{-1}\sum_f\omega_f J_f]\frac{\partial\phi}{\partial t} = \pi\lambda^2\frac{L}{2\pi}\sum_\nu\int d\omega_f c^{-1}\cdot\delta(\nu\omega+\omega_f)\left[\left(\frac{\partial}{\partial J_f}|V_{\nu f}|^2\right)\left(\frac{\partial}{\partial J_f}+\nu\frac{\partial}{\partial J}\right)+|V_{\nu f}|^2\left(\frac{\partial^2}{\partial J_f^2}+\nu\frac{\partial^2}{\partial J\partial J_f}\right)\right.$$

$$+\nu\frac{\partial}{\partial J}|V_{\nu f}|^2\left(\frac{\partial}{\partial J_f}+\nu\frac{\partial}{\partial J}\right)\Big]-\delta(\nu\omega-\omega_f)\left[\left(\frac{\partial}{\partial J_f}|V_{\nu f}|^2\right)\left(\frac{\partial}{\partial J_f}-\nu\frac{\partial}{\partial J}\right)+|V_{\nu f}|^2\left(\frac{\partial^2}{\partial J_f^2}-\nu\frac{\partial^2}{\partial J\partial J_f}\right)-\nu\frac{\partial}{\partial J}|V_{\nu f}|^2\right.$$

$$\left.\left.\times\left(\frac{\partial}{\partial J_f}-\nu\frac{\partial}{\partial J}\right)\right]\right\}\phi\exp(-(kT)^{-1}\sum_f\omega_f J_f). \qquad \text{(II.23)}$$

Let us write this equation in the following form, canceling the exponentials:

$$\partial\phi/\partial t = \pi\lambda^2(L/2\pi)\sum_\nu\int d\omega_f c^{-1}\{\delta(\nu\omega+\omega_f)(I+II)+\delta(\nu\omega-\omega_f)(III-IV)\}, \qquad \text{(II.23a)}$$

where

$$\left.\begin{matrix} I \\ III \end{matrix}\right\} = \left\{\left(\frac{\partial}{\partial J_f}|V_{\nu f}|^2\right)\left(-\frac{\omega_f}{kT}\pm\nu\frac{\partial}{\partial J}\right)+|V_{\nu f}|^2\left(\frac{\omega_f^2}{(kT)^2}\mp\frac{\omega_f}{kT}\frac{\partial}{\partial J}\right)\right\}\phi$$

$$\left.\begin{matrix} II \\ IV \end{matrix}\right\} = \nu\frac{\partial}{\partial J}|V_{\nu f}|^2\left(-\frac{\omega_f}{kT}\pm\nu\frac{\partial}{\partial J}\right)\phi, \qquad \text{(II.24)}$$

i.e., we have carried out the differentiations with respect to J_f indicated in Eq. (II.23), which, since

$$(\partial/\partial J_f)\exp(-(kT)^{-1}\sum\omega_f J_f)$$

$$= -(\omega_f/kT)\exp(-(kT^{-1}\sum\omega_f J_f),$$

means replacing the operator $\partial/\partial J_f$ with $-(\omega_f/kT)$. In Eqs. (II.24), the upper sign corresponds to the upper Roman numeral and the lower sign to the lower one.

Let us consider the expression I. On introducing the

definitions of $|V_{\nu f}|^2$ and

$$|q_f|^2 = J_f/M\omega_f,$$

$$I=\left\{\frac{|\bar{V}_f|^2 J_\nu^2(fr_0)}{M\omega_f}\left(-\frac{\omega_f}{kT}+\nu\frac{\partial}{\partial J}\right)-\frac{|\bar{V}_f|^2 J_\nu^2(fr_0)}{M\omega_f}\frac{J_f\omega_f}{kT}\times\left(-\frac{\omega_f}{kT}+\nu\frac{\partial}{\partial J}\right)\right\}\phi. \quad \text{(II.25)}$$

Since the lattice is assumed to be in equilibrium, we have $\omega_f J_f = kT$ (two degrees of freedom), and hence

$$I=0.$$

In a similar way, we find

$$III=0.$$

Equation (II.23a) is thus reduced to

$$\partial\phi/\partial t=\pi\lambda^2(L/2\pi)\sum_\nu\int d\omega_f c^{-1}\times\{\delta(\nu\omega+\omega_f)II-\delta(\nu\omega-\omega_f)IV\}. \quad \text{(II.26)}$$

This can be further reduced. Because of the different δ functions, we observe that the term with II when integrated will give the same result as the term with $(-IV)$. Hence, we can write

$$\partial\phi/\partial t=2\pi\lambda^2(L/2\pi)\sum_\nu\int d\omega_f c^{-1}\times\left\{\nu\frac{\partial}{\partial J}|V_{\nu f}|^2\left(-\frac{\omega_f}{kT}+\frac{\partial}{\partial J}\right)\delta(\nu\omega+\omega_f)\right\}\phi. \quad \text{(II.27)}$$

This is the equation we shall solve. On integrating (II.27) with respect to ω_f, remembering the δ function, we obtain

$$\frac{\partial\phi}{\partial t}=\frac{\lambda^2 L}{c}\sum_\nu\nu^2\frac{\partial}{\partial J}|V_{\nu f'}|^2\left(\frac{\omega}{kT}+\frac{\partial}{\partial J}\right)\phi, \quad \text{(II.28)}$$

where

$$cf'=-\nu\omega.$$

On inserting the value of $|V_{\nu,f}|^2$ and using $\omega_f J_f = kT$ and our expression for $|\bar{V}_f|^2/\omega_f^2$, we find

$$\frac{\partial\phi}{\partial t}=\frac{\lambda^2 L}{c}\frac{kT}{M}\frac{\partial}{\partial J}\left\{(\beta_1-\beta_2 r_0^2)\sum_\nu\nu^2 J_\nu\left(-\frac{\nu\omega}{c}r_0\right)\times\left(\frac{\omega}{kT}+\frac{\partial}{\partial J}\right)\right\}\phi. \quad \text{(II.29)}$$

The summation is performed using a summation formula due to Schott[4]:

$$\sum_{J=-\infty}^{\infty}\nu^2 J_\nu^2(\nu z)=\frac{z^2(4+z^2)}{8(1-z^2)^{\frac{1}{2}}}\approx\tfrac{1}{2}z^2, \qquad z\ll 1. \quad \text{(II.30)}$$

[4] G. N. Watson, *Theory of Bessel Functions* (Cambridge University Press, New York, 1944), 2nd ed., p. 573.

On inserting (II.30) in (II.29), we obtain

$$\frac{\partial\phi}{\partial t}=\frac{\lambda^2 kT\omega^2}{2c^3\mu}\left\{\frac{\partial}{\partial J}\beta_1 r_0^2\left[\frac{\omega}{kT}+\frac{\partial}{\partial J}\right]-\frac{\partial}{\partial J}\beta_2 r_0^4\left[\frac{\omega}{kT}+\frac{\partial}{\partial J}\right]\right\}\phi, \quad \text{(II.31)}$$

where

$$\mu=M/L.$$

The introduction in this equation of the reduced variable

$$x=\omega J/kT$$

and

$$r_0^2=\theta J; \qquad \theta=2\omega/\gamma,$$

valid in the harmonic approximation, yields

$$\frac{\partial\phi}{\partial t}=\frac{\lambda^2}{2c^3\mu}\beta_1\theta\omega^3\frac{\partial}{\partial x}\left(x-\frac{\beta_2\theta kT}{\beta_1\omega}x^2\right)\left(1+\frac{\partial}{\partial x}\right)\phi. \quad \text{(II.32)}$$

Let us define

$$\tau_c\equiv 2c^3\mu/\lambda^2\beta_1\theta\omega^3=c^3\mu\gamma/\lambda^2\beta_1\omega^4, \quad \text{(II.33)}$$

$$\xi=\beta_2\theta kT/\beta_1\omega. \quad \text{(II.34)}$$

τ_c has dimension time and is a relaxation time for the process of energy exchange of the defect with its surroundings, while ξ is a dimensionless quantity. With these definitions, we can write [Eq. (II.32)]

$$\partial\phi/\partial\tau=(\partial/\partial x)(x-\xi x^2)[1+(\partial/\partial x)]\phi, \quad \text{(II.32a)}$$

where

$$\tau=t/\tau_c$$

is a reduced time variable. This is the equation that governs the relaxation of the particle with the lattice. This process can be thought of as the motion of a particle in a parabolic potential being perturbed by the presence of the surrounding lattice.

This equation is most conveniently solved by perturbation, i.e., we consider ξ to be a perturbation parameter. The unperturbed equation then reads

$$\partial\phi/\partial\tau=(\partial/\partial x)x[1+(\partial/\partial x)]\phi. \quad \text{(II.35)}$$

This is seen to be the equation one obtains when the usual assumption is made, i.e.,

$$|\bar{V}_f|^2/\omega_f^2=\text{const.}$$

From our treatment, it is clear that we can express $|V_f|^2/\omega_f^2$ as a power series in r_0^2, i.e., in the energy of the particle, and it can be shown that when this series is used,

$$|V_f|^2/\omega_f^2=\sum_{j=0}^{\infty}c_j r_0^{2j},$$

the final equation for ϕ will read

$$\partial\phi/\partial\tau=(\partial/\partial x)\left(\sum_{j=0}^{\infty}b_j x^{j+1}\right)[1+(\partial/\partial x)]\phi,$$

where $b_0=1$.

Let us here confine ourselves to the previously treated case $\xi=0$. Proceeding as in Prigogine and Bak[5] we obtain for ϕ

$$\phi=\epsilon^{-x}\sum_n c_n \exp(-n\tau)\ {}_1F_1(-n,1,x), \quad \text{(II.36)}$$

where the summation is over the roots of the equation

$${}_1F_1(-n,1,x^*)=0 \quad \text{(II.37)}$$

considered as an equation in n. x^* is the value of the reduced energy at which the particle escapes the potential minimum. From this a rate constant for the process of escape is calculated as the value of n at the first zero of Eq. (II.37).

The result is (see footnote reference 5)

$$k_0=f(x)\,(\lambda^2\beta_1\gamma x/\mu c^3 m^2)\,\epsilon^{-x}, \quad \text{(II.38)}$$

and for the diffusion constant

$$D=\tfrac{1}{2}a^2k_0=f(x)\,(\lambda^2\beta_1\gamma a^2 x/2c^3m^2\mu)\,\epsilon^{-x}. \quad \text{(II.39)}$$

In these equations β_1, γ, x, and a are the previously introduced quantities. μ is the mass per unit length of the linear chain, and $f(x)$ satisfies

$$0.85<f(x)<1 \quad \text{for} \quad x>5.$$

Here, only the "unperturbed" equation (II.33) has been considered. In the Appendix, we show how a correction term can be obtained by solving Eq. (II.32a) by an ordinary perturbation procedure.

To obtain this result, we have also introduced the approximation of considering the oscillation of the defect as a normal mode, as well as used the harmonic frequency of this oscillation. In the next two sections, the justification of this procedure is investigated by finding the localized modes and their frequencies of a lattice with two and three defects, namely, with an isotope and one and two holes, respectively.

III

This section describes briefly the formalism developed by Montroll and Potts[3] for the investigation of lattices with defects.

We consider a one-dimensional ring of N atoms connected by springs with force constants γ. Then the equations of motion are

$$M\ddot{x}_j-\gamma(x_{j+1}-2x_j+x_{j-1})=0; \qquad j=-[1/2]N+1,\cdots,(1/2)N$$
$$x_{N+j}=x_j. \quad \text{(III.1)}$$

x_j is the displacement of the jth atom from its equilibrium position. If a is the lattice spacing, we can express the displacements as a linear combination of the normal modes:

$$x_j=A_k a\exp[i(\omega_k t+j\varphi_k)] \qquad \varphi_k=2\pi k/N, \quad \text{(III.2)}$$

where

$$\omega_k=2(\gamma/M)^{\frac{1}{2}}\sin\tfrac{1}{2}\varphi_k=\omega_L\sin\tfrac{1}{2}\varphi_k$$

with

$$\omega_L=2(\gamma/M)^{\frac{1}{2}}$$

being the largest frequency in the band. Defects in the lattice give rise to two classes of normal modes: those whose frequencies are slightly disturbed, but remain in the band of "perfect frequencies" and those whose frequencies are displaced out of the band. These latter modes are localized around the defects and their effect on the lattice dies out rapidly with the distance from the defect.

The equations of motion for the localized defects are

$$M\ddot{x}_j-\gamma(x_{j+1}-2x_j+x_{j-1})=D_j x_j, \quad \text{(III.3)}$$

where D is an operator characterizing the lattice defects. As a solution, we assume that

$$x_j=aAu(j)\exp(-i\omega t), \quad \text{(III.4)}$$

where $u(j)$ is a set of dimensionless numbers defined in an infinite lattice by

$$Lu(j)=M\omega^2u(j)+\gamma[u(j+1)-2u(j)+u(j-1)]$$
$$=\sum_k w^{(k)}(k+j)u(k+j) \quad j=0,\pm1,\cdots. \quad \text{(III.5)}$$

The set $u(j)$ are localized around defects so that

$$u(j)\to 0 \quad \text{as} \quad j\to\pm\infty. \quad \text{(III.6)}$$

Equation (III.5) defines the operator L. The $w^k(k+j)$'s characterize lattice defects.

The general solution to (III.5) is obtained by the use of the Green's function $g(j)$, defined by

$$Lg(j)=\begin{cases}\gamma & \text{if } j=0\\ 0 & \text{otherwise.}\end{cases} \quad \text{(III.7)}$$

The solution is then

$$u(j)=\gamma^{-1}\sum_k\sum_l g(j+k-l)w^{(k)}(l)u(l), \quad \text{(III.8)}$$

which is easily verified by substitution in (III.5). If the disturbance has an influence on lattice points $l_1\cdots l_s$, we find the new frequencies and normal modes by successively setting j in (III.8) equal to $l_1, l_2, \cdots, l_s$, and we see that

$$u(j)=\gamma^{-1}\sum_{\beta=1}^{s}\sum_k g(j+k-l_\beta)w^{(k)}(l_\beta)u(l_\beta). \quad \text{(III.9)}$$

It should be noted that the Green's function depends on ω. We have

$$g(j)=\frac{\gamma}{\pi}\int_0^\pi\frac{\cos j\phi\,d\varphi}{2(1-\cos\varphi)+M\omega^2}=\frac{(-1)^j\exp(-|j|z)}{2\sinh z}, \quad \text{(III.10)}$$

where

$$\cosh(1/2)z=\omega/\omega_L=f>1.$$

[5] I. Prigogine and Thor A. Bak, J. Chem. Phys. **31**, 1368 (1959).

As a result of (III.6), we have

$$g(j)\to 0 \quad \text{as} \quad j\to\infty \tag{III.11a}$$

and hence $z>1$. Also, since $z\to\infty$ as $f\to\infty$, we have

$$g(j)\to 0 \quad \text{as} \quad f\to\infty, \quad j \text{ fixed.} \tag{III.11b}$$

Finally, we have, as usual,

$$g(j)=g(-j). \tag{III.11c}$$

We see that if $\mathbf{u}$ is a vector with components $u(l_\beta)$, the s equations for $u(l_1)\cdots u(l_s)$ can be written in the form

$$\mathbf{u}=\mathbf{G}\mathbf{u}, \tag{III.12}$$

where $\mathbf{G}$ is a known matrix. If ψ_ν is the eigenvector of $\mathbf{G}$,

$$\mathbf{G}\psi_\nu=\lambda_\nu\psi_\nu, \tag{III.13}$$

we can express $\mathbf{u}$ as

$$\mathbf{u}=\sum_\nu u_\nu\psi_\nu,$$

and by substitution in (III.12), we obtain

$$\sum_\nu u_\nu\psi_\nu=\sum_\nu u_\nu\psi_\nu\lambda_\nu \tag{III.14}$$

or

$$\sum_\nu u_\nu(1-\lambda_\nu)\psi_\nu=0, \tag{III.15}$$

i.e.,

$$u_\nu(1-\lambda_\nu)=0, \quad \text{all } \nu. \tag{III.16}$$

Hence, if $\mathbf{u}\not\equiv 0$, we find the frequencies of the normal modes by setting

$$\lambda_\nu=1. \tag{III.17}$$

IV

There are two types of defects with which we shall be concerned in this paper. One is the impurity atom of mass M', the other is a hole. If we insert an impurity in the lattice, we generally also change the springs attached to it. Hence, an impurity can be characterized by two parameters,

$$P=\gamma'/\gamma \quad \text{and} \quad Q=M'/M,$$

where γ' is the new spring constant, γ the normal spring constant, M' the mass of impurity, and M that of a lattice atom in the perfect lattice. We shall, as suggested by Montroll and Potts,[3] characterize a hole by $P>1$ and $Q=0$. This means that a hole corresponds to an attraction of the neighboring atoms. This is reasonable, because there is nothing in a hole to yield the normal repulsive force—hence a relative attraction. This means that there will exist a tendency for the adjacent atoms to fall into the hole, and it is precisely this process which is of interest to us, since it can be considered a mechanism for diffusion in a linear chain.

In the following, we confine ourselves to the case of the isotope, i.e., the impurity does not by itself give rise to a force constant different from the usual one.

We shall consider two cases, a symmetrical and an unsymmetrical one. In both cases, an isotope (with 2 and 1 holes, respectively) will give rise to localized modes with frequencies out of the band. In the latter case, however, the amplitude of a heavy isotope will be numerically smaller than that of the lattice atom, and hence will have the smaller tendency to fall into the hole.

(a) Symmetrical Case

We consider the case of the isotopic impurity with mass M' located at the point "0" in the lattice. On either side is a hole, but we describe the hole by a force constant of such a magnitude that the lattice will be stretched, the springs adjacent to the isotope atom will span two lattice spacings. This can be done without altering the geometry of the lattice. In this model, then, the points "−1" and "+1" are really a distance of two lattice spacings away from "0". Equations (III.5) are, in this case,

$$Lu(j)=0 \quad \text{except when } j=0,\pm 1$$

$$Lu(0)=(M-M')\omega^2u(0) + (\gamma-\gamma')[u(1)-2u(0)+u(-1)] \tag{IV.1}$$

$$Lu(-1)=(\gamma'-\gamma)[u(-1)-u(0)] \tag{IV.2}$$

$$Lu(1)=(\gamma'-\gamma)[u(1)-u(0)], \tag{IV.3}$$

where γ' is the new force constant representing a hole. The $w^{(k)}$'s are then

$$w^{(k)}(k+j)=0$$

for all k, j, except

$$w^{(0)}(0)=(M-M')\omega^2-2(\gamma-\gamma')$$
$$w^{(\pm 1)}(\pm 1)=\gamma-\gamma'$$
$$w^{(1)}(0)=w^{(-1)}(0)=\gamma-\gamma'$$
$$w^{(0)}(\pm 1)=\gamma'-\gamma. \tag{IV.4}$$

The solution is

$$\begin{aligned} u(j)=\gamma^{-1}u(0)\{&g(j)[(M-M')\omega^2-2(\gamma-\gamma')] \\ &+(\gamma-\gamma')[g(j+1)+g(j-1)]\} \\ &+u(-1)(1-P)[g(j)-g(j+1)] \\ &+u(1)(1-P)[g(j)-g(j-1)], \end{aligned} \tag{IV.5}$$

where $P=\gamma'/\gamma$. In order to write this equation in more compact form, we use (III.7) to derive another expression for the coefficient of $u(0)$. We have

$$\begin{aligned} &\gamma^{-1}\{g(j)[(M-M')\omega^2-2(\gamma-\gamma')] \\ &\qquad +(\gamma-\gamma')[g(j+1)+g(j-1)]\} \\ &=\gamma^{-1}\{Lg(j)-M'\omega^2g(j)-[Lg(j)-M\omega^2g(j)/\gamma]\gamma'\} \\ &=\begin{cases} 4f^2g(j)(P-Q) & \text{if } j\neq 0 \\ 4f^2g(0)(P-Q)+(1-P) & \text{if } j=0. \end{cases} \end{aligned} \tag{IV.6}$$

Hence, we have for the matrix **G** of (III.12)

$$\mathbf{G}=\begin{vmatrix}(1-P)[g(1)-g(0)] & 4f^2g(1)(P-Q) & (1-P)[g(1)-g(2)]\\ (1-P)[g(0)-g(1)] & 4f^2g(0)(P-Q)+(1-P) & (1-P)[g(0)-g(1)]\\ (1-P)[g(1)-g(2)] & 4f^2g(1)(P-Q) & (1-P)[g(1)-g(0)]\end{vmatrix}. \quad \text{(IV.7)}$$

This is exactly the same matrix as the one obtained by Montroll and Potts,[3] who considered the general case of an impurity distorting the lattice, i.e., having different from normal springs attached to it.

It is easily seen that one eigenvector of this matrix (IV.7) is

$$\psi_1=\{1, 0, -1\} \text{ with } \lambda_1=(1-P)[g(2)-g(0)]. \quad \text{(IV.8)}$$

This is a pulsating mode

$$\leftarrow\cdot\rightarrow,$$

and it can be thought of as the (only) localized mode of a hole.

We are, however, more interested in the other modes. In general, the two remaining characteristic values satisfy the equation

$$\begin{aligned}\lambda^2-\lambda\{&(1-P)([g(1)-g(2)]+[g(1)-g(0)]+1)\\ &+4f^2g(0)(P-Q)\}\\ &+(1-P)^2\{[g(1)-g(2)]+[g(1)-g(0)]\}\\ &+4f^2(1-P)(P-Q)[2g^2(1)-g^2(0)-g(0)g(2)]=0.\end{aligned}$$

On using (III.7), this can also be written

$$\begin{aligned}\lambda^2-\lambda[&(1-P)\{[g(1)-g(2)]+3[g(1)-g(0)]\}\\ &+(1-Q)\{1-2[g(1)-g(0)]\}]\\ &+4f^2g(1)(1-P)(1-Q)=0. \quad \text{(IV.10)}\end{aligned}$$

The characteristic vectors are of the form

$$\psi=\{a, b, a\} \quad \text{(IV.11a)}$$

with

$$a/b=\frac{\lambda+P-1-4f^2g(0)(P-Q)}{2(1-P)[g(0)-g(1)]} \quad \text{(IV.11b)}$$

In order to obtain an approximate expression for the frequency, we put $1-Q\sim 0$ in (IV.10). We then have

$$\lambda\simeq\begin{cases}0\\ (1-P)\{[g(1)-g(2)]+3[g(1)-g(0)]\}.\end{cases} \quad \text{(IV.12)}$$

The nonzero root is the one of interest here. To obtain the frequency, we use (III.17) and set

$$(1-P)\{[g(1)-g(2)]+3[g(1)-g(0)]\}=1. \quad \text{(IV.13)}$$

On using (III.10) for $g(j)$ and setting $y=e^z$, we obtain

$$(y+1)[y^2-y(3P-2)+1-P]=0. \quad \text{(IV.14)}$$

The root $y=e^z=-1$ is discarded. The other two roots are

$$y=\tfrac{1}{2}\{3P-2\pm[P(9P-8)]^{\frac{1}{2}}\},$$

of which one is $\sim 3P-2$ and, since the product of the roots is $1-P$, $P>1$, the other one is negative. Hence the only significant root is

$$e^z\sim 3P-2. \quad \text{(IV.15)}$$

On inserting this, together with $\lambda=1$, in (IV.11b), we obtain

$$a/b=[Q(3P-1)-2P]/2(1-P). \quad \text{(IV.16)}$$

It is easily seen that

$$a/b<0 \text{ for } Q>[2P/(3P-1)],\quad P>1 \quad \text{(IV.17)}$$

and

$$|a/b|<1 \text{ for } Q<[2(2P-1)/(3P-1)],\quad P>1. \quad \text{(IV.18)}$$

Hence the normal mode is of the type $\rightarrow\longleftarrow\rightarrow$, i.e., the impurity and its nearest neighbors are out of phase. Furthermore, for

$$[2P/(2P-1)]<Q<[2(2P-1)/(3P-1)],$$

the amplitude of the defect (isotope) is numerically larger than that of either neighbor lattice atom. If we take the absolute value of the ratio of amplitudes as a measure of the relative tendency to fall into the hole, we see that the defect, under the aforementioned conditions

$$P>1,\quad [2P/(3P-1)]<Q<[2(2P-1)/(3P-1)],$$

has a larger tendency to diffuse in this case.

The frequency is found for this normal mode:

$$\begin{aligned}4f^2&=4\cosh^2(1/2)z=e^z+e^{-z}+2\\ &=(3P-1)^2/(3P-2) \quad \text{(IV.19)}\end{aligned}$$

or

$$\omega=(\gamma/M)^{\frac{1}{2}}[(3P-1)/(3P-2)^{\frac{1}{2}}]. \quad \text{(IV.20)}$$

It is noteworthy that the frequency is independent of the mass of the isotope. This is due to the approximations made in solving the eigenvalue equation, where we essentially put $Q=1$, i.e., $M'=M$. But it is seen that no large error is introduced by using the frequency for harmonic oscillation in the equation for the diffusion coefficient.

(b) Unsymmetrical Case

This is a case corresponding to one isotopic defect and one hole. The isotope is located at the lattice point "0," and the force constant between "0" and "1" is changed from γ to γ'. The equations of motion [i.e., Eqs. (III.5)] are here

$$Lu(j)=0 \quad \text{except for } j=0,1$$

$$Lu(0)=(M-M')\omega^2u(0)+(\gamma-\gamma')[u(1)-u(0)]$$

$$Lu(1)=(\gamma-\gamma')[u(0)-u(1)]. \tag{IV.21}$$

The $w^{(k)}$'s are zero, except

$$w^0(0)=(M-M')\omega^2-(\gamma-\gamma')$$

$$w^{(1)}(1)=w^{(-1)}(0)=-w^{(0)}(1)=\gamma-\gamma', \tag{IV.22}$$

and the solutions of (IV.21) are

$$u(j)=\gamma^{-1}\{u(0)[(M-M')\omega^2g(j)+(\gamma-\gamma')[g(j-1)-g(j)]+u(1)(\gamma-\gamma')[g(j)-g(j-1)]\} \tag{IV.23a}$$

or

$$u(j)=u(0)\{4f^2(1-Q)g(j)+(1-P)[g(j-1)-g(j)]\}+u(1)(1-P)[g(j)-g(j-1)], \tag{IV.23b}$$

where the quantities f, Q, P, have the usual meaning. The matrix $\mathbf{G}$ of (III.12) takes the form

$$\mathbf{G}=\begin{Vmatrix} 4f^2(1-Q)g(0)+(1-P)[g(1)-g(0)] & (1-P)[g(0)-g(1)] \\ 4f^2(1-Q)g(1)+(1-P)[g(0)-g(1)] & (1-P)[g(1)-g(0)] \end{Vmatrix}. \tag{IV.24}$$

Let us, for typographical reasons, introduce the symbols

$$\beta_j=4f^2(1-Q)g(j)$$

$$\epsilon=(1-P)$$

$$g_j=g(j). \tag{IV.25}$$

We can then write

$$\mathbf{G}=\begin{Vmatrix} \beta_0+\epsilon(g_1-g_0) & \epsilon(g_0-g_1) \\ \beta_1+\epsilon(g_0-g_1) & \epsilon(g_1-g_0) \end{Vmatrix}. \tag{IV.24a}$$

The only mode of interest to us is the pulsating mode of a hole (see footnote reference 3), i.e., we are looking for eigenvectors ψ of the form

$$\psi=\{1,a\} \quad a<0.$$

On inserting this in the equations

$$\mathbf{G}\psi=\lambda\psi,$$

we obtain

$$\beta_0+\epsilon(g_1-g_0)+a\epsilon(g_0-g_1)=\lambda \tag{IV.26}$$

$$\beta_1+\epsilon(g_0-g_1)+a\epsilon(g_1-g_0)=\lambda a. \tag{IV.27}$$

On solving for a, we obtain

$$a=\frac{-\beta_0\pm\sqrt{\beta_0^2+4\beta_1\epsilon(g_0-g_1)+4\epsilon^2(g_0-g_1)^2}}{2\epsilon(g_0-g_1)}. \tag{IV.28}$$

As we shall see, the root a_- (where we use the negative sign in the numerator) can be discarded, since the eigenvalue λ_- corresponding to it does not yield a frequency satisfying the physical conditions (III.11a). Using a_+, the corresponding eigenvalue is easily found to be

$$\lambda_+=\tfrac{1}{2}\beta_0+\epsilon(g_1-g_0)+\tfrac{1}{2}[\beta_0^2+4\beta_1\epsilon(g_0-g_1)+4\epsilon^2(g_0-g_1)^2]^{\frac{1}{2}}. \tag{IV.29}$$

On setting $\lambda_+=1$, according to (III.17), we obtain, by rearranging and squaring the equation, and introducing the definitions (IV.25) for β_j and g_j,

$$x^2(1-2\delta\epsilon-\delta)-x(1+4\delta\epsilon+\delta-2\epsilon)-2\delta\epsilon=0$$

$$x\equiv e^s. \tag{IV.30}$$

Here again we approximate the equation by setting $\delta\epsilon=(1-Q)(1-P)\simeq 0$, and the two solutions are

$$x=0$$

$$x=(2P-Q)/Q. \tag{IV.31}$$

The root $x=0$ is discarded because of (III.11a) and the second root is found by substitution to (approximately) satisfy Eq. (IV.29). If we use a_-, the equation for λ_- will be identical with (IV.29) except for a change of sign in front of the square root. Since we square the equation, the equation for x will be identical with (IV.30), but the only root physically possible will not be a solution of (IV.29).

On using (IV.31), we obtain for β_0, β_1 and g_0-g_1

$$\beta_0=P(1-Q)/(P-Q)$$

$$\beta_1=PQ(1-Q)/(2P-Q)(P-Q)$$

$$g_0-g_1=Q/2(P-Q), \tag{IV.32}$$

which, when inserted in (IV.28), yield

$$a_+=[-P(1-Q)+(P-Q)\sqrt{F}]/Q(1-P), \tag{IV.33}$$

$$F=\frac{1}{(P-Q)^2}\left[P^2(1-Q)^2+\frac{2PQ^2(1-Q)(1-P)}{(2P-Q)}+(1-P)^2Q^2\right]. \tag{IV.34}$$

We are interested in cases where $a_+<0$. Since the denominator in (IV.33) is negative ($P>1$ and $Q<P$),

this is obtained when the numerator is positive. There are two cases:

(1) $Q<1$. Here we obtain the inequality

$$[2P(1-Q)/(2P-Q)]<P-1$$

or

$$Q>[2P(2-P)/(1+P)]. \quad \text{(IV.35)}$$

(2) $Q>1$. Here $[-P(1-Q)/(P-Q)]>0$ and the numerator is positive for all Q. The only conditions on Q is then

$$[2P(2-P)/(1+P)]<Q<P. \quad \text{(IV.36)}$$

Let us now consider the numerical value of a_+, confining ourselves to the region of Q in which it is negative, i.e., (IV.36). We have

$$|a_+|=\frac{[P(1-Q)/(P-Q)]-\sqrt{F}}{Q(1-P)/(P-Q)} \quad \text{(IV.37)}$$

$$|a_+|<1:[P(1-Q)/(P-Q)]-[Q(1-P)/(P-Q)] =1>\sqrt{F}$$

or

$$-(1-Q)(1-P)>[Q(1-Q)(1-P)/(2P-Q)]. \quad \text{(IV.38)}$$

(1) $Q<1$. (IV.38) is satisfied for all Q since $P>1$.

(2) $Q>1$. Equation (IV.38) now reads

$$2P<0,$$

which is clearly not satisfied. Hence, we conclude that

$$|a_+| \begin{cases} <1 & \text{for } Q<1 \\ >1 & \text{for } Q>1. \end{cases} \quad \text{(IV.39)}$$

The frequency of the mode is easily found. We get

$$4f^2=4\cosh^2(1/2)z=4P^2/Q(2P-Q)$$

or

$$\omega=(\gamma/M')^{\frac{1}{2}}2P/(2P-Q)^{\frac{1}{2}}. \quad \text{(IV.40)}$$

In this case, we obtain an explicit dependence of ω on the mass of the impurity.

V. DISCUSSION

On summarizing the previous analysis, we may say that we have seen that it is justified to consider as a first approximation the oscillation of a single impurity atom as a normal mode when solving the general Liouville equation, assuming the rest of the lattice to be in equilibrium with a Boltzmann distribution.

Furthermore, it is not unreasonable to use the ordinary harmonic frequency with its square-root dependence on the mass of the atom. This is certainly true within a factor two or three.

The remarkable feature in this approach is the dependency of the relaxation time, and hence of the diffusion coefficient, on the square of the mass, instead of the customary square root. This is here obtained by using a harmonic frequency for the localized mode, and for a different potential the mass dependence of the frequency would be different. However, there is no *a priori* reason to believe that the dependency of the relaxation time τ_c on the fourth power of the frequency would be altered. This is interesting, because a similar expression for the relaxation time for the process of a point defect scattering a phonon, which is precisely the process we consider here, was obtained by Klemens,[6] who used a conventional second-order perturbation technique. As Klemens pointed out, there is no essential difference, as far as the scattering of phonons is concerned, between an impurity and a hole. On this basis and the previous analysis, we can then say that diffusion by a vacancy mechanism is described by the diffusion coefficient (II.37). Because of the approximations introduced, i.e., $Q=M'/M=1$, our results should apply only to isotope diffusion. For the symmetrical case, i.e., with two vacancies surrounding the impurity the isotopic impurity will be the one with the greater tendency to diffuse, irrespective of whether its mass is smaller than or larger than the mass of the normal lattice atom. In the unsymmetrical case, only the light isotope shows a tendency to "diffuse," relative to the normal lattice atom. There is no reason to believe, however, that the qualitative features should be altered by an exact solution of the equations. The present approach therefore predicts a larger isotope effect for diffusion than is expected on the basis of the classical theories. As pointed out in the Introduction, it should be born in mind that classical theories do not consider in detail the interaction between the diffusing mass and the surroundings, whereas the present theory does.

Experimentally, there has not so far been many results in support of the present treatment. The only experiments published so far that showed a behavior deviating from that expected from classical theories are those by Lazarus and Okkerse.[7] Their results on the diffusion of iron isotopes in silver seemed to fit exactly a dependency on the square of the mass. However, the results have later been repudiated,[8] but there seems to be no doubt that the isotope effect in these experiments is more pronounced than was expected. More experiments along these lines should throw some light on this equation.

ACKNOWLEDGMENT

The author gratefully acknowledges many stimulating discussions with Dr. Thor A. Bak.

APPENDIX

In order to solve Eq. (II.32a) by an ordinary perturbation technique, it is convenient to transform it so that the (unperturbed) equation is self-adjoint.

[6] P. G. Klemens, Proc. Phys. Soc. (London) **A68**, 1113 (1955).
[7] D. Lazarus and D. Okkerse, Phys. Rev. **105**, 1677 (1957).
[8] D. Lazarus (private communication).

This will yield the Sturm-Liouville equation for the problem, and from this we can obtain solutions that are orthonormal.

The usual separation of variables

$$\phi(x,\tau)=T(\tau)X(x)$$

yields an equation for X:

$$xX''+(1+x)X'+(1+k)X$$
$$-\xi[x^2X''-(2x+x^2)X'-2xX]=0. \quad (A.1)$$

The substitution

$$X=e^{-x}\varphi(x)$$

yields

$$x\varphi''+(1-x)\varphi'+k\varphi$$
$$-\xi[x^2\varphi''-(3x^2+2x)\varphi'+2x^2\varphi]=0. \quad (A.2)$$

The unperturbed equation is

$$x\psi''+(1-x)\psi'+k\psi=0, \quad (A.3)$$

which is the differential equation satisfied by the confluent hypergeometric function

$$\psi_i=c_1F_1(-k_i,1,x). \quad (A.4)$$

These functions are not orthogonal. Multiplication of Eq. (A.3) by e^{-x} brings the equation on a self-adjoint form:

$$e^{-x}x\psi''+e^{-x}(1-x)\psi'+ke^{-x}\psi=0. \quad (A.3a)$$

The application of Sturm-Liouville theory to this equation yields the result that

$$\int_0^{x^*}e^{-x}\psi_i\psi_j dx=\delta_{ij}, \quad (A.5)$$

where δ_{ij} is the Kronecker δ. Hence, the set $\{e^{-\frac{1}{2}x}\psi_i\}$ forms a complete orthonormal set.

In Eq. (A.2), we now make the substitution

$$\varphi=e^{\frac{1}{2}x}u$$

to obtain

$$xu''+u'+[\tfrac{1}{2}-(\tfrac{1}{4})x]u$$
$$-\xi[x^2u''-(2x^2+2x)u'+(\tfrac{3}{4}x^2-x)u]=-\lambda u. \quad (A.6)$$

We define the operators $\mathcal{P}$ and $\mathcal{R}$ by

$$\mathcal{P}=x(\partial^2/\partial x^2)+(\partial/\partial x)+(\tfrac{1}{2}-\tfrac{1}{4}x)$$
$$\mathcal{R}=x^2(\partial^2/\partial x^2)-2x(x+1)(\partial/\partial x)+x(\tfrac{3}{4}x-1)$$
$$=x[\mathcal{P}-(3+2x)(\partial/\partial x)+(x-\tfrac{3}{2})]. \quad (A.7)$$

We can now write Eq. (A.6) as

$$\mathcal{P}u-\xi\mathcal{R}u=-\lambda u. \quad (A.8)$$

Here, the unperturbed equation

$$\mathcal{P}v=-kv$$

has the solutions

$$v_i=e^{-\frac{1}{2}x}\psi_i$$

with

$$\int_0^{x^*}v_iv_j dx=\delta_{ij}.$$

We are interested in the lowest eigenvalue λ_0. On using the ordinary perturbation procedure, we set

$$\lambda_0=k_0+\xi k_0'+\cdots,$$

where k_0' is given by the usual formula:

$$k_0'=\int_0^{x^*}v_0\mathcal{R}v_0 dx. \quad (A.9)$$

It has not been possible to find this integral in closed form. Thus, if we want to find the correction to the rate constant k_0, only numerical calculation of the integral in (A.9) is possible.

Valence-Bond Resonance Structures for a Triplet State

A. D. McLachlan*

Gates and Crellin Laboratories of Chemistry, California Institute of Technology, Pasadena, California†

(Received April 4, 1960)

Pauling's rules for calculating the singlet ground state of a molecule by the valence-bond method are extended to deal with triplet states.

THE original method of canonical structures developed by Pauling[1] for calculating the resonance energies of conjugated molecules by the valence-bond method was intended only for singlet electronic states. Although the valence-bond theory has not proved as useful for the excited triplet states as for the singlet ground states of molecules, some calculations of electron-coupled spin-spin interactions[2–4] and the proton hyperfine interactions in free radicals[5,6] have successfully used the method.

In this paper we give the rules for setting up canonical structures for triplet wave functions and writing down the energy matrix. The rules for a doublet state with one unpaired electron are simple. First one introduces a dummy orbital O with opposite spin to the radical so that the system (radical+dummy) is in a singlet state. One then calculates the singlet state of the complete system by Pauling's rules, but sets the dummy orbital at infinity with vanishing exchange integrals to all the other atoms. Pauling states that the triplet states can be found similarly by using two dummy orbitals at infinity, O and O'. But this is not quite correct since abstracting two electrons from a singlet molecule can leave it in either a singlet or a triplet state, and the method proposed by Pauling may leave it in a mixture of both. To see this, consider the dummy orbital singlet structures A', B', X', Y', Z' below (Fig. 1). In A' and B', electrons O, O' are bonded in a singlet state so that the four atoms a, b, c, d are also certainly in a singlet state corresponding to the structure A or B. In X', Y', and Z' the spins O, O' are completely uncorrelated so that neither O, O' nor a, b, c, d are in an eigenstate of S^2. However, it is still possible to define a pure triplet electronic state of a molecule which corresponds to each one of the structures like X', Y', and Z'. These triplets are a complete (but arbitrary) linearly independent set of functions. Pauling's dummy method is a useful procedure for finding such a set, but the rules for setting up the energy matrix are quite different.

TRIPLET CANONICAL STRUCTURES

Let us first define a triplet wave function $\psi(ab)\cdots(\bar{i}j)\cdots(pq)$ for a molecule with $2n$ valence electrons and $2n$ atomic orbitals. In it the atoms i, j have unpaired spins while a, $b\cdots p$, q are bonded in pairs with opposed spins. If $\|\,a\alpha b\beta\cdots i\alpha j\alpha\cdots p\beta q\alpha\,\|$ stands for the normalized Slater determinant

$$\|\,a\alpha b\beta\cdots i\alpha j\alpha\cdots p\beta q\alpha\,\| = (2n!)^{-\frac{1}{2}}\sum_P(-)^P \times[a\alpha(1_P)b\beta(2_P)\cdots q\alpha(2n_P)] \quad (1)$$

and we use the notation

$$\|\,ab\,\|\,(\alpha\beta\pm\beta\alpha) = \|\,a\alpha b\beta\,\| \pm \|\,a\beta b\alpha\,\|,$$

the triplet wave functions are defined to be

$$\psi(ab)\cdots(\bar{i}j)\cdots(pq) = \|\,ab\cdots ij\cdots pq\,\|\,(1/\sqrt{2})\,(\alpha\beta-\beta\alpha)\cdots \cdots\left\{\begin{matrix}\alpha\alpha\\(1/\sqrt{2})\,(\alpha\beta+\beta\alpha)\\\beta\beta\end{matrix}\right\}\cdots(1/\sqrt{2})\,(\alpha\beta-\beta\alpha) \quad (2)$$

when S_z is 1, 0, or -1. The function ψ of (2) can be represented by a structure like X, Y, Z (Fig. 2) in which the unpaired orbitals i, j are joined by broken bonds, the paired ones by full bonds. We use plain letters (X) to label structures of the $2n$-electron problem and primes (X') for those of the $(2n+2)$-electron problem with two dummy orbitals. Each triplet structure, like X, is closely related to two others; the corresponding structure X' of the dummy scheme, in which the unpaired orbitals i, j are bonded to O, O', and a

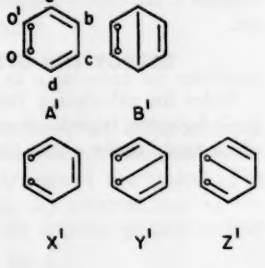

FIG. 1.

* Harkness Fellow of the Commonwealth Fund 1959–1961.
† Contribution No. 2565.

[1] L. Pauling, J. Chem. Phys. **1**, 280 (1933).
[2] M. Karplus, D. H. Anderson, T. C. Farrar, and H. S. Gutowsky, J. Chem. Phys. **27**, 597 (1957).
[3] M. Karplus and D. H. Anderson, J. Chem. Phys. **30**, 6 (1959).
[4] M. Karplus, J. Chem. Phys. **30**, 11 (1959).
[5] M. Karplus, J. Chem. Phys. **30**, 15 (1959).
[6] A. D. McLachlan, J. Chem. Phys. **32**, 1488 (1960).

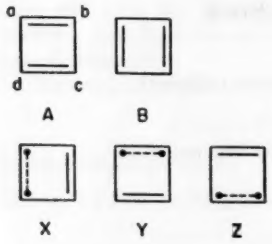

FIG. 2.

singlet structure x in which the broken bond is restored. (Here $x=B$, $y=z=A$.) Furthermore, x itself corresponds to a dummy structure x' with the same bonds in the molecule and O bonded to O'. ($x'=B'$, $y'=z'=A'$). The dummy wave functions $\phi(X')$ and $\phi(x')$ yield a pure triplet state $\chi(X')$ of the $2n$-electron system,

$$\chi(X')=(2/\sqrt{3})[\phi(X')-\tfrac{1}{2}\phi(x')]: \qquad (3)$$

for in $\chi(X')$ the orbitals i, j, O, O' outside the closed shell have the spin wave function

$$\| ijOO' \| \ (1/\sqrt{3})[\alpha\alpha.\beta\beta-\tfrac{1}{2}(\alpha\beta+\beta\alpha)(\alpha\beta+\beta\alpha)+\beta\beta.\alpha\alpha],$$

so that the real molecule is in one or other of the three states $\psi(X)$ defined by (2). If the dummy structures are linearly independent and complete, it is easy to show that the triplet wave functions defined by (3) and the related $\psi(X)$'s are also linearly independent and complete. Furthermore the correspondence

$$\psi(X)\sim\chi(X') \qquad (4)$$

implies that the energy and overlap matrices for the two sets are identical and can be derived from (3) by Pauling's rules for the dummy singlet structures. The rules for writing down triplet canonical structures therefore are:

1. Triplet wave functions $\psi(X)$ of the form (2) correspond to structures X having one broken bond ij whose electrons are unpaired.

2. Each triplet X is derived from a dummy structure X' in which i, j are bonded to O, O'.

3. Arrange the $2n$ orbitals around a circle and then add dummies O, O' next to each other. Now draw every singlet structure X' in which (a) no bonds cross each other, and (b) O is not joined to O'. The derived triplets X are then a complete and linearly independent set.

ENERGY AND OVERLAP MATRICES

Rules for calculating the energy and overlap integrals between triplet canonical structures can be derived fairly easily either from the definitions (2) and (3), or by applying the general theory of McWeeny[7] in his fundamental reassessment of the valence-bond theory. One draws superposition diagrams PQ for each pair of structures P and Q and applies the rules below. However, pairs of structures can be of two types since the broken bonds of P and Q (Fig. 3) may be in the same cycle, (i) or different cycles (1) and (2), (ii). If the diagram contains $(n-r)$ cycles and $[ab]$ stands for the exchange integral between atoms a and b, the overlap matrix elements are given by the formulas

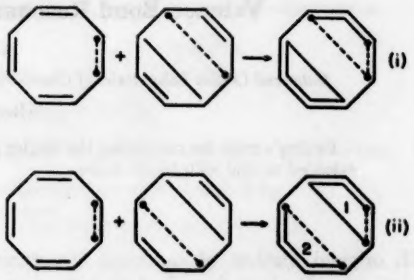

FIG. 3.

$$S_{PP}=1, \qquad S_{PQ}(\mathrm{i})=2^{-r}, \qquad S_{PQ}(\mathrm{ii})=0, \qquad (5)$$

and the energy ones by

$$H_{PP}=\{Q-\tfrac{1}{2}\textstyle\sum(\text{all})[ab]+\tfrac{3}{2}\sum(\text{bonded atoms}) -\tfrac{1}{2}[ij](\text{broken bond})\}; \qquad (6)$$

$$H_{PQ}(\mathrm{i})=2^{-r}\{Q-\tfrac{1}{2}\textstyle\sum(\text{all})[ab] -\tfrac{1}{2}\sum(\text{same cycle, same spin}) +\tfrac{1}{2}\sum(\text{same cycle, opp. spin}) -\sum(\text{same cycle, even No. of bonds}) +\sum(\text{same cycle, odd No. of bonds})\}; \qquad (7)$$

$$H_{PQ}(\mathrm{ii})=2^{-r-1}\{\textstyle\sum[a_1b_2](\text{opp. spin}) -\sum[a_1b_2](\text{same spin})\}. \qquad (8)$$

The "number of bonds" in $H_{PQ}(\mathrm{i})$ refers to the number of actual bonds, not counting the broken one, which lie between two atoms in the same cycle. The symbol $[a_1b_2]$ in $H_{PQ}(\mathrm{ii})$ means that atom a is in cycle 1 and atom b in cycle 2 of the superposition diagram. Atoms at odd positions on the circle are considered to have spin α and even positions β.

ACKNOWLEDGMENTS

I thank Professor Linus Pauling and H. Sternlicht for helpful discussions about these rules.

[7] R. McWeeny, Proc. Roy. Soc. (London) **A223**, 306 (1954).

Activity Coefficients of Electrons and Holes at High Concentrations*

ARTHUR J. ROSENBERG

Lincoln Laboratory, Massachusetts Institute of Technology, Lexington 73, Massachusetts

(Received March 14, 1960)

The use of the mass-action law in connection with solid-state equilibria involving conduction electrons or holes assumes that the chemical potential of the species is related to its concentration by $\mu=\mu^0(T)+kT\ln n$. This approximation can fail at concentrations which are still very small by ordinary chemical standards. The formalism may be preserved in principle by introducing a suitable activity coefficient γ. It is shown theoretically, however, that γ increases almost exponentially with increasing n when $n/\lambda \lesssim 0.1$, where λ is the partition function in the quasi-free-particle approximation. As a consequence, the proper exponent of n in mass-action equations becomes much larger than expected from stoichiometry considerations alone. The use of such equations becomes difficult, therefore, when $n/\lambda \lesssim 0.5$, and entirely unjustified when $n/\lambda \lesssim 10$. The determination of λ, which lies between 10^{18} and 10^{21} cm^{-3} for most semiconductors is discussed from an experimental viewpoint.

SOME time ago it was suggested[1] that conduction electrons and holes in solids should be free to participate in chemical equilibria, and that their concentrations could be used in mass-action equations describing the ionization of crystalline defects. This quasi-chemical approximation is now universally accepted and has proved extraordinarily effective, as, for example, in the elegant studies by Reiss, Fuller, and Morin[2] of the chemical interaction of defects in germanium and silicon.

It is the purpose of this communication to explore the consequences of the fact, noted by Reiss,[3] that the approximation can fail at concentrations which are still dilute by ordinary chemical standards. While the mass-action formalism may be preserved by the use of activity coefficients, it will be shown that the values of these coefficients become proportional to an increasing positive power of the concentration. The exponents of the concentration to be used in the mass-action equation become much larger than predicted from stoichiometry considerations alone, and the utility of the formalism becomes severely restricted.

The mass-action formalism originates in the general condition for chemical equilibrium, i.e.,

$$\sum_i \nu_i \mu_i = 0, \tag{1}$$

where ν_i is the mole number (negative for reactants) and μ_i is the chemical potential of the ith species undergoing a reaction.[4] If the system is composed of *weakly interacting particles*,[5]

$$\mu_i = \mu_i^0(T) + kT\ln n_i, \tag{2}$$

then Eq. (1) *leads directly to the mass-action equation*

$$\prod_i n_i^{\nu_i} = K(T) \tag{3}$$

where the n_i's are concentrations and K is a function of temperature and the choice of standard state alone. At high concentrations, however, the relation between μ_i and n_i frequently departs from Eq. (2). Nevertheless, as long as the deviation can be corrected for by the introduction of an "activity coefficient,"[6] γ_i, so that

$$\mu_i = \mu_i^0(T) + kT\ln n_i + kT\ln\gamma_i, \tag{4}$$

then an analog of Eq. (3) may be written as

$$\prod_i n_i^{\nu_i} = K(T)\prod_i \gamma_i^{-\nu_i}. \tag{5}$$

The only restriction on the γ_i, which are generally a function of both temperature and the concentrations, is that they become unity at low concentrations.

From the standpoint of statistical mechanics, Eq. (2) comes from maximizing the entropy associated with the external degrees of freedom of weakly interacting particles. The usual source of deviations from the equation is the perturbation of the energy levels of a system when the average separation between particles becomes small. This phenomenon is generally treated by introducing a coordinate-dependent potential-energy term $U(q)$ into the Hamiltonian for the system.[5] In most practical cases, the γ's which result in this way are not sensitive functions of the concentrations, and the term

$$\prod_i \gamma_i^{-\nu_i}$$

in Eq. (5) can be taken as a constant for relatively large variations in the n_i's.[6]

In the case of electrons, however, a fundamental deviation from Eq. (2) may occur even where the potential energy is zero throughout the system. The statistical derivation of Eq. (2) assumes that λ_i, the partition function of the ith species, greatly exceeds

* The work reported in this paper was performed by Lincoln Laboratory, a center for research operated by Massachusetts Institute of Technology with the joint support of the U. S. Army, Navy, and Air Force.

[1] C. Wagner and W. Schottky, Z. phys. Chem. **B11**, 163 (1930).

[2] H. Reiss, C. S. Fuller, and F. M. Morin, Bell System Tech. J. **35**, 535 (1956).

[3] H. Reiss, J. Chem. Phys. **21**, 1209 (1953).

[4] S. Glasstone, *Thermodynamics for Chemists* (D. Van Nostrand Company, Inc., Princeton, New Jersey, 1947), p. 273 ff.

[5] S. Glasstone, *Theoretical Chemistry* (D. Van Nostrand Company, Inc., Princeton, New Jersey, 1944), p. 432.

[6] See footnote reference 4, p. 250 ff.

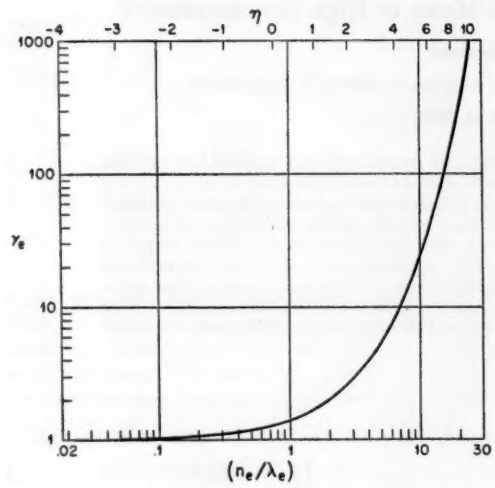

FIG. 1. The activity coefficient of quasi-free electrons and holes. See Eqs. (9) and (18).

n_i. In a potential-free system of particles which are subject to the Pauli exclusion principle, λ_i is given by[5]

$$\lambda_i = g_{\text{int}}(2\pi mkT/h^2)^{\frac{1}{2}}, \tag{6}$$

where g_{int} is the internal degeneracy of particles with mass m and the other symbols have their usual meaning. For particles of atomic mass, λ_i exceeds 10^{24} cm^{-3} at ordinary temperatures, and is thus larger than the maximum accessible concentration for atomic particles, whether or not they are subject to the exclusion principle.

For particles with the free-electron mass, m_e, however, Eq. (6) becomes (with $g_{\text{int}}=2$ for spin degeneracy)

$$\lambda_e = 4.83\times10^{15}T^{\frac{3}{2}} = 2.53\times10^{19} \text{ per cm}^3 \text{ at } 300°\text{K}. \tag{7}$$

Provided that the electron concentration, n_e, remains much less than λ_e, Eq. (2) is applicable in the form

$$\mu_e = -kT\ln\lambda_e + kT\ln n_e. \tag{8}$$

As n_e approaches and exceeds λ_e, however, the added electrons are constrained to occupy states with energy greater than kT. The average energy must increase accordingly, so that μ_e rises more rapidly than indicated by Eq. (2). In the formalism of Eq. (4), therefore, the activity coefficient must rise with increasing n_e.

This may be shown quantitatively by using the exact relation between μ_e and n_e for a free-electron gas[7]:

$$n_e = (2/\pi^{\frac{1}{2}})\lambda_e F_{\frac{1}{2}}\{\eta\} \tag{9}$$

where $\eta \equiv \mu_e/kT$, $F_{\frac{1}{2}}\{\eta\}$ is the integrated Fermi-Dirac function,

$$F_{\frac{1}{2}}\{\eta\} = \int_0^\infty \{x^{\frac{1}{2}}/[1+\exp(x-\eta)]\}dx, \tag{10}$$

and λ_e is given, as before, by Eq. (7). Generalizing Eq. (8) by adding an activity coefficient in the fashion of Eq. (4), one has

$$\mu_e = -kT\ln\lambda_e + kT\ln n_e + kT\ln\gamma_e. \tag{11}$$

Introducing Eq. (9) into Eq. (11) and rearranging terms, one then obtains

$$\gamma_e = \tfrac{1}{2}\pi^{\frac{1}{2}}(\exp\eta/F_{\frac{1}{2}}\{\eta\}). \tag{12}$$

Equation (12) has been evaluated using the tabulated values of $F_{\frac{1}{2}}\{\eta\}$ given by MacDougall and Stoner.[8] The values of γ_e so obtained have been plotted vs (n_e/λ_e) and the corresponding values of η in Fig. 1.

Figure 1 clearly illustrates the early departure of γ_e from unity. Even at $n_e=0.1\lambda_e$, γ_e has risen to 1.03. Beyond this point the rise is nearly exponential; when $n_e=30\lambda_e$, γ_e exceeds 1000.

These results have an important bearing upon the exponent of n_e to be used in the mass-action equation for a reaction involving electrons. Consider, for example, the dissociation,

$$A = A^{z+} + z \text{ electrons}. \tag{13}$$

The corresponding mass-action equation [cf. Eq. (5)] is

$$n_e^z\gamma_e^z(n_{A^{z+}}\gamma_{A^{z+}}/n_A\gamma_A) = K(T). \tag{14}$$

From Fig. 1 it is seen that γ_e can be expressed as

$$\gamma_e = n_e^{y\langle n_e\rangle}, \tag{15}$$

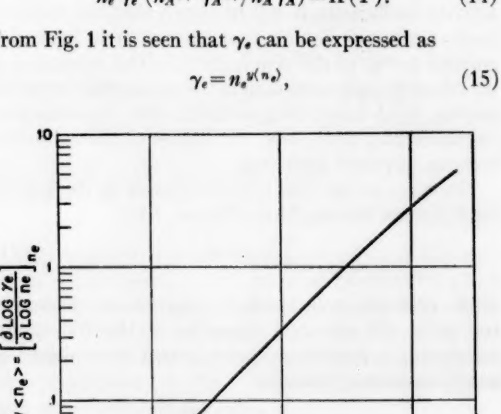

FIG. 2. The variation of $y\langle n_e\rangle$ with electron concentration.

[7] See, for instance (a) W. Shockley, *Electrons and Holes in Semiconductors* (D. Van Nostrand Company, Inc., Princeton, New Jersey, 1950) and (b) J. S. Blakemore, Elec. Commun. **29**, 131 (1952).

[8] J. MacDougall and E. C. Stoner, Phil. Trans. Roy. Soc. (London) **A237**, 350 (1938).

where $y\langle n_e\rangle$, always $\geqslant 0$, is given by

$$y\langle n_e\rangle=[\partial \log\gamma_e/\partial \log n_e]_{n_e}. \quad (16)$$

Equation (16) has been evaluated graphically from Fig. 1 with the results given in Fig. 2. Substituting Eq. (15) into Eq. (14) one obtains

$$n_e^{z[1+y\langle n_e\rangle]}\cdot(n_A^{z+}\gamma_A^{z+}/n_A\gamma_A)=K(T). \quad (17)$$

It is evident, therefore, that the proper exponent for n_e is $[1+y\langle n_e\rangle]$ times the exponent which one would anticipate from stoichiometry considerations. As shown in Fig. 2, the effect can be drastic since $y\langle n_e\rangle$ increases to values well above unity. This must always be taken into account when a mass-action equation is used for electron concentrations exceeding $0.1\lambda_e$ (where $y\langle n_e\rangle$ has already risen to 0.04).

APPLICATION TO REAL SYSTEMS

While the above treatment is based upon the model of a free-electron gas, it can readily be extended to most solids. As long as the potential energy, ψ_e, of the electron is independent of position, each of the equations may be used provided that $(\mu_e-\psi_e)$ is substituted for μ_e. In the normal crystal, however, the potential varies with the periodicity of the lattice.

For those solids in which the wavelength of conducting particles is much larger than the lattice spacing, however, the effective-mass approximation[9] may readily be applied to the estimation of activity coefficients. The results of this treatment are equivalent to those which would be obtained if ψ_e were independent of position but the electron mass were a factor (m^*/m_e) times the free-electron mass, m_e. Thus, by generalizing λ_e to mean

$$\lambda_e=2(2\pi m_e kT)^{\frac{1}{2}}(m^*/m_e)^{\frac{1}{2}}$$

$$=2.53\times10^{19}(T/300)(m^*/m_e)^{\frac{1}{2}}\ \text{cm}^{-3} \quad (18)$$

and taking the zero of energy as the bottom of the conduction band (or the top of the valence band in the case of holes) one may use the results of Figs. 1 and 2 for the calculation of γ and $y\langle n_e\rangle$.

Equation (18) assumes that the effective mass is independent of energy, and that the energy bands are spherically symmetric.[9] In the case of many-valley bands with constant m^*, the treatment is virtually unchanged if one uses the density-of-states effective mass.[10] With variable effective masses the problem is much more difficult; however, the results are qualitatively similar to Figs. 1 and 2 if one employs an average value for m^*. The effective-mass approximation fails completely, however, in the case of solids, like spinels, where the conduction electrons are strongly localized.[11]

The results are equivalent for electrons in the conduction band and holes in the valence band of crystalline solids. The source of the electrons or holes, be it impurity ionization or intrinsic dissociation in a pure semiconductor, is immaterial. Values for the density-of-states effective mass generally lie within 10^{-2} to 10 times that of the free-electron mass, hence λ_e should lie in the range, 2×10^{18} to 6×10^{20} cm^{-3} at room temperature, which corresponds to concentrations between 10^{-4} and 1 at. %. The rapid departure from ideal behavior can occur, therefore, at concentrations which are much smaller than those at which small deviations appear for particles of atomic mass.[6]

When estimates of the effective mass are not available, an approximate value of λ_e (and m_e^*) may be obtained by measuring the Seebeck coefficient (α) and the Hall coefficient (R) at a given temperature.[12] When one kind of current carrier dominates the conductivity, $R=(en_e)^{-1}$. According to the constant-effective-mass approximation [cf. Eq. (9)], therefore,

$$\lambda_e=\pi^{\frac{1}{2}}/2eRF_{\frac{1}{2}}\{\eta\}. \quad (19)$$

The value of η can be obtained from the following equation which applies to simple energy bands[13]:

$$\alpha=-(k/e)\{[(r+2)\cdot F_{r+1}\{\eta\}]/[(r+1)\cdot F_r\{\eta\}]-\eta\}. \quad (20)$$

The value of the parameter r lies between zero and two depending on the scattering mechanism.[14] Thus, $r=0$ for scattering by acoustical phonons, while $r=2$ for ionized-impurity scattering.[15] Tabulated values of the Fermi-Dirac functions, F_0, $F_{\frac{1}{2}}$, F_1, F_2, and F_3 are available in the literature.[8,16] From α and an assumed value of r one obtains η through Eq. (20) and, substituting η into Eq. (19), obtains λ_e. The values of λ_e calculated for $r=0$ and $r=2$ differ by only a factor of 5, so the arbitrary assumption that $r=1$ will give a value of λ_e to a factor of three. Within this uncertainty, this procedure gives an approximate value of λ_e even for solids with nonspherical energy surfaces and variable effective mass.

Using this value of λ_e, one can immediately determine whether the use of electron or hole concentrations in mass-action equations is practical. When $\eta_e/\lambda_e<0.1$, η_e can be used without correction. When $0.1<\eta_e/\lambda_e<1$, the data of Figs. 1 and 2 may be used with discretion to obtain the necessary corrections. When $\eta_e/\lambda_e>1$, the utility of such corrections becomes questionable. When $\eta_e/\lambda_e>10$, the use of the mass-action formalism can no longer be justified.

[9] F. Seitz, *Modern Theory of Solids* (McGraw-Hill Book Company, Inc., New York, 1940), p. 271.
[10] C. Herring, Bell System Tech. J. **34**, 237 (1955), see p. 251.
[11] J. C. Slater, J. Phys. Chem. Solids **8**, 21 (1959).
[12] These measurements are not particularly difficult to carry out on homogeneous, compact solids. For an excellent discussion of the experimental techniques, see Vol. VIB of *Solid State Physics* (Academic Press, Inc., New York, 1959).
[13] R. W. Wright, Proc. Roy. Soc. (London) **A64**, 984 (1951).
[14] See footnote reference 7(a).
[15] E. M. Conwell and V. F. Weisskopf, Phys. Rev. **77**, 388 (1950).
[16] P. Rhodes, Proc. Roy. Soc. (London) **A204**, 396 (1950).

Continuum-Model Treatment of Long-Range Intermolecular Forces. I. Pure Substances*

BRUNO LINDER

Department of Chemistry, The Florida State University, Tallahassee, Florida

(Received March 28, 1960)

A theory is presented whereby the long-range intermolecular forces, including the London dispersion forces, of pure nonelectrolytes may be calculated from optical and dielectric data. The method is based on the continuum-model approach, where one molecule is treated explicitly while the others are replaced by a medium of uniform dielectric. The classical and quantum-mechanical oscillators are used as working models and expressions are derived for computing the cohesive energy appropriate for both types of oscillators. The potential energy based on the quantum-mechanical oscillator is calculated for a number of liquids and is shown to be in fair agreement with the experimental energy of vaporization.

I. INTRODUCTION

THE van der Waals attractive forces are generally attributed to three types of long-range interactions:

(1) interactions between permanent dipoles (orientation effect);

(2) interactions between permanent and induced dipoles (induction effect); and

(3) interactions arising from the mutual polarization of the electron clouds of neighboring atoms or molecules (dispersion effect).

The dispersion effect is, by far, the most important constituent of the van der Waals interaction. It generally outweighs the combined contributions of orientation and induction effects, and is in the absence of permanent dipoles the sole contributor to the total attractive force.

The potential energy of a system of interacting particles can be obtained in two ways. One approach is to sum over the pairwise interactions of all molecules. London[1] used this method to compute the lattice energy for a number of simple nonpolar substances.

Another approach is to consider the interaction between a specific molecule and its entire surrounding which is to be regarded as a uniform infinite dielectric. This method, developed by Martin[2] and Bell[3] and improved by Kirkwood[4] and Bonnor,[5] is restricted to polar molecules and gives only the electrostatic part (orientation and induction effects) of the total interaction energy. Basically, the method consists of calculating the work done in transferring a polar molecule from empty space into a cavity inside the dielectric. The field produced by the polar molecule polarizes the dielectric, which, in turn, sets up a field at the center of the cavity. The interaction energy is then obtained from the coupling between the dipole moment and the local field.

The aim of the present paper is to develop a formalism for calculating the dispersion energies by the continuum method and thus extend this method to the treatment of nonpolar molecules. Nonpolar molecules, if regarded as oscillating dipoles, have vanishing average moments, but the important quantity that always enters into the expression for the interaction energy is the square of the dipole moment (which does not vanish). It is this property that makes the proposed method of attack feasible.

The present approach should have several advantages. First, the total attractive force can at once be gotten without having to sum first over all interactions between individual pairs of molecules. Second, since for a condensed system the total interaction energy (or potential energy) is roughly equal to the energy of vaporization or sublimation, the present method affords a means whereby these thermodynamic quantities can be related to the dielectric properties of the substance. Finally, since the work required to remove a molecule from inside the dielectric into empty space is really a free energy function, one should be able to compute, in case of mixed dielectrics, the free energy of solution and thus relate the activity coefficient to the dielectric properties of the solution.

II. GENERAL THEORY

As a working model consider a spherical molecule of radius a composed of a set of positive and negative charges e. (More will be said later about the exact nature of a; for the time being let a represent a constant of molecular dimensions.) Suppose that the charges are bound isotropically and harmonically to an equilibrium position, which we let coincide with the center of our coordinate system. The rapid oscillations of the electrons about the nuclei give rise to instantaneous dipole moments, the average value of which is zero. Moments of higher order will, in first approximation, not be considered. The motion of the nuclei,

* This research was supported by a grant from The Petroleum Research Fund administered by the American Chemical Society. Grateful acknowledgment is hereby made to the donors of said fund.

[1] F. London, Z. Physik. **63**, 245 (1930); Z. physik. Chem. (Leipzig) **B11**, 222 (1930).

[2] A. R. Martin, Phil. Mag. **8**, 550 (1929); Trans. Faraday Soc. **33**, 191 (1937); see also A. R. Martin and A. C. Brown, Trans. Faraday Soc. **34**, 742 (1938).

[3] R. P. Bell, Trans. Faraday Soc. **31**, 1557 (1931).

[4] J. G. Kirkwood, J. Chem. Phys. **2**, 351 (1934).

[5] W. B. Bonnor, Trans. Faraday Soc. **47**, 1143 (1951).

which is very much slower than that of the electrons, will also be neglected.

Let $\mathbf{r}_i$ denote the position vector of the ith charge. The set of charges will give rise to an instantaneous moment $\mathbf{m}=\sum e_i\mathbf{r}_i$. Now suppose that the molecule is surrounded by a uniform medium of constant dielectric. The field associated with $\mathbf{m}$ interacts with the surrounding dielectric which, in turn, polarizes the molecular sphere. The degree of polarization depends on the dielectric constant ϵ, and is different for time-dependent and static fields. The dielectric constant associated with a varying field is a complex number, but the imaginary part vanishes in two limiting cases: for zero frequency and infinite frequency. The high-frequency dielectric constant ϵ_∞, is to be associated only with the displacement of the electrons from their equilibrium positions, and should satisfy the Maxwell relation, $\epsilon_\infty=n^2$, where n is the refractive index. In addition to the electronic displacements, the static dielectric constant ϵ_0 contains contributions from the atomic polarization of the nuclei and the orientation of the molecules in case of polar molecules. For non-polar molecules, there is very little distinction between the static and high-frequency dielectric constant as the effect of atomic polarization is generally small.

Our main problem is to find an expression for the field at the center of the cavity due to all sources except the charges on the molecule and to determine how this field will interact with the dipole moment $\mathbf{m}$. The problem is complicated by the fact that the dipole is a fluctuating one and the field so produced is also fluctuating. For this reason we wish to consider first the more familiar case of placing a static (permanent) dipole inside a dielectric.

(a) Reaction Field of a Permanent Dipole

The procedure for determining the "reaction" field of a permanent dipole may be found in one of several places.[4–7]. One of the most rigorous derivations was given by Bonnor,[5] whose method of approach can best be adapted to the oscillating dipole.

Basically, one has to determine the potential inside a sphere of radius a which is embedded in a medium of uniform dielectric; the charges on the sphere give rise to a dipole and poles of higher order.[8] The potential is obtained from a solution of the Laplace equation, subject to the conditions that across the spherical boundary the potential and the normal component of the displacement vector be continuous. Bonnor[5] assumed that the displacement vectors inside and outside the sphere are given, respectively, by

$$\mathbf{D}_i=\mathbf{E}_i+4\pi\mathbf{P}_i \tag{1}$$

and

$$\mathbf{D}_o=\epsilon\mathbf{E}_0, \tag{2}$$

where ϵ is the static dielectric constant of the surrounding medium, $\mathbf{P}_i$ the polarization vector of the sphere, and $\mathbf{E}_i$ and $\mathbf{E}_o$ the field strengths inside and outside the sphere. The field in the center of the cavity—the reaction field $\mathbf{R}$—can then readily be determined and reduces, upon neglect of all higher-order moments beyond the dipole moment, to

$$\mathbf{R}=[2(\epsilon-1)/(2\epsilon+1)][(4\pi/3)\mathbf{P}_i+(\boldsymbol{\mu}_0/a^3)], \tag{3}$$

where $\boldsymbol{\mu}_0$ is the dipole moment.

The polarization vector $\mathbf{P}_i$ is the induced moment per unit volume. The total induced moment is $\mathbf{m}=(4\pi/3)\mathbf{P}_ia^3$ and is related to $\mathbf{R}$ by

$$\mathbf{m}=\alpha\mathbf{R}, \tag{4}$$

where α is the polarizability of the sphere and is assumed to be isotropic. If we define a new quantity g by

$$g=[2(\epsilon-1)/(2\epsilon+1)](1/a^3), \tag{5}$$

we have

$$\mathbf{R}=g[\mathbf{m}+\boldsymbol{\mu}_0], \tag{6}$$

which, upon substitution of (4) into (6) and rearrangement, becomes

$$\mathbf{R}=\boldsymbol{\mu}_0g/1-\alpha g. \tag{7}$$

The work done in bringing the sphere inside the dielectric is obtained by integrating the work-element $dW=\frac{1}{4}\mathbf{E}\cdot d\mathbf{D}$; the result is[5]

$$W=-\tfrac{1}{2}\mu_0^2g/1-\alpha g \tag{8}$$

or

$$W=-\tfrac{1}{2}\boldsymbol{\mu}_0\cdot\mathbf{R} \tag{9}$$

Fröhlich[7b] has used the reaction-field to describe also the behavior of a spontaneous moment in an applied field. The reaction field of a spontaneous moment is defined as [see Eq. (6)]

$$\mathbf{R}=g\mathbf{m} \tag{10}$$

and the work function is

$$W=-\tfrac{1}{2}\mathbf{m}\cdot\mathbf{R}. \tag{11}$$

(b) Reaction Field of an Oscillating Dipole

When we try to extend the theory to fluctuating dipoles, we are immediately faced with the difficulty that the dielectric constant is not static. Nor is the dielectric constant the same as high-frequency dielectric constant.

[6] L. Onsager, J. Am. Chem. Soc. **58**, 1486 (1936).

[7] (a) W. F. Brown, Jr., *Handbuch der Physik* (Springer-Verlag, Berlin, 1956), Vol. 17, pp. 1–154; (b) H. Fröhlich, *Theory of Dielectrics* (The Clarendon Press, Oxford, England, 1949); (c) C. J. F. Böttcher, *Theory of Electric Polarization* (Elsevier Publishing Company, New York, 1952).

[8] The treatment as outlined here is, strictly speaking, valid only for a sphere which is large enough to have the same dielectric properties as a macroscopic sphere, that is, a sphere which contains a great many molecules. We shall *formally* treat the sphere as having such properties, but in actual numerical work we shall assume that the derived formulas apply also to a single molecule. Such an assumption is open to criticism.

When an oscillator with a natural frequency ν_0 is placed in a fluctuating field of frequency ν, its polarizability is given by

$$\alpha^* = \alpha\nu_0^2/\nu_0^2 - \nu^2, \tag{12}$$

where α is the static polarizability. This expression is correct only if the frequencies ν_0 and ν differ appreciably, and holds equally well for the classical as the quantum-mechanical oscillator. In fact, this relation is also valid in case of real molecules if one assumes that only one transition probability for induced emission and absorption is effectively possible, an assumption that will be made throughout this work. For the polarizability of a molecule, if assumed to be isotropic, may be written as

$$\alpha^* = \tfrac{2}{3}\sum_k \frac{|\,\mathbf{m}_{ok}\,|^2(E_k - E_0)}{(E_o - E_k)^2 - (h\nu)^2}, \tag{13}$$

where E_o and E_k are the energy levels of the oth and kth quantum states; $|\,\mathbf{m}_{ok}\,|^2$ is the transition probability from the oth to the kth state

$$\left(\boldsymbol{m}_{ok} = \int \psi_0 e\mathbf{r}\psi_k d\tau\right)$$

and h is Planck's constant. If only one transition probability is allowed, the sum in Eq. (13) reduces to a single term. The static polarizability then becomes

$$\alpha = \tfrac{2}{3}\,|\boldsymbol{m}_{ok}\,|^2/(E_k - E_0), \tag{14}$$

which, when substituted into Eq. (13) (with the higher-order terms omitted) yields Eq. (12).

The variation of ϵ with ν is quite complicated, but the dependence of the g factor on the frequency takes a simple form under certain idealized conditions. Let us assume that the "center" molecule has a moment $\mathbf{m}$ and that its frequency of oscillation is ν_i. We shall indicate this by the subscript (ν_i), e.g., $\mathbf{m}_{(\nu_i)}$. This moment gives rise to a field, which at a distance $\mathbf{r}_k$ from the center, may be represented by the following expression:

$$\mathbf{E}_k = (3\mathbf{m}_{(\nu_i)}\cdot\mathbf{r}_k/r_k^5)\,\mathbf{r}_k - (\mathbf{m}_{(\nu_i)}/r_k^3). \tag{15}$$

This field will fluctuate with the same frequency as $\mathbf{m}_{(\nu_i)}$ and induce a moment in each molecule of which the dielectric is composed. For the kth molecule the moment is

$$\mathbf{m}_k = \alpha_k^*\mathbf{E}_k, \tag{16}$$

where the asterisk serves to indicate that the polarizability is not static.

Let us first consider the hypothetical case where all the molecules of the dielectric medium have the same frequency, say, ν_j. The induced moment of the kth molecule can then be written as

$$\mathbf{m}_k = \alpha_j\mathbf{E}_k[\nu_j^2/(\nu_j^2 - \nu_i^2)]. \tag{17}$$

Each moment $\mathbf{m}_k$ gives rise to a field $\mathbf{E}_k'$ at the center of the cavity, which can be represented by

$$\mathbf{E}_k' = \{[(3\alpha_j\mathbf{E}_k\cdot\mathbf{r}_k/r_k^5)]\mathbf{r}_k - (\alpha_j\mathbf{E}_k/r_k^3)\} \times[\nu_j^2/(\nu_j^2 - \nu_i^2)]. \tag{18}$$

The resultant field $\sum_k \mathbf{E}_k'$ is the analog of the reaction field of a static dipole and will be denoted by the symbol $\mathbf{R}^*$. For, if we let ν_i approach zero, the frequencies drop out from expression (18) and the resultant field $\sum_k E_k'(\nu_i=0)$ is simply the reaction field of a static dipole moment $\mathbf{m}_{(\nu_i=0)}$:

$$\mathbf{R} = \sum_k E_k'(\nu_i = 0) = g_j\mathbf{m}_{(\nu_i=0)}. \tag{19}$$

(The subscript j under the g serves to indicate that g belongs to an environment whose polarizability is α_j.) Comparison of (19) with (18) shows that

$$\mathbf{R}^* = g_j\mathbf{m}_{(\nu_i)}[\nu_j^2/(\nu_j^2 - \nu_i^2)]. \tag{20}$$

Our next task is to determine the work function W. The latter may be obtained by coupling $\mathbf{m}_{(\nu_i)}$ with $\mathbf{R}^*$ and is given by

$$W = -\tfrac{1}{2}m^2{}_{(\nu_i)}g_j[\nu_j^2/(\nu_j^2 - \nu_i^2)] \tag{21}$$

or, if we replace $m^2{}_{(\nu_i)}$ by the average square of the dipole moment (which is a function of ν_i), we have

$$W = -\tfrac{1}{2}\langle m_{\nu_i}{}^2\rangle_{\text{Av}}g_j[\nu_j^2/(\nu_j^2 - \nu_i^2)]. \tag{22}$$

This expression, however, is incorrect for the following reason. It is based on the erroneous assumption that the oscillators of the dielectric medium and "center" sphere have uniquely defined frequencies ν_j and ν_i, respectively. In an actual fluid, the molecules will sufficiently perturb each other to give rise to a range of frequencies even though the molecules may all have the same frequency in empty space. Thus it would be more appropriate to speak of a distribution of frequencies (even though the average frequency may be close to the natural frequency of a single oscillator) and to replace Eq. (22) by

$$W = -\tfrac{1}{2}\iint \rho(\nu_i)\rho(\nu_j)\,\langle m_{\nu_i}{}^2\rangle_{\text{Av}}g_j[\nu_j^2/(\nu_j^2 - \nu_i^2)]\,d\nu_i d\nu_j, \tag{23}$$

where $\rho(\nu_i)$ and $\rho(\nu_j)$ are the distribution functions of the frequencies of the "center" sphere and of the dielectric medium. This formula is not applicable when $\nu_i = \nu_j$, but the probability that this will occur should be very small and will be ignored.

The nature of Eq. (23) is such that it exhibits complete reciprocal character for there is a term $\langle m_{\nu_i}{}^2\rangle_{\text{Av}}g_j[\nu_j^2/(\nu_j^2 - \nu_i^2)]$ for every term

$$\langle m_{\nu_j}{}^2\rangle_{\text{Av}}g_i[\nu_i^2/(\nu_i^2 - \nu_j^2)]$$

and vice versa. Advantage may be taken of this fact to eliminate the function $\nu_j^2/(\nu_j^2 - \nu_i^2)$ in Eq. (23), but in order to do so, we must make a distinction between the classical and quantum-mechanical oscillators.

(i) *Classical Harmonic Oscillator*

For the classical oscillator,

$$\langle m_{\nu_i}^2\rangle_{Av}=3kT\alpha_i, \tag{24}$$

where k is Boltzmann's constant and T is the absolute temperature. Substitution of (24) in (23) then yields

$$W=-\tfrac{3}{2}kT\iint\rho(\nu_i)\rho(\nu_j)\alpha_i g_j[\nu_j^2/(\nu_j^2-\nu_i^2)]d\nu_i d\nu_j. \tag{25}$$

This integral can be written as

$$W=-\tfrac{3}{4}kT\iint\rho(\nu_i)\rho(\nu_j)\{\alpha_i g_j[\nu_j^2/(\nu_j^2-\nu_i^2)] +\alpha_j g_i[\nu_i^2/(\nu_i^2-\nu_j^2)]\}d\nu_i d\nu_j \tag{26}$$

because of the reciprocal relation.

It can be shown that the functions $\alpha_i g_j$ and $\alpha_j g_i$ are equivalent. This is easily seen in case of low dielectric constants, for

$$\alpha_i g_j\approx[2(\epsilon_j-1)/3](\alpha_i/a^3)=2\cdot(4\pi/3)\cdot(N/V)(\alpha_i\alpha_j/a^3)$$

and so is $\alpha_j g_i$. (The symbols N and V stand for Avogadro's number and molar volume, respectively.) The equivalence of $\alpha_i g_j$ and $\alpha_j g_i$, however, has general validity, for g_j depends linearly on α_j, as one would conclude from Eq. (19) and the form of Eq. (18), and so an interchange of the indices i and j in $\alpha_i g_j$ produces no new results. This permits us to factor out $\alpha_i g_j$ from the bracketed function in Eq. (26), which then reduces to

$$W=-\tfrac{3}{4}kT\iint\rho(\nu_i)\rho(\nu_j)\alpha_i g_j d\nu_i d\nu_j. \tag{27}$$

The integral gives the average values $\langle\alpha_i\rangle_{Av}$ and $\langle g_j\rangle_{Av}$. The latter is simply the measured g value and we assume that $\langle\alpha_i\rangle_{Av}$ is the same as α of the oscillator in empty space. This assumption is entirely reasonable, for it can be shown that for an assembly of coupled harmonic oscillators, the mean polarizability of a molecule is unaltered by the presence of neighboring molecules. (However, there is a slight deviation in case of real molecules.)[9,10] Thus, Eq. (27) takes the simple form

$$W=-\tfrac{3}{4}kT\alpha g \tag{28}$$

or

$$W=-\tfrac{1}{4}\langle m_0^2\rangle_{Av}g, \tag{29}$$

where $\langle m_0^2\rangle_{Av}$ is the statistical average of the square of the dipole moment in empty space.

(ii) *Quantum-Mechanical Harmonic Oscillator*

For the ground state of the quantal oscillator,

$$\langle m_{\nu_i}^2\rangle_{Av}=\tfrac{3}{2}h\nu_i\alpha_i. \tag{30}$$

The same expression with $h\nu_i$ replaced by the ionization potential I may be used to obtain $\langle m_{\nu_i}^2\rangle_{Av}$ in case of real molecules, provided one assumes that only one frequency, $\nu_{k0}=(E_k-E_0)/h$, corresponding to the ionization energy will make any effective contributions. This approximation was first introduced by London[1] and follows immediately from the definition of polarizability given in Eq. (14).

When the quantal expression for $\langle m_{\nu_i}^2\rangle_{Av}$ is substituted in Eq. (23), we obtain

$$W=-\tfrac{3}{4}h\iint\rho(\nu_i)\rho(\nu_j)\nu_i\alpha_i g_j[\nu_j^2/(\nu_j^2-\nu_i^2)]d\nu_i d\nu_j. \tag{31}$$

which can be written as

$$W=-\tfrac{3}{8}h\iint\rho(\nu_i)\rho(\nu_j)\nu_i\nu_j\{\alpha_i g_j[\nu_j/(\nu_j^2-\nu_i^2)] +\alpha_j g_i[\nu_i/(\nu_i^2-\nu_j^2)]\}d\nu_i d\nu_j. \tag{32}$$

Again, if we replace $\alpha_j g_i$ by $\alpha_i g_j$, we get

$$W=-\tfrac{3}{8}h\iint\rho(\nu_i)\rho(\nu_j)\alpha_i g_j[\nu_i\nu_j/(\nu_i+\nu_j)]d\nu_i d\nu_j. \tag{33}$$

If we further make the reasonable assumption that the average value of ν_i or ν_j is the same as the natural frequency ν_0 of a single oscillator, we obtain

$$W=-\tfrac{3}{16}h\nu_0\alpha g \tag{34}$$

or

$$W=-\tfrac{1}{8}\langle m_0^2\rangle_{Av}g. \tag{35}$$

It is seen that classical and quantal expressions have the same functional form and may be represented by a single formula

$$W=-\gamma\tfrac{1}{2}\langle m_0^2\rangle_{Av}g, \tag{36}$$

where

$\gamma=\frac{1}{2}$ for the classical oscillator

$=\frac{1}{4}$ for the quantum-mechanical oscillator.

Thus, the classical and quantal W values will differ not only because the $\langle m_0^2\rangle_{Av}$ values are different, but also because the γ's are different.

It is interesting to note that Eq. (36) may also be used to represent W of a permanent dipole; here, $\langle m_0^2\rangle_{Av}=\mu_0^2/1-\alpha g$ and $\gamma=1$.

III. CALCULATION OF $\langle m_0^2\rangle_{Av}$

The classical value for $\langle m_0^2\rangle_{Av}$ may be obtained by Eq. (22). However, in any actual numerical computation of the interaction energy, the classical value would be of little use, as the oscillations of the electrons about the nuclei are seldom classically excited at ordinary temperatures. The quantum-mechanical value for $\langle m_0^2\rangle_{Av}$ may be obtained in several ways, one of which [Eq. (30)] was already discussed in connection with the determination of W. The following methods may be

[9] L. Jansen and P. Mazur, Physica **21**, 193 (1955); P. Mazur and L. Jansen, *ibid.* **21**, 208 (1955).

[10] A. Michels, J. de Boer and A. Bijl, Physica **4**, 981 (1937).

used for computing the quantum-mechanical $\langle m_0^2\rangle_{Av}$ values.

(a) From Slater Screening Parameters[11]

In a few simple cases we can calculate $\langle m_0^2\rangle_{Av}=e^2\sum\langle r_i^2\rangle_{Av}$ using Slater screening parameters. Assuming that there is no correlation between the individual electrons in the (spherical) molecule, we obtain

$$\langle r_i^2\rangle_{Av}=\int\psi_i^*r_i^2\psi_i d\tau, \tag{37}$$

where ψ_i is the wave function belonging to the ith electron. The calculations are particularly simple for atoms. On using the Slater orbitals

$$\psi_{n^*,l,m}=r^{n^*-1}\exp[-(Z-S)r/n^*]Y_l^m(\theta,\phi), \tag{38}$$

it is easily seen that

$$\langle r_i^2\rangle_{Av}=[n_i^*/2(Z-S_i)]^2[(2n_i^*+1)(2n^*+2)]. \tag{39}$$

Here, n^* stands for the effective principal quantum number, $Z-S$ the effective nuclear charge, $Y_1^m(\theta,\phi)$ the normalized spherical harmonic, and $\mathbf{r}_i$ is the distance of the ith electron from the nucleus. The unit of length is the Bohr radius $a_0=0.5292$ A.

(b) From Diamagnetic Susceptibility Measurements

There is a direct relation between $\langle m_0^2\rangle_{Av}=\sum_i e^2\langle r_i^2\rangle_{Av}$ and the diamagnetic susceptibility. The molar susceptipility of an atom may be written as[12]

$$\chi=-(e^2N/6m_ec^2)\sum_i\langle r_i^2\rangle_{Av}, \tag{40}$$

where N is Avogadro's number and m_e the electron mass. Substitution of the proper values for e, m, and N results in

$$\langle m_0^2\rangle_{Av}=-8.14\times10^{-30}\chi(\text{esu-cm})^2. \tag{41}$$

(c) From Polarizability Measurements

There are essentially two methods available for determining $\langle m_0^2\rangle_{Av}$ from the polarizability. One is based on the London approximation[1]

$$\langle m_0^2\rangle_{Av}=\tfrac{3}{2}h\nu_0\alpha\approx\tfrac{3}{2}I\alpha, \tag{42}$$

which was already mentioned in the previous section. The second method is based on a formula derived by Kirkwood[13]:

$$\alpha=(4/9a_0)\sum_i\langle r_i^2\rangle_{Av}^2. \tag{43}$$

This expression is greatly simplified if one assumes that only the outer shell electrons make any appreciable contribution to the polarizability, and that they all contribute equally. If we further assume that the number of effective oscillating electrons is n, we get

$$\langle m_0^2\rangle_{Av}=ne^2\sum_i\langle r_i^2\rangle_{Av}=3/2(\alpha a_0n)^{\frac{1}{2}} \tag{44}$$

where a_0 is the unit of length in atomic units.

The effective number of oscillating electrons may be obtained from the values of the oscillator strengths. The classical theory of light absorption predicts the following relation between the polarizability and the oscillator strength[14]:

$$\alpha(\nu)=(e^2/4\pi^2m_e)\sum_i[f_i/(\nu_i^2-\nu^2)], \tag{45}$$

where ν_i is the frequency of the ith electron, ν the frequency of the incident radiation, and f_i the oscillator strength. Classically, f_i is interpreted to mean the effective number of electrons oscillating with frequency ν_i.

The quantal expression for the polarizability in terms of oscillator strength has the same functional form as Eq. (45). However, the quantum-mechanical oscillator strength is related to the transition probabilities for induced absorption and emission. One could make use of the Kuhn-Thomas rule[14] to determine the total number of oscillating electrons. But this would require summing over all discrete and continuous energy states which are difficult to obtain and so this method will not be pursued any further.

When only one frequency makes any considerable contribution to the polarizability, we may write

$$\alpha(\nu)=(e^2/4\pi^2m_e)[n/(\nu_0^2-\nu^2)], \tag{46}$$

where n is the number of effective electrons. Since there is only one variable parameter ν, one can obtain n from a plot of $1/\alpha$ vs ν^2.[15]

Table I lists the approximate values of $\langle m_0^2\rangle_{Av}$ obtained by the various methods discussed herein. It is seen that the $\langle m_0^2\rangle_{Av}$ values based on the London and Kirkwood formulas agree quite well with each other but differ considerably from those obtained from diamagnetic susceptibilities and Slater screening parameters. We believe that the London and Kirkwood formulas are more appropriate for the model adopted here, and we shall use them exclusively in our later numerical computations.

Regardless of which method is used, the $\langle m_0^2\rangle_{Av}$ values will generally be much larger than the μ_0^2 values for permanent dipoles, which are seldom greater than 10^{-35}(esu-cm)^2. Thus, it is only reasonable to expect that the dispersion energy should generally exceed the electrostatic energy.

[11] J. C. Slater, Phys. Rev. **36**, 57 (1930).
[12] See J. H. Van Vleck, *Electric and Magnetic Susceptibilities* (Oxford University Press, New York, 1932), p. 91.
[13] J. G. Kirkwood, Physik. Z. **33**, 57 (1932).
[14] See for example W. Kauzmann, *Quantum Chemistry* (Academic Press, Inc., New York, 1957), pp. 563–577 and 638–647.
[15] A list of n values so obtained may be found in E. A. Moelwyn-Hughes, *Physical Chemistry* (Pergamon Press, New York, 1957), p. 373.

TABLE I. Average values of the instantaneous dipole moment $\langle m_0^2 \rangle_{Av}$ for some nonpolar molecules.

Formula	Substance	Optical polarizability $\alpha \times 10^{24}$ cm^3	Effective No. of oscillating electrons n^e	Ionization potential I (ev)	Molar diamagnetic susceptibility $-\chi_{mol}/\times 10^6$ cc/mole	$\langle m_0^2 \rangle_{Av} \times 10^{36}$ (esu-cm)^2 Based on Eq. (39)	Based on Eq. (41)	Based on Eq. (42)	Based on Eq. (44)
He	Helium	0.207[a]	1.22	24.5[d]	1.38[f]	13.4	11.2	12.2	12.4
Ne	Neon	0.396[a]	2.41	21.53[d]	6.7[f]	45.7	54.5	20.5	24.4
Ar	Argon	1.644[a]	4.35	15.75[d]	18.1[f]	150.9	147	62.3	66.6
Kr	Krypton	2.486[a]	4.93	14.00[d]	37.0[f]	253.9	301	83.6	87.2
Xe	Xenon	4.021[a]	5.63	12.15[d]	59.0[f]	384.7	480	117	119
H_2	Hydrogen	0.81[a]	1.56	15.43[e]	4.0[g]		32.6	30.2	
N_2	Nitrogen	1.742[a]	4.64	15.58[e]	9.57[h]		77.9	65.1	71.1
O_2	Oxygen	1.573[a]	3.13	12.075[e]	...			45.6	55.6
Cl_2	Chlorine	4.61[b]	6.74	11.48[e]	40.5[h]		329	127	140
Br_2	Bromine	6.464[a]	3.95	10.55[e]	64.0[h]		521	164	126
I_2	Iodine			9.41[e]	91.4[h]		744		
CO_2	Carbon dioxide	26.5[b]	5.71	13.79[e]	18.6[h]		151	87.4	101
CS_2	Carbon disulfide	8.566[a]		10.08[e]	41.0[h]		337	196	
CCl_4	Carbon tetrachloride	10.243[a]	15.78	11.47[e]	66.1[h]		538	282	318
$SiCl_4$	Silicon tetrachloride	10.47[c]	19.54	11.6[d]	91.3[h]		743		358
$SnCl_4$	Stannic tetrachloride	13.721[a]	16.43		115.4[h]		939		366
$TiCl_4$	Titanium tetrachloride	14.990[a]		11.7[d]				421	
CH_4	Methane	2.55[a]	4.83	12.99[d]	12.2[g]		99.3	79.8	88.4
C_2H_6	Ethane	4.389[a]	6.55	11.65[d]	27.3[g]		222	123	133.3
C_6H_{12}	Cyclohexane	10.87[b]		9.88[e]	68.0[h]		554	258	256
C_6H_6	Benzene	10.390[a]	10.03	9.245[e]	55.5[h]		452	231	
p-C_8H_{10}	p-Xylene	14.276[a]		8.445[e]				290	
$C_4H_8O_2$	Dioxane	8.566[a]		9.14[e]				188	

[a] Calculated from gaseous molar refractions R_∞ given in A. A. Maryott and F. Buckley, Natl. Bur. Standards Circ. 537 (1953).
[b] *Landolt-Börnstein Tables* (Verlag Julius Springer, Berlin, 1951), Vol. 3, 6th ed., p. 513.
[c] E. A. Moelwyn-Hughes, *Physical Chemistry* (Pergamon Press, New York, 1957), p. 373.
[d] F. H. Field and J. L. Franklin, *Electron Impact Phenomena* (Academic Press, Inc., New York, 1957), p. 108.
[e] K. Watanabe, J. Chem. Phys. **26**, 541 (1957) and "Preliminary table of ionization potentials", Department of Physics, University of Hawaii, May 20, 1957.
[f] J. H. van Vleck, *Electric and Magnetic Susceptibilities* (Oxford University Press, New York, 1932), p. 215.
[g] Footnote reference b, p. 538.
[h] *International Critical Tables* (National Bureau of Standards, New York, 1929), Vol. VI, p. 354.

IV. POTENTIAL ENERGY OF A NONPOLAR SUBSTANCE

The work W is essentially the difference in energy per molecule inside and outside the dielectric and may be identified with the molecular potential energy. The total potential energy of N molecules is therefore

$$U = -\tfrac{1}{2} N \gamma g \langle m_0^2 \rangle_{Av}. \tag{47}$$

The potential energy of a liquid U_l should roughly be equal to the negative of the energy of vaporization $-\Delta E^v$, although this assumes that the rotation, translation, and vibration of each molecule is the same in the liquids as in the gas phase, a condition which is seldom satisfied.

In order to compute the potential energy U_l, we must know the size of the radius a. This is the same as the cavity radius which appears in the Onsager and Böttcher theories of dielectrics.[6,16] Onsager[6] arbitrarily set

$$(4\pi/3) a^3 N = V_l, \tag{48}$$

where V_l is the molar volume of the liquid. We shall do the same in our computation of U_l.

With this definition of a, the Onsager equation for the polarization of the nonpolar dielectrics reduces to the Clausius-Mossotti equation

$$[(\epsilon-1)/(\epsilon+2)]V = (4\pi/3) N\alpha, \tag{49}$$

which holds quite well for a great many liquids and dilute gases.

The value of a could be calculated from the Böttcher equation[16]

$$\frac{\epsilon-1}{\epsilon+2} V = \frac{4\pi}{3} N\alpha \frac{9\epsilon}{(\epsilon+2)[2\epsilon+1-(\alpha/a^3)(2\epsilon-2)]}. \tag{50}$$

However, in order to do so, one must know how ϵ varies with the density or, if only one value of ϵ is available, the latter must be known to a very high degree of accuracy. Unfortunately, no such data are available for liquids like H_2, He, N_2, etc., for which the theory may be expected to hold good.

[16] C. J. F. Böttcher, Physica **9**, 937 (1942); see also footnote reference 7c.

TABLE II. Comparison of the calculated potential energy of some liquids with the experimental energy of vaporization.

Formula	Substance	Temperature °K[a]	Molar volume V_T (cm³)[a]	Dielectric constant ϵ_T[b]	Square of dipole moment[d] $\langle m_0^2\rangle_{Av}\times10^{36}$ (esu-cm)²	Potential energy, $-U_l$ kcal/mole	Energy of vaporization ΔE^v kcal/mole[f]
He	Helium	4.2	32	1.048	12.2	0.053	0.012
Ar	Argon	87	28	1.521	62.3	2.5	1.396
H_2	Hydrogen	20.4	28	1.228	30.2	0.66	0.176
N_2	Nitrogen	77	35	1.434	65.1	1.9	1.18
O_2	Oxygen	90	28	1.483	45.6	1.8	1.45
Cl_2	Chlorine	239	46	2.05	127	5.1	4.40
Br_2	Bromine	298	51	3.06	164	8.4	6.74
CS_2	Carbon disulfide	298	61	2.628	196	7.6	6.1
CCl_4	Carbon tetrahloride	298	97	2.228	282	5.8	7.23
$SiCl_4$	Silicon tetrachloride	298	115	1.99[e]	358[e]	5.6	6.59
$SnCl_4$	Stannic tetrachloride	298	118	2.86	366[e]	7.8	8.95
$TiCl_4$	Titanium tetrachloride	298	111	2.79	421	9.4	9.02
CH_4	Methane	112	38	1.68	79.8	3.0	1.78
C_6H_{12}	Cyclohexane	298	109	2.015	258	4.4	7.30
C_6H_6	Benzene	298	89	2.274	231	5.5	7.39
p-C_8H_{10}	p-Xylene	298	124	2.260	290	4.8	9.53
$C_4H_8O_2$	Dioxane	298	86	2.209	188	4.3	9.8

[a] All values were taken from J. H. Hildebrand and R. L. Scott, *The Solubility of Non-Electrolytes* (Reinhold Publishing Corporation, New York, 1950), 3rd ed., p. 435.
[b] A. A. Maryott and E. R. Smith, Natl. Bur. Standards Circ. 514 (1951).
[c] Calculated from the refractive index n_D given in the *International Critical Tables* (National Bureau of Standards, New York, 1929), Vol. I, p. 103.
[d] All values taken from next to the last column of Table I except as otherwise indicated.
[e] Values taken from last column of Table I.
[f] Computed from heats of vaporization ΔH^v, as given in footnote reference a.

The potential energy shown in Table II was calculated from Eq. (47) using the quantum-mechanical values for $\langle m_0^2\rangle_{Av}$ and $\gamma=\frac{1}{4}$. (The classical values are of no interest.) The $\langle m_0^2\rangle_{Av}$ values for all substances, except the ones for which the ionization potentials are not known, were taken from the next to the last column of Table I. The remaining values were taken from the last column. We have used the static dielectric constant to compute g; in the event the former was not available, we have substituted n_D^2 for ϵ, n_D being the refractive index of the Na–D line.

Comparison with the experimental energies of vaporization given in the last column of Table II shows that all calculated values are of the right order of magnitude and in several instances the agreement is quite good. This is probably all that can be expected considering the approximations made in calculating U_l and the fact that the assumption regarding the equivalence of U_l and $-\Delta E^v$ is at best only a rough approximation.

V. POTENTIAL ENERGY OF A POLAR SUBSTANCE

We have hitherto used the static dielectric constant to compute U_l. We are justified in doing so for we have so far considered only nonpolar substances for which $\epsilon_0\approx\epsilon_\infty$. When we wish to extend this theory to polar substances, however, we must make a distinction between ϵ_0 and ϵ_∞. For, the dispersion energy is associated only with the electronic displacements and so the high-frequency dielectric constant $\epsilon_\infty\approx n^2$ ought to be used. The dispersion energy is only part of the total cohesive energy in polar substances. The remainder is the electrostatic interaction which can be computed from Eq. (8); here, however, one must use the static dielectric constant. If we make the reasonable assumption that there is no appreciable coupling between the electrostatic and dispersion forces, we may write for the total potential energy of a liquid

$$U_l=-(N/2)\{[\mu_0^2g_0/(1-\alpha g_0)]+\tfrac{1}{4}\langle m_0^2\rangle_{Av}g_\infty\}, \quad (51)$$

where

$$g_0=[(2\epsilon_0-2)/(2\epsilon_0+1)](1/a^3)$$

and

$$g_\infty=[(2n^2-2)/(2n^2+1)](1/a^3). \quad (52)$$

One should use the quantum-mechanical values for $\langle m_0^2\rangle_{Av}$.

It is to be expected that, due to the smallness of μ_0^2 as compared with $\langle m_0^2\rangle_{Av}$, the electrostatic energy would contribute little to the total cohesive force. This is indeed the case. Thus, chloroform, with a dipole moment of 1.02 D, has an electrostatic energy of 0.24 kcal/mole at its normal boiling point; the electrostatic energy of chlorobenzene, which has a dipole moment of 1.70 D, is only 0.31 kcal/mole and even acetone, with

a moment of 2.89 D, contributes only 2.6 kcal/mole.[17] The dispersion energies, on the other hand, should be comparable to the dispersion energies of similar nonpolar substances, which run around 5 to 10 kcal/mole. Only for substances for which ϵ_0 is abnormally large (e.g., H_2O) can the electrostatic energy be expected to make a larger contribution than the dispersion energy. Had the classical values been used for $\langle m_0^2 \rangle_{Av}$, the opposite would have been true.

VI. CRITIQUE OF THE CONTINUUM METHOD

The present treatment predicts that both the classical and quantum-mechanical oscillators give rise to "dispersion" energies, but the classical values are much too small and are further temperature dependent. The quantum-mechanical values are of the right order of magnitude and are very easy to compute. In deriving the quantum-mechanical formula, we have made no specific use of quantum mechanics other than to set $\langle m_0^2 \rangle_{Av}$ equal to $3/2h\nu_0\alpha$. From this point of view the treatment may be considered to be semiclassical.

[17] All values for μ_0 and ϵ_0 were taken from footnote reference a of Table I and footnote reference b of Table II, respectively.

The present dispersion formula owes its simple form to a number of approximations. Some were deliberately made in order to simplify the calculations, as, for example, the use of $\frac{3}{2}I\alpha$ for $\langle m_0^2 \rangle_{Av}$; others are inherent in the continuum treatment and no obvious way of improving the theory is evident. The assumptions regarding a uniform medium of constant dielectric and of a "hard" center molecule would fall under the latter category. These assumptions are very unrealistic when applied to an actual fluid; yet, they are the same assumptions that underly the continuum theory of dielectrics, which has met with a great deal of success. The success of the latter is undoubtedly the result of cancellation of errors and it is probable that similar cancellations prevail in the present treatment of dispersion energies.

ACKNOWLEDGMENTS

The author wishes to thank Dr. Robert Kromhout for his valuable comments and criticisms and Dr. Bentz Howard for several stimulating discussions. Thanks are also due to the Petroleum Research Fund for providing financial support.

Crystal Structure of β-Ga_2O_3

S. GELLER

Bell Telephone Laboratories, Inc., Murray Hill, New Jersey

(Received March 23, 1960)

The crystal structure of β-Ga_2O_3 has been determined from single-crystal three-dimensional x-ray diffraction data. The monoclinic crystal has cell dimensions $a=12.23\pm0.02$, $b=3.04\pm0.01$, $c=5.80\pm0.01$ A and $\beta=103.7\pm0.3°$ as originally reported by Kohn, Katz, and Broder [Am. Mineral. **42**, 398 (1957)]. There are 4 Ga_2O_3 in the unit cell. The most probable space group to which the crystal belongs is C_{2h}^3–$C2/m$; the atoms are in five sets of special positions $4i$: $(000, \frac{1}{2}\frac{1}{2}0)\pm(x0z)$. There are two kinds of coordination for Ga^{3+} ions in this structure, namely tetrahedral and octahedral. Average interionic distances are: tetrahedral Ga—O, 1.83 A; octahedral Ga—O, 2.00 A; tetrahedron edge O—O, 3.02 A; and octahedron edge O—O, 2.84 A. Because of the reduced coordination of half of the metal ions, the density of β-Ga_2O_3 is lower than that of α-Ga_2O_3 which has the α-corundum structure. Also the closest approach of two Ga^{3+} ions in β-Ga_2O_3 is 3.04 A which is considerably larger than the closest approach of metal ions in the sesquioxides with the α-corundum-type structure and, in agreement with the results of thermodynamic measurements, the β phase appears to be the structurally more stable one.

The average Ga—O distances in the structure seem to account for the fact that although the Ga^{3+} ion is substantially larger than the Al^{3+} ion its quantitative preference for tetrahedrally coordinated sites when substituted for Fe^{3+} ion in the iron garnets is very nearly the same as that of the Al^{3+} ion.

The structure accounts for a recent result obtained by Peter and Schawlow from paramagnetic-resonance measurements on Cr^{3+}-ion-doped β-Ga_2O_3, namely that the Cr^{3+} ion substitutes for the Ga^{3+} ions in a single set of equivalent octahedral sites.

The magnetic aspects of the β-Ga_2O_3 structure are discussed and it is shown that a possible Fe_2O_3 isomorph could be expected to be at least antiferromagnetic with a Néel temperature of about 700°K Furthermore, a knowledge of the β-Ga_2O_3 structure and of the nature of site preferences of the Ga^{3+} and Fe^{3+} ions in the garnets lead to a prediction regarding the structure of the ferrimagnetic crystals of formula $Ga_{2-x}Fe_xO_3$ recently discovered by Remeika.

INTRODUCTION

MUCH attention has recently been given the sesquioxides of the $3d$ elements particularly in regard to their magnetic nature. Several of these have the α-Al_2O_3 (α-corundum) structure.[1] Crystals of α-Al_2O_3 doped with small amounts of magnetic ions are not only of scientific interest but have important application as MASER materials. Trivalent gallium with $3d^{10}$ configuration is nonmagnetic and therefore a Ga_2O_3 crystal doped with a magnetic ion is also of scientific and possibly technological interest.

In these Laboratories paramagnetic-resonance studies by Peter and Schawlow[2] on Cr^{3+}-ion-doped β-Ga_2O_3 crystals prepared by Remeika[3] indicated that the Cr^{3+} ions had replaced Ga^{3+} ions in crystallographically equivalent octahedral sites. If the Cr^{3+} ions had entered crystallographically nonequivalent octahedral sites, this certainly would have been detected. On the other hand, it would not have been simple to detect tetrahedrally coordinated Cr^{3+} ions.

Since Kohn, Katz, and Broder had shown[4] that the unit cell of β-Ga_2O_3 contained 8 Ga^{3+} ions, then, as will be shown in detail later, these ions must be in at least two sets of crystallographically nonequivalent positions. Because there seemed little reason to expect the Cr^{3+} ions to prefer one set of octahedral sites to another and because the Cr^{3+} ion shows an exclusive preference for octahedral coordination, (see, for example, footnote references 5–7) it appeared reasonable to speculate that the Ga^{3+} ions had two types of coordination in β-Ga_2O_3. If this speculation proved sound, we would have the first clear-cut case in which a ***pure*** sesquioxide contained octahedrally and tetrahedrally coordinated metal ions in the same structure.

With the present interest in the $3d$ transition-metal oxides, it would seem worthwhile to determine the structures of any of those yet unknown. (Indeed there now appears to be good reason to refine ***known*** structures of these oxides to provide needed accuracy for theoretical considerations.) Such knowledge could be important to our understanding of the crystal chemistry of the ions involved. For example, the Fe^{3+} and Ga^{3+} ions with spherical electronic configurations $3d^5$ and $3d^{10}$, respectively, have both octahedral and tetrahedral coordination in the garnets $\{Y_3\}[Fe_2](Fe_3)O_{12}$ and $\{Y_3\}[Ga_2](Ga_3)O_{12}$ and in solid solutions of one of these in the other.[5] Both the Ga^{3+} and Al^{3+} ions are smaller than the Fe^{3+} ion, but the Ga^{3+} is substantially larger than the Al^{3+} ion.[6] Yet when these ions are substituted for the Fe^{3+} ion in the garnets they show very nearly the same quantitative preference for tetrahedral sites.[5,9] The present investigation appears to clarify this observation.

The structure of β-Ga_2O_3 also accounts for its being

[1] R. W. G. Wyckoff, *Crystal Structures*, Vol. II (Interscience Publishers Inc., New York). See also Z. Krist., Strukturbericht **1**, 240 (1931); L. Pauling and S. B. Hendricks, J. Am. Chem. Soc. **47**, 781 (1925); W. H. Zachariasen, Z. Krist., Strukturbericht **2**, 310 (1937).

[2] M. Peter and A. L. Schawlow, Bull. Am. Phys. Soc. Ser. II, **5**, 158 (1960).

[3] J. P. Remeika, J. Appl. Phys. **31**, 263S (1960); See also Conference on Magnetism and Magnetic Materials, Detroit, Michigan, November, 1959, Paper No. S4.

[4] J. A. Kohn, G. Katz, and J. D. Broder, Am. Mineral. **42**, 398 (1957).

[5] M. A. Gilleo and S. Geller, Phys. Rev. **110**, 73 (1958).

[6] S. Geller, J. Appl. Phys. **31**, 30S (1960).

[7] S. Geller, C. E. Miller, and R. G. Treuting, Acta Cryst. **13**, 179 (1960).

[8] S. Geller, Acta Cryst. **10**, 248 (1957).

[9] S. Geller, J. Phys. Chem. Solids (to be published).

the thermodynamically stable room-temperature phase,[10] for its having a lower density than that of the α phase, and allows us to make a speculation regarding the structure of the recently discovered ferrimagnetic (and piezoelectric) $Ga_{2-x}Fe_xO_3$.[3]

DETERMINATION OF THE STRUCTURE

The crystals used in this study were prepared by J. P. Remeika.[3] Powdered specimens gave photographs in agreement with the patterns reported by Kohn *et al.*[4] and by Foster and Stumpf[10] for the β-Ga_2O_3. Most of the crystals photographed were twinned, some multiply, but after some searching one was found from which a small single-crystal segment with long direction along the monoclinic b axis was cleaved. The cell constants[11] $a=12.23\pm0.02$, $b=3.04\pm0.01$, $c=5.80\pm0.01$ A, $\beta=103.7\pm0.3°$ given by Kohn *et al.*[4] are quite accurate for our purposes as established by the complete indexing of the powder pattern taken with Cu$K\alpha$ radiation (see Appendix). The space group to which the crystal belongs was reported by Kohn *et al.* to be C_{2h}^3, which is indeed the *most probable* one and with which all our data are compatible. There are 4 Ga_2O_3 in the unit cell;[4] the x-ray density is therefore 5.94 g/cm.

The crystal photographed with the Weissenberg camera and both Cu$K\alpha$ and Mo$K\alpha$ radiation had the dimensions: length 1.3 mm and cross section 0.09×0.11 mm. The diffraction symmetry was C_{2h}–$2/m$, with systematic absences, hkl, $h+k\neq 2n$. Thus the possible space groups are C_{2h}^3–$C2/m$, C_s^3–Cm and C_2^3–$C2$. The space group Cm would require two equivalent atoms related by the symmetry plane to be at a maximum distance from each other of 1.52 A thus indicating that the crystal cannot possibly belong to this space group.

The corresponding intensities on the even-numbered (Weissenberg) layers about the b axis were very similar as were those on the odd-numbered layers. Thus the structure appeared to be layered at one-half the b axis. It was therefore unlikely that the heavy atoms would be at combinations of positions such that the y coordinates differed by other than multiples of $\frac{1}{2}b$, (although, of course very small deviations might occur). In such a case the positions of $C2$ with $y=0$ or $\frac{1}{2}$ become special positions of $C2/m$. Negative tests for piezo- and pyroelectricity supported the conclusion that the most probable space group for the crystal is $C2/m$.

In $C2/m$, the general positions and positions e–h would require two equivalent atoms related by the symmetry plane to be at 1.52 A from each other. Thus atoms could not be in any of these positions.

The intensities were estimated visually by comparison with a calibrated intensity scale and by cross comparison of intensities on various photographs. Intensities of zero-level data taken with Mo$K\alpha$ radiation were averaged with those taken with Cu$K\alpha$ radiation when observable with both radiations. (The small dispersion corrections for Ga would not have a significant effect.) Because no really new information was obtainable from other than the zero and first layers, intensities on these were the only ones quantitatively estimated.

Because absorption of both radiations by the crystal was high ($\mu_{CuK\alpha}=299$ cm^{-1}, $\mu_{MoK\alpha}=255$ cm^{-1}), it was necessary to use a small crystal (see above). Thus maximum exposure times for the photographs taken with Mo$K\alpha$ radiations were 102, 90, 70, and 90 hr for the zero through third layers, respectively. With Cu$K\alpha$ radiation, the maximum exposure times were about 20 hr. Absorption corrections were applied assuming the crystal to be cylindrical with an average radius of 0.05 mm. The absorption correction tables used were those of Bond[12] and applied to the first layer in accordance with the formula given by Bond.[12] (see also footnote reference 13). Lorentz-polarization-Tunell rotation-factor corrections were also applied.[14]

A Patterson projection on (010) clearly showed the peaks resulting from Ga—Ga interactions, and it appeared that all atoms must lie in the symmetry planes, and occupy five sets of positions $4i$: (000, $\frac{1}{2}\frac{1}{2}0$)$\pm(x0z)$. It was also clear that the contributions from the Ga^{3+} ions would determine most of the phases. It was necessary to consider the first-layer data for the purpose of distinguishing the most probable among homomorphic (010) projections. A (010) Fourier synthesis, a generalized Patterson projection using the $h1l$ data, a generalized Fourier projection with the $h1l$ data, and a pseudo-three-dimensional difference synthesis aided in determining the oxygen-ion positions. The pseudo-three-dimensional synthesis was done as follows: The contributions of the Ga^{3+} ions were subtracted from the observed structure factors. These had been scaled on the basis that, as indicated, the contributions of oxygens were generally not large. Thus some intuition entered into this scaling and as will be seen appeared to be quite sound. The remainders assumed to be the oxygen contributions, but of course containing numerous error contributions, were used in the synthesis. Each such amplitude, $h0l$, and $h1l$ was counted once in the synthesis. As expected, some spurious peaks occurred. Nevertheless, having obtained fairly accurate positions of the Ga^{3+} ions, the results of this synthesis together with structural considerations led to a determination of the oxygen trial parameters.

The trial parameters (for refinement) are given in Table I. It should be mentioned that the oxygen-ion positions were expected to be quite inaccurate, the idea being to save the author time by allowing the IBM 704 computer to do *all* of the refining.

[10] L. M. Foster and H. C. Stumpf, J. Am. Chem. Soc. **73**, 1590 (1951).

[11] Our designation of the axes is in keeping with the convention $c<a$ for the monoclinic cell.

[12] W. L. Bond, Acta Cryst. **12**, 375 (1960).

[13] M. J. Buerger and N. Niizeki, Am. Mineral. **43**, 726 (1958).

[14] I am indebted to Dr. R. G. Treuting for programing the calculation of the corrected relative squared structure amplitudes and relative structure amplitudes on the IBM 704 computer.

TABLE I. Trial parameters.

Atom	Coordinates		B, A²
	x	z	
Ga_I	0.087	−0.204	0.2
Ga_{II}	0.341	−0.312	0.2
O_I	0.153	0.092	0.8
O_{II}	0.492	0.248	0.8
O_{III}	0.829	0.443	0.8

REFINEMENT OF THE STRUCTURE

Refinement of the structure was carried out with the Busing-Levy[15] least-squares program for the IBM 704 computer. Only *h0l* and *h1l* amplitudes were used. In the first refinement cycles 824 data were included. All observed amplitudes were weighted unity; all unobserved amplitudes included at one-half threshold value were weighted 0.01. Two scale factors corresponding to the two k values (zero and first layers about b) of the data were refined. Both of these were started at 1.000 and are the scale factors mentioned earlier. Atomic scattering factors used for the structure amplitude calculations were those of Thomas and Umeda[16] for Ga^{3+} and for O^{2-} those given by Berghuis *et al.*[17] for O arbitrarily modified such that $f_{O^{2-}}=10$ at $\sin\theta/\lambda=0$ and $f_{O^{2-}}=f_O$ at $\sin\theta/\lambda\geq 0.20$.

Convergence was attained within three cycles: in the final cycle, the largest change in any coordinate was 0.003 A by O_{II} in the a direction. The weighted R factor was 0.171 for the data calculated on the basis of the parameters of the second cycle. The final scale factors were 0.988 and 0.997 with σ's of 0.010, meaning that these are not significantly different from 1.000.

Examination of the calculated and observed data indicated some large discrepancies in the high-angle data taken with the Mo$K\alpha$ radiation. These data had been taken with Kodak type *KK* film, which unfortunately has rather large grain size. Small weak spots are difficult to see in this case; the difficulty is more pronounced when the α_1, α_2 doublet is resolved. Because the data were plentiful, it was decided to omit a large portion of the high-angle reflections. The total data were therefore reduced from 824 to 522. Two least-squares cycles were run. The largest difference in coordinates between the results so obtained and those obtained previously was 0.005 A for atom O_{III} in the a direction. The final parameters with their standard deviations are given in Table II.

The weighted R factor calculated by the Busing-Levy program was 0.166. However, if unobserved reflections are excluded; the R factor

$$\sum | F_{obs}-F_{calc} | / \sum | F_{obs} |$$

for the *hOl* reflections is 0.143 and for the *h1l*, 0.130. The comparison of calculated and observed structure amplitudes is given in Table III.

INTERATOMIC DISTANCES AND ANGLES

The estimated standard deviations of the positions of the atoms are 0.004, 0.004, 0.033, 0.028, and 0.028 A for Ga(I), Ga(II), O(I), O(II), and O(III), respectively. These standard deviations of position should be considered as radii of circles in the mirror planes. Standard deviations in bond lengths were computed taking into consideration the angle made between the bond direction and the symmetry planes. The interatomic distances and their standard deviations are given in Table IV.

The important angles are given in Table V. Individual standard deviations were not calculated for these, but an estimate of the standard deviation of an O—Ga—O angle is 1.3° and of a Ga—O—Ga angle, 0.9°.

DESCRIPTION OF THE STRUCTURE

The arrangement of the ions in the β-Ga_2O_3 structure is shown in Figs. 1 and 2. The oxygen ions are arranged in a "distorted cubic" close-packed array. There are two crystallographically nonequivalent gallium and three nonequivalent oxygen ions in the unit cell. Each Ga_I^{3+} ion is surrounded by a distorted tetrahedron of oxygen ions: one O_I^{2-} at 1.80 A, two O_{II}^{2-} ions at 1.83 A, and one O_{III}^{2-} ion at 1.85 A (average 1.83 A). Each Ga_{II}^{3+} ion is surrounded by a highly distorted octahedron of oxygen ions: two O_I^{2-} at 1.95 A, one O_{II}^{2-} ion at 1.95 A, one O_{III}^{2-} ion at 2.02 A, and two O_{III}^{2-} ions at 2.08 A (average 2.00 A). A tetrahedron shares *only* corners with other tetrahedra in the b-axis direction and with octahedra in other directions. An octahedron shares edges with adjacent octahedra in the b axis direction and in roughly the [102] direction: the shared edges are, respectively, O_I–O_{III} and O_{III}–O_{III}, each of length 2.67 (Table IV). The distance 2.67 A is the shortest O–O distance in the structure. This is

TABLE II. Final parameters.

	Scale factors		Standard deviations		
1	0.984		0.013		
2	0.988		0.014		

Atom	Coordinates		B, A²	$\sigma(x)$	$\sigma(z)$	$\sigma(B)$
	x	z				
Ga_I	0.0904	−0.2052	0.33	0.0002	0.0005	0.05
Ga_{II}	0.3414	−0.3143	0.28	0.0002	0.0005	0.05
O_I	0.1674	0.1011	0.76	0.0019	0.0041	0.32
O_{II}	0.4957	0.2553	0.43	0.0016	0.0034	0.25
O_{III}	0.8279	0.4365	0.46	0.0015	0.0034	0.25

[15] W. R. Busing and H. A. Levy, ORNL Central Files Memorandum 59-4-37 (April, 1959).
[16] L. H. Thomas and K. Umeda, J. Chem. Phys. **26**, 293 (1957).
[17] J. Berghuis, I. J. M. Haanappel, M. Potters, B. O. Loopstra: C. H. MacGillavry, and A. L. Veenendaal, Acta Cryst. **8**, 478 (1955).

TABLE III. Calculated and observed amplitudes.

k=0

	h=0		h=2		h=4		h=6		h=8		h=10		h=12		h=14		h=16		h=18		h=20		h=22		h=24		h=26		h=28	
l	Obs.	Calc.	Obs.	Calc.	Obs.	Calc.	Obs.	Calc.	Obs.	Calc.	Obs.	Calc.	Obs.	Calc.	Obs.	Calc.	Obs.	Calc.	Obs.	Calc.	Obs.	Calc.	Obs.	Calc.	Obs.	Calc.	Obs.	Calc.	Obs.	Calc.
0		440	< 9	-1	93	-126	57	53	23	-26	<13	1	125	116	<19	2	84	-77	<20	9	19	24	<19	1	33	28	<20	2	35	-34
$\bar{1}$	22	-18	47	33	97	-141	67	-66	112	145	30	36	82	-66	<14	-5	22	-23	25	-23	53	55	20	20	43	<46	18	-11		
$\bar{2}$	117	-151	107	-123	45	45	48	46	<12	-2	<13	10	77	-62	83	-69	57	50	45	45	<19	29	<19	-11	<19	-9	30	-26		
$\bar{3}$	<10	6	27	-27	76	62	122	111	69	-58	109	-93	38	31	42	34	<17	8	40	33	<19	-18	51	-49	<19	20	49	36		
$\bar{4}$	24	30	136	178	17	-23	76	64	35	28	46	-39	15	15	100	100	<17	-13	48	-61	<19	14	<18	12	<19	3	24	31		
$\bar{5}$	<13	-2	17	8	19	20	144	-109	26	-27	136	107	<13	4	50	-42	<14	5	41	-35	<19	-15	51	55	<19	6	41	-39		
$\bar{6}$	23	28	107	-96	57	-49	52	40	<15	10	<13	13	19	16	78	-61	40	-42	49	47	<19	22	<19	-20	<19	-20				
$\bar{7}$	16	-21	<12	-6	14	-23	63	52	63	59	65	-47	46	-46	<18	21	<18	14	<19	14	<19	27	<19	-22						
$\bar{8}$	61	-64	26	34	81	81	<17	-21	17	-21	<18	7	40	-34	24	22	66	64	<18	-18	29	36	<19	11						
$\bar{9}$	41	42	<18	-7	25	17	<18	5	78	-72	<19	-3	74	63	<18	-9	<19	-18	<19	5	27	-34	<18	-4						
$\bar{10}$	43	44	<19	12	54	-59	<19	-18	<19	22	<19	-2	22	17	<19	11	47	-47	<19	-20										
$\bar{11}$	<19	-23	<19	-2	<19	-11	<19	-15	43	40	22	29	33	-32	<18	-19	<19	12	<18	3										
$\bar{12}$	24	-15	30	-36	30	29	30	36	<19	-14	<19	-2	<18	-4																
1			53	30	145	145	70	-49	125	-130	34	31	61	51	<10	0	24	28	<18	-11	55	-53	<19	14	42	42				
2			43	38	88	75	19	-18	<13	-2	46	-41	83	-75	33	36	62	59	30	-29	22	-22	<19	-1	<18	-23				
3			82	-72	72	-65	108	105	73	62	79	-64	22	-21	<17	-2	<18	-21	38	39	25	31	38	-41						
4			113	-104	<20	16	<19	4	<16	-8	88	84	17	18	74	-69	<19	-3	38	30	<19	3	<18	18						
5			99	86	17	-18	123	-103	22	15	49	50	<18	-3	<19	15	<19	-3	43	-44	<19	5	39	39						
6			72	61	14	-17	< 7	-7	30	-17	64	-56	<19	17	48	54	<19	-20	22	-27	<18	3								
7			44	-42	57	52	35	58	30	-42	22	-28	<19	10	<19	-13	<19	19	23	31										
8			<18	-7	<18	17	<18	-6	38	43	<19	23	39	-47	<19	-13	23	29												
9			<19	-13	64	-66	<19	1	39	39	<19	0	<19	3	<18	1														
10			<19	-10	<19	-11	<19	-5	38	-34	<19	4	39	40																
11			<19	21	42	43	<19	-22	29	-27																				
12			<18	18	<17	-1																								

k=1

	h=1		h=3		h=5		h=7		h=9		h=11		h=13		h=15		h=17		h=19		h=21		h=23		h=25	
l	Obs.	Calc.	Obs.	Calc.	Obs.	Calc.	Obs.	Calc.	Obs.	Calc.	Obs.	Calc.	Obs.	Calc.	Obs.	Calc.	Obs.	Calc.	Obs.	Calc.	Obs.	Calc.	Obs.	Calc.	Obs.	Calc.
0			21	17	110	-101	132	-112	51	53	56	61	21	-27	<20	-9	28	-21	45	-45	30	28	46	41	22	-26
$\bar{1}$			135	-136	29	33	23	24	25	20	69	69	18	-31	79	-79	<21	25	45	45	<23	-4	<23	8	<22	-4
$\bar{2}$	63	55	88	-88	14	14	161	181	<15	-11	95	-86	<18	21	<20	1	<21	4	59	61	<23	-3	57	51	<23	6
$\bar{3}$	55	-46	143	145	14	14	42	-40	16	13	67	-69	19	-30	96	87	<21	16	55	-52	<23	-4	<23	-7	<23	-11
$\bar{4}$	<15	1	35	41	26	27	96	-96	72	-71	43	56	22	32	<20	-16	<21	3	22	-32	33	-37	33	36	<23	28
$\bar{5}$	71	87	58	-59	65	-61	17	17	<18	3	22	31	46	54	24	-36	40	-56	<23	26	30	30	<23	-1	<22	13
$\bar{6}$	<18	-12	<18	10	63	-64	24	28	121	105	<20	-22	55	-49	22	15	<22	-11	<23	10	38	51	<23	-11	45	-39
$\bar{7}$	79	-94	<20	-11	68	79	<20	-6	<20	-11	<21	9	56	-62	<22	-11	59	67	<23	-2	38	-34	<23	3	<21	-15
$\bar{8}$	<21	10	<21	-7	27	36	<21	19	68	-69	25	-32	26	40	<23	9	<23	-3	<23	8	32	-34	<22	-23	41	34
$\bar{9}$	71	53	45	41	50	-39	<22	-22	<22	5	<23	-5	30	31	<23	33	<23	-31	<22	20	<21	14				
$\bar{10}$	<23	-11	<23	6	<23	-6	46	-41	33	29	70	55	<23	-19	<23	-20	<23	6	<22	-13						
$\bar{11}$	<23	-2	73	-57	<23	3	52	40	<23	-9	<23	3	<23	2	55	-45	<22	1	47	42						
$\bar{12}$	<22	-6	<22	2	<22	-6	29	28	<22	8	54	45	<22	-11												
1	209	162	79	61	80	-62	<14	-2	51	-47	38	-41	78	80	36	38	58	-57	<23	-16	<23	5	<23	-11	22	24
2	64	-57	14	-11	180	174	18	14	97	-98	<18	12	<20	18	<21	-1	59	52	<23	8	57	-50	<23	-1		
3	138	-143	31	30	40	35	<16	2	53	57	19	-16	80	-79	<22	15	47	49	<23	-3	<23	0	<22	-1		
4	15	20	47	-53	95	-96	31	35	58	67	20	-25	<21	-19	<22	-8	46	-39	<23	15	45	43				
5	58	66	38	-47	<18	-17	<19	-13	29	-33	38	49	36	46	37	-45	<23	-26	<23	14	<22	-6				
6	<19	-16	96	93	20	29	77	-74	<22	-5	26	26	<23	0	23	31	<23	14								
7	<20	10	27	35	<21	-4	22	31	<23	-3	42	-58	<23	3	30	42	<22	0								
8	<23	-20	40	-63	<22	15	42	53	<23	-16	<23	-22	<23	-2												
9	<23	-28	<23	-22	<23	3	<23	-19	<23	22	23	40														
10	42	43	30	29	50	-44	<23	-15	<23	25																
11	38	28	<23	-2	<22	12	<22	2																		

TABLE IV. Interatomic distances and standard deviations.

	Atom pair (No.)	Distance, A	σ, A		Atom pair (No.)	Distance, A	σ, A
Ga_IO_4 tetrahedron	Ga—O_I	1.80	0.03	$Ga_{II}O_6$ octahedron	Ga—O_I(2)	1.95	0.03
	Ga—O_{II}(2)	1.83	0.01		Ga—O_{II}	1.95	0.03
	Ga—O_{III}	1.85	0.03		Ga—O_{III}	2.02	0.03
	O_I—O_{II}(2)	2.93	0.04		Ga—O_{III}(2)	2.08	0.02
	O_I—O_{III}	3.13	0.04		O_I—O_I	3.04	0.01
	O_{II}—O_{II}	3.04	0.01		O_I—O_{II}(2)	2.90	0.04
	O_{II}—O_{III}(2)	3.02	0.03		O_I—O_{III}(2)	2.85	0.04
					O_I—O_{III}(2)	2.67	0.04
					O_{II}—O_{III}(2)	2.89	0.03
					O_{III}—O_{III}(2)	2.67	0.04
					O_{III}—O_{III}	3.04	0.01
Shortest Ga–Ga distances	Ga_I—Ga_I(2)	3.04	0.01	Averages	Ga_I—O	1.83	
	Ga_{II}—Ga_{II}(2)	3.04	0.01		Ga_{II}—O	2.00	
	Ga_{II}—Ga_{II}(2)	3.11	0.01		O—O, octahedron	2.84	
	Ga_I—Ga_{II}	3.28	0.01		O—O, tetrahedron	3.02	
	Ga_I—Ga_{II}(2)	3.30	0.01				
	Ga_I—Ga_{II}(2)	3.33	0.01				
	Ga_I—Ga_{II}(2)	3.45	0.01				

TABLE V. Bond angles.

Within a tetrahedron (involve only Ga_I)

2 O_I—Ga—O_I	107.6°
O_I—Ga—O_I	117.8
O_{II}—Ga—O_{II}	112.0
2 O_{II}—Ga—O_{III}	110.2

Within an octahedron (involve only Ga_{II})

O_I—Ga—O_I	102.7°
2 O_I—Ga—O_{II}	96.1
2 O_I—Ga—O_{III}	91.9
2 O_I—Ga—O_{III}	83.1
2 O_{II}—Ga—O_{III}	91.5
O_{III}—Ga—O_{III}	94.1
2 O_{III}—Ga—O_{III}	81.4

Ga_I—O—Ga_{II} (tetrahedral-octahedral) angles

2 Ga—O_I—Ga	123.3°	(2 different Ga_{II}'s)
2 Ga—O_{II}—Ga	123.0	(2 different O_{II}'s)
2 Ga—O_{III}—Ga	122.3	(2 different Ga_{II}'s)
Ga—O_{III}—Ga[a]	115.4	

Ga_I—O—Ga_I (tetrahedral-tetrahedral) angles

2 Ga—O_{II}—Ga	112.0°	(2 different O_{II}'s)

Ga_{II}—O—Ga (octahedral-octahedral) angles

2 Ga—O_{III}—Ga	98.4°	(2 different Ga_I's)
2 Ga—O_{III}—Ga	98.4	(2 different O_{III}'s)
Ga—O_I—Ga	102.7	
Ga—O_{III}—Ga	94.1	

[a] Ga_I and Ga_{II} in same plane.

in agreement with the observation[18] that in ionic structures, the mutual repulsion of the positive ions tends to reduce the length of shared edges of anion polyhedra.

Because of the short b axis, there are two O_I^{2-} and two O_{III}^{2-} ions (along the b axis) at corners of an octahedron. The structure cannot possibly then have two O_{II}^{2-} ions at the remaining corners of the octahedron, since these must lie in the mirror plane containing the Ga_{II}^{3+} ion within the octahedron. Thus there is only one O_{II}^{2-} ion at a corner of the octahedron, the remaining corner being occupied by a third O_{III}^{2-} ion.

At the corners of the tetrahedron, there are two O_{II}^{2-} ions which are along the b axis, the other corners being occupied by an O_I^{2-} and an O_{III}^{2-} ion each lying in the mirror plane containing the Ga_I^{3+} ion within the tetrahedron.

Thus each O_I^{2-} ion is at the corner of two octahedra and one tetrahedron; each O_{II}^{2-} ion is at the corner of one octahedron and two tetrahedra; and each O_{III}^{2-} ion is at the corner of three octahedra and one tetrahedron. *If* the octahedra and tetrahedra were regular, it would be doubtful that such a structure could exist, because the sums of the bond numbers of the bonds at all oxygen ions would not be 2 (see footnote reference 18). They would be: at O_I^{2-}, $1\frac{3}{4}$, at O_{II}^{2-}, 2; and at O_{III}^{2-}, $2\frac{1}{4}$. However, the polyhedra are probably not regular. In fact, the four bonds to O_{III}^{2-} are the longest ones: Ga_I–O_{III}=1.85 A, Ga_{II}–O_{III}=2.08(2) and 2.02

[18] L. Pauling, *Nature of the Chemical Bond* (Cornell University Press, Ithaca, New York, 1960), 3rd ed., Chap. 13, Sec. 6.

A, whereas those to O_I^{2-} are the shortest ones: Ga_I–O_I = 1.80 A and Ga_{II}–O_I = 1.95 A(2). The Ga_I–O_{II} distance 1.83 A is equal to the average Ga_I–O distance, but the Ga_{II}–O_{II} distance, 1.95 A, is 0.05 A shorter than the average Ga_{II}–O distance. Thus the sum of the bond numbers of the bonds to an O_{II}^{2-} ion is somewhat greater than two, but not importantly so (see footnote reference 20).

Actually, the statistical calculation tells us that: there are no significant differences in Ga_I–O distances, nor in the Ga_{II}–O_I and Ga_{II}–O_{II} distances, nor in the two Ga_{II}–O_{III} distances. The shorter Ga_{II}–O_{III} distance is only possibly significantly different from the Ga_{II}–O_I and Ga_{II}–O_{II} distances. However the long Ga_{II}–O_{III} distance is significantly larger than the shortest distances. Unfortunately, the oxygen ions contribute little to the intensities in comparison with gallium ions and it is unlikely that much greater reliability can be attained even from more accurate intensity data. Also it would appear to be quite difficult to obtain crystals of the aluminum isomorph designated as θ-Al_2O_3[19,20]; none have as yet been reported.

Nevertheless, the aforementioned criterion defined by Pauling[18] indicates that the oxygen polyhedra must be irregular and therefore that the calculated distances are perhaps better than indicated by the standard deviations.

DISCUSSION

1. Comparison with α-Corundum Structure

The β-Ga_2O_3 structure (Figs. 1 and 2) appears to be quite different from that of α-Ga_2O_3 which has the α-corundum structure. The latter has the oxygen ions in approximately hexagonal close-packed array with all the Ga^{3+} ions octahedrally coordinated to O^{2-} ions. Also in the α phase, octahedra share edges and faces

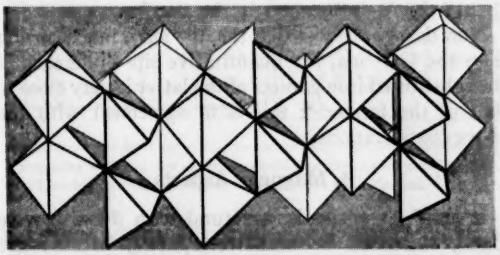

FIG. 1. Perspective view of the arrangement of the oxygen octahedra and tetrahedra in β-Ga_2O_3.

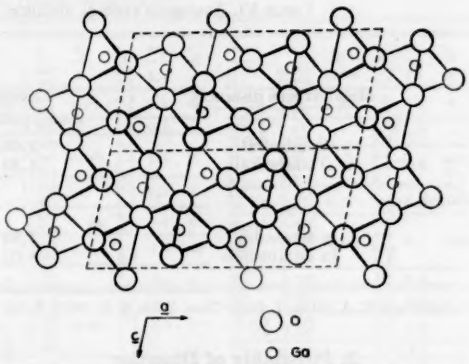

FIG. 2. Plan view of the β-Ga_2O_3 structure. Lines connecting atoms indicate the manner in which the octahedra and tetrahedra are constructed from and joined by the oxygen atoms in the three consecutive symmetry planes. Only the upper faces of the polyhedra are depicted. For increased clarity, this figure should be studied simultaneously with Fig. 1.

which brings the metal ions very near each other. Accurate atomic positional parameters for α-Ga_2O_3 have not been determined. However, in Fe_2O_3,[1] the closest approach of two Fe^{3+} ions through a shared octahedral face is 2.88 A and through a shared edge 2.96 A.[21] In β-Ga_2O_3 no faces are shared between polyhedra and the shortest Ga^{3+}–Ga^{3+} distance is 3.04 A.

Now it is recognized that usually structures in which faces of polyhedra are shared are less stable than those in which edges are shared, which in turn are less stable than structures in which only corners are shared.[18] Thus, one would expect the β phase to be more stable than the α phase. Foster and Stumpf have shown[10] that although the α-Ga_2O_3 forms at lower temperatures than does β-Ga_2O_3, the α phase is metastable. In the case of alumina, it appears that the α phase forms at higher temperatures than the θ (isostructural with β-Ga_2O_3) just the reverse of the gallia. Yet it appears that although seen rarely in comparison with the α phase, the θ-Al_2O_3 is the thermodynamically stable phase at room temperature[19] and that although α-Al_2O_3 is thermodynamically metastable at room temperature the $\alpha \rightarrow \theta$ transition of Al_2O_3 is "infinitely" sluggish at such temperature.

As one might expect, the lower average coordination in the β-Ga_2O_3 is accompanied by a lower density; the volumes per Ga_2O_3 in the α and β phases are 47.8 and 52.8 A^3, respectively.

[19] H. C. Stumpf, A. S. Russell, J. W. Newsome, and C. M. Tucker, Ind. Eng. Chem. **42**, 1398 (1950).

[20] The lattice constants of this phase derived by the present author from the powder data given by Stumpf *et al.*[19] are a = 11.83±0.02, b = 2.92±0.01, c = 5.64±0.01 A, and β = 104.0±0.5°. The powder data, however, are not completely correct, the most outstanding discrepancy being that of d_{001} which should be 5.47 A as against the reported 5.25 A. Also it is possible that some observable lines have been omitted; one of these is the [40$\bar{1}$] reflection.

[21] Recent accurate work on Ti_2O_3 and V_2O_3 by Nordmark[22] has led to the Me–Me distances: 2.55 and 2.64 A, respectively, across the shared face and 2.99 and 2.88 A, respectively, across the shared edge. In any case, the closest approach of Ga^{3+} ions in β-Ga_2O_3 is substantially greater than that of the metal ions in any of the α phases.

[22] C. Nordmark, in Final Technical Report, "Studies on the crystal chemistry of titanium, vanadium and molybdenum oxides at elevated temperatures" by A. Magnéli *et al.*, University of Stockholm (October, 1959), p. 16. See also R. E. Newnham and Y. M. de Haan, American Crystallographic Association Meeting, Washington, D. C., January, 1960, Paper No. D-5.

TABLE VI. Analogous average distances and ranges in β-Ga_2O_3 and in yttrium-iron garnet.

Metal-oxygen distances	β-Ga_2O_3 Averages	β-Ga_2O_3 Range	YIG[a] Averages	YIG[a] Range
Octahedral	2.00 A	1.95–2.08 A	2.00 A	All equal
Tetrahedral	1.83	1.80–1.85	1.88	All equal
O–O distances				
In octahedron	2.84	2.67–2.90	2.84	2.68–2.99 A
In tetrahedron	3.02	2.93–3.13	3.06	2.87–3.16

[a] S. Geller and M. A. Gilleo, J. Phys. Chem. Solids **3**, 30 (1957); **9**, 235 (1959).

2. Possibility of Disorder

That the structure is ordered appears to be established by the paramagnetic-resonance work by Peter and Schawlow[2] on Cr^{3+}-ion-doped β-Ga_2O_3, in which it is found that the Cr^{3+} ions prefer only one set of octahedral sites. It is likely that these ions replace the Ga_{II}^{3+} ions in octahedrally coordinated sites: There is not enough space for foreign ions in the remaining octahedrally coordinated holes. Thus it is improbable that there is the type of disorder which would allow drastic change in the environment of any of the Ga_I^{3+} and Ga_{II}^{3+} ions.

3. Importance of β-Ga_2O_3 Structure Relative to Substitution of Ga^{3+} and Al^{3+} for Fe^{3+} Ions in Yttrium-Iron Garnet

The Ga^{3+} and Fe^{3+} ions have very similar crystal chemistry. Both ions have spherical electronic configuration and are of very nearly the same size, the Ga^{3+} ion being somewhat smaller than Fe^{3+} ion in most structures. The relative radii derived from the perovskitelike compounds[8] put the Ga^{3+} ion $CN(6)$ radius at 0.015 A less than that of the Fe^{3+} ion. This does not mean that average metal-oxygen distances will be exactly the same in different structures. For example, the relative ionic radii derived from the perovskitelike compounds are applicable to the garnets,[5,23,24] but the $CN(6)$ metal-oxygen distances in the garnets are uniformly somewhat larger than the sums of these radii.

Although the structure of yttrium-gallium garnet, $\{Y_3\}[Ga_2](Ga_3)O_{12}$ has not yet been refined, that of yttrium-iron garnet has[25]; it is of interest to compare some analogous distances in this garnet structure with those of β-Ga_2O_3. The averages and ranges of these analogous distances are compared in Table VI. It is seen that the average Ga_{II}—O distance in β-Ga_2O_3 is the same as the octahedral Fe—O distance in yttrium-iron garnet. On the other hand, the average Ga_I–O distance in β-Ga_2O_3 is substantially smaller than the tetrahedral Fe–O distance in the garnet. The average O–O distances of the octahedra in the two structures are equal but the average O–O distance in the GaO_4 tetrahedron in β-Ga_2O_3 is shorter than the average O–O distance in the FeO_4 tetrahedron of the garnet. Now from the least-squares calculations, the aforementioned differences are not significant. However, on a crystal chemical basis, there is reason to believe that the differences are meaningful.

We have shown previously[5] that when the Ga^{3+} ion is substituted for the Fe^{3+} ion in the garnets, it shows a great preference for the tetrahedral $[CN(4)]$ site. Also there is indication that when Fe^{3+} is substituted for the Ga^{3+} ion in yttrium-gallium garnet, it greatly prefers the octahedral $[CN(6)]$ site.[26] We have also mentioned elsewhere that the ratios of effective size of ions in different coordinations may differ and probably depend largely on the nuclear charge and external electronic configuration of the atom.[23,24] The ratios of tetrahedral to octahedral Fe—O distances in yttrium-iron garnet is 0.94; in $Y_3Al_2Al_3O_{12}$[27] the analogous Al–O ratio is 0.91, in β-Ga_2O_3 the ratio of tetrahedral to octahedral average Ga–O distances is 0.91, in fact very similar to that of the Al–O distances in the aluminum garnet.

Now despite the fact that the Al^{3+} ion is much smaller than the Ga^{3+} ion, the quantitative site preference in the substituted iron garnets of the latter is very close to that of the former[5,9]: this is in agreement with the above considerations.

4. Magnetic Aspects

If an Fe_2O_3 phase isostructural with β-Ga_2O_3 were found, it should be antiferromagnetic, because the Ga_I–O–Ga_{II} angles of about 123° (Table V) are (and presumably the Fe_I–O–Fe_{II} angles would be) favorable to superexchange interaction[9,25,28,29] and the network of octahedra and tetrahedra involving these favorable angles continues throughout the structure.[29] Counting the possible significant magnetic interactions we find

[23] S. Geller, R. M. Bozorth, M. A. Gilleo, and C. E. Miller, J. Phys. Chem. Solids **12**, 111 (1960).
[24] S. Geller and D. W. Mitchell, Acta Cryst. **12**, 936 (1959).
[25] S. Geller and M. A. Gilleo, J. Phys. Chem. Solids **3**, 30 (1957); **9**, 235 (1959).
[26] S. Geschwind, Phys. Rev. Letters **3**, 207 (1959).
[27] E. Prince, Acta Cryst. **10**, 787 (1957).
[28] M. A. Gilleo, Phys. Rev. **109**, 777 (1958).
[29] M. A. Gilleo, J. Phys. Chem. Solids (to be published).

TABLE VII. β-Ga_2O_3 powder data (Cu$K\alpha$ radiation).

hkl	d_c	d_o	I_c	ΣI_c	I_o
200	5.982	-	0.0	0.0	-
001	5.635	5.62	1.6	1.6	VW
201	4.679	4.67	3.8	3.8	W
201	3.877	3.86	2.0	2.0	VW
400	2.971	2.95	21.7	22.8	VS
110	2.945		1.1		
401	2.930	2.92	26.1	26.1	VS
002	2.817	2.81	27.5	45.5	VVS
202			18.0		
111	2.675	2.66	12.7	12.7	W-M
111	2.549	2.536	50.2	50.2	VVS
310	2.412	-	0.2	0.2	-
401	2.403	2.390	17.7	17.7	M-S
311	2.343		29.1		
202	2.340	2.332	1.1	31.8	S
402	2.340		1.6		
311	2.109	2.100	4.5	8.2	W-M
112	2.098		3.7		
601	2.024	2.018	2.4	2.4	W
600	1.980		1.5		
112	1.979	1.971	3.4	13.1	M
312	1.978		8.2		
203	1.927	-	.3	0.3	-
511	1.885	-	1.1	1.1	-
003	1.878		0.0		
510	1.872	1.865	4.8	4.8	M
402	1.838	1.831	2.5	3.4	W
602	1.838		0.9		
403	1.791	1.788	1.6	1.6	VW
601	1.744	1.736	1.0	1.0	VVW
312	1.718	-	0.0	0.1	-
512	1.716		0.1		
511	1.685	1.677	2.8	4.7	W-M
203	1.680		1.9		
113	1.628	1.622	1.4	1.4	VW
313	1.598	1.595	13.2	13.2	M-S
603	1.560	1.559	3.7	3.7	W
113	1.543	1.539	11.8	11.8	M
801	1.528	1.525	5.9	16.4	M-S,
020	1.520		10.5		Br.
711	1.512	-	0.2	0.2	-
800	1.485	1.479	0.2	3.5	W-M
710	1.482		3.3		
220	1.473		0.0		
513	1.470		0.1		
021	1.468	-	0.0	0.2	-
602	1.465		0.1		
802	1.465		0.0		
204	1.450	1.449	7.9	7.9	M
221	1.446	-	0.2	0.2	-
403	1.441		1.0		
512	1.440	1.436	14.9	31.9	VS
712	1.440		16.0		
004	1.409		0.2		
403	1.409	-	0.1	0.4	-
221	1.405		0.1		
313	1.388	-	0.4	0.4	-
711	1.366	-	0.0	0.0	-
801	1.359		3.5		
420	1.353	1.355	1.7	9.2	M,Br.
421	1.349		4.0		
022	1.338	1.336	2.4	5.6	W-M
222	1.338		3.1		
803	1.328		0.7	0.7	-
204	1.303		2.1		
604	1.303		0.8		
713	1.302	1.301	0.6	3.8	W-M
113	1.301		0.0		
313	1.301		0.3		
421	1.285	1.281	4.1	4.1	W
222	1.275	-	0.6	1.3	-
224	1.275		0.7		
114	1.243		0.1		
513	1.243	-	0.2	0.4	-
911	1.241		0.1		
603	1.226	1.223	1.9	2.1	W
10,0,1	1.223		0.2		
513	1.217	-	0.4	1.2	-
621	1.215		0.8		
712	1.212		0.1		
912	1.212	1.209	0.0	1.0	VVW,
910	1.211		0.9		Br.
620	1.206		0.2		
802	1.202	-	0.0	0.2	-
10,0,2	1.201		0.0		
223	1.193	-	0.2	0.2	-
10,0,0	1.188		0.0		
023	1.182	-	0.0	0.0	-
422	1.171		1.0		
622	1.171	1.168	0.4	1.6	VW,
404	1.170		0.1		Br.
804	1.170		0.1		
423	1.159	-	0.8	0.8	-
205	1.159		0.0		
405	1.148		0.1		
314	1.147	1.146	0.9	4.2	W-M
714	1.146		2.8		
621	1.146		0.4		
913	1.136	-	0.0	0.0	-
911	1.134	1.132	0.8	1.9	W
10,0,3	1.132		1.3		
223	1.127	-	0.8	0.9	-
005	1.127		0.0		
10,0,1	1.111	-	0.1	0.1	-
605	1.098	1.098	1.7	1.7	W
623	1.089	1.086	2.2	2.2	VVW
315	1.083	-	1.0	1.0	-
821	1.077	1.075	3.6	5.7	W-M,
115	1.074		2.1		Br.
820	1.062		0.0		
205	1.062	1.061	1.0	1.0	VW
713	1.062		0.0		
515	1.057		1.0		
622	1.055	-	0.1	1.1	-
822	1.055		0.0		
803	1.050	1.048	0.5	5.6	M
224	1.049		5.1		
423	1.046	-	0.7	0.7	-
11,1,1	1.043	1.043	1.3	1.3	VVW
604	1.038	-	0.0	0.2	-
10,0,4	1.037		0.2		
514	1.037		2.5		
914	1.036		1.3		
912	1.034		2.7		
11,1,2	1.034	1.033	2.1	10.0	M-S,
024	1.033		0.1		Br.
424	1.033		0.1		
115	1.033		1.2		
805	1.022	-	0.1	0.1	-
11,1,0	1.018	1.015	0.5	1.1	VW
12,0,1	1.017		0.6		
821	1.013		2.9		
10,0,2	1.012	1.011	0.2	3.6	W
12,0,2	1.012		0.5		
130	1.010		0.0		
715	1.003		0.1		
824	1.000	1.000	0.6	1.3	VW
131	0.997		0.6		
11,1,3	0.992		1.3		
131	0.990		2.5		
12,0,0	0.990	0.989	1.9	8.3	M-S,
224	0.989		1.9		Br.
624	0.989		0.7		
330	0.982	-	0.1	0.1	-
406	0.980		0.0		
331	0.977		0.5		
12,0,3	0.977	0.976	1.3	1.8	VW
315	0.969	-	0.6	0.6	-
11,1,1	0.965		0.5		
208	0.964	0.964	1.3	2.1	W
406	0.963		0.3		
331	0.958	-	0.4	0.5	-
132	0.957		0.1		
623	0.954		2.1		
10,2,1	0.953	0.952	0.2	2.3	W
132	0.944		0.3		
332	0.944	0.945	0.8	1.1	VVW
822	0.943		0.0		
10,2,2	0.943		0.0	0.0	-
006	0.939		0.1		
606	0.939		0.2		
12,0,1	0.938	0.937	0.3	1.8	W
10,2,0	0.936		0.0		
10,0,5	0.936		1.2		
331	0.934	-	0.1	0.1	-
915	0.932		0.0		
530	0.932		0.6		
913	0.930	0.929	1.0	2.9	W,Br.
714	0.930		0.4		
11,1,2	0.929		0.9		
424	0.927	-	0.0	0.1	-
824	0.927		0.1		
225	0.921		0.0		
315	0.921	-	0.0	0.0	-
804	0.919		0.0		
12,0,2	0.919		0.0		
425	0.916		0.1	0.1	-
10,0,3	0.911		0.6		
332	0.911		0.0		
532	0.911	0.910	0.0	3.8	W,Br.
115	0.910		0.0		
515	0.910		1.3		
10,2,3	0.908		1.9		
531	0.906	-	0.5	0.5	-
025	0.905		0.0		
133	0.897		0.3		
10,2,1	0.897		0.2		
13,1,1	0.896		0.3		
11,1,2	0.896		0.1		
206	0.895	0.895	0.6	1.8	VVW,
13,1,2	0.895		0.2		Br.
804	0.895		0.0		
515	0.895		0.1		
605	0.893		1.8		*
333	0.892	0.892	2.8	7.3	M,Br.
625	0.890		2.7		
133	0.882		2.9		
116	0.880	0.880	0.1	3.3	W
716	0.880		0.3		
731	0.876	-	0.1	0.2	-
13,1,0	0.875		0.1		
13,1,3	0.873	-	0.3	0.3	-
12,0,2	0.872		1.0		
14,0,2	0.872		0.8		
225	0.871	0.870	1.9	4.7	M
14,0,1	0.870		0.0		
730	0.870		1.0		
533	0.868	-	0.0	0.0	-
823	0.864	-	1.0	1.0	-
532	0.861	0.861	4.7	9.8	M-S,
732	0.861		5.1		Br.
624	0.857		0.0		
10,2,4	0.857	-	0.4	0.8	-
11,1,3	0.856		0.4		
14,0,3	0.853	-	0.5	0.5	-
12,0,3	0.850		0.0		
333	0.850	-	0.2	0.4	-
14,0,0	0.849		0.0		
825	0.848		0.2		
12,2,1	0.845	0.845	1.4	1.4	VW
731	0.845		0.0		
10,2,2	0.843	0.843	0.5	1.7	VW
12,2,2	0.842		1.2		
406	0.840	-	0.1	0.1	-
10,0,6	0.840		0.0		
13,1,1	0.837		2.9		
316	0.835	0.835	4.0	12.0	M-S,
916	0.835		5.1		Br.
914	0.833	0.834	2.1	2.6	W,Br.
13,1,1	0.833		0.5		
12,2,0	0.830		2.3		
733	0.829	0.829	0.4	3.1	W-M
134	0.829		0.0		
334	0.829		0.4		
407	0.828	-	0.1	0.1	-
207	0.824	-	0.0	0.1	-
425	0.823		0.1		
12,2,3	0.822	-	0.4	0.5	-
11,1,3	0.821		0.1		
715	0.819	-	0.1	0.1	-
10,0,4	0.818	0.818	1.9	1.9	W
14,0,1	0.818	0.817	2.7	3.4	W†
607	0.816		0.7		
226	0.814	0.814	3.9	4.9	W-M†
426	0.814		1.0		
134	0.813		0.2		
534	0.813	-	0.3	0.6	-
934	0.812		0.1		
14,0,1	0.811	-	0.0	0.1	-
805	0.810		0.1		
533	0.806	-	0.4	0.6	-
007	0.805		0.2		
732	0.804		0.1		
932	0.804	-	0.0	0.7	-
930	0.804		0.6		
12,0,3	0.801		0.2		
026	0.800	-	0.2	0.5	-
317	0.800		0.1		
626	0.799		0.9		
12,2,1	0.798	0.798	1.4	8.8	M
10,2,5	0.797		6.3		
517	0.795	0.796	4.9	4.9	W†
807	0.790	0.789	1.5	9.8	M
117	0.788		8.1		
13,1,2	0.787		0.3		
15,1,2	0.787	-	0.0	0.3	-
824	0.787		0.0		
12,2,4	0.786	-	0.2	0.2	-
334	0.784		1.6		
734	0.784	0.784	5.1	13.3	M-S
15,1,1	0.784		6.6		
516	0.783		0.9		†
11,1,5	0.783	0.782	0.5	8.4	W,Br.
13,1,5	0.783		3.3		
10,2,3	0.782		3.7		
935	0.781		0.1		
931	0.780	-	1.4	1.6	-
606	0.780		0.0		
12,0,5	0.780		0.1		
717	0.778	-	0.1	0.1	-
15,1,3	0.775	0.775	15.7	15.7	M-S

* Beginning with this line the α_1, α_2 doublet on the powder photograph was resolved.
† α_2 Line from previous reflection overlaps α_1 of this reflection.

that there are six interactions of a tetrahedrally coordinated ion with octahedrally coordinated ions and six interactions of an octahedrally coordinated ion with tetrahedrally coordinated ions. Thus there would be six important magnetic interactions per magnetic ion. From the recent paper by Gilleo,[28] one would estimate a Néel temperature of about 700°K for an Fe_2O_3 phase isostructural with β-Ga_2O_3.

Now, the facts that: (1) the β-Ga_2O_3 structure appears to be favorable to antiferromagnetic interaction, (2) that Fe^{3+} ion has a crystal chemistry similar to that of Ga^{3+} ion, and (3) that the Fe^{3+} ion would prefer octahedral sites if substituted for Ga^{3+} in yttrium-gallium garnet, all would immediately indicate the possibility of producing a ferrimagnetic material from solid solutions of Fe_2O_3 in β-Ga_2O_3. However, experiments made by Remeika *prior* to the determination of this structure, indicated that not much Fe^{3+} ion could be made to dissolve in β-Ga_2O_3 by solid-solid reaction,[30] not enough, that is, to produce strong enough interac-

[30] J. P. Remeika (private communication).

TABLE VIII. Comparison of some relative diffractometer and calculated intensities.

hkl	I_0	I_c
400 110	1	1
$40\bar{1}$	0.23	1.15
002 $20\bar{2}$	0.40	2.00
$11\bar{1}$	0.01	0.56
111	0.05	2.19

tion. On the other hand, Remeika has discovered a new structure of formula $Ga_{2-x}Fe_xO_3$ which is ferrimagnetic (and also piezoelectric).[3] Crystals have been made with composition $x=0.7$ to 1.4, and these have been reported by Wood[31] to belong to space group C_{2v}^9–$Pc2n$ with eight formula units per cell. Thus there must be in this crystal four sets of metal ions in the general positions, the only positions, in the space group. Because the crystal with $x=1.0$ is still quite ferrimagnetic (n_B at 4.2°K and $H=\infty$ is 0.95)[3] the indication is that the metal ions in the structure show a site preference which gives the net moment. Because both Fe^{3+} and Ga^{3+} ions have spherical electronic configurations, and the difference in their $CN(6)$ radii is presumably much smaller than the difference in their tetrahedral radii, there is the strong implication that there are in the $Ga_{2-x}Fe_xO_3$ two kinds of coordinations for the metal ions.

ACKNOWLEDGMENTS

In addition to the acknowledgments made in the text, the author wishes to thank Dr. M. Peter for discussions regarding the paramagnetic-resonance study of Cr^{3+}-ion-doped β-Ga_2O_3, Professor A. Magnéli for permission to quote some results of the work on V_2O_3 and Ti_2O_3, Dr. E. A. Wood for permission to quote the space group of $Ga_{2-x}Fe_xO_3$, and H. J. Seubert for making the drawings.

[31] E. A. Wood (to be published).

APPENDIX

β-Ga_2O_3 Powder Data

The data obtained from the x-ray diffraction powder pattern of pulverized β-Ga_2O_3 crystals taken with Cu$K\alpha$ radiation are in good agreement with those of Kohn *et al.*[4] However, there are some minor discrepancies. Furthermore, a knowledge of the structure allows us to index the pattern more adequately, although the indexing of the highest-angle lines may still be in some doubt.

In Table VII, the calculated spacings and intensities[32] are compared with those observed. The calculations were carried out with an IBM 704 program devised by Dr. R. G. Treuting. Several calculations of spacings with slightly different values of lattice constants indicated that the values given by Kohn *et al.*[4] are good to within the limits of error specified. Calculations of spacings only were carried out with a separate IBM 704 program also devised by Dr. Treuting.

It will be noticed immediately that the observed intensities given are only qualitative. It would appear that quantitative intensity measurements taken with a diffractometer would be called for. Attempts were made to do this, but preferred orientation difficulties indicated that obtaining a proper pattern would indeed be a time-consuming project.

A finely divided powder all of which passed through a 400-mesh sieve, was used as the specimen for the revolving specimen holder of the Norelco diffractometer. Examination of Table VIII, in which the intensity of the ({400}, {110}) reflection is taken as unity and several others are compared with it, is indicative of the extreme effect.

Examination of the powder specimen with a microscope (144×) indicated that the crystallites were needle- or platelike with the needle axis or plate tending to lie flat. The rotating specimen photographed with the Norelco 114.6 cm camera indicated a much more random distribution of crystallites and gave qualitative intensities in much better agreement with the calculated ones.

[32] The expression for the calculated relative intensities is $I_c=(p/4)LPF^2\times10^{-4}$ where p is the multiplicity, L the Lorentz factor, P the polarization factor, and F the structure amplitude.

Molecular Structure of Lithium Chloride Dimer. Thermodynamic Functions of Li_2X_2 (X = Cl, Br, I)

S. H. Bauer, Tadashi Ino, and Richard F. Porter

Department of Chemistry, Cornell University, Ithaca, New York

(Received February 29, 1960)

Our electron diffraction apparatus has been suitably modified for the study of vapors at high temperatures. A furnace and auxiliary power supply have been constructed, and a serviceable design for a sample container, with a nozzle, has been developed.

Data on two systems have been obtained. The diffraction pattern produced by cesium chloride vapor is that expected for a diatomic molecule; the interatomic distance determined in this experiment checks with the microwave value. In lithium chloride vapor, dimers predominate. Their structure is diamond shape (planar) with

$$Li\text{–}Cl = 2.23 \pm 0.03 \text{ A}$$

$$Cl\text{–}Cl = 3.61 \pm 0.03 \text{ A}$$

$$\angle ClLiCl = 108° \pm 4°.$$

The dimensions of the lithium halide dimers are compared and their thermodynamic functions tabulated.

INTRODUCTION

THE existence of appreciable concentrations of dimeric species in the vapors of alkali halides has been demonstrated by several investigators using a variety of experimental methods such as molecular beams,[1] mass spectrometry,[2] torsion-effusion,[3] and vapor density[4] techniques. The combined experimental data indicate that the stabilities of the dimers (i.e., the absolute value of the dimerization energy) increase as their mean dimensions decrease.[5] For halides with a common alkali metal, the dimerization energy increases in the sequence iodide to fluoride; for halides with a common halogen, the dimerization energy increases in the sequence cesium to lithium. These trends are to be expected for any model in which the dominant forces are ionic. In the theoretical papers of Milne and Cubicciotti[6] and of Berkowitz,[7] an "ionic" model is postulated for the alkali halide dimers, in which the principal term in the binding energy is the Coulombic interaction between the positive alkali ions and the negative halogen ions. The most stable configuration theoretically is one in which the dimer assumes a planar diamond shaped structure. The analyses of Milne and Cubicciotti and of Berkowitz permitted the estimation of dimerization energies and of the structural parameters for the dimers. Where comparisons can be made, the energies computed agree reasonably well with each other and with those obtained experimentally. However, the interatomic distances obtained by the two methods differ markedly in some cases and await comparison with measured values.

In this paper we are reporting on an electron diffraction investigation of dimeric lithium chloride. For such a study this system affords a definite advantage since the concentration of dimers exceeds that of the monomers by several fold, under conditions suitable for electron diffraction. Akischin and Rambidi[8] have reported structural results on other alkali halide vapors; these will be discussed below.

EXPERIMENTAL

The electron diffraction apparatus previously described[9] has been modified to accommodate a high-temperature nozzle assembly. A diagram of the crucible, heating elements, and radiation shields is shown in Fig. 1. Not shown in the drawing is a metal bellows which connects plates *h* and *f* with springs and screw spacers to permit changing the elevation and tilt of the entire furnace assembly; *e* designates the wall of the water-cooled sample section of the electron diffraction apparatus. An important feature of the apparatus is the design of the radiation shields surrounding the sample container. Since the distance between the top of the nozzle and the intersection point of the vapor jet with the electron beam is critical, it was necessary to make the top covers conical and closely spaced at the central opening (clearance, 0.020 in.). With this arrangement,

[1] R. C. Miller and P. Kusch, J. Chem. Phys. **25**, 860 (1956); **27**, 981 (1957); M. Eisenstadt, G. M. Rothberg, and P. Kusch, *ibid.*, **29**, 797 (1958).

[2] L. Friedman, J. Chem. Phys. **23**, 477 (1955); J. Berkowitz and W. A. Chupka, J. Chem. Phys. **29**, 653 (1958); R. C. Schoonmaker and R. F. Porter, *ibid.* **30**, 283 (1959); *ibid.* **29**, 1070 (1958); T. A. Milne, H. Klein, and D. Cubicciotti, J. Chem. Phys. **28**, 718 (1958).

[3] A. C. Pugh and R. F. Barrow, Trans. Faraday Soc. **54**, 671 (1958).

[4] C. Beusman, U. S. Atomic Energy Commission Document, ORNL-2323 (1957); S. Datz and W. T. Smith, Jr., J. Phys. Chem. **63**, 938 (1959); J. L. Barton and H. Bloom, *ibid.* **63**, 1785 (1959).

[5] S. H. Bauer, R. M. Diner, and R. F. Porter, J. Chem. Phys. **29**, 991 (1958).

[6] T. A. Milne and D. Cubicciotti, J. Chem. Phys. **29**, 846 (1958).

[7] J. Berkowitz, J. Chem. Phys. **29**, 1386 (1958).

[8] P. A. Akischin and N. G. Rambidi, Zhur. Neorg. Khim. **3**, 2599 (1958); **4**, 718 (1959).

[9] J. M. Hastings and S. H. Bauer, J. Chem. Phys. **18**, 13 (1950).

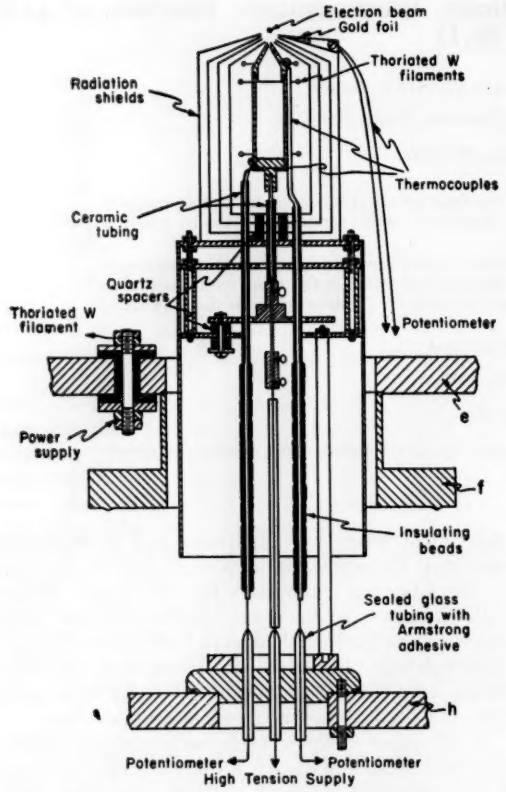

FIG. 1. Side view of furnace, showing crucible, heating elements thermocouple locations, radiation shields, etc. "Gold foil" designates location of reference sample.

it was possible to place four tantalum shields around the sample container, with a minimum of shielding extending above the tip of the nozzle. A support for an etched gold foil used for calibrating the voltage and sample-plate distance is mounted on a line with the crucible axis. A CO_2-cooled copper shield surrounds this assembly. Coaxially, about one centimeter above the nozzle, there is a cooled inverted copper boat for condensing the ejected material. The shield and boat are attached to the upper portion of the electron diffraction unit. Details of construction of the crucible head (jet nozzle) are shown in Fig. 2.

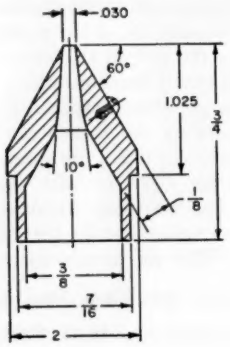

FIG. 2. Details of crucible head (nozzle).

For the study of lithium chloride, nozzles and sample containers constructed of inconel were found to be satisfactory. For temperatures below 800°C the sample containers were heated by radiation from three surrounding filaments. To obtain higher temperatures, electron bombardment from filaments was used to supplement the power input. For example, the temperature of the crucible was raised from 850° to 1400°C in about 3 min with an electron bombardment power of 150 w. Since the current through two of the filaments can be individually controlled, it is possible to adjust the heating currents so that the temperature of the nozzle is slightly higher than that of the body of the crucible. It was not difficult to attain temperatures

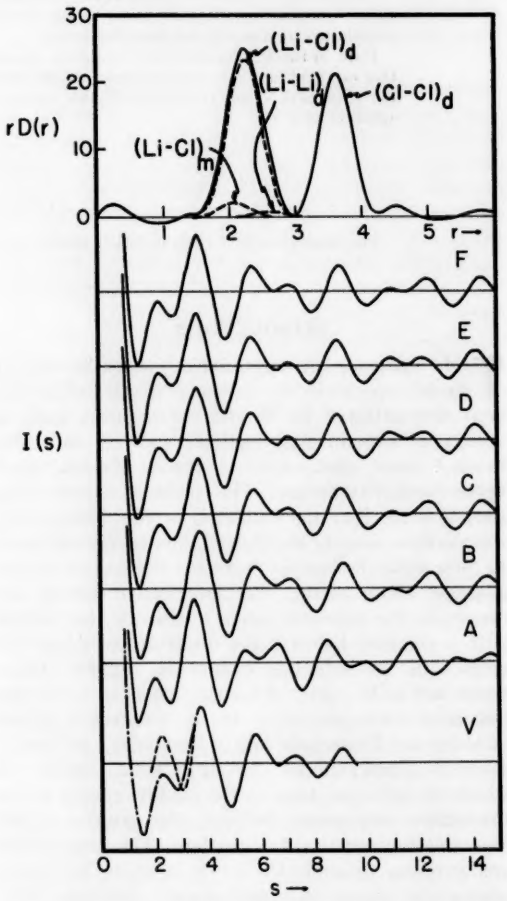

FIG. 3. Visual and computed intensity curves for lithium chloride vapor; $s \equiv (4\pi/\lambda) \sin \theta/2 \equiv (\pi/10q)$.

TABLE I. s_{cal}/s_{obs} for various models.

max	min	s_{obs}	*A*	*B*	*C*	*D*	*F*	*E*
1		2.24	0.916	1.006	1.006	1.006	1.162	1.028
	1	2.99	0.853	0.936	0.936	0.920	1.054	0.970
2		3.70	0.959	1.010	1.014	1.000	1.095	1.027
	2	4.85	0.934	1.002	0.990	0.974	1.052	1.005
3		5.75	0.948	1.021	1.009	1.000	1.096	1.026
	3	6.60	0.905	1.008	1.000	1.019	1.121	1.037
4		7.25	0.921	0.993	0.988	0.982	1.144	1.048
	4	8.09	0.939	1.007	1.001	0.989	1.094	1.004
5		9.04	0.946	1.018	1.007	0.995	1.087	1.007
Weighted Av			0.928	1.005	0.997	0.991	1.105	1.022
Weighted mean deviation / Weighted Av			0.0184	0.0125	0.0113	0.0144	0.0241	0.0168
Deduced distances								
Cl–Cl			3.62	3.61_8	3.60_9	3.61_7	3.63_5	3.60_7
Li–Cl			2.14	2.21	2.23	2.27_9	2.43_1	2.24_8

around 1800°K, but even at 1700°K the blackbody radiation emerging from the top small openings in the radiation shields at the point where diffraction of electrons occurs causes an unacceptable amount of fogging of the photographic plates. Due to the relatively low densities of the gases studied, it was necessary to take exposures ranging from one to ten minutes. Hence, it was essential that operating pressures in the system be of the order of 10^{-5} mm of Hg and that the electron beam remain stable both with respect to accelerating voltage and geometric position over extended periods. The crucible and shields were degassed prior to filling with the sample, which was thoroughly degassed in an auxiliary vacuum system. In the absence of a valve for confining the vapor to the crucible, rough control of the rate of sample effusion was obtained by control of the crucible heating power.

The apparatus was first tested with cesium chloride, since the Cs—Cl bond distance is known very accurately from microwave data,[10] and the vapor contains a negligible fraction of dimers. Diffraction patterns of CsCl vapor were photographed (no sector was used) with the sample at 700° and 800°C. At these temperatures, the vapor pressures of CsCl are about 0.5 and 6.5 mm of Hg, respectively. The photographs had the appearance of a simple $\sin sr/sr$ function and showed five rings. Plates of varying density were measured visually. The measurements confirmed that the system is essentially monomeric in the vapor phase. The deduced Cs—Cl distance is 2.93±0.03 A. Within the specified limits of precision, this checks with the microwave data from which the distance is deduced to be 2.9062±0.0001 A, but differs considerably from the first electron diffraction measurements reported by Maxwell, Hendricks, and Mosley.[11] These data are also in substantial agreement with the recent electron diffraction value, 2.91±0.01 A, reported by Akischin and Rambidi.[8] The closest anion-cation separation in the crystal is 3.566 A.

Diffraction patterns of lithium chloride vapor were taken with the crucible at about 820°C; no sector was used. At this temperature, the vapor pressure is approximately 5 mm Hg. The accelerating voltage was 50 kv; the sample-plate distance was 23.5 cm. With an electron beam current of about $(2–4)\times10^{-8}$ amp, exposures ranging from 30 sec to 5 min gave a large gradation in photographic densities on medium lantern-slide plates.

The photographs showed six rings. The positions of the maxima and minima were measured with a

TABLE II.

Monomer	Cl–Cl	Li–Cl	∠ ClLiCl	Remarks
A	3.90 A	2.31 A	115°	Berkowitz model
B	3.60	2.20	110°	
C	3.62	2.24	107.5°	best model
D	3.65	2.30	105°	
E	3.53	2.20	100°	
F	3.29	2.20	97°	*M* and *C* model

[10] A. Honig, M. L. Stitch, and M. Mandel, Phys. Rev. **92**, 901 (1953).

[11] L. R. Maxwell, S. B. Hendricks, and V. M. Moseley, Phys. Rev. **52**, 968 (1937).

TABLE III. Comparison of experimental and calculated distances in lithium halide dimers.

	Observed					Computed				
X	Li–Li	X–X	Li–X	∠XLiX	Ref	Li–Li	X–X	Li–X	∠XLiX	Ref
Cl	2.64 A	3.61 A	2.23 A	108°±4°	This work	2.91 A 2.46	3.29 A 3.90	2.20 A 2.31	97° 115	6 7
Br	2.70	3.85	2.35	110±4	15	3.10 2.60	3.50 4.20	2.34 2.47	97 116	6 7
I	2.71	4.30	2.54	116±4	15	3.37 2.71	3.88 4.52	2.57 2.64	98 118	6 7

comparator, and the relative intensities were estimated visually; the position of the first maximum could not be measured reliably. The intensity curve is shown in Fig. 3, V, and the data are summarized in Table I.

ANALYSIS OF THE DATA

To obtain a radial distribution curve, an intensity curve was computed for a diamond-shaped model, with Cl–Cl=3.62 A and Li–Cl=2.24 A. The computed intensity curve $0<q<10$ was then spliced onto the experimental curve, using the region $10<q<14$ for matching the intensity scale. The composite curve was then inverted by means of

$$2\pi^2 rD(r) = (\pi/10)^2 \sum_{q=1}^{n} qI(q)\exp[-\gamma^2(\pi q/10)^2]\sin(\pi q/10)r$$

with γ adjusted so that $\exp[-\gamma^2(3\pi)^2]=0.1$; $q=(10/\pi)s$. The resulting curve is shown at the top of Fig. 3. The peak at 3.62 A can be readily identified with Cl–Cl distance in the dimer; the peak at 2.23 A is a composite of Li–Li and Li–Cl peaks in all the species.

To begin with, we assumed that the vapor consists of a mixture of monomers, dimers, and trimers and that the structures of the dimers and trimers are planar with diamond and hexagonal symmetries, respectively. The intensity of scattered electrons may then be weighted as follows:

$$(1+\alpha+\beta)^{-1}\left[\frac{f^+f^-}{r_{+-}}\right]_{\text{monomer}} + \frac{\alpha}{1+\alpha+\beta}\left[\frac{4f^+f^-}{r_{+-}}+\frac{f^-f^-}{r_{--}}+\frac{f^+f^+}{r_{++}}\right]_{\text{dimer}} + \frac{\beta}{1+\alpha+\beta}\left[\frac{6f^+f^-}{(r_{+-})_a}+\frac{3f^+f^+}{r_{++}}+\frac{3f^-f^-}{r_{--}}+\frac{3f^+f^-}{(r_{+-})_b}\right]_{\text{trimer}},$$

where α is the dimer/monomer ratio, β is the trimer/monomer ratio, f^+ and f^- are scattering factors ($\approx Z^+$, Z^-), and the r's are distance parameters characteristic of the three species. For the trimer $(\text{Li–Cl})_a$ and $(\text{Li–Cl})_b$ represent the shortest and longest Li–Cl distances, respectively. Calculations were made using the experimental values of $\alpha=3.70$ and $\beta=0.26$ obtained by Miller and Kusch[1] for a sample temperature of 870°K. The distances used in the dimer and trimer terms were those computed theoretically by Milne and Cubicciotti[6]; a Li–Cl distance of 2.02 A was used for the monomer.[12] Approximate relative scattering contributions were found to be $(\text{Li–Cl})_m=3\%$, $(\text{Li–Cl})_d=42\%$, $(\text{Li–Cl})_t=5\%$, $(\text{Cl–Cl})_d=40\%$, and $(\text{Cl–Cl})_t=7\%$; the Li–Li distances and the long Li–Cl distance in the trimer contribute collectively about 3%. Hence, for the foregoing conditions about 84% of the scattering by all Li–Cl atom pairs and about 93% of the scattering by all Cl–Cl atom pairs are caused by the dimer. Since the temperature at which scattering was observed was roughly 200°K higher than that at which the vapor composition has been determined by Miller and Kusch, a temperature correction to α and β should be applied. Although experimental errors in the thermochemical data do not allow for a very precise correction, values of α and β at 1090°K were estimated as follows. A value of $\Delta H°$ (vaporization) for the monomer was obtained by a third law treatment of Miller and Kusch's vapor pressure data for the monomer and the tabulated free energy functions for gaseous and liquid LiCl.[13] This value was combined with the heats of dissociation of the dimer and trimer to deduce heats of vaporization for these two species. The values obtained were $\Delta H°_{1000}(m)=46$ kcals per mole of monomer, $\Delta H°_{1000}(d)=40$ kcals per mole of dimer, and $\Delta H°_{1000}(t)=50$ kcals per mole of trimer. Recalculation then indicates that α could fall as low as 2.0 and β could rise to about 0.4 at 1090°K. On the basis of these estimates of α and β, the dimer contributes about 70% of the total scattering due to all Li–Cl atom pairs and about 66% of the total scattering due to all Cl–Cl pairs. It should be emphasized that the errors of 10% in distance parameters used in the foregoing calculations will not affect the general argument that the major fraction of the observed scattering is due to the dimeric species.

The radial distribution curve provides a measure of the relative scattering contributions of (dimer and trimer)/monomer. Since the area contributed to a radial distribution curve by each type of atom pair, plotted on a $r^2D(r)$ scale, is $g_{ij}Z_iZ_j$, one may subtract

[12] A. Honig, *et al.*, Phys. Rev. **96**, 629 (1954).
[13] National Bureau of Standards Report 6484 (supplement to NBS report 6297), July (1959).

from the peak at 2.24 A the $(Li–Cl)_d$ and $(Li–Li)_d$ contributions, as deduced from the magnitude of the $(Cl–Cl)_d$ peak (assuming no appreciable trimer concentration). The residue is scattering due to the monomer. A rough estimate of the dimer/monomer ratio thus obtained is 2.5.

A not easily answered question which is inherent to this type of an electron diffraction study is the actual monomer/dimer/trimer composition in the jet at the point of diffraction. The percent dissociation changes after exit into the high vacuum region. Since the temperature as well as the gas density decrease, we cannot calculate the net effect. In addition, it has been recently pointed out[14] that in such a jet, segregation of the heavier molecular species occurs along the jet axis. In our experiment, the electron beam intersects the jet about two millimeters above the tip of the nozzle, and thus it samples a section of the jet which has been enriched in the higher molecular-weight components. The radial distribution curve shows no peaks which may be identified solely with the trimer. From the $rD(r)$ curve, one may deduce that the Cl–Cl distance is 3.62 A and the Li–Cl distance is 2.24 A in the dimer.

The final structure was deduced from a comparison of the observed intensity curve (V) with those computed for several models (Table II). For these computations no trimer contribution was inserted, and the dimer/monomer ratio was set at 3/1. These approximations have no effect on the quantitative conclusions.

We have not computed intensity curves for planar models with unequal Li–Cl distances, in which the dimer consists of a pair of weakly associated monomers with their dipoles antiparallel. Due to the limited range in q of the recorded diffraction patterns, the deduced radial distribution peaks are correspondingly broad (half-width$\approx$0.5 A). Hence, these data do not allow us to distinguish between four Li–Cl contributions at 2.23 A and the sum of two each at $(2.23+\delta)$ and $(2.23-\delta)$, with δ as large as 0.1 A. To answer this question one must resort to the theoretical computations[6,7] which clearly indicate that the symmetrical structure has the lowest energy. For selection of the best model the shape of the intensity curve for $q>20$ is critical. Of the curves listed C is in best agreement with the pattern as observed visually. For this model, the observed and computed positions of the maxima and minima are compared in Table I. In the best structure

$$Cl–Cl=3.61\pm0.03\text{ A} \qquad Li–Li=2.64\text{ A}$$

$$Li–Cl=2.23\pm0.03\text{ A} \qquad \angle ClLiCl=108°\pm4°.$$

DISCUSSION OF THE STRUCTURES OF THE ALKALI HALIDE DIMERS

The Li–Cl distance in the dimer appears to be approximately midway between that found in the monomer (2.02 A[12]) and in the crystal (2.566 A). A comparison between the measured and computed distances in the lithium halide dimers is presented in Tables III and IV.

TABLE IV. Comparison of experimental distances in monomer, dimer, and crystal, for the lithium halides.

X	$(Li–X)_m$[12]	$(Li–X)_d$	$(Li–X)_c$	2(radius X^-)[16]	$(X–X)_d$
Cl	2.02 A	2.23 A	2.570 A	3.62 A	3.61 A
Br	2.1704	2.35	2.751	3.90	3.85
I	2.3919	2.54	3.00	4.32	4.30

The work by Akischin and Rambidi[15] on the lithium halides has recently come to our attention. These investigators observed an angular dependence of scattered intensity for lithium bromide vapor which resembles the pattern reported here for lithium chloride except for a change of scale. On the basis of such data, they deduced the structural parameters for Li_2Br_2 and Li_2I_2, as is summarized in Table III. However, the intensity curves Akischin and Rambidi reported for the fluoride and chloride vapors appear to be slightly distorted $\sin x/x$ functions. The $D(r)$ curves deduced therefrom showed only one strong peak which was assigned to the Li–X scattering. This we find difficult to explain since we would anticipate, on the basis of theory[6,7] and experiment,[1] that at corresponding temperatures the chloride would have a greater concentration of dimers than the bromide, etc. Perhaps these investigators were not successful in preventing the continuum radiation produced by the crucible and heating elements from introducing a spurious background in their photographs which may have reduced their resolution to such an extent that the distinctive features failed to show up. As demonstrated in the foregoing, the dominant contribution in the electron diffraction pattern of lithium chloride is that caused by the dimer.

The close correspondence between the sum of the radii for anion-anion contact[16] and the measured values may be fortuitous and may be limited to the lithium halides. Certainly a number of factors both repulsive and attractive must be balanced in an adequate theory with which one might predict these structures with confidence. Such a theory is not yet available. In this instance, the structures appear to be the more sensitive criteria since both M and C and B's models give satisfactory agreement between the calculated and observed dissociation energies.

Akischin and Rambidi[2] have made extensive electron diffraction studies of other alkali halide vapors and have reported structural data for the monomeric species of K, Rb, and Cs salts. These workers have noted, how-

[14] P. C. Waterman and S. A. Stern, J. Chem. Phys. **31**, 405 (1959).

[15] P. A. Akischin and N. G. Rambidi, Vestnik Moskov. Univ. Ser. Mat. Mekhan. Astron. Fiz. i Khim. **13**, 223 (1958); Z. Phys. Chem. **213**, 111 (1960).

[16] L. Pauling, *The Nature of the Chemical Bond* (Cornell University Press, Ithaca, New York, 1939), p. 326.

TABLE V. Molecular parameters for thermodynamic functions.

Formula	Li_2Cl_2	Li_2Br_2	Li_2I_2
Molecular Wt	84.794	173.712	267.700
σ	4	4	4
g_0 (electronic)	1	1	1
Rotational constants			
A	0.6842 cm^{-1}	0.6591 cm^{-1}	0.6545 cm^{-1}
B	0.07356	0.02882	0.01437
C	0.06642	0.02761	0.01406
Vibrational frequencies			
A_g	662 cm^{-1}	576 cm^{-1}	501 cm^{-1}
A_g'	662	576	501
B_{1g}	318	202	148
B_{1u}	260	230	200
B_{2u}	374	329	294
B_{3u}	411	365	360

TABLE VIa. Thermodynamic functions for Li_2Cl_2 (ideal).

T°K	$-(F°-H_0°)/T$	$(H°-H_0°)/T$	$S°$	$C_p°$
298.16	56.17	11.66	67.83	16.11
400.00	59.79	12.99	72.78	17.49
500.00	62.80	13.97	76.77	18.24
600.00	65.42	14.72	80.14	18.70
700.00	67.73	15.31	83.04	18.99
800.00	69.81	15.78	85.59	19.18
900.00	71.69	16.17	87.86	19.32
1000.00	73.41	16.49	89.90	19.42
1200.00	76.47	16.99	93.46	19.56
1400.00	79.11	17.36	96.48	19.64
1600.00	81.45	17.65	99.10	19.69
1800.00	83.54	17.88	101.43	19.73
2000.00	85.44	18.07	103.51	19.76
2500.00	89.51	18.41	107.92	19.80
3000.00	92.89	18.64	111.58	19.82
3500.00	95.78	18.81	114.59	19.83
4000.00	98.30	18.94	117.24	19.84
4500.00	100.53	19.04	119.58	19.85
5000.00	102.54	19.12	121.67	19.85

ever, that in some of these systems the scattering intensity curves as a function of scattering angle do not correspond exactly to a simple diatomic molecule and have suggested that the dimeric species contribute to the scattering to some extent. Indeed from the slight shifts in peak positions they obtained reasonable estimates of the percent dimer present, in spite of the fact that in making such an estimate they used a questionable procedure.

THERMODYNAMIC FUNCTION FOR THE DIMERS

Now that the molecular dimensions of the dimers have been measured, one can compute with some certainty the rotational contributions to the partition functions. The vibrational frequencies still must be obtained mostly by estimation procedures. The molecular parameters used in the following computations are listed in Table V. With regard to the values selected for the fundamentals, the Ag and $A'g$ modes were assumed to be equal to the stretching frequency in the monomer[17]; B_{1g} has been computed[5] on basis of a plausible model, with parameters adjusted to fit the experimental dissociation energy. The frequencies deduced for the B_{1u} mode by BDP[5] appear to be too high, but the values suggested by Berkowitz[7] are much too low; the corresponding values in Table V are three-quarters of the estimates made by BDP. For B_{2u} and B_{3u}, the Berkowitz frequencies were used, except for

TABLE VIb. Thermodynamic functions for Li_2Br_2 (ideal).

T°K	$-(F°-H_0°)/T$	$(H°-H_0°)/T$	$S°$	$C_p°$
298.16	61.00	12.47	73.48	16.91
400.00	64.86	13.76	78.62	18.04
500.00	68.03	14.68	82.72	18.63
600.00	70.78	15.37	86.15	18.99
700.00	73.19	15.91	89.09	19.21
800.00	75.34	16.33	91.67	19.36
900.00	77.28	16.67	93.96	19.46
1000.00	79.06	16.96	96.01	19.54
1200.00	82.19	17.39	99.58	19.64
1400.00	84.89	17.72	102.61	19.70
1600.00	87.28	17.97	105.25	19.74
1800.00	89.41	18.17	107.57	19.77
2000.00	91.33	18.33	109.66	19.79
2500.00	95.45	18.62	114.08	19.82
3000.00	98.87	18.82	117.69	19.83
3500.00	101.78	18.97	120.75	19.84
4000.00	104.32	19.08	123.40	19.85
4500.00	106.57	19.17	125.74	19.86
5000.00	108.60	19.23	127.83	19.86

TABLE VIc. Thermodynamic functions for Li_2I_2 (ideal).

T°K	$-(F°-H_0°)/T$	$(H°-H_0°)/T$	$S°$	$C_p°$
298.16	64.44	13.07	77.51	17.43
400.00	68.46	14.32	82.78	18.39
500.00	71.76	15.18	86.94	18.88
600.00	74.58	15.83	90.41	19.17
700.00	77.06	16.32	93.38	19.35
800.00	79.27	16.70	95.97	19.47
900.00	81.25	17.02	98.27	19.55
1000.00	83.06	17.27	100.33	19.61
1200.00	86.25	17.67	103.92	19.69
1400.00	88.99	17.96	106.96	19.74
1600.00	91.41	18.19	109.59	19.77
1800.00	93.56	18.36	111.92	19.79
2000.00	95.50	18.51	114.01	19.81
2500.00	99.66	18.77	118.43	19.83
3000.00	103.10	18.95	122.05	19.84
3500.00	106.03	19.08	125.11	19.85
4000.00	108.59	19.17	127.76	19.86
4500.00	110.85	19.25	130.10	19.86
5000.00	112.88	19.31	132.19	19.86

[17] S. A. Rice and W. Klemperer, J. Chem. Phys. **27**, 573, 643 (1957).

the iodides for which his numbers were reduced (×.91) so that these conform to the ratio of (exp/theo) for the monomers.

The heat capacity, entropy, enthalpy, and free energy functions were computed by Dr. Russell E. Duff at the LASL on an IBM 704 using a program set up by Sitney[18] for the ideal gas, rigid rotor, simple harmonic oscillator approximations. These are summarized in Table VI and differ from the values given in NBS, preliminary report No. 6484.

[18] L. R. Sitney, Report distributed by LASL (LA-2278) on May 8, 1959, Pubco-I, An IBM 704 code for computing the ideal thermodynamic functions of a polyatomic gas molecule.

ACKNOWLEDGMENTS

This work was supported by the Office of Naval Research. We also wish to thank Dr. R. E. Duff for the computation of the thermodynamic functions and Mr. Robert LaVilla for his assistance with the early stages of the modification of the electron diffraction apparatus.

THE JOURNAL OF CHEMICAL PHYSICS VOLUME 33, NUMBER 3 SEPTEMBER, 1960

Open First-Order Stochastic Processes

PAUL J. GANS

Noyes Chemical Laboratory, University of Illinois, Urbana, Illinois

(Received April 1, 1960)

The solution of the general open first-order stochastic process representing the relaxation of an open multistate system is obtained by the generalization of a method of Krieger and Gans. The result is valid for a system containing an arbitrary number of absorbing and semiabsorbing states as well as allowing the presence of any number of emitting states. The stability of the solution is discussed in terms of the matrix of the transition probabilities. This is done with the aid of a theorem of Lévy and Hadamard. The result is applied to the corresponding closed system as well as the present work.

1. INTRODUCTION

THE relaxation of a multistate system by means of a first-order process has been studied by many authors using a variety of methods.[1] One convenient method is to represent the system as a finite collection of cells in a suitable space. The cells are assumed to be populated by "particles" allowed to move under a probability law. The state of the system at any time t may then be specified by $\mathbf{N}$, an r-dimensional vector whose components $n_i (i=1, \cdots, r)$ are the occupation numbers of the r cells. The transition probabilities governing the movement of particles between arbitrary cells are, for a first-order process, taken to be

$$p_{ij}=\alpha_{ij}n_i, \tag{1.1}$$

where p_{ij} is the probability per unit time per particle of a transition from cell i to cell j, and α_{ij} is a factor depending upon i and j but is independent of $\mathbf{N}$ and t. Siegert,[2] Shuler,[3] and Krieger and Gans[4] have given solutions for the general closed relaxation process defined by Eq. (1.1). On the other hand, only certain types of open (in the sense of allowing particle exchange with surroundings) systems have been investigated. The properties of an open one-cell system are well known.[5] Gans[6] has studied some simple open few-celled systems. Montroll and Shuler[7] have investigated the relaxation of a system of diatomic molecules with an absorbing cell or state in order to allow the removal of particles from the system. Kim[8] has extended the work of Montroll and Shuler to the case of the general first-order relaxation process with a single absorbing state. It is the purpose of this paper to generalize a previous theory[4] to allow ingress or egress of a particle to or from *any* cell in the system. Thus, any state may be partially or totally absorbing, and particles may enter the system at any point.

If a particle sink or bath be denoted by the index zero, then a suitable definition of an absorbing state is one for which

$$p_{i0}=\alpha_{i0}n_i, \qquad \alpha_{i0}\neq 0, \tag{1.2}$$

is satisfied. If α_{i0} is not zero for a particular i, and no particle may leave that cell for any other cell, ($\alpha_{ij}=0$ for all $j=0$), then cell i is absorbing in the sense of Montroll and Shuler.[7] Otherwise the state is semi-absorbing.

[1] See E. W. Montroll and K. E. Shuler, Advances in Chem. Phys. **1**, 361 (1958); and M. Lax, Revs. Modern Phys. **32**, 25 (1960) for extensive lists of references.
[2] A. J. F. Siegert, Phys. Rev. **76**, 1706 (1949).
[3] K. E. Shuler, Phys. Fluids **2**, 442 (1959).
[4] I. M. Krieger and P. J. Gans, J. Chem. Phys. **32**, 247 (1960).
[5] See for example W. Feller, *An Introduction to Probability Theory and its Applications* (John Wiley & Sons, Inc., New York, 1957), 2nd ed., Vol. I, Chap. 17.
[6] P. J. Gans, thesis, Case Institute of Technology, 1959.
[7] E. W. Montroll and K. E. Shuler, footnote reference 1.
[8] S. K. Kim, J. Chem. Phys. **28**, 1057 (1958).

The simplest way to allow the entry of particles into the system from an infinite source or bath[9] is to take p_{0j}', the probability per particle per unit time for transfer from the bath to cell j, to be constant. That is

$$p_{0j}'=\beta_j, \tag{1.3}$$

where the constant β_j depends only on j.

2. DIFFERENCE EQUATION

The mathematical details follow the method of Krieger and Gans.[4] Let δt be a time interval so small that at most one transition can take place in δt. Then the difference equation relating the probability $P(\mathbf{N}; t+\delta t)$ that the system is in the state $\mathbf{N}$ at $t+\delta t$ to the probability $P(\mathbf{N}', n_i+1, n_j-1; t)$ that the system was in a state $(\mathbf{N}', n_i+1, n_j-1)$ at time t (where $\mathbf{N}'$ is the reduced vector derived from $\mathbf{N}$ by the removal of the specifically mentioned components n_i and n_j) is just

$$\begin{aligned}P(\mathbf{N}; t+\delta t)=&\sum_{i=1}^{r}\sum_{j=1}^{r}{}'P(\mathbf{N}', n_i+1, n_j-1; t)\,p_{ij}\delta t\\&+\sum_{i=1}^{r}P(\mathbf{N}', n_i+1; t)\,p_{i0}\delta t+\sum_{j=1}^{r}P(\mathbf{N}', n_j-1; t)\,p_{0j}'\delta t\\&+\Big[1-\sum_{i=1}^{r}\sum_{j=0}^{r}{}'p_{ij}\delta t-\sum_{j=1}^{r}p_{0j}'\delta t\Big]P(\mathbf{N}; t),\end{aligned} \tag{2.1}$$

where primed summations indicate omission of the term $j=i$. The last term in Eq. (2.1) is the probability of no change in the system to the first order in δt. On using the equations of Sec. 1, (2.1) becomes

$$\begin{aligned}P(\mathbf{N}; t+\delta t)-P(\mathbf{N}; t)=&\sum_{i=1}\sum_{j=1}{}'P(\mathbf{N}', n_i+1, n_j-1; t)\\&\cdot\alpha_{ij}(n_i+1)\delta t+\sum_{i=1}P(\mathbf{N}', n_i+1; t)\alpha_{i0}(n_i+1)\delta t\\&+\sum_{j=1}P(\mathbf{N}', n_j-1; t)\beta_j\delta t-\sum_{i=1}\sum_{j=0}P(\mathbf{N}; t)\alpha_{ij}n_i\delta t\\&-\sum_{j=1}{}'P(\mathbf{N}; t)\beta_j\delta t.\end{aligned} \tag{2.2}$$

Dividing both sides by δt and letting δt approach zero leads to

$$\begin{aligned}\partial P(N; t)/\partial t=&\sum_{i=1}\sum_{j=1}{}'P(N', n_i+1, n_j-1; t)\alpha_{ij}(n_i+1)\\&+\sum_{i=1}P(N', n_i+1; t)\alpha_{i0}(n_i+1)+\sum_{j=1}P(N', n_j-1; t)\beta_j\\&-\sum_{i=1}\sum_{j=0}P(N; t)\alpha_{ij}n_i-\sum_{j=1}P(N; t)\beta_j,\end{aligned} \tag{2.3}$$

which is the differential-difference equation for the system.

3. GENERAL SOLUTION

The differential-difference equation (2.3) can be solved by means of generating functions. Introduction of an appropriate generating function transforms the equation into a first-order partial differential equation solvable by standard methods. The generating function $G(\mathbf{X}; t)$, where $\mathbf{X}$ is an r-component vector, is defined by

$$G(\mathbf{X}; t)=\sum_{n_1=0}^{\infty}\cdots\sum_{n_r=0}^{\infty}P(\mathbf{N}; t)\prod_{i=1}^{r}x_i^{n_i}, \tag{3.1}$$

with x_i a component of $\mathbf{X}$. The $P(\mathbf{N}; t)$ are assumed to satisfy the normalization relation

$$\sum_{n_1=0}^{\infty}\cdots\sum_{n_r=0}^{\infty}P(\mathbf{N}; t)=1, \tag{3.2}$$

so that $G(\mathbf{X}; t)$ exists for all $|x_i|\leqq 1$.

The transformation of Eq. (2.3) is effected by multiplying both sides by

$$\prod_i x_i^{n_i}$$

and summing over all values of all n_i. This leads to

$$\begin{aligned}\partial G/\partial t=&\sum_{i=1}\sum_{j=1}{}'\alpha_{ij}(x_j-x_i)\,(\partial G/\partial x_i)\\&+\sum_{i=1}\alpha_{i0}(1-x_i)\,(\partial G/\partial x_i)+\sum_{j=1}\beta_j(x_j-1)G,\end{aligned} \tag{3.3}$$

where G has been written for $G(\mathbf{X}; t)$.

The set of transition probabilities α_{ij} $(i, j=1, \cdots, r)$ form a matrix $\boldsymbol{\alpha}$ with undefined diagonal elements α_{ii}. Since the α_{ii} do not appear in Eq. (3.3), they may arbitrarily be taken to be

$$\alpha_{ii}=-\alpha_{i0}-\sum_{j=1}{}'\alpha_{ij}=-\sum_{j=0}\alpha_{ij}, \tag{3.4}$$

so that Eq. (3.3) may be written

$$\partial G/\partial t=\sum_{i=1}\sum_{j=0}\alpha_{ij}x_j(\partial G/\partial x_i)+\sum_{j=1}\beta_j(x_j-1)G, \tag{3.5}$$

where $x_0\equiv 1$.

The general solution of Eq. (3.5) is obtained by the method of characteristics.[10] The set of simultaneous ordinary differential equations subsidiary to Eq. (3.5) is

$$dt/1=\{-dx_i/\sum_{j=0}\alpha_{ij}x_j\}=d\,\ln G/\sum_{j=1}\beta_j(x_j-1), \tag{3.6}$$

where the bracketed term is really r terms, one for each value of i. If an arbitrary set of multipliers b_{ki} is chosen, then it can be shown that

$$dt=\sum_{i=1}b_{ki}dx_i/\sum_{i=1}b_{ki}\sum_{j=0}\alpha_{ij}x_j, \tag{3.7}$$

since

$$dx_i=dt\sum_{j=0}\alpha_{ij}x_j, \tag{3.8}$$

[9] Only infinite baths need be considered. If the bath were of finite extent, a new cell indexed $r+1$ could be defined and first-order transitions allowed between it and any other cell.

[10] F. H. Miller, *Partial Differential Equations* (John Wiley & Sons, Inc., New York, 1941).

for all i. If r sets of multipliers are chosen, Eq. (3.6) becomes

$$dt=\{-\sum_{i=1}^{r}b_{ki}dx_i/\sum_{i=1}^{r}b_{ki}\sum_{j=0}\alpha_{ij}x_j\}=d\ln G/\sum_{j=1}\beta_j(x_j-1). \tag{3.9}$$

The multipliers are arbitrary, but if the condition

$$\sum_{i=1}^{r}b_{ki}(\alpha_{ij}-\lambda_k\delta_{ij})=0 \tag{3.10}$$

is imposed (where δ_{ij} is the Kroneker delta), Eq. (3.9) becomes immediately integrable. Equation (3.10) is essentially a set of simultaneous equations having solutions $b_{ki}\neq 0$ if the λ_k are chosen as the eigenvalues of the α matrix. Reversing the order of summation in Eq. (3.7) and using Eq. (3.10) yields

$$\sum_{i=1}b_{ki}dx_i/\sum_{i=1}b_{ki}\sum_{j=0}\alpha_{ij}x_j=\lambda_k^{-1}d\ln\sum_{j=1}b_{kj}(x_j-1), \tag{3.11}$$

and so Eq. (3.9) becomes

$$dt=\{-\lambda_k^{-1}d\ln\sum_{j=1}b_{kj}(x_j-1)\}=d\ln G/\sum_{j=1}\beta_j(x_j-1). \tag{3.12}$$

There are $r+1$ integral of the system. These are

$$I_k=\lambda_k t+\ln\sum_{j=1}b_{kj}(x_j-1),\qquad (k=1,\cdots,r),$$

$$J=\ln G+B^{-1}\sum_{j=1}\beta_j\sum_{k=1}\lambda_k^{-1}B^{kj}\exp(I_k-\lambda_k t), \tag{3.13}$$

with $B=\det(b_{kj})$ and B^{kj} the cofactor of the element b_{kj}. The general solution may then be expressed as

$$G=\phi(I_1, I_2, \cdots, I_r, J), \tag{3.14}$$

where ϕ is an arbitrary function determined by the boundary conditions.

4. SOLUTION FOR KNOWN INITIAL POPULATIONS

Let m_i be the value of n_i at $t=0$, and let G^0, I_k^0, and J^0 be the corresponding values of G, I_k, and J. Then from Eqs. (3.13) and (3.14),

$$I_k^0=\ln\sum_j b_{kj}(x_j-1), \tag{4.1}$$

$$J^0=\ln G^0+B^{-1}\sum_j\beta_j\sum_k\lambda_k^{-1}B^{kj}\exp I_k^0, \tag{4.2}$$

$$G^0=\phi(I_1^0, I_r^0, \cdots, I_r^0, J^0). \tag{4.3}$$

The boundary condition for known initial population,

$$P(\mathbf{N};0)=\delta(\mathbf{N},\mathbf{M}), \tag{4.4}$$

with the components of $\mathbf{M}$ being the r values m_i, becomes, under the transformation (3.1),

$$G(\mathbf{X};0)=G^0=\prod_i x_i^{m_i}. \tag{4.5}$$

The r simultaneous equations (4.1) may be solved for x_j to give

$$x_j=1+B^{-1}\sum_k B^{kj}\exp I_k^0, \tag{4.6}$$

while Eq. (4.2) may be written as

$$G^0=\exp\{J^0-B^{-1}\sum_j\beta_j\sum_k\lambda_k^{-1}B^{kj}\exp I_k^0\}. \tag{4.7}$$

Substitution of these two expressions into Eq. (4.5) yields

$$\exp\{J^0-B^{-1}\sum_j\beta_j\sum_k\lambda_k^{-1}B^{kj}\exp I_k^0\}=\prod_i\{1+B^{-1}\sum_k B^{kj}\exp I_k^0\}^{m_i}, \tag{4.8}$$

Since the functional relationship ϕ between G and the integrals I_k and J is independent of time, I_k and J may be written for I_k^0 and J^0, which leads to

$$G(\mathbf{X};t)=\exp\{B^{-1}\sum_j\beta_j\sum_k\lambda_k^{-1}B^{kj}[\exp(\lambda_k t)-1]\cdot\sum_i b_{xi}(x_i-1)\}\prod_i\{1+B^{-1}\sum_j(x_j-1)\cdot\sum_k B^{ki}b_{kj}\exp(\lambda_k t)\}^{m_i}, \tag{4.9}$$

as the solution for $G(\mathbf{X};t)$.

The average population of a cell is given by

$$\langle n_s\rangle=(\partial\ln G/\partial\ln x_s)_{x=1}=\sum_{n_1=0}^{\infty}\cdots\sum_{n_r=0}^{\infty}n_s P(\mathbf{N};t); \tag{4.10}$$

thus

$$\langle n_s\rangle=B^{-1}\sum_j\beta_j\sum_k\lambda_k^{-1}B^{kj}[\exp(\lambda_k t)-1]b_{ks}+B^{-1}\sum_i m_i\sum_k B^{ki}b_{ks}\exp(\lambda_k t). \tag{4.11}$$

In the limit of infinite time, these become

$$G(x;\infty)=\exp\{-B^{-1}\sum_j\beta_j\sum_k\lambda_k^{-1}B^{kj}\sum_i b_{ki}(x_i-1)\}, \tag{4.12}$$

and

$$\langle n_s\rangle_\infty=-B^{-1}\sum_j\beta_j\sum_k\lambda_k^{-1}B^{kj}b_{ks}, \tag{4.13}$$

respectively. It should be noted that $\langle n_s\rangle_\infty$ is different from zero if and only if not all of the β_j are zero. Hence, if Eq. (4.13) is nonzero, it is in reality a steady state solution and not an equilibrium solution.

5. STABILITY OF THE SOLUTION

The transition probability matrix α occurs both in the closed relaxation theory[4] (with $\alpha_{ii}=-\sum_{j=1}'\alpha_{ij}$) and in the present work (with $\alpha_{ii}\leq-\sum_{j=1}'\alpha_{ij}$, the equality holding only when $\alpha_{i0}=0$ for a given i). Since terms of the sort $\exp(\lambda_k t)$ occur in all terms in the expressions for $\langle n_s\rangle$ in both cases, true equilibrium can

occur if and only if $Re(\lambda_k) \leq 0$ for all k. The case $Re(\lambda_k) > 0$ clearly represents an "unphysical" situation as the cell population would then tend to infinity with time. Therefore, it is desirable to see what may be deduced about the nature of λ_k without placing restrictive assumptions on the transition probabilities for each of

$$\text{Case I:} \qquad \alpha_{ii} = -\sum_{j=1} \alpha_{ij} \tag{5.1}$$

and

$$\text{Case II:} \qquad \alpha_{ii} \leqq -\sum_{j=1} \alpha_{ij}. \tag{5.2}$$

A theorem of Lévy and Hadamard[11] is suitable for the purpose.

Since $(\alpha_{ij} - \lambda_k \delta_{ij}) = 0$, r vectors $\mathfrak{y}_k$ exist such that not all components of any vector μ_k are zero.[12] Then, since $\sum_j (\alpha_{ij} - \lambda_k \delta_{ij}) \mu_{kj} = 0$ holds for all i and k,

$$\lambda_k \mu_{ki} = \sum_j \mu_{kj} \alpha_{ij} = \mu_{ki} \alpha_{ii} + \sum_j{}' \mu_{kj} \alpha_{ij}. \tag{5.3}$$

Because $\mathfrak{y}_k \neq 0$, there is a component μ_{kj} of maximum modulus. Let that component be μ_{ki}. Then

$$\lambda_k - \alpha_{ii} = \sum_j{}' \alpha_{ij} (\mu_{kj}/\mu_{ki}), \tag{5.4}$$

and

$$\begin{aligned} |\lambda_k - \alpha_{ii}| &= \left| \sum_j{}' \alpha_{ij} (\mu_{kj}/\mu_{ki}) \right| \leq \sum_j{}' |\alpha_{ij} (\mu_{kj}/\mu_{ki})| \\ &= \sum_j{}' \alpha_{ij} |\mu_{kj}/\mu_{ki}|; \end{aligned} \tag{5.5}$$

thus

$$|\lambda_k - \alpha_{ii}| \leq \sum_j{}' \alpha_{ij}, \tag{5.6}$$

which is essentially the theorem of Lévy and Hadamard. It can be seen that the eigenvalues λ_k are all contained in the union of circles with centers at α_{ii} and radii $\sum_j{}' \alpha_{ij}$. In addition, Eq. (5.6) implies that

$$|\alpha_{ii}| - \sum_j{}' \alpha_{ij} \leq |\lambda_k| \leq \sum_j{}' \alpha_{ij} \tag{5.7}$$

and hence

$$\min |\lambda_k| \geq |\alpha_{ii}| - \sum_j{}' \alpha_{ij}. \tag{5.8}$$

For case I, Eq. (5.6) shows that $\mathrm{Re}(\lambda_k) \leqq 0$. Since $\det(\alpha_{ij}) = 0$, λ_k must be zero for at least one value of k.[13] In case II it is known that $\alpha_{i0} \neq 0$ for at least one value of i. Then, from Eq. (5.6), $\mathrm{Re}(\lambda_k) \leqq 0$ as before, but from Eq. (5.8),

$$\min |\lambda_k| \geq |\alpha_{ii}| - \sum_j{}' \alpha_{ij} > 0. \tag{5.9}$$

Thus $\lambda_k < 0$ for all k. Clearly then, the solutions for both cases are bounded.

In summary then, this paper has presented the general solution for the open first-order relaxation problem allowing an arbitrary number of absorbing, semiabsorbing, and emitting states. It has been shown that the corresponding closed system always approaches equilibrium, with at most damped oscillations. Also, it has been shown that the open system approaches equilibrium if and only if $\beta_j = 0$ for all j with solution $\mathbf{N} = 0$. Otherwise the open system approaches a steady state.

ACKNOWLEDGMENT

I would like to thank my wife for extensive help in the preparation and typing of the manuscript.

[11] E. Bodewig, *Matrix Calculus* (Interscience Publishers, New York, 1956), p. 57.

[12] The μ_k are the transpose of the vectors b_k occurring both in this paper and that by Krieger and Gans (footnote reference 4).

[13] This has been shown in general by Siegert (footnote reference 2); and by Shuler (footnote reference 3) and Kim (footnote reference 8) under the assumption of detailed balance.

Nitric Oxide-Fluorine Dilute Diffusion Flame

DONALD RAPP* AND HAROLD S. JOHNSTON

University of California, Berkeley, California

(Received March 14, 1960)

The dilute diffusion flame method for measuring the rates of fast gas reactions has been used to study the reaction $2NO+F_2=2ONF$. The reaction proceeds with the emission of visible light, and photographic methods were used to obtain concentration profiles in space. The results were interpreted in terms of the mechanism

$$NO+F_2 \longrightarrow ONF+F \text{ (rate determining)}$$

$$NO+F \underset{\text{Fast}}{\rightleftharpoons} ONF^* \rightarrow ONF+h\nu$$

$$ONF^* \xrightarrow{(M)} ONF.$$

The interpretation of results is somewhat ambiguous. The observed rate may be that for the first step, in which case the rate constant has a pre-exponential factor of 6×10^{11} cc/mole-sec and an activation energy of 1.5 ± 1.0 kcal between room temperature and dry ice temperature. Alternatively the observed rate may be a composite of at least four of the elementary steps given above. With a reasonable assignment of rate constants for the succeeding steps, the first alternative is favored, although the margin of safety is not great.

THEORY OF DIFFUSION FLAMES

POLANYI'S dilute diffusion flame technique for measuring the rates of fast gas reactions has been used in a wide variety of applications.[1-6] The procedure consists of allowing one gas (the nozzle reactant) to stream out of a nozzle into an atmosphere containing the atmosphere reactant. For low-flow rates and low pressures the flow is mainly by diffusion. Ordinarily the atmosphere reactant concentration is large compared to the concentration of nozzle reactant in the inlet stream so that C_A (the atmosphere reactant concentration) can be considered constant in space. The nozzle reactant reacts as it diffuses spherically outward; its steady-state differential equation is

$$D_N\nabla^2C_N+\nabla\cdot\mathbf{V}C_N-kC_AC_N=0, \quad (1)$$

and if the middle term is negligible, the concentration is given by

$$C_N=(A/r)\exp(-\omega r), \quad (2)$$

where V is the velocity, $\omega^2=(kC_A/D_N)$, k is the bimolecular rate constant for reaction, D_N is the nozzle reactant diffusion coefficient, and A is a constant when r is large compared to the nozzle radius r_0 and small compared to the container dimensions.

The usual procedure[3] is to assume C_N is given by (2) even for small radii down to the nozzle opening, and to replace the cylindrical nozzle source by a small hypothetical spherical source of radius r_0. Garvin and Kistiakowsky[2] showed the proper way to evaluate $A=r_0C_N(r_0)$ by equating the total influx of nozzle reactant to the total rate at which reaction is occurring in the flame. One measures C_N at some large radius R, and ω is determined. The diffusion coefficient can be calculated from kinetic theory,[7] and thus the rate constant is determined. For (2) to be valid for small r one must use very slow nozzle flow rates and low reaction chamber pressures so that diffusion is comparable to bulk flow near the nozzle opening. Heller[5] and Warhurst[6] proposed on empirical grounds that V_0/D_N must be less than about 12 cm^{-1}, where V_0 is the linear velocity of gas flow inside the nozzle. Reed and Rabinovitch[3] have examined this question theoretically and concluded that there are many instances where higher values of V_0/D_N should give reliable results. Kistiakowsky and co-workers[8] have obtained good results with $V_0/D_N=20$.

The method used in this work does not depend on the nozzle boundary condition. Instead, it utilizes (2) at two large radii R_1 and R_2, so that

$$C_N(R_1)/C_N(R_2)=(R_2/R_1)\exp[-\omega(R_1-R_2)]. \quad (3)$$

Thus (2) is used only in the range of r where it is most nearly valid, at large distances from the nozzle opening. Because the measurements have been confined to this region, we feel justified in using much higher

* Present Address: Lockheed Missile Systems Division, Palo Alto, California.

[1] M. Polanyi, *Atomic Reactions* (Williams and Norgate, London, 1932).

[2] D. Garvin and G. B. Kistiakowsky, J. Chem. Phys. **20**, 105 (1952).

[3] J. F. Reed and B. S. Rabinovitch, J. Phys. Chem. **61**, 598 (1957).

[4] F. T. Smith and G. B. Kistiakowsky, J. Chem. Phys. **31**, 621 (1959).

[5] W. Heller, Trans. Faraday Soc. **33**, 1556 (1937).

[6] E. Warhurst, Trans. Faraday Soc. **35**, 674 (1939).

[7] J. O. Hirschfelder, C. F. Curtiss, R. B. Bird, and E. L. Spotz, *Thermodynamics and Physics of Matter*, edited by F. D. Rossini (Princeton University Press, Princeton, New Jersey, 1955), pp. 339–418.

[8] G. B. Kistiakowsky, Discussions Faraday Soc. **17**, 92 (1954).

values of V_0/D_N, (i.e., 30 to 80 cm^{-1}).[9] At these high velocities, C_N will certainly not be spherically symmetric at small radii, but this is not necessary for our purposes.

The relative value of the diffusion term and the velocity term in (1) at the large values of the radius used in this study can be estimated by simple approximate considerations. In the absence of a velocity term the concentration distribution is given by (2) and the contribution of diffusion to the rate is $D_N\nabla^2C_N = D_N\omega^2C_N$. In the absence of diffusion the radial velocity term is approximately the product of the linear velocity in the nozzle times the ratio of nozzle cross section πr_0^2 to the surface area of a sphere of radius r (observations were typically made at $r=8r_0$), that is, $V(r) = V_0(r_0^2/4r^2)$. The contribution of the velocity term to the rate is

$$-\nabla\cdot\mathbf{V}C_N = C_N[(2+\omega r)/r^3][V_0r_0^2/4].$$

For the velocity term to be negligible we must have

$$1 \gg [(2+\omega r)/\omega^2 r][r_0^2/4r^2](V_0/D_N).$$

In our experiments, at best we had $V_0=925$ cm/sec., $D_N=29.3$ cm^2/sec, $\omega=6.1$ cm^{-1}, and $r=1$ cm, giving the satisfactory result that $1 \gg 0.03$. At worst, however, we had $V_0=2050$, $D_N=23.1$, $\omega=3.5$, and $r=0.6$ cm, giving $1 \gg 0.29$. Under the worst of conditions, the assumption behind the use of (2) limits our ability to determine a rate constant to more than one significant figure.

The high-flow rates were necessary in our experiments to obtain a high light emission rate without increasing the concentration of fluorine in the nozzle gas unduly, since the high heat of reaction (75 kcal/mole) produces a temperature rise proportional to the fluorine concentration. The actual temperature rise in the experiments had to be kept to a minimum since (2) and (3) are isothermal equations.

In taking a photograph of a flame, the camera automatically integrates the light emission along a sighting path perpendicular to the nozzle axis. As Garvin[10] has shown, the integral of C_N along such a path gives the ratio

$$I(R_1)/I(R_2) = K_0(\omega R_1)/K_0(\omega R_2), \qquad (4)$$

where K_0 is the zero order Bessel function of the second kind. The integral I is

$$\int_{-\infty}^{+\infty} (r'^2 - r^2)^{-\frac{1}{2}} \exp(-\omega r')\, dr'.$$

The relationship of (4) to (3) can best be seen by using the expansion for the Bessel function of large arguments

$$K_0(\omega r) = (\pi/2\omega r)^{\frac{1}{2}} \exp(-\omega r)\{1 - [1^2/1!(8\omega r)] + \cdots\}. \qquad (5)$$

For $1 < \omega r$ we find

$$I(R_1)/I(R_2) = (R_2)/R_1)^{\frac{1}{2}} \exp[-\omega(R_1 - R_2)]. \qquad (6)$$

For our values of R, which are close to one another, (6) is only slightly different from (3). In the reaction of nitric oxide with fluorine the light emitting species is not the nozzle reactant. However (6) still holds for the relative intensity at two points on the film if the concentration of emitting species is proportional to the nozzle reactant concentration in space for the region of R used in the measurements. In appendix II we shall present evidence for the proportionality of the emitting species concentration to the nozzle reactant concentration, the emitting species being interpreted as an excited electronic state of ONF, and the nozzle reactant being F_2.

EXPERIMENTAL METHOD

The apparatus consisted of storage tanks for each reactant, connected through flow meters and needle valves to the reaction chamber, which was a copper cylinder (5 cm diam and 25-cm long) containing an axial 1.8 mm diam stainless steel tube as a nozzle.[11] The reaction chamber was connected through a needle valve to a heated tower containing sodium hydroxide and sodium chloride to dispose of nitrosyl fluoride in the products, and then to a cold trap and vacuum pump. The pressure in the reaction chamber was measured by means of a dibutyl phthalate manometer protected by a cold trap.

The atmosphere storage tank contained roughly 90% nitrogen and 10% nitric oxide, and the nozzle reactant storage tank contained approximately 99% nitrogen and 1% fluorine. The pressures in these tanks were of the order of hundreds of mm Hg. The gases were connected directly through flowmeters to needle valves which maintained the pressure in the reaction chamber at about 3 mm Hg. A calcium fluoride window (5 cm diam) on the reaction chamber facing the nozzle outlet provided a view of the emission from the flame to an "Exacta" camera (f2 lens, Ansco Super Hypan film). A series of runs lasting from 5 to 40 min was made for various pressures and flowrates. Time exposure photographs were taken of each run. The long exposure times were necessary to obtain sufficient film blackening.

Several methods for analyzing the films are given in footnote 11; only the best will be discussed here. Several photographs corresponding to various exposure times were taken of a flame having constant flow and

[9] There was no indication of any turbulence in the flow, even at the highest velocities. This is understandable if one computes the Reynolds number for the gas flow in the nozzle. The Reynolds number for a gas at low pressure is given by $2r_0v/D = \mathrm{Re}$, and it is an empirical fact that turbulence begins to set in for $\mathrm{Re} > 2000$. Even at the highest velocities used in this work the highest value of Re was 10. Thus the flow was essentially laminar for all experiments reported in this paper.

[10] D. Garvin, J. Chem. Phys. **24**, 1256 (1956).

[11] D. Rapp, Ph.D. Dissertation, University of California, Berkeley, 1960.

TABLE I. Experimental conditions and results.

Reaction chamber							
P mm	$C_A \times 10^8$ moles/cc	D_N cm²/sec	V_0 cm/sec	ω cm^{-1}	T °K	$k \times 10^{-10}$ cc/mole-sec	τ_{exp} min
4.2	2.2	35	1040	5.8	300	5.3	1 3- 9-18
3.2	1.4	46	1490	3.9	300	4.8	2 - 5-10-20
5.0	2.3	29	925	6.5	300	6.0	2 - 5-10-20
3.8	1.4	20	1085	3.1	195	0.8	5 -10-20
3.0	1.3	25	1640	4.1	195	1.8	2.5- 5-10-20
3.0	1.1	22	1635	2.6	195	1.3	5 -10-20-40
2.9	1.5	23	2050	3.5	195	1.9	10-20-40

F_2-Storage			NO-Storage		
P mm	% F_2	f ml/min at storage pressure	P	% NO	f ml/min at storage pressure
290	0.093	23	230	15.7	47
270	0.093	27	210	15.7	40
255	0.093	14	200	15.7	21
240	0.093	26	190	15.7	25
230	0.093	33	180	15.7	43
220	0.093	33	155	15.7	37
210	0.093	43	135	15.7	47

pressure conditions. The negatives were analyzed for relative film blackening by using a recording microphotometer in appropriate passes through the flame picture.[12] Microphotometer traces of a series of photographs of a single flame are shown in Fig. 1. The concentration of emitting species falls off roughly exponentially from the nozzle outlet, so that the longer exposure time pictures "see" farther out into the flame. For sufficiently high exposures the saturation limit of the film is reached. In general, film blackening is not proportional to film exposure. The film exposure in the general case is a complicated function of light intensity and exposure time. However, since the reciprocity effect[13] was found to be negligible under the conditions involved in these experiments, the film exposure reduces to the simple product of light intensity and exposure time ($I \cdot \tau_{exp}$). There is thus a one-to-one correspondence between film blackening and film exposure. If we therefore take points corresponding to the same film blackening along various curves of constant exposure time in Fig. 1, the ratio of intensities at two such points is inversely proportional to the ratio of exposure times. But since the ratio of intensities is given by (6), we obtain

$$(R_2/R_1)^{\frac{1}{2}} \exp[-\omega(R_1-R_2)] = (\tau_{exp})_2/(\tau_{exp})_1. \quad (7)$$

In Fig. 1, for example, the ratio of exposure times is 4, and the radii are 0.41 cm and 0.70 cm. Thus

$$4 = (0.70/0.41)^{\frac{1}{2}} \exp[-\omega(0.29)],$$

and ω is calculated to be 3.9 cm^{-1}. If we use the known values of C_A and D_N, we calculate k since $\omega^2 = (kC_A/D_N)$. This procedure was followed in all the runs which are listed in Table I. The statistical average of the data in Arrhenius form $k = A \exp(-E/RT)$ give $A = 6 \times 10^{11}$ cc/mol-sec, and $E = 1.5$ kcal/mol. It is estimated that $E = 1.5 \pm 1$ within the limits of error in this experiment.

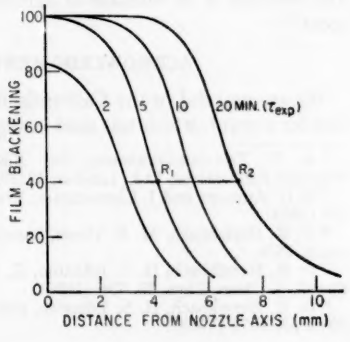

FIG. 1. Microphotometer traces of a series of photographs of a single flame.

[12] The apparent flame center from which radii are measured is located slightly downstream of the nozzle outlet. This apparent center was located by making a microphotometer pass down the nozzle axis and recording the point of maximum film blackening. Typically, the apparent center was about 1–2 nozzle radii below the nozzle outlet. The distortion from spherical shape was small at large radii, as may be seen from the photographs of flames reproduced in footnote 11. The microphotometer runs shown in Fig. 1 were obtained by making passes perpendicular to the nozzle axis at a distance downstream of the nozzle outlet corresponding to the apparent flame center. It was assumed that slight inaccuracies in lining up the flame negatives under the microphotometer light beam were responsible for the fact that slightly different values of k are obtained from different sets of time-exposures of the same flame.

[13] The effect whereby under some conditions film blackening depends on both I and τ_{exp}, and not merely on the simple product $I \cdot \tau_{exp}$.

DISCUSSION

In the reactions of nitric oxide with bromine and chlorine,[14] a direct termolecular mechanism predominates at low temperatures; also, a two-step bimolecular mechanism occurs in the reaction of nitric oxide with chlorine, but the slow first step is inhibited by an activation energy of 20 kcal.[15] It becomes important at high temperatures and low nitric oxide pressures. However in the reaction of nitric oxide with fluorine, the "slow" first step of the bimolecular mechanism has an activation energy of only about 1.5 kcal, and thus the termolecular mechanism is negligibly slow even at dry ice temperature. To put this statement into quantitative terms, let us compare the experimental second-order pre-exponential factor of 6×10^{11} cc/mol-sec with theoretical pre-exponential factors for bimolecular and termolecular mechanisms. We shall have to compare $\mathbf{A}^{(Bi)}$ with $C_{NO}\cdot\mathbf{A}^{(Ter)}$ in the two cases. Herschbach[16] calculated $\mathbf{A}^{(Bi)}$ as 5.6×10^{11} cc/mol-sec using the methods given in footnote reference 17. This was done three years prior to the experimental work, and is in remarkably good agreement with the experimental result, 6×10^{11}.

Using consistent force constants and the recently proposed general method of evaluating the classical phase integral[18] for the two activated complexes

Bimolecular 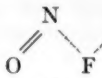

Termolecular

we have calculated pre-exponential factors

$$\mathbf{A}^{(Bi)}=12\times10^{10}\text{ cc/mol-sec},$$

$$\mathbf{A}^{(Ter)}=1.5\times10^{10}\text{ cc}^2/\text{mol}^2\text{-sec},$$

and since $C_{NO}=10^{-8}$ mol/cc under experimental conditions, $\mathbf{A}_{Ter}\cdot C_{NO}=1.5\times10^{2}$ cc/mol-sec. This indicates that even if its activation energy were zero, the termolecular mechanism would be too slow by a factor of about 10^8. Note that the calculated termolecular pre-exponential factor for the reaction between nitric oxide and chlorine is in substantial agreement with experiment.[16]

ACKNOWLEDGMENT

We are grateful to the California Research Corporation for a grant, which was used in support of this work, and to the Office of Naval Research and the National Science Foundation for support.

APPENDIX I

TEMPERATURE DISTRIBUTION

In the treatment given in previous sections we have assumed the reaction chamber was isothermal, and that the concentration of emitting species was proportional to the nozzle reactant concentration in the part of the flame where measurements were taken. We shall attempt to justify each of these assumptions in turn.

The reaction of nitric oxide with fluorine is highly exothermic, 75 kcal/mol,[19] and the heat of reaction produces a temperature rise in the vicinity of the nozzle outlet.

To calculate the magnitude of this effect, we follow Garvin and Kistiakowsky.[2,10] The temperature distribution in the flame is found to be

$$T-T_s=(B/\omega)(1-e^{-\omega r})/(\omega r), \tag{8}$$

where T_s is the temperature at the surface of the walls, and the constant B is evaluated in footnote reference 10. In typical runs, (B/ω) was about 20°C, and $T-T_s$ was about 10°C in the region of r where measurements were made. This 10° temperature rise was considered negligible for this reaction with such a low activation energy, and in addition the temperature rise is about the same at each of the two temperatures at which the experiments were carried out.

APPENDIX II

RELATION BETWEEN REACTANTS AND LIGHT EMITTING SPECIES

Finally, we must decide of what reaction we have measured the rate. Let us assume that the mechanism is

$$\mathrm{ON}+\mathrm{F}_2 \underset{k_2}{\overset{k_1}{\rightleftharpoons}} \mathrm{ONF}+\mathrm{F}$$

$$\mathrm{ON}+\mathrm{F} \underset{k_4}{\overset{k_3}{\rightleftharpoons}} \mathrm{ONF}^* \xrightarrow{k_5} \mathrm{ONF}+h\nu$$

$$\mathrm{ONF}^*+\mathrm{N}_2 \xrightarrow{k_6} \mathrm{ONF}+\mathrm{N}_2.$$

All bimolecular reaction rate constants are expressed in cc/mol-sec, and unimolecular rate constants are in sec^{-1}. We shall attempt to justify this mechanism by interpreting the experimental rate constant as k_1, and assigning reasonable values to the other rate constants.

We assume (a) k_1 is the experimental rate constant, 6×10^{10}; (b) k_2 is essentially zero because the reaction is 15 kcal endothermic; (c) k_3 is a collision rate constant, 2×10^{14}; (d) k_4 is the same as the known rate constant

[14] A. F. Trotman-Dickenson, *Gas Kinetics* (Butterworths Scientific Publications, Ltd., London, 1955), pp. 265–267.
[15] P. G. Ashmore and J. Chanmugam, Trans. Faraday Soc. **49**, 270 (1953).
[16] D. R. Herschbach, M. S. Thesis, Stanford University, California, 1956.
[17] D. R. Herschbach, H. S. Johnston, K. S. Pitzer, and R. E. Powell, J. Chem. Phys. **25**, 736 (1956).
[18] D. R. Herschbach, H. S. Johnston, and D. Rapp, J. Chem. Phys. **31**, 1652 (1959).
[19] H. S. Johnston and H. J. Bertin, Jr., J. Am. Chem. Soc. **81**, 6402 (1959).

for the dissociation of *excited* N_2O *molecules*,[20] 2×10^{10}; (e) from semiquantitative estimates of the absolute sensitivity of the film, it was estimated that only about one reaction in 10^5 produced a quantum of light, so that the rate of step 5 is assumed to be 10^{-5} that of step 6; (f) k_6 is taken to be the collision constant, 2×10^{14}. The typical value of C_{NO} was 10^{-8} moles/cc, and that for C_{N_2} was 10^{-7} moles/cc. Furthermore, we assume (g) the same diffusion coefficient, $D=30$ cm²/sec, for F_2, F, and (ONF)*. The conservation equations for these species are

$$\nabla^2 C_{F_2}-\omega_1^2 C_{F_2}=0 \tag{9}$$

$$\nabla^2 C_F-\omega_3^2 C_F+\omega_4^2 C_*+\omega_1^2 A e^{-\omega_1 r} \tag{10}$$

$$\nabla^2 C_*-\omega_t^2 C_*+\omega_3^2 C_F \tag{11}$$

where $\omega_1^2=k_1C_{NO}/D=20$, $\omega_3^2=k_3C_{NO}/D=6.7\times10^4$, $\omega_4^2=k_4/D=6.7\times10^8$, $\omega_5^2=k_5/D=1$ to 10, $\omega_6^2=k_6C_{N_2}/D=6.7\times10^5$, and $\omega_t^2=\omega_4^2+\omega_5^2+\omega_6^2=6.7\times10^8$. The solution to (9) is of course (2). Equations (10) and (11) form a set of coupled linear differential equations which can be solved by well known techniques.[21] One first transforms to new concentration variables given by $u_t=C_t r$. Then denoting u_F by x, u_* by y, and Dr by d/dr, Eqs. (10) and (11) transform to

$$(D_r^2-\omega_3^2)x+\omega_4^2 y=-A\omega_1^2 e^{-\omega_1 r} \tag{10'}$$

$$\omega_3^2 x+(D_r^2-\omega_t^2)y=0. \tag{11'}$$

After multiplying (10′) through by ω_3^2, and (11′) by $(D_r^2-\omega_3^2)$, the resulting equations are subtracted one from another, to give a single equation in y

$$[D_r^4-(\omega_3^2+\omega_t^2)D_r^2+(\omega_3^2\omega_t^2-\omega_3^2\omega_4^2)]y = \omega_1^2\omega_3^2 A e^{-\omega_1 r}. \tag{12}$$

The solution for y is

$$y=B\exp(-\omega_1 r)+K_1\exp[-(\omega_t^2+\omega_3^2)^{\frac{1}{2}}r] +K^2\exp\{-[\omega_3^2(\omega_5^2+\omega_6^2)/(\omega_3^2+\omega_t^2)]^{\frac{1}{2}}r\}. \tag{13}$$

where K_1 and K_2 are constants fixed by the nozzle boundary condition, and the constant B is $A\omega_1^2[\omega_6^2-(\omega_1^2\omega_t^2/\omega_3^2)]^{-1}$. If this expression is used in (11′), one can solve for x to yield

$$x=[(\omega_t^2-\omega_1^2)/\omega_3^2]B\exp(-\omega_1 r-K_1\exp[-(\omega_t^2+\omega_3^2)^{\frac{1}{2}}r.] +K_2(\omega_t^2/\omega_3^2)\exp\{-[\omega_3^2(\omega_5^2+\omega_6^2)/(\omega_3^2+\omega_t^2)]^{\frac{1}{2}}r\}. \tag{14}$$

The term multiplying r in the exponent in (13) and (14) is 4.5 for B, 2.6×10^4 for K_1, and 8.2 for K_2. Clearly the exponent multiplying K_1 is such that this term is always negligible. If the term in K_2 were negligible compared to that in B, then the product emitter would have the same distribution in space as the reactant fluorine, and the observed rate constant could be interpreted as k_1. Also the ratios of reactants and intermediates would be given by

$$C_F/C_{F_2}=(\omega_t^2/\omega_3^2)(B/A)=0.6$$

$$C_*/C_{F_2}=B/A=6\times10^{-5}.$$

At one centimeter, the exponential term multiplying B is 1/90 and that multiplying K_2 is 1/2800; and this appears to confirm that the observed rate is that of the first step of the mechanism. However, the terms in the exponent multiplying K_2 are based on assumed values for the rate constants and are subject to considerable uncertainty.

A test of the hypothesis given in this appendix is to calculate ω from flame photographs at various r to see if it is constant. This has been done for the various sets of runs, and although there is some scatter, there are no trends. For example, in Fig. 1, ω is 3.7 calculated from the 10 and 20 min runs, 4.1 from the 5 and 10 min runs, and 3.9 from the 5 and 20 min runs. In some runs the scatter was worse, and in others, better. Most of the error is attributed to misalignment of the various negatives in the microphotometer.

We are deeply grateful to D. Garvin and R. A. Jacobsen of Princeton University for advice and assistance in the preparation of this appendix.

[20] H. S. Johnston and J. R. White, J. Chem. Phys. **22**, 1969 (1954).

[21] H. W. Reddick and F. A. Miller, *Advanced Math for Engineers* (John Wiley & Sons, Inc., New York, 1949).

Spin Exchange in Biradicals*

D. C. REITZ AND S. I. WEISSMAN

Washington University, St. Louis, Missouri

(Received February 1, 1960)

The electron spin resonance spectra of four isotopically labeled biradicals have been observed. The hyperfine splittings demonstrate independence of the halves.

MOST paramagnetic organic molecules contain an odd number of electrons. Their magnetic properties are well accounted for by the contributions from a single electronic spin, i.e., their ground electronic states are almost pure doublets. The small number of even electron paramagnetic molecules have not, on the other hand, been so sharply classified. The even electron paramagnetic molecules are, for the most part, formed by joining together two odd electron molecules in such a way that the features of the structure responsible for the stability of the orginial odd electron molecules are preserved. Studies have been made of the static magnetic susceptibilities of such biradical molecules and of the catalysis of the interconversion of ortho and para hydrogen.

Since the development of the method of magnetic resonance, new information not accessible to the older methods has been obtained for several biradicals. Hutchison and co-workers[1] demonstrated that the intensity of the resonance absorption of hydrocarbon I at room temperature corresponded to about 4% of the molecules being paramagnetic. Sloan, Jarrett, and Vaughan[2] showed that the magnetic resonance spectra of liquid solutions of a series of biradicals exhibit proton hyperfine splittings, and that the spectra suggest strongly that the two halves of these biradicals are "uncoupled." A simple explanation of the small magnetism is that the paramagnetic state is a thermally excited triplet. However, classification as a triplet state implies a degree of coupling between halves not compatible with the hyperfine splittings.

Our investigations include measurements of C^{13} hyperfine splittings, determination of variation of spectra with temperature, and estimates of the absolute intensity of the absorption.

We consider first how the hyperfine splittings and the coupling between the halves of a biradical are related. As a particularly simple example we may think of a pair of one-electron atoms with nuclei of spin $\frac{1}{2}$ maintained at various fixed distances from each other. In the extreme case where the atoms are close together, the system will be in either a singlet or a triplet electronic state. The former has no resonance absorption. This latter would yield a symmetrical hyperfine spectrum of three lines with intensity ratio 1:2:1. When the atoms are far apart the hyperfine spectrum is simply a pair of lines—the spectrum of isolated atoms.

The set of states appropriate for coupled two-electron systems may be used for the description of the separated atoms. The states in which both electron spins of the separated atom are in the same spin state are pure triplet, but the two states in which one spin is up and the other down are the sum and difference of the corresponding singlet and triplet functions. While such mixtures are not good stationary state functions for a system consisting of only two electron spins, they are appropriate in the separated atom limit where the electron-nuclear hyperfine interactions dominate in determining the spin configuration.

We now give a simplified account of the magnetic resonance spectrum of a pair of electrons coupled to a pair of nuclei of equal charges.

The orbital interaction of the electron may be expressed in the familiar way as a spin interaction; only the isotropic part of the hyperfine interaction will be considered. Designate σ_1 and σ_2 as the Pauli spin operators for the two electrons; I_A and I_B the spin operators for the two nuclei. Let H_0 be the spin-independent part of the Hamiltonian, with solutions

$$\alpha\phi_A, \beta\phi_B; \qquad \beta\phi_A, \alpha\phi_B; \qquad \alpha\phi_A, \alpha\phi_B; \qquad \beta\phi_A, \beta\phi_B.$$

ϕ_A is a space function associated with nucleus A, ϕ_B is an equivalent function for nucleus B, and α and β are the two spin functions. The functions are normalized and antisymmetrized with respect to exchange of the labels of the electrons. Each represents a particular orientation of electron spin in the neighborhood of each nucleus.

Now consider the effects of electron exchange and of hyperfine interactions. The former may be represented as $J\sigma_1\cdot\sigma_2$. For our purposes it is convenient to use the operator $\sigma_A\cdot\sigma_B$ in which σ_A and σ_B are the spin operators for the occupants of ϕ_A and ϕ_B, respectively.

The hyperfine interaction is

$$-(8\pi/3)\{\sigma_1\cdot[I_A\delta(\mathbf{r}_1-\mathbf{r}_A)+I_B\delta(\mathbf{r}_1-\mathbf{r}_B)]$$
$$+\sigma_2\cdot[I_A\delta(\mathbf{r}_2-\mathbf{r}_A)+I_B\delta(\mathbf{r}_2-\mathbf{r}_B)]\}.$$

* This work was supported by the U. S. Air Force through the Air Force Office of Scientific Research of the Air Research and Development Command under contract. Reproduction in whole or in part is permitted for any purpose of the U. S. Government.

[1] C. A. Hutchison, Jr., A. Kowalsky, R. C. Pastor, and G. W. Wheland, J. Chem. Phys. **20**, 1485 (1952).

[2] H. S. Jarrett, G. J. Sloan, and W. R. Vaughn, J. Chem. Phys. **25**, 697 (1956).

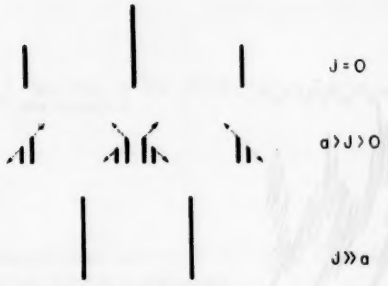

FIG. 1. Splittings for two electrons coupled to one nucleus with $I=\frac{1}{2}$ and one with $I=0$.

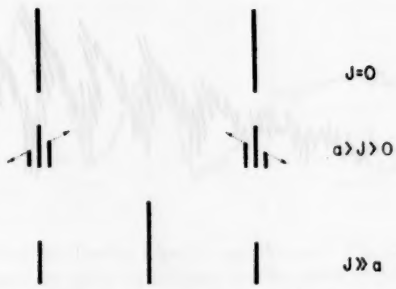

FIG. 2. Splittings for two electrons coupled to two nuclei each with $I=\frac{1}{2}$.

In the approximation in which ϕ_A vanishes at r_B and ϕ_B vanishes at r_A and the overlap between ϕ_A and ϕ_B is neglected, the hyperfine term becomes

$$a(\sigma_A \cdot I_A + \sigma_B \cdot I_B)$$

where

$$a = -(8\pi/3)\mu_e\mu_n \mid \phi_A(r_A) \mid^2$$

and μ_e and μ_n are the magnetic moments of electron and nucleus, respectively.

The total Hamiltonian is now

$$\mathcal{H}_0 + J\sigma_A \cdot \sigma_B + a(\sigma_A \cdot I_A + \sigma_B \cdot I_B).$$

We consider three cases: (a) Neither nucleus has spin. (b) Nucleus A has spin $\frac{1}{2}$ and nucleus B has spin zero. (c) Nuclei A and B have identical moments and spin $\frac{1}{2}$. The solutions for case (a) are obvious. They are the familiar singlet and triplet functions.

The triplet states are split in an external field and yield a single line (anisotropic spin-spin interactions are neglected). The solution for case (b) when $J \ll a$, i.e., for spin-exchange rate small compared with hyperfine frequency, lead to a spectrum consisting of a symmetrical triplet with intensity ratios 1:2:1. The central line arises from spin transitions on the side of the molecule which does not have a nuclear spin; the two outside lines from the spin transitions on the side which contains a nuclear spin. As the exchange rate increases the lines split (with splitting of order J), and finally when $J \gg a$ the spectrum becomes a doublet of half the splitting of the original spectrum. Each spin spends half its time on the side of the molecule which contains the nuclear spin. The details of the change from one spectrum to another are given in Fig. 1.

For the case when each side of the molecule contains a nucleus of spin $\frac{1}{2}$, the spectrum consists of two lines for slow exchange (each electron remains in the vicinity of one nucleus) and of three lines with intensities 1:2:1 when the spin migrates rapidly from one side of the molecule to the other. Details of the changes in the spectrum are given in Fig. 2.

EXPERIMENTAL PROCEDURES AND RESULTS

The radicals here discussed are:

I

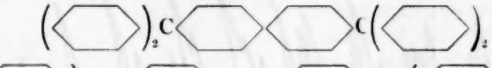

II

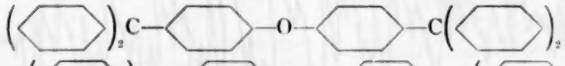

III

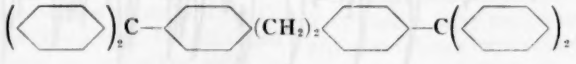

IV

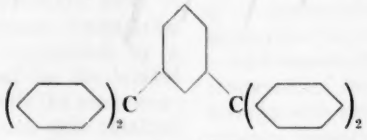

I, II, and III were labeled at both methyl carbons with C^{13}. The procedure (to be described below) yielded a mixture containing 16% of unlabeled material (case a), 48% with one C^{13} (case b) and 36% with two C^{13} (case c). The spectrum for such a mixture should have consisted of five lines with intensity ratio 9:24:34:24:9 in the limit of rapid exchange and of three lines with ratio 3:4:3 for slow exchange. IV was labeled in only one position so that 40% of the molecules contained no C^{13} and 60% contained one C^{13}. The expected spectra are one of three lines with half the usual C^{13} splitting in ratio 3:4:3 for fast exchange

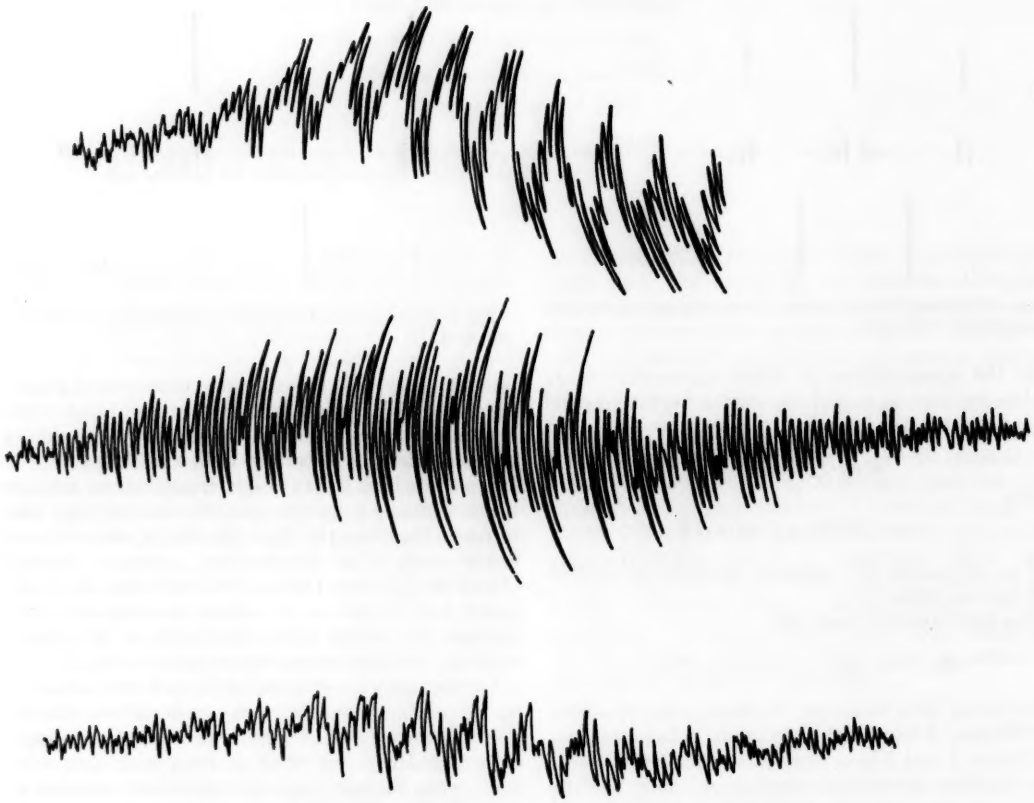

FIG. 3. Spectrum of I at 297°K (top); 265°K (center); 221°K (bottom).

FIG. 4. Spectrum of II at 263°K (top); 215°K (bottom).

FIG. 5. Spectrum of III, 297°K, 60% C^{13}, low resolution.

and one of three lines with the usual C^{13} splitting in ratio 3:14:3 for slow exchange.

Preparation of Labeled Biradicals

Compound I was prepared by the following sequence of reactions:

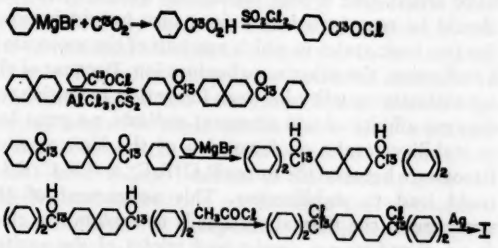

II and III were prepared by analogous reactions through the benzoylation of diphenylether and diphenylethane, respectively.

Compound IV was labeled with C^{13} at only one of the methyl positions. It was prepared as follows:

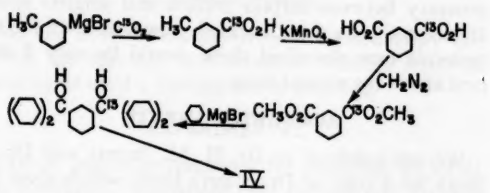

In the case of compounds I, II, and III, the intermediate diketones were isolated and crystallized; for IV the diester was isolated and crystallized. The dihalogen derivatives were not isolated as crystalline solids in the preparation of the labeled compounds. Preparation of the biradicals from unlabeled compounds by a procedure identical with those used for the labeled compounds resulted in biradicals with the same magnetic resonance spectra as those which were obtained from large scale preparation with isolation and purification of the intermediate dihalides. Our unlabeled biradicals were identical in their magnetic and optical properties with those described by Jarrett, Soan, and Vaughn.[2]

Conversion of the dihalides to biradicals was carried out under high vacuum conditions by the techniques described by Lewis, Lipkin, and Magel.[3] The radicals produced by such techniques are far more stable than those prepared by the more conventional methods. A sample of I, stored in the dark, has been stable for one year.

Magnetic Measurements

Magnetic resonance spectra of dilute liquid solutions under conditions of the highest resolutions available to us were recorded. The solvent in each case was either toluene, dimethoxyethane, or tetrahydrofuran. The spectra were the same in all solvents. Most of the measurements were made in a small magnet with magnetic field inhomogeneity of about 0.3 oe over the sample. Repetition of the measurements with an improved instrument which permitted resolution of about 0.03 oe revealed a complex hyperfine structure, each radical possessing its distinctive spectrum. At 0.3 oe resolution the resonances of I, II, III, and IV are hardly distinguishable from each other.

Figures 3 and 4 show the resonances of I and II (normal isotopic abundance) in toluene at several different temperatures. The sharpening of lines with decreasing temperature is more marked than for most other radicals. Figure 5 shows the resonance of III with 60% C^{13} in the methyl position.

Crude measurements were made of the variation in intensity of the resonances with temperature, of the absolute spin susceptibility of I and III, and of the variation of spin susceptibility with concentration at constant temperature.

Relative to C^{13} splitting, the spectra in each case corresponded to independence of the two spins: $J < A = 7\times10^{7}$ sec^{-1}. Since the proton splittings have not been analyzed it is not impossible that J may be in the range of the proton splittings, i.e., J could be as high as a few megacycles per second.

All resonance diminished in intensity with decreasing temperature. Because of the rapid decrease in line breadth with decreasing temperature (Figs. 3 and 4) accurate measurements of dependence of susceptibility on temperature are difficult. The variation of intensity with temperature corresponds to an energy interval of 2 to 3 kcal/mole between the magnetic state and the normal paramagnetic state. The estimates of total spin

[3] G. N. Lewis, D. Lipkin, and T. T. Magel, J. Am. Chem. Soc. **66**, 1579 (1944).

susceptibility correspond to energy intervals in the same range.

Absolute susceptibilities were measured by comparison of the integrated absorptions of solutions of biradical and peroxylamine disulphonate of known concentrations. Cavity Q, filling factor, microwave power, and modulation amplitudes were made equal for the biradical solution and the standard samples. Microwave power levels were sufficiently low so that no appreciable saturation was observed.

DISCUSSION OF THE RESULTS

Our results require for each of the molecules described here an energy level scheme consisting of a singlet normal state and a singlet and triplet effectively degenerate with each other about 10^{13} cps above the normal state. The situation is markedly different from the one existing in single crystals of cupric acetate where an excited triplet state exhibits a tight spin coupling compatible with the singlet-triplet separation.[4]

Since the results for the biradicals are unexpected and not easily explained, we have had some suspicions concerning the chemical identity of the substances whose resonances we have studied. In order to eliminate the possibility that a small percentage of the dihalides from which the hydrocarbons are made were only half reduced, we carried out the reduction of IV with an excess of sodium to produce a diamagnetic solution of dinegative ions. The biradical was regenerated by removal of the sodium with mercury. The spectra obtained by this treatment were identical with those obtained by normal reduction with silver amalgam.

The correspondence of the intensities of the hyperfine components in each case to the abundance of C^{13} in the $C^{13}O_2$ used in the preparation supports but does not conclusively prove that the synthesis proceeded according to the sequences indicated in the section on the preparations. For compounds I, II, and III both methyl carbons originate in the carbon dioxide with which a Grignard intermediate is treated. In compound IV, one of the methyl carbons originates in the CH_3 group of *meta*-bromotoluene while the other comes from carbon dioxide. Nevertheless, the intensities of the hyperfine components indicated that the two methyl carbons originating from the two different sources have identical roles in the biradicals.

A polymerization process which leads to large molecules with spins effectively at the ends or a dissociation which leads to an ordinary radical is not excluded.

We should note that the hyperfine splittings from the biradical porphyrindine indicates independence of the two halves,[5] while the temperature dependence of susceptibility of the crystalline material shows that the magnetic state is 0.6 kcal above the normal state.[6]

A satisfactory explanation (if we have not made a chemical blunder) of the phenomena must account not only for the position of the magnetic state of the biradicals some 2013 kcal above the normal state but for the mixing of the singlets and triplets. We have no explanation which is completely acceptable to us or to the many people with whom we have discussed the problem. We note a few of the suggestions which have arisen. One is that the normal diamagnetic state should be represented as a resonance hybrid between the two ionic states in which one-half of the molecule is a carbanion, the other a carbonium ion. Because of the approximate equality between ionization potential and electron affinity of odd alternant radicals, no great loss in stability results on formation of the ionic species. Resonance between the forms $R_3C^+R_3C^-$ and $R_3C^-R_3C^+$ could lead to stabilization. This assignment of the structure of the normal state fails to explain the close degeneracy between singlet and triplet of the excited state, but at least it does not preempt the states necessary for forming the degenerate set.

Another suggestion has been that the excited magnetic states should be identified with Pariser's[7] $^3\Omega^-$ and $^1\Omega^-$ states. Pariser has shown that within the approximations of his treatment of alternant systems a degeneracy between certain triplets and singlets exists. It has not been demonstrated, however, that for the molecule here described these should lie only 2 or 3 kcal above the normal state.

ACKNOWLEDGMENTS

We are indebted to Dr. H. M. Jarrett and Dr. S. Sloan for a copy of Dr. Sloan's thesis which gives detailed information concerning the preparation and properties of the biradicals.

We are grateful to Dr. A. McLachlan for calling to our attention Pariser's result on the degeneracy between certain singlets and triplets.

[4] B. Bleaney and K. D. Bowers, Proc. Roy. Soc. (London) **A218**, 451 (1952).

[5] K. H. Hauser, Z. Naturforsch. **14a**, 425 (1959).

[6] E. Muller and I. Muller-Rodloff, Ann. **521**, 81 (1935).

[7] R. Pariser, J. Chem. Phys. **24**, 250 (1956).

Kinetics of the Alpha Radiolysis of Carbon Monoxide

P. S. RUDOLPH AND S. C. LIND

Chemistry Division, Oak Ridge National Laboratory, Oak Ridge, Tennessee*

(Received April 11, 1960)

The radiolytic decomposition of CO induced by alpha particles appears to be initiated by two reactive species, CO^+ and CO^*. The products of the reaction are CO_2 and the solids $(C_3O_2)_x$ and graphite. Carbon dioxide formed during the reaction depletes the CO^+ by charge transfer. Thus, when CO_2 pressure becomes sufficiently high, CO^* only initiates reaction. The reaction mechanism suggested is consistent with previous ionization and photochemical studies in the CO system.

INTRODUCTION

THE study of the effect of foreign gases on the rate of gas-phase radiolytic reactions has been restricted to added gases, particularly chemically inert gases.[1-4] In many cases the inert additive increases the rate of chemical reaction in proportion to its stopping power.[1,5] The radiolytic polymerization of acetylene is accelerated by all the rare gases[1] but is retarded by benzene vapor.[2,3] These effects have been explained on the basis of charge-transfer reactions. Acceleration results when charge transfers to the reactant from the additive and retardation occurs when charge transfers to the additive. An exceptional case is the radiolytic condensation of CO in the presence of Xe. In this instance Xe, as additive, has *no* effect on the reaction rate.[4]

In this paper we examine the effect of CO_2 (a gaseous product) on the rate of condensation of CO initiated by alpha particles. The equation,

$$3\,CO \rightsquigarrow CO_2 + \text{solids} \qquad (1)$$

shows the over-all stoichiometry.[4,6] As ordinarily observed, the reaction rate decreases steadily from its initial value until a limiting rate is attained.

EXPERIMENTAL

Carbon monoxide prepared by dropping HCOOH onto hot H_2SO_4,[7] was passed over Drierite and Ascarite and condensed in liquid nitrogen, the middle fraction only was retained. Purity was checked by combustion with O_2 on a hot Pt filament and by vapor phase chromatography, the minimum purities so indicated were 99.6% and 99.9% respectively.[8]

Carbon dioxide prepared by thermal decomposition of $NaHCO_3$,[7] was passed over Drierite and through a trap immersed in CO_2 slush. A sample of the CO_2 so prepared was completely absorbed by dry KOH heated to incipient fusion.[6]

The reaction vessels were small (ca $2\frac{1}{2}$-cm diam) volume-calibrated bulbs *B*, shown schematically in Fig. 1. Radon was condensed into the sphere by liquid nitrogen through small-diameter tubing *T*, which was then sealed off under vacuum. The reactant gas was subsequently forced into the reaction vessel through the three-way stopcock *S*, by mercury from a leveling bulb (not shown) and the stopcock was closed. The reaction vessel was placed in a lead-shielded constant temperature ($25.0° \pm 0.1$) bath. Total gas pressure was always measured with mercury set at the internal index point *I*. Between readings the mercury level was maintained at the fidicual line *F*, etched on the 1-mm capillary

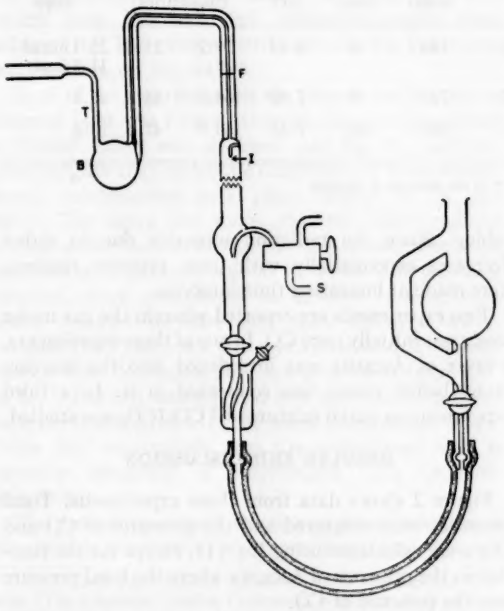

FIG. 1. Schematic diagram of the reaction vessel and manometric system.

* Operated for the U. S. Atomic Energy Commission by the Union Carbide Corporation.

[1] S. C. Lind and D. C. Bardwell, J. Am. Chem. Soc. **48**, 1575 (1926).

[2] S. C. Lind and P. S. Rudolph, J. Chem. Phys. **26**, 1768 (1957).

[3] P. S. Rudolph and C. E. Melton, J. Chem. Phys. **32**, 586 (1960).

[4] P. S. Rudolph and S. C. Lind, J. Chem. Phys. **32**, 1572 (1960).

[5] S. C. Lind, J. Phys. Chem. **58**, 800 (1954).

[6] S. C. Lind and D. C. Bardwell, J. Am. Chem. Soc. **47**, 2675 (1925).

[7] A. Farkas and H. W. Melville, *Experimental Methods in Gas Reactions* (MacMillan and Company, Ltd., London, 1939), p. 161.

[8] The authors are grateful to J. W. Boyle and R. Hornbeck for making these analyses.

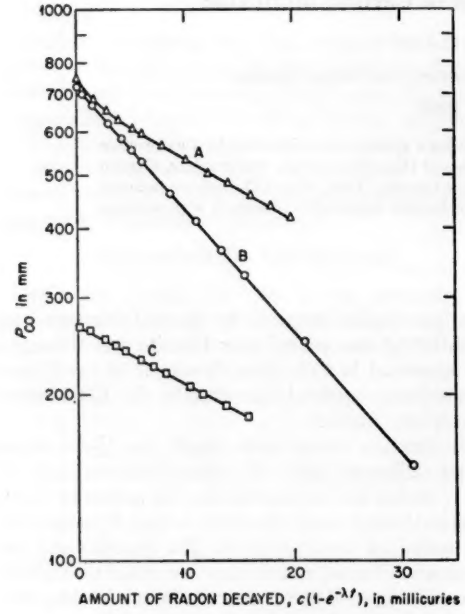

FIG. 2. The dependence of CO pressure on the amount of radon decayed normalized to a 2-cm diam sphere.

	P_{CO}° (mm)	$P_{CO_2}^{\circ}$ (mm)	Volume (cc)	Initial Radon Actual (E_0) (millicuries)	Initial Radon Normalized (c) (millicuries)	Slope
A	748	0	8.43	79.2	21.6	25.1 initial 11.5 final
B[a]	723	0	7.89	160.8	45.8	22.1
C	265	88	7.51	160.0	47.1	10.6

[a] In the presence of Ascarite.

tubing. Since the radiation intensity due to radon decreases exponentially with time, pressure readings were made at increasing time intervals.

Two experiments are reported wherein the gas under study was initially pure CO. In one of these experiments, a layer of Ascarite was introduced into the reaction vessel before radon was condensed in it. In a third experiment an initial mixture of 3 CO:1CO_2 was studied.

RESULTS AND DISCUSSION

Figure 2 shows data from three experiments. Total pressures were measured and the pressures of CO and CO_2 were calculated using Eq. (1), except for the reaction in the presence of Ascarite where the total pressure was the pressure of CO.

In these reactions, the reaction rate is a function of the fraction of radon remaining at any time t (i.e., $e^{-\lambda t}$). The first-order reaction rate constant is given[9] by

$$k=(2.30/E_0)\times(\Delta \log P_{CO}/(\Delta e^{-\lambda t}), \qquad (2)$$

where E_0 is the initial amount of radon in curies, P_{CO} is the CO pressure in mm at any time t, and λ, the decay constant for Rn, is 7.551×10^{-3} hr^{-1}. It has been shown[10] that k is proportional the the ion yield, M/N, the decrease in number of molecules of CO per ion pair formed in the CO.

The reaction rate in a system such as this varies inversely with the square of the diameter of the reaction vessel.[10] All the data presented in Fig. 2 are normalized to a sphere of 2-cm diam. The normalizing factor $2^2/D^2$ is incorporated in

$$c=4E_0/2.30D^2, \qquad (3)$$

where D is the diameter of the reaction vessel. Thus, the slopes of the curves plotted in Fig. 2 are the reaction rates and are comparable.

The initial decrease in rate of CO disappearance shown by change of slopes of curve A, Fig. 2, is characteristic of studies on initially pure CO both in this work and in previously reported work.[6] This decrease to a terminal value suggests that initially two mechanisms are involved and that as product CO_2 is formed one of the mechanisms is inhibited. The evident suggestion[11] is that two different species, CO^+ and CO^* are the important reactants. Because CO^+ has a higher ionization potential than CO_2, the CO^+ can transfer its charge to CO_2 and thus become deactivated, leaving only CO^* to react at a constant rate.

In such event removal of CO_2 from the reaction region should give constant k (as evidenced by slope) over the whole course of the experiment equal to the initial k in the experiments in which CO_2 is allowed to accumulate in initially pure CO. Curve B, Fig. 2, shows the results of a typical experiment in which Ascarite present in the reaction zone removed CO_2 as rapidly as it was formed. The slope of line B is approximately the same as the initial slope of curve A (22.1 and 25.1, respectively); the respective M/N's are 2.8 and 3.2.

We further reasoned that if the retardation were due to CO_2, the initial presence of more than 6% of CO_2 should give a slope equal to the final slope of the experiments in which CO_2 is formed and allowed to accumulate. The results of an experiment performed to test this conclusion are shown in curve C, Fig. 2. In this case the initial mixture was 3CO:1CO_2. The final slope of curve A and the slope of line C are in good agreement (11.5 and 10.6, respectively); the M/N's are 1.5 and 1.4, respectively.

The three experiments discussed here give data in agreement with the explanation of retardation on the

[9] S. C. Lind, J. Phys. Chem. **16**, 592 (1912).
[10] S. C. Lind, J. Am. Chem. Soc. **41**, 531 (1919).
[11] R. L. Platzman (private communication); cf. H. Eyring, J. O. Hirschfelder, and H. S. Taylor, J. Chem. Phys. **4**, 479, 570 (1936).

basis of charge transfer. Although energy considerations alone are insufficient criteria for postulating a charge transfer reaction,[3] mass spectrometric studies[12] in this Laboratory using mixtures of CO and $C^{13}O_2$, and $C^{13}O$ and CO_2 in a dual-leak research mass spectrometer[13] have shown the reaction

$$CO^+ + CO_2 \rightarrow CO + CO_2^+ \quad (4)$$

to be about 80% efficient. Thus, the suggestion that charge transfer is responsible for the retardation is consistent with the available physical data.

The energy W necessary to produce an ion pair in CO gas is, as for any other gas, greatly in excess of the ionization potential. Any kinetic scheme for the radiolysis of CO should take into consideration the total energy expended in the gas and thus include processes subsequent to both ionization and excitation. Numerous reactions can be written for the various reactive species thus formed. The formation of parent ion and dissociation of parent ion, both spontaneous and collision induced, have been reported in mass spectrometric studies on CO.[14] The formation of excited species, their dissociation into reactive intermediates and the reactions of these intermediates to produce observed products have been postulated from the photolysis of CO.[15] Qualitative studies in a mass spectrometer in this Laboratory[12] at high pressures (approximately 0.1 mm in the ionization chamber) suggest that ionic species react as follows:

$$CO^+ + CO \rightarrow CO_2^+ + C \quad (5)$$

$$O^+ + CO \rightarrow CO_2^+ \quad (6)$$

$$C^+ + CO \rightarrow C_2O^+ \quad (7)$$

and/or,

$$CO^{+*} + CO \rightarrow C_2O^+ + O. \quad (8)$$

The intermediate ion C_2O^+ probably reacts with CO to give $C_3O_2^+$. The product ions are finally neutralized and the C and C_3O_2, whether produced from ionic or excited species, polymerize to yield solid products. Early workers[6] concluded from a material balance that the solid products were $(C_3O_2)_x$ and carbon. The carbon, as graphite was subsequently confirmed by x-ray diffraction studies.[16]

The numerous intermediates disappear in a variety of reactions to yield final products with various efficiencies which seem (as can be judged from lack of dependence of k on CO pressure in experiments such as represented by line B, Fig. 2) to be independent of CO concentration.

[12] P. S. Rudolph and C. E. Melton (unpublished). These authors thank Dr. G. A. Ropp, of this Laboratory, for preparing the isotopically labeled gases.

[13] C. E. Melton and G. A. Ropp, J. Am. Chem. Soc. **80**, 5573 (1958).

[14] C. E. Melton and G. F. Wells, J. Chem. Phys. **27**, 1132 (1957).

[15] K. Faltings, W. Groth, and P. Harteck, Z. physik. Chem. **B41**, 15 (1938).

[16] J. H. L. Watson, M. Vanpee, and S. C. Lind, J. Phys. Chem. **54**, 391 (1950).

FIG. 3. Photograph of a large reaction sphere showing the Tyndall effect and solid products which have settled to the bottom.

Previous workers[6] in their study of the alpha radiolysis of CO observed a coherent film evenly distributed on the inner surface of the reaction vessel. This film was inert to water and acid and alkaline solutions. Subsequent attempts by the previous workers and by the present authors failed to produce this coherent film, yet the reality of the film cannot be denied as it was peeled from the wall and photomicrographs were taken of it.[17] The evenly distributed film was formed by condensation on the wall.[18]

In all of the experiments of the present study, when a beam of light was focused through the reaction sphere a Tyndall Effect was observed (see Fig. 3). Such results indicate that under the conditions of these experiments condensation took place largely in the gas phase. The figure also shows that the solid products settled to the bottom of the reaction sphere. The solid products were partially soluble in water. The resulting solution, when evaporated to dryness without heat under reduced pressure and then sublimed under vacuum at 92°, gave a white crystalline solid. This solid melted with decomposition (gas evolution) from 133° to 137°. Purified malonic acid in a check melting point tube decarboxylated over the same temperature range. From this we conclude that the unhydrated solid is partially composed of polymerized C_3O_2 (malonic anhydride).

The possibility of back reaction as an explanation of the initial retardation was considered but did not

[17] S. C. Lind, *The Chemical Effects of Alpha Particles and Electrons* (The Chemical Catalog Company, Inc., New York, 1928), p. 153.

[18] Polymerization at the wall was also postulated by P. Harteck and S. Dondes [J. Chem. Phys. **23**, 902 (1955)].

explain all the experimental evidence. In a separate experiment, a reaction vessel containing solid condensation products was evacuated and a charge of radon was condensed in it. Large quantities of CO_2 were evolved and new solid condensation products formed. If back reaction involving CO_2 and solid products were the explanation of the observed retardation in the experiment with pure CO (cf. curve A, Fig. 2), then the initial yield in the experiment with CO_2 initially present (cf. curve C, Fig. 2) should have decreased as solid products were formed. No change in slope was observed in this experiment. Further, if back reaction were the explanation one might expect ultimate establishment of an equilibrium between the forward reaction and the back reaction. At such "equilibrium" no pressure change would be observed. Such an effect, however, has never been observed, even though some experiments were continued to over 50% utilization of the CO.

CONCLUSIONS

This study presents evidence supporting the view that the alpha radiolysis of CO proceeds through ionic and excited species and that the active ionic species CO^+ is deactivated by charge transfer to the product CO_2. There is no evident depletion of the excited species.

ACKNOWLEDGMENTS

We thank Professor Milton Burton of Notre Dame University for constructive criticism of the manuscript.

THE JOURNAL OF CHEMICAL PHYSICS VOLUME 33, NUMBER 3 SEPTEMBER, 1960

Force Constants for NH_4^+ and ND_4^+*

S. SUNDARAM†

Laboratory of Molecular Structure and Spectra, Department of Physics, The University of Chicago, Chicago, Illinois

(Received March 21, 1960)

Normal coordinate analysis, for XY_4-type molecules of T_d symmetry, has been carried out by the Wilson *FG*-matrix method. Following Dennison, using the spectral data on NH_4^+ and ND_4^+, the anharmonicity factors have been calculated. The constants of the most general quadratic potential-energy function have been obtained for the ammonium ion.

NORMAL COORDINATE ANALYSIS

THE normal vibrations of tetrahedral XY_4-type molecules have been studied, using the Wilson *FG*-matrix method,[1] by Meister and Cleveland.[2] These molecules have T_d symmetry and give rise to one nondegenerate a_1-type vibration, one doubly degenerate e-type vibration, and two triply degenerate t_2-type vibrations. The number of internal coordinates that can be used in the construction of the symmetry coordinates will be 10, including the changes in the four XY bonds and in the six YXY interbond angles. Hence there is one redundant coordinate.

If one assumes the most general quadratic potential-energy function for this type of molecule, analytical expressions relating the valence force constants (f) to the symmetry force constants (F) may be obtained from the transformation,[3]

$$f=\tilde{U}FU, \tag{1}$$

where U is the matrix formed by the coefficients of the internal coordinates in the symmetry coordinates and f, F are also the force constant matrices.

In the present investigation, the symmetry coordinates are the same as those given by Meister and Cleveland.[2] The following analytical expressions have been derived:

$$f_d=(F_{11}+3F_{44})/4, \tag{2}$$

$$f_{dd}=(F_{11}-F_{44})/4, \tag{3}$$

$$df_{d\alpha}=F_{34}/8^{\frac{1}{2}}=-df_{d\alpha}', \tag{4}$$

$$d^2f_\alpha=(2F_{22}+3F_{33})/6, \tag{5}$$

$$d^2f_{\alpha\alpha}=-F_{22}/6, \tag{6}$$

$$d^2f_{\alpha\alpha}'=(2F_{22}-3F_{33})/6, \tag{7}$$

where F_{11}, F_{22}, and F_{33}, F_{34}, F_{44} are the potential-energy matrix elements corresponding to a_1, e, and t_2 vibrations.

ANHARMONICITY FACTORS

If one considers the data from a pair of molecules like XH_4 and XD_4, one sees that in order to satisfy product rule,[4] the harmonic wave numbers (ω) have

* This work was assisted by the Geophysics Research Directorate of the Air Force Cambridge Research Center, Air Research and Development Command.

† Present address: Ganeshnagar, Pudukkottah, South India.

[1] E. B. Wilson, Jr., J. Chem. Phys. **7**, 1047 (1939); **9**, 76 (1941).

[2] A. G. Meister and F. F. Cleveland, Am. J. Phys. **14**, 13 (1946)

[3] R. Gold, J. M. Dowling, and A. G. Meister, J. Mol. Spectroscopy **2**, 9 (1958).

[4] O. Redlich, Z. physik. Chem. **B28**, 371 (1935).

TABLE I. Vibrational wave numbers and anharmonicity factors for NH_4^+ and ND_4^+.

Type	NH_4^+ (cm^{-1})	x_{ii}	ND_4^+ (cm^{-1})	x_{ii}
a_1	3041	0.116	2214	0.085
e	1710	0.015	1215	0.011
l_2	3138	0.059	2350	0.045
	1403	0.059	1066	0.045

to be calculated using the observed fundamentals (ν) and the anharmonic constants x_{ii}. Following Dennison,[5] one may write

$$\omega_i=\nu_i(1+x_{ii}), \tag{8}$$

and

$$\omega_i^*=\nu_i^*[1+x_{ii}(\nu_i^*/\nu_i)], \tag{9}$$

where ω_i, ν_i and ω_i^*, ν_i^* correspond to XH_4 and XD_4, respectively. ω_i^*/ω_i can also be expressed in terms of the ratio of the kinetic-energy matrices. Thus, a determination of x_{ii} and therefore ω_i, ω_i^* would be possible from a knowledge of ν_i, ν_i^*, and the G-matrix elements. Such a procedure has been followed in the present investigation and the anharmonic constants have been calculated. Table I summarizes the vibrational spectral data[6] and the calculated anharmonicity factors for NH_4^+ and ND_4^+.

POTENTIAL ENERGY CONSTANTS

With the eight fundamental vibrational wave numbers for NH_4^+ and ND_4^+, one can set up eight equations by expanding the secular determinant. When harmonic wave numbers (ω) are used, only five out of the above eight equations will be distinct and therefore the five symmetry force constants can be unambiguously determined. In the present investigation, by the method outlined in the foregoing, the five symmetry force constants and, therefore, all the constants of the most general quadratic potential energy function have been calculated.

TABLE II. Potential-energy constants of NH_4^+ and NH_3.[a]

Constant	NH_4^+	NH_3
f_d	6.3857	6.9402
f_{dd}	0.1544	0.1597
$f_{d\alpha}$	0.0192	0.1018
$f_{d\alpha'}$	−0.0192	0.2336
f_α	0.4240	0.6058
$f_{\alpha\alpha}$	−0.0995	−0.0562
$f_{\alpha\alpha'}$	−0.0258	

[a] The constants are in 10^5 dynes cm^{-1}.

The results are given in Table II. Comparing these constants with those obtained for NH_3 and ND_3 by Sundaram *et al.*,[7] one finds there is close agreement in the case of the constants for the NH or ND stretchings and the interaction between stretchings. However, in the case of the ammonium ion, the constant for the bending mode is appreciably less than in NH_3 and ND_3. The constants listed in Table II are transferable to NT_4^+ and the partially deuterated and tritiated ions. The results for these will be reported elsewhere.

[5] D. M. Dennison, Revs. Modern Phys. **12**, 175 (1940).
[6] I. Nakagawa and S. Mizushima, Bull. Chem. Soc. Japan **28**, 589 (1955).
[7] S. Sundaram, F. Suszek, and F. F. Cleveland, J. Chem. Phys. **32**, 251 (1960).

Out-of-Plane CH Vibrations in Some Polynuclear Aromatic Hydrocarbons

MILAN RANDIĆ*

Institute "Rudjer Boskovic," Zagreb, Yugoslavia

(Received March 28, 1960)

The out-of-plane CH bands in a number of polynuclear aromatic molecules are analyzed. The CH bonds are considered as coupled oscillators. With each group of n neighboring CH bonds an $n\times n$ subdeterminant and a single vibrational frequency was associated. The method is applied to the methyl-1,2-benzanthracenes. Observed spectra agree with calculated frequencies well, and thus support the idea that observed CH bands are caused by splitting of n identical coupled oscillators. The spectra of some other polynuclear aromatic hydrocarbons are discussed as well.

THE infrared spectra of polynuclear aromatic compounds are complex, having many bands, and it does not seem to be feasible to attempt a complete interpretation of their spectra. However, there are some regions in which characteristic group vibrations appear such as

3100–3000 cm^{-1}	CH stretching
1650–1450 cm^{-1}	skeletal stretching
900– 650 cm^{-1}	out-of-plane CH bendings.

The absorption spectrum as a whole is typical of each compound and is used for identification purposes, but in some instances useful correlations of the group frequencies with molecular structure can be made. Large molecules with a number of identical bonds or groups of atoms, such as C—C and CH_2 groups in n paraffins, or CH groups in polyenes and polyphenyls might be thought of as essentially systems of identical coupled oscillators. A number of observed frequencies can then be interpreted as due to splitting of original degeneracies. These assumptions proved qualitatively very useful in the assignment of vibrational frequencies of n paraffins.[1]

In this paper we specifically consider the out-of-plane CH vibrations in some polynuclear aromatics. The procedure is as follows:

1. The complete secular determinant is written for a given system of identical oscillators in which it is assumed that only adjacent oscillators are directly coupled and that there is no coupling between rings.

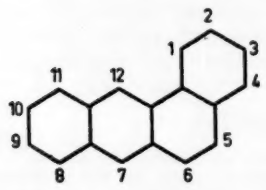

FIG. 1. 1,2-Benzanthracene, numbering of hydrogens.

2. The determinant is split into a number of smaller $n\times n$ subdeterminants, each corresponding to a group of n adjacent CH bonds.

3. Each $n\times n$ subdeterminant gives n different frequencies. However, selection rules and intensity considerations limit the number of frequencies observed strongly in the infrared spectrum, so that each subdeterminant gives rise to a single important frequency as far as the spectrum is concerned.

As an example we shall first examine the 900–650 cm^{-1} region of the spectra of methyl-1,2-benzanthracenes. Benzanthracene (Fig. 1) itself has 12 hydrogen atoms and we shall consider all 12 methyl monosubstituents. It is assumed that CH_3 substitution does not appreciably affect the chemical environment of the rest of the molecule. In the case of 1-methyl-1,2-benzanthracene the secular determinant may be written formally as[2]:

	2	3	4	5	6	7	8	9	10	11	12
2	x	1	0								
3	1	x	1								
4	0	1	x								
5				x	1						
6				1	x						
7						x					
8							x	1	0	0	
9							1	x	1	0	
10							0	1	x	1	
11							0	1	1	x	
12											x

* Presented at the 1st Congress of Pure and Applied Chemistry of Yugoslavia, held at Zagreb, June 14–18, 1960.

[1] See for example J. K. Brown, N. Sheppard, and D. M. Simpson, Phil. Trans. Roy. Soc. (London) **A247**, 35 (1954).

[2] G. Herzberg, *Infrared and Raman Spectra of Polyatomic Molecules* (D. Van Nostrand and Company, Inc., Princeton, New Jersey, 1945), p. 69.

TABLE I. The number of subdeterminants for methyl-1,2-benzanthracenes.

Position of CH_3 substituent	1×1	2×2	3×3	4×4	Type
1	2	1	1	1	*A*
2	3	2	0	1	*B*
3	3	2	0	1	*B*
4	2	1	1	1	*A*
5	3	0	0	2	*C*
6	3	0	0	2	*C*
7	1	1	0	2	*D*
8	2	1	1	1	*A*
9	3	2	0	1	*B*
10	3	2	0	1	*B*
11	2	1	1	1	*A*
12	1	1	0	2	*D*

where $x=(K-m\omega^2)/K'$ and $\omega=2\pi\nu$. K represents the force constant of the restoring force characterizing a single CH bond and K' measures the interaction between two neighboring CH bonds. The foregoing determinant can be split into two 1×1, one 2×2, one 3×3, and one 4×4 subdeterminant. Each of these determinants will give a set of vibrational frequencies. Other monosubstituted methyl derivatives of benzanthracene can be treated in the same way. The number of subdeterminants in each case, after the secular determinant has been broken down, is given in Table I. In this way we see that there are only four different types of spectra (designated with *A*, *B*, *C*, and *D*) to be expected in the 900–650 cm^{-1} region for all 12 substituted methyl-1,2-benzanthracenes. All possible frequencies have to be obtained as roots of small subdeterminants and these appear in four different combinations only.

This is to be expected since there are, in the foregoing approximation, four types of equivalent hydrogen atoms in respect to methyl substitution (see Table II). For example atoms 1, 4, 8, and 11 if substituted with CH_3 will all give the same number of $n\times n$ subdeterminants, and therefore the same pattern in the infrared spectra, (i.e., spectra type *A*). By numbering sets of equivalent H atoms we can therefore predict how many different types of spectra (i.e., types of different patterns in the infrared spectra in the corresponding region) we can expect for any polynuclear aromatic molecule.

TABLE II. Equivalent H atoms on nearest neighbor approximation.

Equivalent H atoms				Type of spectra
1	4	8	11	*A*
2	3	9	10	*B*
5	6			*C*
7	12			*D*

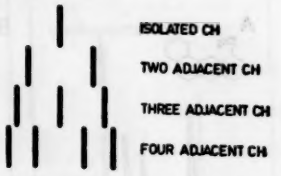

FIG. 2. Frequency distribution for n adjacent CH oscillators.

CALCULATION OF INDIVIDUAL FREQUENCIES

For the calculation of the individual frequencies we have to know the potential field. In this case we have to know the characteristic force constant for single CH out-of-plane vibration and coupling constant K' between two adjacent CH bonds. The subdeterminants

$$\begin{vmatrix} x & 1 & 0 & 0 \\ 1 & x & 1 & 0 \\ 0 & 1 & x & 1 \\ 0 & 0 & 1 & x \end{vmatrix} = 0 \quad \text{etc.,}$$

give us the well-known distribution of frequencies (Fig. 2). These subdeterminants are in fact the so-called Tchebishev polynomials, and can easily be solved, giving[3] $x=2\cos k\pi/(n+1)$. With each of these frequencies a definite vibrational mode is associated. To see which of the foregoing frequencies is prominent in the spectrum the intensity of the vibrational modes has to be considered. The intensity depends on the square of the magnitude of electric dipole change during the vibration. It is clear that the mode in which all hydrogens move out-of-plane in phase induces the largest change in dipole moment during the vibration, while other modes have relatively small vibrating dipole due to partial cancellation of the contributions from individual CH bonds. In benzene, for example, only the A_{2u} out-of-plane CH vibration is allowed, all others being forbidden on account of symmetry properties only. In larger molecules with little or no symmetry similarly most of the intensity is found in one band, i.e., one band of the set is dominant. With this assumption each subdeterminant is characterized by a single dominant frequency. In other words, each group

TABLE III. Methyl-1,2-benzanthracenes: the type of spectra and the assignment of infrared bands.

1×1	2×2	3×3	4×4	Type	Number of bands
2	1	1	1	*A*	4
3	2	0	1	*B*	3
3	0	0	2	*C*	2
1	1	0	2	*D*	3
880	820	780	750 cm^{-1}		Assignment

[3] See for example T. H. Goodwin and V. Vand, J. Chem. Soc. 1683 (1955).

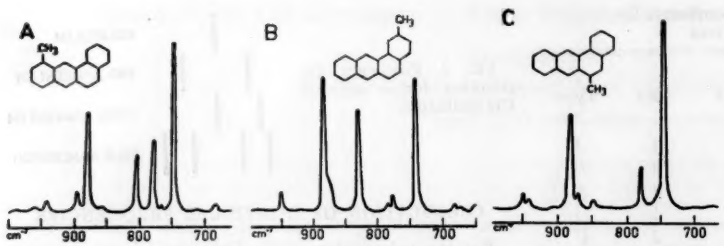

FIG. 3. Infrared spectra of methyl-1,2-benzanthracenes; [Reproduced from the *Chemical Application of Spectroscopy* (Interscience Publishers, Inc., New York; by kind permission)].

of n adjacent CH bonds of polynuclear aromatics is characterized by a single frequency in the region 900 cm^{-1}–700 cm^{-1}, which is due to the in-phase CH out-of-plane vibrational mode. These frequencies are different for each subdeterminant and their relative intensities will also depend on the number each subdeterminant repeats in a secular determinant for a given molecule. In a recent paper Zbinden[4] discussed the relative intensity distribution in a band series associated with a system of n coupled oscillators. He derived a general formula, treating the absorption process as a forced vibration of the system in a classical way, and obtained the maximum intensity (i.e., the strongest absorption band) for the in-phase vibration of the coupled oscillators. For the other vibrational modes the intensity falls off very rapidly. This result can be applied to our problem as well, and it supports the foregoing assumption of a single dominant frequency characterizing each group of n adjacent CH bonds.

In the case of methyl-1,2-benzanthracenes the type of spectra, the number of expected bands and the infrared assignments are given in Table III. Frequencies are in agreement with those found in benzene rings with the equivalent number of heavy substituents.[5] There is a complete agreement between the number of observed[6] absorption bands in the 900–700 cm^{-1} region and those predicted in Table III (Fig. 3). The main features of the spectra in this region are thus explained, although some bands are double or split.[6]

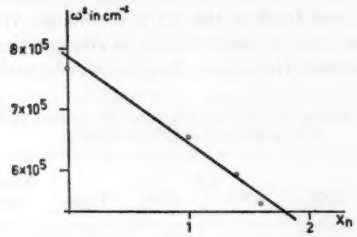

FIG. 4. Maximal root x_n of the $n\times n$ subdeterminant against the observed ω^2.

[4] R. Zbinden, J. Mol. Spectroscopy **3**, 654 (1959).
[5] L. J. Bellamy, *The Infrared Spectra of Complex Molecules* (Methuen and Company, Ltd., London, England, 1958), Chap. 5.
[6] R. N. Jones and C. Sandorfy, in *Chemical Applications of Spectroscopy, Technique of Organic Chemistry* (Interscience Publishers, Inc., New York, 1956), Figs. 81–86, pp. 402–405.

It is beyond this simple approximation to discuss such small effects.

The assignment of the spectra: The absorption between 830–810 cm^{-1} which is associated with CH vibrations at position 3 and 4, and the 750 cm^{-1} associated with the presence of four vicinal CH bonds[7] may be said to be due to 2×2 and 4×4 subdeterminants, respectively. In addition, we can assign the absorption of single CH and three CH groups at 880 cm^{-1} and 780 cm^{-1}. This is then a complete assignment of the out-of-plane CH bendings sufficient to explain the spectra of all methyl-1,2-benzanthracenes. It should be stressed that the complete assignment of frequencies to different $n\times n$ subdeterminants is *consistent* with the predicted distribution of frequencies of identical coupled oscillators (Fig. 2), and was reached independently. This is therefore a strong support to the proposed origin and the assignment of CH out-of-plane absorption bands.

We shall obtain individual frequencies by solving each of $n\times n$ subdeterminants and then taking the greatest root, which corresponds to the in-phase vibration. The frequencies are given then by

$n\times n$	
1	$\omega^2=K/m$
2	$\omega^2=(K+K')/m$
3	$\omega^2=(K+1.414K')/m$
4	$\omega^2=(K+1.618K')/m$
5	$\omega^2=(K+1.732K')/m$

If we plot a diagram with maximal roots x_n against the observed ω^2 we should obtain a straight line if the above assumptions are correct. The slope of the

TABLE IV. Observed and calculated CH out-of-plane frequencies for methyl-1,2-benzanthracenes.

n	Observed	Calculated
1	880 cm^{-1}	890 cm^{-1}
2	820 cm^{-1}	810 cm^{-1}
3	780 cm^{-1}	780 cm^{-1}
4	750 cm^{-1}	760 cm^{-1}

[7] See work cited in footnote 6, p. 404.

TABLE V. The number of subdeterminants, the number of bands and observed frequencies for some polynuclear aromatics.

	1×1	2×2	3×3	4×4	Number of bands	Observed (cm^{-1})
Naphthalene	0	0	0	2	1	830
Anthracene	2	0	0	2	2	720 880
Phenanthrene	0	1	0	2	2	730 810
Benzanthracene	2	1	0	2	3	740 800 880

line will give us the coefficient K'. The main force constant is given with the value of ω^2 for $x_n=0$. Using the relation

$$\lambda=(K+x_nK')/m,$$

where $\lambda=(\nu/1303)^2$ one obtains K and K' in 10^5 d/cm if ν is given in cm^{-1} and m in atomic units. From the plot ω^2 against x_m (Fig. 4), we have

$$K=0{,}468$$

$$K'=-0{,}080.$$

A comparison can be made with benzene[8]

$$K=0{,}378$$

$$K'=-0{,}057.$$

This is a fair comparison showing the same magnitudes. The complete comparison is not possible due to different assumptions involved in the force fields. Using the obtained force constants we can calculate frequencies which are given in Table IV. These frequencies differ only for ± 10 cm^{-1} from the experimental ones and this is within the accuracy of empirical regularities for characteristic frequencies. For that reason the approximate treatment of the foregoing vibrations is justified.

OTHER POLYNUCLEAR MOLECULES

Naphthalene, anthracene, phenanthrene, and benzanthracene will now be discussed. The number of subdeterminants for each of these molecules is given in Table V. In the last column the number of absorption bands in each case is given. The observed frequencies

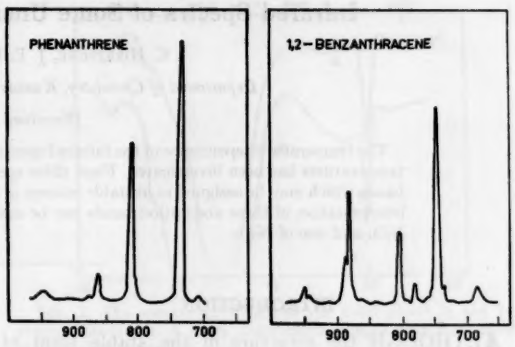

FIG. 5. Infrared spectra of phenanthrene and 1,2-benzanthracene. [Reproduced from the *Chemical Application of Spectroscopy* (Interscience Publishers, Inc., New York, by kind permission).]

are added and some of the spectra shown in Fig. 5. For the spectra of other molecules see footnote 6.

From the spectra of these molecules, again, we see a very good agreement between the number of bands predicted and observed. The assignment of bands is easy to make if a comparison with general results of methyl benzanthracenes is made, but since these molecules are not so closely related we are not surprised to find some deviations (the relative shifts of the absorption bands).

Other molecules can be analyzed in a similar manner. In some cases, like dimethyl-1,2-benzanthracene, more lines are observed[6] than expected, but one should bear in mind that other bands corresponding to different types of vibrations, might appear in the same region. Steric hindrance will also cause some complications, as is seen from a comparison of the spectra of para and meta polyphenyls against ortho polyphenyls.[9] In the case of methyl-1,2-benzanthracenes we did not discuss the over-crowding of certain atoms. The substitution of 1 and 12 will cause some steric hindrance and this will possibly reflect itself in some complexity of the spectra.

ACKNOWLEDGMENT

The author wishes to thank Dr. Norman Sheppard (Cambridge, England) for his general advice and discussions in connection with this work.

[8] F. A. Miller and B. L. Crawford, J. Chem. Phys. **14**, 282 (1946).

[9] J. E. Stewart and M. Hellmann, J. Research Natl. Bur. Standards **60**, 125 (1958).

Infrared Spectra of Some Unstable Isomers of N_2O_4 and N_2O_3*

I. C. HISATSUNE, J. P. DEVLIN, AND YASUO WADA†

Department of Chemistry, Kansas State University, Manhattan, Kansas

(Received April 4, 1960)

The temperature dependence of the infrared spectra of N_2O_4 and N_2O_3 in the solid phase at liquid-nitrogen temperatures has been investigated. From these spectra of both ^{14}N and ^{15}N isotopic molecules, absorption bands which may be assigned to unstable isomers of these nitrogen oxides have been identified. A reasonable interpretation of these absorption bands can be made by assuming the existence of two unstable forms of N_2O_4 and one of N_2O_3.

INTRODUCTION

ALTHOUGH the structure of the stable form of N_2O_4 in the gas, liquid, and solid phases is known to be planar and symmetric,[1–3] Fateley, Bent, and Crawford[4] have shown recently that unstable forms of this molecule can be stabilized by matrix isolation method using liquid helium as refrigerant. These investigators were also able to identify two infrared absorption bands of an unstable isomer of N_2O_3.

We have been carrying out similar studies of these unstable isomers of N_2O_4 and N_2O_3 using liquid nitrogen refrigerant, however, and have found many more absorption bands which can be assigned reasonably to these unstable molecules. Our investigations, which were preceded by a careful study of the spectra of the stable forms of these nitrogen oxides and in which both isotopes of nitrogen were used, are not only consistent with the results of Fateley, Bent, and Crawford, but they provide convincing evidence that such unstable isomers are trapped in the solid even at liquid-nitrogen temperatures.

EXPERIMENTAL

Gas samples were taken from Matheson Company compressed gas cylinders and purified according to the methods described previously.[3] Samples of N_2O_3 were prepared by reacting purified nitric oxide and purified oxygen. The ^{15}N isotopic molecules were prepared by reacting purified oxygen with 99.4% ^{15}N enriched nitric oxide obtained from the Isomet Corporation. Partial oxidation of this nitric oxide was carried out first to form $^{15}N_2O_3$, and after the completion of its study the sample was completely oxidized by using excess oxygen to form $^{15}N_2O_4$. The original sample of ^{15}NO contained a considerable amount of nitrous oxide, but no attempts were made to remove this impurity from our samples. Furthermore, ^{15}N nitrogen oxides were recovered after each run and used repeatedly without further purification.

The spectra were taken with a Perkin-Elmer 12B spectrometer which has been modified for double-pass operation. LiF, NaCl, KBr, and CsBr prisms were used, and these were calibrated according to the method of Downie *et al.*[5] Before and after each run on the Perkin-Elmer 12B instrument, the spectrum of the sample was also recorded with a Perkin-Elmer 137 Infracord spectrometer. The low-temperature cells used in these runs were similar to those used before.[3]

The absorption bands associated with unstable nitrogen oxide species were identified in the following manner. A gaseous sample was first condensed on the cold-cell window after the window had attained the minimum temperature with liquid-nitrogen refrigerant. Under routine operations, our cells gave minimum temperatures of about −160°C, although with higher concentrations of N_2O_3, the temperature was slightly higher because of the appreciable vapor pressure of nitric oxide solid. (In order to obtain higher concentrations of N_2O_3, we used an excess of NO over NO_2 in most of the runs.) The spectrum of this condensed sample was recorded, and then the sample was allowed to warm slowly. The N_2O_4 and N_2O_3 samples were warmed, respectively, to about −80°C and about −120°C. These warming sequences were carried out once or more depending on the amount of sample which was condensed on the window. After each warming the samples were recooled to the minimum temperatures. The spectrum of this annealed sample was recorded and compared to that obtained with the unannealed sample.

RESULTS AND INTERPRETATION

Dinitrogen Tetroxide

Typical Infracord spectra of a sample of $^{14}N_2O_4$ condensed rapidly from the gas phase and of the same sample after annealing are shown in Fig. 1. Similar spectra in the 14-μ region and in the CsBr prism region are shown in Figs. 2 and 3. The most intense absorption bands in these spectra arise from the fundamentals of

* This research was sponsored in part by the Geophysics Research Directorate, Air Force Cambridge Research Center, and in part by the Division of Sanitary Engineering Service, Public Health Service.

† National Science Foundation Cooperative Graduate Fellowship, 1959–60.

[1] D. W. Smith and K. Hedberg, J. Chem. Phys. **25**, 1282 (1956).

[2] J. S. Broadley and J. M. Robertson, Nature **164**, 915 (1949).

[3] R. G. Snyder and I. C. Hisatsune, J. Mol. Spectroscopy **1**, 139 (1957).

[4] W. G. Fateley, H. A. Bent, and B. Crawford, Jr., J. Chem. Phys. **31**, 204 (1959).

[5] A. R. Downie, M. C. Magoon, R. Purcell, and B. Crawford, Jr., J. Opt. Soc. Am. **43**, 941 (1953).

the stable planar form (V_h) of N_2O_4. The frequencies of these fundamentals in gas, liquid, and solid phases are listed in Table I. In this table, frequencies in parentheses have been estimated from combination or overtone bands, and the torsional frequency, which is assumed here to be the same in all phases and isotopic species, has been deduced from entropy calculations.[3,6] The frequencies of the $^{15}N_2O_4$ in the gas and liquid phases and the Raman frequencies of the same isotopic molecule in the solid phase are those reported by Begun and Fletcher.[7] The remaining observed frequencies in this table have been obtained in our Laboratory. The Raman frequencies of the solid $^{14}N_2O_4$ have been obtained with the spectrograph and low-temperature apparatus described earlier.[8]

In Table II the frequencies of the absorption bands which disappeared on annealing the solid are given. The values in the first column are those reported by Fateley *et al.*[4] Since these absorption bands were all

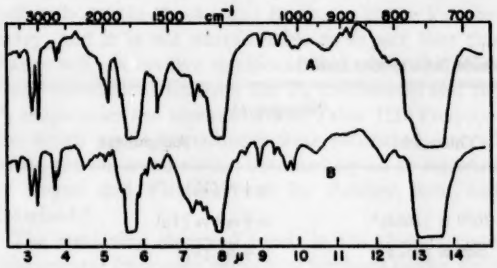

FIG. 1. Infracord spectra of $^{14}N_2O_4$ in the solid phase. Spectrum *A* is from an unannealed solid and *B* from the same sample after annealing.

observed to disappear irreversibly when the solid samples were annealed, they cannot arise from any phase transitions in the solid. Furthermore, we have been particularly careful in our experimental technique so that we may justifiably rule out the possibility that these bands may arise from impurities in our samples. Thus, we are left with the only reasonable conclusion that these absorption bands must be associated with some unstable species of N_2O_4. The agreement between our results and those of Fateley *et al.*,[4] where comparison is possible, is good, and we may take this fact as further support of our conclusion that unstable isomers of N_2O_4 have been trapped in our solid samples even at the temperatures used in this work.

Beside the stable V_h symmetry form of N_2O_4, the two likely isomers of this molecule are the twisted form which still retains the NN bond and the nitrosyl

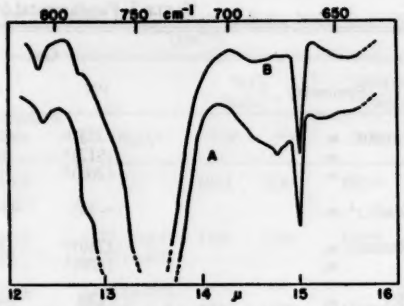

FIG. 2. The spectra of $^{14}N_2O_4$ in the solid phase in the 14-μ region. Spectrum *A* from unannealed sample and *B* from the sample after annealing.

nitrate form ($ONONO_2$). In the twisted form, the symmetry of the isomer may be either V_d when the twist angle is 90° or V when the angle has some intermediate value between 0° and 90°. Another planar symmetric ring form of the molecule has been suggested by Longuet-Higgins,[9] but the observed frequencies do not appear to be consistent with this structure.

The V symmetry selection rules predict eight infrared active fundamentals and the V_d symmetry only five. These fundamentals are expected to lie very close to the corresponding infrared bands of the stable V_h symmetry isomer. Detection of all such bands in our spectra in the presence of an overwhelming excess of the stable V_h isomer is not possible. Thus, it is difficult to decide from the difference in selection rules and from our infrared data which of the two symmetries is the correct one for the twisted form of the N_2O_4 isomer. We prefer, however, to interpret our results in terms of the V_d symmetry for the twisted isomer of N_2O_4. This choice is based on the structure of B_2Cl_4 which is isoelectronic with N_2O_4. Experimental evidence shows that B_2Cl_4 is planar in the crystal phase[10] but it changes to a V_d symmetry in the liquid and gas phases.[11] It

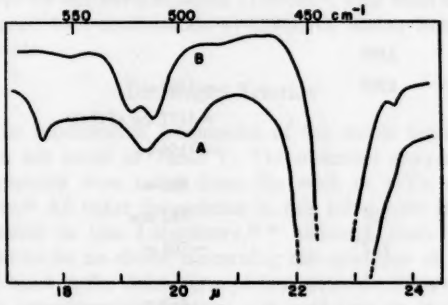

FIG. 3. The spectra of $^{14}N_2O_4$ in the solid phase in the 20-μ region. Spectrum *A* from unannealed sample and *B* from sample after annealing.

[6] I. C. Hisatsune, *Proceedings of the International Meeting on Molecular Spectroscopy, Bologna, Italy, September*, 1959 (Pergamon Press, New York, to be published).

[7] G. M. Begun and W. H. Fletcher, Symposium on Molecular Structure and Spectroscopy, Columbus, Ohio, June, 1959.

[8] I. C. Hisatsune and R. V. Fitzsimmons, Spectrochim. Acta **15**, 206 (1959).

[9] H. C. Longuet-Higgins, Nature **153**, 408 (1944).

[10] M. Atoji, P. J. Wheatley, and W. N. Lipscomb, J. Chem. Phys. **27**, 196 (1957).

[11] D. E. Mann and L. Fano, J. Chem. Phys. **26**, 1665 (1957).

TABLE I. Fundamental frequencies of the V_h symmetry N_2O_4 (cm^{-1}).

Symmetry		Gas		Liquid		Solid	
		^{14}N	^{15}N	^{14}N	^{15}N	^{14}N	^{15}N
A_g (Raman)	ν_1	(1373)[b]	(1350)[b]	1380	1360[c]	1382	1363[c]
	ν_2	(812)[b]	(800)[b]	809	797[c]	812	800[c]
	ν_3	(260)[b]	(260)[b]	265	264[c]	275	273[c]
A_u (Inact.)[a]	ν_4	(~50)	(~50)	(~50)	(~50)	(~50)	(~50)
B_{1g} (Raman)	ν_5	(1710)[b]	(1670)[b]	1712	1672[c]	1721	1683[c]
	ν_6	(480)[b]	(478)[b]	481	478[c]	495	487[c]
B_{1u} (IR)	ν_7	430	~420[c]	~438	416[c]	439	428
B_{2g} (Raman)	ν_8	(675)[b]	(641)[b]	666	654[c]	671	(655)[b]
B_{2u} (IR)	ν_9	1748	1707[c]	1737	1703[c]	1730	1700
	ν_{10}	~385	~377[c]	(380)[b]	(~350)[b]	369	350
B_{3u} (IR)	ν_{11}	1261	1251[c]	1253	1248[c]	1253	1242
	ν_{12}	750	739[c]	743	735[c]	737	732

[a] Estimated from entropy calculations.[3,6]
[b] Estimated from combination or overtone absorption bands.
[c] G. M. Begun and W. H. Fletcher.[7]

TABLE II. Frequencies of unstable N_2O_4 species (cm^{-1}).

Nitrogen-14		Nitrogen-15	
FBC[a]	This work	This work	Assignment
	2935 w (2997)[b]		$\nu_5+\nu_7$ (V_d)
		~2679 w (2663)[b]	$\nu_5+\nu_6+\nu_8$ (V_d)
		2549 w (2572)[b]	$\nu_5+2\nu_8$ (V_d)
	2536 w (2530)[b]		$\nu_2+\nu_7$ (V_d)
		2352 m (2333)[b]	$\nu_7+\nu_8$ (V_d)
	1961 ms (1961)[b]	1935 m (1921)[b]	$\nu_5+\nu_8$ (V_d)
1829			NO stretch ($ONONO_2$)
1718	~1715 w	1682 ms	ν_7 (V_d)
1645			NO stretch ($ONONO_2$)
	1576 m (1564)[b]	1523 ms (1542)[b]	$\nu_2+\nu_6$ (V_d)
		1366 ?	NO stretch ($ONONO_2$)
1290			NO stretch ($ONONO_2$)
1282	~1280 w	1270 m	ν_5 (V_d)
	~1177 vw (1174)[b]		$\nu_8+\nu_9$ (V_d)
	~1156 vw		Combination band ($ONONO_2$)
	882 w		NO_2 wag ($ONONO_2$)
787	782 mw	773 ms	NO_2 deformation ($ONONO_2$)
752	~765 m	742 w	ν_6 (V_d)
		683 ?	NO_2 wag ($ONONO_2$)
	~679 m	651 w	ν_8 (V_d)
	564 w	554 w	NO_2 wag ($ONONO_2$)
	~495 w	~494 w	ν_9 (V_d)
	295 w	293 w	NO_2 wag ($ONONO_2$)

[a] W. G. Fateley, H. A. Bent, and B. Crawford.[4]
[b] Calculated.

should be pointed out, however, that another isoelectronic species, the oxalate ion, appears to change from the V_h symmetry to the V symmetry[12] instead, but in this case the spectroscopic assignment is far from being conclusive. Another evidence in favor of the V_d symmetry for the twisted isomer is that if the symmetry was V, then Fateley *et al.* should have observed another absorption band in the 1750-cm^{-1} region. However, they reported only one band at 1718 cm^{-1}. In view of these arguments, the choice of V_d symmetry for the twisted N_2O_4 appears to be justified.

The selection rules according to the V_d symmetry predict that there will be five infrared active fundamentals, two of which are of B_2 class and three of degenerate E class. The most significant difference between this prediction and that from the stable V_h symmetry is that the Raman active modes in B_1 and B_2 classes of V_h symmetry now become infrared active modes of E class symmetry. The vibrational modes in the A_g, A_u, and B_{3u} of V_h symmetry transform, respectively, to the A_1, A_2, and B_2 classes in the V_d symmetry, and it is not unreasonable to expect that this change will not involve significant shifts in frequencies. These correlations between the V_h frequencies and the V_d frequencies are summarized in Table III. Frequencies which are in parentheses were estimated, but all others are observed values obtained by us or reported by Begun and Fletcher[7] and by Fateley, Bent, and Crawford.[4]

The remaining observed bands in the characteristic fundamental frequency regions of nitrogen oxides have been assigned to the $ONONO_2$ isomer. This isomer had been proposed by Fateley *et al.* with considerable confidence, and our data give additional support to their

TABLE III. Fundamental frequencies of the V_h and V_d isomers of N_2O_4 in the solid phase (cm^{-1}).

V_h Isomer			V_d Isomer		
	^{14}N	^{15}N	^{14}N	^{15}N	
A_g(Raman)	1382	1363[a]	(1382)	(1363)	A_1(Raman)[c]
	812	800[a]	(812)	(800)	
	275	273[a]	(275)	(273)	
A_u(Inact.)[c]	(≈50)	(≈50)	(≈60)	(≈60)	A_2(Inact.)[c]
B_{1g}(Raman)	1721	1683[a]			
	495	487[a]			
B_{1u}(IR)	439	428	1718[b]	1682	E(IR and Raman)
B_{2g}(Raman)	671	(655)[c]	≈679	651	
B_{2u}(IR)	1730	1700			
	369	350	≈495	≈494	
B_{3u}(IR)	1253	1242	1282[b]	1270	B_2(IR)
	737	732	752[b]	742	

[a] G. M. Begun and W. H. Fletcher.[7]
[b] W. G. Fateley, H. A. Bent, and B. Crawford.[4]
[c] Estimated.

[12] M. J. Schmelz, T. Miyazawa, S. Mizushima, T. J. Lane, and J. V. Quagliano, Spectrochim. Acta **9**, 51 (1957).

TABLE IV. Observed fundamentals of N_2O_5, N_2O_3, and $ONONO_2$ (cm^{-1}).

Characteristic Mode	$^{14}N_2O_5$[a]	N_2O_3 (solid)[b] ^{14}N	N_2O_3 (solid)[b] ^{15}N	$ONONO_2$ (solid) ^{14}N	$ONONO_2$ (solid) ^{15}N
NO stretch (nitrosyl)	...	1863	1830	1829[d]	...
NO stretch (nitro)	1752 (solid)	1589	1546	1645[d]	...
	1700 (solid)				
NO stretch (nitro)	1316 (solid)			...	1366?
	1248 (solid)	1297	1277	1290[d]	...
NO stretch	860 (gas)	...	...	882	...
NO_2 deformation	737 (solid)	783	771	787[d]	773
	719 (solid)				
NO_2 wag		627	614	...	683?
	580 (gas)	...	...	564	554
	458 (gas)	407[c]	397[c]		
	357 (gas)	313	308	295	293

[a] Solid frequencies by W. G. Fateley *et al.*,[4] gas by I. C. Hisatsune (unpublished). Assignment of low-frequency bands tentative.
[b] I. C. Hisatsune and co-workers.[13,14]
[c] Tentatively assigned to NO wag.
[d] W. G. Fateley, H. A. Bent, and B. Crawford.[4]

confidence. Although the present data is not substantial, we may still show the reasonableness of the proposal of Fateley *et al.* by extending their comparison of the frequencies of this isomer to N_2O_3 and N_2O_5. Such comparison is shown in Table IV. In this table the N_2O_5 gas-phase frequencies are from the unpublished result obtained by one of us (I.C.H.). The frequencies of N_2O_3 are those obtained in this Laboratory.[13,14]

The complete assignments of the observed bands of unstable N_2O_4 isomers are summarized in Table II. Attempts were made to assign all frequencies other than those due to fundamentals to combination bands of the twisted isomer. Satisfactory assignments were possible except for one band at about 1156 cm^{-1}. This band was assigned to a combination of $ONONO_2$ isomer fundamentals.

Dinitrogen Trioxide

The fundamental frequencies of the stable form of N_2O_3 are listed in Table V. The observed gas-phase frequencies were taken from the work of D'Or and Tarte.[15] All other frequencies in this table have been obtained in this Laboratory.[13,14] Although there appears to be no doubt concerning the existence of the NN bond in the stable form of this molecule, the available experimental data are not sufficient to decide whether the molecule is planar or nonplanar. The

[13] I. C. Hisatsune and K. H. Rhee, *Proceedings of the International Meeting on Molecular Spectroscopy, Bologna, Italy, September*, 1959 (Pergamon Press, New York, to be published).
[14] I. C. Hisatsune and J. P. Devlin, Spectrochim. Acta (to be published).
[15] L. D'Or and P. Tarte, Bull. soc. roy. sci. Liège **22**, 276 (1953).

TABLE V. Fundamental frequencies of N_2O_3 (cm^{-1}).

Gas Infrared[a]	Solution Infrared[c]	Solution Raman[d]	Solid Infrared ^{14}N	Solid Infrared ^{15}N	Assignment
1830	1841	1849	1863	1830	NO stretch
1615	1611	1600	1589	1546	NO stretch
1309	1291	1291	1297	1277	NO stretch
770	768	772	783	771	NO_2 deformation
...	624	614	627	614	NO_2 wag
430	(400)[b]	(400)[b]	407	397	NO wag
(350)[b]	(330)[b]	(330)[b]	313	308	NO_2 wag
(260)[b]	(260)[b]	253	(265)[b]	(262)[b]	NN stretch

[a] L. D'Or and P. Tarte.[15]
[b] Estimated from combination or overtone bands.
[c] I. C. Hisatsune and K. H. Rhee.[13]
[d] I. C. Hisatsune and J. P. Devlin.[14]

planarity of both the solid dimer of nitric oxide[16] and N_2O_4 suggests, however, that it is not unreasonable to expect that the stable form of N_2O_3 in the solid phase is also planar.

A typical Infracord spectrum of solid $^{14}N_2O_3$ sample and the spectrum of the same sample annealed at about $-116°C$ and recooled to $-150°C$ are shown in Fig. 4. Similar spectra in the 14-μ region and the CsBr prism region are shown in Figs. 5 and 6. These N_2O_3 samples were obtained by condensing a gaseous mixture of NO_2 and excess NO. This excess NO was necessary to suppress the concentration of N_2O_4, which we were never able to eliminate completely in thick solid samples. Since solid NO has an appreciable vapor pressure even at liquid-nitrogen temperature, use of such excess prevented us from studying very thick samples of N_2O_3. In runs with such thick samples, the temperature of the cold window rose gradually as the spectrum was being taken, and before a complete scan could be made many of the unstable bands had already disappeared or weakened considerably in intensity. Furthermore, in these thick samples it was not possible to prevent the loss of some of the sample during the annealing process so that bands associated with unstable species could be identified only with a great deal of difficulty and uncertainty. These experimental difficulties account for the fact that we were not able to obtain extensive spectroscopic data on the unstable species of N_2O_3.

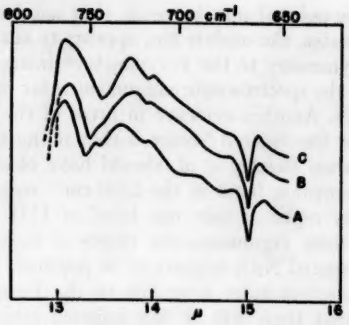

FIG. 5. The spectra of $^{14}N_2O_3$–$^{14}N_2O_4$ in the solid phase in the 14-μ region. Spectrum *A* is from an unannealed solid at $-144°C$, Spectrum *B* from the same sample at $-117°C$, and Spectrum *C* from the same sample after recooling to $-145°C$.

In Table VI, the frequencies of absorption bands, which may be assigned to some unstable forms of N_2O_3, are listed. These bands disappear irreversibly and, thus, cannot be attributed to crystal phase transition such as the one reported by Reed and Lipscomb.[17] The broad total absorption observed in many of our runs with thick samples in the low frequency region of the spectrum (cf. Fig. 6) indicates that there may be more unstable bands in this region, although we were not able to identify any.

The number of observed bands is hardly enough to make a conclusive assignment, but a reasonable interpretation of these bands can be made by relying on the characteristic frequencies of vibrational modes in nitrogen oxides. Furthermore, only one plausible isomer of N_2O_3 of ONONO structure need be assumed to explain these absorption bands. As Fateley *et al.* pointed out, this isomer should have two bands in the N=O

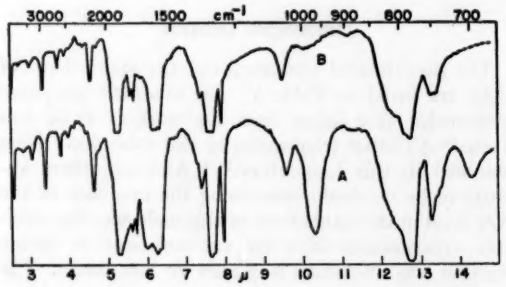

FIG. 4. Infracord spectra of $^{14}N_2O_3$–$^{14}N_2O_4$ in the solid phase. Spectrum *A* from an unannealed sample and *B* from the same sample after annealing.

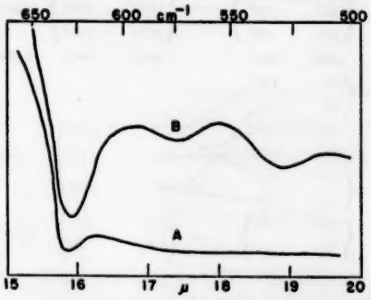

FIG. 6. The spectra of $^{14}N_2O_3$–$^{14}N_2O_4$ in the solid phase in the 18-μ region. Spectrum *A* from unannealed solid at $-164°C$ and *B* from the same sample after annealing and recooling.

[16] W. J. Dulmage, E. A. Meyers, and W. N. Lipscomb, Acta Cryst. **6**, 760 (1953).

[17] T. B. Reed and W. N. Lipscomb, Acta Cryst. **6**, 781 (1953).

stretch region. However, beside the two bands at 1900 cm^{-1} and 1830 cm^{-1} observed by these authors, we find another band of moderate intensity in this region. The 1900-cm^{-1} band appears somewhat too high for the N=O stretching frequency since even in FNO the corresponding frequency is 1844 cm^{-1}.[18] Furthermore, Fateley *et al.* reported that the intensity of the 1900 cm^{-1} band was much lower than that of 1830 cm^{-1}. It seems reasonable, therefore, to choose 1830 and 1677 cm^{-1} bands for the two N=O stretching modes of the ONONO isomer. This choice is, moreover, in line with the 1829 and 1645 cm^{-1} assigned to simliar modes in $ONONO_2$. The remarkable band at 964 cm^{-1} and the lowest frequency band at 699 cm^{-1} can then be assigned to the N—O stretching and NO_2 deformation modes respectively. In nitric[19] and nitrous[20] acids, the N—O stretching frequencies are reported to be, respectively, 925 and 856 cm^{-1}.

[18] R. J. Woltz, E. A. Jones, and A. H. Nielsen, J. Chem. Phys. **20**, 378 (1952).
[19] H. Cohn, C. K. Ingold, and H. G. Poole, J. Chem. Soc. (London) **1952**, 4272.
[20] L. H. Jones, R. M. Badger, and G. E. Moore, J. Chem. Phys. **19**, 1599 (1951).

TABLE VI. Absorption bands of unstable N_2O_3 species (cm^{-1}).

$^{14}N_2O_3$	$^{15}N_2O_3$	Assignment
1900[a]	...	2×964 = 1928 or other combination
1830[a]	...	N=O stretch
1677 ms	1648 s	N=O stretch
964 s	947 m	N—O stretch
699 mw	693 m	NO_2 deformation

[a] W. G. Fateley, H. A. Bent, and B. Crawford.[4]

SUMMARY

Neither our present investigations nor those of Fateley, Bent, and Crawford[4] by themselves appear conclusive in establishing the existence of the interesting isomers of N_2O_4 and N_2O_3. However, from these data combined and with the considerable amount of information which has now accumulated on the stable forms of these nitrogen oxides, we are perhaps justified in concluding that the existence of these isomers is no longer questionable. At least, the earlier authors need not regard the staggered N_2O_4 with healthy skepticism any more.

Spin Densities in Organic Free Radicals*

THOMAS H. BROWN,† D. H. ANDERSON,‡ AND H. S. GUTOWSKY

Noyes Chemical Laboratory, University of Illinois, Urbana, Illinois

(Received March 30, 1960)

The proton hyperfine constants obtained from proton magnetic resonance spectra of polycrystalline free radicals and from valence bond calculations of π-orbital spin densities are compared for the free radicals α,α'-diphenyl-β-picryl hydrazyl, and *tris*-*p*-chlorophenylaminium perchlorate. Two lines are observed in the proton magnetic resonance spectra, one shifted upfield and one downfield from the normal resonance frequency. These are assigned to the *ortho* and *para* protons, and the *meta* protons of the free radicals, respectively. Though the agreement between theory and experiment is not quantitative for the hyperfine constants, the theoretical and experimental ratios of hyperfine constants agree within experimental error. This serves to verify the existence of positive and negative spin densities and the signs of some of the relationships involved.

I. INTRODUCTION

THE nuclear spin-electron spin coupling in organic free radicals is an important source of detailed information concerning molecular electronic structure. Usually, the nuclear hyperfine coupling constant a_i is obtained by observing the splitting of the electron magnetic resonance spectrum.[1,2] The experimental value is then compared with the results of calculations for various theoretical models of the free radical. In this paper we are concerned with proton hyperfine constants obtained from observations of the *nuclear* magnetic resonance shifts in the solid free radicals α, α'-diphenyl-β-picryl hydrazyl (DPPH) and *tris*-*p*-chlorophenylaminium perchlorate (TPPAP). A brief account has been given[3] of such observations and preliminary valence-bond calculations which demonstrated the existence of both positive and negative proton coupling constants in DPPH. Similar observations are reported here for TPPAP and the details of the calculations are presented for both substances.

In these substances, we consider the values of a_i to be determined very largely by the contact term[4]

$$a_i=(8\pi/3h)g_e g_i \beta_e \beta_N [\Psi(0)]_i^2, \qquad (1)$$

where $[\Psi(0)]_i^2$ is the density of the unpaired electron at the ith nucleus, and the g and β are the g factors and magnetons for the electron and nucleus. The calculations of the coupling constants are conveniently expressed in terms of the spin densities[5–8] ρ_i at the various nuclei in a radical. For protons attached to carbon atoms in an aromatic ring, the proton hyperfine splitting results from a $\sigma-\pi$ exchange interaction,[5,9–11] for which McConnell[5–7] has given an approximate semiempirical relation between the π-electron spin density at the carbon and a_H. This relation,

$$a_H=-22.5\rho_C, \qquad (2)$$

where a_H is the splitting in gauss of the electron resonance, is *approximately* independent of the substituents in the aromatic system. We will calculate ρ_C from the wave function and then use Eq. (2) to obtain values of a_H for comparison with experiment.

Simple valence bond and molecular orbital calculations have been attempted for a number of free radicals[5,6,8–16]; however, the agreement with experiment varies considerably from radical to radical. Two general types of radicals have been distinguished. These are the even-alternate radicals, of which the aromatic hydrocarbon negative ions[17,18] are examples, and the odd-alternate radicals such as DPPH,[19,20] perinaphthyl,[21]

* Acknowledgment is made to the donors of the Petroleum Research Fund, administered by the American Chemical Society, and to the Office of Naval Research and E. I. du Pont de Nemours and Company for partial support of this research.

† Postdoctoral Fellow, Division of General Medical Sciences, United States Public Health Service.

‡ Now at Sandia Corporation, Albuquerque, New Mexico.

[1] C. Kikuchi and V. W. Cohen, Phys. Rev. **93**, 394 (1954).

[2] C. A. Hutchinson, R. C. Pastor, and A. G. Kowalsky, J. Chem. Phys. **20**, 534 (1952).

[3] H. S. Gutowsky, H. Kusumoto, T. H. Brown and D. H. Anderson, J. Chem. Phys. **30**, 860 (1959). Independent experimental evidence for the negative sign in Eq. (2) and for negative spin densities on carbon atoms has been obtained in several studies; see footnote reference 42 and prior work cited there.

[4] E. Fermi, Z. Physik **60**, 320 (1930).

[5] H. M. McConnell, J. Chem. Phys. **24**, 632, 764 (1956).

[6] H. M. McConnell and H. H. Dearman, J. Chem. Phys. **28**, 51 (1958).

[7] H. M. McConnell and D. B. Chesnut, J. Chem. Phys. **28**, 107 (1958); **27**, 984 (1957).

[8] H. S. Jarrett and G. J. Sloan, J. Chem. Phys. **22**, 1783 (1954).

[9] B. Venkataraman and G. K. Fraenkel, J. Chem. Phys. **24**, 737 (1956).

[10] R. Bersohn, J. Chem. Phys. **24**, 1066 (1956); Arch. sci. (Geneva) **11**, 12 (1958).

[11] S. I. Weissman, J. Chem. Phys. **25**, 890 (1956).

[12] P. Brovetto and S. Ferroni, Nuovo cimento **5**, 142 (1957).

[13] H. M. McConnell, J. Chem. Phys. **28**, 1188 (1958); **29**, 244 (1958).

[14] D. B. Chesnut, J. Chem. Phys. **29**, 43 (1958).

[15] G. J. Hoijtink, Mol. Phys. **1**, 157 (1958).

[16] A. D. McLachlan, Mol. Phys. **1**, 233 (1958).

[17] R. L. Ward and S. I. Weissman, J. Am. Chem. Soc. **76**, 3612 (1954).

[18] R. C. Pastor and J. Turkevich, J. Chem. Phys. **23**, 1731 (1955).

[19] A. N. Holden, C. Kittel, F. R. Merritt, and W. A. Yager, Phys. Rev. **77**, 147 (1950).

[20] C. H. Townes and J. Turkevich, Phys. Rev. **77**, 148 (1950).

[21] P. B. Sogo, M. Nakazaki, and M. Calvin, J. Chem. Phys. **26**, 1343 (1957).

and the triphenyl aminium salts.[22,23] For radicals of the first type, the results of molecular orbital[5,24] and valence-bond calculations[25] agree with experiment and with each other, though not always to the extent that one might wish. However, for odd-alternate radicals, simple molecular orbital calculations yield positive spin densities of reasonable magnitude or zero values depending upon the position in the molecule.[6,10] The valence-bond calculations, on the other hand, yield both positive and negative spin densities, all of reasonable magnitude, with the negative spin densities occurring at those positions which were zero in the molecular orbital case.[5-7,10,12,13] Inasmuch as we present experimental evidence for the existence of negative spin densities, we employ a valence-bond approach in our calculations.

II. EXPERIMENTAL PROCEDURE AND RESULTS

The experimental magnitudes and signs of the proton hyperfine constants reported here were determined by observing the proton magnetic resonance spectra of solid molecular free radicals. The magnitudes of the hyperfine constants in free radicals are usually obtained from the hyperfine splittings observed in electron magnetic resonance spectra. The energy levels involved are given by the expression

$$E=g_e\beta_e H_0 m_S-\sum_i g_i\beta_N H_0 m_i+\sum_i a_i g_e\beta_e m_S m_i, \quad (3)$$

where a_i in the hyperfine interaction term is here the splitting in gauss of the electron magnetic resonance by the ith nucleus.[26] The selection rules for electron magnetic resonance are $\Delta m_S=\pm 1$ and $\Delta m_i=0$; and for nuclear magnetic resonance, $\Delta m_S=0$ and $\Delta m_i=\pm 1$. The symmetry of the hyperfine interaction in the plus and minus values of m_S and m_i makes it impossible to determine the sign of a_i from the splittings and transition frequencies. Changing the sign of a_N simply interchanges the hyperfine components within the NMR spectrum and also within the electron resonance.

However, at thermal equilibrium, the upper energy levels are labeled by their decreasing population, and the order of the levels does depend upon the sign of a_N. This difference produces small differences in the intensities of the hyperfine components of both the electron and nuclear magnetic resonances, which in principle could be used to establish the sign of a_N. Unfortunately, the differences in intensity produced by changing the sign of a_N are of the order of one part in 10^3 and too small for practical use except at very low temperatures. A more readily observed effect results[3,7] when the hyperfine structure is averaged out by some dynamic process, such as a short electron T_1 or by electron exchange as in our experiments on solid DPPH and TPPAP. In this case, the hyperfine splitting term becomes

$$\sum_i a_i g_e\beta_e\langle m_S\rangle_i m_i, \quad (4)$$

where $\langle m_S\rangle_i$ is the average value of m_S in radicals with nuclear spin states defined by m_i. The value of $\langle m_S\rangle_i$ is determined by the populations of the $m_S=+\frac{1}{2}$ and $m_S=-\frac{1}{2}$ states for which the i nuclear spins have specific values m_i; in particular we find that

$$\langle m_S\rangle_i=\sum_{m_S} N_{S_i} m_S/\sum_{m_S} N_{S_i}\cong -g_e\beta_e H_0/4kT. \quad (5)$$

The N_{S_i} are the populations of radicals in which the electron and nuclear spin states are m_S and m_i. The last step in Eq. (5) makes the reasonable approximations that $kT\gg|g_e\beta_e H_0|\gg|g_i\beta_N H_0|$, $|a_i g_e\beta_e|$. Upon substituting Eqs. (4) and (5) in Eq. (3), we find that the ΔE corresponding to nuclear magnetic resonance, i.e., $\Delta m_i=\pm 1$, $\Delta m_S=0$, is given as

$$\Delta E=g_i\beta_N H_0+a_i g_e\beta_e(g_e\beta_e H_0/4kT). \quad (6)$$

The net effect of the averaged hyperfine interaction is thus a displacement of the ith nuclear resonance by an amount and direction depending upon the sign and magnitude of a_i. The effect is similar to the Knight shift[27] produced by the conduction electrons in metals and also to the dynamic averaging of other types of NMR splittings and shifts.[28] The averaging out of the hyperfine splitting occurs when either the electron exchange time τ or the electron T_1 is short enough that its reciprocal exceeds $a_i g_e\beta_e$. In our experiments, the proton resonance was observed with a fixed frequency spectrometer,[29] in which case Eq. (6) predicts a difference,

$$\Delta H=H^*-H_0=-a_i(\gamma_e/\gamma_H)(g_e\beta_e H_0/4kT), \quad (7)$$

between H^*, the magnetic field required for the resonance of the ith group of protons in the radical, and H_0, the resonance field for protons not subjected to any hyperfine interaction. The γ are the magnetogyric ratios $g\beta$.

Of the two free radicals considered here, the experimental results for α,α'-β-picryl hydrazyl (DPPH) have been reported previously.[3] For *tris*-*p*-chlorophenylaminium perchlorate[23] (TPPAP), the derivative of the proton resonance was observed[29] at 77°K in a polycrystalline sample at 26.90 Mc. The integrated line shape, as given in Fig. 1, can be resolved into two components with the same intensity but different widths, one shifted upfield by 3.90 gauss and the other downfield by 2.30 gauss from the proton resonance in a diagmagnetic reference sample. For this particular radical, there are only two types of protons, the *ortho*

[22] R. S. Codrington, J. D. Olds, and H. C. Torrey, Phys. Rev. **95**, 607A (1954).
[23] R. I. Walter, J. Am. Chem. Soc. **77**, 5999 (1955).
[24] E. de Boer, J. Chem. Phys. **25**, 190 (1956).
[25] T. H. Brown, H. S. Gutowsky and J. C. Schug (to be published).
[26] Absolute values are used for g_e, g_N, β_e, and β_N.
[27] W. D. Knight, Phys. Rev. **76**, 1259 (1949).
[28] H. S. Gutowsky, D. W. McCall and C. P. Slichter, J. Chem. Phys. **21**, 279 (1953); H. S. Gutowsky and A. Saika, *ibid.* **21**, 1688 (1953).
[29] H. S. Gutowsky, L. H. Meyer and R. E. McClure, Rev. Sci. Instr. **24**, 644 (1953).

and *meta* ring protons, and the assignments are simpler than in the case of DPPH. In the latter, under the same conditions as for TPPAP, the four proton resonance components expected were only partially resolved into two components of unequal widths but having the same intensity, one shifted upfield by 2.95 gauss, the other downfield by 1.75 gauss.[3] The assignments are based upon the results of the theoretical calculation discussed in the next section.

III. CALCULATION OF SPIN DENSITIES

A typical structure for each of the two free radicals considered is given by Formulas (I) and (II), respectively. The calculations

DPPH

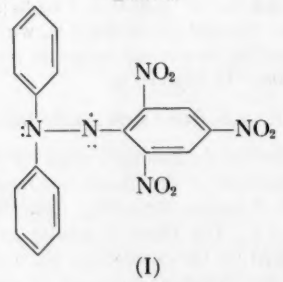

(I)

TPPAP

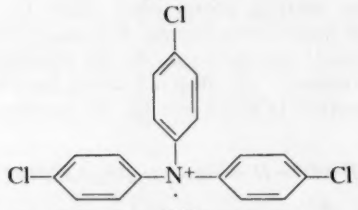

(II)

of the ground-state wave functions are quite similar to those reported previously for triphenyl methyl.[12] For our two radicals, only the mono-phenyl aminyl fragment need be considered in detail. The rules developed by Pauling and Wheland[30] can then be used to extend the results to the biphenyl and triphenyl cases. For the mono-phenyl aminyl fragment, the three types of structures which enter into the ground state are Formulas (III)–(V):

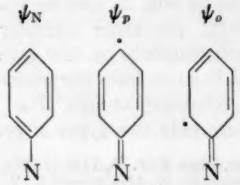

(III) (IV) (V)

[30] L. Pauling and G. Wheland, J. Chem. Phys. **1**, 362 (1933).

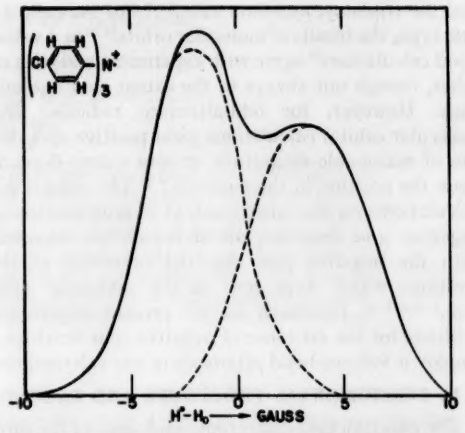

FIG. 1. The proton magnetic resonance absorption observed at 26.90 Mc in polycrystalline *tris-p*-chlorophenylaminium perchlorate (TPPAP) at 77°K. H^* is the magnetic field applied to the sample while H_0 (~6310 gauss) is that at which the proton resonance occurred in a diamagnetic reference, corrected for bulk magnetic susceptibility differences.

The wave function is the linear combination given by Eq. (8),

$$\Psi = c_1\psi_N + c_2\psi_p + c_3\psi_o, \tag{8}$$

where ψ_N represents the contribution of structures where the unpaired electron is on the nitrogen atom, ψ_p on the *para* position, and ψ_o on the *ortho* positions. It is important to note that, within the framework of simple valence bond theory, it is not possible to draw structures which have the unpaired electron on the *meta* ring positions.

By using simple valence-bond theory, which considers only near-neighbor interactions, and simple overlap, the coefficients c_1, c_2, and c_3 may be obtained. From these, using the spin-density operator given by McConnell,[7]

$$(\rho_A)_{ij} = \langle \psi_i \mid \boldsymbol{P}_A \mid \psi_j \rangle = (1/S_z)\langle \psi_i \mid \sum_k \Delta_A(k)\boldsymbol{S}_{kz} \mid \psi_j \rangle, \tag{9}$$

the spin densities in the various orbitals may be obtained. In Eq. (9), $(\rho_A)_{ij}$ represents the contribution to the π-orbital spin density at atom A from structures i and j. The total π-orbital spin density at atom A, ρ_A, is then obtained by the appropriate use of Eq. (8). The values of the spin densities given by Eq. (9) can be obtained by modification of the Pauling rules concerning the coefficients of exchange integrals from superpositions diagrams.[6,12] We now consider in detail the calculations and results obtained for the two free radicals.

A. DPPH

The usual structural formula for DPPH is Formula (I). However, even though the unpaired electron is allotted to the nitrogen adjacent to the picryl ring, it is

clear that, in order for the radical to be stable, the unpaired electron must be considerably delocalized over both sets of ring systems. Stability of this type is evidenced in the contrast between the triphenyl methyl radical and the considerably more reactive phenyl methyl radical. In addition, electron magnetic resonance studies[2] indicate large spin densities on both the central nitrogen atoms of DPPH. The only plausible way in which the unpaired electron can migrate onto the phenyl rings and onto the other nitrogen is to assume that an ionic structure contributes to the molecular wave function. Therefore, we represent the ground state of DPPH as a superposition of the two structures, Formulas (VI) and (VII):

$$\phi_2\ddot{N}-\dot{\ddot{N}}-P \qquad \phi_2\overset{\cdot+}{\ddot{N}}-\overset{\cdot-}{\ddot{N}}-P,$$

(VI) (VII)

where ϕ is a phenyl ring and P a picryl ring. The coordinate pair of electrons on each nitrogen atom has been drawn in for clarity. The fact that (VI) allows migration *only* onto the picryl ring and (VII) *only* onto the phenyl rings, suggests that the calculation may be decomposed into two parts involving the monophenyl aminyl (MPA) and the biphenyl aminium (BPA) fragments. As a further simplification, the nitro groups on the picryl ring as well as the positive charge on the aminium nitrogen will not be considered. The problem has thus become one of calculating the unpaired electron spin densities of MPA and BPA, Formulas (VIII) and (IX). Each fragment will be assigned 0.5 electron, which assumes

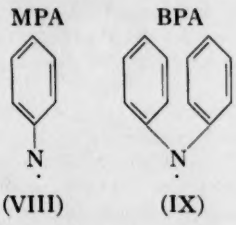

(VIII) (IX)

that (VIII) and (IX) make approximately equal contributions to the ground-state wave function. This assumption will be considered in the discussion section.

TABLE I. Electron spin densities at the nitrogen and carbon nuclei in the monophenyl aminyl (MPA) and biphenyl aminium (BPA) fragments. The values were calculated via Eqs. (8) and (9) using 1.2 for the ratio α of the carbon-nitrogen to the carbon-carbon exchange integral.[a]

	ρ_N	ρ_{IC}	ρ_o	ρ_m	ρ_p
MPA	+0.300	−0.160	+0.185	−0.100	+0.190
BPA	+0.266	−0.129	+0.131	−0.060	+0.122

[a] ρ_{IC} is the spin density at the carbon to which the nitrogen is attached; ρ_o, ρ_m, and ρ_p are the spin densities at the carbons *ortho*, *meta*, and *para* to the 1-carbon.

TABLE II. Electron spin densities at the nitrogen and carbon nuclei in *tris*-*p*-chlorophenylaminium perchlorate as a function of α, the ratio of the carbon-nitrogen and carbon-carbon exchange integrals.[a]

$\rho \backslash \alpha$	0.5	0.8	1.0	1.2	1.5	2.2
ρ_N	+0.800	+0.646	+0.562	+0.484	+0.430	+0.331
ρ_{IC}	−0.191	−0.224	−0.228	−0.219	−0.227	−0.215
ρ_o	+0.135	+0.181	+0.200	+0.213	+0.225	+0.239
ρ_m	−0.076	−0.096	−0.104	−0.109	−0.113	−0.116
ρ_p	+0.140	+0.171	+0.182	+0.189	+0.193	+0.192
ρ_o/ρ_m	−1.78	−1.89	−1.93	−1.96	−1.99	−2.06

[a] ρ_{IC} is the spin density at the carbon to which the nitrogen is attached; ρ_o, ρ_m, and ρ_p are the spin densities at the carbons *ortho*, *meta*, and *para* to the 1-carbon.

The absolute values of the energy levels are not required; all that is needed to solve the secular equation which leads to the ground-state wave function is the ratio α of the carbon-nitrogen to the carbon-carbon exchange integral. By using a value of 1.2 for this ratio, which is based on an analysis of bond energies, the following values are obtained for the coefficients in Eq. (8):

	c_1	c_2	c_3
MPA	−0.334	−0.254	−0.280
BPA	−0.134	−0.117	−0.138.

The effect of varying the ratio of the exchange integrals will be discussed in more detail in the following section.

By combining Eqs. (8) and (9), the spin densities at the various nitrogen and carbon nuclei can be expressed in terms of the coefficients c_1, c_2, and c_3. The results for the two fragments, using the numerical values of c_1, c_2, and c_3 given above for $\alpha = 1.2$, are listed in Table I.[31] A comparison of these results with experiment will be given in the concluding section.

B. TPPAP

The calculation of the spin densities in TPPAP, of which a typical structure is (II), proceeds in a fashion similar to the calculations for DPPH and triphenyl methyl.[12] The preliminary calculations for TPPAP neglect the effect of the chlorine substituents.[32] Because of the uncertainty in the value of the carbon-nitrogen exchange integral involving the charged nitrogen and because the assignment of the proton shifts observed for this radical is unambiguous, the calculations were performed using several values of α, the ratio of the carbon-nitrogen to carbon-carbon exchange in-

[31] The results for DPPH are slightly different from those reported earlier in footnote reference 3. The details of the ground-state wave function calculation and the expressions for the spin densities in DPPH may be found elsewhere, David H. Anderson, Ph.D. thesis, University of Illinois, 1959. The formulas for ρ_{IC} on pp. 90 and 114 are in error, which changes slightly the numerical results reported therein.

[32] This assumption seems to be a reasonable first approximation in light of the relatively small effect chlorine has on the proton hyperfine constants in substituted semiquinones, as shown by the experimental results of B. Venkataraman, B. G. Segal, and G. K. Fraenkel, J. Chem. Phys. **30**, 1006 (1959).

TABLE III. Experimental and theoretical values for the proton hyperfine splitting constant in DPPH and TPPAP, in units of gauss splitting of the electron spin resonance.

Radical	Type of proton	Theory[a,b]	Expt[c]
DPPH	*ortho* (phenyl)	−2.94	−1.63
	para (phenyl)	−2.74	−1.63
	meta (phenyl)	+1.55	+0.97
	meta (picryl)	+2.55	+0.97
	$(ortho)_{Av}/(meta)_{Av}$	−1.82	−1.68
TPPAP	*ortho*	−4.77	−2.16
	meta	+2.29	+1.27
	(*ortho*)/(*meta*)	−1.96	−1.70

[a] See footnote reference 31.

[b] Calculated for $\alpha=1.2$; see Table II and footnote reference 38 for other values for TPPAP.

[c] The values for DPPH are from the two proton resonance lines resolved, each of which presumably has two unresolved components.

tegral. The results are listed in Table II. It should be pointed out that in the calculations reported here for both radicals the rules used to obtain the spin densities at the various carbon positions were modified when considering the central nitrogen atoms.[33]

IV. DISCUSSION

By means of Eq. (7), values for the proton hyperfine constant a_H, including the sign, can be obtained from the proton shifts observed in the solid free radicals. Also, Eq. (2) can be used to calculate a_H from the theoretical spin densities at the carbons. Table III lists such theoretical values, for $\alpha=1.2$, as well as the experimental values from the proton shifts. The assignments for the experimental results were made by comparing the experimental values with the relative magnitudes of the theoretical results.

A. DPPH

The results in Table III indicate that the proton hyperfine constants are negative at the *ortho* and *para* positions and positive at the *meta* positions. Unfortunately, the theoretical values of a_H for DPPH are based upon such an approximate model that better agreement between the experimental and theoretical magnitudes probably cannot be expected. It should also be noted that the dipolar contribution to the proton shift was neglected in the calculation. However, even though the magnitudes of a_H depend upon good values for exchange integrals, relative electron affinities of the aromatic rings, and other quantities which are difficult obtain, the resulting errors in a_H tend to be systematic, as shown in Table II. Consequently, it is better to compare the ratios of the splitting constants than their magnitudes.

The proton resonance observed upfield is assigned to the unresolved absorption of the four *ortho* and two *para* protons and that downfield, to the four *meta* (phenyl) and two *meta* (picryl) protons. The ratio of these shifts is −1.68. To obtain a comparable theoretical value, we take the weighted averages of the corresponding a_H and obtain a theoretical ratio of −1.82. The agreement between these ratios is excellent inasmuch as the difference between the two is within the intrinsic error of decomposing the experimental curve into components. The approximate agreement between the experimental and theoretical a_H, and the quantitative agreement between the experimental and theoretical ratios confirm the existence of positive and negative spin densities.

The results actually give us more information since the theoretical values leave little doubt that the *ortho* and *para* protons have shifts which are larger in magnitude than those of the *meta* protons. The experiments demonstrate that the upfield proton shift is larger than the downfield. Therefore, the upfield shift is assigned to the *ortho* and *para* protons. However, in view of Eq. (7), a_H for the upfield protons must be ***negative***. But the approximate valence bond treatment shows that the *ortho* and *para* carbon spin densities are ***positive***, and hence the sign of a_H is the ***opposite*** of the spin density on the adjacent carbon, as given in Eq. (2). The ratio of the *ortho* and *para* spin densities are relatively insensitive to the parameters in the calculation, so this conclusion seems unambiguous.

Now let us return to our rather arbitrary assignment of 0.5 electron, each, to the MPA and BPA fragments used in the theoretical treatment. The actual electron distribution can be represented to a better approximation by alloting a different fraction of the unpaired electron to each fragment. However, if the fractions differed very much from 0.5, the agreement between the experimental and theoretical ratios of a_H for the *ortho* and *meta* protons would suffer,[34] indicating that the assignment of 0.5 electron to each fragment is a good approximation.

A final point concerns the relative electron spin densities on the nitrogen atoms. Our theoretical results summarized in Table I give an electron spin density which is 13% greater at the nitrogen adjacent to the picryl ring than at the nitrogen adjacent to the phenyl rings. Recent detailed studies of the hyperfine splittings by the two central nitrogen atoms in solutions of DPPH indicate that they are not equal.[35] The ratio of the two nitrogen hyperfine constants was found to be 0.82± 0.01. Because of the different bonding of these two atoms and the effects of the nitro groups on the picryl ring, one would expect the ratio of the nitrogen hyperfine constants to differ somewhat from the ratio of the π-orbital spin densities given here. In addition, the contributions to the nitrogen splittings from spin densities on adjacent atoms are not known, but the

[33] T. H. Brown and J. C. Schug (unpublished results).

[34] The theoretical ratio can be fitted to the observed ratio of −1.68 by assigning different fractions of an electron to the two fragments; this gives 0.525 and 0.475 electrons to MPA and BPA, respectively.

[35] R. M. Deal and W. S. Koski, J. Chem. Phys. **31**, 1138 (1959).

agreement of the theoretical ratio of the nitrogen spin densities ($\rho_N/\rho_{N'}=0.89$)[36] with the ratio of experimental hyperfine constants, 0.82, is, however, encouraging. The experimental results obtained so far do not indicate which nitrogen atom has the greater hyperfine constant.[35] Recently, both the isotropic and anisotropic contributions to the nitrogen hyperfine constants in DPPH have been investigated in experiments[37] on dilute single crystals containing N^{15}. There is, however, an ambiguity in the interpretation of the hyperfine tensor such that there are two choices for the isotropic and anisotropic contributions to $a_{N'}$, i.e., for the β-nitrogen, and two values for the ratio $a_N/a_{N'}$. Studies in liquid solution of the N^{15} DPPH are needed, apparently, to resolve the question, or else detailed calculations of the hyperfine constants from the π-orbital spin densities.

B. TPPAP

With this free radical, as in the case of DPPH, the quantitative agreement between the theoretical and experimental values of the proton hyperfine constant is not too good. However, the ratio of the theoretical hyperfine constants as given in Table III agrees well with experiment and can, in fact, be fitted by varying the parameter α as shown in Table II.[38] Though it is probably not meaningful to fit the theoretical value of the ratio to experiment, the agreement between theory and experiment supports the existence of both positive and negative spin densities.[3] In addition, it is concluded that the sign of a_H is opposite to the sign of the observed proton shift and of the theoretical spin densities at the carbons.[3] These conclusions are the same as those reached in the case of DPPH and should hold quite generally for this type of free radical.

In contrast to the case of DPPH, the comparison between theory and experiment for TPPAP can be made without considering unresolved lines and average values of shifts, except insofar as they might arise from nonequivalence of protons in the crystal unit cell. Within the existing framework of the calculation, one might first consider the value of the ratio of exchange integrals α, discussed previously. It is seen, however, from Table II that, though α has a small effect on the spin densities at the *ortho* and *meta* positions, it can not provide the factor of two which is necessary for quantitative agreement between theory and experiment.

However, the spin density on the nitrogen atom is quite sensitive to the value of α. It is possible that comparison of theoretical values for a_N obtained from the spin densities given here, with experimental results[39] will serve to determine the best value of α. In this way values for some of the integrals occurring in the valence bond theory may possibly be obtained from good experimental values of hyperfine constants.

Though the measurements of the proton shifts in free radicals give the sign of the hyperfine constant as well as a value for its magnitude, a more accurate method for determining the latter is the measurement of electron magnetic resonance splittings. A comparison of the results of the two methods would be useful in the present case in determining the extent of the dipolar contribution to the proton shifts in the solid free radicals and as a further check on the results of the theoretical calculations. Unfortunately, in the case of both TPPAP[39] and DPPH,[2,35] no proton splittings of the electron magnetic resonance have been resolved.[40] It is clear, however, from the number of nonequivalent magnetic nuclei present, that in DPPH there may be as many as 17 875 transitions. All that is necessary to account for the apparent absence of proton splittings, therefore, is to assume that the protons have several much smaller hyperfine constants than the central nitrogen nuclei. Kaplan,[41] in fact, has ascribed the width of the rather broad nitrogen hyperfine lines to unresolved proton lines, using the values given previously for a_H.[3]

In the case of TPPAP, however, one would predict a maximum of only 147 lines in the electron magnetic resonance spectrum, neglecting the chlorine nuclei. The value of a_N is fairly large, about 10 gauss,[39] and even if the proton splittings cannot be resolved completely, the general shape of the envelope of partially resolved lines is sensitive to the values of a_H. In particular, it may be possible to differentiate between the theoretical and experimental sets of values for a_H given in Table III.

C. General Comments

Further comment is warranted on the relatively poor quantitative agreement between the calculated and experimental spin densities for both radicals, even

[36] A ratio $\rho_N/\rho_{N'}=0.93$ was obtained for DPPH by R. Bersohn, footnote reference 10, using a molecular orbital calculation. This result, however, suffers from the difficulties mentioned in the introduction.

[37] R. W. Holmberg, R. Livingston and W. T. Smith, J. Chem. Phys. 33, 540 (1960).

[38] The effect of varying α in the DPPH calculations gives results similar to those in Table II (see footnote reference 31). A more complete calculation using all of the canonical structures for the phenyl aminium fragment gives agreement between the theoretical and experimental ratios for a value of α of 1.0; T. H. Brown and J. C. Schug (unpublished calculations).

[39] O. R. Gilliam, R. I. Walter and V. H. Cohen, J. Chem. Phys. 23, 1540 (1955).

[40] *Note added in proof.* Partial resolution of the proton hyperfine splitting has just been reported by Y. Deguchi [J. Chem. Phys. 32, 1584 (1960)] for DPPH in carefully purified solvents. A continuous series of fairly regular splittings of about 0.45 gauss is observed in addition to the much larger splittings of 10 gauss produced by the N^{14} nuclei. The intensity distribution leads us to suggest that each nitrogen hyperfine component is split by the protons into a series of lines extending over a range of about 15 gauss, certainly no less than the N^{14} splitting of 10 gauss. The extent to which the protons should split each N^{14} hyperfine component is given by $\Sigma_H \mid a_H \mid$. The values for a_H obtained from our observations of the proton shifts in solid DPPH are given in Table III. They lead to a value for $\Sigma_H \mid a_H \mid$ of 15.6 gauss which agrees with our interpretation of the ESR spectrum reported by Deguchi.

[41] J. I. Kaplan; (private communication).

though ratios of the densities at the various ring carbons agree reasonably well. There is some evidence[33] that valence-bond structures in addition to those considered here and in earlier treatments of odd-alternant radicals may contribute appreciably to the ground state of DPPH and TPPAP. The extent to which they also contribute to the spin densities is presently being investigated. Also, it should be remembered that in the calculation of the hyperfine coupling and proton shifts we neglected the anisotropic contribution, which arises mainly from the electron-spin, nuclear-spin dipolar interaction.[42]

The contribution can be of the same order[42] as the isotropic interaction which we also treat. However, in polycrystalline samples such as we used, the anisotropic component of the hyperfine interaction tensor would produce a distribution of proton resonance shifts and hence broaden the proton resonance, and perhaps shift its center of gravity as well. It is difficult to determine experimentally the extent of such broadening, because of the partial resolution of the proton resonance components in DPPH and TPPAP. However, the second moments of the two proton resonance components for TPPAP, in Fig. 1, suggest that any "anisotropy broadening" is a modest fraction ($<\frac{1}{2}$) of the isotopic shift. Moreover, the fact that the proton resonance components are symmetrical indicates that any anisotropy is itself "symmetrical" about the average shift, which must, therefore, be that from the isotropic part of the hyperfine splitting.

To be sure, these arguments are qualitative and subject to considerable experimental uncertainty. They are nonetheless compatible with the detailed treatment by McConnell *et al.*[42] of the proton hyperfine splitting tensor in the $CH(CO_2H)_2$ radical in a single crystal of malonic acid. In any event, the existence of "anisotropy broadening" of the proton resonance in TPPAP is supported by the upfield proton line, in Fig. 1, which is not only shifted more than the downfield line but also is appreciably broader. Part of this greater breadth can arise from larger proton-proton dipolar broadening, which would be expected for the *ortho* protons. In addition, the proton spin-lattice relaxation times are short enough to broaden the proton resonances appreciably; attempts to measure them by rf pulse methods indicate that they are of the order of 100 μsec. Such relaxation no doubt arises from the large magnetic fields produced at the protons by the electrons and the resultant broadening would be proportional to the proton resonance shift. In conclusion, if the crystal structure were known in detail and the proton lines could be completely resolved in experiments at higher fields and lower temperatures, it should be possible in principle to obtain all three diagonal components of a nuclear hyperfine splitting tensor from a study of the nuclear resonance shifts and absorption line shapes in a polycrystalline free radical.

[42] H. M. McConnell, C. Heller, T. Cole, and R. W. Fessenden, J. Am. Chem. Soc. **82**, 766 (1960). We are indebted to a kindly referee who pointed out the relevance of this work to ours.

ACKNOWLEDGMENTS

We wish to express our thanks to Professor Martin Karplus for helpful discussions and to John Schug for assistance in some of the calculations. Our appreciation is extended to Professor R. I. Walter for generously supplying the samples of the *tris-p*-chlorophenylaminium perchlorate used in our experiments.

THE JOURNAL OF CHEMICAL PHYSICS VOLUME 33, NUMBER 3 SEPTEMBER, 1960

Nuclear Magnetic Resonance Spectra of Systems of the A_3B_2C Type: Proton Magnetic Resonance Spectra and the Absolute Signs of the Proton-Proton Spin Coupling Constants in Ethyl Acetylene and Ethyl Mercaptan

P. T. NARASIMHAN* AND MAX T. ROGERS

Kedzie Chemical Laboratory, Michigan State University, East Lansing, Michigan

(Received March 17, 1960)

The high-resolution proton magnetic resonance spectra of ethyl acetylene and ethyl mercaptan have been studied at both 40 Mc and 60 Mc. Theoretical analysis of these spectra as systems of the A_3B_2C type enables one to determine the relative signs of the proton-proton spin coupling constants in these molecules. It is thus shown that the spin coupling constants $J_{CH_3-CH_2}$ and J_{CH_2-CH} are of opposite sign in ethyl acetylene, while $J_{CH_3-CH_2}$ and J_{CH_2-SH} in ethyl mercaptan are of the same sign. Making use of the results of the valence bond theory regarding the absolute sign of $J_{CH_3-CH_2}$ the present analysis has made possible determinations of the absolute sign of J_{CH_3-CH} and J_{CH_2-SH} in ethyl acetylene and ethyl mercaptan, respectively.

I. INTRODUCTION

THE relative signs of nuclear spin-spin coupling constants in some molecules have been obtained recently[1–12] from high resolution nuclear magnetic resonance (NMR) spectra. There is increasing theoretical interest in the signs of these spin coupling constants but it has as yet not been possible to obtain directly the absolute signs of coupling constants experimentally. It can be shown that the usual form of the Hamiltonian used for the theoretical calculation of NMR spectra is such that when the signs of all the coupling constants in the Hamiltonian for a system are reversed, the theoretical spectrum remains unchanged. Thus it is not possible to determine experimentally from the NMR spectra alone the absolute signs of the spin coupling constants.

At the present time, proton-proton spin couplings are by far easier to handle theoretically[13–19] than couplings involving other nuclei. On the basis of molecular orbital theory McConnell[14] has deduced that long-range proton-proton spin couplings have positive sign. Thus one would expect all long-range proton-proton spin couplings in a molecule to have the same signs, namely, the positive sign. However, the work of Alexander,[3] and others,[6–9] has shown conclusively that long range proton spin-spin couplings may have opposite signs in certain molecules, and thus points to the fact that such spin couplings could indeed have a negative absolute sign. In a later work, McConnell[16] has shown by means of valence bond theory that in even-alternant hydrocarbon systems one might expect an alternation in the sign of long-range proton spin-spin coupling due to π-electrons. Experimental evidence for this is not conclusive at present since the σ-electron couplings presumably mask the effect. One point of interest that may be noted here is that in hydrocarbons where long-range proton-proton spin couplings of opposite sign are met with there are generally present doubly- or triply-bonded carbon atoms. The sign of the nuclear spin coupling constant between the two protons in the CH_2 fragment was at one time thought to be negative[10] but a later work[18] has disproved this.

Recently valence bond theory has been successfully employed by Karplus and co-workers[17–19] for the calculation of some proton spin-spin coupling constants. The long-range spin coupling constant for protons in ethane has thus been calculated,[19] and the results shown to be in good agreement with available experimental data. Since the valence-bond theory also yields a positive sign for the long-range proton spin coupling constant ($J_{CH_3-CH_3}$) in ethane, one might conclude that $J_{CH_3-CH_2}$ for protons in an ethyl group has the positive sign. In this connection it may be mentioned here that from a complete analysis of the high-resolution proton magnetic resonance spectrum of pure ethyl alcohol as an A_3B_2C system we have shown recently[11] that the proton-

* Present address: Noyes Chemical Laboratory, University of Illinois, Urbana, Illinois.

[1] G. A. Williams and H. S. Gutowsky, J. Chem. Phys. **25**, 1288 (1956).

[2] H. S. Gutowsky, C. H. Holm, A. Saika, and G. A. Williams J. Am. Chem. Soc. **79**, 4596 (1957).

[3] S. Alexander, J. Chem. Phys. **28**, 358 (1958).

[4] B. Bak, J. N. Shoolery, and G. A. Williams, J. Mol. Spectroscopy **2**, 525 (1958).

[5] R. E. Richards and T. Schaefer, Proc. Roy. Soc. (London) **A246**, 429 (1958).

[6] G. A. Williams and H. S. Gutowsky, J. Chem. Phys. **30**, 717 (1959).

[7] R. W. Fessenden and J. S. Waugh, J. Chem. Phys. **30**, 944 (1959).

[8] F. S. Mortimer, J. Mol. Spectroscopy **3**, 335, 528 (1959).

[9] A. D. Cohen and N. Sheppard, Proc. Roy. Soc. (London) **A252**, 488 (1959).

[10] N. Sheppard and J. J. Turner, Proc. Roy. Soc. (London) **A252**, 506 (1959).

[11] P. T. Narasimhan and M. T. Rogers, J. Chem. Phys. **31**, 1428 (1959).

[12] P. T. Narasimhan and M. T. Rogers, J. Chem. Phys. **31**, 1430 (1959).

[13] H. M. McConnell, J. Chem. Phys. **23**, 2454 (1955).

[14] H. M. McConnell, J. Chem. Phys. **24**, 460 (1956). See corrections to some of the equations in this paper by G. A. Williams, Ph.D. thesis, University of Illinois, 1956.

[15] H. M. McConnell, J. Mol. Spectroscopy **1**, 11 (1957).

[16] H. M. McConnell, J. Chem. Phys. **30**, 126 (1959).

[17] M. Karplus, D. H. Anderson, T. C. Farrar, and H. S. Gutowsky, J. Chem. Phys. **27**, 597 (1957).

[18] M. Karplus and D. H. Anderson, J. Chem. Phys. **30**, 6 (1959).

[19] M. Karplus, J. Chem. Phys. **30**, 11 (1959).

TABLE I. Spin eigenfunctions of the A_3B_2C system.[a]

$\Sigma I_z=3$	$\Sigma I_z=2$	$\Sigma I_z=1$	$\Sigma I_z=0$
QTd States			
$\phi_1=Q_3T_1d_1$	$\phi_1=Q_3T_1d_{-1}$	$\phi_1=Q_3T_{-1}d_1$	$\phi_1=Q_1T_{-1}d_1$
	$\phi_2=Q_3T_0d_1$	$\phi_2=Q_1T_0d_1$	$\phi_2=Q_{-1}T_0d_1$
	$\phi_3=Q_1T_1d_1$	$\phi_3=Q_{-1}T_1d_1$	$\phi_3=Q_{-3}T_1d_1$
		$\phi_4=Q_3T_0d_{-1}$	$\phi_4=Q_3T_{-1}d_{-1}$
		$\phi_5=Q_1T_1d_{-1}$	$\phi_5=Q_1T_0d_{-1}$
			$\phi_6=Q_{-1}T_1d_{-1}$
QS$_0$d States			
$\phi_1=Q_3S_0d_1$	$\phi_1=Q_3S_0d_{-1}$	$\phi_1=Q_1S_0d_{-1}$	
	$\phi_2=Q_1S_0d_1$	$\phi_2=Q_{-1}S_0d_1$	
DTd States (Doubly degenerate)			
$\phi_1=D_1T_1d_1$	$\phi_1=D_{-1}T_1d_1$	$\phi_1=D_{-1}T_1d_{-1}$	
	$\phi_2=D_1T_1d_{-1}$	$\phi_2=D_{-1}T_0d_1$	
	$\phi_3=D_1T_0d_1$	$\phi_3=D_1T_0d_{-1}$	
		$\phi_4=D_1T_{-1}d_1$	
DS$_0$d States (Doubly degenerate)			
	$\phi_1=D_1S_0d_1$	$\phi_1=D_{-1}S_0d_1$	
		$\phi_2=D_1S_0d_{-1}$	

[a] The eigenfunctions for states with negative ΣI_z values are obtained by reversing the signs of the subscripts of the correspondng positive ΣI_z functions. Thus, for $\Sigma I_z=-1$ of the *QTd* state, we get $\phi_1=Q_{-3}T_1d_{-1}$, and so on.

proton spin coupling constants $J_{CH_3-CH_2}$ and J_{CH_2-OH} are of the same sign. From the results of the valence-bond theory concerning the absolute sign of $J_{CH_3-CH_2}$ in an ethyl group we have, therefore, deduced that J_{CH_2-OH} in pure ethyl alcohol also has a positive sign.

The example given above regarding the determination of the sign of the coupling constants in pure ethyl alcohol points to the fact that the positive sign of the spin-spin coupling constant for protons in the ethyl group could be used advantageously for obtaining the signs of other coupling constants[20] in a molecule containing an ethyl group. We have consequently investigated the high-resolution proton magnetic resonance spectra of ethyl acetylene and ethyl mercaptan at both 40 Mc and 60 Mc. By analyzing these spectra as being of A_3B_2C type, we have obtained the relative signs of the coupling constants in these two molecules. From the known sign of $J_{CH_3-CH_2}$ the signs of other spin coupling constants have been obtained. Since, as mentioned earlier, these spectra have to be analyzed as A_3B_2C systems, we shall present next the details of this analysis.

II. NMR SPECTRUM OF THE A_3B_2C SYSTEM

The compounds studied in this investigation may be classified as A_3B_2C types where A_3 denotes the protons in the CH_3 group, B_2 those in the CH_2 group, and C the other proton in the molecule. The following analysis is more general in that it can be applied to any system of nuclei (spin $\frac{1}{2}$) composed of three equivalent nuclei (A_3) chemically shifted from another set of two equivalent nuclei (B_2), and yet another nucleus C. Let the resonance frequencies of the three chemically shifted groups of nuclei in the absence of any spin coupling be ν_A, ν_B and ν_C. Also, let the coupling constant for the nuclear spin-spin interaction between groups A and B be designated by J_{AB}, and we have also spin coupling constants J_{AC} and J_{BC} to describe the appropriate interactions. As mentioned earlier, all the three nuclei in group A are assumed to be equivalent, so that any spin-spin interaction within this group, even if present, will not affect our results.[21] Similarly, the two nuclei in the B group are assumed to be equivalent in this sense. Now, we can write the Hamiltonian of the system in an uniform magnetic field as

$$\hat{H}=\sum_{i=1}^{6}H_i, \tag{1}$$

where

$$H_1=-\nu_A I_z(A) \tag{1a}$$

$$H_2=-\nu_B I_z(B) \tag{1b}$$

$$H_3=-\nu_C I_z(C) \tag{1c}$$

$$H_4=J_{AB}[\mathbf{I}(A)\cdot\mathbf{I}(B)] \tag{1d}$$

$$H_5=J_{AC}[\mathbf{I}(A)\cdot\mathbf{I}(C)] \tag{1e}$$

$$H_6=J_{BC}[\mathbf{I}(B)\cdot\mathbf{I}(C)]. \tag{1f}$$

In the above expressions I_z is the z component (in the direction of the field) of the spin-angular momentum vector $\mathbf{I}$ of the nucleus, and accordingly $I_z(A)$ represents the total value of the z component for all the three spins in group A. The Hamiltonian (1) has been written such that the energy levels are expressed in units of cps. The terms H_1, H_2, and H_3 in the Hamiltonian describe the interaction of the A, B, and C groups of nuclei with the external magnetic field while H_4, H_5, and H_6 correspond to the nuclear spin-spin interactions within the system. One can get solutions for the energy levels corresponding to Hamiltonian (1) and also calculate the transition frequencies and probabilities by using approximate methods, as for example, perturbation methods. The perturbation method has been employed by Arnold[22] and Anderson[23] for the calculation of the proton NMR spectrum of pure ethyl alcohol (A_3B_2C) at 30.5 Mc. However, when the spin coupling constants involved are comparable to the chemical shifts, one cannot rely safely on results obtained by perturbation methods. In particular, if one is interested in the relative signs of the spin coupling

[20] A very similar approach has been made recently independently by N. Sheppard and J. J. Turner. See reference 10.

[21] H. S. Gutowsky, D. W. McCall, and C. P. Slichter, J. Chem. Phys. **21**, 279 (1953).

[22] J. T. Arnold, Phys. Rev. **102**, 136 (1956).

[23] W. A. Anderson, Phys. Rev. **102**, 151 (1956).

constants it is better to avoid any approximation in the theoretical procedure involved in the calculation of the spectra, because of the fact that usually the differences in the calculated spectra using different signs of coupling constants are not very great. On this account we shall concern ourselves here with the problem of obtaining a complete solution of the Hamiltonian without making use of approximations.

In order to calculate the NMR spectrum of the system described by the Hamiltonian (1) we have to obtain the various energy levels and the corresponding stationary-state eigenfunctions, and then, by using well-known selection rules[24] we can obtain the NMR transition frequencies and relative intensities. We may start out by using as zero-order eigenfunctions the simple product spin functions for the six nuclei which will be $2^6=64$ in number. These product spin functions would themselves be stationary-state eigenfunctions if there were no spin-spin interaction terms in the Hamiltonian. However, these terms bring about some mixing among the simple product functions, and in order to write down the stationary-state eigenfunctions one has to use linear combinations of the zero-order spin functions. Since the total z-component of the spin angular-momentum of the system, which may be written as $I_z(A)+I_z(B)+I_z(C)=\sum I_z$, is a good quantum number there is no mixing between states having different values of $\sum I_z$. This fact enables one to factor the secular equation

$$|H_{mn}-E_n\delta_{mn}|=0,\quad \delta_{mn}=1 \text{ if } m=n,\quad =0 \text{ if } m\neq n, \quad (2)$$

corresponding to the various allowed values of $\sum I_z$. For the A_3B_2C system we have, therefore, secular equations for values of $\sum I_z$ from $+3$ to -3. For setting up the secular equations, one has to evaluate the various matrix elements H_{mn}. The method of evaluating the relevant matrix elements has been widely discussed[23–28] and, as has been pointed out by McConnell, *et al.*,[24] it is often convenient, when molecular or group symmetry is present, to transform the simple product spin eigenfunctions into symmetry eigenfunctions by application of group theory.[27] In the present case of the A_3B_2C system, the three equivalent nuclei of the A group have a characteristic group symmetry (D_{3h}), while those of the B group have symmetry ($D_{\infty h}$). The simple product spin eigenfunctions corresponding to these groups can, therefore, be transformed into the appropriate symmetry functions, and thus the eigenfunctions for the whole A_3B_2C system can be written as the various products of symmetry functions of groups A and B and the two spin functions of the C group. In a previous work[29] we obtained the product symmetry functions for the A_3B_2 system; we can now write the spin functions for the A_3B_2C system in the manner outlined above. We shall use here the earlier notation[29,30] based on the multiplicity character for writing the eigenfunctions. Table I gives the various eigenfunctions thus obtained, which are grouped according to their $\sum I_z$ values. In Table II are given the various matrix elements between these functions. The matrix elements involving H_1, H_2, and H_3 are easily obtained[23–28], but the matrix elements for H_4, H_5, and H_6 have been obtained in the present work by making use of the expanded form, as for example,

$$\langle m|H_3|n\rangle=[\mathbf{I}(A)\cdot\mathbf{I}(B)]_{mn}=[I_z(A)]_{mn}[I_z(B)]_{mn}+[I_y(A)]_{mn}[I_y(B)]_{mn}+[I_z(A)]_{mn}[I_z(B)]_{mn}. \quad (3)$$

The matrix elements for the x, y and z components of the angular momentum have been evaluated by making use of the generalized angular momentum matrices for the various "spin-particles." The concept of spin particle has been explained in detail elsewhere[29,30] and we need not go into it further. Details of constructing the above-mentioned angular momentum matrices are well known,[31] and have also been dealt with elsewhere.[29–30] It may, however, be noted here that the three nuclei of A may have $\sum I=\frac{3}{2}$ or $\frac{1}{2}$, namely, the quartet (Q) or doublet (D) states, while the nuclei of B may have $\sum I=1$ or 0, and correspondingly the triplet (T) or singlet (S_0) states. The two states of C are represented by d_1 or d_{-1}. According to the scheme in Table I there are 24 spin functions in the QTd states, and 8 in the QS_0d states. The DTd and DS_0d states are doubly degenerate, so that there are 24 spin functions in DTd and 8 in DS_0d states. The QTd, QS_0d, DTd, and DS_0d states do not mix with one another, and thus considerable factoring of the secular determinant is achieved. Table II gives the matrix elements for these functions corresponding to the Hamiltonian (1); the numbering of the functions is the same as that in Table I. The following substitutions have been made: $\nu_A-\nu_B=\delta_{AB}$; $\nu_B-\nu_C=\delta_{BC}$. The energy expressions are given relative to ν_A. The matrix elements for the various states involving $\sum I_z=-1$, -2, and -3 are easily obtained by means of simple rules[32] from the ones given in Table II for $\sum I_z=+1$, $+2$, and $+3$. Hence, these have not been included here.

The evaluation of the eigenvalues and eigenvectors of the various secular determinants enables one to then calculate the NMR transition frequencies and relative intensities. For the evaluation of the latter, we make use of the x components of the spin angular momenta;

[24] H. M. McConnell, A. D. McLean, and C. A. Reilly, J. Chem. Phys. **23**, 1152 (1955).
[25] N. K. Banerjee, T. P. Das, and A. K. Saha, Proc. Roy. Soc. (London) **A226**, 490 (1954).
[26] H. J. Bernstein, W. G. Schneider and J. A. Pople, Can. J. Chem. **35**, 65 (1957).
[27] E. B. Wilson, J. Chem. Phys. **26**, 60 (1957).
[28] J. A. Pople, W. G. Schneider, and H. J. Bernstein, *High Resolution Nuclear Magnetic Resonance* (McGraw-Hill Book Company, Inc., New York, 1959).
[29] P. T. Narasimhan and M. T. Rogers, J. Am. Chem. Soc. **82**, 34 (1960).
[30] D. R. Whitman, Ph.D. thesis, Yale (1957).
[31] L. I. Schiff, *Quantum Mechanics* (McGraw-Hill Book Company, Inc., New York, 1949).
[32] P. L. Corio, J. Chem. Phys. **29**, 682 (1958).

TABLE II. Matrix elements for the A_3B_2C system.

	Diagonal elements	Off-diagonal elements
	QTd States	
$\Sigma I_z=3$	$H_{11}=-3\nu_A+\frac{3}{2}\delta_{AB}+\frac{1}{2}\delta_{BC}+\frac{3}{2}J_{AB}+\frac{3}{4}J_{AC}+\frac{1}{2}J_{BC}$	
$\Sigma I_z=2$	$H_{11}=-2\nu_A+\frac{1}{2}\delta_{AB}-\frac{1}{2}\delta_{BC}+\frac{3}{2}J_{AB}-\frac{3}{4}J_{AC}-\frac{1}{2}J_{BC}$	$H_{12}=H_{21}=\frac{1}{2}\sqrt{2}J_{BC}$
	$H_{22}=-2\nu_A+\frac{1}{2}\delta_{AB}+\frac{1}{2}\delta_{BC}+\frac{3}{4}J_{AC}$	$H_{13}=H_{31}=\frac{1}{2}\sqrt{3}J_{AC}$
	$H_{33}=-2\nu_A+\frac{1}{2}\delta_{AB}+\frac{1}{2}\delta_{BC}+\frac{1}{2}J_{AB}+\frac{1}{4}J_{AC}+\frac{1}{2}J_{BC}$	$H_{23}=H_{32}=\frac{1}{2}(6)^{\frac{1}{2}}J_{AB}$
$\Sigma I_z=1$	$H_{11}=-\nu_A-\frac{1}{2}\delta_{AB}+\frac{1}{2}\delta_{BC}-\frac{1}{2}J_{AB}+\frac{3}{4}J_{AC}-\frac{1}{2}J_{2C}$	$H_{12}=H_{21}=H_{45}$
	$H_{22}=-\nu_A+\frac{1}{2}\delta_{AB}+\frac{1}{2}\delta_{BC}+\frac{1}{4}J_{AC}$	$=H_{34}=\frac{1}{2}(6)^{\frac{1}{2}}J_{AB}$.
	$H_{33}=-\nu_A+\frac{1}{2}\delta_{AB}+\frac{1}{2}\delta_{BC}-\frac{1}{2}J_{AB}-\frac{1}{4}J_{AC}+\frac{1}{2}J_{BC}$	$H_{14}=H_{41}=H_{25}$
	$H_{44}=-\nu_A-\frac{1}{2}\delta_{AB}-\frac{1}{2}\delta_{BC}-\frac{1}{2}J_{AC}$	$=H_{52}=\frac{1}{2}\sqrt{2}J_{AB}$.
	$H_{55}=-\nu_A+\frac{1}{2}\delta_{AB}-\frac{1}{2}\delta_{BC}+\frac{1}{2}J_{AB}-\frac{1}{4}J_{AC}-\frac{1}{2}J_{BC}$	$H_{23}=H_{32}=\sqrt{2}J_{AB}$
		$H_{24}=H_{42}=\frac{1}{2}\sqrt{3}J_{AC}$
		$H_{35}=H_{53}=J_{AC}$
		All others are zero.
$\Sigma I_z=0$	$H_{11}=-\frac{1}{2}\delta_{AB}+\frac{1}{2}\delta_{BC}-\frac{1}{2}J_{AB}+\frac{1}{4}J_{AC}-\frac{1}{2}J_{BC}$	$H_{12}=H_{21}=H_{56}$
	$H_{22}=\frac{1}{2}\delta_{AB}+\frac{1}{2}\delta_{BC}-\frac{1}{4}J_{AC}$	$=H_{65}=\sqrt{2}J_{AB}$.
	$H_{33}=\frac{1}{2}\delta_{AB}+\frac{1}{2}\delta_{BC}-\frac{1}{2}J_{AB}-\frac{3}{4}J_{AC}+\frac{1}{2}J_{BC}$	$H_{14}=H_{41}=H_{36}$
	$H_{44}=-\frac{3}{2}\delta_{AB}-\frac{1}{2}\delta_{BC}-\frac{3}{2}J_{AB}-\frac{3}{4}J_{AC}+\frac{1}{2}J_{BC}$	$=H_{63}=\frac{1}{2}\sqrt{3}J_{AC}$.
	$H_{55}=-\frac{1}{2}\delta_{AB}-\frac{1}{2}\delta_{BC}-\frac{1}{4}J_{AC}$	$H_{15}=H_{51}=H_{26}$
	$H_{66}=\frac{1}{2}\delta_{AB}-\frac{1}{2}\delta_{BC}-\frac{1}{2}J_{AB}+\frac{1}{4}J_{AC}-\frac{1}{2}J_{BC}$	$=H_{62}=\frac{1}{2}\sqrt{2}J_{BC}$.
		$H_{23}=H_{32}=H_{45}$
		$=H_{54}=\frac{1}{2}(6)^{\frac{1}{2}}J_{AB}$.
		$H_{25}=H_{52}=J_{AC}$
		All others are zero.
	QS$_0$d States	
$\Sigma I_z=2$	$H_{11}=-2\nu_A+\frac{1}{2}\delta_{AB}+\frac{1}{2}\delta_{BC}+\frac{3}{4}J_{AC}$	
$\Sigma I_z=1$	$H_{11}=-\nu_A-\frac{1}{2}\delta_{AB}-\frac{1}{2}\delta_{BC}-\frac{3}{4}J_{AC}$	$H_{12}=H_{21}=\frac{1}{2}\sqrt{3}J_{AC}$
	$H_{22}=-\nu_A+\frac{1}{2}\delta_{AB}+\frac{1}{2}\delta_{BC}+\frac{1}{4}J_{AC}$	
$\Sigma I_z=0$	$H_{11}=-\frac{1}{2}\delta_{AB}-\frac{1}{2}\delta_{BC}-\frac{1}{4}J_{AC}$	$H_{12}=H_{21}=J_{AC}$
	$H_{22}=\frac{1}{2}\delta_{AB}+\frac{1}{2}\delta_{BC}-\frac{1}{4}J_{AC}$	
	DTd States (Double degenerate)	
$\Sigma I_z=2$	$H_{11}=-2\nu_A+\frac{3}{2}\delta_{AB}+\frac{1}{2}\delta_{BC}+\frac{1}{2}J_{AB}+\frac{1}{4}J_{AC}+\frac{1}{2}J_{BC}$	
$\Sigma I_z=1$	$H_{11}=-\nu_A+\frac{3}{2}\delta_{AB}+\frac{1}{2}\delta_{BC}-\frac{1}{2}J_{AB}-\frac{1}{4}J_{AC}+\frac{1}{2}J_{BC}$	$H_{12}=H_{21}=\frac{1}{2}J_{AC}$
	$H_{22}=-\nu_A+\frac{1}{2}\delta_{AB}-\frac{1}{2}\delta_{BC}+\frac{1}{2}J_{AB}-\frac{1}{4}J_{AC}-\frac{1}{2}J_{BC}$	$H_{13}=H_{31}=\frac{1}{2}\sqrt{2}J_{AB}$
	$H_{23}=-\nu_A+\frac{1}{2}\delta_{AB}+\frac{1}{2}\delta_{BC}+\frac{1}{4}J_{AC}$	$H_{23}=H_{32}=\frac{1}{2}\sqrt{2}J_{BC}$
$\Sigma I_z=0$	$H_{11}=\frac{1}{2}\delta_{AB}-\frac{1}{2}\delta_{BC}-\frac{1}{2}J_{AB}+\frac{1}{4}J_{AC}-\frac{1}{2}J_{BC}$	$H_{12}=H_{21}=H_{34}$
	$H_{22}=\frac{1}{2}\delta_{AB}+\frac{1}{2}\delta_{BC}-\frac{1}{4}J_{AC}$	$=H_{43}=\frac{1}{2}\sqrt{2}J_{BC}$.
	$H_{33}=-\frac{1}{2}\delta_{AB}-\frac{1}{2}\delta_{BC}-\frac{1}{4}J_{AC}$	$H_{13}=H_{31}=H_{24}$
	$H_{44}=-\frac{1}{2}\delta_{AB}+\frac{1}{2}\delta_{BC}-\frac{1}{2}J_{AB}+\frac{1}{4}J_{AC}-\frac{1}{2}J_{BC}$	$=H_{42}=\frac{1}{2}\sqrt{2}J_{AB}$.
		$H_{23}=H_{32}=\frac{1}{2}J_{AC}$
		All others are zero.
	DS$_0$d States (Doubly degenerate)	
$\Sigma I_z=1$	$H_{11}=-\nu_A+\frac{1}{2}\delta_{AB}+\frac{1}{2}\delta_{BC}+\frac{1}{4}J_{AC}$	
$\Sigma I_z=0$	$H_{11}=\frac{1}{2}\delta_{AB}+\frac{1}{2}\delta_{BC}-\frac{1}{4}J_{AC}$	
	$H_{22}=-\frac{1}{2}\delta_{AB}-\frac{1}{2}\delta_{BC}-\frac{1}{4}J_{AC}$	$H_{12}=H_{21}=\frac{1}{2}J_{AC}$

matrix methods are convenient for this problem. Details of these are to be found in footnote references 29 and 30. Incidentally, it may be noted that since the states involving DTd and DS_0d functions are doubly degenerate, the relative intensities for these have to be doubled. The largest determinant to be solved is 6×6 for the QTd states and 4×4 for DTd states. We have been able to carry out the above computations and obtain theoretical spectra of A_3B_2C type systems by means of a program coded for the high-speed electronic digital computer MISTIC at Michigan State University.

III. EXPERIMENTAL

Pure liquid samples of ethyl acetylene and ethyl mercaptan were degassed and sealed in 5 mm o.d. Pyrex tubes. The sample of ethyl acetylene was kindly supplied by the National Bureau of Standards, Washington. The proton magnetic resonance spectra were recorded at 40 Mc with a Varian V-4300B high-resolution spectrometer and at 60 Mc by means of the V-4311 RF-unit. The usual sample spinning technique and sideband modulation were employed.

IV. RESULTS

The values of the various chemical shifts and coupling constants for ethyl acetylene and ethyl mercaptan could be obtained more easily from the 60 Mc spectra (Figs. 1 and 2) than from the 40 Mc spectra (Figs. 3 and 4). However, for the determination of the relative signs of the coupling constants it was found advantage-

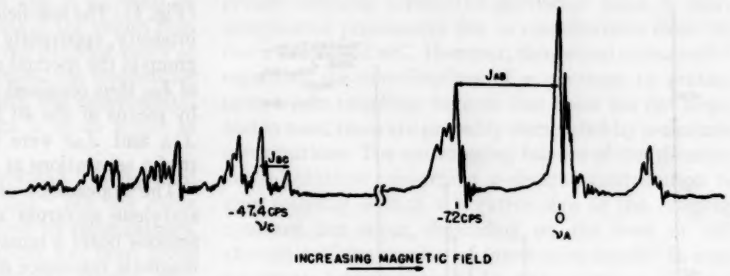

FIG. 1. The high resolution proton magnetic resonance spectrum of ethyl acetylene at 60 Mc.

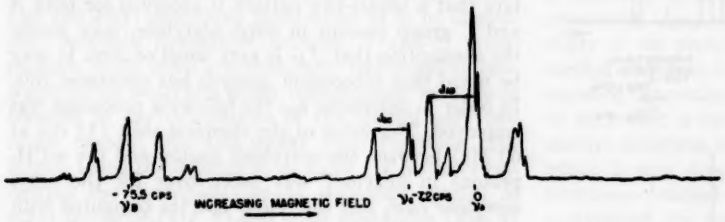

FIG. 2. The high resolution proton magnetic resonance spectrum of ethyl mercaptan at 60 Mc.

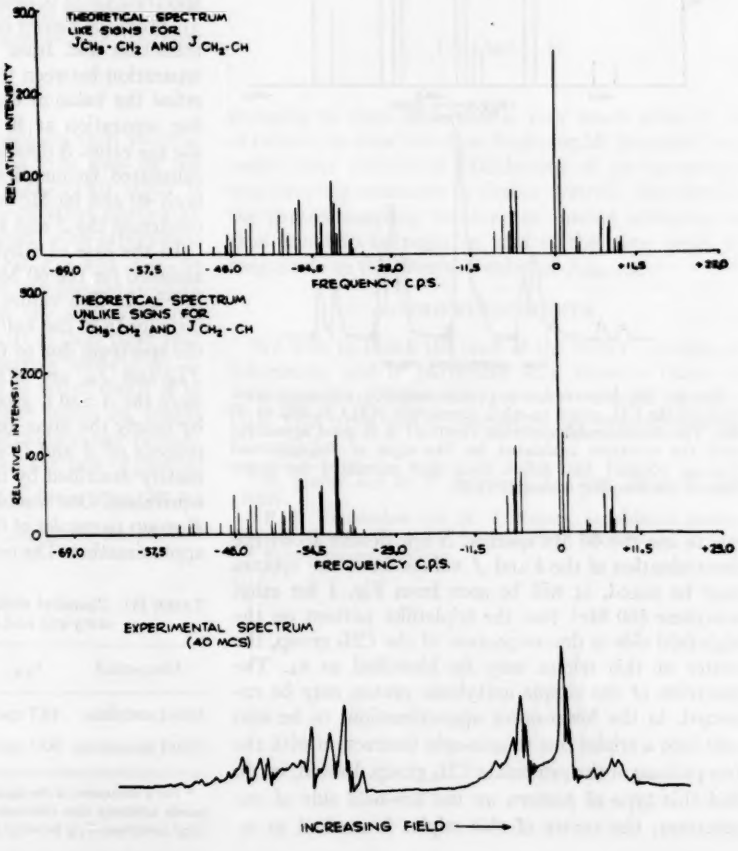

FIG. 3. The high-resolution proton magnetic resonance spectrum of ethyl acetylene at 40 Mc. The spectrum calculated for unlike signs of the coupling constants $J_{CH_3-CH_2}$ and J_{CH_2-CH} (center) agrees better with the experimental spectrum (bottom) than does the spectrum calculated for unlike signs of the coupling constants (top).

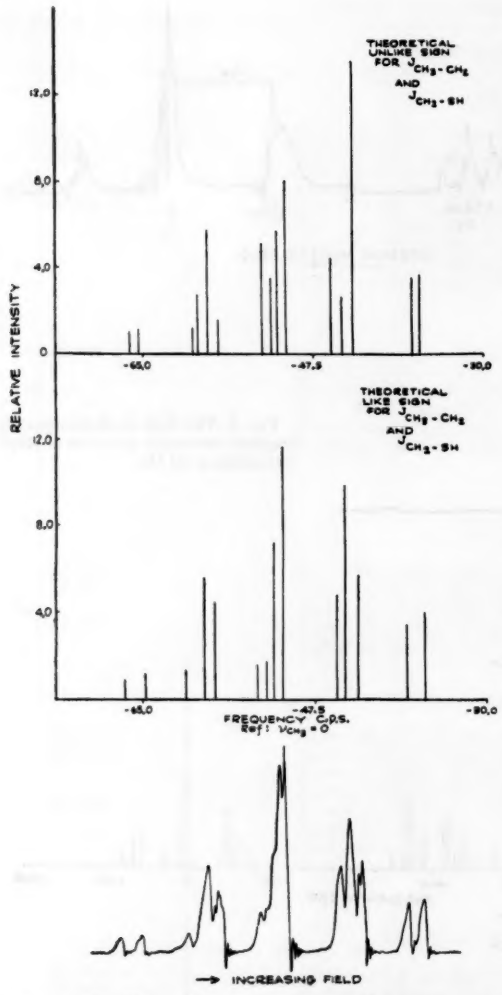

FIG. 4. The high-resolution proton magnetic resonance spectrum of the CH_3 group in ethyl mercaptan (CH_3CH_2SH) at 40 Mc. The experimental spectrum (bottom) is in good agreement with the spectrum calculated for like signs of $J_{CH_3-CH_2}$ and J_{CH_2-SH} (center) but differs from that calculated for unlike signs of the coupling constants (top).

ous to use the 40 Mc spectra. A few details about the determination of the δ and J values from the spectra may be noted. It will be seen from Fig. 1 for ethyl acetylene (60 Mc) that the tripletlike pattern on the high-field side is due to protons of the CH_3 group, the center of this triplet may be identified as ν_A. The spectrum of the simple acetylenic proton may be expected, in the lower-order approximation, to be also split into a triplet due to spin-spin interaction with the two protons of the proximate CH_2 group. Indeed, we do find this type of pattern on the low-field side of the spectrum; the center of this triplet is marked as ν_C (Fig. 1). The low-field line of this triplet is enhanced in intensity, apparently due to its being closer to the CH_2 group in the spectral sense (see reference 23). The value of δ_{BC} thus obtained at 60 Mc could also be confirmed by means of the 40 Mc spectrum. The magnitudes of J_{AB} and J_{BC} were also initially obtained from the triplet separations at 60 Mc.

The appearance of the high-field part of the ethyl acetylene spectrum at 60 Mc due to the CH_3 group protons bears a remarkable resemblance to the proton magnetic resonance spectrum of the CH_3 group in pure ethyl alcohol (A_3B_2C) at 15 Mc with comparable δ_{AB} and also J_{AB}. This observation, combined with the fact that a triplet-like pattern is observed for both A and C group protons in ethyl acetylene, may justify the assumption that J_{AC} is very small or zero. It may be noted that subsequent analysis has confirmed this. In order to determine δ_{BC} the following procedure was employed. The value of the chemical shift (12 cps at 60 Mc) between the acetylenic proton and the α-CH_2 protons in hexyne-1 was taken over for the ethyl acetylene case, and the A_3B_2C spectra computed with both like and unlike signs for J_{AB} and J_{BC}. It was soon apparent that the line falling at the lowest field on the spectrum could be assigned to a QTd transition ($\sum I_z 2 \rightarrow 3$). From the known expression for the frequency of this transition and from the experimental value for the separation between this line and ν_A, it was possible to refine the value of δ_{BC}. A similar measurement of this line separation at 40 Mc made it possible to confirm the δ_{BC} value. A detailed comparison of the theoretically calculated frequencies and intensities of the lines at both 40 and 60 Mc with the experimental spectra has confirmed the J and δ values given in Table III.

In the case of ethyl mercaptan, ν_A, ν_B, and ν_C were assigned for the 60 Mc spectrum in the manner shown in Fig. 2. The values of J_{AB} and J_{BC} were obtained initially from the line spacings of the high-field side of the spectrum due to CH_3 and SH group protons. Since J_{AB} and J_{BC} are of nearly the same magnitude, and since the A and C group protons are chemically shifted by nearly the same amount, the spin interaction of the protons of A and C with those of B may be approximately described by taking the A and C protons to be equivalent. One would then expect the spectrum of the B group to consist of five main peaks in the lower-order approximation. The center of the B group of lines would

TABLE III. Chemical shift and coupling constant data for ethyl acetylene and ethyl mercaptan (40 Mc).[a]

Compound	δ_{AB}	δ_{BC}	J_{AB}	J_{AC}	J_{BC}
Ethyl acetylene	40.7 cps	−9.1 cps	7.2 cps	0 cps	2.4 cps
Ethyl mercaptan	50.3 cps	−42.7 cps	7.2 cps	0 cps	7.7 cps

[a] For a discussion of the signs of these constants see text. Note that by our purely arbitrary sign convention, $\delta_{AB}=\nu_A-\nu_B=0-(-40.7)=+40.7$ cps for ethyl acetylene; δ_{AB} for ethyl mercaptan similarly has a positive sign.

correspond to ν_B and, as shown in Fig. 2, ν_B could be assigned in this manner. Refinements of the values thus obtained were made possible from the detailed study of the analytical expressions for the transition frequencies and intensities, and comparison with the experimental spectra. A summary of the results is to be found in Table III.

The value of J_{AB} for ethyl mercaptan was reported previously by Bothner-By and Glick[33] but the value of J_{BC} was apparently not determined by these authors. The value of δ_{AB} in ethyl mercaptan has been given earlier[34] as 1.07 ppm. (Benzene solution: approx. 50% by vol.). The values given here are for pure liquids in a sealed tube at room temperature. In both ethyl acetylene and ethyl mercaptan there seems to be no observable spin-spin interaction between A and C group protons. Since there are, then, only two coupling constants in the molecules under consideration we have to consider in our calculations of the spectra only two cases, namely, like and unlike signs for these constants. Using the data given in Table III, we have calculated the theoretical proton resonance spectra of ethyl acetylene (Fig. 3) and ethyl mercaptan (Fig. 4) at 40 Mc for the two cases of like and unlike signs for J_{AB} and J_{BC}. The theoretical spectra have been compared with the experimentally obtained spectra for the determination of the relative signs of the coupling constants.

V. DISCUSSION

For ethyl acetylene the agreement between theoretical and experimental spectra is seen to be good for the case of unlike signs for J_{AB} and J_{BC}. This result is quite interesting, since in the case of ethyl mercaptan and also ethyl alcohol,[11] the agreement with experiment is best when one uses like signs for J_{AB} and J_{BC}. As mentioned in the Introduction, we can use the positive sign of $J_{CH_2-CH_2}$ for determining the signs of other coupling constants in a molecule. It is thus clear that J_{CH_2-CH} in ethyl acetylene is negative while J_{CH_2-SH} in ethyl mercaptan is positive. The latter result is in line with McConnell's conclusions[14] based on simple MO theory regarding the sign of long-range proton-proton spin coupling constants. But the case of proton-proton coupling across the acetylenic bond is more complicated presumably due to contributions from the two π bonds of C≡C. However, theoretical estimates[15,16] regarding the contributions of π electrons to proton-proton spin couplings suggest that these are not large, and in most cases are probably dominated by σ-electron contributions. The encouraging feature of the theoretical calculations concerning π-electron contribution to spin coupling is that a negative sign of the coupling constant can occur, depending on the even or odd character of the number of intervening bonds (in even alternant hydrocarbons.) In any event, a detailed description of the electronic structure of the molecule is necessary in order to make quantitative estimates concerning J_{CH_2-CH} in ethyl acetylene. A theoretical study of the proton-proton spin coupling constant in methyl acetylene would probably be of help in understanding the results obtained here. It may be of interest to note that a recent determination[35] of J_{CH_3-CH} in methyl acetylene has yielded a value of 2.8 ± 0.3 cps, which is very close to the value for J_{CH_2-CH} in ethyl acetylene obtained in the present work. Also, in several acetylenes[36] the value of J_{CH_3-CH} is very nearly 2.4 cps. These results suggest that the electronic structure of the

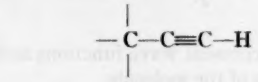

grouping in these molecules is very much alike. It is of interest to note here that Professor M. Karplus[37] has made some theoretical calculations of proton-proton spin coupling constants in similar systems. The sign of the proton coupling constant in methyl acetylene is thus found to be negative, and of the same order of magnitude as the observed value of J_{CH_2-CH}.

ACKNOWLEDGMENTS

We wish to thank the staff of the MISTC computer laboratory, and in particular Mrs. Beverly Davis of Michigan State University, for their valuable cooperation. This work was supported by the Atomic Energy Commission.

[33] A. A. Bothner-By and R. E. Glick, J. Chem. Phys. **25**, 362 (1956).

[34] B. P. Dailey and J. N. Shoolery, J. Am. Chem. Soc. **77**, 3977 (1957).

[35] N. Muller and D. E. Pritchard, J. Chem. Phys. **31**, 768 (1959).

[36] P. T. Narasimhan and M. T. Rogers, unpublished results. See also reference 28, p. 247 for J_{CH_2-CH} in hexyne-1.

[37] Private communication.

Concise Method for Forming Two-Center Integrals of Operators*

J. M. ROBINSON

Department of Physics, Texas College of Arts and Industries, Kingsville, Texas

(Received February 22, 1960)

Two-center integrals of operators for Slater-type atomic orbitals are concisely expressed in terms of O functions which arise directly from the integral representation in spherical polar coordinates. The O functions are expressible in terms of A and B functions which lend themselves nicely to machine programs. Their greatest asset is their convenient correlation of A and B functions with Slater-type atomic orbitals and operators expressed in spherical polar coordinates. Examples are given for dipole-moment and quadrupole-moment operators.

IN computing expectation values for molecules of various observables, we have, from a fundamental postulate of quantum mechanics,[1]

$$(\bar{l}) = \int \phi^*(L)\phi dv \Big/ \int \phi^*\phi dv,$$

which results in the need for evaluating integrals of the form

$$I = \int \phi_i(L)\phi_j dv, \tag{2}$$

where ϕ_i and ϕ_j represent wave functions assigned to a particular electron of the molecule.

This paper concerns itself with a concise method of evaluating two-center integrals arising from the insertion of an operator between two such Slater-type atomic orbitals. Numerous authors[2–6] have devised auxiliary functions for two-center integral evaluations using letters as a convenient means of representing the auxiliary functions, hence the integral. In many cases there is a marked similarity between these auxiliaries. The O functions defined in this paper are indeed similar to Kotani's Is[2], Kastler's Ls, Ms, and Ns[3], Coulson's Js[4], and Roothan's Cs[5]. Most of these auxiliaries differ only by a simple multiplier. The reason for the definition of the O function is to simplify the evaluation of operator integrals expressed in spherical polar form in terms of functions which lend themselves nicely to high-speed digital computers.

Consider the coordinate system defined in Fig. 1, where

$$r_a = (\lambda+\omega)R/2, \qquad r_b = (\lambda-\omega)R/2,$$
$$\cos\theta_a = (1+\lambda\omega)/(\lambda+\omega), \quad \cos\theta_b = (1-\lambda\omega)/(\lambda-\omega), \tag{3}$$
$$\sin\theta_a = [(\lambda^2-1)(1-\omega^2)]^{\frac{1}{2}}/(\lambda+\omega),$$
$$\sin\theta_b = [(\lambda^2-1)(1-\omega^2)]^{\frac{1}{2}}/(\lambda-\omega),$$

and

$$dv = R^3(\lambda^2-\omega^2)/8 \cdot d\lambda d\omega d\phi,$$

in elliptical coordinates.

Then for a two-center integral of the general form

$$I = \int (\text{Slater-type function})\ L\ (\text{Slater-type function})\, dv,$$

the integral can be reduced with little effort to

$$I = N \int \frac{r_a^{\,x}\cos^c\theta_a \sin^v\theta_a \epsilon^{-\rho_1 r_a} r_b^{\,y}\cos^q\theta_b \sin^w\theta_b \epsilon^{-\rho_2 r_b} dX}{r_a^{\,2} r_b^{\,2}} \cdot \int f(\phi)\, d\phi, \tag{4}$$

where $dX = r^2 \sin\theta d\theta dr$. This can be simplified to

$$I = NI(r,\theta)\cdot I(\phi). \tag{5}$$

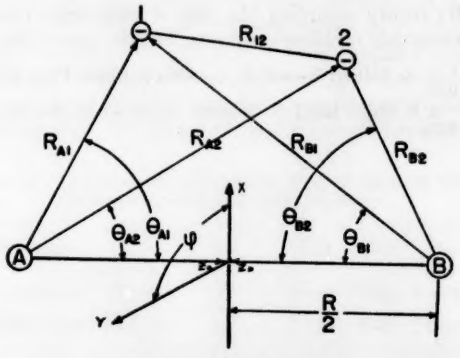

FIG. 1. Coordinate system.

* This work was supported in part by National Science Foundation.

[1] H. Margenau and G. M. Murphy, *The Mathematics of Physics and Chemistry* (D. Van Nostrand, Inc., Princeton, New Jersey, 1956), p. 326.

[2] M. Kotani, *et al.*, *Table of Molecular Integrals* (Maruzen Company, Ltd., Tokyo, 1955).

[3] D. Kastler, "Theorie quantique de la molecule *HF*," Doctoral dissertation, University of Saarbrucken.

[4] C. A. Coulson, Proc. Cambridge Phil. Soc. **38**, 210 (1941).

[5] K. Rudenberg, C. C. J. Roothan, and W. Jaunzemis, J. Chem. Phys. **24**, 201 (1956).

[6] J. Miller, J. M. Gerhauser, and F. A. Matsen, *Quantum Chemistry Integrals and Tables* (University of Texas Press, Austin, Texas, 1958).

On transforming to elliptical coordinates, the integral $I(r,\theta)$ can be evaluated to give

$$I(\Delta_1,\Delta_2)=(R/2)^h O_{fg}^{cde}(\Delta_1,\Delta_2), \tag{6}$$

where

$$\Delta_1=(\rho_1+\rho_2)R/2, \qquad \Delta_2=(\rho_1-\rho_2)R/2 \tag{7}$$

and

$$O_{fg}^{cde}(\Delta_1,\Delta_2)=\int_1^\infty\int_{-1}^{+1}(\lambda+\omega)^c(\lambda-\omega)^f(1+\lambda\omega)^d \cdot(1-\lambda\omega)^g[(\lambda^2-1)(1-\omega^2)]^e\epsilon^{-\Delta_1\lambda}\epsilon^{-\Delta_2\omega}d\omega d\lambda \tag{8}$$

with the correlation

$$h=(x-s+y-t+3); \qquad c=(x-s-d-v+1);$$
$$f=(y-t-g-w+1); \qquad e=(w+v)/2;$$

for

$$s\gtrless 1, \qquad t\gtrless 1. \tag{9}$$

These O functions can be easily expanded into a series of products of $A_n(\Delta_1)$ and $B_m(\Delta_2)$ functions where A and B are defined by

$$A_n(\Delta_1)=\int_1^\infty\lambda^n\epsilon^{-\Delta_1\lambda}d\lambda; \qquad B_m(\Delta_2)=\int_{-1}^{+1}\omega^m\epsilon^{-\Delta_2\omega}d\omega. \tag{10}$$

The A and B functions are easily evaluated on a digital computer using recursion relations[7] or series expansions.[6]

Some examples of applications would be dipole-moment calculations involving integral evaluations of the form[8]

$$(\bar{M})=I=\int(\text{Slater orbital})\,r_a\cos\theta_a\,(\text{Slater orbital})\,dv.$$

Consider the case of the orbitals $1s_{a1}$ and $2s_{b1}$. Using our previous definition

$$(1s_{a1}\,2s_{b1}\mid M_{a1})=NI(r,\theta)I(\phi),$$

where

$$I(r,\theta)=\int\epsilon^{-\rho_1 r_{a1}}(r_{a1}\cos\theta_{a1})r_{b1}\epsilon^{-\rho_2 r_{b1}}dX_1,$$

we find

$$I(r,\theta)=(R/2)^5O_{20}^{110}(\Delta_1,\Delta_2)$$

where

$$O_{20}^{110}(\Delta_1,\Delta_2)=A_4B_1+A_3(B_0-B_2)-A_2(B_1+B_3) -A_1(B_2-B_4)+A_0B_3,$$

and hence, finally,

$$(1s_{a1}2s_{b1}\mid\bar{M}_{a1})=2(\rho_1^3\rho_2^5/3)^{\frac{1}{2}}(R/2)^5O_{20}^{110}(\Delta_1,\Delta_2).$$

[7] H. Eyring, J. Walter, and G. E. Kimball, *Quantum Chemistry* (John Wiley & Sons, New York, 1954).

[8] R. P. Hurst, J. Miller, and F. A. Matsen, J. Chem. Phys. **26**, 1092 (1957).

Quadrupole-moment calculations involve integral evaluations of the form[9]

$$(\bar{Q}_{a1})=I=\int(\text{Slater orbital})[r_{a1}^2(1-3\cos^2\theta_{a1}) +2r_{a1}R\cos\theta_{a1}]\cdot(\text{Slater orbital})\,dv.$$

Consider the case of the orbitals $2s_{a1}$ and $2p_{sb1}$. On using our previous definition, we find

$$(2s_{a1}2p_{sb1}\mid\bar{Q}_{a1})=N\int r_{a1}\epsilon^{-\rho_1 r_{a1}}[r_{a1}^2(1-3\cos^2\theta_{a1}) +2r_{a1}R\cos\theta_{a1}]r_{b1}\cos\theta_{b1}\epsilon^{-\rho_2 r_{b2}}dX\int d\phi,$$

which can be integrated to yield

$$(2s_{a1}\,2p_{sb1}\mid\bar{Q}_{a1})=2(\rho_1^5\rho_2^5/3)^{\frac{1}{2}}[(R/2)^7O_{11}^{400}(\Delta_1,\Delta_2) -3(R/2)^7O_{11}^{220}(\Delta_1,\Delta_2)+2R(R/2)^6O_{11}^{210}(\Delta_1,\Delta_2)],$$

where

$$O_{11}^{400}(\Delta_1,\Delta_2)=-A_6B_1+A_5(B_0-3B_2)+A_4(3B_1-2B_3) +2A_3(B_4+B_2)+A_2(3B_5-2B_3)-A_1(3B_4-B_6)-A_0B_5,$$
$$\cdots$$

where

$$A_n=A_n(\Delta_1) \quad\text{and}\quad B_m=B_m(\Delta_2).$$

As an example of two-electron two-center integrals, electron-repulsion calculations involve integrals of the form

$$(1/r_{ij})=I=\iint(\text{Slater orbitals})\,(1/r_{ij}) \times(\text{Slater orbitals})\,dv_1dv_2,$$

where r_{ij} is the interelectronic distance.

Consider the hybrid integral $(1s_{a1}1s_{a1}\mid 1/r_{ij}\mid 1s_{a2}1s_{b2})$. On using the $1/r_{ij}$ expansion for $l=0$, $m=0$, one has

$$(1s_{a1}1s_{a1}\mid 1/r_{ij}\mid 1s_{a2}1s_{b2})=N^*\iint\epsilon^{-\rho_1 r_{a1}}\epsilon^{-\rho_2 r_{a1}}[1/r_>]\epsilon^{-\rho_3 r_{a2}} \cdot\epsilon^{-\rho_4 r_{b2}}dX_1dX_2,$$

where integration of ϕ_1 and ϕ_2 has been performed. Radial integration of r_{a1} yields

$$I(r_{a2},\theta_{a2})=16N/(\rho_1+\rho_2)^3\int\left[\frac{\epsilon^{-\rho_3 r_{a2}}\epsilon^{-\rho_4 r_{b2}}}{r_{a2}} -\frac{\epsilon^{-(\rho_1+\rho_2+\rho_3)r_{a2}}\epsilon^{-\rho_4 r_{2b}}}{r_{a2}}-(\rho_1+\rho_2)/2\epsilon^{-(\rho_1+\rho_2+\rho_3)r_{a2}}\epsilon^{-\rho_4 r_{b2}}\right]dX_2,$$

[9] M. Kotani *et al.*, J. Phys. Soc. Japan **12**, 708 (1957).

which can be immediately written as

$$(1s_{a1}1s_{a1} \mid 1/r_{ij} \mid 1s_{a2}1s_{b2}) = 16(\rho_1^3\rho_2^3\rho_3^3\rho_4^3)^{\frac{1}{2}}/(\rho_1+\rho_2)^3 \cdot[(R/2)^2 O_{10}^{000}(\Delta_1', \Delta_2') - (R/2)^2 O_{10}^{000}(\Delta_1, \Delta_2) - [(\rho_1+\rho_2)/2]\cdot(R/2)^3 O_{10}^{100}(\Delta_1, \Delta_2)]$$

where

$$\Delta_1' = (\rho_3+\rho_4)R/2, \qquad \Delta_2' = (\rho_3-\rho_4)R/2,$$

$$\Delta_1 = (\rho_1+\rho_2+\rho_3+\rho_4)R/2,$$

and

$$\Delta_2 = (\rho_1+\rho_2+\rho_3-\rho_4)R/2.$$

In conclusion, it will be noted that the exponents of s and t in Eq. (4) are bounded to insure integration in terms of the A and B functions only. The introduction of other auxiliary functions as well as the A and B functions could increase the upper bound of s and t.[2-6]

THE JOURNAL OF CHEMICAL PHYSICS VOLUME 33, NUMBER 3 SEPTEMBER, 1960

CN Stretching Bands in the Raman Spectra of Some Group Ib and Group IIb Complex Cyanides*

G. W. CHANTRY AND R. A. PLANE

Department of Chemistry, Cornell University, Ithaca, New York

(Received February 29, 1960)

The Raman spectra of solutions containing cuprous, argentous, and mercuric ions together with cyanide ions indicate the presence of the di-, tri-, and tetra-coordinated complexes. The spectra from solutions containing zinc and cadmium ions, respectively, with cyanide ions could be investigated in concentrations where only the tetra-coordinated complex is observed.

THE complex species formed in aqueous solution between cyanide ions and various cations of the copper and zinc groups have been the subject of a number of investigations by a variety of methods.[1] Most of these depend on the measurements of a property of a single species and infer the presence of complex species through the systematic variation of this property with changing composition of the solution. Techniques of this sort are open to criticism and may lead to incorrect formulation of complex species.[2] Unequivocal results can only be obtained when it is possible to study some property of each complex species independently of the other species present. Such a method is the infrared technique of Jones and Penneman[3] who were able to show, for example, that $Ag(CN)_4^{-3}$ is a dominant species in solutions with a high ratio of cyanide ion to argentous ions, although all previous investigations had failed to show this species.

The cyanide complexes formed by the Ib and IIb elements are in the main of quite high symmetry [e.g., linear $M(CN)_2$ tetrahedral $M(CN)_4$] and therefore, studies of infrared and Raman spectra are complementary and results obtained from one can serve to check those from the other. The Raman technique, like the infrared technique, is free from the objections just mentioned. For these reasons, the systems examined by Jones and Penneman have been investigated using Raman spectrophotometry. The CN stretching bands of the complexes are generally shifted to higher frequencies compared with free cyanide ion and although these shifts are relatively large, there is still a considerable degree of overlapping. In order to resolve such spectra into the component bands so that an analysis may be made, a photoelectric spectrophotometer is a great advantage. The use of such an instrument is also desirable since the degree of depolarization of all bands can be rapidly and accurately measured, thus allowing separation of coincident bands which differ in degree of depolarization. Such separations make it possible to determine the concentration of free cyanide ion even when the band due to this ion is coincident with a band due to a complex species. The concentration of free cyanide ion is important in the present studies since it gives, by difference, the amount of bound cyanide ion and hence the average formula of the complex present. This, in turn, renders the assignment of the various bands almost certain.

The measurements reported in this paper concern the

* This research was supported by the U. S. Air Force through the Air Force Office of Scientific Research of the Air Research and Development Command.

[1] Cf. J. Bjerrum, G. Schwarzenbach, and L. G. Sillen, "Stability constants of metal ion complexes," Part II, Chemical Society special publication No. 7, 1958.

[2] T. F. Young and A. C. Jones, Ann. Rev. Phys. Chem. **1952**, 275.

[3] L. H. Jones and R. A. Penneman, J. Chem. Phys. **22**, 965 (1954).

CN stretching bands in aqueous solutions of Cu(I), Ag(I), Zn(II), Cd(II), and Hg(II) at varying ratios of cyanide ion to metal ion.

EXPERIMENTAL

Measurements were made with a Cary model-81 Raman spectrophotometer; the spectra being excited mostly with the 4358-A line of the mercury arc, though occasional use was made of the 4047-A line. Reagents were prepared as follows. Cuprous cyanide was made from commercial cuprous chloride which was first purified by a standard method.[4] This was then dissolved in concentrated potassium chloride solution. On addition of potassium cyanide solution, a white gelatinous precipitate of cuprous cyanide formed. The precipitate was washed repeatedly with water followed by alcohol and ether. The resulting dry powder contained no chloride and was stable when stored in a desiccator. Silver, zinc, and cadmium complex cyanides were made in solution by the addition of A. R. potassium cyanide solutions to the solutions of the appropriate A. R. metal-ion nitrate. Mercury complexes were made by dissolving A. R. mercuric oxide in potassium cyanide solution.

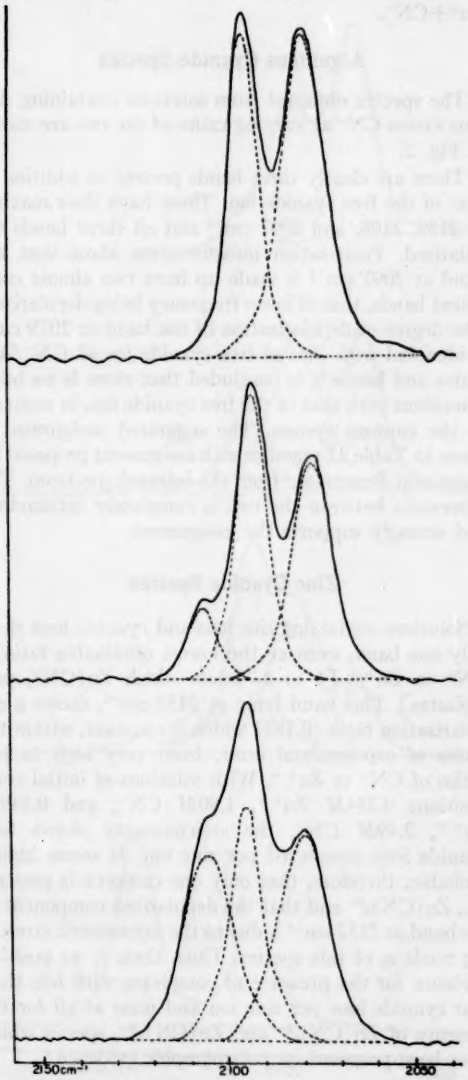

FIG. 1. Raman spectra of Cu(I)–CN^- complexes at increasing (bottom to top) $CN^-/Cu(I)$ ratio.

RESULTS AND DISCUSSION

Cuprous Cyanide Species

The spectra obtained from cuprous ion plus excess cyanide ion at ratios of the two varying up to 5.01 F CN^-/0.544 F Cu(I) are shown in Fig. 1.

Two bands in addition to the free-cyanide-ion band (2079 cm^{-1}) are evident. These have their maxima at 2094 and 2106 cm^{-1}. Polarization measurements and intensity measurements plus stoichiometric relations show that there are three other bands present also. The reasons for this statement are as follows. The depolarization ratio of the band at 2079 cm^{-1}, even at the highest CN^-/Cu^+ ratio, is very much in excess of that for the free cyanide ion ($\rho_{CN^-}=0.086$). If one assumes that this is because of the coincidence of a depolarized band ($\rho=6/7$), then it follows that the residual intensity of the band due to free CN^- demands that four cyanide ions per cuprous ion have complexed. Since it is presumed that the highest complex formed is $Cu(CN)_4^{3-}$, this result strongly confirms the assumption that the band coincident with that of free cyanide ion is depolarized

At the highest CN^-/Cu^+ ratio used, the band at 2094 cm^{-1} is completely polarized ($\rho=0$) and hence this must be assigned to a species of tetrahedral or

TABLE I.

Species	Frequency cm^{-1}	Assignment	ρ_n
$Cu(CN)_3^{-2}$	2094	ν sym, ν asym	>0.00
$Cu(CN)_4^{-3}$	2094	ν sym	0.00
$Ag(CN)_2^{-1}$	2139	ν sym	0.270
$Ag(CN)_3^{-2}$	2108	ν sym, ν asym	0.290
$Ag(CN)_4^{-3}$	2097	ν sym, ν asym	0.310
$Zn(CN)_4^{-2}$	2152	ν sym, ν asym	0.185
$Cd(CN)_4^{-2}$	2141	ν sym, ν asym	0.210
$Hg(CN)_4^{-2}$	2140	ν sym, ν asym	0.300

[4] *Inorganic Syntheses, Vol. II* edited by W. C. Fernelius (McGraw-Hill Book Company, Inc., New York, 1946).

TABLE II.

Species	Raman spectrum (cm^{-1})	Infrared spectrum[a] (cm^{-1})
$Cu(CN)_2^{-1}$	ν sym = 2106 ν asym = ...	ν sym = ... ν asym = 2125
$Cu(CN)_3^{-2}$	ν sym = 2094 ν asym = 2094	ν sym = ... ν asym = 2094
$Cu(CN)_4^{-3}$	ν sym = 2094 ν asym = 2079	ν sym = ... ν asym = 2076
$Ag(CN)_2^{-1}$	ν sym = 2139 ν asym = ...	ν sym = ... ν asym = 2135
$Ag(CN)_3^{-2}$	ν sym = 2108 ν asym = 2108	ν sym = ... ν asym = 2105
$Ag(CN)_4^{-3}$	ν sym = 2097 ν asym = 2094	ν sym = ... ν asym = 2092
$Zn(CN)_4^{-2}$	ν sym = 2152 ν asym = 2152	ν sym = ... ν asym = 2149
$Cd(CN)_4^{-2}$	ν sym = 2141 ν asym = 2141	ν sym = ... ν asym = 2140
$Hg(CN)_2$	ν sym = 2190 ν asym = ...	ν sym = ... ν asym = 2190 (in CH_3OH)
$Hg(CN)_3^{-1}$	ν sym = 2160 ν asym = 2160	ν sym = ... ν asym = 2161
$Hg(CN)_4^{-2}$	ν sym = 2140 ν asym = 2140	ν sym = ... ν asym = 2143

[a] L. H. Jones and R. A. Penneman, J. Chem. Phys. **22**, 965 (1954); R. A. Penneman and L. H. Jones, *ibid.* **24**, 293 (1956); R. A. Penneman, R. L. M. McCullough, and L. H. Jones, paper No. 76 presented to the Division of Inorganic Chemistry of the American Chemical Society, Atlantic City, New Jersey, 1959, and private communication.

higher symmetry (See Table I). It is strongly presumptive that this band is ν_1 of the known tetrahedral molecule $Cu(CN)_4^{3-}$. If this is the case, the depolarized band at 2079 cm^{-1} must be ν_6 of this molecule (the triply degenerate asymmetric stretch of the CN bonds.)

At lower CN^-/Cu^+ ratios the degree of depolarization of the band at 2094 cm^{-1} increases and the stoichiometry, based on the intensity of the free-cyanide-ion line shows that between three and four cyanide ions per cuprous ion have complexed. This suggests that the complex $Cu(CN)_3^{2-}$ is being formed. In Raman scattering it is generally observed that symmetric stretching modes are more intense than asymmetric ones. In infrared absorption the converse is generally true. Since a strong band is found in the infrared experiments at 2094 cm^{-1} and a strong one in the Raman experiments at the same frequency, it is probable that the symmetric and asymmetric stretching frequencies of $Cu(CN)_3^-$ are coincident. It might be expected, however, that the symmetric CN stretching mode of this molecule would have a degree of depolarization different from zero, but as its exact value is unknown, it is not possible to determine the intensities of the two modes separately. The band at 2106 cm^{-1} is very plausibly ascribed to the linear $Cu(CN)_2^{1-}$ molecule. The suggested assignment for the cuprous complexes is given in Table II.

The only other detailed Raman study is that of Chiorboli and Testa[5] who were unable to detect the two lower species but agree with the present assignment for $Cu(CN)_4^{3-}$. Table II also lists the infrared results of Penneman and Jones,[6] and inspection of this table shows that there is complete agreement between the two assignments. This agreement is, therefore, strong evidence for the presence of the three species $Cu(CN)_2^-$, $Cu(CN)_3^{2-}$, and $Cu(CN)_4^{3-}$ in the aqueous system $Cu^+ + CN^-$.

Argentous Cyanide Species

The spectra obtained from solutions containing Ag^+ plus excess CN^- at varying ratios of the two are shown in Fig. 2.

There are clearly three bands present in addition to that of the free cyanide ion. These have their maxima at 2139, 2108, and 2097 cm^{-1} and all three bands are polarized. Polarization measurements show that the band at 2097 cm^{-1} is made up from two almost coincident bands, that of lower frequency being depolarized. The degree of depolarization of the band at 2079 cm^{-1} is identical with that of free cyanide for all CN^-/Ag^+ ratios and hence it is concluded that there is no band coincident with that of the free cyanide ion, in contrast to the cuprous system. The suggested assignment is given in Table II together with assignment proposed by Jones and Penneman[3] from the infrared spectrum. The agreement between the two is completely satisfactory and strongly supports the assignment.

Zinc Cyanide Species

Solutions containing zinc ions and cyanide ions show only one band, even at the lowest obtainable ratio of CN^- to Zn^{++} [4 to 1, below which $Zn(CN)_2$ precipitates]. This band lying at 2152 cm^{-1}, shows a depolarization ratio (0.185) which is constant, within the limits of experimental error, from very high to low ratios of CN^- to Zn^{++}. With solutions of initial compositions 0.284*M* Zn^{++}, 1.90*M* CN^-, and 0.149*M* Zn^{++}, 2.49*M* CN^-, the stoichiometry shows four cyanide ions complexed per zinc ion. It seems highly probable, therefore, that only one complex is present, i.e., $Zn(CN)_4^{2-}$ and that the depolarized component of the band at 2152 cm^{-1} is due to the asymmetric stretching mode ν_6 of this species. Thus, there is no positive evidence for the presence of complexes with less than four cyanide ions per zinc ion and none at all for the presence of $Zn(CN)_5^{3-}$ and $Zn(CN)_6^{4-}$, species which have been proposed on polarographic evidence.[1]

[5] P. Chiorboli and C. Testa, Ann. chim. (Rome) **47**, 639 (1957).
[6] R. A. Penneman and L. H. Jones, J. Chem. Phys. **24**, 293 (1956).

Cadmium Cyanide Species

Solutions containing cadmium ions and cyanide ions differ slightly from the corresponding zinc solutions since they can be prepared with a cyanide-ion to metal-ion ratio somewhat less than 4 to 1.[7] However, such solutions are light sensitive and apparently contain a colloidal suspension; hence, Raman spectra could only be obtained from solutions in which the ratio was greater than 4 to 1. In these solutions a single band was observed at 2141 cm^{-1} which had a constant depolarization ratio of 0.210 throughout the range of cyanide-ion to cadmium-ion ratio investigated. Stoichiometric measurements (at 2.77M CN^- and 0.491M Cd^{++}) indicate that only the tetracyano complex forms. The band at 2141 cm^{-1} is, therefore, assigned to this substance and since the depolarization ratio is constant and different from zero, it follows that the asymmetric stretching frequency ν_3 must be coincident with the symmetric ν_1. No evidence was found for the lower complex $Cd(CN)_3^{1-}$ which Penneman and Jones[8] have detected in solutions with cyanide-ion to cadmium-ion ratios less than 4 to 1. However, since the

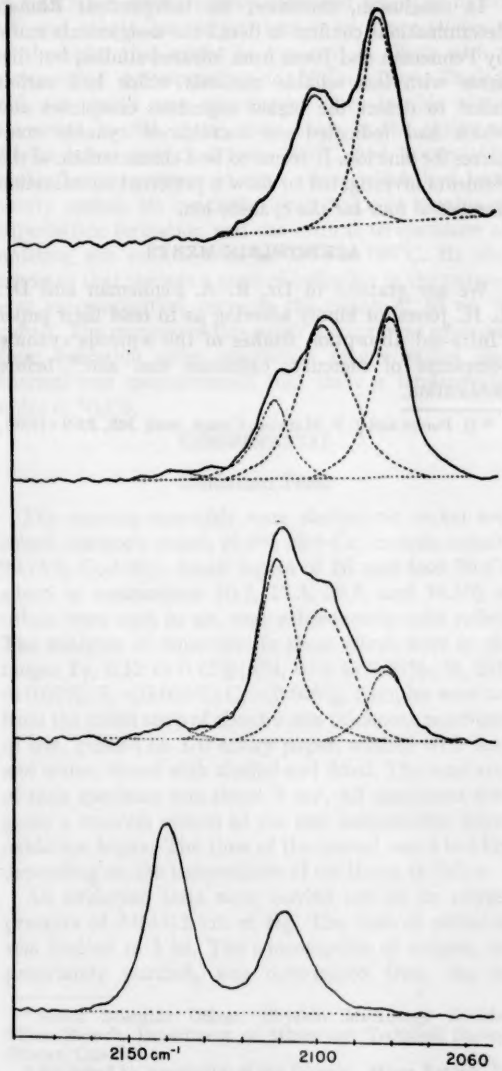

FIG. 2. Raman spectra of Ag(I)–CN^- complexes at increasing (bottom to top) CN^-/Ag(I) ratio.

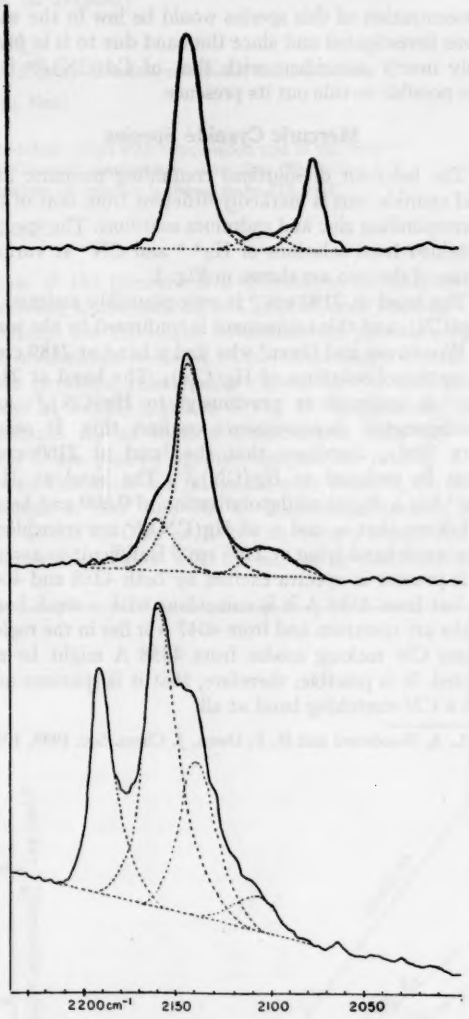

FIG. 3. Raman spectra of Hg(II)–CN^- complexes at increasing (bottom to top) CN^-/Hg(II) ratio.

[7] A. S. Corbet, J. Chem. Soc. **129**, 3190 (1926).

[8] R. A. Penneman, R. L. McCullough, and L. H. Jones, Paper No. 76 presented to the Division of Inorganic Chemistry of the American Chemical Society, Atlantic City, New Jersey, 1959, and private communication.

concentration of this species would be low in the solutions investigated and since the band due to it is probably nearly coincident with that of $Cd(CN)_4^{2-}$ it is not possible to rule out its presence.

Mercuric Cyanide Species

The behavior of solutions containing mercuric ions and cyanide ions is markedly different from that of the corresponding zinc and cadmium solutions. The spectra obtained from solutions of Hg^{++} and CN^- at various ratios of the two are shown in Fig. 3.

The band at 2190 cm^{-1} is very plausibly assigned to $Hg(CN)_2$ and this assignment is confirmed by the work of Woodward and Owen[9] who find a band at 2189 cm^{-1} in methanol solutions of $Hg(CN)_2$. The band at 2140 cm^{-1} is assigned as previously[9] to $Hg(CN)_4^{2-}$ and stoichiometric measurements confirm this. It seems very likely, therefore, that the band at 2160 cm^{-1} must be assigned to $Hg(CN)_3^{1-}$. The band at 2140 cm^{-1} has a degree of depolarization of 0.300 and hence it follows that ν_6 and ν_1 of $Hg(CN)_4^{2-}$ are coincident. The weak band lying at 2105 cm^{-1} is difficult to assign. It is present in spectra excited by both 4358 and 4047 A, but from 4358 A it is coincident with a weak band in the arc spectrum and from 4047 A it lies in the region where CN rocking modes from 4358 A might be expected. It is possible, therefore, that it is spurious and not a CN stretching band at all.

The suggested assignment is given in Table II together with the infrared assignment of Penneman, McCullough, and Jones.[8] It is seen that the agreement is excellent. The assignment is, however, in but partial agreement with that of Poulet and Mathieu.[10] We do not find it necessary to postulate the species $Hg_2(CN)_6^{2-}$. Their evidence for such a species is the complexity of the Raman spectra of solutions containing a ratio of CN^- ion to Hg^{++} ion of 3 to 1. Our quantitative measurements show that the complexity is due completely to the simultaneous presence of the three simple species.

In conclusion, therefore, the independent Raman determinations confirm in detail the assignments made by Penneman and Jones from infrared studies, but disagree with less reliable methods which had earlier failed to detect the higher argentous complexes and which had indicated six coordinated cyanide complexes for zinc ion. It seems to be a characteristic of the elements investigated to show a preferred coordination number of four for the cyanide ion.

ACKNOWLEDGMENTS

We are grateful to Dr. R. A. Penneman and Dr. L. H. Jones for kindly allowing us to read their paper "Infra-red absorption studies of the aqueous cyanide complexes of mercury, cadmium and zinc" before publication.

[9] L. A. Woodward and H. F. Owen, J. Chem. Soc. **1959**, 1055.

[10] H. Poulet and J. P. Mathieu, Compt. rend. **248**, 2079 (1959).

Detection of Order in Ni_3Co†

Y. L. YAO*

Department of Mines and Technical Surveys, Mines Branch, Physical Metallurgy Division, Ottawa, Canada

(Received March 30, 1960)

Measurements of the variation of oxidation rate of nickel-cobalt alloys with composition and of the variation of saturation magnetization and thermal emf of Ni_3Co with temperature show that Ni_3Co has a tendency to order at low temperatures. The critical temperature of ordering is shown to be 773±1°C.

INTRODUCTION

VARIOUS workers have examined alloys of nickel and cobalt, but so far there is no direct evidence of the order that might be expected in alloys with a composition corresponding to Ni_3Co. Thus, Taylor[1] did not detect any superlattice lines in this alloy. However, he did report that alloys in the region of Ni_3Co, when quenched from 900°C, had appreciably higher lattice parameters than alloys which had been slowly cooled. He concluded that Ni_3Co is capable of superlattice formation and the critical temperature of ordering was estimated to be 750° to 780°C. He also reported that there is a marked inflection in the parameter vs composition curve in the region of 30 wt % cobalt. The purpose of this paper is to present evidence from oxidation rates, saturation magnetization and thermal emf measurements that there is tendency to order in Ni_3Co.

EXPERIMENTAL

Oxidation Tests

The starting materials were electrolytic nickel and cobalt (cathode nickel, 99.9% Ni+Co; cathode cobalt, 99.75% Co+Ni). Small ingots of Ni and four Ni-Co alloys of composition 10.2, 19.3, 28.9, and 38.3% of cobalt were cast in air, and subsequently cold rolled. The analyses of impurities in these alloys were in the range: Fe, 0.12 to 0.22%; Cu, 0.02 to 0.03%; Si, 0.01 to 0.02%; S, <0.003%; C, <0.006%. Samples were cut from the rolled strip of about 2 mm thickness, machined to size, ground on 3/0 emery paper, washed with soap and water, rinsed with alcohol and dried. The total area of each specimen was about 9 cm^2. All specimens were given a vacuum anneal at the test temperature before oxidation began. The time of the anneal was 3 to 6 hrs, depending on the temperature of oxidation to follow.

All oxidation tests were carried out at an oxygen pressure of 2.0±0.1 cm of Hg. The time of oxidation was limited to 3 hr. The consumption of oxygen, appropriately purified, was determined from the decrease of the pressure of a differential oil manometer according to the method of Campbell and Thomas.[2]

Except for the initial deviation, the parabolic time law of oxidation holds for Ni and these alloys. One set of such parabolic relationship curves for Ni and these alloys at 1000°C is shown in Fig. 1. The parabolic rate constants K_P at various temperatures from 600° to 1000°C are plotted against composition in Fig. 2. It is seen that there is a minimum near the 20% Co composition at 600° and 700°C. The disturbance is still seen at 800°C. Only at 1000°C is there a steady rise of the rate of oxidation with the increasing cobalt content.

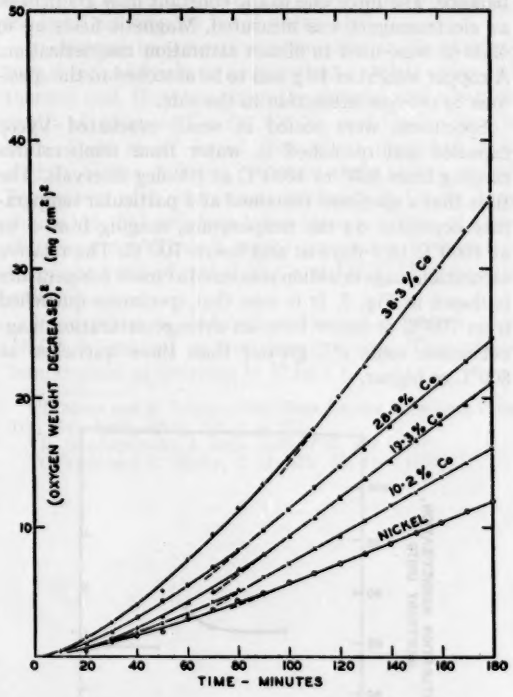

FIG. 1. Parabolic time-law plot for oxidation of Ni-Co alloys at 1000°C during three hours under oxygen pressure of 2 cm of mercury.

* Senior Scientific Officer, Physical Metallurgy Division, Mines Branch, Department of Mines and Technical Surveys, Ottawa, Canada.

† Published by permission of the Director, Mines Branch, Department of Mines and Technical Surveys, Ottawa, Canada.

[1] A. Taylor, J. Inst. Metals 77, 585 (1950).

[2] W. E. Campbell and U. B. Thomas, Trans. Electrochem. Soc. 91, 623 (1947).

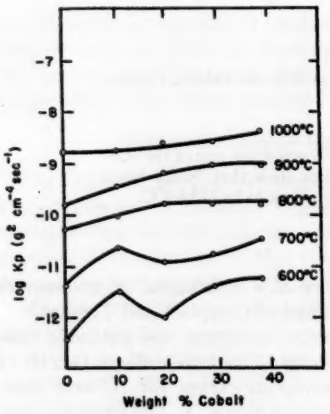

FIG. 2. Parabolic rate constants of Ni-Co alloys.

Saturation Magnetization

A small ingot of Ni-Co alloy with 25.0 wt % Co was cast in vacuum, and wire of 0.2-mm diam was drawn from it. A specimen of suitable length, cemented to a quartz wire, was hung from one arm of a chemical balance. The force due to the constant field gradient of an electromagnet was measured. Magnetic fields up to 4500 oe were used to obtain saturation magnetization. A copper weight of 10 g had to be attached to the specimen to prevent attraction to the side.

Specimens were sealed in small evacuated Vycor capsules and quenched in water from temperatures ranging from 300° to 1000°C at 100-deg intervals. The time that a specimen remained at a particular temperature depended on the temperature, ranging from 3 hr at 1000°C to 4 days at and below 700°C. The relative saturation magnetization measured at room temperature is shown in Fig. 3. It is seen that specimens quenched from 700°C or below have an average saturation magnetization some 2% greater than those quenched at 800°C or higher.

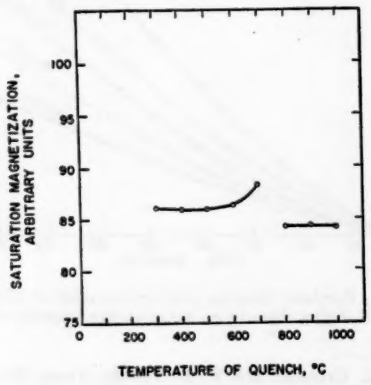

FIG. 3. Effects of quenching temperature on the saturation magnetization of Ni_3Co.

Thermal emf

The 25% Co alloy in the form of wire, prepared for magnetic tests, was welded with an iron and a constantan wire to form a triple junction. The hot junction was placed in the constant temperature section of a tube furnace. Through suitable vacuum seals, the other ends of the wires were immersed in a water-ice freezing mixture and connected to a potentiometer with binding posts for three elements of the two thermocouples, constantan being a common element. By switching from iron-constantan to Ni_3Co-constantan thermocouple, the relationship between thermal emf and temperature of Ni_3Co was found. The error of the measurement of temperature was estimated to be ± 1°C, by previous calibrating with a platinum-13% rhodium thermocouple.

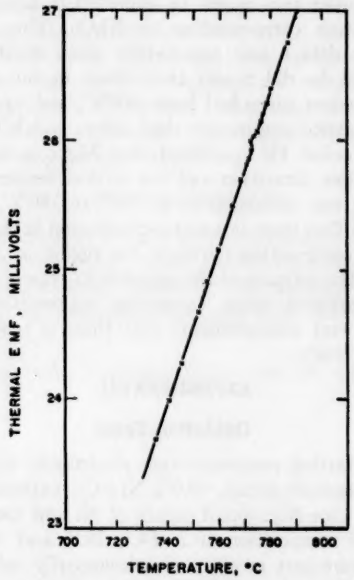

FIG. 4. Thermal emf of Ni_3Co relative to constantan at the reference junction of 0°C.

To relieve stresses, the hot junction was heated in vacuum at 900°C for 4 hr and furnace-cooled. Because it was indicated by our magnetic measurements that there was ordering of Ni_3Co between 700° and 800°C and by Taylor's x-ray work[1] that ordering occurred between 750° and 780°C, the temperature of the hot junction was slowly raised from room temperature to 730°C and kept constant at this temperature for 4 days. The heating was then conducted at a rate of about 25°C per hour in the temperature range from 730° to 790°C. It is seen in Fig. 4 that thermal emf varies linearly with temperature in this range except for a small disturbance between 770° and 780°C. The behaviour is reversible on cooling.

DISCUSSION

An oxidation anomaly in Ni-Co alloys similar to that described above was observed by Smeltzer.[3] He studied the reactions of an 11% Co alloy with oxygen from 500° to 800°C and of a 25% alloy from 400° to 800°C. The usual Arrhenius plot, whether the rate constants were derived from a parabolic or a cubic relationship, of the 11% alloy was linear; but for the 25% alloy, again derived from either relationship, two linear sections were connected by a smooth curve in the temperature range of approximately 560° to 640°C. He explained the continuous variations of the temperature coefficients of the oxidation constants in this temperature range by the transformation from the ferromagnetic to paramagnetic state, the Curie point of the 25% alloy being 635°C.

The anomaly could also be explained on the basis of the oxidation rate of the random Ni_3Co being greater than that of the ordered one. It is well known that Tammann recognized the existence of ordered copper-gold alloys from their chemical reactivity towards nitric acid four years before the pioneer investigation of superlattice lines of these alloys by Bain. That the reactivity of the random Cu_3Au towards aqueous ferric chloride solution is greater than that of the ordered one was further demonstrated by Papazian *et al.*[4]

Unfortunately, Smeltzer's investigation covered only two alloys and for the 11% Co alloy the lowest temperature of oxidation was 500°C. From his results, it is not possible to infer whether a similar anomaly is associated with the magnetic transformation in the 11% alloy, the Curie point of which is 490°C. From our results (Fig. 2), it appears that the anomaly in the 20% Co alloy, the Curie point of which is 580°C, may extend to 700°C and that in the 30% alloy, the Curie point of which is 675°C, it may extend to 800°C. Both alloys are already in the paramagnetic state at these temperatures.

It has been shown that the change of room-temperature saturation magnetization of a ferromagnetic alloy by heat treatment reveals the presence of order.[5] This is especially significant in Ni_3Co, because its components have similar x-ray scattering powers. Conversely, with the knowledge of crystal structure of the ordered alloy, the effect of order on saturation moment can be estimated. Smoluchowski[6] interpreted the saturation moment of the disordered alloy as the sum of the saturation moments of the various local electron concentration fluctuations of a chosen number of atoms. The distribution of the two kinds of atoms in the group was assumed to be binomial and each moment obtained from the semiempirical Slater-Pauling plot. For the perfectly ordered alloy, the distribution was according to the chemical composition. Thus, the increases of the saturation moments of Fe_3Ni and FeCo by ordering were estimated to be 8 and 1%, respectively, as compared with the experimental values of 6 and 4%. A similar calculation yields a result of no change of the saturation moment of Ni_3Co by ordering, the ordered phase of Ni_3Co being assumed to be isomorphous with that of Fe_3Ni. That the curve in the Slater-Pauling plot between cobalt and nickel is a straight line accounts for the difference. From Fig. 3 the increase is about 2%. However, in view of the highly approximated theory, the small discrepancy is not unexpected.

In contrast to saturation magnetization, no satisfactory theories have been advanced to correlate order and thermal emf. However, from the thermal emf measurements of alloys in Cu-Zn, Cu-Ni, and Cu-Ni-Zn systems, Dahl *et al.*[7] found that alloys quenched have slightly higher or lower emf than those slowly cooled. By analogy with similar measurements in Cu_3Au, they concluded that ordering takes place in alloys of these three systems. Thus it seems reasonable to associate the slight jump of emf of Ni_3Co at 773°C (Fig. 4) with ordering.

In conclusion, indirect evidence indicated that Ni_3Co is ordered at low temperatures. The critical temperature of ordering is 773 ± 1°C.

[3] W. W. Smeltzer, Acta Met. **7**, 191 (1959).
[4] H. Papazian and R. A. Lad, Trans. Am. Inst. Mining, Met. Petrol. Engrs. **206**, 1340 (1956).
[5] T. Muto and Y. Takagi, *Solid State Physics* (Academic Press, Inc., New York, 1955), Vol. 1, p. 193.
[6] R. Smoluchowski, J. phys. radium **12**, 389 (1951).
[7] O. Dahl and E. Starke, Z. Metallk. **50**, 410 (1959).

Collisional Deactivation of Vibrationally Excited *sec*-Butyl-d_1 Radicals Produced by Chemical Activation*

R. E. HARRINGTON,† B. S. RABINOVITCH, AND M. R. HOARE

Department of Chemistry, University of Washington, Seattle 5, Washington

(Received March 1, 1960)

Vibrationally excited *sec*-butyl-d_1 radicals have been produced by addition of D atoms to *cis*-butene-2. The radicals, which have a narrow range of internal energy E, undergo either collisional stabilization (S) or decomposition (D) with specific rate k_E. The ratio D/S has been studied as a function of pressure down to 0.005 mm at 25°. Using calculated values of k_E, information is obtained about vibrational transitions upon collision of excited radicals with butene molecules, under different assumptions regarding the form of the transition probability function. It is shown that in these cases the average energy transferred is at least 8.5 kcal/mole, and quite probably much more, which supports the conventional Lindemann collisional activation-deactivation assumption of strong collisions in this case.

WHILE theories of vibrational energy transfer between molecules in collision have been proposed for the low-energy region of importance in ultrasonic dispersion,[1] and attempts have been made to extend these at least qualitatively to the higher energies at which chemical reaction can occur,[2] little is known about the actual probabilities of transfer from highly excited vibrational states of polyatomic molecules, and little progress may be expected until there is a substantial body of experimental data.[3] This paper is directed to this need.

Much of the existing information on the relative collisional efficiencies of gas molecules for vibrational energy transfer at high energies comes from the study of inert gas effects in unimolecular reactions,[4] and reverse recombination events.[5] The relation of vibrational transition probabilities to the calculation of unimolecular reaction rates is extremely complicated, except under various limiting assumptions and conditions[6–9] (which include the case of the Lindemann assumption below). The reverse deduction of transition probabilities from rate measurements is even more difficult and, in the absence of additional information, essentially ambiguous. Nevertheless an insight into the energy-transfer process may be gained in this way. Consider the special case where the collisional transfer probability vanishes except when the average vibrational energy transferred ΔE is large compared to the mean energy $\langle E-E_0\rangle$ of species above the critical energy E_0 (the conventional Lindemann assumption). Then on the average $1/\beta$ collisions will be experienced by an activated molecule before a deactivation transition is induced, where β is an "all or nothing" collisional deactivation efficiency (and may be a function of energy). Since β appears in both the rates of activation and deactivation, the high pressure rate will not be affected by its value. However, its average value enters the low pressure rate and may be determined in principle, subject to the Lindemann assumption, by rate measurements at limiting low pressures.

If the Lindemann condition is not valid and small increments of energy are exchanged, the rates of activation and deactivation may be related to transition probabilities through nonequilibrium theory[6–8]; the probability of reaction being dependent on the mean passage time for a random walk through the activated region. If an activated species capable of decomposition is produced photochemically or by chemical activation,[10] the probability of stabilization relative to reaction, (S/D), reflects its mean passage time out of the activated region, and will in general be a complicated function of pressure and specific reaction probability. If Lindemann deactivation occurs, (S/D) will be proportional to the collision number ω and hence to the pressure p, as $p\to 0$. On the other hand, if a molecule may only lose energy in decrements ΔE less than $\langle E-E_0\rangle$, then at limitingly low pressures the probability of losing the successive decrements ΔE needed for deactivation becomes extremely small. For example, if species were formed at a single energy $E=E_0+n\Delta E$, and if the reaction probability k_E were a constant for $E>E_0$, then it is readily shown that

* Acknowledgment is made to the donors of the Petroleum Research Fund administered by the American Chemical Society, for partial support of this work. Abstracted in part from a Ph.D. thesis to be presented by R.E.H. to the Graduate School, University of Washington, Seattle, Washington.

† Shell Oil predoctoral fellow.

[1] (a) Z. Slawsky, R. N. Schwartz, and K. F. Herzfeld, J. Chem. Phys. **20**, 1591 (1952); (b) K. F. Herzfeld and T. A. Litovitz, *Absorption and Dispersion of Ultrasonic Waves* (Academic Press, Inc., New York, 1959).

[2] B. H. Mahan, J. Phys. Chem. **62**, 100 (1958).

[3] M. Boudart and J. T. Dubois, J. Chem. Phys. **23**, 223 (1955).

[4] M. Volpe and H. S. Johnston, J. Am. Chem. Soc. **78**, 3903 (1956).

[5] D. L. Bunker and N. Davidson, J. Am. Chem. Soc. **80**, 5090 (1958).

[6] R. J. Rubin and K. E. Shuler, J. Chem. Phys. **25**, 59, 68 (1956); E. W. Montroll and K. E. Shuler, Advances in Chem. Phys. **1**, 361 (1958).

[7] S. K. Kim, J. Chem. Phys. **28**, 1057 (1958).

[8] B. Widom, J. Chem. Phys. **31**, 1387 (1959).

[9] E. E. Nikitin and N. D. Sokolov, J. Chem. Phys. **31**, 735 (1959).

[10] (a) B. S. Rabinovitch and R. W. Diesen, J. Chem. Phys. **30**, 735 (1959); (b) B. S. Rabinovitch, D. H. Dills, W. H. McLain, and J. H. Current, *ibid.* **32**, 493 (1960).

$S/D \propto p^n$ as $p \to 0$. This would represent a catastrophic fall in S/D at low pressures if n were much greater than unity. This is an extreme case, and where $k_E \to 0$ as $E \to E_0$, and a distribution of energy jump sizes is allowed, the change in S/D would be less marked.

In this paper are presented the results of a study of the unimolecular decomposition of chemically activated *sec*-butyl-d_1 radicals produced at 25° from D+*cis*-butene-2, at pressures down to 0.005 mm Hg. No deviation from linearity of S/D with pressure was found. We may use this result together with an assumed rate constant k_E to obtain information about the transition probabilities. Using a k_E of the Marcus type,[11] a lower limit is set to the average amount of energy transferred per collision in the activated region, for particular assumed forms of the energy transition probability distribution function. In this experiment, at low heat bath temperature, attention may be confined to the deactivation process, which is a useful simplification.

EXPERIMENTAL METHOD

Recently we have described the study of vibrationally excited alkyl radicals arising by the addition of H atoms to simple olefins, such as butene,[10]

$$H + C_4H_8 \rightarrow CH_3\dot{C}HCH_2CH_3^*.$$

If excited from a heat bath at low temperature the radicals are relatively monoenergetic. By using different isomers of the olefin with either hydrogen or deuterium atoms, the radical energy may be varied. *Sec*-butyl-d_1 radicals employed here are produced with minimum total vibrational energy of 43 kcal/mole from D atoms+*cis*-butene-2.[12] This corresponds to a minimum excess energy ($E - E_0$) of 10 kcal above the critical energy for decomposition to propylene plus methyl. By measuring the relative amounts of products arising from collisional stabilization and decomposition of the radicals, it is possible to determine the quantity D/S as a function of pressure.

$$CH_3\dot{C}HCH_2CH_3^* \xrightarrow{D(k_E)} \cdot CH_3 + C_3H_6$$

$$\xrightarrow{S(\omega)} CH_3\dot{C}HCH_2CH_3.$$

For monoenergetic radicals, the experimentally observed average rate constant $k_a = \omega \cdot D/S$ should be independent of pressure if deenergization follows the Lindemann probabilities; lesser efficiency would give rise to increase of k_a with decline of pressure. Expression of the data in terms of k_a, rather than D/S, permits inspection of the results more readily.

Apparatus and Procedure

The details of the experimental arrangement and procedure have been described previously,[10,12] as has the determination of the amounts of stabilization and decomposition of excited butyl radicals.

Because virtually all D atoms reach the wall of the 1 l reactor vessel at the lower pressures used here, it was necessary to ensure that reflection of D atoms occurred and that formation of stabilized butyl radicals was not a consequence of the heterogeneous addition of D atoms to the double bond in the presence of a heat sink. A similar possibility was excluded earlier in a study of H atoms with ethylene[10b]; it was stringently tested here by experiments over a suitable range of pressures with a packed vessel (3.5 g of Pyrex glass fibers, having surface area tenfold greater than the wall, was distributed homogeneously throughout the 1 l reactor), and in experiments done in a small 85 ml reactor.

It is assumed, as may be supported on theoretical grounds, that inefficiency of the principal reaction of stabilized radicals at low pressures, namely

$$C_4H_8D + \cdot CH_3 \rightarrow i\text{-pentane},$$

does not lead to an error in estimation of the amount of the collisional stabilization process. Similarly, there seems little evidence to support the significance of the reaction sequence

$$D + C_4H_8D \rightarrow C_4H_8D_2^* \rightarrow \text{decomposition products}.$$

In any case, the amount of stabilization product measured is thus a lower limit to the true amount, which would accentuate any departure from the Lindemann collisional assumption of strong collisions.

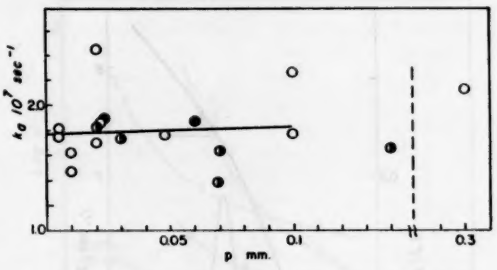

FIG. 1. Plot of k_a vs pressure. ⊙ 1 l reactor; ◑ small reactor; ● packed 1 l reactor.

RESULTS AND DISCUSSION

The experimental results at 25°C are summarized as a plot of k_a *vs* p in Fig. 1. The data extend down to an S/D ratio of 0.0057 at the lowest pressure used, 0.0050 mm, where $\omega = 1.01 \times 10^8$ sec^{-1}. The collision diameters used for butyl and *cis*-butene-2 are those given previously.[10] The data at 0.1 mm and below are fitted by a line of almost zero slope, so k_a is sensibly constant and shows *no increase* at lower pressures. The probable error of an individual measurement is ~10% and this may be taken as the upper limit of any rise in k_a at the lowest pressure.

[11] R. A. Marcus, J. Chem. Phys. **20**, 359 (1952).
[12] R. E. Harrington, B. S. Rabinovitch, and R. W. Diesen, J. Chem. Phys. **32**, 1245 (1960).

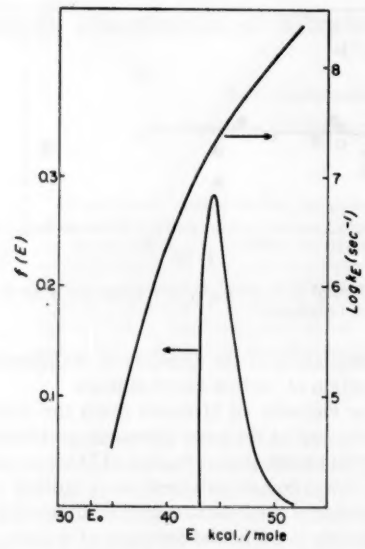

FIG. 2. Plot of $f(E)$ vs E and $\log_{10}k_E$ vs E.

The low pressure limiting value of $k_a=1.8\times10^7$ sec^{-1} is a little less than that previously adopted,[12] but the difference is within experimental error.

The results obtained with a packed vessel and a small vessel (Fig. 1) show that no wall effect occurs and that addition to the double bond is a homogeneous process. Barring coincidental compensation of opposing factors, the data also support theoretical prediction that radiative transitions are negligible even at the longest collision times (10^{-5} sec).

Calculation of D/S for Different Transition Probability Functions

Since *no* effect of collisional inefficiency is evident, the data can only provide an estimate of the lower limit to the average amount of energy transferred per collision from butyl to *cis*-butene-2 molecules. This estimate depends, of course, on the assumed distribution of collisional transfer probabilities. The consequence of different distributions will now be examined.

In order to find the steady-state population of each element of the activated region, and hence the over-all degree of reaction, we use the activation distribution function $f(E)$ and the specific dissociation probabilities k_E previously calculated by quantum-statistical summation[12] (Fig. 2). The number of vibrational energy levels for the butyl-d_1 radical (for 31 vibrational degrees of freedom) has been found by a simplified direct count[12] to be of the order of 10^{11} to 10^{12} per kcal at the energies concerned, so that the activated region may be regarded as a continuum. Define $P(E,\epsilon)d\epsilon$ as the probability that a molecule initially at E will undergo transition to an element $d\epsilon$ at ϵ in one second. Both the specific dissociation probability and transition probabilities are taken to be explicit functions of the *total* internal energy of the molecules. The steady-state population of the molecules N_E is given by the solution of the integral equation:

$$-dn_E/dt=n_Ek_E-f(E)+\int_0^\infty\{n_EP(E,\epsilon)-n_\epsilon P(\epsilon,E)\}d\epsilon=0, \quad (1)$$

where $n_E=N_E/R$, R being the total amount of excitation per second, and $f(E)dE$ is the fractional activation initially to the element dE at E. The physical constraints, *viz.* that

$$\int_0^\infty P(E,\epsilon)d\epsilon=\beta\omega$$

and

$$\int_0^\infty f(E)dE=1,$$

ensure that solutions to (1) exist.

If the activated region is divided into discrete subregions, values of k_i and f_i being assigned to each region and values of P_{ij} to each pair of regions, by suitable averaging, and the integral is replaced by a summation, Eq. (1) reduces to a set of linear equations. This in no way implies a particular quantum structure for the activated region; and by taking a sufficient number of subregions the solution of Eq. (1) may be approached as closely as desired. (In practice subregions 1 kcal wide were used.) The population of the ith region is given by

$$n_i=(f_i+\sum_{j\neq i}P_{ji}n_j)/(k_i+\beta\omega). \quad (2)$$

Now whatever the form of P_{ij} it must satisfy the detailed balance condition, for limitingly small subregions,

$$P_{ij}/P_{ji}=\exp\{-(E_j-E_i)/RT\}\cdot g_j/g_i.$$

It is shown later that, in the present case, transitions involving only several kcal may be neglected, so that we may put $P_{ij}\gg P_{ji}$ throughout, thus treating the problem as one of a system of molecules cascading in steps through the activated region without reactivation. This obviates the necessity of simultaneously solving the set of Eqs. (2) since, by starting with the highest excitation level, all the steady-state populations n_i may be obtained successively. From the populations n_i the ratio D/S is obtained directly

$$D=R\sum n_ik_i; \qquad S=R-D; \qquad (D/S)=\sum n_ik_i/(1-\sum n_ik_i).$$

Two simple and extreme models for P_{ij} were used: a "stepladder" model and an "exponential" model. Calculated values of D/S were then expressed as a

ratio $\gamma=(D/S)/(D/S)_L$ where $(D/S)_L$ is the value to be expected under the naive Lindemann assumption used in the computation of k_a. The calculations refer to the lowest experimental pressure (0.005 mm) and 25°C.

The stepladder model is defined by

$$\left.\begin{aligned} P_{ij}&=\beta\omega; \quad i-j=m \\ &=0; \quad i-j\neq m \end{aligned}\right\}$$

and represents a simple cascade in steps of m kcal.[13] Values of γ calculated for different m are plotted in Fig. 3 for k_i, and also for a reduced value $k_i/25$ which seems a generous estimate of possible uncertainty in calculated k_i values. D/S increases very rapidly with decrease in ΔE as would be expected.

In the exponential model, we consider a distribution of the form $P_{ij}=\beta\omega a\exp(-a(j-i))$. P_{ij} is normalized to the effective collision number $\beta\omega$ and represents an average jump size of $1/a$ kcal. Results are given for three different values of a in Fig. 2. We will not be concerned here with the physical implications of these two models.

Allowing a possible 10% experimental error in the value $\gamma=1$ at a pressure of 0.005 mm, the calculated results set limits to the nature of the transitions. We may conclude:

(a) If the de-energization is strictly of the stepladder type with equally spaced transitions occurring on every collision ($\beta=1$), then the size of the jumps must be ≥ 11.5 kcal. Allowance of a decreased value of k_i by a factor of 25 reduces the lower limit to 8.5 kcal.

(b) With an exponential distribution of jump sizes, an average jump of ~50 kcal would be required to reproduce the results for $\beta=1$. This distribution is so flat as to be virtually linear over a range of 10 kcal, and its application to the case $k_i/25$ is a scarcely necessary.

These findings may be explained in terms of statistical redistribution of vibrational energy of collision partners.[13]

If a value of $\beta<1$ is allowed, there is a corresponding uncertainty in deductions of transition probabilities, since the kinetic experiments do not distinguish between slow deactivation due to elastic collisions and that due to cascade through very closely spaced levels. Studies of the ultrasonic relaxation of molecules comparable to the butyl radical show[14] that deactivation of the lowest excited vibrational state can occur within 5

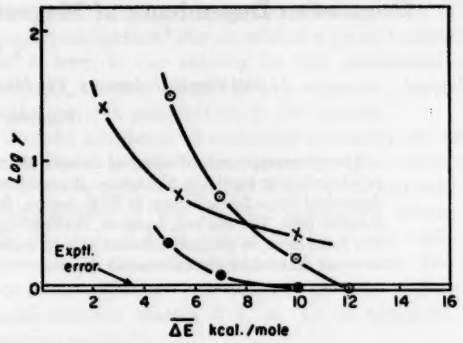

FIG. 3. Plot of $\log_{10}\gamma$ vs ΔE, the average energy transferred per effective collision. ⊙ stepladder model, $\beta=1$; ● stepladder model using $k_i/25$ and $\beta=1$; × exponential model, $\beta=1$.

collisions. It may be that an equal collisional efficiency operates for transitions between more widely spaced levels. In any case, a value of $\beta<1$ only forces a larger jump size than the minima already cited, in those collisions where a significant transition does take place, and a value of $\beta\ll 1$ cannot be tolerated.

It is clear that although butyl radicals may possibly lose energy in small steps, and notwithstanding the possibility of a high quantum-mechanical transition probability for such a process, nevertheless the results obtained here indicate the existence of a parallel mode of deactivation by large steps which effectively determine the kinetics at low pressures. Insofar as it may be valid to extend this conclusion to other unimolecular reactions of complex molecules,[3] we may surmise that Lindemann activation-deactivation is effective in such cases and that no reformulation of this aspect of unimolecular reaction theory is required. It would be desirable, however, to extend these experiments to molecular, as opposed to radical, species, to test this hopeful surmise.

In several recent papers dealing with the mercury photosensitized production of alkyl radicals by addition of H atoms to alkenes, a hot radical energy effect has been invoked to explain the nature of the radical disproportionation and recombination results.[15] Since ~10^5–10^8 collisions with inert hydrocarbon molecules must intervene between the formation and fruitful collision of a radical, it seems likely that the observed results are not to be simply interpreted as energy effects even though an excess energy for recombination, disproportion is only in respect to the average thermal energy.

[13] P_{ij} is taken independent of i (i.e., β independent of energy) as a useful simplification, since the range of i is limited.

[14] C. J. Franck and A. Eucken, Z. physik. Chem. **B20**, 460 (1933), and interaction of reactive species which may undergo reaction.

[15] J. D. Lambert and R. Salter, Proc. Roy. Soc. (London) **A253**, 277 (1959).

[16] P. J. Boddy and J. C. Robb, Proc. Roy. Soc. (London) **A249**, 518 (1959); R. A. Back, Can. J. Chem. **37**, 1834 (1959).

Orientation Dependence of Magnetic Hyperfine Structure in Free Radicals*

S. M. BLINDER

Applied Physics Laboratory, The Johns Hopkins University, Silver Spring, Maryland

(Received February 18, 1960)

The anisotropic part (B term) of the spin Hamiltonian for a free radical is averaged to zero when there is rapid molecular tumbling. Otherwise, it combines with the isotropic part (A term) to produce orientation-dependent hyperfine splittings in ESR spectra. In the high-field case, the electron is strongly coupled to the external field. The nucleus, however, is effectively coupled to the electron's tensor field. Consequently, the two spins have, in general, different axes of quantization. Applying first-order perturbation theory, expressions are derived for the orientation dependence of the resonance in a single crystal and for the line shape in a powder.

THIS note will be concerned with orientation-dependent hyperfine structure arising from magnetic interaction between nuclear and electron spins in molecular systems. Zeldes *et al.*[1] have recently given results applying to hybridized $s-p$ orbitals. We shall present here a more generalized treatment, applicable to cases of lower symmetry as well.

Under conditions generally obtaining in electron spin resonance (ESR) spectroscopy, the dominant contribution to the magnetic energy of the system comes from Zeeman coupling of the electron spins with the field. Secondary contributions may arise from a variety of sources, most important being magnetic coupling with nuclear spins. Also possible are spin-rotational and nuclear quadrupole interactions as well as nuclear Zeeman coupling. In a great many free-radical studies, these latter are, however, entirely absent or of negligible magnitude.[2]

In atomic systems, anisotropic contributions to hyperfine interaction vanish by virtue of the spherical symmetry. Also, in liquids and gases, these terms are generally averaged to zero by high-frequency molecular reorientations.[3] In both cases, only the residual isotropic interaction (Fermi contact term) is observed. The resultant energy levels are then given by the Breit-Rabi formula.[4] Orientation-dependent terms are, in contrast, often the dominant feature of ESR spectra of crystals. Powders or glassy solids, of course, exhibit statistical averages of these anisotropies.

Recent measurements of ESR angular dependence in oriented single crystals[5] have made possible the evaluation of new molecular parameters. Detailed information on the distribution of the unpaired electron, e.g., the extent of delocalization, is thus made available. We shall attempt to relate these constants to observed orientation-dependent spectra. As might be expected, molecular symmetry plays an important role in determining the number and relative magnitude of such parameters: some vanish, others become degenerate as the symmetry increases.

We shall limit our consideration to the case of a single unpaired electron interacting with a single magnetic nucleus. The results may be generalized to interactions involving a group of identical nuclei in equivalent or nearly equivalent chemical environments. Extension of the treatment to include multiple electrons or multiple nonequivalent nuclei is straightforward but will not be carried out here.

The well-known spin Hamiltonian for Zeeman and magnetic hyperfine interactions[6] is written in the following form:

$$\mathcal{H}(\mathbf{S},\mathbf{I}) = -g\mu_0\mathbf{H}\cdot\mathbf{S} + A\mathbf{S}\cdot\mathbf{I} + \mathbf{S}\cdot\mathfrak{B}'\cdot\mathbf{I} - g_I\mu_N\mathbf{H}\cdot\mathbf{I} \quad (1)$$

with

$$A\mathbf{S} = -gg_I\mu_0\mu_N(8\pi/3)\langle\sum_k\delta(\mathbf{r}_k)\mathbf{S}_k\rangle \quad (2)$$

and

$$\mathfrak{B}' = -gg_I\mu_0\mu_N\langle 3\mathbf{r}\mathbf{r}r^{-5} - \mathfrak{I}r^{-3}\rangle. \quad (3)$$

$\mathbf{H}$ represents the static magnetic field. μ_0 and μ_N are, respectively, the Bohr and nuclear magnetons; g and g_I, the electronic and nuclear spectroscopic splitting factors referred to their respective magnetons. $\mathbf{S}$ and $\mathbf{I}$ represent the electron and nuclear spin vector operators. $\mathbf{r}_k$ is here the position vector of electron k in a *space-fixed* coordinate system with origin at the magnetic nucleus. $\mathfrak{I}$ is the unit diadic. The four parts of (1) represent, respectively, the electronic Zeeman energy, the isotropic and anisotropic hyperfine interactions, and the nuclear Zeeman energy.

We have assumed implicitly in writing (1), that the electron magnetic moment is due entirely to spin.

* This work supported by the Bureau of Naval Weapons, Department of the Navy.

[1] H. Zeldes, G. T. Trammel, R. Livingston, and R. H. Holmberg, J. Chem. Phys. **32**, 618 (1960).

[2] Nuclear quadrupole coupling might be important in radicals containing Cl or I nuclei. The nuclear Zeeman energy may become comparable with the hyperfine terms in a very large field or for a nucleus several shells removed from an F center. See N. W. Lord, Phys. Rev. Letters **1**, 511 (1958).

[3] S. I. Weissman, J. Chem. Phys. **22**, 1378 (1954).

[4] G. Breit and I. I. Rabi, Phys. Rev. **38**, 2082 (1931).

[5] D. K. Ghosh and D. H. Whiffen, Mol. Phys. **2**, 285 (1959); T. Cole, C. Heller, and H. M. McConnell, Proc. Natl. Acad. Sci. U. S. **45**, 525 (1959); H. M. McConnell, T. Cole, C. Heller, and R. W. Fessenden, J. Am. Chem. Soc. **82**, 766 (1960); I. Miyagawa and W. Gordy, J. Chem. Phys. **30**, 1590 (1959); **32**, 255 (1960).

[6] See, for example, A. Abragam and M. H. L. Pryce, Proc. Roy. Soc. (London) **A205**, 135 (1951); S. M. Blinder, J. Mol. Spectroscopy **5**, 17 (1960).

Orbital momenta, neglecting the important case of linear molecules,[7] are partially or completely "quenched" by asymmetric molecular or crystal fields. Furthermore, we have ignored the possible anisotropy in the electronic g factor.[8] Should the anisotropy in g be comparable to that in the hyperfine coupling, our treatment of angular dependence would have to be generalized. We shall not attempt here to analyze this exceedingly complicated situation.

The expectation value brackets in (2) and (3) denote averages over the complete molecular wave function. The bracket in the B term is effectively an integral over the orbital of the unpaired electron. The A term, however, will, in general, include contributions from other orbitals as a consequence of exchange polarization.[9] For an orbital with no s character, the A term is due entirely to this mechanism. Accordingly, A may be positive or negative, depending on the net spin polarization at the nucleus.

To take advantage of molecular symmetry, we effect a coordinate transformation from the space-fixed axes XYZ to the molecule-fixed axes xyz coincident with the principal axes of the traceless symmetric tensor $\mathfrak{B}'$. The direction of $\mathbf{H}$ is chosen as the Z axis while the figure axis of the molecule serves as the z axis. The two coordinate systems are related by the orthogonal transformation matrix $\mathfrak{Q}(\theta, \phi, \chi)$ in terms of the Eulerian angles.[10]

$$\mathfrak{Q}(\theta\phi\chi)=\begin{bmatrix}\cos\theta\cos\phi\cos\chi-\sin\phi\sin\chi & \cos\theta\sin\phi\cos\chi+\cos\phi\sin\chi & -\sin\theta\cos\chi\\ -\cos\theta\cos\phi\sin\chi-\sin\phi\cos\chi & -\cos\theta\sin\phi\sin\chi-\cos\phi\cos\chi & \sin\theta\sin\chi\\ \sin\theta\cos\phi & \sin\theta\sin\phi & \cos\theta\end{bmatrix} \tag{4}$$

Consequently, we may write

$$\mathfrak{B}'=\mathfrak{Q}^{-1}\cdot\mathfrak{B}\cdot\mathfrak{Q}, \tag{5}$$

the $\mathfrak{B}$ tensor being diagonal in the principal axes system

$$\mathfrak{B}=\begin{pmatrix}B_1 & 0 & 0\\ 0 & B_2 & 0\\ 0 & 0 & B_3\end{pmatrix} \tag{6}$$

with

$$B_1=-gg_I\mu_0\mu_N\langle(3x^2-r^2)/r^5\rangle, \quad \text{etc.} \tag{7}$$

and

$$B_1+B_2+B_3=0. \tag{8}$$

We shall confine further considerations to the following set of conditions. (1) The electron spin Zeeman coupling constitutes the dominant energy contribution to the Hamiltonian (1) (large external field). (2) The only interactions leading to hyperfine structure are the A and B terms (nuclear quadrupole and molecular rotation effects are neglected). (3) The nuclear Zeeman energy is negligible in comparison with the hyperfine terms. (4) Anisotropy in the electronic g factor is negligible compared to that arising from hyperfine interaction (hence orbital momenta are effectively "quenched").

It is most convenient to treat the hyperfine interaction by perturbation theory. Accordingly, we write

$$\left.\begin{aligned}\mathfrak{IC}_0(\mathbf{S})&=-g\mu_0HS_z\\ \mathfrak{V}(\mathbf{S},\mathbf{I})&=A\mathbf{S}\cdot\mathbf{I}+\mathbf{S}\cdot\mathfrak{Q}^{-1}\cdot\mathfrak{B}\cdot\mathfrak{Q}\cdot\mathbf{I}.\end{aligned}\right\} \tag{9}$$

We shall consider only first-order contributions of the perturbation operator $\mathfrak{V}(\mathbf{S}, \mathbf{I})$. Second-order terms, in addition to being more tedious to evaluate, are comparable in magnitude to the neglected nuclear Zeeman term.[11]

Matrix elements are first evaluated in the M_S, M_I quantization scheme, with respect to the fixed Z axis. In this representation $\mathfrak{IC}_0$ is diagonal. The unperturbed energy levels (no hyperfine coupling) are given by

$$E^{(0)}(M_S)=-g\mu_0HM_S, \tag{10}$$

each being $(2I+1)$-fold degenerate. First-order contributions are now computed by diagonalization of each $(2I+1)\times(2I+1)$ block of $\mathfrak{V}$ diagonal in M_S. This is equivalent to finding an effective axis of quantization for $\mathbf{I}$ by the following procedure.[12]

We write for $\mathfrak{V}$

$$\mathfrak{V}(M_S,\mathbf{I})=M_S(AI_z+\mathbf{k}\cdot\mathfrak{Q}^{-1}\cdot\mathfrak{B}\cdot\mathfrak{Q}\cdot\mathbf{I}), \tag{11}$$

this being now a diagonal matrix element in $\mathbf{S}$ but remaining an operator function in $\mathbf{I}$. Expanding the

[7] R. A. Frosch and H. M. Foley, Phys. Rev. **88**, 1337 (1952); R. Beringer, E. B. Rawson, and A. F. Henry, *ibid.* **94**, 343 (1954).

[8] B. Bleaney, Phil. Mag. **42**, 441 (1951).

[9] Isotropic hyperfine interaction by exchange polarization is discussed by: Abragam and Pryce, footnote reference 6; H. M. McConnell and D. B. Chesnut, J. Chem. Phys. **28**, 107 (1958); M. H. Cohen, D. A. Goodings, and V. Heine, Proc. Phys. Soc. **73**, 811 (1959); S. M. Blinder, Bull. Am. Phys. Soc. **5**, 14 (1960); Phys. Rev. (to be published).

[10] We employ the definition of these angles as given in E. B. Wilson, J. C. Decius, and P. C. Cross, *Molecular Vibrations* (McGraw-Hill Book Company, Inc., New York, 1955), pp. 285–286. θ and ϕ are the spherical polar coordinates of the z axis relative to the Z axis while χ represents the orientation of the molecule about the z axis. Physically it is evident that the hyperfine energy is independent of ϕ.

[11] See footnote 14, however.

[12] The component of $\mathbf{I}$ along $\mathbf{H}$ is not a constant of the motion unless the B term is small *wrt* the nuclear Zeeman energy (or when $\mathfrak{B}=0$).

tensor product in the B term, we obtain

$$\mathcal{U}(M_S, \mathbf{I}) = M_S(\alpha I_X + \beta I_Y + \gamma I_Z) \tag{12}$$

with

$$\alpha = Q_{11}Q_{13}B_1 + Q_{21}Q_{23}B_2 + Q_{31}Q_{33}B_3$$
$$\beta = Q_{12}Q_{13}B_1 + Q_{22}Q_{23}B_2 + Q_{32}Q_{33}B_3$$
$$\gamma = A + Q_{13}^2B_1 + Q_{23}^2B_2 + Q_{33}^2B_3.$$

Multiplying and dividing (12) by

$$K = (\alpha^2+\beta^2+\gamma^2)^{\frac{1}{2}},$$

we may regard α/K, β/K, γ/K as direction cosines for an axis Z'; consequently

$$\mathcal{U}(M_S, \mathbf{I}) = KM_SI_Z'. \tag{13}$$

Since $\mathbf{I}$ is quantized in the same way about any axis fixed in space,

$$E^{(1)}(M_S, M_I') = KM_SM_I', \tag{14}$$

M_I' being the Z' component of $\mathbf{I}$. Thus the Hamiltonian $\mathcal{H}_0+\mathcal{U}$ is diagonalized to first order in the hybrid M_S, M_I' representation.

The axis Z' represents physically the direction of the magnetic field as the nucleus—the averaged field of the unpaired electron. It is in this field that the nuclear spin is effectively quantized. We note that the operator I_Z', hence the quantum number M_I', is implicitly dependent upon the orientation of the molecule. Thus a molecule will not, in general, maintain the same value of M_I' if subjected to a hypothetical reorientation. In a large ensemble of molecules there will exist an equilibrium distribution of nuclear spin states for each orientation. Except at temperatures $\ll 1°$K, this distribution will be very nearly statistical, thus virtually independent of orientation. The M_I' quantization, to summarize, is valid either for a single molecule in a fixed orientation or for an ensemble of molecules with statistical distribution of orientations and of M_I'-states.

Of the three parameters $B_1B_2B_3$, only two are independent by virtue of the vanishing trace. It is convenient to define two axuiliary parameters as follows

$$B \equiv \tfrac{1}{2}B_3 = -\tfrac{1}{2}(B_1+B_2)$$
$$C \equiv \tfrac{1}{2}(B_1-B_2). \tag{15}$$

K is then given by

$$K^2 = \begin{cases} A^2+2AB(3\cos^2\theta-1)+B^2(3\cos^2\theta+1) \\ \quad +C^2\sin^2\theta+2C(A-B)\sin^2\theta(\cos^2\chi-\sin^2\chi). \end{cases} \tag{16}$$

When z represents a threefold or higher axis of rotation, in particular, for cylindrical symmetry, B_1 and B_2 become degenerate, C vanishes, and χ dependence is removed in first order. C is thus a measure of deviation from cylindrical symmetry.[13]

[13] It is convenient to label the principal axes in such way that $|B|>|C|$. However, should one of the principal moments vanish, choose $B=0$, $|C|>0$.

For $C=0$, (14) and (16) may be written

$$E^{(1)}(M_S, M_I') = [A^2+2AB(3\cos^2\theta-1)+B^2(3\cos^2\theta+1)]^{\frac{1}{2}}M_SM_I'. \tag{17}$$

This is rigorous for cylindrical symmetry, an approximation for nearly cylindrical symmetry ($|C| \ll |B|$). The selection rules for magnetic dipole transitions are given by

$$\Delta M_S = 0, \qquad \Delta M_I' = \pm 1 \text{ (NMR transition)}$$

or

$$\Delta M_S = \pm 1, \qquad \Delta M_I' = 0 \text{ (ESR transition)}.$$

No combination lines appear to first order. However, since $M = M_S + M_I$ is not a constant of the motion (as it is in the Breit-Rabi treatment), simultaneous nuclear-electronic transitions can occur in higher order, giving rise to satellite lines.[14] Presuming that the above selection rules apply, the observed hyperfine components are given by

$$\nu(\theta) = \frac{E^{(1)}(M_S, M_I') - E^{(1)}(M_S-1, M_I')}{h}$$
$$= [A^2+2AB(3\cos^2\theta-1)+B^2(3\cos^2\theta+1)]^{\frac{1}{2}}M_I', \tag{18}$$

ν being referred to the center of the resonance and A, B expressed in frequency units. For an oriented single crystal, then, (18) gives the resonance frequencies as a function of orientation,

Several special cases are of interest. For $B=0$ there is, of course, no orientation dependence. When $B=-2A$, the angular dependence also vanishes, to accuracy of first order. When $|A| \gg |B|$, the root in (18) may be expanded to yield

$$\nu(\theta) \approx [A+B(3\cos^2\theta-1)]M_I', \tag{19}$$

whereas, when $|B| \gg |A|$,[15]

$$\nu(\theta) \approx [B(3\cos^2\theta+1)^{\frac{1}{2}} + A(3\cos^2\theta-1)(3\cos^2\theta+1)^{-\frac{1}{2}}]M_I'. \tag{20}$$

In a powder, a statistical distribution of single crystal orientations is observed. We denote the theoretical shape of the powder spectrum (ignoring other factors contributing to line shape) by $g(\nu)$. This is the sum of $2I+1$ component line shape functions, one for each M_I'

$$g(\nu) = \sum_{M=-I}^{I} g_M(\nu). \tag{21}$$

[14] G. T. Trammell, H. Zeldes, and R. Livingston, Phys. Rev. **110**, 630 (1958). In certain circumstances the second-order spectrum can actually be more intense than the first-order spectrum. See Miyagawa and Gordy (1960), footnote reference 5.

[15] This case obtains for a p orbital having little or no contact hyperfine interaction (via exchange polarization). A similar equation is derived in footnote reference 1.

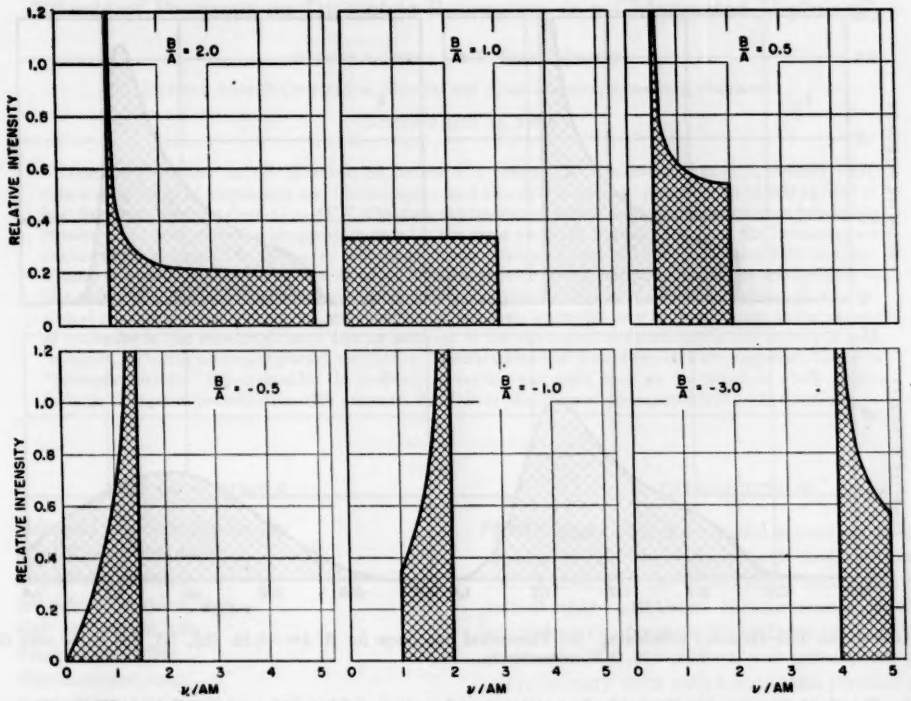

FIG. 1. Theoretical line shapes. Each figure shows a single hyperfine component ($M \neq 0$) of the powder spectrum.

If each component function is normalized to unity [with $g_0(\nu)=\delta(\nu)$], $g(\nu)$ is normalized to $2I+1$. The fraction of molecules (or crystallites) having polar angle between θ and $\theta+d\theta$ is $\frac{1}{2}\sin\theta d\theta$. We denote the corresponding resonance frequencies by ν and $\nu+d\nu$. Consequently, we may write

$$g_M(\nu)d\nu=\tfrac{1}{2}\sin\theta d\theta, \tag{22}$$

ν being implicitly dependent on θ through (18). Solving (18) for $\cos\theta$ and differentiating with respect to ν, we find

$$g_M(\nu)=g_{-M}(\nu)=-\tfrac{1}{2}d\cos\theta/d\nu$$
$$=-\tfrac{1}{2}\frac{1}{M(6AB+3B^2)^{\frac{1}{2}}}\frac{\nu/M}{[(\nu/M)^2-(A-B)^2]^{\frac{1}{2}}}, \tag{23}$$

$(\nu/M)^2$ being restricted to values between $(A-B)^2$ and $(A+2B)^2$. Only non-negative values of $g_M(\nu)$ are physically meaningful. For convenience, we may label the high-field ($\nu>0$) part of the spectrum with $M>0$, the low-field part ($\nu<0$) with $M<0$. Accordingly, a normalized hyperfine component line shape is given by

$$g_M(\nu)=\frac{1}{|M||6AB+3B^2|^{\frac{1}{2}}}\frac{\nu/M}{|(\nu/M)^2-(A-B)^2|^{\frac{1}{2}}} \tag{24}$$
$$|A-B|\leq\nu/M\leq|A+2B|, \qquad (B/A)>0 \text{ or } <-2$$
$$|A+2B|\leq\nu/M\leq|A-B|, \qquad -2<(B/A)<0.$$

The function becomes infinite at $\nu=|A-B|M_I'$. This frequency corresponds to the most probable molecular orientation ($\theta=\pi/2$), The shape of $g_M(\nu)$ is characterized by a single parameter, B/A, and is thus dependent only on the relative signs of A and B, not at all on their absolute signs. In Fig. 1 are sketched theoretical powder line profiles for several values of the parameter.[16] For $B/A>0$ or <-2, the infinity in $g_M(\nu)$ occurs at the smallest allowed value of $|\nu|$. whereas, for $-2<B/A<0$, it is at the largest $|\nu|$. The case $B/A=+1$ is exceptional. In general (excepting the region $-2<B/A<0$), the larger $|B|$, the broader the powder spectrum and the poorer the spectroscopic resolution.

In the absence of the B term, e.g., in fluid medium, the resonance frequencies are given by $\nu=AM_I'$. The intensity maxima in the powder are, as we have seen, close to $|A-B|M_I'$.[17] If a free radical is studied in both fluid and powder media, the constants $|A|$ and $|A-B|$ may be assigned from the positions of the peaks alone.[18] The absolute value of B is then either

[16] These line shapes are qualitatively similar to certain NMR powder spectra. See, for example, G. E. Pake, J. Chem. Phys. **16**, 327 (1948).

[17] For the more general case ($C\neq 0$), the corresponding frequencies are given by

$$\nu=[(A-B)^2+C^2]^{\frac{1}{2}}M_I'.$$

[18] N. W. Lord and S. M. Blinder, Bull. Am. Phys. Soc. **5**, 72 (1960).

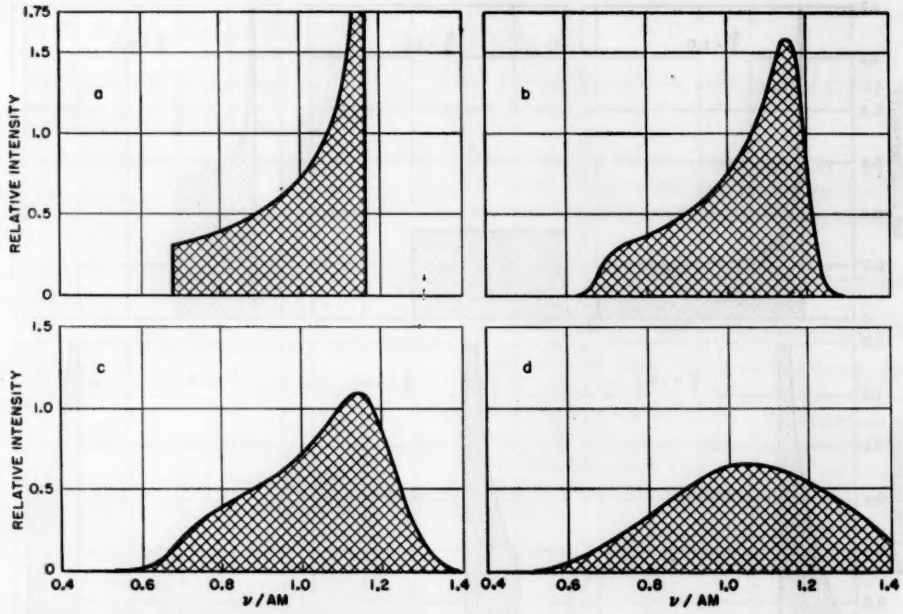

FIG. 2. Line shapes with Gaussian broadening. (a) Theoretical line shape for $B/A=-0.16$. (b), (c), (d) Same with Gaussian broadening corresponding to $\sigma/A=0.04$, 0.08, 0.20, respectively.

$|A|\pm|A-B|$. A choice may presumably be made on the basis of observed powder line shape, if not from theoretical considerations. If the absorption derivative is observed, peaks may appear at the frequencies $|A+2B|M_I'$ as well.

In discussing line shape we have thus far neglected other contributory factors: anisotropy in g, dipolar broadening, unresolved hyperfine structure, field inhomogeneity, as well as various exchange, saturation, and relaxation effects. The line shape from all factors excluding hyperfine angular dependence may generally be represented by either a Gaussian or a Lorentzian distribution function (provided the g anisotropy is not too large, in which case the line shape would be asymmetric). Presuming that the line broadening is not altered in the transition from fluid to solid, the observed intensity distribution $g_{\text{exp}}(\nu)$ may be represented as an integral transform of one of the above theoretical line shapes $g(\nu)$

$$g_{\text{exp}}(\nu)=\int d\nu' G(\nu-\nu')g(\nu'), \tag{25}$$

where $G(\nu-\nu')$ is a normalized Gaussian or Lorentzian function inferred from the liquid ESR spectrum. It should be noted that the maxima in $g(\nu)$ may be shifted by this transform. In Fig. 2 we illustrate the effect of increasing Gaussian broadening (as measured by the standard deviation σ) on the shape of a powder line. We may generalize that larger values of σ cause greater shifts in the observed resonance peaks (the shift of peaks due to overlap of components must also be considered). Furthermore, as σ increases, so does the symmetry of the line, its shape approaching that of the Gaussian.

Some of the results in this paper have been applied to analysis of ESR spectra of diphenylpicrylhydrazyl (DPPH) and picrylaminocarbazyl in fluid and solid media.[19]

ACKNOWLEDGMENTS

The author is indebted to Dr. C. K. Jen, Dr. F. J. Adrian, and Dr. N. W. Lord for invaluable discussions on the subject of this paper and to Dr. Ralph Livingston and his colleagues for a preprint of their article.

[19] N. W. Lord and S. M. Blinder (to be published).

Effects of Pressure on Dielectric Relaxation in a Chlorinated Diphenyl*

THOMAS A. PERLS AND L. BRUCE WILNER

Lockheed Aircraft Corporation, Missiles and Space Division, Sunnyvale, California

(Received April 15, 1960)

Data are presented on the dielectric properties of a commercial chlorinated diphenyl, Aroclor 1260, over a wide range of frequencies and temperatures, and also over a range of pressures up to 200 kg/cm² at four fixed temperatures from 17 to 51°C. The data are compared with acoustical-relaxation data previously obtained, and with viscosity-temperature data for the same material. Similar data, from the literature, are evaluated for glycerol. The ratio η/τ_D is calculated over a range of temperatures for Aroclor 1260 and over a range of pressures for glycerol. The Aroclor 1260 data provide strong evidence against the applicability to this material of Debye's simple hydrodynamic model of a spherical dipole in a viscous medium. A distribution of relaxation times is observed, and it is pointed out that, while this may be due, in part, to the variety of molecules in the Aroclor, it may also be ascribed to the variety of configurations in the vicinity of each molecule, including various degrees of association. Several additional lines of research are suggested. The term "piezopermittivity" is proposed for the property of certain materials, such as the Aroclors, which results in large changes in permittivity with pressure. Possible applications of piezopermittivity are discussed.

LIST OF SYMBOLS

a	radius of spherical dipole, cm
A	area of test blob, cm²
A_0	empirical constant
B	empirical constant, deg
d	slab separation, cm
D	dissipation factor
D_0	displacement, cm
f	frequency, cps
F	force, dynes
$i=$	$(-1)^{\frac{1}{2}}$
k	Boltzmann constant, 1.38×10^{-16} erg/deg
K	"Modulus" η/τ_D, dynes/cm²
p	pressure, kg/cm²
P	shearing rate, radians/sec
S	shearing stress, dynes/cm²
t	time, sec
T	absolute temperature, deg Kelvin.
T_∞	empirical reference temperature, deg. Kelvin.
β	empirical exponent
$\delta=$	$\tan^{-1}D$
ϵ^*	complex dielectric constant
ϵ'	real part of the dielectric constant
ϵ''	imaginary part of the dielectric constant
ϵ_∞	limiting, high-frequency value of the dielectric constant
ϵ_0	limiting, low-frequency value of the dielectric constant
η	viscosity, dyne sec/cm², or poises
τ	generalized relaxation time, sec
τ_D	dielectric relaxation time, sec
τ_{dipole}	dielectric relaxation time computed from local field at elementary dipoles, sec
τ_0	empirical dielectric relaxation time, sec
τ_p	acoustical relaxation time, sec
ω	angular frequency, rad/sec

* This work was done as part of the LMSD General Research Program.

INTRODUCTION

THE study of dielectric and acoustical relaxation in liquids has made important contributions to our understanding of the liquid state, and it has been suggested[1] that additional measurements would be of interest on the pressure dependence of these relaxation frequencies.

Preliminary work with a sinusoidal pressure generator (SPG) on acoustical relaxation[2] in both glycerol and a chlorinated diphenyl, namely diphenyl metachloride (Aroclor No. 1260),[3] had shown a surprisingly large pressure dependence in Aroclor. The SPG data for Aroclor 1260 showed that the average acoustical relaxation time shifted by approximately a factor of ten toward lower frequencies with increase in static pressure over the range from 4 to 175 atmospheres.

Data in the literature for several chlorinated diphenyls on the changes in the complex dielectric constant with frequency and temperature [4,5] were compared with the acoustic relaxation data for Aroclor 1260 previously obtained[2] and showed a similar dependence on temperature: the average relaxation time decreases by a factor of ten for an increase in temperature of 5 to 13°C, the smaller required temperature range corresponding to higher viscosity.

Data were therefore obtained on the dielectric properties of the batch of Aroclor 1260 which had been used in the acoustic tests, and the computed dielectric relaxation times are compared in Fig. 1 with data from footnotes 4 and 5. It was found that the observed re-

[1] K. F. Herzfeld and T. A. Litovitz, *Absorption and Dispersion of Ultrasonic Waves* (Academic Press, Inc., New York and London, 1959).

[2] T. A. Perls, D. O. Miles, and L. B. Wilner, J. Acoust. Soc. Am. **32**, 274 (1960).

[3] On the average, this material is very nearly hexachlorobiphenyl.

[4] A. H. White and S. D. Morgan, J. Franklin Inst. **216**, 635 (1933).

[5] W. Jackson, Proc. Roy. Soc. (London) **153**, 158 (1936).

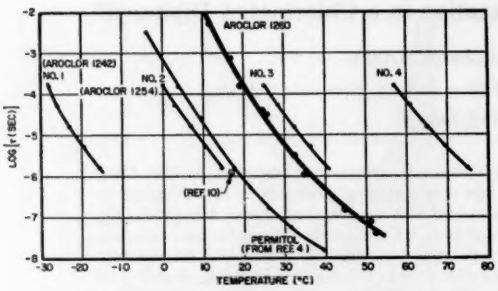

FIG. 1. Dielectric relaxation time vs temperature for several chlorinated diphenyls. Curves marked numbers 1, 2, 3, and 4 are replotted from data in footnote 4. Chlorinated diphenyls number 1 and 2 are identified as Aroclor 1242 and Aroclor 1254, respectively, in "The Aroclors," Application Data Bulletin No. O–P–115, Monsanto Chemical Company, Organic Chemicals Division, St. Louis, Missouri. The pentachlorobiphenyl [see footnote 18, and T. A. Litovitz and T. Lyon, J. Acoust. Soc. Am. **26,** 577 (1954)] and biphenyl pentachloride [see T. Litovitz and T. Lyon, J. Acoust. Soc. Am. **30,** 856 (1958)] used in the ultrasonic work of Litovitz and co-workers is Aroclor 1254 (personal communication from T. A. Litovitz).

laxation frequencies near room temperature were very nearly the same in acoustic and dielectric measurements performed with low static pressures. (Footnote 1 gives a comparison of ultrasonic and dielectric relaxation times for six liquids at atmospheric pressure and shows that $\tau_D > \tau_p$ in all cases, except for glycerol, where $\tau_D = \tau_p$ within the experimental errors.)

Because of the large observed pressure effect for the SPG Aroclor 1260 measurements, and in view of data in the literature[6] showing a dielectric relaxation effect with pressure in "chlorodiphenyl,"[7] it appeared of fundamental interest to determine the pressure dependence of the dielectric relaxation time for our material, particularly since data on this effect for liquids other than the chlorinated diphenyls showed relatively small changes. For example, published data for glycerol show a change in the average dielectric relaxation time of approximately 10% at 0°C over a pressure range of approximately 200 atmospheres,[8] and of a factor of 5 at 5°C for a pressure change of approximately 3500 atmospheres.[9] The paper by Gilchrist *et al.*[10] gives data for glycerol in the range from −60 to −34°C showing relaxation times increasing by factors of 4.0 to 2.45, respectively, for a pressure increase of 1000 kg/cm².

MEASUREMENTS

Data were obtained in a small pressure vessel (provided with electrical connections and a thermocouple well), in which the pressure was raised by means of a hydraulic jack. The pressure was transmitted to the inside of the vessel through a rubber diaphragm, and the main body of the vessel was filled with mercury in order to reduce thermal changes associated with the pressure changes. The test liquid was floated on the mercury, and a small parallel-plate capacitor was immersed in the liquid. The real part of the capacitance and the dissipation factor $D = \tan\delta = \epsilon''/\epsilon'$ of the system were measured with a General Radio Type 716–C Capacitance Bridge over the frequency range from 30 to 300 000 cps. This arrangement proved sufficiently sensitive to determine capacitance and dissipation data with a repeatability better than 0.1%, so that the peaks in the dissipation curves could be determined to a frequency accuracy of the order of 1%. Overlapping measurements, in the frequency range from 50 000 cps to 10 Mc were observed with a Boonton Q-Meter, type 260A.[11]

It turned out, under these conditions, that the most severe problem was temperature stability, and it was found essential to keep the temperature changes of the test liquid within ±0.2°C during a test run. The results of measurements near 25°C are shown in Fig. 2. (No significant sensitivity to electric field amplitude was observed in the range from 47 to 4600 volts rms/cm.)

Figure 3 shows the relaxation times vs absolute pressure at several temperatures and includes a plot, for comparison, of the preliminary SPG data[2] obtained at 20°C. It should be noted that the dielectric relaxation times, at high pressure and at the two highest temperatures, are shown as a range. This range represents the experimental observation that the frequency for maximum dissipation decreased with time, under these conditions, thus reflecting a gradual increase in the relaxation time. (Near 51°C, and 210 kg/cm² this increase was by a factor of 1.5 in 1 hour.[12]) This observation is in agreement with considerations of the "glass transition" given by Herzfeld and Litovitz,[1] and may provide a method for the study of the kinetics of the stabilization of the structure of liquids for condi-

[6] P. Caillon and E. Groubert, Compt. rend. **242,** 1855 (1956).
[7] In all probability a material very much like Aroclor No. 1254, pentachlorobiphenyl, see Fig. 1.
[8] F. E. Harris, E. W. Haycock, and B. J. Adler, J. Chem. Phys. **21,** 1943, (1953).
[9] K. P. Scaife, Proc. Phys. Soc. (London) **B68,** 790 (1955).
[10] A. Gilchrist, J. E. Early, and R. H. Cole, J. Chem. Phys. **26,** 196 (1957).

[11] The difference in frequency between the peaks of the D and ϵ'' curves is of the order of 10%, and it is the peak of the ϵ'' curves which is generally used to determine the frequency $f = 1/(2\pi\tau_D)$. Data in the literature are, however, given in terms of either D or ϵ'', and the difference, log 1.1 = 0.04, barely detectable on the scale of Fig. 1, has been ignored in the present paper. It should be noted, in this connection, that use of the empirical relaxation expression of Cole and Cole [K. S. Cole and R. H. Cole, J. Chem. Phys. **9,** 341 (1941)] and Davidson and Cole [D. W. Davidson and R. H. Cole, J. Chem. Phys. **19,** 1484 (1951)], $\epsilon^* = \epsilon_\infty + (\epsilon_0 - \epsilon_\infty)/(1 + i\omega\tau_0)^\beta$, amounts to a yet different definition of τ_0, which differs from the usual τ_D by a factor depending on β through the relation $\tau_0 = \tau_D \tan[\pi/2(1+\beta)]$. Thus, for $\beta = 0.6$, $\tau_0 = 1.5\,\tau_D$ [see for example, T. A. Litovitz and D. Sette, J. Chem. Phys. **21,** 17 (1953)].

[12] This change in τ_D is much too large to be accounted for by any temperature changes due to the adiabatic compression (heating) and subsequent cooling of the test liquid. The total temperature change measured by a thermocouple immersed in the Aroclor, during the time the pressure was near 210 kg/cm², was 0.3°C, which accounts for a change in τ_D by only 5%.

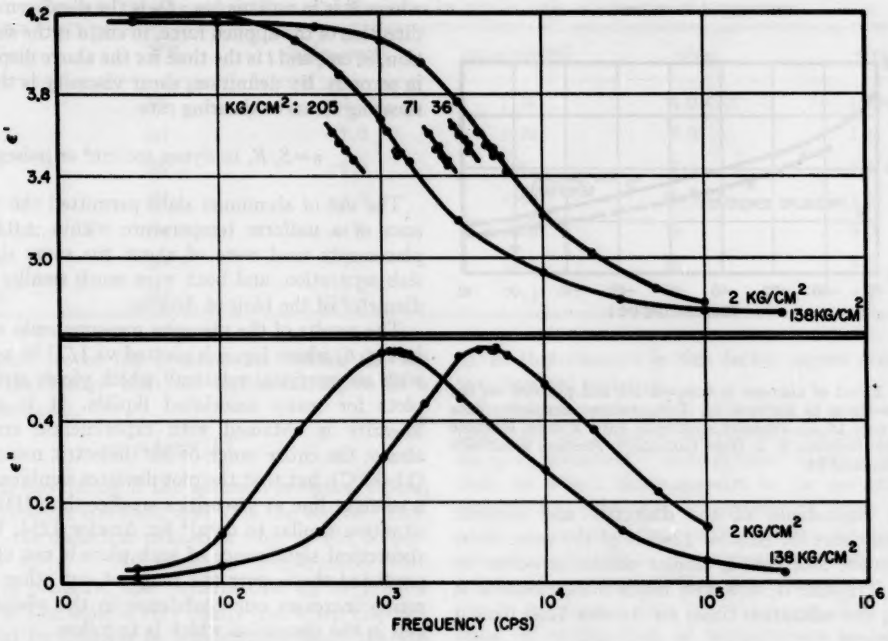

FIG. 2. Dependence of the real and imaginary parts of the dielectric constant on Aroclor 1260 on frequency, at pressures up to 200 atmospheres.

tions of temperature and pressure near the glass transition. The reduced drift, near 35°C, and the fact that none was observed at the lower temperatures is readily explained by the greatly increased time required for structural rearrangements under these conditions.

The average change in the logarithm of the dielectric relaxation time for changes in pressure of 200 atmospheres and for changes in temperature of 1°C are plotted versus temperature in Fig. 4 and similar data from the literature[8–10,13,14] are shown for glycerol in Fig. 5.[15] Data on the pressure sensitivity of the acoustic relaxation time of Aroclor 1260 and glycerol are indicated as points on Figs. 4 and 5. It is seen that the

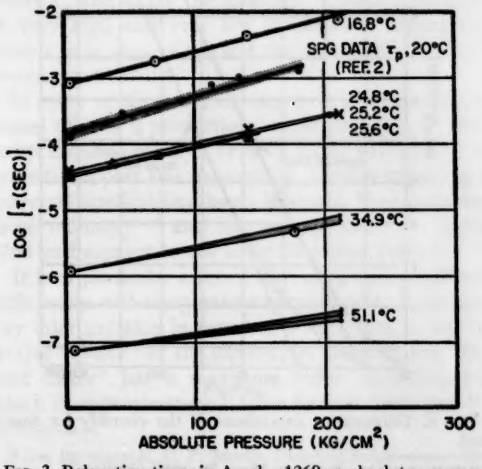

FIG. 3. Relaxation times in Aroclor 1260 vs absolute pressure.

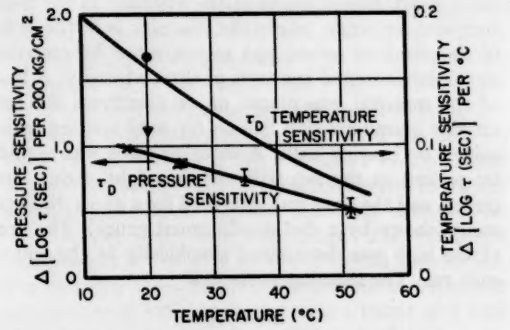
τ_D TEMPERATURE SENSITIVITY
τ_D PRESSURE SENSITIVITY
PRESSURE SENSITIVITY Δ [LOG τ (SEC)] PER 200 KG/CM²
TEMPERATURE SENSITIVITY Δ [LOG τ (SEC)] PER °C
TEMPERATURE (°C)

FIG. 4. Effect of changes in temperature and pressure on the relaxation times in Aroclor 1260. τ_D temperature sensitivity from Fig. 1. τ_D pressure sensitivity from Fig. 3. τ_p temperature sensitivity, from footnote 2, ●. τ_p pressure sensitivity from footnote 2, ▼.

[13] A. K. Schulz, Z. Naturforsch. **9a**, 944 (1954).
[14] T. A. Litovitz, E. H. Carnevale, and P. A. Kendall, J. Chem. Phys. **26**, 465 (1957).
[15] Note that the quantities plotted are essentially

$$d(\log_{10}\tau)/dp = \log_{10}e\, d\tau/(\tau dp) = 0.434\, d\tau/(\tau dp)$$

and

$$d(\log_{10}\tau)/dT = 0.434 d\tau/(\tau dT).$$

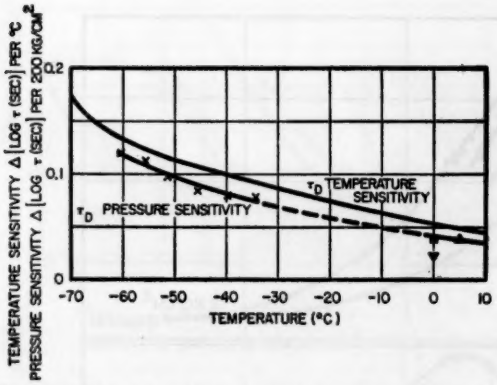

FIG. 5. Effect of changes in temperature and pressure on the relaxation times in glycerol. τ_D Temperature sensitivity data from footnote 13. τ_D Pressure sensitivity data × from footnote 10; ■ from footnote 8; ▲ from footnote 9. Pressure sensitivity ▼ from footnote 14.

pressure dependence of the dielectric and acoustic relaxation times for Aroclor 1260 is of the same order of magnitude and that a similar condition exists for glycerol. Pressure is, however, much more effective in changing the relaxation times for Aroclor 1260 than it is for glycerol.

Because of the importance of the shear viscosity in any consideration of dielectric[16,17] and ultrasonic[18,19] relaxation in viscous liquids, data were obtained for the viscosity of our sample of Aroclor 1260 over the temperature range from 0 to 88°C. Low-viscosity values, between 0.4 and 50 poises were measured with a commercial viscometer, Fenske Routine, size 300.[20] On the other hand, measurement of the viscosity in the room temperature range, where the viscosity is of the order of thousands of poises, was accomplished by reverting to the fundamental concepts of shear viscosity. A blob of the material was placed on an aluminum slab and another aluminum slab laid on top with spacing maintained by bearing balls. A shearing force was applied by pulling on the top slab with a weight, string, and pulley, and the time was measured for a given displacement (shown by a dial displacement gauge). The area of the blob was determined graphically at the end of each run. The shearing stress was

$$S=F/A$$

where S is in dynes/cm²; F is the applied force, in dynes; and A is the area of the blob, in cm². The shearing rate was

$$R=D_0/dt$$

where R is in radians/sec; D_0 is the displacement in the direction of the applied force, in cm; d is the slab separation, in cm; and t is the time for the above displacement, in seconds. By definition, shear viscosity is the ratio of shearing stress to shearing rate.

$$\eta=S/R, \text{ in dynes sec/cm}^2 \text{ or poises.}$$

The use of aluminum slabs permitted the maintainance of a uniform temperature within ±0.1°C. Displacements used were of about the same size as the slab separation, and both were much smaller than the diameter of the blob of Aroclor.

The results of the viscosity measurements are shown in Fig. 6, where $\log_{10}\eta$ is plotted vs $1/T^3$ in accordance with an empirical relation[21] which yields straight line plots for many associated liquids. It is seen that linearity is obtained with experimental errors over almost the entire range of our dielectric measurements (11–53°C), but that the plot deviates significantly from a straight line at viscosities smaller than 100 poises, a situation similar to data[18] for Aroclor 1254. While the theoretical significance of such plots is not clear,[21] the predicted shape over the range of our other measurements increases our confidence in the viscosity data and in the discussion which is to follow.

DISCUSSION OF RESULTS

It is of interest to examine the changes in both viscosity, η, and dielectric relaxation time, τ_D, as either

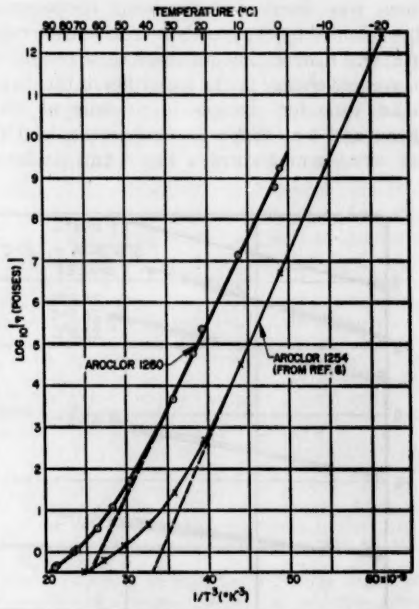

FIG. 6. Temperature dependence of the viscosity for Aroclor 1260.

[16] P. Debye, *Polar Molecules* (The Chemical Catalogue Company, 1929).
[17] W. Kauzmann, Revs. Modern Phys. **14**, 12 (1942).
[18] T. A. Litovitz, T. Lyon, and L. Peselnick, J. Acoust. Soc. Am. **26**, 566 (1954).
[19] T. A. Litovitz, J. Acoust. Soc. Am. **29**, 648 (1957).
[20] Manufactured by Cannon Instrument Company, State College, Pennsylvania.
[21] T. A. Litovitz, J. Chem. Phys. **20**, 1088 (1952).

TABLE I. Viscosity and dielectric relaxation times for Aroclor 1260, as a function of temperature.

t°C	T°K	$\log[\tau_D(\text{sec})]$	$\log[\eta(\text{poises})]$	η/τ_D	$\eta/\tau_D T$
55	328	−7.5	1.10	4.0×10^{9}	1.2×10^{6}
48	321	−7.0	1.70	5.0	1.6
36.5	309.5	−6.0	2.87	7.4	2.4
28	301	−5.0	4.00	10	3.3
21.8	294.8	−4.0	5.10	13	4.3
15.8	288.8	−3.0	6.15	14	4.9
10.2	283.5	−2.0	7.12	13	4.7

the temperature or the pressure are varied. On the basis of the Debye relation[16] (spherical dipole in a viscous medium),

$$\tau_D = 4\pi\eta a^3/kT$$

where a is the radius of the assumed spherical dipole; k is Boltzmann's constant; and T is the absolute temperature; the dielectric relaxation time should be proportional to η/T. At constant temperature, with changes in pressure, this requires that τ_D be proportional to η. The same is very nearly true when viscosity is changed by changes in temperature, since the viscosity changes by a factor of 10^{10} for a change in absolute temperature of approximately 35%.

It should not be expected, however, that this relation applies to pure polar liquids, because, theoretically, the assumed hydrodynamic model is not realistic in this case, and, experimentally, a substitution of measured values of τ_D, η, and T leads to values of a which are much too small.[22] The introduction of the maximum correction for the field acting at the elementary dipoles leads to:

$$\tau_{\text{dipole}} = \tau_D(\epsilon_\infty+2)/(\epsilon_0+2)$$

where ϵ_∞ and ϵ_0 are the dielectric constants measured at very high and very low frequencies, respectively. Since $\epsilon_\infty<\epsilon_0$, $\tau_{\text{dipole}}<\tau_D$, and the calculated value of a becomes yet smaller.

In spite of these discrepancies, it is frequently assumed that τ_D is proportional to either η or η/T, and a comprehensive survey[17] of such data, as of 1942, appears to support this assumption. Doubts regarding its universal applicability have, however, been expressed, more recently,[10,19] and the present data for Aroclor 1260 lend support to the latter view. See Table I.

It is of particular interest that η/τ_D and $\eta/\tau_D T$ vary sufficiently with temperature to make quite implausible any interpretation in terms of a reduction in the "effective volume" of the dipoles. In addition, the "local field factor" has a maximum value $(\epsilon_\infty+2)/(\epsilon_0+2)$, which is approximately 1.3 for Aroclor 1260 (see Fig. 2), so that changes in this factor cannot account for the observed variation.

In this connection, it is of interest to compare literature data for glycerol, on viscosity vs pressure[23] and on τ_D vs pressure,[8–10] since glycerol is one of the materials for which there appears to be no appreciable variation in η/τ_D over a temperature range of about 110°C in which both η and τ_D change by 8 orders of magnitude.[13,17] Since the viscosity-pressure data are tabulated at 30 and 75°C, it is necessary to extrapolate the τ_D vs pressure data into this range. This is readily done by noting that, at temperatures at least 60°C above T_∞, τ_D depends on temperature in accordance with the empirical relation[24] $\log\tau_D = A_0 + B/(T-T_\infty)$, hence

$$d(\log\tau_D)/dT = -B/(T-T_\infty)^2.$$

In view of the similar trend for the Temperature and Pressure sensitivity curves, in Fig. 5, a log-log plot of $d(\log\tau_D)/dp$ vs $T-T_\infty$ should only require a suitable choice of T_∞ to produce a straight line with a slope of −2. The best fit is obtained with $T_\infty = -150$°C (123°K) for glycerol, over the range from −60°C to 0°C (see Fig. 7) and provides an extrapolated value of $d(\log\tau_D)/dp$ at 30°C of 0.030 per 200 kg/cm². Since the data on which the smooth line of Fig. 7 is based were obtained for pressure changes ranging from 200 kg/cm² to several thousand kg/cm², it appears that this extrapolated value should apply over this range. The computed values shown in Table II are based on this assumption. It is seen that the ratio η/τ_D, for glycerol at a constant temperature of 30°C, varies by over a factor of 2 with changes in pressure from 1 to 4000 kg/cm².

It is thus seen that the changes in the ratio η/τ_D observed for Aroclor 1260 at different temperatures are *not* to be considered an isolated anomaly to a general rule requiring strict constancy of this ratio under all conditions. While there appears to be no simple relation between η/τ_D and temperature for Aroclor 1260, it is

[22] See, for example, C. P. Smyth, *Dielectric Behavior and Structure* (McGraw-Hill Book Company, Inc., New York, 1955).

[23] *International Critical Tables*, (McGraw-Hill Book Company, Inc., New York, 1930), Vol. VII, p. 223, quoting Bridgman, Proc. Am. Acad. Arts Sci. 61, 55 (1926).

[24] See, for example, W. Dannhauser and R. H. Cole, J. Chem. Phys. 23, 1762 (1955).

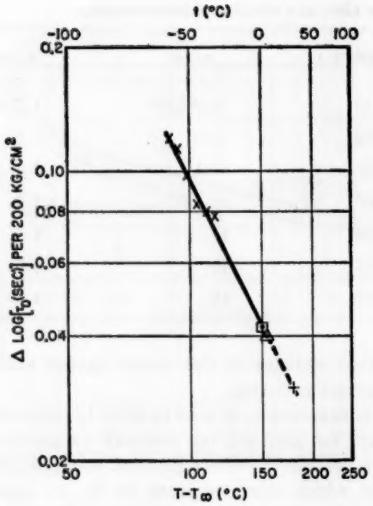

FIG. 7. Extrapolation of glycerol τ_D—pressure data to 30°C. $T_\infty = -150$°C (123°K)

remarkable that the change in η/τ_D, for glycerol, appears to be essentially linear with pressure up to at least 4000 kg/cm².

Qualitatively, at least, the observed phenomena can be accounted for by changes in the "short-range order" in the vicinity of each dipole, such as are discussed by Herzfeld and Litovitz[1] in connection with acoustical relaxation. The changes in η/τ_D appear to require the introduction of a modulus K, such that $\eta = K\tau_D$, where K is independent of temperature but increases with pressure, for glycerol, while it increases with decreasing temperature, for Arocolor 1260. (Plans are being made to obtain viscosity-pressure data, to determine the relation between K and pressure for this material.) It is seen that K can be thought of as a measure of the degree of interference of neighboring molecules with the orientation of dipoles, with "closer packing" at high pressures (and at low temperatures, for some materials) increasing this interference.

APPLICATIONS OF PIEZOPERMITTIVITY

The term "piezopermittivity" is proposed for the property of certain substances which results in large changes in dielectric constant (or "permittivity") with pressure. This usage is analogous to "piezoelectricity," the separation of electrical charges under pressure, and "piezoresistivity" the change in electrical resistivity due to pressure.

The "pressure sensitivity" of Aroclor 1260 makes possible a variety of instrumentation applications of this material for example by the use of its "piezopermittivity" at a fixed temperature and operating frequency. The variety of response curves obtainable is illustrated in Fig. 8 for Aroclor 1260.[25] It appears, in addition, that the desired operating frequency and temperature may be preselected from frequency response and other considerations, and that a fluid of the Aroclor series could then be found for which the capacitance-pressure curve has the desired shape. Thus, for example, fair linearity and high sensitivity are given at 127 kcps and 19.1°C for the Aroclor 1254-like material of footnote 6. Considerable difficulties arise, however, in many practical applications of the piezopermittivity of the Aroclors, since, in addition to a relatively large change in dielectric constant with temperature (1°C is equivalent to approximately 30 kg/cm²), there is a change in shape of the capacitance-pressure curves with temperature.

TABLE II. Viscosity and dielectric relaxation times for glycerol, at 30°C, as a function of pressure.

p(kg/cm²)	$\log \eta$	$\log \tau_D$	$\log \eta - \log \tau_D$	η/τ_D
1	0.580	−9.100	9.680	4.78×10^9
500	0.714	−9.025	9.739	5.48
1000	0.840	−8.95	9.790	6.16
2000	1.077	−8.80	9.877	7.52
4000	1.516	−8.50	10.016	10.4

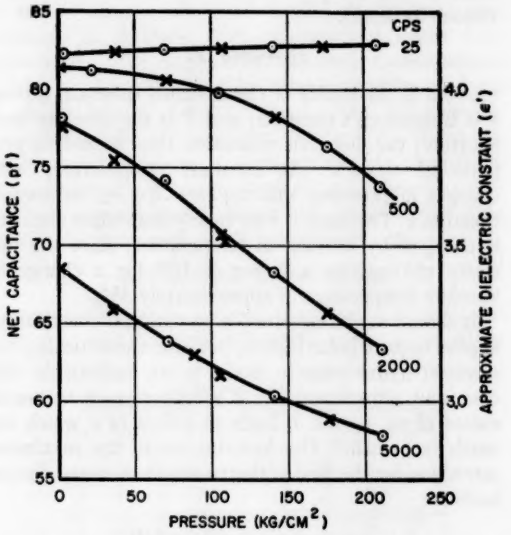

FIG. 8. Capacitance vs pressure for parallel-plate capacitor in Aroclor 1260, at 25.6±0.2°C.

CONCLUSION

Aroclor 1260 is a useful material for the study of relaxation phenomena in liquids. Both acoustical and di-

[25] The increase of the dielectric constant with pressure, at low frequencies, is in agreement with published data on many materials [see, for example, W. E. Danforth, Phys. Rev. 38, 1224 (1931)], while its decrease with pressure, in the relaxation region, is related to the increase of τ_D with pressure (see Fig. 2).

electric relaxation are readily observed near room temperature at frequencies accessible to relatively simple equipment. The inter-relations of temperature, pressure, and the acoustical and dielectric relaxation times give clues to much fundamental information about the liquid state.

In the present paper, data were presented on the dielectric behavior of Aroclor 1260 with temperature (between 10 and 55°C) and pressure (between 1 and 200 kg/cm^2). These data were compared with acoustical-relaxation and viscosity-temperature data for the same material. For purposes of comparison, similar data, from the literature, were evaluated for glycerol.

It was found that (1) the pressure dependence of the dielectric and acoustical relaxation times is nearly the same for Aroclor 1260, and about an order of magnitude larger than for glycerol.

(2) A plot of $\log_{10}\eta$ vs $1/T^3$ for Aroclor 1260 yields a straight line over a wide range of viscosities, in accordance with an empirical relation of Litovitz, but that significant deviations occur at temperatures above 50°C.

(3) The ratios η/τ_D and $\eta/\tau_D T$ for Aroclor 1260 decrease significantly with increasing temperature, a situation which cannot reasonably be interpreted as a change of either the "effective volume" of the dipoles or the "local field factor," and thus provides strong evidence against the simple hydrodynamic model of a spherical dipole in a viscous medium.

(4) A similar change in η/τ_D occurs in literature data for glycerol, as the pressure is changed at constant temperature.

(5) The large piezopermittivity of the Aroclors may have practical applications in the field of Instrumentation, particularly where temperature changes can be minimized or compensated for.

Much remains to be done, and some examples are given below. Data on viscosity vs pressure, at several temperatures should contribute greatly to a theoretical understanding of the effects involved. Results should be extended to higher pressures, as suggested by previous investigators.[10] A closer examination of the slow time-dependent effects observed in the present work may provide data for a direct study of structural relaxation times. The distribution of relaxation times observed for the chlorinated diphenyls has often been ascribed,[22] at least in part, to the "variety of molecules of which they consist." The distribution width, for glycerol, is however very nearly the same, and the individual molecules for this substance are generally considered identical. The distribution, in this case, is thought to be due to the variety of configurations in the vicinity of each molecule,[1] including various degrees of association. It would thus be of interest to obtain dielectric, acoustical, and viscosity data on molecular fractions of the Aroclors, to determine whether the observed distributions of relaxation times become appreciably narrower.

ACKNOWLEDGMENTS

A. A. Beltran compiled a preliminary bibliography on the "Influence of Pressure on Dielectric Constants" which was of great help to us. We wish to thank the Monsanto Chemical Company for kindly providing the sample of Aroclor 1260, and P. G. Benignus of that organization for giving us additional references to publications related to the Aroclors. We also wish to acknowledge stimulating discussions with C. B. Hearns, D. O. Miles, and, particularly, T. A. Litovitz.

Comments on Hypervelocity Wave Phenomena in Condensed Explosives*

R. F. CHAIKEN

Aerojet General Corporation, Azusa, California

(Received April 15, 1960)

The occurrence of hypervelocity wave phenomena in condensed explosives during shock initiation to detonation is discussed in terms of an adiabatic reaction model for the chemical energy release (i.e., the detonation reaction). On the basis of the model, the chemical reaction exhibits an apparent induction time resulting in a sudden release of energy behind the initiating shock front. It is believed that this energy release leads to a propagated high-pressure reaction wave which moves in the shock compressed explosive at a "super-velocity" (i.e., greater than the normal steady-state velocity) to overtake the initiating shock front. The proposed explanation is consistent with the reported observations of hypervelocity wave phenomena in detonating liquid nitromethane and single crystals of PETN.

THE direct observation of hypervelocity wave phenomena during detonation initiation by strong shocks in single crystals of PETN and liquid nitromethane have been reported by Holland, Campbell, and Malin[1] and by Cook, Pack, and Gey,[2] respectively.

Holland *et al.* noted, by means of streak camera photography of shock impacted large crystals of PETN, that the growth of detonation towards steady state apparently proceeded in several stages. First, a relatively low-velocity wave front (5.56 mm/μsec) appeared which abruptly changed to a very high-velocity compression wave ($\sim$10.45 mm/μsec). Within $\sim$0.5 μsec, the high-velocity front changed to an apparent steady-state detonation (8.28 mm/μsec) which consumed the crystal, No explanation was offered as to the nature of these events.

From similar space-time high-speed camera studies of the shock initiation to detonation in nitromethane, Cook and his co-workers observed a "flash across" phenomena in which an apparent wave of luminescence originated in the explosive behind the initial compression front, and propagated at a reported velocity of $\sim$35 mm/μsec to overtake the initial compression front. This "flash across" phenomena was interpreted as a heat transfer wave caused by a sudden increase in the thermal conductivity of the shock compressed nitromethane. The phenomenon was taken as a direct observation of the "heat pulse" which Cook, Keyes, and Filler[3] had predicted.

Several years prior to the CPG (i.e., Cook, Pack, and Gey) studies, the author carried out a streak camera study of the shock initiation to detonation in nitromethane.[4] At that time, evidence was found to indicate the existence of a hypervelocity wave moving behind the initiating shock front. It was suggested that the detonation reaction wave originated behind the initial compression front, and traveled at a "supervelocity" in the compressed explosive to overtake the initiating shock front.

The author believes that this detonation initiation process could be an alternate explanation for the "flash across" phenomena observed by CPG, and at the same time offers an explanation for the velocity steps in PETN which were observed by Holland *et al.*

Figure 1 depicts a space-time plot of the wave phenomena occurring during detonation initiation in nitromethane based upon the author's studies.[4] Referring, for the time being, only to time zones I and II, D_i is the initiating shock velocity (i.e., the velocity of the shock wave entering the explosive from an external source); D' is the hypervelocity wave velocity; u is the velocity imparted to the explosive by the initiating shock wave; τ is the time lag after compression, for any element of fluid at an initial distance S from the point where the initiating shock front enters the explosive, to reach the observed luminous stage; τ_0 refers to the observed time lag for the fluid element at $S=0$.

In the time zones I and II, CPG's observations apparently coincide with the author's except for the magnitude and interpretation of τ_0 and D'.

On assuming that D_i and D' are independent of S (i.e., negligible attenuation of the wave fronts in the explosive), it is possible to express τ as a linear function of S.

From Fig. 1 the following relations hold:

$$S=u(\tau_0-\tau)+S' \tag{1}$$

and

$$S'=D'\Delta t=\Delta S_1+u\Delta t. \tag{2}$$

From the Rankine-Hugoniot (R–H) relationships for one-dimensional steady-state shock propagation,

$$\Delta S_1=(V/V_0)S, \tag{3}$$

* This work was supported by the Advanced Research Projects Agency under a contract monitored by the Office of Naval Research.

[1] T. E. Holland, A. W. Campbell, and M. E. Malin, J. Appl. Phys. **28**, 1212 (1957).

[2] M. A. Cook, D. H. Pack, and W. A. Gey, *Seventh Symposium (International) on Combustion* (Butterworth Scientific Publications, London, 1959), p. 820.

[3] M. A. Cook, R. Keyes, and A. S. Filler, Trans. Faraday Soc. **52**, 363 (1955).

[4] R. F. Chaiken "The kinetic theory of detonation of high explosives," M. S. thesis, Polytechnic Institute of Brooklyn, Brooklyn, New York (1958); also submitted to the Eighth Symposium (International) on Combustion, Pasadena, California (1960).

where V/V_0=the ratio of specific volumes across the shock front (subscript 0 referring to the initial state).

Equations (1)–(3) can be rearranged to yield

$$\tau=\tau_0-(S/u)[D'(1-V/V_0)-u]/[D'-u]. \quad (4)$$

From the R–H equations, $u/D_i=1-V/V_0$; therefore, Eq. (4) becomes

$$\tau=\tau_0-[(D'/D_i-1)/(D'-u)]S. \quad (5)$$

Equation (5) is the same as CPG's experimental equation, i.e.,

$$\tau=\tau_0-a'S, \quad (6)$$

where a' is a positive constant having the measured value of ~ 1.7 μsec/cm. For this value of a', and taking $D'=35$ mm/μsec and $u=0.45\ D_i$, the initiating shock velocity in CPG's experiments turns out to be ~ 5.3 mm/μsec. This value of D_i falls within the range of values studied by the author.

In Fig. 2, a plot of a' vs D' is given for the conditions $D_i=5.3$ mm/μsec and $u=2.4$ mm/μsec. Superimposed upon this curve are the results of the two studies. It is seen that CPG's values for a' and D' differ by the respective factors of ~ 0.25 and ~ 3 from the author's values. However, it is easily seen that in the range of $a'=1.7$ μsec/cm, it would be very difficult to calculate an accurate value for D' on the basis of an experimentally measured a'. This might be a reason for the discrepancy in the two sets of results.

It is interesting to note that if one assumes that the chemical reaction wave resulting in D' has a velocity comparable to a steady-state detonation velocity (D_s) at the shock density ($\rho=1/V$), it might be possible to obtain an estimate of D' from extrapolated $D_s(\rho)$ data. From the work of Campbell, Malin, and Holland[5] on

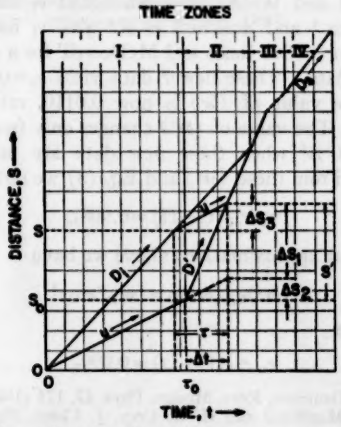

FIG. 1. Space-time plot of wave propagation upon shock initiation of detonation. D_i=initiating shock velocity. u=velocity imparted to the mass by D_i. D'="hypervelocity" wave velocity. D_s=steady-state detonation velocity.

[5] A. W. Campbell, M. E. Malin, and T. E. Holland, J. Appl. Phys. **27**, 963 (1956).

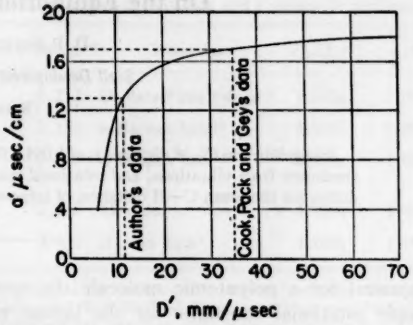

FIG. 2. Plot of a' vs D'. $a'=(D'/D_i-1)/(D'-\mu)$. $D_i=5.3$ mm/μsec. $\mu=2.4$ mm/μsec.

the detonation velocity of nitromethane as a function of initial temperature the following expression for $D_s(\rho)$ can be obtained:

$$D_s=2.78\times 10^3\rho+3110 \text{ m/sec.} \quad (7)$$

Estimating that $\rho\simeq 2.1$ g/cm^3 for $D_i\simeq 5.3$ mm/μsec, yields a steady-state detonation velocity of 8.86 mm/μsec. Since this reaction wave would be traveling in a moving medium,

$$D'=D_s+u\simeq 11.5 \text{ mm/}\mu\text{sec} \quad (8)$$

which is consistent with the author's value.

The formation of a propagated "supervelocity" reaction wave is also consistent with an adiabatic reaction model in which the chemical reaction rate exhibits an apparent induction time (τ_0). After τ_0 seconds pass, the molecules of explosive which were first compressed by the initiating shock front suddenly decompose. The rapid release of energy propagates a high-pressure reaction wave moving with velocity $D'>D_i$ behind the initiating shock front. This "supervelocity" reaction wave overtakes the initiating shock front and passes into the unshocked region. The detonation reaction in the nitromethane which has not yet been compressed is then greatly overinitiated (i.e., it occurs with a higher than steady-state velocity), and the detonation front rapidly decays to its normal steady-state value. Thus referring to time zones III and IV in Fig. 1, a small portion of the explosive will be consumed by a detonation front moving at a hypervelocity before steady state is achieved. This general picture now explains the detonation steps in PETN.[1] Additional support for this general description of the detonation initiation process comes from the recent work by Hubbard and Johnson.[6] Calculations of the shock initiation detonation conditions utilizing time-dependent one-dimension hydrodynamic equations with an Arrhenius form of chemical energy release indicate the formation of a hypervelocity reaction wave behind the initiating shock front.

[6] H. W. Hubbard and M. H. Johnson, J. Appl. Phys. **30**, 765 (1959).

On the Equilibrium C-H Distance in Methane

D. P. STEVENSON AND JAMES A. IBERS

Shell Development Company, Emeryville, California

(Received April 18, 1960)

An equilibrium C—H distance r_e of 1.091±0.002 A has been calculated with the aid of a normal coordinate treatment from vibrational and rotational spectroscopic data on CH_4 and CD_4. From these results we also derive for the mean C—H distance, of interest in electron diffraction studies, the value 1.102±0.002 A.

IN general for a polyatomic molecule the spectroscopic rotational constants for the lowest vibrational state are functions of several motion-modified bond distances, and consequently only "effective" distances can be derived. However, for CH_4 (and other tetrahedral XY_4 molecules) the single rotational constant B_0 is given by

$$B_0=3h/(64\pi^2mcr_{zy}^2) \tag{1}$$

and thus from B_0 of CH_4 one may obtain directly a value of $r_{-2}=\langle r^{-2}(\text{C—H})\rangle^{-\frac{1}{2}}$ where the average is over the motions which result from zero-point energy. (As before[1] we use the notation $r_n=\langle r^n\rangle^{1/n}$.) Moreover, for CH_4 there are sufficient spectroscopic data to allow a value of r_e, the equilibrium distance, to be derived from r_{-2}(C—H). Previously[2] we found an r_e of 1.080 A for CH_4, but unfortunately we committed a numerical error in making the calculation. Moreover, we were unaware of newer spectroscopic data for CH_4 which affect the apparent value of the ratio r_e/r_{-2}. In this paper we re-evaluate this ratio, derive a value for r_e, and finally make some comparisons with electron diffraction results on C—H distances in normal alkanes.

The relation between r_e and r_n is[1]

$$r_{\pm n}=r_e\{1+(\langle\delta r\rangle/r_e)-[(1\mp n)/2r_e^2]\langle\delta r^2\rangle+\cdots\}, \tag{2}$$

where the $\langle\delta r^i\rangle$ are in the present case the mean-ith deviations of the C—H distance from equilibrium, and where, in accordance with arguments presented earlier,[1] we have justifiably neglected higher order terms. For $n=-2$, then, we have upon simple inversion

$$r_e/r_{-2}=1-(\langle\delta r\rangle/r_{-2})+\tfrac{3}{2}(\langle\delta r^2\rangle/r_{-2}^2). \tag{3}$$

Evaluation of the $\langle\delta r^i\rangle$ from spectroscopic data is discussed in detail in our previous paper.[1] From the normal coordinate treatment of the vibrations one relates the $\langle\delta r^i\rangle$ for C—H in CH_4 to the moments of the normal coordinates, and the moments of the normal coordinates are evaluated from the spectroscopic data. In this evaluation it is assumed that the anharmonicity of the pure stretching vibration ν_1 results from the cubic term of the potential function, and so the first moment of the normal coordinate associated with ν_1 is nonzero. Anharmonicities of the other vibrations are assumed to result from quartic and higher even terms of the potential function, and thus the first moments of the other normal coordinates are zero. We then find

$$\langle\delta r\rangle=\tfrac{3}{4}(x_e/2\alpha_1)^{\frac{1}{2}}, \tag{4}$$

where $\alpha_j=4\pi^2\mu_j'\omega_jc/h$, ω_j is the frequency for infinitesimal amplitude and μ_j' is the reduced mass of the vibration j, and x_e is the anharmonicity coefficient in the quadratic [in $(v+\frac{1}{2})$] expression for the vibrational energy levels. We also find

$$\langle\delta r^2\rangle=(b_1/\alpha_1)+(b_3/\alpha_3)+(b_4/\alpha_4), \tag{5}$$

where the coefficients b_1, b_3, and b_4, are given in our previous paper.[1] Note, as one would expect, $\langle\delta r^2\rangle$ is independent of ν_2, the symmetric bending vibration.

We use Dennison's[3] approximate formula

$$2x_e=[(m_D/m_H)^{\frac{1}{2}}-(\nu_H/\nu_D)]/[(\nu_H/\nu_D)-1] \tag{6}$$

to obtain a value for the x_e to be associated with ν_1 for CH_4. Previously we used the frequencies of MacWood and Urey[4] of 2084.7 and 2914.2 cm^{-1} for ν_1 of CD_4 and CH_4. These data give $x_e=0.0199$. However, Shepherd and Welsh[5] have reassigned ν_1 for CD_4 as 2107.8 cm^{-1} and Stoicheff *et al.*[6] give ν_1 for CH_4 as 2916.5 cm^{-1}. (See Jones and McDowell[7] for a summary of such data.) These newer data yield $x_e=0.0391$ for CH_4. The value of $\langle\delta r\rangle$ is now 0.0110, rather than 0.0079 A. The value of $\langle\delta r^2\rangle$ changes only from 0.0072 to 0.0071 A^2 when these new data are taken into account. From these $\langle\delta r^i\rangle$ and Eq. (3) we obtain

$$r_e/r_{-2}(\text{C—H})=0.998_9. \tag{7}$$

Within our approximations above we have

$$\langle\delta r^i\rangle_H/\langle\delta r^i\rangle_D=(m_D/m_H)^{\frac{1}{2}}$$

and hence

$$r_e/r_{-2}(\text{C—D})=0.999_2. \tag{8}$$

[1] J. A. Ibers and D. P. Stevenson, J. Chem. Phys. **28**, 929 (1958).

[2] D. P. Stevenson and J. A. Ibers, Ann. Rev. Phys. Chem. **9**, 359 (1958).

[3] D. M. Dennison, Revs. Modern Phys. **12**, 175 (1940).

[4] G. E. MacWood and H. C. Urey, J. Chem. Phys. **4**, 402 (1936).

[5] G. G. Shepherd and H. L. Welsh, J. Mol. Spectroscopy **1**, 277 (1957).

[6] B. P. Stoicheff, C. Cumming, G. E. St. John, and H. L. Welsh, J. Chem. Phys. **20**, 498 (1952).

[7] L. H. Jones and R. S. McDowell, J. Mol. Spectroscopy **3**, 632 (1959).

In Table I we collect together available data on the rotational constants of CH_4 and CD_4. We also list the values of r_{-2} derived from the constants, and the values of r_e which are obtained from the ratios above. It is clear that there are disagreements among the separate rotational constants, but there seems no basis for our attempting a detailed analysis of the reliabilities of the individual values. However, we have not included the data of Kaylor and Nielsen[8] on CD_4, for these data appear to be far out of line. (See Shepherd and Welsh[5] for some possible reasons why this is so.) A simple average of the data of Table I gives r_e for C—H of 1.091_2 and r_e for C—D of 1.090_0 A. On the basis of the five r_e values of the table we think it reasonable to take

$$r_e = 1.091 \pm 0.002 \text{ A}.$$

It is interesting to note that if one assumes CH_3D to be a perfect tetrahedron, then from the data of Boyd and Thompson[9] (and also of Ginsburg and Barker[10]) one obtains $r_{-2} = 1.0924$ A, in good agreement with the data of the table.

In his electron diffraction studies Bartell usually reports distances which are r_1's. [Bartell[11] uses the notation $r_g(0)$, rather than r_1.] We obtain from the data above the following r_1 values: 1.102 ± 0.002 A for the C—H in CH_4; 1.099 ± 0.002 for the C—D in CD_4.[12] Although an electron diffraction study of CH_4 and CD_4 is in progress,[13] the results are not yet available to us.

TABLE I. Rotational constants and r values for methane.

Substance	$B_0(\text{cm}^{-1})$	Remarks	r_{-2}(A)[a]	r_e(A)
CH_4	5.252	IR data,[b] analysis of [c]	1.093_1	1.091_8
	5.253	ν_2 Raman band[d]	1.093_0	1.091_7
	5.270	ν_2 Raman band[e]	1.091_3	1.090_0
CD_4	2.64_7	IR data[f]	1.089_2	1.088_2
	2.631	Raman data[g]	1.092_5	1.091_6

[a] Use was made of the tabulation of fundamental constants of E. R. Cohen, K. M. Crowe and J. W. M. DuMond, *Fundamental Constants of Physics* (Interscience Publishers, Inc. New York, 1957), in the conversion of B_0 to r_{-2}.
[b] J. P. Cooley, Astrophys. J. **62**, 73 (1925).
[c] W. H. J. Childs, Proc. Roy. Soc. (London) **153**, 555 (1936).
[d] Footnote 6.
[e] T. Feldman, J. Romanko, and H. L. Welsh, Can. J. Phys. **33**, 138 (1955).
[f] A. H. Nielsen and H. H. Nielsen, Phys. Rev. **54**, 118 (1938).
[g] Footnote 5.

However, Bartell and co-workers[14] find r_1 values for C—H in *n*-butane, *n*-pentane, *n*-hexane, and *n*-heptane of 1.108 ± 0.004, 1.118 ± 0.004, 1.118 ± 0.006, and 1.121 ± 0.007 A, respectively. Bartell suggests from these data that the methyl C—H might be shorter than the methylene C—H, and the fact that our calculated r_1 for CH_4 is shorter than the observed r_1's for the higher alkanes is consistent with this suggestion. Bartell's[14] experimental values of $\langle \delta r^2 \rangle$ for the alkanes, which vary from 0.0061 to 0.0071 A^2, are in essential agreement with the value of 0.0071 A^2 derived here for CH_4 from spectroscopic data.

ACKNOWLEDGMENT

We wish to thank L. S. Bartell for questioning our original value of r_e.

[8] H. M. Kaylor and A. H. Nielsen, J. Chem. Phys. **23**, 2139 (1955).
[9] D. R. J. Boyd and H. W. Thompson, Proc. Roy. Soc. (London) **A216**, 143 (1953).
[10] N. Ginsburg and E. F. Barker, J. Chem. Phys. **3**, 668 (1935).
[11] L. S. Bartell, J. Chem. Phys. **23**, 1219 (1955).
[12] Note in accordance with (2) that the values of r_1 derived from r_{-2} values are independent of $\langle \delta r \rangle$ and hence of assumptions concerning anharmonicities of the vibrations.
[13] L. S. Bartell (private communication, 1960).
[14] R. A. Bonham, L. S. Bartell, and D. A. Kohl, J. Am. Chem. Soc. **81**, 4765 (1959).

Secondary Positive Ion-Emission from Platinum*

R. C. BRADLEY, A. ARKING,† AND D. S. BEERS‡

Laboratory of Atomic and Solid State Physics, Cornell University, Ithaca, New York

(Received July 30, 1959)

Mass analysis of the secondary particles ejected from Pt surfaces by inert gas ion bombardment or by heating revealed species characteristic of the base metal, of certain bulk and surface impurities, and of the bombarding beam (so-called "reflected" ions). The Pt^+ ions seemed to come directly from the substrate rather than from surface compounds. Their yield increased with temperature, bombarding ion energy, and bombarding ion mass. The ratio of sputtered Pt ions to sputtered neutrals is estimated to be of the order of 1 to 1000 at room temperature. The kinetics of the formation and desorption of a certain surface compound [possibly $Pt(CO)_2$] was studied by secondary ion analysis. The compound formed spontaneously on the surface from the background gas in the instrument (CO at 10^{-8} mm Hg). Its formation rate was greatly enhanced by inert gas ion bombardment. It desorbed readily at 1000°C with an activation energy of 0.74 ± 0.05 ev. The "reflected" ions appeared to be sputtered rather than reflected. Their energy was always extremely low (<1 ev) and the dependence of their yield on ambient gas pressure and target temperature is consistent with the notion that they originated from inert gas atoms trapped in the surface layers.

INTRODUCTION

IT has previously been shown that the analysis of secondary ions ejected from metal surfaces by the impact of positive inert gas ions provides interesting information on sputtering, surface and bulk compositions, and surface and bulk kinetics.[1,2] Much of this information is relevant to other fields of interest such as, for example, corrosion, catalysis, and the achievement of high vacua by ion gauge pumping.

The present paper briefly reports the results of some experiments on a platinum surface using this technique. It was the objective here to increase our knowledge and understanding of the nature and properties of secondary ions in general, and also to learn to what further extent they can be used as a tool for studying gas-solid interfaces. More detailed accounts of these experiments are given in the papers by Beers,[3] and Bradley and Arking.[4]

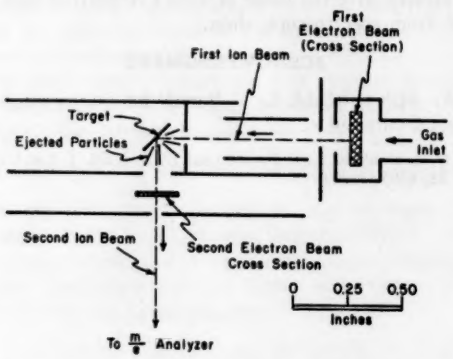

FIG. 1. Diagram showing the electrode geometry in the ion source region of the mass spectrometer. Inert gas ions are generated in the first electron beam and are accelerated and focused onto the target. Changed particles ejected from the target are mass analyzed directly. Uncharged particles must first be ionized by the second electron beam before they can be mass analyzed.

EXPERIMENTAL

The experimental arrangement is fully described in footnote 2. Therefore we include here only a diagram of the ion source region of the sector field mass spectrometer which was built for these studies (Fig. 1). The target is a commercial polycrystalline platinum foil located on the axis of the instrument. It may be bombarded by a monoenergetic inert gas ion beam with any energy up to 1000 ev; it may also be heated by an electric conduction current to any temperature up to its melting point. Ions released from its surface—either by ion bombardment or simple heating or both—can be mass analyzed directly. Neutral particles released are more difficult to study since they must first be ionized by electron bombardment—a very inefficient process[5]—before they can be mass analyzed.

Under normal operating conditions the pressure of inert gas in the spectrometer is of the order of 10^{-5} mm Hg, and the partial pressure of the principal gaseous impurity (CO) is about 10^{-8} mm Hg. Partial pressures of other gaseous impurities (CO_2, N_2, etc.) are 10^{-10} mm Hg or less.

* This research was supported by the U. S. Air Force through the Air Force Office of Scientific Research of the Air Research and Development Command.

† Present address: NASA Thoeretical Division, 8719 Colesville Road, Silver Spring, Maryland.

‡ Present address: RCA Research Laboratories, Princeton, New Jersey.

[1] R. E. Honig, J. Appl. Phys. **29**, 549 (1958).

[2] R. C. Bradley, J. Appl. Phys. **30**, 1 (1959).

[3] D. S. Beers, Technical Report No. 10 (Cornell University, March 1, 1959) AFOSR-TN-59-151.

[4] R. C. Bradley and A. Arking, Technical Report No. 11 (Cornell University, May 1, 1959) AFOSR-TN-59-271.

[5] The chance that an atom or molecule will be ionized by the electron beam depends on its energy, the electron flux, and the ionization cross section. An order of magnitude calculation indicates that the chance is approximately 1 in 10 000 for the conditions here.

RESULTS AND DISCUSSION

The particles removed from the platinum surface by ion bombardment, evaporation, or both are listed in Table I. These are seen to consist of ions and atoms characteristic of the base metal, of certain bulk impurities, of certain surface impurities, and of the bombarding beam.

A. Platinum

Pt peaks due to both sputtered ions and sputtered neutrals were observed. The peaks due to neutrals could be studied separately from those due to ions either by biasing out the ions or else by noting the changes in peak height when the ionizing electron beam was turned on and off. The peak due to ions was generally about 10 times larger than that due to neutrals. Considering the low efficiency for detecting the neutrals,[5] we estimate that the actual ratio of sputtered Pt ions to neutrals was of the order of 1 to 1000.

The yield[6] of Pt^+ as a function of temperature for two different bombarding conditions is shown in Fig. 2. There was no evidence of any hysteresis in these measurements (provided that the Pt was flashed to 1300°C before each measurement), and we take this to mean that these ions were sputtered from the base metal and were not fragments of surface compounds. The positive temperature coefficient is consistent with Wehner's sputtering studies of Pt.[7] However, the secondary ion yields show a much more rapid increase with temperature than do his sputtering yields (or our neutral atom yields), and from this we conclude that the fraction of sputtered particles leaving as ions increases with increasing temperature. It is interesting to note that the opposite effect was found for Mo.[2]

B. Bulk Impurities

The alkali metals (first row of Table I) almost invariably appear in the mass spectrum of ions sputtered[1,2] or evaporated[8] from metal surfaces. This is because their ionization potentials are low compared to the work function of most surfaces, a condition which renders them extremely susceptible to surface ionization. They are hence easily detected even though their concentration in the base metal may be very low. In the present case, spectroscopic analysis of the platinum sample indicated that these impurities were present in an amount less than 1 part in 10^5; nevertheless their mass peaks were comparable in size to the Pt^+ peak itself. The Ca^+ peak is less often observed but is not unexpected from a substrate with a work function as high as that of Pt (~5–6 ev).

From the manner in which the peak heights change as a function of temperature and time one can compute activation energies for volume diffusion and desorption of these impurities. This analysis has been described in a previous paper[9] and hence will not be repeated here.

None of the other bulk impurities known from spectroscopic analysis to be present (of which Pb and Zn with concentrations of 0.02% each were the most abundant) could be detected.

TABLE I. Particles removed from Pt by sputtering and by evaporation. During sputtering the Pt temperature was 20°C, during evaporation it was about 1300°C.

	Sputtered particles	Evaporated particles
Ions only	Li, Na, K, Ca, $PtO(CO)$	Li, Na, K, Ca
Neutrals only[a]	H_2O, O_2, CO_2	H_2O, O_2, CO_2, and A or Xe
Ions and neutrals[b]	C, N, O, CO, N_2, Pt, A or Xe	C, O

[a] The mass 18 and 32 peaks (H_2O and O_2), when present at all, were just barely detectable.

[b] For all species in this row except Pt, the neutral peaks predominated, indicating that the fraction of these particles which left the surface as ions was considerably less than 10^{-4}.

C. Surface Compounds

Only one species with a mass ratio higher than that of Pt (195 amu) was discernible in the secondary ion spectrum, and this had a mass ratio corresponding quite closely to the carbonyl fragment $PtO(CO)^+$.[10] That it came from a surface compound was apparent from the fact that it was reduced to a very low level by a high temperature flash (1300°C) but returned spontaneously when the surface was allowed to remain at room temperature for several hours. This compound was evidently formed by a chemical reaction between the clean Pt surface and the background impurity gas in the instrument (principally CO).

[6] "Yield" as used here is defined as the ratio of peak height to bombarding ion current. True yields—that is, the ratios of ejected to incident particles—were not measured. "Peak height", "yield," and "collector current" are used interchangeably provided the bombarding ion current was kept constant.

[7] G. K. Wehner, Phys. Rev. **108**, 35 (1957).

[8] H. B. Wahlin, Phys. Rev. **34**, 164 (1929); L. P. Smith, *ibid.* **35**, 381 (1930).

[9] R. C. Bradley, Phys. Rev. **117**, 1204 (1960).

[10] In footnotes 2 and 4 we referred to this peak as PtO_3^+, which differs from $PtO(CO)^+$ by 4 atomic mass units. Although the latter provides a better fit to the data, we did not find it listed among the known compounds of platinum and so hesitated to use it. However, it has become increasingly clear, as more data have become available, that secondary ions of surface compounds are usually fragments. For example, from a Mo surface we did not find the common trioxide at all but we did find MoO_2^+; from Cu we found CuO^+ instead of the expected Cu_2O^+. In the light of these other studies it seems quite reasonable, therefore, that the peak was a fragment of the compound $Pt(CO)_2$. This would also be more consistent with the fact that the background impurity gas in the instrument was CO rather than O_2. In any event, even though there may still exist some question as to the true identity of the peak, we believe that the technique we have used for studying it is of general interest and will be applicable to other studies of surface kinetics.

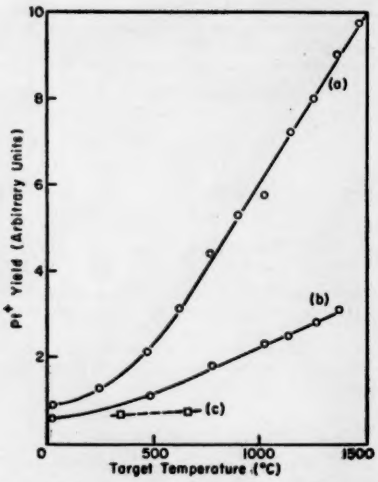

FIG. 2. Pt^+ yield as a function of temperature for different bombardment conditions. Curve (a): Xe^+ bombardment (870 ev incident ion energy, 10 $\mu a/cm^2$ incident ion current density). Curve (b): A^+ bombardment (1000 ev, 30 $\mu a/cm^2$). Curve (c) has been taken from Wehner's data (footnote 7), and shows how the *total* sputtering yield of Pt depends on temperature for Hg^+ bombardment (300 ev, >3 ma/cm^2).

The surface kinetics of this compound was studied in the following way. The Pt surface was first flashed to 1350°C for about a minute to remove adsorbed impurities.[11] A reproducible amount of the compound was then generated on the surface at room temperature, using a technique which will be described presently. Finally, with the ion beam on, the Pt was suddenly heated at time $t=0$ to a predetermined temperature (e.g., 1000°C) and the yield was measured as a function of time thereafter (Fig. 3). The initial high yield decayed exponentially to a steady-state value with a decay constant that depended only on the temperature and not on the bombarding parameters, indicating that at these high temperatures the depletion was due primarily to desorption rather than to sputtering. A plot of the decay constant as a function of the reciprocal of the absolute temperature gave an activation energy for this depletion of 0.74 ± 0.05 ev (see Fig. 4).

The existence of a nonzero steady state value of the yield showed that a replenishment process was also active during these runs which at steady state just balanced the depletion. In the temperature range 1000°–1200°C the rate of replenishment was found to have little if any dependence on the temperature, which probably means that in this range the rate controlling process for replenishment was the arrival of CO molecules from the background gas (about 10^{-2} monolayer/second).

[11] Platinum is a metal notoriously difficult to clean. When we refer to our Pt surfaces as "clean," we merely mean that we did not find any evidence of surface contamination in our studies. This is of course is no proof that there were no contaminations present.

It was interesting to find that the formation of the compound on the surface at room temperature was assisted by the inert gas ion bombardment. Ten minutes bombardment of a freshly flashed surface by a 1000 ev, 10 $\mu a/cm^2$ ion beam resulted in a peak that otherwise would have required a full day to form—an enhancement of over 100 times in the rate of formation of the compound. What makes this effect interesting is that it constitutes a reversal of the usual state of affairs. Normally, ion bombardment is counted on to clean the surfaces of solids[12]; in the present case it not only failed to clean the surface, it actually helped contaminate it. Considering the fact that ion bombardment agitates and disrupts surface atoms, perhaps it is not too surprising to find that chemical reactions can also be activated by the process. As far as we are aware, however, this is the only case where such an occurrence has actually been reported and studied.

This effect was exploited for generating a reproducible amount of the compound on the surface prior to $t=0$ for the desorption studies discussed above. The experimental procedure consisted simply of (a) flashing the Pt surface to clean it, (b) ion bombarding it at room temperature for 15 minutes, and (c) heating it at $t=0$ to the predetermined temperature.

The emission characteristics of the $PtO(CO)^+$ ions were unusual. Their yield was proportional to the bombarding current as expected for a sputtering process. However, it also increased exponentially with temperature, which is not normal for sputtering and indeed suggests that the emission was thermally activated.

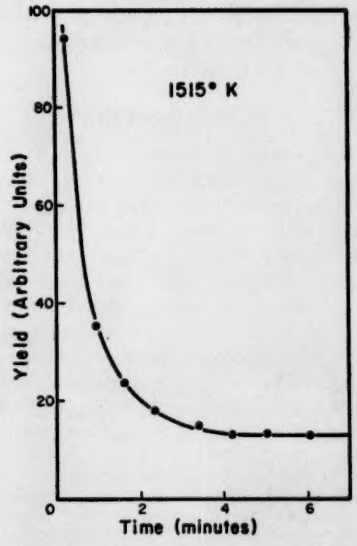

FIG. 3. $PtO(CO)^+$ yield as a function of time for a typical desorption run.

[12] See, for example, H. E. Farnsworth *et al.* J. Appl. Phys. **26**, 252 (1955).

In fact the "activation energy" corresponding to this exponential increase turned out to be the same as that for desorption to within the experimental error (see Fig. 4). This means that in addition to being proportional to the bombarding ion current, the yield of these ions was also proportional to the flux of desorbing molecules. A possible explanation for this result is that a fraction of the desorbing molecules suffered ionizing collisions with the incident ions—or possibly with the secondary electrons ejected by the incident ions. The number of such collisions would be proportional to both the ion current and the desorption rate as required.

D. Gaseous Impurities

The gas released by heat or ion bombardment (see second and third rows of Table I) had the same mass spectrum and the same peak-height ratios as the background gas. We may conclude, then, that these gases were surface rather than bulk impurities.

The only ions which appeared under simple heating (aside from Ca and the alkali metals) had m/e ratios of 12 and 16 and are thought to be fragments of the CO molecules on the surface.[13]

The inert gas atoms evolved by simple heating (see second row of Table I) occurred only after a period of ion bombardment of the surface and may be presumed to be particles of the primary beam which were driven into the surface. The rate of release of this gas was found to increase exponentially with temperature provided that the release rate was kept sufficiently low so that the source of gas did not become appreciably depleted in the time needed to make a series of measurements. The activation energy associated with this release was about 1.6±0.2 ev. We interpret this to be the energy needed for the Pt atoms on the surface to rearrange themselves and in so doing to uncover and release the trapped gas.

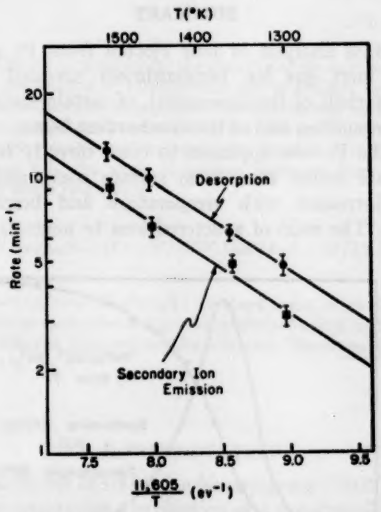

FIG. 4. Semilog plots for the determination of activation energies. The upper plot gives the exponential decay constant as a function of $1/kT$ (converted to reciprocal electron-volts). The slope of this line is the activation energy for desorption: 0.74±0.05 ev. The lower plot is the emission rate of secondary $PtO(CO)^+$ ions as a function of $1/kT$ for a given coverage. It can be seen that the slopes of the two lines are the same to within the experimental uncertainty.

[13] It has been concluded from infrared studies that CO chemisorbs as a molecule on a Pt surface, the bonding taking place through the C atom. See, for example, R. P. Eischens *et al.*, J. Chem. Phys. **22**, 1786 (1954).

TABLE II. Properties of "reflected" Xe ions as a function of incident ion energy.

Incident ion energy	Relative yield	Energy spread at half-height (ev)	Retarding potential at half-height[a] (volts)
100	1.00	0.35	−1.08
300	0.96	0.55	−1.10
600	1.21	0.63	−1.25
900	1.08	0.86	−1.08

[a] Uncorrected for contact potential. A one volt contact potential difference between the Mo collector and the Pt target would be a reasonable value.

E. Reflected Ions

The inert gas ions released during ion bombardment (third row of Table I) correspond to the bombarding ions themselves and are generally referred to as "reflected" ions. Relatively few studies have been devoted to ion reflection[14] and the process is not well understood. The experiments to be described now were on the reflection of singly charged Xe ions[15] from Pt.

The yield of the reflected Xe^+ ions (that is, the ratio of collector current to target current) was independent of the target current and the bombarding energy (to within 10%) in the range 100–900 ev (see Table II). It depended on the ambient Xe pressure and the target temperature (see Fig. 5) in a manner which could be represented by the following empirical equation:

$$\text{Yield} \propto \{[1+53\exp(-0.43\ \text{ev}/kt)] \times[1+(1.5\times10^{-6}\ \text{mm Hg}/p)]\}^{-1}.$$

The numerical constants were obtained by curve fitting and are probably good to about 10–20%.

[14] Most of the early work on ion reflection has been summarized in H. S. W. Massey and E. H. S. Burhop, *Electronic and Ionic Impact Phenomena* (Clarendon Press, Oxford, 1952); p. 560. More recent observations and discussions are given by H. D. Hagstrum, Phys. Rev. **89**, 244 (1953); C. Brunnée, Z. Physik **147**, 161 (1957); O. v. Roos, *ibid.* **147**, 210 (1957); P. M. Waters, Phys. Rev. **111**, 1053 (1958); and R. E. Honig, footnote 1. The present work and that of Honig are the only ones in which the ions were studied with a mass analyzer.

[15] To avoid an admixture of Xe^{++} in the bombarding ion beam the electron energy in the first ion source was kept low.

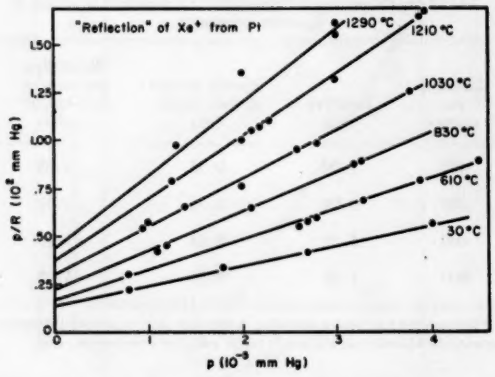

FIG. 5. A plot of (pressure p)/(Reflected ion yield R) vs p for several different target temperatures. The points are the data; the straight lines are given by the equation in the text.

The above equation is of the same form as Langmuir's adsorption equation[16] which suggests that the "reflected" ions came from inert gas atoms that were trapped on the surface. This may seem at first to be a puzzling result inasmuch as the adsorption of Xe on Pt should be very small at these temperatures. However, it is known that under the action of ion bombardment, trapping mechanisms other than classical chemisorption or physisorption are active (ion burial, for example[17,18]) and under these circumstances there seems little reason to doubt that the concentration of inert gas on the "surface" would be different from that which would exist in the absence of the bombardment.

Further support for this hypothesis is provided by a more recent study[19] in which a target was bombarded first with one gas and then with another. For the first minute or two of the second bombardment period a peak due to the first gas was observed.

The energy spread of the reflected ions, as measured by a retarding potential technique, was always less than 1 ev (see Fig. 6 and Table II). There was a slight increase in the spread with increasing bombarding energy. There was also a small increase with increasing temperature, most of which can be accounted for by the voltage drop across the target due to the heating current. The spread was slightly greater for a surface not recently flashed, an effect which is doubtless attributable to patches of different work function on the Pt. The spread was not affected by the ambient gas pressure in the range involved, showing that scattering of the beam in the analyzer tube was negligible. This last is important because the yield would have been affected by such scattering.

The average energy of the reflected ions could not be obtained from retarding potential measurements to closer than one or two electron volts because of the unknown contact potential difference between the target and the collector. However, it was very low compared to the bombarding energy, certainly no larger than the uncertainty imposed by the contact potential difference. In fact, considering that the energy spread was less than 1 ev it seems safe to conclude that the average energy was also less than 1 ev.

In comparing these results on ion reflection with those of other workers we are impressed with the dissimilarity between the behavior of reflected inert gas ions and that of reflected alkali metal ions,[14] the only two types that have been studied. In the case of the former the reflected ions are of low energy and depend on the ambient gas pressure. In the case of the latter, some of the ions are energetic and are unaffected by the pressure. It seems very likely that the term "reflection" is a misnomer as applied to the inert gas studies, and that the ions measured were sputtered rather than reflected.[20] The truly reflected inert gas particles, some of which ought to have appreciable energy, are evidently neutral and so escape detection. In the case of alkali metal ions, however, true reflection is observable because the ions are not neutralized by the metal surface.

SUMMARY

1. Mass analysis of ions ejected from Pt surfaces under inert gas ion bombardment revealed species characteristic of the base metal, of certain surface and bulk impurities, and of the bombarding beam.

2. The Pt ions appeared to come directly from the substrate rather than from surface compounds. The yield increased with temperature and bombarding energy. The ratio of sputtered ions to neutrals is esti-

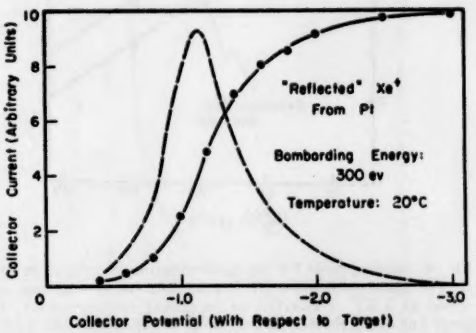

FIG. 6. The solid curve is a typical retarding potential plot for the reflected ions. The abscissa is the measured voltage difference between the final collector and the target (uncorrected for contact potential difference). The dashed curve is obtained by differentiating the solid curve, and hence shows the energy distribution.

[16] I. Langmuir, J. Am. Chem. Soc. **40**, 1361 (1918).
[17] E. Brown and J. H. Leck, Brit. J. Appl. Phys. **6**, 161 (1956).
[18] J. H. Carmichael and E. A. Trendelenburg, J. Appl. Phys. **29**, 1570 (1958).
[19] R. C. Bradley and E. Ruedl, Bull. Am. Phys. Soc. **5**, 16 (1959).

[20] As a matter of fact, since most of the previous studies did not involve mass analysis the so-called reflected ions may well have been secondary ions of various sorts.

mated to be of the order of 1 to 1000 at room temperature and somewhat higher (less than an order of magnitude) at high temperatures.

3. The only easily observable bulk impurity ions were those with low ionization potentials (Na, K, Ca, etc.)—the same ones that are observed in thermionic emission studies.

4. The presence of a surface impurity [possibly $Pt(CO)_2$] was revealed by a peak at approximately 240 amu which is tentatively identified as $PtO(CO)^+$. From a study of this peak as a function of temperature and time it was found that the compound formed spontaneously on the surface—probably due to a background of CO in the instrument, that the formation rate could be greatly enhanced by ion bombardment, and that the compound desorbed readily at 1000°C with an activation energy of 0.74±0.05 ev. In the range 1000°–1200°C the yield of the $PtO(CO)^+$ ions was found to be proportional to both the desorption rate and the bombarding ion current, suggesting post-desorption ionization by the bombarding beam.

5. Following a period of ion bombardment, inert gas could be released from the surface by heating to 1300°C. The activation energy for this release was 1.6±0.2 ev.

6. Secondary inert gas ions characteristic of the bombarding beam are usually referred to as "reflected" ions. However, the evidence presented here is more consistent with the notion that they are sputtered from surface layers rather than reflected. Their energy and energy spread are always extremely low (<1.0 ev) and their abundance depends on the ambient inert gas pressure and target temperature in a manner suggestive of Langmuir adsorption.

THE JOURNAL OF CHEMICAL PHYSICS VOLUME 33, NUMBER 3 SEPTEMBER, 1960

Streaming Birefringence of Rigid Macromolecules in General Two-Dimensional Laminar Flow

HAROLD WAYLAND

Division of Engineering, California Institute of Technology, Pasadena, California

(Received March 25, 1960)

Quantitative expressions for the direction of the angle of isocline and for the amount of birefringence due to a dilute solution of rigid macromolecules in a general two-dimensional laminar flow are derived. If E is the principal strain rate and Λ_0 is the angle between the streamline direction and the direction of the principal strain rate axis, the angle of isocline, measured from the first principal strain rate axis is

$$\chi = -(E \sin 2\Lambda_0/6D)\{1-(E^2/27D^2)[\sin^2 2\Lambda_0+(24b^2/35)]+\cdots\},$$

where $b=[(a_1^2-a_2^2)/(a_1^2+a_2^2)]$ is a shape factor for an ellipsoid of revolution of semimajor axis a_1 and semiminor axis a_2 and D is the rotary diffusion constant for this ellipsoid. The amount of birefringence is

$$\Delta n=(4\pi/15)(cGEb/nD)\{1-(E^2/18D^2)[\sin^2 2\Lambda_0+(6b^2/35)]+\cdots\},$$

where n is the mean index of refraction of the solution, c the volume concentration of the macromolecules, and $G=g_1-g_2$ is the optical anisotropy of the ellipsoids.

It is seen that if the principal strain rate is not at 45° to the streamline at the point of observation, this will make itself felt in the position of the angle of isocline before it influences the amount of birefringence.

Detailed expressions for the effect of polydispersity show that there is a simple relationship between the birefringence and angle of isocline measured in Couette flow and these quantities measured in general two-dimensional flow only if (a) $\Lambda_0=45°$ in the general flow or (b) the birefringence and angle of isocline values are linear with strain rate.

I. INTRODUCTION

THE theory of streaming birefringence (SBR) due to the orientation distribution of a population of rigid ellipsoidal particles due to pure shear flow has been developed by Peterlin and Stuart[1,2] for solutions so dilute that particle interactions can be neglected. Several situations arise in which it would be desirable to have a similar solution for general two-dimensional laminar flow: the use of the SBR of a dilute colloidal solution for studying the character of a two-dimensional laminar flow has never been placed on a sound theoretical basis; a complete understanding of SBR apparatus such as that of Kuhn, Oswald, and Kuhn[3] demands an analysis of a situation in which a flow due to a pressure drop is superposed on a Couette flow; and the possibility of studying relaxation effects in a steady state situation presents itself if the SBR of converging and diverging flow is understood theoretically.

[1] A. Peterlin and H. A. Stuart, Z. Physik **112**, 1, 129 (1939).
[2] A. Peterlin and H. A. Stuart, *Hand- und Jahrbuch der Chemischen Physik* (Becker u. Erler, Leipzig, 1943), Bd VIII, Abt. 1B.
[3] W. Kuhn, H. Oswald, and H. Kuhn, Helv. Chim. Acta **36**, 1209 (1953).

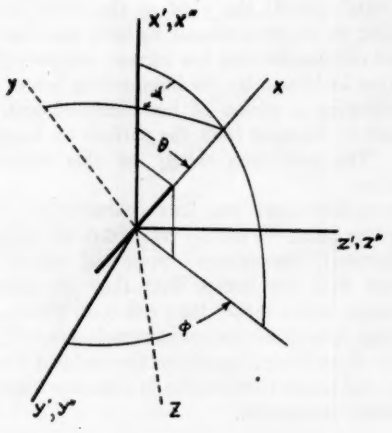

FIG. 1.

II. DERIVATION OF THE EQUATION FOR THE DISTRIBUTION FUNCTION

Let us consider a population of identical ellipsoids of revolution with semi-axes $a_1 \neq a_2 = a_3$. The xyz coordinate system (Fig. 1) is taken fixed in the particle with a_1 lying in the x direction. Two other coordinate systems will be used: $x'y'z'$ and $x''y''z''$ which both have the same origin as the xyz system and which are coincident with each other at the point of observation. The $x'y'z'$ system always retains the same orientation relative to the streamlines, and is the fundamental system with respect to which we shall want to derive the orientation distribution of the family of ellipsoids. The $x''y''z''$ system remains parallel to itself as its origin moves with the particle. The angular position of the ellipsoid can best be described by the Euler angles θ, ϕ, ψ referred to the $x''y''z''$ axes, where θ and ϕ are the colatitude and azimuthal angles, respectively, of the axis a_1 and ψ gives the rotational position of the particle about its axis of symmetry. The value of ψ will not enter into the expression for the SBR, hence it will be sufficient to obtain the orientation distribution function for the particle population as a function of θ, ϕ, $b=[(a_1^2-a_2^2)/(a_1^2+a_2^2)]$ and the hydrodynamic parameters.

If there were no flow, Brownian motion would tend to make the angular distribution uniform. The flux density due to Brownian motion is

$$\mathbf{i}_{dif} = -D\nabla F, \tag{1}$$

where D is the rotary diffusion constant, ∇ the gradient operator in the angular variables of spherical coordinates, and $F(\theta, \phi)$ is the angular distribution function. The hydrodynamic forces on the particle due to the flow field introduce a transport flux density $\mathbf{i}_{str}$,

$$\mathbf{i}_{str} = F\dot{\theta}\mathbf{e}_\theta + F\dot{\phi}\sin\theta\mathbf{e}_\phi. \tag{2}$$

For the steady state we must have

$$\operatorname{div}(\mathbf{i}_{str}+\mathbf{i}_{dif}) = 0. \tag{3}$$

To obtain an expression for $\mathbf{i}_{str}$ we shall take advantage of Jeffery's[4] work on the motion of ellipsoidal particles in a viscous fluid. Jeffery obtained a first integral of the equations of motion of a general ellipsoid when immersed in an arbitrary viscous flow provided that the motion of the particle was sufficiently slow that the linearized Navier-Stokes equations could be used. The undisturbed velocity field in the neighborhood of the particle, referred to the xyz coordinate system is

$$\delta\mathbf{V} = S\delta\mathbf{r} + \tfrac{1}{2}[\nabla\times\mathbf{V}]\times\delta\mathbf{r}, \tag{4}$$

where $\mathbf{V} = \mathbf{i}u + \mathbf{j}v + \mathbf{k}w$ is the velocity vector, S the rate of strain matrix ($e_{xx} = \partial u/\partial x$, $e_{xy} = \frac{1}{2}(\partial u/\partial y + \partial v/\partial x)$, $\cdots$), and $\nabla\times\mathbf{V} = \mathbf{i}\xi + \mathbf{j}\eta + \mathbf{k}\zeta$. In this notation the angular velocities $\omega_1, \omega_2, \omega_3$ of an ellipsoid of revolution about the x, y, z axes, respectively, when immersed in the flow described by Eq. (4), will be

$$\begin{aligned} \omega_1 &= \tfrac{1}{2}\xi \\ \omega_2 &= \tfrac{1}{2}\eta - be_{zx} \\ \omega_3 &= \tfrac{1}{2}\zeta + be_{xy}. \end{aligned} \tag{5}$$

The flow itself is most easily defined in terms of the axes $x''y''z''$ which are fixed in direction. Knowing the flow relative to the double-primed axes, the necessary strain rates and rotational components for insertion in Eq. (5) can readily be computed for any given orientation of the particle. The required angular velocities can then be referred to the $x'y'z'$ system (which will be rotating if the streamlines are curved). We shall assume

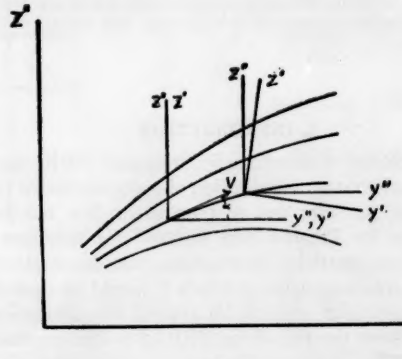

FIG. 2.

[4] G. B. Jeffery, Proc. Roy. Soc. (London) **A102**, 161 (1922–1923).

a two-dimensional flow parallel to the $y''z''$ plane (and likewise to the $y'z'$ plane), Fig. 2. This means that $u''=0$ and both v'' and w'' are independent of x''. The only nonvanishing strain rate and rotation components will be $e_{y''y''}$, $e_{y''z''}$, $e_{z''z''}$, and ξ''. Let the direction cosines of the coordinate system xyz referred to the system $x''y''z''$ be $(l_1m_1n_1)$, $(l_2m_2n_2)$, and $(l_3m_3n_3)$, respectively. To obtain the required angular velocities from Eq. (5) we need compute only ξ, η, ζ, e_{xz}, and e_{xy}.

$$e_{xz}=e_{y''y''}m_1m_3+e_{y''z''}(m_1n_3+m_3n_1)+e_{z''z''}n_1n_3$$

$$e_{xy}=e_{y''y''}m_1m_3+e_{y''z''}(m_2n_1+m_1n_2)+e_{z''z''}n_1n_2$$

$$\xi=\xi''\cos\theta;\quad \eta=-\xi''\sin\theta\cos\psi;\quad \zeta=\xi''\sin\theta\sin\psi. \tag{6}$$

We can now write the expression for ω_1, ω_2, and ω_3 and solve them for $\dot\theta$ and $\dot\phi$ to obtain

$$\begin{aligned}\dot\theta&=\omega_2\sin\psi+\omega_3\cos\psi\\&=b\sin\theta\cos\theta[e_{y''y''}\cos^2\phi+e_{z''z''}\sin^2\phi\\&\qquad+2e_{y''z''}\sin\phi\cos\phi]\\&=b\sin\theta\cos\theta[e_{y''y''}\cos2\phi+e_{y''z''}\sin2\phi]\end{aligned} \tag{7}$$

$$\dot\phi=\tfrac{1}{2}\xi''-b[e_{y''y''}\sin2\phi-e_{y''z''}\cos2\phi]. \tag{8}$$

These expressions can be considerably simplified if we refer the flow system to the first local principal rate of strain axis, i.e., with the axis associated with the strain rate $+E$ where E is the magnitude of the principal strain rate at the point under observation. This is done by introducing a new azimuthal angle

$$\lambda=\phi-\beta \tag{9}$$

where

$$\tan2\beta=e_{y''z''}/e_{y''y''}. \tag{10}$$

Equations (7) and (8) reduce to

$$\begin{aligned}\dot\theta&=Eb\sin\theta\cos\theta\cos2\lambda\\\dot\phi&=\tfrac{1}{2}\xi''-Eb\sin2\lambda\end{aligned} \tag{11}$$

where

$$E^2=e_{y''z''}{}^2+e_{y''y''}{}^2.$$

As a family of particles passes the observation point the axes $x'y'z'$ fixed in direction with respect to the streamlines will be rotating relative to the axes $x''y''z''$ which remain parallel to themselves in all positions. This solid body rotation will not contribute to the change in orientation distribution of the family of particles and must be subtracted out. If the rate of rotation is such that inertial effects can be neglected and if the rate of change of streamline curvature is negligible we can write

$$\Omega=V/\rho=(v^2+w^2)^{\frac{1}{2}}/\rho, \tag{12}$$

where Ω is the angular velocity of the $y'z'$ coordinate system relative to the $y''z''$ system and ρ is the radius of curvature of the streamline passing through the point of observation measured at the point. If $\tan\alpha$ is the slope of the streamline at the observation point in the $y''z''$ coordinate system,

$$\Omega=V(d\alpha/ds)=V(d/ds)\tan^{-1}(w/v), \tag{13}$$

where ds is taken along the streamline. Performing the calculation we find

$$\begin{aligned}\Omega&=\tfrac{1}{2}(w_{y''}-v_{z''})+\tfrac{1}{2}(w_{y''}+v_{z''})\cos2\alpha\\&\qquad+\tfrac{1}{2}(w_{z''}-v_{y''})\sin2\alpha\\&=\tfrac{1}{2}\xi''+e_{y''z''}\cos2\alpha-e_{y''y''}\sin2\alpha\\&=\tfrac{1}{2}\xi''+E(\sin2\beta\cos2\alpha-\cos2\beta\sin2\alpha)\\&=\tfrac{1}{2}\xi''+E\sin2(\beta-\alpha)\\&=\tfrac{1}{2}\xi''+E\sin2\Lambda_0.\end{aligned} \tag{14}$$

The quantity $\beta-\alpha=\Lambda_0$ is just the angle between the principal strain rate axis and the streamline direction at the point of observation. The expressions for $\dot\theta$ and $\dot\phi$ referred to the $x'y'$ axes now become

$$\begin{aligned}\dot\theta'&=\dot\theta=Eb\sin\theta\cos\theta\cos2\lambda\\\dot\phi'&=\dot\phi-\Omega=-E(b\sin2\lambda+\sin2\Lambda_0).\end{aligned} \tag{15}$$

The expression for the particle flux density referred to the $x'y'z'$ axes, due to the given hydrodynamic flow, can now be written explicitly.

$$\begin{aligned}\mathbf{i}_{str}&=F\dot\theta'\mathbf{e}_{\theta'}+F\dot\phi'\sin\theta'\mathbf{e}_\lambda\\&=E[Fb\sin\theta\cos\theta\cos2\lambda\mathbf{e}_\theta\\&\qquad-F(b\sin2\lambda+\sin2\Lambda_0)\sin\theta\mathbf{e}_\lambda].\end{aligned} \tag{16}$$

Equation (3), referred to the moving coordinate system, becomes

$$\operatorname{div}\{E[Fb\sin\theta\cos\theta\cos2\lambda\mathbf{e}_\theta-F(b\sin2\lambda+\sin2\Lambda_0)\sin\theta\mathbf{e}_\lambda]-D\nabla F\}=0. \tag{17}$$

It is convenient to rewrite this in the form

$$\begin{aligned}\nabla^2F=(E/D)\{&-3b\sin^2\theta\cos2\lambda F\\&+b\sin\theta\cos\theta\cos2\lambda(\partial F/\partial\theta)\\&-(\sin2\Lambda_0+b\sin2\lambda)(\partial F/\partial\lambda)\}=\sigma\mathbf{W}F,\end{aligned} \tag{18}$$

where $\mathbf{W}$ is the differential operator in curly brackets of Eq. (18) and $\sigma=E/D$.

III. SOLUTION FOR THE DISTRIBUTION FUNCTION

For small values of σ, Eq. (18) can be solved by an expansion in zonal harmonics.[1,2,5] Assume

$$F=F_0+\sum_{j=1}^{\infty}\sigma^j F_j \tag{19}$$

where

$$F_j=\sum_{n=0}^{j}a_{n0,j}P_{2n}(\cos\theta)+\sum_{n=1}^{j}\sum_{m=1}^{n}(a_{nm,j}\cos 2m\lambda + b_{nm,j}\sin 2m\lambda)\,P_{2n}^{2m}(\cos\theta). \tag{20}$$

Substituting Eq. (20) in Eq. (18) and equating like powers of σ we have

$$\nabla^2 F_{j+1}=\mathbf{W}F_j; \qquad j=0, 1, 2, 3, \cdots. \tag{21}$$

Starting with $F_0=1/4\pi$ we can solve successively for the various F_j with the following results:

$$F_0=1/4\pi$$

$$F_1=(b/4\pi)\,(\tfrac{1}{2}\sin^2\theta\cos 2\lambda)$$

$$F_2=(b^2/4\pi)\left[(\tfrac{1}{16}\sin^4\theta-\tfrac{1}{30})-\frac{\sin 2\Lambda_0}{6b}\sin^2\theta\sin 2\lambda+\tfrac{1}{16}\sin^4\theta\cos 4\lambda\right]$$

$$F_3=(b^3/4\pi)\left\{\left[\frac{1}{2^6}\sin^6\theta-\left(\frac{1}{2^2\cdot 3\cdot 5}-\frac{\sin 2\Lambda_0}{2\cdot 3^2 b^2}\right)\sin^2\theta\right]\cos 2\lambda-\frac{\sin 2\Lambda_0}{2\cdot 3\cdot 5b}\sin^4\theta\sin 4\lambda+\frac{1}{2^3\cdot 19}\sin^6\theta\cos 6\lambda\right\}$$

$$F_4=\sum_{n=1}^{4}a_{n0,4}P_{2n}+\sum_{n=1}^{4}\sum_{m=2}^{n}[a_{nm,4}\cos 2m\lambda+b_{nm,4}\sin 2m\lambda]P_{2n}^{2m}+\frac{b^4}{4\pi}\left\{\frac{-71\sin 2\Lambda_0}{2^6\cdot 3^2\cdot 5\cdot 7b}\sin^6\theta+\frac{13\sin 2\Lambda_0}{2^3\cdot 3^2\cdot 5^2\cdot 7b}\sin^4\theta+\frac{4\sin 2\Lambda_0}{3\cdot 5^2\cdot 7b}+\frac{\sin^2 2\Lambda_0\sin^2\theta}{2\cdot 3^2 b^2}\right\}\sin 2\lambda. \tag{22}$$

Only the terms in $\sin 2\lambda$ and $\cos 2\lambda$ (the latter has a zero coefficient) were calculated in detail for F_4 since these are the only terms entering into the SBR theory.

IV. ANGLE OF ISOCLINE AND ORIENTATION FACTOR FOR THE MONODISPERSE CASE

The direction of the isoclinic axis and the orientation factor can be calculated from the integrals A and B where

$$A=\int_0^{\pi}\int_0^{2\pi}F(\theta,\lambda)\,\sin^3\theta\sin 2\lambda\,d\lambda\,d\theta=\frac{-4E^2\sin 2\Lambda_0}{90}\frac{b}{D^2}\left[1-\frac{E^2b^2}{9D^2}\left(\tfrac{11}{35}+\frac{\sin^2 2\Lambda_0}{b^2}\right)+\cdots\right]$$

$$B=\int_0^{\pi}\int_0^{2\pi}F(\theta,\lambda)\,\sin^3\theta\cos 2\lambda\,d\lambda\,d\theta=\frac{2Eb}{15D}\left[1-\frac{E^2b^2}{9D^2}\left(\tfrac{3}{35}+\frac{\sin^2 2\Lambda_0}{b^2}\right)+\cdots\right]. \tag{23}$$

The position of the angle of isocline referred to the first principal rate of strain axis will be given by

$$\tan 2\chi=\frac{A}{B}=-\frac{E\sin 2\Lambda_0}{3}\left(1-\frac{8E^2b^2}{315}+\cdots\right) \tag{24}$$

from which

$$\chi=-\frac{E\sin 2\Lambda_0}{6D}\left[1-\frac{E^2}{27D^2}\left(\sin^2 2\Lambda_0+\frac{24b^2}{35}\right)+O\left(\frac{E^4}{D^4}\right)\right]. \tag{25}$$

The quantity $2E\sin 2\Lambda_0=\gamma_s$ is simply the shear rate parallel to the streamline, so we can rewrite (25) as

$$\chi=-\frac{\gamma_s}{12D}\left[1-\frac{1}{27D^2}\left(\frac{\gamma_s^2}{4}+\frac{24b^2}{35}E^2\right)+\cdots\right]. \tag{26}$$

The amount of birefringence, Δn, is given by[1,2]

$$\Delta n=2\pi c[(g_1-g_2)/n](A^2+B^2)^{\frac{1}{2}}=\frac{4\pi}{15}\frac{G}{n}\frac{cEb}{D}\left[1-\frac{E^2}{18D^2}\left(\sin^2 2\Lambda_0+\frac{6b^2}{35}\right)+O\left(\frac{E^4}{D^4}\right)\right]=\frac{4\pi}{15}\frac{G}{n}\frac{cEb}{D}\left[1-\frac{1}{18D^2}\left(\frac{\gamma_s^2}{4}+\frac{6b^2}{35}E^2\right)+\cdots\right] \tag{27}$$

where c is the volume concentration of the ellipsoidal particles, n the mean index of refraction of the solution, and $(g_1-g_2)=G$ the optical anisotropy factor for the particles.

For Couette flow, $\Lambda_0=\pm\pi/4$ and Eqs. (26) and (27) reduce to the classical solution of Peterlin and Stuart. For a general two-dimensional flow the angle between the streamline direction and the principal strain rate axis may differ from 45°. This will affect the direction of the angle of isocline no matter how small the principal strain rate E, but will influence the amount of birefringence only when the birefringence ceases to be linear with strain rate.

V. INFLUENCE OF POLYDISPERSITY

For a polydisperse medium made up of a discrete set of components a subscript i will be used to distinguish among these components. Assuming no hydrodynamic

[5] S. T. Demetriades, J. Chem. Phys. **29**, 1054 (1958).

interactions among the components in the mixture, the angle of isocline will be given by[6]

$$\tan 2\chi=\frac{\sum c_iG_iA_i}{\sum c_iG_iB_i}$$

$$=\frac{\dfrac{-4E^2\sin 2\Lambda_0}{90}\sum_i\dfrac{c_iG_ib_i}{D_i^2}\left[1-\dfrac{E^2b_i^2}{9D_i^2}\left(\dfrac{11}{35}+\dfrac{\sin^2 2\Lambda_0}{b_i^2}\right)+\cdots\right]}{\dfrac{2E}{15}\sum_i\dfrac{c_iG_ib_i}{D_i}\left[1-\dfrac{E^2b_i^2}{9D_i^2}\left(\dfrac{3}{35}+\dfrac{\sin^2 2\Lambda_0}{b_i^2}\right)+\cdots\right]}$$

$$=-\frac{\gamma_s}{6}\left\{\frac{\sum_i\dfrac{c_iG_ib_i}{D_i^2}}{\sum_i\dfrac{c_iG_ib_i}{D_i}}-\frac{E^2}{9\cdot 35}\left[\frac{11\sum_i\dfrac{c_iG_ib_i}{D_i}\sum_i\dfrac{c_iG_ib_i^3}{D_i^4}-3\sum_i\dfrac{c_iG_ib_i}{D_i^2}\sum_i\dfrac{c_iG_ib_i^3}{D_i^3}}{\left(\sum_i\dfrac{c_iG_ib_i}{D_i}\right)^2}\right]\right.$$

$$\left.-\frac{\gamma_s^2}{36}\left[\frac{\sum_i\dfrac{c_iG_ib_i}{D_i}\sum_i\dfrac{c_iG_ib_i}{D_i^4}-\sum_i\dfrac{c_iG_ib_i}{D_i^2}\sum_i\dfrac{c_iG_ib_i}{D_i^3}}{\left(\sum_i\dfrac{c_iG_ib_i}{D_i}\right)^2}\right]+\cdots\right\},\quad(28)$$

or

$$\chi=-\frac{\gamma_s}{12}\left\{\frac{\sum_i\dfrac{c_iG_ib_i}{D_i^2}}{\sum_i\dfrac{c_iG_ib_i}{D_i}}-\frac{E^2}{9}\left[\frac{\frac{11}{35}\sum_i\dfrac{c_iG_ib_i}{D_i}\sum_i\dfrac{c_iG_ib_i^3}{D_i^4}-\frac{3}{35}\sum_i\dfrac{c_iG_ib_i}{D_i^2}\sum_i\dfrac{c_iG_ib_i^3}{D_i^3}}{\left(\sum_i\dfrac{c_iG_ib_i}{D_i}\right)^2}\right]\right.$$

$$\left.-\frac{\gamma_s^2}{36}\left[\frac{\left(\sum_i\dfrac{c_iG_ib_i}{D_i^2}\right)^3+3\left(\sum_i\dfrac{c_iG_ib_i}{D_i}\right)^2\sum_i\dfrac{c_iG_ib_i}{D_i^4}-3\sum_i\dfrac{c_iG_ib_i}{D_i}\sum_i\dfrac{c_iG_ib_i}{D_i^2}\sum_i\dfrac{c_iG_ib_i}{D_i^3}}{3\left(\sum_i\dfrac{c_iG_ib_i}{D_i}\right)^3}\right]+\cdots\right\}.\quad(29)$$

Similarly

$$\Delta n=2\pi/n\{[\textstyle\sum_i c_iG_iA_i]^2+[\sum_i c_iG_iB_i]^2\}^{\frac{1}{2}}$$

$$=\frac{4\pi E}{15n}\sum_i\frac{c_iG_ib_i}{D_i}\left\{1-\frac{E^2}{105}\frac{\sum_i\dfrac{c_iG_ib_i^3}{D_i^3}}{\sum_i\dfrac{c_iG_ib_i}{D_i}}-\frac{\gamma_s^2}{72}\left[\frac{2\sum_i\dfrac{c_iG_ib_i}{D_i}\sum_j\dfrac{c_jG_jb_j}{D_j^3}-\left(\sum_i\dfrac{c_iG_ib_i}{D_i^2}\right)^2}{\left(\sum_i\dfrac{c_iG_ib_i}{D_i}\right)^2}\right]\right\}.\quad(30)$$

As long as experimental data taken in Couette calibration are linear the presence of polydisperisty does not affect the relationship between SBR in general two-dimensional flow and that in Couette flow; beyond the linear region there is no simple connection between data obtained in Couette flow and that obtained in general two-dimensional flow unless $\Lambda_0=45°$.

[6] C. Sadron, J. phys. radium 9, 381 (1938).

THE JOURNAL OF CHEMICAL PHYSICS VOLUME 33, NUMBER 3 SEPTEMBER, 1960

Green and Purple Sulfur: Electron-Spin Resonance Studies*

H. E. RADFORD, *National Bureau of Standards, Washington, D. C.*
AND
F. O. RICE, *Catholic University of America,† Washington, D. C.*

(Received April 22, 1960)

Electron spin resonance absorption has been found in the colored deposits formed by condensing heated sulfur vapor on cold surfaces. Complexities in the resonance spectrum give evidence for the existence in the cold deposits of at least two types of trapped sulfur radicals with differing degrees of internal magnetic anisotropy. Measurements of the intensity and stability of the resonance absorption yield information on the radical trapping process.

ELECTRON spin resonance (ESR) absorption has been discovered in several ordinary sulfur-containing materials,[1,2] as well as in pure sulfur itself in molten form.[3] In each case the absorption has been traced to small steady-state concentrations of sulfur radicals. The presence of sulfur radicals has also been conjectured in the strikingly colored deposits formed by the sudden condensation of hot sulfur vapor on a chilled surface.[4] Reported here are the results of ESR measurements on this "colored sulfur."

I. EXPERIMENT

Colored sulfur deposits were prepared by vacuum distillation of purified sulfur[5] onto a surface cooled by liquid nitrogen; just before striking the cold surface the sulfur vapor passed through a section of quartz tubing heated by an electric furnace. Several deposits were made, at furnace temperatures ranging from 400° to 1100°K; corresponding deposit colors ranged from the normal sulfur yellow through dark green to purple-black, with intermediate gradations. Suitable ESR samples, labeled by furnace temperature, were made by scraping the deposits off the cold surface and packing them into small quartz tubes; the whole operation was performed under liquid nitrogen. Most of the ESR measurements were made at 3.2-cm wavelength, but measurements on a few samples were repeated at 1.3-cm wavelength. Both spectrometers were of the microwave bridge type, using straight crystal detection, magnetic field modulation, and narrow band amplification. A rectangular TE_{012} microwave sample cavity was used at 3.2 cm; a circular cylindrical TE_{011} cavity was used at 1.3 cm. Both cavities were drilled to receive the sulfur sample tubes, and were cooled by a liquid-nitrogen jacket.

Figure 1 shows a typical colored sulfur ESR spectrum recorded at 3.2 cm. The spectrometer traces out an approximate first derivative of the absorption spectrum; this is represented by part (a) of the figure, and part (b) shows the reconstructed absorption spectrum. The three well-defined features of the derivative spectrum are labeled with g factors, calculated by inserting the measured values of microwave frequency and magnetic field strength into the relation $h\nu = g\mu_0 H$. Spectra recorded at 1.3 cm differed from that of Fig. 1 chiefly in over-all width: measured between outside peaks of the derivative recording the width was 65 gauss at 3.2 cm and 157 gauss at 1.3 cm. These widths are in strict proportion with the magnetic field strengths required to establish resonance; indeed, the 1.3 cm spectra are described by the same three g factors as those of Fig. 1. The width of the narrow central absorption peak did not differ significantly in the 3.2 and 1.3 cm spectra.

The ESR absorption intensity of colored sulfur depends strongly on the furnace temperature maintained during the deposition process. Absorption signals rise above the spectrometer noise level for a furnace temperature of about 550°K, and grow rapidly as the furnace temperature is raised to the neighborhood of 800°K. From 800° to 1100°K little further change occurs in the signal amplitudes. The corresponding variation of the total absorption intensity (the second integral of the derivative recording) with furnace temperature appears in the semilogarithmic plot of Fig. 2. The ordinates here refer to numbers of radicals, determined by weighing, in samples of diphenyl picryl hydrazyl (DPPH) which, when substituted for 100-mg samples of colored sulfur, gave equal total ESR absorption. On this scale, the highest concentration of unpaired electrons in the colored sulfur deposits was about one per 500 sulfur atoms, within an uncertainty of perhaps a factor of two. The lowest observable concentration was over a thousand times smaller.

Accompanying the rise in total absorption intensity with furnace temperature there is a systematic change in the distribution of intensity over the spectrum. At temperatures lower than 700°K the central absorption

* This research was performed under the National Bureau of Standards Free Radicals Research Program, supported by the Department of the Army.

† Present address: Georgetown University, Washington, D. C.

[1] D. M. Gardner and G. K. Fraenkel, J. Am. Chem. Soc. **77**, 6399 (1955); **78**, 6411 (1956).
D. J. E. Ingram and M. C. R. Symons, J. Chem. Soc. **1957**, 2435.

[3] D. M. Gardner and G. K. Fraenkel, J. Am. Chem. Soc. **78**, 3279 (1956).

[4] F. O. Rice and C. Sparrow, J. Am. Chem. Soc. **75**, 848 (1953); F. O. Rice and J. Ditter, *ibid.* **75**, 6066 (1953).

[5] Purified by the method of R. F. Bacon and R. Fanelli, Ind. Engr. Chem. **34**, 1043 (1942).

peak is 5 gauss wide and contributes about 10% of the total absorption; as the furnace temperature is increased from 700° to 900°K the central peak broadens to a maximum of 20 gauss, where it appears to account for about 75% of the total absorption. Higher furnace temperatures have no further effect on the intensity pattern. No comparable change with furnace temperature occurs in the shapes of the outer peaks of Fig. 1(a), nor in the amplitude of one relative to the other.

The characteristic differences in the spectra of samples prepared at different temperatures above 700°K can be completely removed by warming the samples from 77° to 195°K (dry ice temperature). Differences in the total absorption intensity and differences in the detailed shape of the spectra, all stable indefinitely at 77°K, are removed in a few minutes by this treatment, leaving a set of ESR spectra which are indistinguishable from the original spectrum associated with a furnace temperature of 700°K. A notable feature of this residual component of ESR absorption is its relative stability: only a moderate further decay in absorption intensity takes place if, after the initial rapid warming, the samples are kept at 195°K for several succeeding hours. Subsequent tests, prompted by these observations, showed that colored sulfur also could be condensed on a surface cooled by dry ice instead of liquid nitrogen. The ESR spectra did not differ noticeably from those of the deposits warmed to dry ice temperature after first being condensed on the colder surface.

Colored sulfur deposits were also prepared by condensing the products of an electric discharge in sulfur vapor on a surface cooled by liquid nitrogen. The discharge was excited by a 2450 Mc diathermy generator and was stabilized by admixing helium gas to the sulfur vapor stream. The deposits, which had a red-brown color, gave essentially the same ESR spectrum as that of Fig. 1, although with evidence of additional absorption toward the high-field side of the spectrum. A similar reddish color was observed in solid sulfur subjected to γ irradiation at 77°K, but no ESR absorption was detected in this material. This "red sulfur," like the other colored forms, is stable only at low temperatures; when warmed to room temperature it reverts—explosively in the case of irradiated sulfur—to the normal yellow color of solid sulfur.

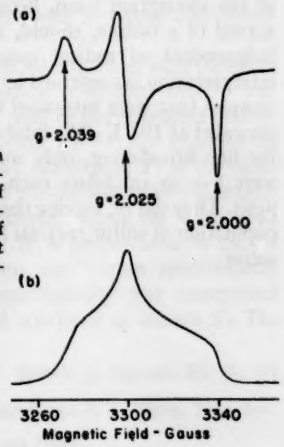

FIG. 1. The electron spin resonance spectrum, at a microwave frequency of 9328 Mc, of colored sulfur. Part (a) represents a derivative recording of the absorption spectrum. Part (b) shows a numerical integration of (a).

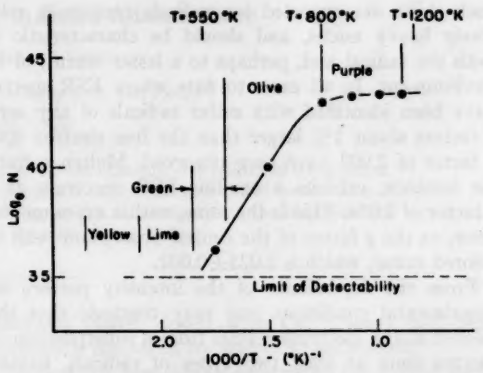

FIG. 2. Empirical "excitation function" for the paramagnetism of colored sulfur. The natural logarithm of the integrated ESR absorption intensity is plotted against the reciprocal of the furnace temperature used in preparing the colored sulfur deposit. The intensity scale refers to numbers of DPPH radicals which produce an integrated absorption intensity equal to that of a 100 mg sulfur sample. Also indicated by this figure is the dependence on furnace temperature of the deposit color.

II. DISCUSSION

Measurements of the vapor pressure[6] and magnetic susceptibility[7] of hot sulfur vapor show that it consists to a large extent of diatomic sulfur in its triplet (diradical) ground state. In view of the well-recognized possibility of trapping radicals in low-temperature solids,[8] it is thus reasonable to presume that trapped sulfur radicals of one sort or another are responsible for the ESR absorption of colored sulfur. Certainly, the strength of magnetic properties produced in a cold deposit by trapping thermally generated radicals should depend on the furnace temperature used, and these magnetic properties should disappear if the cold deposit is warmed sufficiently; these are two salient characteristics of colored sulfur.

Somewhat more direct evidence for the presence of sulfur radicals in colored sulfur is offered by the ESR spectrum itself. Although hyperfine structure, useful in identifying the spectra of other radicals, is absent in this case (the predominant isotope S^{32} has no nuclear spin), the localization of unpaired electrons on sulfur nuclei is clearly indicated by a shift of the ESR spectrum from the location of the free electron spin resonance. Generally ascribed to spin-orbit interactions,

[6] H. Braune, S. Peter, and V. Neveling, Z. Naturforsch. **6a**, 32 (1951).
[7] A. B. Scott, J. Am. Chem. Soc. **71**, 3145 (1949).
[8] J. L. Franklin and H. P. Broida, Ann. Rev. Phys. Chem. **10**, 145 (1959).

such shifts are expected for radicals containing relatively heavy nuclei, and should be characteristic of both the radical and, perhaps to a lesser extent, of its environment. In all cases to date where ESR spectra have been identified with sulfur radicals of any sort, g factors about 1% larger than the free electron spin g factor of 2.002 have been observed. Molten sulfur,[8] for instance, exhibits a one-line ESR spectrum at a g factor of 2.024. This is the same, within experimental error, as the g factor of the central absorption peak of colored sulfur, which is 2.025 ± 0.002.

From the dependence of the intensity pattern on experimental conditions, one may conclude that the colored sulfur spectrum results from a superposition of spectra from at least two types of radicals, having slightly different magnetic properties. One type produces the central absorption peak and, judging from the numerical value and apparent isotropy of its g factor, it is probably the same long-chain polysulfur diradical as that identified in molten sulfur. There is no other independent evidence for the presence of polysulfur chains in the cold deposit, but it is perhaps significant that the deposit, when warmed to room temperature, is found to consist partly of "amorphous sulfur," whose rubberlike properties are characteristic of polymer chains.

The second feature of the ESR spectrum, the broad asymmetric absorption band, may be attributed to a second group of sulfur radicals which have slightly differing magnetic properties. Since the width of the band increases in strict proportion with the resonance field strength, the breadth of the absorption must reflect a spread in g factors, and not the averaged effects of anisotropic fine structure, which would be independent of magnetic field. In its simplest interpretation, the band may be assigned to a single type of radical with an anisotropic magnetic moment. Frozen into the solid in a randomly oriented way, such radicals would exhibit an ESR absorption bounded by values of magnetic field which correspond to the g factor extrema. Sample calculations show that the observed absorption profile can be fitted fairly well by theory with the assumption that the radicals have axial magnetic symmetry. The calculated absorption is distributed in such a way that $g_{||}$ and $g_{\perp}$, the g factors in directions respectively parallel and perpendicular to the symmetry axis of the radical, are given very nearly by the locations of the absorption derivative maxima. From Fig. 1 they are: $g_{||} = 2.000 \pm 0.002$, $g_{\perp} = 2.039 \pm 0.002$, where the quoted uncertainty is of experimental origin.

The ESR results alone do not permit any sort of precise identification of the radical type (or types) responsible for this broad absorption, but they do serve to limit somewhat the possibilities. Most important, the absence of detectable fine structure rules out diradical sulfur aggregates small enough to show an appreciable anisotropic spin-spin interaction. Excluded would be diatomic sulfur, as well as polymer chains of up to, say, eight or ten atoms. This is not to say that such radicals do not exist in the cold deposit, but rather that if in fact they are present in sizeable numbers, their ESR absorption spectra do not possess features sharp enough to be detected. It is quite likely that, because of its strong anisotropic spin-spin interaction, diatomic sulfur would be undetectable no matter what its concentration in a solid like colored sulfur, which has no visible crystalline structure. On the other hand, chainlike aggregates of four, six, or eight sulfur atoms with an unpaired electron localized near each end of the chain might exhibit only a small anisotropic spin-spin interaction, and such radicals would contribute ESR absorption with characteristic, field-independent breadths. In the buildup of long diradical chains from the incoming diatomic vapor, it is reasonable that some such short-chain intermediate product might be stabilized in the cold deposit; the ESR spectrum, however, offers no sign of these radicals.

The abrupt saturation of trapped radical populations at the higher furnace temperatures, shown by Fig. 2, is caused by the self-limiting effect of radical recombination in the deposit. This is supported by two independent pieces of evidence. First, the central line of the ESR spectrum broadens rapidly as population saturation sets in, and attains a characteristic width at complete saturation. This broadening is probably caused by spin-spin interactions between neighboring radicals. Absent in a dispersed, unsaturated radical population, the broadening would increase with radical concentration to an upper limit set by the stability of two neighboring radicals against mutual annihilation (the width of the absorption band, being determined chiefly by a spread of g factors, should, as observed, be relatively independent of radical concentration). Second, this interpretation is confirmed by the behavior of the sulfur samples that were saturated with radicals at 77°K and annealed at 195°K. The interacting radicals responsible for line broadening, only marginally stable at 77°K, were free to annihilate each other in the warmed deposit. They did so, leaving the same, stable, unsaturated population of sulfur radicals in every sample of colored sulfur.

THE JOURNAL OF CHEMICAL PHYSICS VOLUME 33, NUMBER 3 SEPTEMBER, 1960

Nuclear Magnetic Resonance in Solid Adamantane

DAVID W. MCCALL AND DEAN C. DOUGLASS

Bell Telephone Laboratories, Inc., Murray Hill, New Jersey

(Received April 26, 1960)

Proton magnetic resonance studies of solid adamantane reveal the existence of a rotational transition at about −130°C. The activation energy associated with the rotational transition is found to be about 5 kcal/mole. Theoretical and experimental second moments agree if it is assumed that the molecules are rigidly fixed below the transition and rotate freely above the transition.

THE hydrocarbon adamantane is a remarkable substance. The structure is tetrahedral, a CH group at each corner and a connecting CH_2 group along each edge, but molecular models reveal that the compound is quite spherical. Although the formula is $C_{10}H_{16}$ adamantane melts (sealed tube) at 267°C, while normal decane melts at −31°C. Since adamantane presumably possesses intermolecular forces which are not very different from other saturated hydrocarbons, this behavior suggests a low entropy of fusion associated with a rotational transition in the solid. With these features in mind, the proton magnetic resonance spectrum has been studied for the powdered material as a function of temperature. The resonance is found to be quite broad at temperatures below −130°C, between −130° and −110°C the resonance narrows, and above −110°C the resonance width remains approximately constant up to the highest temperature studied (about 70°C). This line width reduction will be shown to be consistent with a transition from a rigid crystal lattice to a rotator phase, but no information concerning the packing in either form has been deduced.

A Varian Associates variable frequency spectrometer and 12-in. magnet system were employed. The resonances were observed at 15 Mc. The specimen temperature was controlled by means of a gas flow system, previously described,[1] and it was necessary to encapsulate the powder in glass capillary tubes. The temperature was measured with a copper-constantan thermocouple.

Saturation measurements were made at each temperature and T_1, the spin-lattice relaxation time,[2,3] was estimated as follows. The peak of the resonance derivative curve is maximized when $\gamma^2 H_1^2 T_1 T_2 = \frac{1}{2}$, where H_1 is the radio-frequency field amplitude, T_2 is the spin-spin relaxation time,[2,3] and γ is the proton gyromagnetic ratio. T_2 was taken as $2/\sqrt{3}\gamma\delta H$, where δH is the peak to peak resonance width. H_1 is proportional to the "rf field" meter deflection on the Varian spectrometer and the constant of proportionality was determined by measuring a standard specimen of known T_1. The standard (water doped with Cu^{++} ions) had been previously measured by spin-echo techniques.[4]

In practice, one simply determines the rf field meter reading μ_m, which corresponds to the maximum derivative signal (from the phase sensitive detector), and the resonance width δH is obtained at suitably small modulations[5] amplitude. T_1 is then determined from $T_1 = 2.42 \times 10^5 \delta H/\mu_m^2$, where δH is in gauss and T_1 is in seconds. The constant of calibration may be considerably in error but relative values for T_1 will not be affected.

Second moments have been computed and corrected for saturation[6] and finite modulation amplitude.[7] The sum of the corrections was less than 30% of the reported second moment in every case.

The specimen was kindly supplied by Professor Schleyer, Princeton University.[8]

Figure 1 shows the second moment of the resonance as a function of temperature. Figure 2 shows the spin-lattice relaxation time T_1 as function of the inverse absolute temperature. It is apparent that motional processes are responsible for the narrowing of the

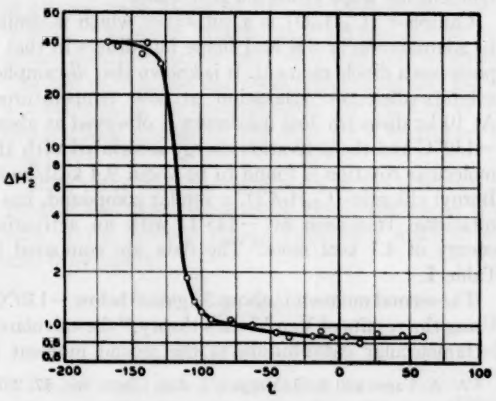

FIG. 1. The second moment (in gauss²) of the proton resonance in adamantane as a function of temperature.

[1] D. W. McCall and W. P. Slichter, J. Polymer Sci. **26**, 171 (1957).
[2] N. Bloembergen, E. M. Purcell, and R. V. Pound, Phys. Rev. **73**, 679 (1948).
[3] F. Bloch, Phys. Rev. **70**, 460 (1946).

The method used was the 180°–90° technique. See H. Y. Carr and E. M. Purcell, Phys. Rev. **94**, 630 (1954).
[5] This is "sweep" in Varian terminology.
[6] D. W. McCall, J. Appl. Phys. **29**, 739 (1958).
[7] E. R. Andrew, Phys. Rev. **91**, 425 (1953).
[8] Paul Schleyer, J. Am. Chem. Soc. **79**, 3292 (1957).

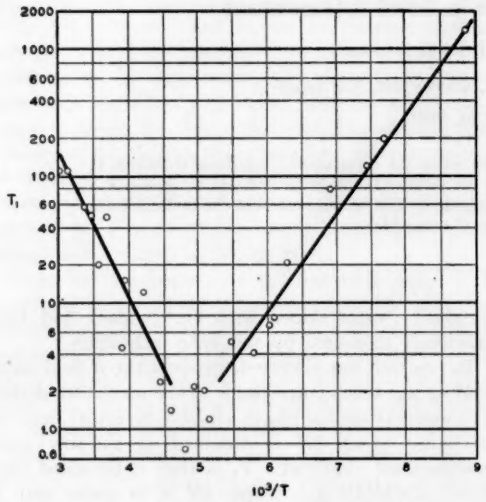

FIG. 2. The spin-lattice relaxation time (in seconds) of the proton resonance of adamantane as a function of reciprocal absolute temperature.

resonance observed near −130°C. At the knee of the second moment-temperature curve, the correlation time for the motion is given by[2] $\tau_c \sim 1/\gamma\Delta H_2 \sim 6\times10^{-6}$ (−130°C), and at the T_1 minimum $\tau_c \sim 1/\omega_0 \sim 10^{-8}$ sec (−65°C). ω_0 is 2π times the resonance frequency. Assuming that τ_c varies in accordance with the Arrhenius relation, $\tau_c = \tau_0 \exp(E/RT)$, these values yield about 5.8 kcal/mole for the activation energy E. Activation energies may also be computed from the slopes of the straight line portions of Fig. 2 and the low-temperature slope yields 4.1 kcal/mole. The high temperature slope yields 5.6 kcal/mole.

Camphor ($C_{10}H_{16}O$) is a substance which is similar to adamantane in size and shape but differs in that it possesses a dipole moment. It is known that *dl*-camphor exhibits dielectric relaxation at low temperatures.[9] At 10 kc dielectric loss maximum is observed at about −130°C and the activation energy associated with the molecular rotation is found to be about 9.4 kcal/mole. Bornyl chloride ($C_{10}H_{17}Cl$), a similar compound, has a rotational transition at −145°C with an activation energy of 4.7 kcal/mole.[9] The data are compared in Table I.

The second moment is about 39 gauss^2 below −130°C. Using the results of Van Vleck's theory,[10] the calculated intramolecular contribution to the second moment is

[9] W. A. Yager and S. O. Morgan, J. Am. Chem. Soc. **57**, 2071 (1935).

[10] J. H. Van Vleck, Phys. Rev. **74**, 1168 (1948).

TABLE I.

Compound	Transition temperature (°C)	Activation energy (kcal/mole)
Adamantane	−130	6
dl-Camphor	−130	9
Bornyl chloride	−145	5

31.5 gauss.[2] (Tetrahedral bond angles, $r_{CC}=1.54$ A, and $r_{CH}=1.07$ A were assumed for this calculation.) The intermolecular contribution was computed in a rather novel way. Molecular rotation can have no effect on the second moment[11] and, therefore, we have simply employed Van Vleck's powder formula with the assumption of free rotation of all the molecules. This yields about 7 gauss^2, in good agreement with the experimental value.

Above the transition the second moment is about 0.9 gauss^2 which indicates that the intramolecular contributions have been entirely eliminated by molecular rotation. The intermolecular effect for the rotator phase has been computed and is found to be about 0.95 gauss^2, again in good agreement with experiment. Note that the two intermolecular calculations are quite different. In the rigid phase a fictitious rotation was introduced into the final Van Vleck formula (where it has no effect) to avoid the necessity of knowing the orientations of the individual molecules. In the rotator phase calculation the dipolar Hamiltonian is averaged before the second moment is computed.

The crystal structure of adamantane is cubic close-packed, which is quite unusual for an organic compound.[12] Such packing is common, however, in substances composed of spherical units, e.g., metals and salts. Adamantane is nearly spherical in shape and nonpolar. Furthermore, the molecules are rotating, which tends to increase the spherical aspect. It would be of interest to determine the crystal structure below the transition temperature. If the structure is not close-packed at low temperatures, it might be inferred that the rotation plays an important part in determining the molecular arrangement.

ACKNOWLEDGMENTS

The authors are indebted to Dr. S. Meiboom, Dr. W. P. Slichter, Dr. E. Wasserman, Dr. J. W. Nielsen, and Professor Schleyer for assistance in this work.

[11] G. E. Pake in *Solid State Physics*, edited by F. Seitz and D. Turnbull (Academic Press, Inc., New York, 1956), Vol. 2, p. 45.

[12] W. Nowacki, Helv. Chim. Acta **28**, 1233 (1945).

THE JOURNAL OF CHEMICAL PHYSICS VOLUME 33, NUMBER 3 SEPTEMBER, 1960

Separation of Boron Isotopes. IV. The Methyl Sulfide-BF_3 System*

A. A. PALKO AND J. S. DRURY

Chemistry Division, Oak Ridge National Laboratory, Oak Ridge, Tennessee

(Received March 18, 1960)

The exchange of boron between BF_3 (gas) and the dimethyl sulfide-BF_3 complex (liq.) was studied from −20°C to +26°C. The single stage separation factor changed from 1.056 to 1.031 over this temperature range with B^{10} concentrating in the liquid phase. Vapor pressures of dimethyl sulfide and of various mixtures of BF_3 and dimethyl sulfide were determined. ΔH for the reaction BF_3 (gas) + Me_2S (liq.) → $BF_3 \cdot Me_2S$ (liq.) was estimated to be −10.1 kcal/mole over the above temperature range. The melting point of the 1:1 complex was −19.6°C.

INTRODUCTION

A SYSTEMATIC study has been undertaken of chemical reactions by which boron isotopes may be separated. Systems involving gaseous BF_3 and oxygen-containing addition compounds have been reported previously.[1,2] Present studies are concerned with reactions between BF_3 and sulfur complexes of BF_3. Data for the *n*-butyl sulfide-BF_3 complex are contained in Part III of this series.[3]

Dimethyl sulfide reacts readily with BF_3 to form the 1:1 complex, liberating 10.1 kcal of heat for each mole of complex formed. The complex is a clear, colorless liquid which melts at −19.6°C. It reacts violently with water and methanol, liberating HF. Excess BF_3 dissolves only slightly in the 1:1 complex. In the vapor state the complex is almost completely dissociated into BF_3 and methyl sulfide.[4] When carefully prepared, $Me_2S \cdot BF_3$ is quite stable. No irreversible decomposition was noticed during these studies even though certain solutions were observed for several weeks.

EXPERIMENTAL

Materials

The BF_3 used in these experiments was from the same batch of gas as was used for the *n*-butyl sulfide experiments, and was treated in the manner described previously.[3]

The dimethyl sulfide was experimental grade material supplied by Crown Zellerbach Corporation, Camas, Washington, and was better than 99.8% pure. It had the following physical characteristics: melting point, −98.3°C; boiling point, 37.1°C; n_D^{20}, 1.4349; d_4^{20}, 0.847. To remove final traces of water and mercaptan, the Me_2S was refluxed for several hours over freshly cut sodium and copper shot.[5] The sulfide was then fractionated in a still packed with glass helices. A center cut was distilled directly into the reaction flask as needed.

Separation Factor

The single stage separation factor α for the dimethyl sulfide-BF_3 system is the isotopic equilibrium constant for the reaction:

$$B^{10}F_3(\text{gas}) + B^{11}F_3 \cdot Me_2S(\text{liq.}) \rightleftharpoons B^{11}F_3(\text{gas}) + B^{10}F_3 \cdot Me_2S(\text{liq.})$$

and may be written

$$\alpha = (B^{10}/B^{11})\text{liq.}/(B^{10}/B^{11})\text{gas.}$$

The procedure and apparatus for determining α was the same as that used for the *n*-butyl sulfide and anisole systems and may be found elsewhere.[2,3]

Vapor Pressure

A series of vapor pressure measurements were made at several mole ratios of BF_3 to Me_2S from −20 to +26°C. The same experimental apparatus and procedure described earlier[1] was used with one exception. The 300 ml reaction flask was replaced by one having a total volume of approximately 50 ml. Use of the smaller flask eliminated the need for a correction for free BF_3.

Since there was little agreement in the literature regarding the vapor pressure of Me_2S, the vapor pressure of the purified Crown Zellerbach material was also determined.

RESULTS

Separation Factor

Single stage isotopic separation factors were determined at four temperatures, −20, −10, 0, and 26°C. Results are shown in Table I.

If it is assumed that $\log \alpha$ vs $1/T$ is essentially linear over the observed temperature range, these data may be expressed by the following least squares equation:

$$\log \alpha = (16.9/T) - 0.0440. \quad (1)$$

* This paper is based on work performed for the U. S. Atomic Energy Commission by Union Carbide Corporation.

[1] R. M. Healy and A. A. Palko, J. Chem. Phys. **28**, 211 (1958).
[2] A. A. Palko, R. M. Healy, and L. Landau, J. Chem. Phys. **28**, 214 (1958).
[3] A. A. Palko, J. Chem. Phys. **30**, 1187–1189 (1959), Part III.
[4] W. A. G. Graham and F. G. A. Stone, J. Inorg. Nuclear Chem. **3**, 164 (1956).
[5] D. W. Osborne, R. N. Doescher, and D. M. Yost, J. Am. Chem. Soc. **64**, 169–172 (1942).

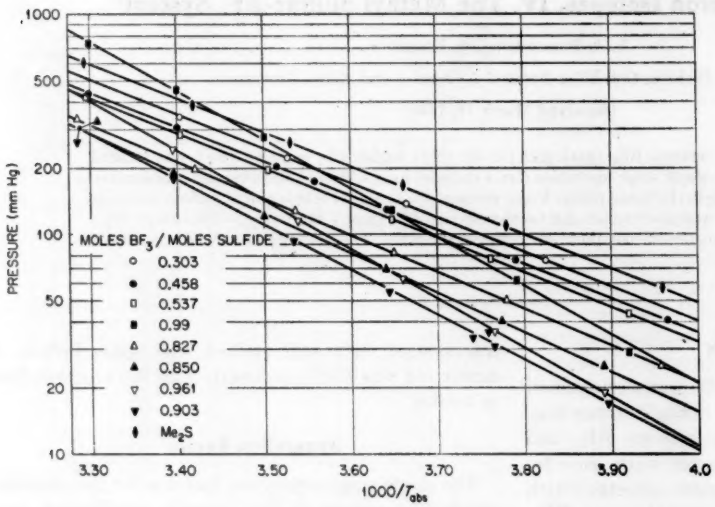

FIG. 1. Vapor pressure of various compositions of the system BF_3+ *n*-methyl sulfide.

Vapor Pressure

Vapor pressure measurements over the temperature range −20°C to +26°C were obtained for pure methyl sulfide and several solutions containing various mole ratios of BF_3 to Me_2S. These data are shown in Fig. 1. Least square curves of the form $\log P = a - (b/T)$ were fitted to the experimental points. Values for the constants of these curves are given in Table II.

DISCUSSION

Separation Factor

The exchange of boron between BF_3 gas and liquid $Me_2S \cdot BF_3$ results in the concentration of boron-10 in the liquid phase. The isotopic separation factor is comparable to that obtained in the Bu_2S and anisole systems.

Graham and Stone[4] have estimated that the $Me_2S \cdot BF_3$ complex is 96.2 to 97.4% dissociated in the vapor phase over the temperature range 12–34°C. If this observation is valid, the isotopic equilibrium constants for the observed exchange reaction should be some 3 to 5% higher than the measured separation factors. In this paper, however, no distinction can be made between the separation factor and the isotopic equilibrium constant since the error involved in the mass analysis is considerably greater than the difference between these two quantities.

From the temperature dependence of the separation factors, estimates may be made of heat and entropy changes associated with the isotopic exchange reaction. Equation (1) leads to $\Delta H = +77$ cal/mole, $\Delta F_{273.1} = -23$ cal/mole, and $\Delta S_{273.1} = +0.20$ e.u./mole.

TABLE I. Single stage separation factor as a function of temperature for the Me_2S-BF_3 system.

	26°C	0°C	−10°C	−20°C
	1.036	1.043	1.033	1.059
	1.030	1.039	1.049	1.056
	1.029	1.045	1.048	1.057
α	1.029	1.039	1.055	1.055
		1.039	1.044	1.054
		1.039	1.058	1.056
α (95% C.I.)	1.031	1.041	1.048	1.056
	±0.007	±0.005	±0.008	±0.002

Vapor Pressure

At low temperatures, the addition of BF_3 to Me_2S results in a progressive lowering of the vapor pressure of the system until a mole ratio of approximately 0.9 BF_3/Me_2S is reached. Further addition of BF_3 causes a rapid increase in system pressure. This characteristic

TABLE II. Vapor pressure of Me_2S-BF_3 solutions from −20°C to +26°C($\log P = a - (b/T)$.

Composition of solution (moles BF_3/mole Me_2S)	a	b	ΔH reaction (2.303 Rb) kcal/mole
0.303	7.837	1557	7.1
0.458	7.780	1556	7.1
0.537	7.819	1577	7.2
0.827	7.989	1665	7.6
0.850	8.377	1796	8.2
0.903	9.241	2056	9.4
0.961	9.982	2236	10.2
0.990	10.164	2209	10.1
Pure Me_2S	7.878	1546	7.1

places the Me_2S system at a disadvantage, in comparison with the Bu_2S or anisole systems, as far as practical application is concerned, since it interferes with the establishment of an efficient product reflux mechanism. Despite this disadvantage, the $Me_2S \cdot BF_3$ complex could still be used to separate boron isotopes by employing a distillation process such as that used by the Hooker[6,7] Chemical Company. Since the effective enrichment factor for the chemical exchange reaction involving the $Me_2S \cdot BF_3$ complex is almost twice that of the $Me_2O \cdot BF_3$ complex, fewer enrichment stages and a smaller reflux ratio should be required to produce a given yield of boron-10 with the $Me_2S \cdot BF_3$ complex than with the $Me_2O \cdot BF_3$ complex.

The heat change for the reaction

$$Me_2S \cdot BF_3(\text{liq.}) \rightleftharpoons BF_3(\text{gas}) + Me_2S(\text{liq.}) \qquad (2)$$

may be computed from the vapor pressure data given in the first three columns of Table II. These results are shown in the last column of Table II. Thus the heat of reaction of the 1:1 mole ratio complex is 10.1 kcal $mole^{-1}$. By correcting Eq. (2) for the heat of vaporization of Me_2S and using data for the 0.99 mole fraction complex, a "heat of vaporization" of $Me_2S \cdot BF_3$(liq.) may be obtained. This value, 17.18 kcal/mole, includes also the heat of association of the complex since the complex is almost completely dissociated in the vapor phase.

The vapor pressure listed in Table II for the 0.99 mole fraction complex is greater by more than a factor of 2 than that reported as the saturation pressure of liquid $(CH_3)_2S \cdot BF_3$ by Graham and Stone.[4] It appears that this discrepancy may be due to the use by those investigators of a small sample of complex in a tensimeter possessing a relatively large free volume. Under such conditions, the composition of the complex actually measured would be somewhat less than the 1:1 mole ratio of reactants initially introduced into the tensimeter. If the mole ratio of BF_3 to Me_2S in the liquid complex were only altered from 1.0 to 0.9 through such circumstances, the measured vapor pressure over the solution would be reduced by a factor of 2.

[6] Hooker Electrochemical Company, Chem. Engr. **64**, 148 (1957).
[7] A. L. Conn and J. E. Wolf, I.E.C. **50**, Pt. 2, 1231–1234 (1958).

THE JOURNAL OF CHEMICAL PHYSICS VOLUME 33, NUMBER 3 SEPTEMBER, 1960

Separation Theorem for Degenerate Eigenvalues

D. W. DAVIES
Chemistry Department, University College of North Staffordshire, Keele, Staffordshire, England

(Received April 18, 1960)

An algebraic theorem concerning the separation of the eigenvalues of a matrix is discussed for degenerate eigenvalues in variation calculations. It is shown that the occurrence of degenerate eigenvalues in a given approximation does not prevent the application of the theorem to the determination of upper bounds for exact eigenvalues in physical problems.

THE theorem that the eigenvalues of the leading minors of a symmetric matrix separate the eigenvalues of the matrix itself has been known in algebra for many years.[1] The form that the theorem takes for degenerate eigenvalues has been discussed by Browne.[2] The importance of the theorem for variation calculations in quantum mechanics was pointed out by Hylleraas and Undheim,[3] and a more detailed discussion has been given by Macdonald.[4] A recent discussion of the whole question of finding bounds for the eigenvalues of excited states has been given by Löwdin.[5]

These discussions of variation calculations do not, however, explicitly consider degenerate eigenvalues, and the object of the present paper is to show how a theorem established by Browne[2] applies to variation calculations. The method used is similar to that given by Macdonald.[4] Let $\mathcal{H}$ be a Hermitian operator, which may be the Hamiltonian of a physical problem, and let $\mathcal{E}$ and Ψ be the corresponding sets of correct eigenvalues and eigenvectors, respectively, then

$$\mathcal{H}\Psi = \mathcal{E}\Psi. \qquad (1)$$

Let ψ^m, the mth approximation to Ψ, be expanded in terms of a set of m orthonormal basis functions ϕ_j, thus,

$$\psi^m = \sum_{j=1}^{m} c_j{}^m \phi_j. \qquad (2)$$

[1] See, for example, G. Salmon, *Modern Higher Algebra* (Hodges, Foster, and Company, Dublin, 1876), p. 44.
[2] E. T. Browne, Am. J. Math. **52**, 843 (1930).
[3] E. A. Hylleraas and B. Undheim, Z. Physik **65**, 759 (1930).
[4] J. K. L. Macdonald, Phys. Rev. **43**, 830 (1933).
[5] P.-O. Löwdin, *Advances in Chemical Physics* (Interscience Publishers, Inc., New York, 1959), Vol. 2, p. 264 *et seq.*

Let E^m be the mth approximation to $\mathcal{E}$, given by

$$E^m=\int\psi^{m*}\mathcal{H}\psi^m d\tau, \tag{3}$$

where the * indicates the complex conjugate, and $d\tau$ is a volume element in the configuration space. If the c_j^m are varied to minimize E^m subject to the condition that the ψ^m remain normalized, the standard result is obtained that

$$\sum_j(H_{ij}^m-\delta_{ij}E^m)c_j^m=0, \qquad i,j=1,2,\cdots m, \tag{4}$$

whence

$$D^m(E^m)\equiv \mathrm{Det}[H_{ij}^m-\delta_{ij}E^m]=0, \tag{5}$$

where

$$H_{ij}^m=\int\phi_i^*\mathcal{H}\phi_j d\tau. \tag{6}$$

Thus a set of $E^m=E_1^m, \leq E_2^m\cdots\leq E_m^m$ is obtained from Eq. (5), and a corresponding set of $\psi^m=\psi_1^m$, ψ_2^m, $\cdots$, ψ_m^m from Eq. (4). The ψ^m are orthogonal if none of the E^m are degenerate, and they may always be made orthogonal if there are degenerate E^m. They will be taken as orthonormal in what follows.

To obtain the $(m+1)$th approximation to Ψ, ψ^{m+1} may be written

$$\psi^{m+1}=\sum_{j=1}^m c_j^{m+1}\psi_j^m+c_{m+1}^{m+1}\phi_{m+1}, \tag{7}$$

where ϕ_{m+1} is a normalized function orthogonal to the ψ^m.

Consider the determinant $D^{m+1}(E)$ given by

$$D^{m+1}(E)\equiv \mathrm{Det}[H_{ij}^{m+1}-\delta_{ij}E], \qquad i,j=1,2,\cdots,m+1, \tag{8}$$

where

$$H_{ij}^{m+1}=\int\psi^{m*}\mathcal{H}\psi^m d\tau=\delta_{ij}E_i^m \qquad (i,j\leq m),$$

$$H_{ij}^{m+1}=\int\phi_{m+1}{}^*\mathcal{H}\psi_j{}^m d\tau=h_i^* \qquad (i=m+1),$$

$$H_{ij}^{m+1}=\int\psi_i{}^{m*}\mathcal{H}\phi_{m+1}d\tau=h_i \qquad (j=m+1),$$

$$H_{ij}^{m+1}=\int\phi_{m+1}{}^*\mathcal{H}\phi_{m+1}d\tau=h_{m+1} \qquad (i,j=m+1), \tag{9}$$

as the ψ^m have been calculated so as to make H_{ij}^m diagonal. Thus,

$$D^{m+1}(E)\equiv(h_{m+1}-E)\prod_j(E_j^m-E) -\sum_j|h_i|^2\Big[\prod_{j\neq i}(E_j^m-E)\Big] \qquad i,j=1,2,\cdots m \tag{10}$$

and

$$D^{m+1}(E_r^m)\equiv-|h_r|^2\prod_{j\neq r}^m(E_j^m-E_r^m). \tag{11}$$

In general $h_r\neq 0$, and if none of the E^m are degenerate, $D^{m+1}(E_r^m)\neq 0$, and the eigenvalues of the $(m+1)$th approximation are all different from those of the mth.

If, however, E_r^m is p-fold degenerate, having the values E_r^m, E_{r+1}^m, $\cdots E_{r+p-1}^m$, from Eq. (11) $D^{m+1}(E_r^m)$ vanishes, and the mth and $(m+1)$th approximations have the same eigenvalue E_r^m. Let E_s^{m+1} be this eigenvalue in the $(m+1)$th approximation. The degeneracy of E_s^{m+1} must now be investigated.

As $D^{m+1}(E)$ vanishes for $p\geq 2$ it must have $(p-1)$ factors (E_r^m-E) or $(E_s^{m+1}-E)$. From Eq. (10)

$$\begin{aligned}D^{m+1}(E)&=(E_s^{m+1}-E)^p(h_{m+1}-E)\prod_{j\neq r,r+1,\cdots r+p-1}(E_j^m-E)\\&\quad-(E_s^{m+1}-E)^p\sum_{i\neq r,r+1,\cdots r+p-1}|h_i|^2\Big[\prod_{j\neq i,r,r+1,\cdots r+p-1}(E_j^m-E)\Big]\\&\quad-(E_s^{m+1}-E)^{p-1}\sum_{i\neq r,r+1,\cdots r+p-1}|h_i|^2\Big[\prod_{j\neq i,r,r+1,\cdots r+p-2}(E_j^m-E)\Big]\\&\equiv[E_s^{m+1}-E]^{p-1}[(E_s^{m+1}-E)(d_1-d_2)-d_3]\\&\equiv(E_s^{m+1}-E)^{p-1}D^{m+2-p}(E).\end{aligned} \tag{12}$$

Now $d_3\neq 0$ for $E=E_s^{m+1}$, thus E_s^{m+1} is not a root of $D^{m+2-p}(E)$, but it is a $(p-1)$-fold root of $D^{m+1}(E)$. The nondegenerate roots of $D^{m+2-p}(E)$ will be separated by those of $D^m(E)$ in accordance with the theorem given at the beginning.

The case $h_r=0$ has so far been excluded. As ϕ_{m+1} is not linearly dependent on ψ^m, in general h_r will vanish only if ψ_r^m is an exact eigenvector, or if ϕ_{m+1} and ψ_r^m belong to different irreducible representations or the symmetry group of the Hamiltonian. It is clear that if h_r does vanish, the rth solution is unchanged in passing from the mth to the $(m+1)$th approximation, and E_s^{m+1} will be p-fold degenerate. Thus the following theorem is proved: a p-fold degenerate eigenvalue in

the mth approximation will remain an eigenvalue in the $(m+1)$th approximation, but, provided that the matrix components of the operator between the m basis functions used in the mth approximation and the additional function used in the $(m+1)$th approximation do not vanish, its degeneracy in the $(m+1)$th approximation will be $(p-1)$-fold.

The importance of the separation theorem for quantum mechanics lies in the fact that the set of basis functions can be made complete as $m\to\infty$, from which it follows that each approximate eigenvalue E_r^m is an upper bound to the exact value $\mathcal{E}_r$. The theorem proved above shows that this result is unaffected by the occurrence of degenerate E^m.

THE JOURNAL OF CHEMICAL PHYSICS VOLUME 33, NUMBER 3 SEPTEMBER, 1960

Activator Center in Magnesium Fluorogermanate Phosphors

G. KEMENY AND C. H. HAAKE

Research Department, Westinghouse Electric Corporation, Bloomfield, New Jersey

(Received March 14, 1960)

The Mn^{4+} center in mainly octahedral symmetry has been studied in magnesium fluorogermanate phosphors. Emission and absorption spectra and the temperature dependence of various parameters have been evaluated. Absorption takes place from the $^4A_2$ ground state into the $^4F_2$, $^4F_1$, and higher excited states whereas both emission bands, which lie in the red region of the spectrum, correspond to transitions from the split $^4F_2$ state to the ground state. Electrons in $^4F_1$ and higher quartet states decay nonradiatively into the $^4F_2$ state. The crystal field parameters Dq for the absorption and emission are 2400 and 1600 cm^{-1}, respectively. The electronic and vibrational structure, the temperature dependence and kinetics of emission can be explained by a configurational (normal) coordinate diagram. This coordinate is associated with the distortions from octahedral symmetry and is thus different from that associated with the octahedral crystal field parameter Dq.

INTRODUCTION

THE behavior of $3d^3$ ions octahedrally surrounded by oxygen or other anions has been extensively studied in the past.[1–4] However, experimental studies are usually restricted to absorption measurements. Not often are systems available in which the $3d^3$ ion also emits radiation. Such a system, however, is found in magnesium fluorogermanate, a phosphor used for color correction of high-pressure mercury-vapor lamps.[5,6] The activator is Mn in the quadrivalent state $(3d^3)$[7] and paramagnetic resonance measurements indicate a surrounding, most likely by oxygen ions, of octahedral symmetry.[8] Under such conditions crystal field theory can aid in interpreting the physical properties of the system. Knowing the splitting of the electron energies of the $3d^3$ ion in an octahedral field as a function of the crystal field parameter (Dq) from theory[2] and having measured absorption and emission spectra of magnesium fluorogermanate, one can give a general description of the activator center.

EXPERIMENTAL

The emission spectrum of magnesium fluorogermanate activated with Mn, which is independent of the wavelengths of excitation,[5] was measured at various temperatures between −185° and +150°C with a monochromator-photomultiplier system and corrected for relative number of quanta. (See Figs. 1 and 2). Two groups of emission peaks are clearly visible. Increasing temperature increases the intensity of the group around 630 mμ, but decreases that of the group around 660 mμ. The wave numbers of the individual peaks have been determined as well as possible from careful and detailed measurements (Table I). Question marks beside some of the wave numbers indicate uncertainties due to poor resolution.

The peaks *a*, *b*, *d*, *e*, *f*, and *g* are clearly resolved, at least at 78°K. Peak *h* appears only as a hump and, therefore, its exact position is uncertain. At room temperature peak *d* seems to be a superposition of two peaks as judged by its non-Gaussian appearance. Another peak *c* has, therefore, been listed whose exact position is uncertain. Since, however, at 78°K peak *d* appears purely Gaussian, its position is well known. At this temperature peak *c* is negligibly small.

There is also a faint green emission with a broad peak at about 550 mμ, which, however, does not arise from the Mn^{4+} center. As a matter of fact, at least at room temperature, the intensity of the green emission decreases with increasing Mn concentration.

[1] R. Finkelstein and J. H. van Vleck, J. Chem. Phys. **8**, 790 (1940).
[2] Y. Tanabe and S. Sugano, J. Phys. Soc. Japan **9**, 766 (1954).
[3] L. E. Orgel, J. Chem. Phys. **23**, 1004 (1955).
[4] D. S. McClure, J. Phys. Chem. Solids **3**, 311 (1957).
[5] L. Thorington, J. Opt. Soc. Am. **40**, 579 (1950).
[6] C. H. Haake, J. Electrochem. Soc. **106**, 866 (1959).
[7] F. A. Kröger and J. van den Boomgaard, J. Electrochem. Soc. **97**, 377 (1950).
[8] J. G. Castle, Jr. (private communication).

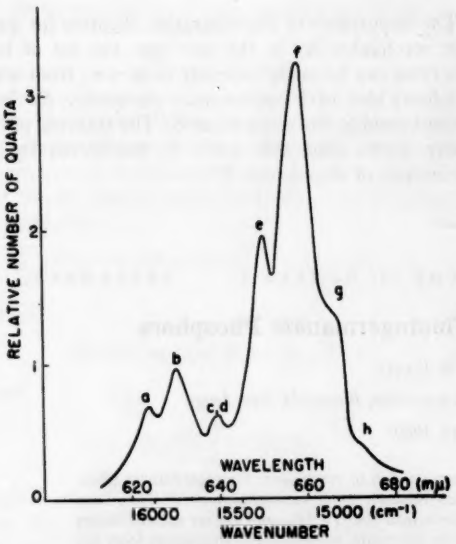

FIG. 1. Emission spectrum of magnesium fluorogermanate (Mn) measured at room temperature.

The absorptance spectrum $A(\lambda)$ was obtained from the reflectance $R(\lambda)$ of quasi-infinitely thick phosphor plaques as $1-R(\lambda)$ (Fig. 3). Three absorptance peaks appear at about 24 000 cm^{-1} (418 mμ), 35 000 cm^{-1} (285 mμ), and 42 500 cm^{-1} (235 mμ). In Fig. 4 are shown in relative values the total number of quanta emitted from a magnesium fluorogermanate phosphor screen (density: 2 mg/cm^2) as a function of temperature with the exciting wavelengths 313, 365, and 405 mμ as parameters. Although the plots for 313 and 405 mμ look very similar, there is a strong increase of emission with increasing temperature for 365 mμ excitation leading to a pronounced peak.

The temperature dependence of the transmittance for the exciting radiation of the same wavelengths and through the same phosphor screen is shown in Fig. 5. Again, the 365-mμ radiation exhibits a transmittance differing considerably from those of the other two wavelengths shown (313 and 405 mμ).

The phosphorescence decay is purely exponential. Measurements of decay times at various temperatures resulted in the following values:

3.48 msec at −125°C,

3.40 msec at −60°C,

3.31 msec at +28°C,

2.48 msec at +165°C.

THEORY

Ions incorporated in a crystal lattice are subjected to internal electric fields (crystal fields) which cause splitting and mixing of the electron energy levels of the isolated ions.[9] The extent to which this occurs depends on the strength of the crystal field and the geometrical arrangement of the neighboring ions. Tanabe and Sugano[2] have calculated the splitting of energy levels of ions in the $3d^3$ configuration subjected to an octahedral crystal field. Since in the present system the activator is Mn^{4+} ($3d^3$ configuration)[7] and paramagnetic resonance measurements indicate octahedral symmetry around the Mn ion,[8] Tanabe and Sugano's calculations apply here. In Fig. 6 part of the energy diagram for the Mn^{4+} ion has been extracted from Tanabe and Sugano's paper. The diagram shows the electronic energy difference ΔE relative to the $^4A_2$ ground state as a function of the parameter Dq of the crystal field strength.

In principle optical absorption in the center can occur from the $^4A_2$ ground state into doublet or quartet states. However, the energies observed at the absorptance maxima (Fig. 3) can only be fitted into the Dq diagram if transitions into doublet states are excluded. Moreover, transitions into doublets are far less probable because of the necessary spin flip. Thus, the center absorbs at $Dq \approx 2400$ cm^{-1} into the states $^4F_2$ (24 000 cm^{-1}) and $^4F_1$ (35 000 cm^{-1}). In Fig. 6 the energy difference between $^4A_2$ and $^4F_1$ actually appears to be about 33 600 cm^{-1}. This value follows when both absorption energies are correlated to the same value of Dq. The discrepancy of 4% is, however, not serious, since the theory which leads to the Dq diagram is only approximate. The assignment of the third peak is uncertain. It might be mentioned here that Tanabe and Sugano[2] have reported a similar third peak. They, too, were unable to specify exactly the corresponding excited state, although they assumed it to be a quartet.

Return to the ground state $^4A_2$ follows a strong lattice relaxation, i.e., a lowering of Dq. This strong relaxation would be incompatible with transitions into the doublet states. Regardless of whether absorp-

TABLE I. Peak positions of emission spectrum of magnesium fluorogermanate.

Peak	λ(mμ)	$10^{-4}\,\bar{\nu}(cm^{-1})$
a	624	1.60_3
b	631	1.58_6
c	638 ?	1.56_7 ?
d	640	1.56_3
e	651	1.53_8
f	659	1.51_8
g	667	1.49_9
h	672 ?	1.48_8 ?

[9] H. A. Bethe, Ann. Physik 3, 133 (1929).

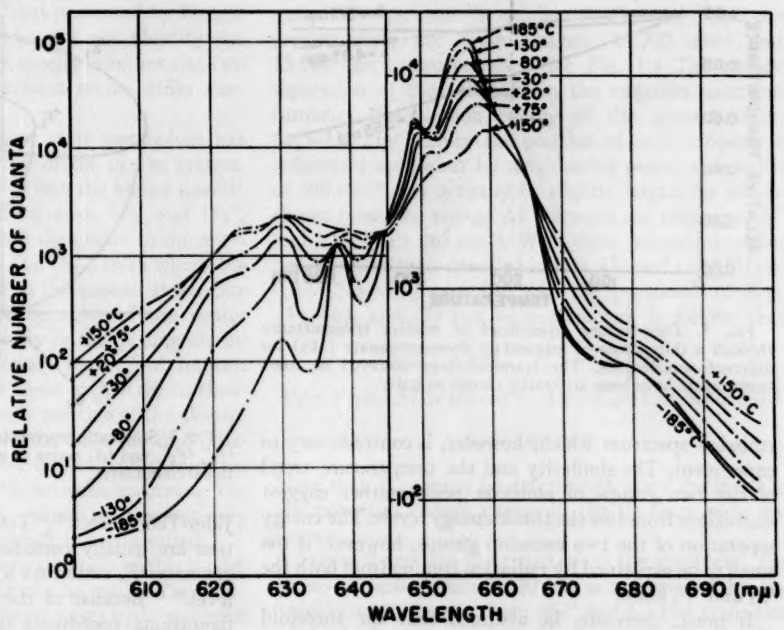

FIG. 2. Temperature dependence of emission spectrum of magnesium fluorogermanate (Mn). (Monochromator resolution is lower than that chosen for the spectrum in Fig. 1.)

tion takes place into the lower or the higher quartet states, the emission spectrum always exhibits the same shape with an energy centering around 15 500 cm^{-1}. Thus only one excited state is involved in the emission. This most likely is the $^4F_2$ state. Electrons in the higher quartet states lose energy in a radiationless manner until they reach the $^4F_2$ state. The mechanism of this transition cannot be represented in this Dq diagram, since at no value of Dq (except at $Dq=0$) are the energies of the two excited states equal. Energy crossover, therefore, must involve another degree of freedom not shown in the diagram of Fig. 6. Even when absorption occurs into the $^4F_2$ state the Dq diagram cannot distinguish between the lattice relaxation in the excited state and that in the ground state. This feature as well as the structure of the emission spectrum evolves from consideration of the total energy of the center.

The total energy scheme actually has as many configurational dimensions as there are nonequivalent normal coordinates excepting those of rigid motion of the center. As long as the motion of the ions preserve the octahedral symmetry of the center, a single normal coordinate (Q_1) suffices in the scheme. It is this coordinate Q_1 which is associated with the Dq in Fig. 6. Different values of Q_1 correspond to different distances between the surrounding ions and the Mn ion and thus induce different crystal field intensities characterized by the parameter Dq.

Thus if the center were in perfect octahedral symmetry, only one group of peaks would appear in the

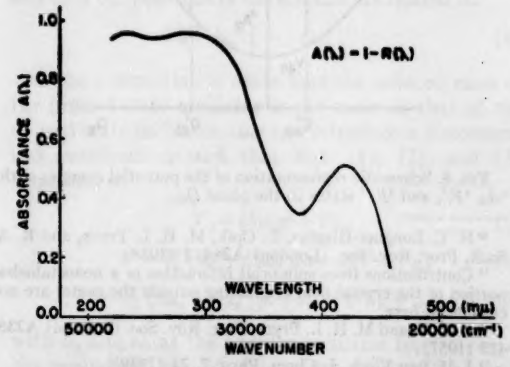

FIG. 3. Absorptance spectrum of magnesium fluorogermanate (Mn) at room temperature.

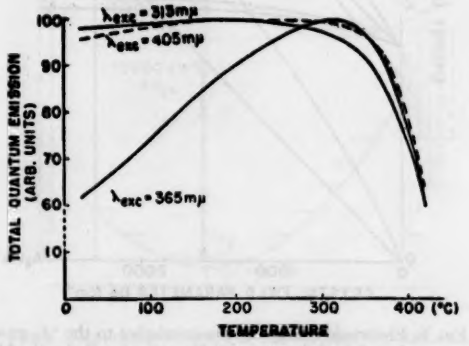

FIG. 4. Total quantum emission of a screen of magnesium fluorogermanate (Mn) as a function of temperature for different wavelengths of excitation. (Normalized to maximum.)

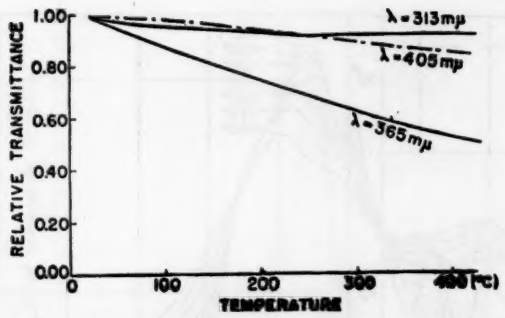

FIG. 5. Temperature dependence of relative transmittance through a thin screen of magnesium fluorogermanate (Mn) for different wavelengths. The transmittances observed at room temperature have been arbitrarily chosen as unity.

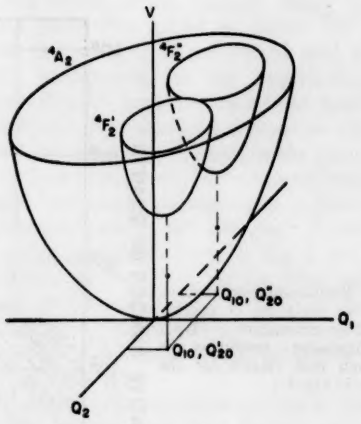

FIG. 7. Schematic representation of the potential energies of the $^4F_2'$, $^4F_2''$, and $^4A_2$ states as a function of two normal configurational coordinates.

emission spectrum which, however, is contradictory to experiment. The similarity and the temperature trend of the two groups of emission peaks rather suggest transitions from two electronic energy levels. The energy separation of the two emission groups, however, is too small to be explained by radiation coming from both the $^4F_2$ and $^4F_1$ state.

It must, therefore, be assumed that the threefold degenerate $^4F_2$ state is split, since the $^4A_2$ ground state is not degenerate. Such a splitting can be caused by the Jahn-Teller effect.[10,11] Tetragonal and/or trigonal distortion are usually considered to split the threefold degenerate $^4F_2$ state into a twofold and a nondegenerate level.[12,13] Because of the distortion an additional configurational coordinate (Q_2) must be introduced. Thus the potential energies now appear as paraboloids rather than parabolas (see Fig. 7). This model of the Mn

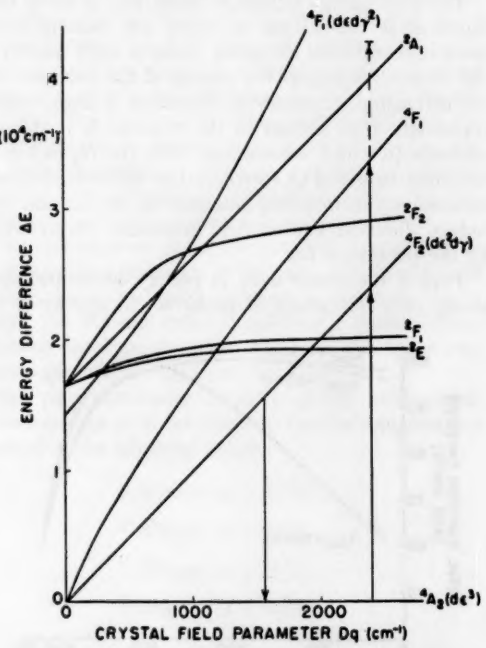

FIG. 6. Electronic energy difference relative to the $^4A_2$ ground state as a function of the crystal field parameter Dq for the Mn^{4+} ion in octahedral symmetry. (Only eight states are shown.)

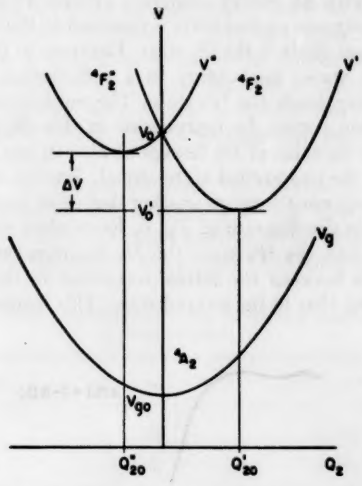

FIG. 8. Schematic representation of the potential energies of the $^4A_2$, $^4F_2'$, and $^4F_2''$ states in the plane Q_{10}.

[10] H. C. Longuet-Higgins, U. Opik, M. H. L. Pryce, and R. A. Sack, Proc. Roy. Soc. (London) **A244**, 1 (1958).

[11] Contributions from spin-orbit interaction or a nonoctahedral portion of the crystal field originating outside the center are not considered here.

[12] U. Opik and M. H. L. Pryce, Proc. Roy. Soc. (London) **A238**, 425 (1957).

[13] J. H. van Vleck, J. Chem. Phys. **7**, 72 (1939).

center is more elaborate than that presented by Kröger and van den Boomgaard,[7] who did not identify the electronic states nor did they specify whether the two excited states from which emission occurs differ electronically or vibrationally.

The minimum of the ground state paraboloid has been arbitrarily placed at the origin of the system. Absorption occurs at $Q_1=Q_2=0$ into the higher quartet states of which only the lowest ones, $^4F_2'$ and $^4F_2''$, are shown here. The system will then relax to the minimum either at Q_{10}, Q_{20}' or at Q_{10}, Q_{20}'', from where the electrons return radiatively into the ground state. One can attempt to describe the behavior of the center either "solely" in the Q_1 or solely in the Q_2 diagram by projecting the paraboloids onto "planes" of interest through certain values of $Q_2=$ const or $Q_1=$ const. However, although at least the crude position of the absorption and emission energies can be depected in Q_1 diagrams, in the present case they do not lend themselves to explaining the features of the emission spectrum. The Q_2 diagram through the Q_{10} plane as schematically shown in Fig. 8, on the other hand, is better suited.

Before going into the numerical details of this model, certain theoretical statements can be made. The Jahn-Teller effect introduces only linear terms in the potential energy. Therefore, the force constants, K_e, which were equal before the splitting, remain equal. Thus the parabolas of the $^4F_2$ state exhibit the same curvature. In the Q_2 diagram shown in Fig. 8 these and the ground-state parabolas represent the potential energies

$$V_g=\tfrac{1}{2}K_0Q_2^2+V_{g0}, \tag{1}$$

$$V'=\tfrac{1}{2}K_eQ_2^2-aQ_2+V_0, \tag{2}$$

$$V''=\tfrac{1}{2}K_eQ_2^2+(\tfrac{1}{2}a)Q_2+V_0. \tag{3}$$

Since the average energy of the three $^4F_2$ levels remains unchanged by the Jahn-Teller effect, the linear term of the doubly degenerate state is half that of the non-degenerate one. It follows from Eq. (2) and (3) that

$$2(dV''/dQ_2)_{(Q_2=0)}=-(dV'/dQ_2)_{(Q_2=0)}$$

and thus the positions of the minima are related by

$$2\,|\,Q_{20}''\,|=|\,Q_{20}'\,|. \tag{4}$$

If the assumption is made that the reduced mass of the ground-state oscillator is the same as that of the excited state oscillator, one can introduce a dimensionless coordinate x such that Eqs. (1), (2), and (3) transform to

$$V_g=\tfrac{1}{2}\hbar\omega_g x^2+V_{g0}, \tag{5}$$

$$V'=\tfrac{1}{2}[(\hbar\omega_e)^2/\hbar\omega_g](x-x_0')^2+V_0', \tag{6}$$

$$V''=\tfrac{1}{2}[(\hbar\omega_e)^2/\hbar\omega_g](x+x_0'')^2+V_0'+\Delta V, \tag{7}$$

with ω_g and ω_e as the angular oscillator frequencies of the ground and excited states, respectively. The energy separations between the minima of V' and V'' and the ground state are approximately 15 200 cm^{-1} and 15 900 cm^{-1}, respectively. (See Fig. 1.) The energy separation of the subpeaks in the emission spectrum furnishes the phonon energy of the ground state: $\hbar\omega_g\approx 180$ cm^{-1}. Since the position of each subpeak is influenced somewhat by neighboring peaks, this value of 180 cm^{-1} may actually be slightly larger. As will be shown later, the energy ΔV between the minima of V' and V'' equals 265 cm^{-1}. With these numerical values and the conditions specified in Eqs. (2) and (3) $[V'(x=0)=V''(x=0)]$ and Eq. (4) the parabolas of Eqs. (5), (6), and (7) can be constructed. It follows that

$$|\,x_0'\,|=2.54 \qquad |\,x_0''\,|=1.27$$

$$V_0'-V_{g0}=1.57_8\times10^4\ cm^{-1} \qquad V_0-V_{g0}=1.61_3\times10^4\ cm^{-1}$$

$$\hbar\omega_e=140\ cm^{-1}.$$

Note that V_{g0} cannot be determined, since the shape of the potential energy curves in the Q_1 diagram is unknown.

Figure 9 explains the structure of the spectrum. The group of peaks around 630 mμ is represented by the transitions a, b and c from $^4F_2''$ to $^4A_2$. The transition of the highest energy from the lowest phonon level of $4F_2''$ occurs into the lowest phonon level of $^4A_2$, thus limiting the number of discernible transitions toward shorter wavelengths. More transitions are possible (and observed) from $^4F_2'$ to $^4A_2$. Transitions from the second phonon level of $^4F_2'$ do not introduce new peaks but broaden the existing ones. They are, therefore, not shown in Fig. 9. The occupancy of both excited states $^4F_2'$ and $^4F_2''$ is in thermal equilibrium. Thus it is clear

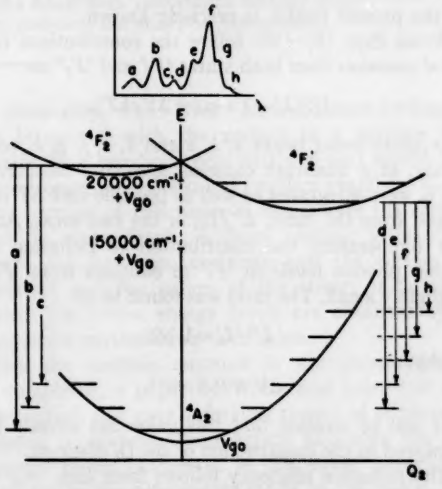

FIG. 9. Total energy diagram of $^4A_2$, $^4F_2'$, and $^4F_2''$ as a function of Q_2 (corresponding to x). Individual emission peaks are correlated to specific transitions.

that increasing temperature causes the intensity of the emission in the group around 630 mμ to increase at the expense of the emission intensity of the group around 660 mμ (Fig. 2).

The kinetics of luminescence is of the first order. The differential equation is simply

$$dn/dt=\alpha I-n'\gamma-n''\gamma-n'\gamma_q\exp(-V_q/kT), \quad (8)$$

where n' and n'' are the number of the excited ions in $^4F_2'$ and $^4F_2''$, respectively, their sum being n; α is the absorption coefficient for the exciting radiation of the intensity I; γ is the probability of radiative transitions $^4F_2'$, $^4F_2''\rightarrow{}^4A_2$; γ_q is the probability of nonradiative transitions $^4F_2'\rightarrow{}^4A_2$ via the cross-over of the respective parabolas; and V_q is the quenching energy between the minimum of V' and the cross-over of V' and V_g. With thermal equilibrium between the excited states and also equal phonon energies and with $^4F_2''$ being doubly degenerate one finds

$$n''/n'=2\exp(-\Delta V/kT) \quad (9)$$

and hence

$$n=n'+n''=n'[1+2\exp(-\Delta V/kT)]. \quad (10)$$

The radiative transitions are of the dipole type.[2] These transitions are possible because of the breakdown of the parity selection rule induced by the hemihedral part of the crystal field.[2] Since the transition matrix elements between the $^4F_2$ states and the ground state are almost identical, the transition probabilities γ for the present purposes, can be considered equal. In this respect the present kinetics equations differ from those given by Kröger and van den Boomgaard.[7] These authors also left undecided the question of the weight of occupancy in the excited states $^4F_2'$ and $^4F_2''$ which, in the present model, is precisely known.

From Eqs. (8)–(10) follow the contributions to the total emission from both states $^4F_2'$ and $^4F_2''$ as

$$L''/L'=2\exp(-\Delta V/kT).$$

The areas under peaks *a*, *b*, *c* and *d*, *e*, *f*, *g*, *h*, respectively, of a quantum emission spectrum measured at 78°K were integrated as well as possible and ΔV determined from the ratio, L''/L', of the two areas. At this low temperature the contribution of radiation from higher phonon levels in $^4F_2'$ to emission from $^4F_2''$ is negligibly small. The ratio was found to be

$$L''/L'\approx 1/69$$

so that

$$\Delta V\approx 265\ \text{cm}^{-1}.$$

It will be recalled that this value has already been employed in the construction of the Q_2 diagram.

The radiation efficiency follows from Eqs. (8)–(10) as

$$\eta=\left\{1+\frac{\gamma_q\exp(-V_q/kT)}{\gamma[1+2\exp(-\Delta V/kT)]}\right\}^{-1}. \quad (11)$$

With this equation the temperature dependence of total emission (Fig. 4) can be evaluated for temperatures above that of maximum luminescence. Averaging over the values of γ_q and V_q as obtained from evaluating each plot separately one finds

$$\gamma_q\approx 10^{12}\ \text{sec}^{-1}$$

and

$$V_q\approx 1.1\times 10^4\ \text{cm}^{-1}.$$

Here γ^{-1} was taken as the decay time of phosphorescence at low temperature. ($\gamma=1/\tau=287\ \text{sec}^{-1}$). The observable decay time τ is actually a function of temperature as follows with Eqs. (8)–(10) from

$$\tau^{-1}=-d\ln(n')/dt=\gamma+\frac{\gamma_q\exp(-V_q/kT)}{1+2\exp(-\Delta V/kT)} \quad (12)$$

but at low temperature τ is constant. That this is very nearly so has already been shown by Kröger and van den Boomgaard[7] and is confirmed by the present measurements. The slight decrease of τ with increasing temperature in a region where the second term of Eq. (12) is still ineffective is probably due to an increasing asymmetry of the instantaneous positions of the Mn-ion with respect to the surrounding oxygen ions.[2]

The wavelength effect on the temperature dependence of total emission (Fig. 4) below the temperature range where quenching sets in, can be easily understood. The atomic absorption coefficient α is proportional to the probability of transitions from the ground to the excited states and to the probability of having the level in which absorption takes place occupied. The action of α is reflected in the total emission in the temperature range where quenching can not yet interfere. If the wavelength of absorption lies in or near a peak of the absorption spectrum, the transition takes place mostly from the lowest level of the ground state and α should not or only slightly depend on temperature. This is observed in Fig. 4 for $\lambda=313$ and 405 mμ. These wavelengths are near absorption peaks, as can be seen in Fig. 3. On the other hand excitation by 365 mμ most likely occurs from higher phonon levels of the ground state as indicated by the remoteness of 365 mμ from the wavelengths of peak absorption. Thus the occupancy probability in α and hence the emission intensity rises strongly with increasing temperature. Actually this temperature dependence of α continues irrespective of the quenching action. This follows from the temperature dependence of the transmittance through a thin magnesium fluorogermanate (Mn) screen (Fig. 5). The transmittance is almost constant for 313 and 405 mμ ($\alpha\approx$ const), but drops sharply with increasing temperature for 365 mμ, i.e., with increasing α.

SUMMARY

The energies observed at the absorption maxima of the manganese-activated magnesium fluorogermanate phosphor can be well fitted into the Dq diagram derived

by Tanabe and Sugano for $3d^3$ ions in octahedral crystal field symmetry. Whereas the absorption involves three excited states, emission occurs only from one state ($^4F_2 \rightarrow {}^4A_2$), the transition from the higher quartet states to $^4F_2$ being radiationless.

The crystal field symmetry, however, is not perfectly octahedral. The detailed structure of the emission spectrum can be explained in a potential energy scheme only after the introduction of a second normal coordinate associated with a lowered symmetry. This lowered symmetry induces a splitting of the $^4F_2$ state into two levels. The degeneracy of $^4F_2$, however, is threefold so that one of the split levels is still doubly degenerate. This knowledge facilitates the evaluation of the kinetics of luminescence. The final equations together with experimental data give information about the energy separation of the two levels of the $^4F_2$ state, the probability of nonradiative transitions from $^4F_2'$ to $^4A_2$, and the quenching energy.

The atomic absorption in the center is proportional to the transition probability and the occupancy probability of the ground-state level. Whereas the former is nearly constant, the latter can be strongly temperature sensitive. If higher phonon states are involved, as for instance with 365 mμ excitation, the absorption and thus also the emission rise steeply with increasing temperature. This may well be the reason for similar phenomena observed with other phosphor systems, e.g., Zn_2SiO_4:Mn[14] or ZnS[Zn].[15]

[14] C. H. Haake, unpublished measurements.
[15] G. F. J. Garlick, *Luminescent Materials* (Oxford University Press, New York, 1949), p. 105.

THE JOURNAL OF CHEMICAL PHYSICS VOLUME 33, NUMBER 3 SEPTEMBER, 1960

Second-Order Perturbation Calculation of the Hindered Rotator Model for Adsorbed Hydrogen

ARTHUR A. EVETT

Department of Physics, University of Arizona, Tucson, Arizona

(Received March 4, 1960)

A refinement of the previously reported models for adsorbed hydrogen is presented, based on the assumption that each hydrogen atom interacts with the adsorbent by a van der Waals force of the Lennard-Jones type. The calculation is accomplished by using the previous model based on a parabolic potential well interaction, for which exact wave functions are obtained, as the zeroth-order approximation and then carrying out a second-order perturbation calculation to obtain accurate results for the Lennard-Jones type interaction. The results lead to the conclusion that agreement with data on ortho-para hydrogen separation coefficients can be obtained only by assuming a magnitude for the rotational barrier which is inconsistent with data on adsorption energies. To eliminate this discrepancy a perturbing term involving a hindrance to rotation in the plane parallel to the surface is introduced and a second-order perturbation analysis shows that such a term can lead to agreement with both separation coefficient and adsorption energy data.

EXPERIMENTAL measurements on adsorbed hydrogen at low temperatures have shown that a considerable enrichment of orthohydrogen relative to parahydrogen occurs in the adsorbed phase compared to the gas phase at the same temperature.[1,2] Determinations of the separation coefficient s, defined by $s=([p]/[o])_{gas}/([p]/[o])_{adsorbed}$ where $[p]$ and $[o]$ designate the concentrations of para and ortho, range from 1.67 to TiO_2 at 90°K to about 16 on Al_2O_3 at 20°K.

Explanations of this phenomenon have been based on considering the hydrogen molecule as a rigid rotator which is hindered by the force field of the adsorbent surface. Sandler[1] treated the limiting case of the hydrogen being hindered completely so as to rotate in a plane only, while Evett[3] assumed each hydrogen atom interacted with the surface in a manner describable by a parabolic potential well and solved the resulting quantum-mechanical problem exactly.

The purpose of this paper is to consider the earlier model[3] in more detail. A more realistic interaction between the hydrogen molecule and the surface is introduced and the values of the energy differences between the lowest energy levels are obtained by a second-order perturbation calculation.

After the analysis reported in the present paper was completed, a paper by White and Lassettre[4] appeared which also gave a detailed theory of ortho-para hydrogen separation. Their article also uses the unperturbed model considered in the earlier paper[3] but the nature of the refinements made on the model and

[1] Y. L. Sandler, J. Phys. Chem. **58**, 58 (1954); J. Chem. Phys. **29**, 97 (1958).
[2] C. M. Cunningham and H. L. Johnston, J. Am. Chem. Soc. **80**, 2377 (1958).
[3] A. A. Evett, J. Chem. Phys. **31**, 565 (1959).
[4] D. White and E. N. Lassettre, J. Chem. Phys. **32**, 72 (1960).

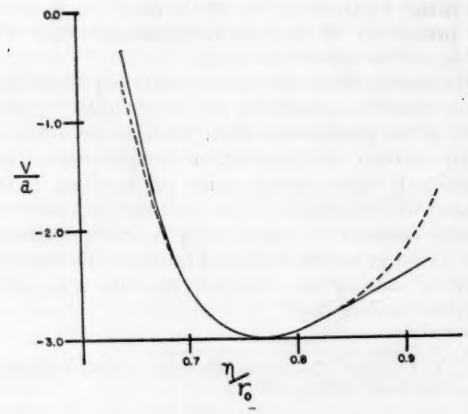

FIG. 1. Comparison of the Hill-type interaction as expressed in Eq. (2) with its fourth power Taylor series expansion as expressed in Eq. (3). The solid curve is the Hill interaction and the dashed curve is its Taylor series expansion. Both curves are for $\cos\theta=0$.

the techniques for handling the refinements are different from those reported in the present paper. White and Lassettre employ a variational procedure and use a Morse-type interaction potential. In the present paper the more accurate Lennard-Jones type interaction is considered, as was proposed by Hill,[5] and a second-order perturbation analysis is employed rather than a variational procedure. The results based on the Lennard-Jones interaction lead to the conclusion that agreement with experimental data can be obtained only by assuming a particular type of hindrance to rotation in a plane parallel to the surface, and the effect of this type of hindrance on the separation coefficient is computed. It is shown that this over-all model, with reasonable parameters, gives excellent agreement with experiment.

THE MODEL

Let z be the perpendicular distance of the center of the molecule from the adsorbent surface. The molecule is assumed to be free to move in a plane parallel to the surface.[6] Let θ be the angle between the z axis and the axis of the homonuclear diatomic molecule, and let ϕ be the angle between some reference plane containing the z axis and a plane containing both the z axis and the molecular axis. The molecule-adsorbent interaction potential is assumed to be given by

$$V=-V_0+\tfrac{1}{2}K\eta^2+\lambda^2\Lambda\xi^2+c_1\eta^3+c_2\eta^4+c_3\eta\xi^2 +c_4\eta^2\xi^2+c_5\xi^4. \quad (1)$$

In Eq. (1), V_0, K, λ^2, c_1, c_2, c_3, c_4, and c_5 are constants, $\Lambda=h^2/8\pi^2I$ with I denoting the moment of inertia of the molecule, $\xi=\cos\theta$, and $\eta=z-z_0$ with z_0 some constant. An interaction potential of this type would arise if *each atom* in the molecule contributed an interaction potential of the form of

$$-V_0/2+\tfrac{1}{4}K(z_a-z_0)^2+\gamma(z_a-z_0)^3+\beta(z_a-z_0)^4,$$

where z_a is the distance of the atom from the surface. Alternately, Eq. (1) can be looked upon as the first few terms in a power series expansion of a more accurate interaction potential. For example, Hill[6] showed that, if one assumes each atom in the molecule interacts with each atom in the adsorbent by means of the Lennard-Jones 6–12 exponent van der Waals interaction, then the molecule-surface potential is closely represented by

$$V=a\left\{\frac{-r_0^3}{(z+\xi d/2)^3}+\frac{-r_0^3}{(z-\xi d/2)^3} +\tfrac{1}{15}\left[\frac{r_0^9}{(z+\xi d/2)^9}+\frac{r_0^9}{(z-\xi d/2)^9}\right]\right\}. \quad (2)$$

Here r_0 is the separation at the minimum of the interaction potential between one atom of the molecule and one atom of the adsorbent, and d is the interatomic separation in the molecule. Expansion of Eq. (2) in a Taylor series about the minimum of V at $z=z_0$, $\xi d/2=0$

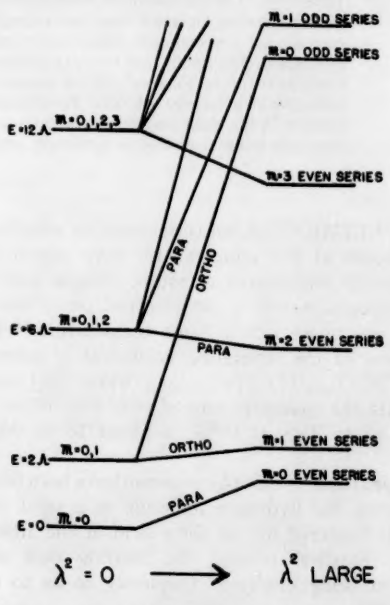

FIG. 2. Correlation of the rotational energy levels of the free rigid rotator ($\lambda^2=0$) with the energy levels of the plane oscillator limit for large λ^2. The quantity λ^2 is proportional to the amplitude of the hindrance to rotation. The diagram is highly schematic.

[5] A discussion of the necessity of relaxing this restriction, along with the consequences, is discussed later in the paper.

[6] T. L. Hill, J. Chem. Phys. **16**, 181 (1948).

gives

$$V=-2.982a+68.82a\eta^2/r_0^2+17.205ad^2\xi^2/r_0^2-450a\eta^3/r_0^3$$
$$+1961.5a\eta^4/r_0^4-337.5ad^2\eta\xi^2/r_0^3+2942.2ad^2\eta^2\xi^2/r_0^4$$
$$+122.6ad^4\xi^4/r_0^4. \quad (3)$$

Note that Eq. (3) is a special case of Eq. (1).

Figure 1 compares the Hill-type interaction curve as given by Eq. (2) with its fourth power Taylor series expansion as given by Eq. (3). Both curves are for $\xi=0$.

SOLUTION OF THE UNPERTURBED PROBLEM

The earlier paper[7] obtained the three lowest energy levels for a rigid rotator in a potential well given by the first three terms in Eq. (1). The last five terms in Eq. (1) will be treated as perturbations of the original potential, and their effect on the energy levels will be determined by a second-order perturbation calculation. Actually, the η^3 and η^4 terms affect all rotational levels the same, and since only energy differences between the lowest levels are of significance for the present problem, the contributions of these terms can be neglected. Consequently the only effective perturbing terms are the last three in Eq. (1). As shown in the earlier paper[8] the unperturbed problem is separable and the wave functions can be expressed in the form $H(\eta)\Phi^m(\phi)R(\xi)$, where the $H(\eta)$ are the normalized solutions (Hermite polynomials) to the linear harmonic oscillator, $\Phi^m(\phi)=C\exp(\pm im\phi)$ where $m=0, 1, 2, \cdots$, and $R(\xi)=(1-\xi^2)^{m/2}F(\xi)$. It is assumed that H, Φ, and R are individually normalized over the range of their arguments.

For each choice of m there exists a sequence of functions $F(\xi)$ which is even in the argument ξ [this sequence is denoted by $F(k, m; e)$] and a sequence of functions $F(\xi)$ which is odd in the argument ξ [this sequence is denoted by $F(k, m; o)$]. Thus, the $m=0, 1, 2, \cdots$ corresponds to the quantum number in $\Phi^m(\phi)$, the e or o signifies whether the even or odd sequence is involved, and k denotes which particular function in the sequence is being considered. The range of values for k is $k=1, 2, 3, \cdots$.

As λ^2 approaches infinity, the rotational motion of the unperturbed problem becomes similar to a type of plane oscillator and the allowed rotational energy levels satisfy the formula:[8] $E_{rot}=[(n+\frac{1}{2})2\lambda+m^2]\Lambda$, where $n=0, 1, 2, \cdots$. If $\lambda^2=0$, the rotational problem reduces to that of a free rigid rotator. In Fig. 2 the correlation between the free rotator energy levels with the rotational energy levels at large values of λ^2 is represented schematically.

For moderate values of λ^2, the lowest energy levels are those arising from the even F for $m=0$ and $m=1$. For adsorption phenomena at low temperatures (less than 100°K) only these lowest levels enter in significantly, but higher levels are needed to complete the perturbation calculation. The higher levels would also be of interest for other applications or for adsorption phenomena at higher temperatures. A tabulation of $\mu=$(unperturbed rotational energy)$/\Lambda$ for various values of λ^2 for several states is given in Table I. The notation for the μ symbols is completely analogous to that explained for the F symbols. These values were obtained by using an IBM–650 computer to find the roots of the continued fractions which give the solutions to this problem.[8,9]

TABLE I. Rotational energies for lowest levels as a function of the hindrance to rotation. $\mu=$(rotational energy)$8\pi^2I/h^2$.

λ^2	$\mu(1,0;e)$	$\mu(2,0;e)$	$\mu(3,0;e)$	$\mu(1,1;e)$	$\mu(2,1;e)$
0	0.00000	6.00000	20.0000	2.00000	12.0000
2	0.61131	7.08426	21.0201	2.38266	12.9379
4	1.12773	8.22571	22.0548	2.73411	13.8815
6	1.57116	9.40196	23.1046	3.05900	14.8264
8	1.95921	10.59477	24.1699	3.36118	15.7690
10	2.30504	11.79039	25.2513	3.64390	16.7063
12	2.61819	12.97873	26.3494	3.90979	17.6359
14	2.90552	14.15246	27.4645	4.16108	18.5561
16	3.17207	15.30630	28.5969	4.39959	19.4653
18	3.42153	16.43651	29.7463	4.62685	20.3624
20	3.65670	17.54051	30.9126	4.84414	21.2466
22	3.87974	18.61667	32.0951	5.05254	22.1174
24	4.09233	19.66409	33.2928	5.25296	22.9744

λ^2	$\mu(1,2;e)$	$\mu(1,3;e)$	$\mu(1,0;o)$	$\mu(1,1;o)$
0	6.00000	12.0000	2.00000	6.00000
2	6.27822	12.2183	3.17213	6.84172
4	6.54250	12.4293	4.28713	7.65315
6	6.79425	12.6334	5.34390	8.43527
8	7.03474	12.8312	6.34274	9.18921
10	7.26504	13.0231	7.28525	9.91621
12	7.48612	13.2095	8.17419	10.61756
14	7.69882	13.3098	9.01309	11.29461
16	7.90386	13.5673	9.80594	11.94872
18	8.10191	13.7393	10.55691	12.58121
20	8.29353	13.9071	11.27006	13.19339
22	8.47923	14.0709	11.94920	13.78649
24	8.65947	14.2311	12.59784	14.36170

[7] See reference in footnote 3. The quantity K used in Eq. (1) in the present article is twice the quantity denoted by the symbol K in the earlier paper.

[8] T. L. Hill, J. Chem. Phys. **16**, 181 (1948), Appendix I; A. A. Evett, J. Chem. Phys. **31**, 1419 (1959).

[9] Energy levels can also be determined from tables given in Stratton, Morse, Chu, Chittle, and Corbato, *Spheroidal Wave Functions* (The Technology Press of Massachusetts Institute of Technology and John Wiley & Sons, Inc., New York, 1956).

TABLE II. Coefficients of the power series expansion for F.

$$F(k, m) = \sum_{\delta=0}^{\infty} a(k, m)_{2\delta}\xi^{2\delta}.$$

			$\lambda^2=6$		
δ	$a(1,0)_{2\delta}$	$a(2,0)_{2\delta}$	$a(3,0)_{2\delta}$	$a(1,1)_{2\delta}$	$a(2,1)_{2\delta}$
0	0.88555	0.6893	0.7646	0.95365	0.7737
1	−0.69567	−3.2406	−8.8323	−0.50497	−4.9618
2	0.18602	1.2634	12.9716	0.10059	1.5555
3	−0.02486	−0.2018	−3.1088	−0.01066	−0.2056
4	0.00198	0.0179	0.3408	0.00071	0.0155
5	−0.00011	−0.0010	−0.0221	−0.00004	−0.0008
6		0.0000	0.0010		

			$\lambda^2=12$		
δ	$a(1,0)_{2\delta}$	$a(2,0)_{2\delta}$	$a(3,0)_{2\delta}$	$a(1,1)_{2\delta}$	$a(2,1)_{2\delta}$
0	0.98376	0.6493	0.7341	1.01689	0.7560
1	−1.28784	−4.2138	−9.6716	−0.97103	−5.9104
2	0.62083	3.0999	17.1350	0.36225	3.5319
3	−0.15543	−0.9600	−7.4952	−0.07338	−0.9086
4	0.02373	0.1668	1.5771	0.00937	0.1344
5	−0.00243	−0.0186	−0.1994	−0.00082	−0.0131
6	0.00018	0.0015	0.0170	0.00005	0.0009
7	−0.00001	−0.0001	−0.0010		

			$\lambda^2=18$		
δ	$a(1,0)_{2\delta}$	$a(2,0)_{2\delta}$	$a(3,0)_{2\delta}$	$a(1,1)_{2\delta}$	$a(2,1)_{2\delta}$
0	1.04559	0.6505		1.06476	0.7518
1	−1.78876	−5.3460		−1.39849	−6.9025
2	1.18403	5.6252		0.73787	5.9378
3	−0.41895	−2.5394		−0.21502	−2.2340
4	0.09197	0.6489		0.03992	0.4869
5	−0.01371	−0.1073		−0.00513	−0.0700
6	0.00147	0.0124		0.00049	0.0072
7	−0.00013	−0.0011		−0.00003	−0.0005
8	0.00001	0.0001			

The functions $F(\xi)$ can be obtained in the form of a power series:

$$F(k, m; e) = \sum_{\delta=0}^{\infty} a(k, m; e)_{2\delta}\xi^{2\delta}.$$

A recursion relation[10] serves to determine the coefficients $a(k, m; e)_{2\delta}$:

$$a(k, m; e)_{2\delta+2} = \{a(k, m; e)_{2\delta}[(2\delta+m+1)(2\delta+m) - \mu(k, m; e)] + a(k, m; e)\lambda^2\}/(2\delta+2)(2\delta+1).$$

In Table II is included a listing of the coefficients $a_{2\delta}$ for some of the states. For the rest of the paper, only even states will be considered, so the e or o will be omitted.

SOLUTION OF THE PERTURBED PROBLEM

With the foregoing data one can calculate the matrix elements required to determine the energies of the perturbed problem, using standard second-order perturbation theory. Table III displays the pertinent matrix elements. Dirac's symbolism[11] is used to identify matrix elements. Explicit use of these matrix elements will be made in this paper only for the Hill-type van der Waals interaction in the form of Eq. (3); however they would serve equally well for computations on the more general situation described by Eq. (1). The following numerical values were substituted to correspond to the case of adsorbed hydrogen: $d=0.74\times10^{-8}$ cm, $r_0=3.0\times10^{-8}$ cm, $A=1.208\times10^{-14}$ erg, $\lambda^2=6$. With these values, Eq. (3) becomes (omitting the terms in η^3 and η^4 for the reasons mentioned previously):

$$V = -20.65\times10^{-14} + 10{,}586\eta^2/2 + 7.248\times10^{-14}\xi^2 - 4.740\times10^{-8}\eta\xi^2 + 13.77\times10^3\eta^2\xi^2 + 3.142\times10^{-14}\xi^4.$$

The total energy of each level will have the form:

Energy = -20.65×10^{-14} + (unperturbed vibrational) + (unperturbed rotational) + (vibrational-rotational perturbation),

or, more explicitly, for states corresponding to the

TABLE III. Matrix elements for the perturbation calculation.

Matrix element	$\lambda^2=6$	$\lambda^2=12$	$\lambda^2=18$
$\langle R(1,0) \mid \xi^2 \mid R(1,0)\rangle$	0.2066	0.1496	0.1209
$\langle R(2,0) \mid \xi^2 \mid R(1,0)\rangle$	−0.2313	−0.1805	−0.1498
$\langle R(3,0) \mid \xi^2 \mid R(1,0)\rangle$	−0.0298	−0.0383	
$\langle R(1,0) \mid \xi^4 \mid R(1,0)\rangle$	0.0971	0.0565	0.0385
$\langle R(2,0) \mid \xi^4 \mid R(1,0)\rangle$	−0.1774	−0.1237	−0.0921
$\langle R(1,1) \mid \xi^2 \mid R(1,1)\rangle$	0.1564	0.1291	0.1110
$\langle R(2,1) \mid \xi^2 \mid R(1,1)\rangle$	−0.1824	−0.1578	−0.1395
$\langle R(1,1) \mid \xi^4 \mid R(1,1)\rangle$	0.0579	0.0418	0.0320
$\langle R(2,1) \mid \xi^4 \mid R(1,1)\rangle$	−0.1123	−0.0898	−0.0737

[10] A. H. Wilson, Proc. Roy. Soc. (London) **118A**, 628 (1928).

[11] P. A. M. Dirac, *The Principles of Quantum Mechanics* (Oxford University Press, London, 1947), third edition.

lowest unperturbed vibrational energy:

$$E(1,m)=-20.65\times10^{-14}+h\nu_0/2+\mu(1,m)\Lambda$$
$$+3.857\times10^{-14}\langle R(1,m)\mid\xi^2\mid R(1,m)\rangle$$
$$+3.142\times10^{-14}\langle R(1,m)\mid\xi^4\mid R(1,m)\rangle$$
$$-6.290\times10^{-27}\left\{\frac{\langle R(1,m)\mid\xi^2\mid R(1,m)\rangle^2}{h\nu_0}\right.$$
$$\left.+\frac{\langle R(2,m)\mid\xi^2\mid R(1,m)\rangle}{h\nu_0+[\mu(2,m)-\mu(1,m)]\Lambda}+\cdots\right\}$$
$$-14.88\times10^{-28}\left\{\frac{\langle R(2,m)\mid\xi^2\mid R(1,m)\rangle^2}{[\mu(2,m)-\mu(1,m)]\Lambda}+\cdots\right\}$$
$$-2.975\times10^{-27}\left\{\frac{\langle R(1,m)\mid\xi^2\mid R(1,m)\rangle^2}{2h\nu_0}\right.$$
$$\left.+\frac{\langle R(2,m)\mid\xi^2\mid R(1,m)\rangle^2}{2h\nu_0+[\mu(2,m)-\mu(1,m)]\Lambda}+\cdots\right\}$$
$$-9.872\times10^{-28}\left\{\frac{\langle R(2,m)\mid\xi^4\mid R(1,m)\rangle^2}{[\mu(2,m)-\mu(1,m)]\Lambda}+\cdots\right\}. \quad (4)$$

In Eq. (4) only those matrix elements are included which are required to maintain accuracy to within 10^{-16} erg in the perturbation rotational-vibrational energy. The symbol ν_0 denotes the unperturbed frequency of vibration of the molecule in the z direction in the potential well near the surface. With the above parameters, $\nu_0=8.95\times10^{12}$ sec^{-1}. The frequency ν_0 should not be confused with that of the *internal* vibrational motion of the molecule.

For the lowest $m=0$ level, Eq. (4) yields $-20.65\times10^{-14}+2.965\times10^{-14}+\mu(1,0)\Lambda$ for the unperturbed energy and 0.13×10^{-14} for the additional perturbation energy. For the lowest $m=1$ level, the unperturbed energy is $-20.65\times10^{-14}+2.965\times10^{-14}+\mu(1,1)\Lambda$ and the additional perturbation energy is 0.28×10^{-14}. So

$$E(1,1)-E(1,0)=[\mu(1,1)-\mu(1,0)]\Lambda$$
$$+0.15\times10^{-14}\text{erg}. \quad (5)$$

The effect of the perturbation is to increase the separation of the levels with a corresponding lowering of the predicted separation coefficient from approximately 5.8 for the unperturbed problem[3] at 20°K to about 3.5 for the perturbed problem at the same temperature.

The total adsorption energy of the ground state for the model with the specified parameters is approximately 15.7×10^{-14} erg, or 2250 cal/mole. Hence, the situation analyzed above corresponds to a hydrogen molecule adsorbed on the surface with an adsorption energy of 2250 cal/mole and a vibrational frequency of the molecule of 8.95×10^{12} sec^{-1}. But the theoretical separation coefficient would be 3.5 as opposed to an experimental value of about 16. Choosing a larger λ^2 would improve the agreement between the theoretical and experimental separation coefficients, but this would also imply a larger adsorption energy. However, the 2250 cal/mole implied by the choice of $\lambda^2=6$ is already close to the upper limit to a reasonable value for physical adsorption. So it appears that the model is capable of yielding results only about $\frac{1}{5}$ as large as the experimental value for the separation coefficient, if the parameters are kept in a reasonable range. The necessity of using an unreasonably large value for the amplitude of the rotational barrier in order to get agreement with experiment is also confirmed by the results of White and Lassettre.[4]

INCORPORATION OF A ϕ-HINDRANCE TERM

To eliminate this large discrepancy, various other types of perturbing terms were tried in the model. To be satisfactory, a perturbing term must be very effective in bringing the lowest ortho level in the adsorbed state closer to the lowest para level. Only one type of term could be found which satisfied this criterion, and this term can be interpreted in a very plausible way.

The model, as treated so far, contains no hindrance to rotation as the angle ϕ varies. However the adsorbent surface certainly is not strictly planar, as is implied in the model, but rather it is undoubtedly very "bumpy." So one would expect a ϕ hindrance to rotation. The functional dependence of this ϕ hindrance potential must be of the form $V_\phi=D\cos2\phi$ in order to be highly effective in increasing the separation coefficient. Such a term removes the degeneracy of the levels described by the wave functions $\Phi^1(\phi)=(e^{\pm i\phi})/(2\pi)^{\frac{1}{2}}$, so it is necessary to introduce the functions $(\sin\phi)/\pi^{\frac{1}{2}}$ and $(\cos\phi)/\pi^{\frac{1}{2}}$ in place of the exponential functions. The perturbation energy arising from V_ϕ for the lowest $m=0$ state is

$$E(1,0)_\phi$$
$$=-\frac{D^2}{2}\left\{\frac{\langle R(1,2)\mid R(1,0)\rangle^2}{[\mu(1,2)-\mu(1,0)]\Lambda}+\frac{\langle R(2,2)\mid R(1,0)\rangle^2}{[\mu(2,2)-\mu(1,0)]\Lambda}\right.$$
$$\left.+\cdots\right\};$$

the perturbation energy from V_ϕ for the $(\sin\phi)/\pi^{\frac{1}{2}}$, $m=1$ state is[12]

$$E(1,-1)_\phi=-(D/2)$$
$$-\frac{D^2}{4}\left\{\frac{\langle R(1,3)\mid R(1,1)\rangle^2}{[\mu(1,3)-\mu(1,1)]\Lambda}+\frac{\langle R(2,3)\mid R(1,1)\rangle^2}{[\mu(2,3)-\mu(1,1)]\Lambda}\right.$$
$$\left.+\cdots\right\};$$

and the perturbation energy from V_ϕ for the

[12] To distinguish the $\sin\phi$ state from the $\cos\phi$ state, the m value in the symbols will be taken as -1 for $\sin\phi$ state and $+1$ for the $\cos\phi$ state.

$(\cos\phi)/(\pi)^{\frac{1}{2}}$, $m=1$ state is

$$E(1,1)_\phi = E(1,-1)_\phi + D.$$

Note that there is a first-order perturbation energy for the $m=1$ states, but not for the $m=0$ state. This accounts for the effectiveness of the $\cos 2\phi$ perturbing term in changing the relative positions of the $m=0$ and $m=1$ states.

For simplicity, the small second-order contributions to these perturbation energies were computed by using the $R(\xi)$ functions appropriate to the free rigid rotator to evaluate the matrix elements. For the accuracy desired here (to within 10^{-16} erg) and for small values of λ^2 the use of the true unperturbed $R(\xi)$ is not necessary. The final expressions for the E_ϕ are (in cgs units):

$$\begin{aligned}
&[m=0] \quad E(1,0)_\phi = -0.06D^2\times 10^{14}\\
&[m=1] \quad E(1,-1]_\phi = -D/2 - 0.02D^2\times 10^{14}\\
&[m=1] \quad E(1,1)_\phi = +D/2 - 0.02D^2\times 10^{14}. \qquad (6)
\end{aligned}$$

Suppose the amplitude of the ϕ hindrance is $\frac{1}{6}$ the amplitude of the θ hindrance for $\lambda^2=6$. Then $D=1.208\times 10^{-14}$ erg. Substitution of this value into Eq. (6) and combining with Eq. (5) leads to the following energy differences:

$$E(1,-1)-E(1,0)=1.16\Lambda$$

$$E(1,1)-E(1,0)=2.16\Lambda.$$

These differences yield a separation coefficient of about 14 at $T=20°$K, which compares favorably with the experimental value of 16 on Al_2O_3 impregnated with a paramagnetic salt.[2]

White and Lassettre[4] discussed the very scanty data on deuterium separation coefficients, so it is of interest to apply the above theory to adsorbed deuterium. A highly tentative separation coefficient of 2.4 for deuterium adsorbed on pure alumina was deduced from experimental data reported by Cunningham, Chapin, and Johnston.[13] This is to be compared to the value of 16 obtained for hydrogen adsorbed on alumina impregnated with a paramagnetic salt. Assuming the same adsorption energy and θ-hindrance potential as was used above for hydrogen adsorption, but assuming no ϕ hindrance of the form $D\cos 2\phi$, the perturbation analysis leads to a separation coefficient of 2.4 for deuterium. This agrees with the experimental value. So one would be led to conclude, on the basis of the foregoing theory, that the impregnation of the alumina with the salt introduced a ϕ-hindrance potential such that its Fourier series expansion includes a term of the form $D\cos 2\phi$ with the D having a value of approximately 10^{-14} erg. The fact that a D value of zero gives agreement with experiment for adsorption on pure alumina indicates that any ϕ-hindrance potential that exists at the adsorption sites on pure alumina has no appreciable contribution from a term of the form of $D\cos 2\phi$. This does not rule out a hindrance having the form $D\cos 4\phi$ or $D\cos 6\phi$, etc., since such terms have little effect on separation coefficients. For example, if an adsorption site was centered between four identical adsorbent atoms placed at the corners of a square, then the ϕ hindrance would be predominantly of the form $D\cos 4\phi$ and the separation coefficient for such a surface would differ little from that computed neglecting the ϕ hindrance completely. However if one or two of the atoms around the adsorption site were not alike or were not spaced so as to be at the corners of a square, then a $D\cos 2\phi$ term would very likely be present and consequently a large separation coefficient would be expected.

[13] C. M. Cunningham, D. S. Chapin, and H. L. Johnston, J. Am. Chem. Soc. **80**, 2382 (1958).

CONCLUSIONS

The foregoing calculations show that agreement with experimental data can be obtained with a hindered rotator model using reasonable parameters. In order that the adsorption energies be less than 2500 cal/mole, one must use θ hindrances with amplitudes less than about 7×10^{-14} erg, because the adsorption energies and the θ hindrances are correlated by the nature of van der Waals forces. However, a θ hindrance of this magnitude is not sufficient to account for the experimental data on separation coefficients for adsorbed hydrogen. Incorporation into the model of a ϕ-hindrance term with the form $V_\phi = D\cos 2\phi$, with D about 10^{-14} erg, brings the theoretical separation coefficient into close agreement with the experimental value for hydrogen adsorbed on alumina impregnated with a paramagnetic salt. The same model with the same parameters except for setting the amplitude of the $\cos 2\phi$ term in the ϕ-hindrance potential equal to zero gives agreement with the experimental value for deuterium adsorbed on pure alumina.

The extreme sensitivity of the separation coefficient on the $\cos 2\phi$ contribution to the ϕ-hindrance potential should enable one to estimate fairly closely the amplitube of this term from experimental data on separation coefficients. Therefore, accurate data of this type would be valuable in determining the rotational behavior of adsorbed hydrogen at low temperatures. In this way some insight could be gained into the detailed nature of the adsorption sites.

THE JOURNAL OF CHEMICAL PHYSICS VOLUME 33, NUMBER 3 SEPTEMBER, 1960

Quantum Mechanical (Phase Shift) Analysis of Differential Elastic Scattering of Molecular Beams*

RICHARD B. BERNSTEIN

Department of Chemistry, University of Michigan, Ann Arbor, Michigan

(Received March 9, 1960)

For a spherically symmetrical intermolecular potential $V(r)=\epsilon f(r/\sigma)$ the quantum calculation of the elastic scattering cross section $d\sigma(\theta)/d\Omega$ in the c.m. system is carried out as follows. For a given relative velocity (or deBroglie wavelength) and an assumed $V(r)$, the radial wave equation is integrated for successive values of the angular momentum quantum number l, yielding the phase shifts η_l. Then $d\sigma(\theta)/d\Omega$ is computed in terms of the series of η_l's in the standard way. A general computational program (following that of K. Smith) is outlined for the evaluation of the radial wave function and the phase shifts, utilizing an IBM 704 computer. Calculations are presented for the L-J (12,6) potential function. The results may be concisely represented using the framework provided by the semiclassical treatment of Ford and Wheeler, i.e., in terms of a set of reduced phase constants vs reduced angular momenta at various reduced relative kinetic energies K. Tables and graphs are presented from which the phases may be obtained, to a good approximation, for any given ϵ, σ and K. Computation of the differential and total cross sections from the phase shifts is then readily accomplished.

The results are compared with the classical and semiclassical treatments. The problem of tunneling and orbiting is discussed.

INTRODUCTION

FOR molecules interacting according to a spherically symmetrical potential

$$V(r)=\epsilon f(r/\sigma), \tag{1}$$

the quantum mechanical problem of the elastic scattering of molecular beams is already solved, in principle, by the standard Mott-Massey theory.[1] For a given relative velocity v (or deBroglie wavelength λ) and an assumed $V(r)$ the radial wave function is integrated for successive values of the angular momentum quantum number l, yielding the phase constants η_l. Then the differential elastic scattering cross sections (in the c.m. system) $d\sigma(\theta)/d\Omega$ are computed in terms of the η_l's by the standard equation[1]

$$\frac{d\sigma(\theta)}{d\Omega}\equiv I(\theta)=\frac{1}{4k^2}\{[\sum_l(2l+1)\,\sin 2\eta_l P_l(\cos\theta)]^2 + [\sum_l(2l+1)\,(\cos 2\eta_l-1)\,P_l(\cos\theta)]^2\}, \tag{2}$$

where $k=2\pi/\lambda=\mu v/\hbar$, μ is the reduced mass, and v is the initial relative speed; P_l is the Legendre function.

In connection with the problem of the elastic scattering of electrons, Kenneth Smith[2] has developed a computational program for evaluating the radial wave function from which the phase shifts may be calculated. This program has now been adapted to the molecular beam scattering problem, and extensive calculations have been carried out and are here reported for the commonly used Lennard-Jones (12, 6) potential function, which may be expressed by

$$V^*(x)=f(x)=4(x^{-12}-x^{-6}), \tag{3}$$

where $x=r/\sigma$ and $V^*=V/\epsilon$ is the reduced potential.

METHOD

The differential equation for the radial wave function $R(r)$ is usually written[1,3] in terms of $G(r)=rR(r)$ as

$$d^2G_l(r)/dr^2+[k^2-U(r)-l(l+1)/r^2]G_l(r)=0, \tag{4}$$

where

$$k(=\mu v/\hbar)=(2\mu E/\hbar^2)^{\frac{1}{2}}, \qquad U(r)=(2\mu/\hbar^2)\,V(r), \tag{5}$$

and $E=\frac{1}{2}\mu v^2$ is the initial relative kinetic energy.

The following dimensionless parameters are introduced:

$$A=k\sigma \quad \text{and} \quad B=(2\mu/\hbar^2)\epsilon\sigma^2. \tag{6}$$

Eq. (4) becomes

$$d^2y/dx^2+[A^2-Bf(x)-l(l+1)/x^2]y=0, \tag{7}$$

where $y(x)\equiv G_l(r)$. Alternatively, Eqs. (4) and (7) may be written in terms of the reduced relative kinetic energy, defined as

$$K=E/\epsilon=A^2/B. \tag{8}$$

Here B may be considered an independent variable, with either A or K as the second independent variable. Then

$$d^2y/dx^2+[1-f(x)/K-\beta^2/x^2]A^2y=0, \tag{9}$$

where a reduced angular momentum function

$$\beta=[l(l+1)]^{\frac{1}{2}}/A \tag{10}$$

has been introduced. The "reduced effective potential"

* The author acknowledges with thanks financial support of this work from the United States Atomic Energy Commission, Division of Research, and from the Alfred P. Sloan Foundation.

[1] N. F. Mott and H. S. W. Massey, *The Theory of Atomic Collisions* (Clarendon Press, Oxford, England, 1949), 2nd ed.

[2] Kenneth Smith, private communication, June 24, 1959. The computational scheme is outlined briefly in a report by K. Smith, W. F. Miller, and A. J. Mumford, Argonne Natl. Lab., February 9, 1960.

[3] See, for example, L. I. Schiff, *Quantum Mechanics* (McGraw-Hill Book Company, Inc., New York, 1955), 2nd ed.

TABLE I. ($A=20$; $B=125$.)

l	x_s	Δx	y_0'	η_{calc}
0	0.70	0.005	1	−16.933
	0.65	0.005	10^{-30}	−16.933
	0.60	0.005	10^{-30}	−16.935
	0.60	0.020	10^{-30}	−16.947
1	0.70	0.005	1	−15.420
	0.70	0.010	1	−15.419
	0.60	0.010	10^{-30}	−15.421
20	0.65	0.005	10^{-30}	+2.219
	0.60	0.005	10^{-30}	+2.219

V_{eff}^* may be defined by the relation

$$Z=V_{eff}^*=\left[V(r)+\frac{l(l+1)}{r^2}\frac{\hbar^2}{2\mu}\right]\Big/\epsilon$$

$$=f(x)+\frac{l(l+1)}{Bx^2}. \quad (11)$$

Thus Eq. (7) may also be written

$$d^2y/dx^2+(K-Z)By=0. \quad (12)$$

For r sufficiently large so that $|U(r)|\ll k^2$, the solutions of Eq. (4) are[1,3]

$$G_l(r)\sim(\pi kr/2)^{\frac{1}{2}}[\cos\eta_l J_{l+\frac{1}{2}}(kr)$$

$$+(-1)^l\sin\eta_l J_{-l-\frac{1}{2}}(kr)], \quad (13)$$

where the J's refer to the usual half-odd-order Bessel functions.

In terms of the reduced parameters,

$$y=c[\cos\eta_l\, j_l(Ax)-\sin\eta_l\, n_l(Ax)], \quad (14)$$

where $j_l(z)$ and $n_l(z)$ are the spherical Bessel and spherical Neumann functions, respectively, and c is a constant independent of x. The phase shifts η_l are defined[1] in terms of the asymptotic solutions of Eq. (4) as $r\to\infty$:

$$G_l(r)\sim\sin[kr-(\pi l/2)+\eta_l], \quad (15)$$

or

$$y\sim\sin[Ax-(\pi l/2)+\eta_l]=\sin[A(x+\eta_l^*)-(\pi l/2)], \quad (16)$$

where $\eta_l^*=\eta_l/A$.

The η_l's may be found from a knowledge only of the zeros of y at large x. From Eq. (14), if x_n is the nth zero of y, then

$$\eta_l=\arctan[j_l(Ax_n)/n_l(Ax_n)]. \quad (17)$$

Thus, the procedure is as follows. Apparent phase shifts are calculated for successive zeros of y and are compared; when the difference between successively determined η_l values becomes negligible it may be considered that the condition ($|U(r)|\ll k^2$) necessary for the validity of Eq. (14) has been attained and that η_l has been evaluated.

The procedure outlined thus far (which is standard in the field of nuclear scattering) has also been employed by a number of workers[4–7] interested in the low temperature properties (especially the second virial coefficient) of helium. In the present instance, the computations were facilitated by the use of an IBM 704 computer. The standard Runge-Kutta-Gill (RKG) method was employed for the numerical integration of the wave equation.

A few features of the present computational program may be noted. First, regarding the boundary conditions, it was advantageous to modify the assumed potential so that for $x<x_s$, $V=\infty$ (and thus $y=0$), while for $x\geq x_s$, $V=\epsilon f(x)$ as usual. For the L-J (12, 6) case, it was found that all zeros of y (and thus the phase shifts) were substantially independent of x_s for $x_s\leq 0.7$ (corresponding to $V^*\geq 255$). In addition, it was noted[2] that any arbitrary value of the initial slope, y_0', could be used; the zeros of y are independent of y_0'. Lastly, as regards the interval size Δx in the RKG integration, it was found that for $\Delta x\leq 0.005$, the zeros and phases were essentially independent of Δx; in most cases even 0.01 was adequate. The integration was carried out to a sufficiently large x (typically in the range from 5 to 15) such that the differences between successive apparent phases were consistently less than some

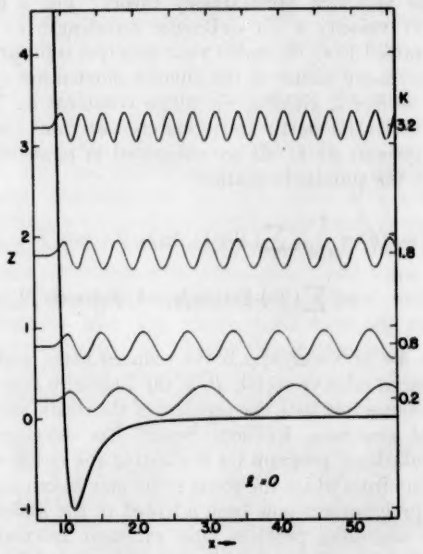

FIG. 1. Reduced effective potential and radial wave functions for $B=125$ and $l=0$.

[4] H. S. W. Massey and R. A. Buckingham, Proc. Roy. Soc. (London) **A168**, 378 (1938).
[5] J. De Boer and A. Michels, Physica **6**, 409 (1939).
[6] (a) R. A. Buckingham, J. Hamilton, and H. S. W. Massey, Proc. Roy. Soc. (London) **A179**, 103 (1951); (b) R. A. Buckingham, A. R. Davies, and D. C. Gilles, Proc. Phys. Soc. (London) **71**, 457 (1958).
[7] J. De Boer, Repts. Progr. Phys. **12**, 351 (1949).

predetermined value (usually <0.0002 rad). The computation time was usually ≤ 1 min.

Table I summarizes some of the results illustrating the independence of the calculated phase shift, η_{calc}, upon x_s and Δx for one of the least favorable cases (small ratio of λ/σ). On the basis of a number of check calculations made under varying conditions, it is estimated that the probable error in η_{calc} is ± 0.002 rad.

The program for $d\sigma(\theta)/d\Omega$ calculated from the phases yielded values at 1° intervals in θ from 0° to 179°. This program was checked by a few direct calculations and by duplicating a number of calculations in the literature.

RESULTS AND DISCUSSION

The results of the present study may conveniently be presented in two parts. Part A summarizes a detailed investigation of the radial wave functions, phase shifts and scattering cross sections for one particular example, the parameters for which correspond to the H_2–Hg system. The scattering of H_2 beams by Hg has been measured by Knauer[8] while classical cross section calculations are available[9] for the L-J (12, 6) potential. Part B involves the transformation of these results into a form of more general applicability. The method employed takes advantage of certain of the features of the semiclassical treatment of Ford and Wheeler[10] and consists of the evaluation of a set of reduced phase constants vs reduced angular momenta at various reduced relative kinetic energies K. With the use of the tables and graphs presented, it is possible to construct a set of phase shifts η_l for any L-J (12, 6) system of given ϵ, σ and K. Only in a certain region of η-l-K space (where the mapping has not been sufficiently extensive) would it be necessary to perform any direct phase calculations; otherwise, the phases may be satisfactorily estimated by the use of the tables within ± 0.04 rad.

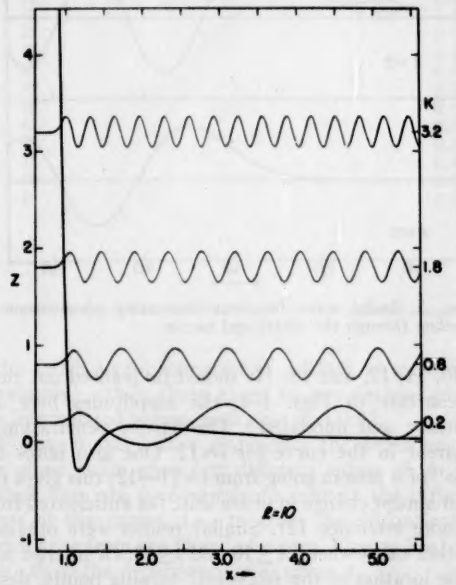

FIG. 2. Reduced effective potential and radial wave functions for $B=125$ and $l=10$.

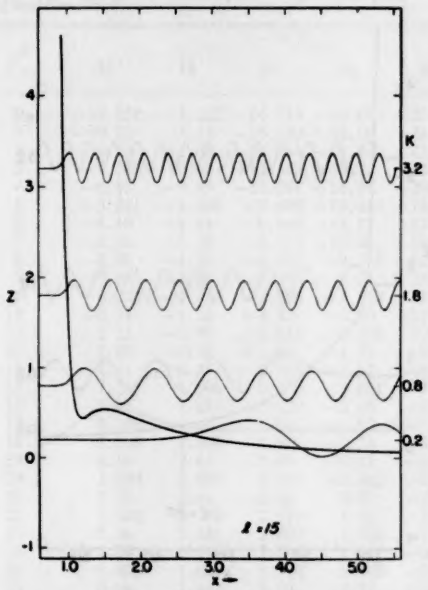

FIG. 3. Reduced effective potential and radial wave functions for $B=125$ and $l=15$.

A. Calculations for the System: H_2—Hg

The L-J (12, 6) parameters for the H_2–Hg system are taken[9] to be: $\epsilon=2.46\times10^{-14}$ erg, $\sigma=2.91\times10^{-8}$ cm; thus, one obtains the value of $B=124.1$ [from Eq. (6)]. Figures 1–4 show plots of the reduced effective potential Z vs x for the rounded value $B=125$ and $l=0$, 10, 15, and 20.

Although only the zeros of y are needed for evaluation of the phases, the complete radial wave function was an optional byproduct of the phase calculation. A number of representative wave functions were thus computed, as listed in Table II. Plotted on Figs. 1–4 are a few of the calculated radial wave functions $y(x)$, all drawn with the same asymptotic ($x\rightarrow\infty$) amplitude, and vertically placed to indicate the reduced relative kinetic energy K. Shown are wave functions for $K=0.2$, 0.8, 1.8, and 3.2, which correspond to $A=5$, 10, 15, and 20, respectively. The asymptotic ($x\rightarrow\infty$) wavelengths are inversely proportional to A. The classical turning points (i.e., the distance of closest

[8] F. Knauer, Z. Physik **80**, 80 (1933); **90**, 559 (1934).
[9] H. U. Hostettler and R. B. Bernstein, J. Chem. Phys. **31**, 1422 (1959).
[10] K. W. Ford and J. A. Wheeler, Ann. Phys. **7**, 259, 287 (1959).

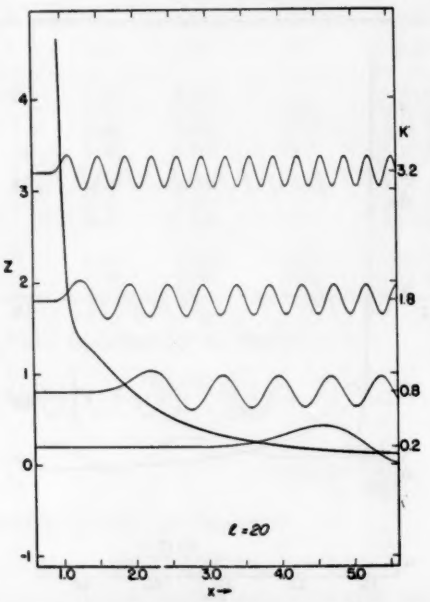

FIG. 4. Reduced effective potential and radial wave functions for $B=125$ and $l=20$.

approach) are located at the first inflection point in the wave function [from Eq. (12), $y''=0$ when $Z=K$]. The distortion of the wave function in the region of the attractive well and the influence of the centrifugal barrier are to be noted.

The wave functions reveal a number of interesting features, particularly with regard to the classical phenomena of orbiting[11] and rainbow scattering,[12] associated with the existence of the hump in the effective potential curve. Hirschfelder *et al.*[11] have shown classically that for the L-J (12, 6) potential, orbiting will occur for any $K\leq 0.8$ at some particular value (dependent on K) of the reduced angular momentum, if $\beta^2 K\leq 2.4624$. In terms of the classical deflection function $\Theta(b)$ this corresponds to a certain impact parameter b_0 for which $\Theta(b_0)\rightarrow-\infty$. For $K>0.8$ the deflection function goes only to a finite minimum, giving rise to rainbow scattering rather than orbiting. In the present notation and for $B=125$ the conditions for classical orbiting are therefore as follows: $A^2/B\leq 0.8$, or $A\leq 10$, and l less than some value l_0 given approximately by $l_0\cong(2.4624B)^{\frac{1}{2}}\cong 17.5$ {obtained using Eq. (10), approximating $[l_0(l_0+1)]^{\frac{1}{2}}$ by l_0}.

As pointed out by Ford and Wheeler,[12] penetration of the centrifugal barrier (tunneling) should occur for K slightly less than Z in the region of the hump. Wave functions illustrating this effect are shown in Fig. 5. Plotted are the curves for $K=0.20$ ($A=5$) with

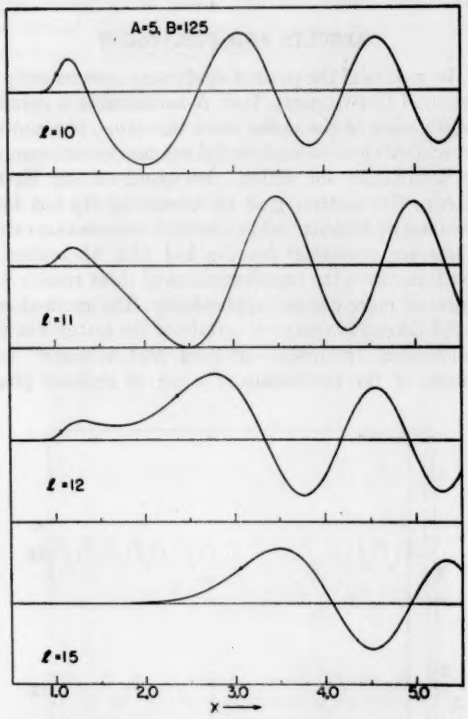

FIG. 5. Radial wave functions illustrating phenomenon of tunneling through the centrifugal barrier.

$l=10$, 11, 12, and 15. (It should be pointed out that, in contrast to Figs. 1–4, the amplitudes here are arbitrary and unrelated.) The barrier penetration is apparent in the curve for $l=12$. One also notes the "loss" of a zero in going from $l=11\rightarrow 12$; this gives rise to an abrupt change in phase shift (as anticipated from footnote reference 12). Similar results were obtained in other cases where $A\leq 10$ and $l\leq 17$. Of interest also is the location of the (classical) turning points, designated on the curves by small circles; the x on the curve for $l=12$ is, of course, classically inaccessible.

Table III is a summary of the phase shifts (in radians) for the present example ($B=125$). The values quoted with three decimal places are computed phase

TABLE II. List of wave functions computed for $B=125$.

A	l
3	0, 2, 4, 6, 7, 8, 10
5	0, 2, 5, 9, 10, 11, 12, 15, 20, 25, 30
7	8, 10, 11, 12, 13, 14, 15, 16, 17, 20
9	0, 12, 13, 14
10	0, 3, 5, 8, 10, 15, 16, 17, 18, 20
15	0, 3, 10, 15, 20
20	0, 1, 2, 3, 4, 5, 6, 7, 8, 10, 15, 20, 25, 30, 40, 50

[11] J. O. Hirschfelder, C. F. Curtiss, and R. B. Bird, *Molecular Theory of Gases and Liquids* (John Wiley & Sons, Inc., New York, 1954), pp. 553–557.

[12] See footnote reference 10, pp. 313–322.

TABLE III. Phase shifts (η_l) for $B=125$.

l \ A	3	5	7	9	10
0	+2.551	−0.484	−3.140	−5.565	−6.716
1	−3.92	+0.95	−1.69	−4.10	−5.24
2	4.994	2.179	−0.371	−2.731	−3.86
3	5.82	3.263	+0.84	−1.47	−2.572
4	6.427	4.175	1.90	−0.33	−1.38
5	6.75	4.906	2.814	+0.727	−0.297
6	6.653	5.440	3.62	1.69	+0.68
7	6.302	5.758	4.25	2.50	1.56
8	3.603	5.826	4.713	3.168	2.336
9	3.329	5.526	5.01	3.74	3.02
10	3.246	4.557	5.097	4.152	3.521
11	0.064	3.788	4.928	4.43	3.90
12	0.041	0.406	4.473	4.509	4.168
13	0.027	0.25	3.817	4.395	4.254
14	0.019	0.157	0.872	4.043	4.150
15	0.013	0.110	0.490	3.212	3.805
16		0.079	0.331	1.371	2.977
17		0.06	0.236	0.780	1.550
18		0.05	0.17	0.533	0.919
19		0.04	0.13	0.37	0.64
20		0.027	0.102	0.292	0.468
21		0.02	0.08	0.23	0.35
22		0.02	0.06	0.18	0.27
23		0.02	0.05	0.14	0.21
24		0.01	0.04	0.11	0.17
25		0.009	0.033	0.092	0.142
26		0.01	0.03	0.08	0.12
27		0.01	0.02	0.06	0.10
28		0.01	0.02	0.05	0.08
29		0.01	0.02	0.04	0.07
30		0.004	0.014	0.037	0.057
31				0.03	0.05
32				0.03	0.05
33				0.02	0.04
34				0.02	0.03
35				0.017	0.026
36					0.02
37					0.02
38					0.02
39					0.02
40					0.014
41					0.01
42					0.01
43					0.01
44					0.01
45					0.008

l \ A	15	18	20	24	30
0	−12.051	−15.022	−16.933	−20.634	−25.941
1	−10.56	−13.52	−15.420	−19.10	−24.38
2	−9.13	−12.08	−13.964	−17.639	−22.85
3	−7.750	−10.69	−12.547	−16.22	−21.41
4	−6.45	−9.35	−11.197	−14.84	−20.00
5	−5.231	−8.060	−9.898	−13.483	−18.60
6	−4.10	−6.84	−8.662	−12.17	−17.29
7	−3.06	−5.70	−7.471	−10.93	−16.02
8	−2.06	−4.63	−6.351	−9.767	−14.78
9	−1.08	−3.61	−5.278	−8.63	−13.56
10	−0.223	−2.640	−4.266	−7.535	−12.392
11	+0.54	−1.76	−3.32	−6.50	−11.24
12	1.22	−0.97	−2.431	−5.504	−10.16
13	1.80	−0.24	−1.61	−4.55	−9.09
14	2.31	+0.45	−0.846	−3.67	−8.08
15	2.731	1.096	−0.156	−2.851	−7.10
16	3.03	1.63	−0.472	−2.10	−6.20
17	3.209	2.06	1.03	−1.40	−5.32
18	3.260	2.400	1.503	−0.75	−4.50
19	3.18	2.65	1.89	−0.11	−3.70
20	2.880	2.800	2.219	+0.440	−2.981
21	2.39	2.84	2.46	0.92	−2.30
22	1.836	2.750	2.576	1.32	−1.65
23	1.36	2.531	2.607	1.656	−1.08
24	1.04	2.196	2.531	1.92	−0.55
25	0.808	1.809	2.344	2.105	−0.04
26	0.64	1.453	2.08	2.23	+0.41
27	0.51	1.165	1.768	2.26	0.800
28	0.42	0.944	1.469	2.184	1.12
29	0.35	0.774	1.213	2.05	1.38
30	0.298	0.642	1.008	1.874	1.592
31	0.25	0.54	0.840	1.66	1.736
32	0.21	0.46	0.707	1.447	1.819
33	0.18	0.39	0.600	1.25	1.843
34	0.16	0.33	0.51	1.07	1.81
35	0.135	0.284	0.432	0.925	1.739
36	0.12	0.24	0.37	0.81	1.64
37	0.10	0.21	0.32	0.70	1.51
38	0.09	0.18	0.28	0.61	1.37
39	0.08	0.16	0.25	0.53	1.23
40	0.069	0.144	0.219	0.464	1.094
41	0.06	0.13	0.20	0.41	0.97
42	0.05	0.11	0.17	0.36	0.86
43	0.04	0.10	0.15	0.32	0.77
44	0.04	0.09	0.14	0.28	0.69
45	0.038	0.080	0.12	0.255	0.62
46	0.03	0.07	0.11	0.23	0.55
47	0.03	0.06	0.10	0.21	0.50
48	0.03	0.05	0.08	0.19	0.46
49	0.03	0.05	0.08	0.17	0.42
50	0.023	0.047	0.070	0.150	0.368

shifts (with a probable error of ±0.002, as mentioned previously), while those given to two decimal places are interpolated values, with a pe of ±0.02.

Figures 6 and 7 show graphically the dependence of the phase shifts upon l at different values of A. The dotted lines are used simply to connect the different parts of the curves, i.e., to cross the discontinuities which arise from the "loss" of a zero. Figures 8(a) and 8(b) show the dependence of η_l upon A.

As generally understood, the short-range repulsive part of the potential is responsible for the negative low-order phases, while the long-range attractive part gives rise to the positive higher-order phases. As the relative kinetic energy is decreased the influence of the attractive well becomes dominant; conversely, as the collision energy increases the negative phases predominate. The low-order phases tend to approach those[13] for the rigid-sphere case (where, for example, $\eta_0=-A$). Inspection of Table III also shows that the value of l corresponding to a maximum in η_l is a linear function of A (i.e., in the present example, for $A>3$, $l_{max}=A+3$).

For the higher collision energies, as the semiclassical approximation becomes more valid, the initial slopes $(d\eta/dl)_0$ are found to approach the expected value of

[13] H. S. W. Massey and C. B. O. Mohr, Proc. Roy. Soc. (London) **A141**, 434 (1933).

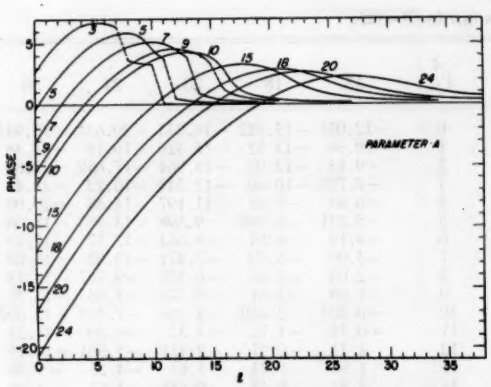

FIG. 6. Phase constant vs angular momentum quantum number.

$\pi/2$. Using the semiclassical correspondence relation,

$$\Theta(l)=2(d\eta/dl), \tag{18}$$

for the deflection function, $\Theta(l)$ was calculated for several values of A; the curves were quite similar to those calculated[9] classically, differing primarily in the region near the minimum in Θ.

A comparison of quantum vs classical calculation of the scattering cross sections is shown in Fig. 9. Plotted is the angular dependence of the scattering calculated [from Eq. (2)] for the case of $A=14.1$ ($K=1.6$) using phases interpolated from Figs. 6–8, compared with the classically calculated[9] curve for the same K. The predicted[14] discontinuity at the characteristic angle χ_s (designated "rainbow scattering" in footnote reference 10) is not evident in the quantum calculation.

In Fig. 10 Knauer's[8] experimental data are compared with the quantum calculation for $A=18$ ($K=2.6$), which corresponds fairly closely with the "most probable" value of A under the conditions of the experiments. Properly, one should average over the appropriate distribution of relative velocities, which would, of course, destroy most or all of the undulating character of the quantum curve, and give more nearly the observed monotonic dependence of $d\sigma/d\Omega$ upon θ. In addition, phenomena connected with rotation of the H_2 molecule and the spin of the protons will tend to wash out the structure that would be expected for the scattering of one ideal, monoenergetic, $J=0$ system by another.

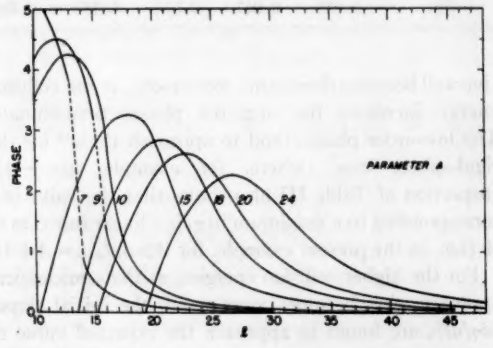

FIG. 7. Phase constant vs angular momentum quantum number.

[14] E. A. Mason, J. Chem. Phys. **26**, 667 (1957).

B. Generalization in Terms of Reduced Parameters

In the Ford-Wheeler[12] semiclassical treatment the

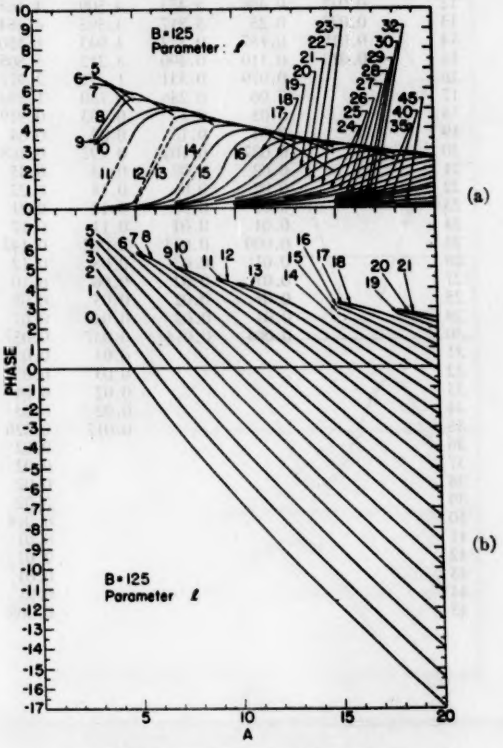

FIG. 8. Phase constant vs velocity parameter, A.

reduced phase constant is defined as

$$\eta^*=\eta/(\mu v\sigma/\hbar)=\eta/A. \tag{19}$$

This is the same as the η^* used in Eq. (16).

For fixed v, the deflection function is given[12] by

$$\Theta=2(d\eta^*/db^*), \tag{20}$$

where b^* is the reduced impact parameter,[11] $b^*=b/\sigma$. The reduced centrifugal potential analogous to the term $l(l+1)/x^2B$ in Eq. (11) is Kb^{*2}/x^2, so that the reduced angular momentum is Kb^{*2}. The previously defined [Eq. (10)] reduced angular momentum function β is then identified with b^*.

According to the semiclassical treatment, a set of curves of η^* vs b^* for various values of K should be unique (i.e., independent of the deBroglie wavelength or of ϵ). In footnote reference 10 (p. 317) two such curves (for $K=0.4$ and 1.6) together with the corresponding deflection functions are shown.

Referring back to the quantum treatment, it is not obvious from Eq. (9) that, for a given K and β, a unique reduced phase constant η^* [Eq. (16)] would be obtained independent of A (or B). In this connection, it is interesting to note the implication of the semiclassical treatment, i.e., that specification of B and K suffices to determine $\eta^*(b^*)$ and thus $\Theta(b^*)$. In the quantum treatment, Eq. (9) suggests that $\eta^*(\beta)$ *might* require the specification of A as well as B and K, i.e., a wavelength dependence of the reduced phase constants (which would presumably disappear with increasing A).

Figure 11 shows the results of the present calculations (for $B=125$) plotted as η^* vs β for various K's. The dotted curves identify the abscissa β as distinct from β' (defined later) wherever the two are different. These η^* vs β curves are unsatisfactory for two reasons. First, the semiclassical constraint on initial slopes,

$$(d\eta^*/db^*)_0=\pi/2, \tag{21}$$

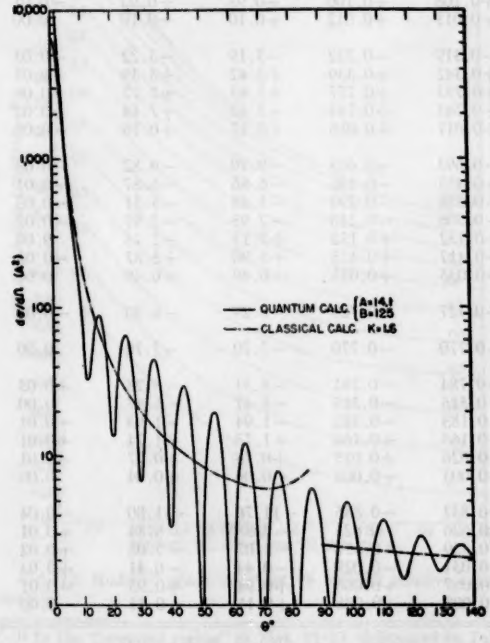

FIG. 9. Classical vs quantum calculation of the scattering of H_2 by Hg in the idealization where both systems are considered to have zero angular momentum. In actuality the undulations will be partly washed out by effects associated with the rotation of the H_2 molecule, the spin of the protons, and the difficulty of securing monoenergetic beams.

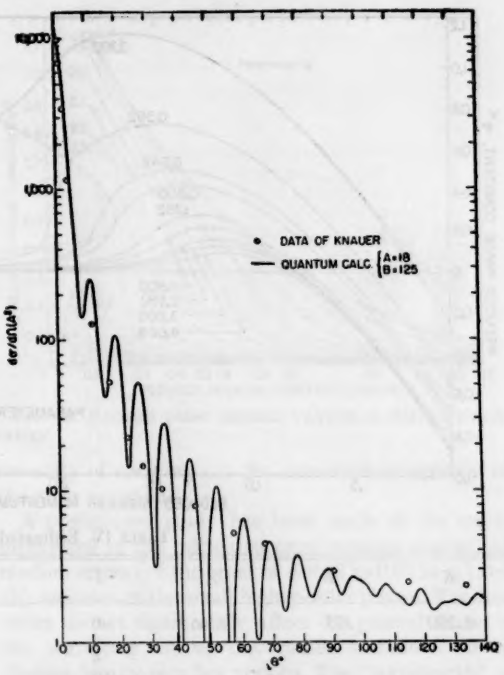

FIG. 10. Scattering of H_2 by Hg at 295°K. (See the remark on the quantum calculations in the caption of Fig. 9.)

is not satisfied (in fact, an inflection point is noted at small β); second, calculations of η_l made with different B and the same K yielded points (β, η^*) which were not on the same iso-K curve.

It is well known[1,10,15,16] that increased accuracy is obtained in the JWKB approximation for the phases by replacing (in the centrifugal potential term) the quantity $l(l+1)$ by $(l+\frac{1}{2})^2$ (the so-called Langer modification).[16] In order to take advantage of as much as possible of the framework of the semiclassical treatment, a modified reduced angular momentum function was defined as

$$\beta'=(l+\tfrac{1}{2})/A. \tag{22}$$

Of course, for large l, $\beta'\cong\beta\cong l/A$, (as implied in footnote reference 10, p. 318).

The solid curves in Fig. 11 refer to abscissa β'. These curves are found to satisfy the condition of Eq. (21). Moreover, at low β' they agree closely with the iso-K curves of η^* vs b^* plotted in footnote reference 10, p. 317. (However, for b^* greater than that corresponding to the maximum in η^*, the differences become appreciable.)

The important question, however, is not the extent of the agreement with the semiclassically estimated

[15] K. W. Ford, D. L. Hill, M. Wakano and J. A. Wheeler, Ann. Phys. 7, 239 (1959).
[16] R. E. Langer, Phys. Rev. 51, 669 (1937).

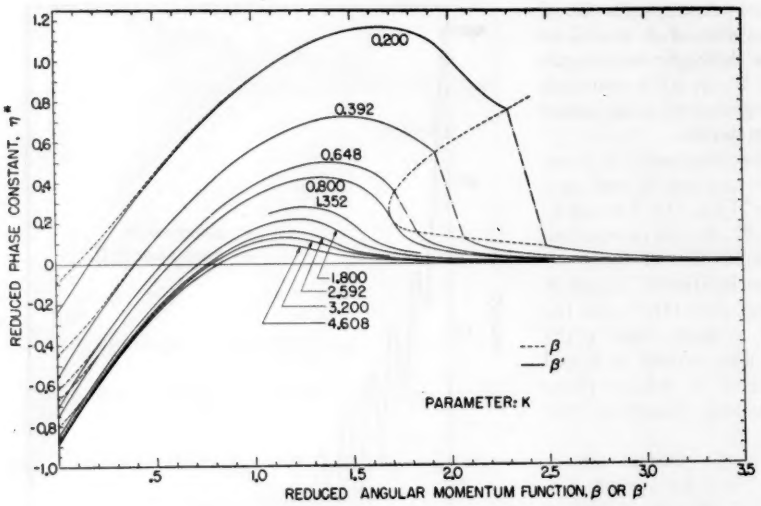

FIG. 11. Reduced phase constant vs reduced angular momentum functions.

TABLE IV. Estimated vs calculated phase shifts.

K	B	A	l	η_{calc}^*	η_{est}^*	η_{calc}	η_{est}	$\eta_{est}-\eta_{calc}$
0.200	375	8.66	0	−0.155	−0.157	−1.34	−1.36	−0.02
			2	+0.176	+0.174	+1.52	+1.51	−0.01
			5	+0.591	+0.586	+5.12	+5.08	−0.04
			10	+1.052	+1.046	+9.11	+9.05	−0.06
			20	+0.108	+0.106	+0.93	+0.92	−0.01
			30	+0.011	+0.012	+0.10	+0.10	0.00
0.267	375	10.00	0	−0.319	−0.322	−3.19	−3.22	−0.03
			5	+0.342	+0.339	+3.42	+3.39	−0.03
			10	+0.783	+0.777	+7.83	+7.77	−0.06
			20	+0.743	+0.744	+7.43	+7.44	+0.01
			30	+0.017	+0.016	+0.17	+0.16	−0.01
0.800	250	14.14	0	−0.693	−0.695	−9.79	−9.82	−0.03
			2	−0.485	−0.486	−6.86	−6.87	−0.01
			3	−0.388	−0.390	−5.48	−5.51	−0.03
			5	−0.208	−0.210	−2.95	−2.97	−0.02
			10	+0.152	+0.152	+2.15	+2.15	0.00
			20	+0.417	+0.415	+5.90	+5.87	−0.03
			30	+0.035	+0.035	+0.49	+0.49	0.00
1.200	62.5	8.66	0	−0.727	−0.728	−6.29	−6.30	−0.01
1.600	62.5	10.00	0	−0.770	−0.770	−7.70	−7.70	0.00
1.800	62.5	10.61	0	−0.784	−0.781	−8.31	−8.28	+0.03
			2	−0.515	−0.515	−5.47	−5.47	0.00
			5	−0.183	−0.182	−1.94	−1.93	+0.01
			10	+0.163	+0.164	+1.73	+1.74	+0.01
			20	+0.026	+0.025	+0.28	+0.27	−0.01
			30	+0.003	+0.003	+0.04	+0.04	0.00
3.200	62.5	14.14	0	−0.832	−0.835	−11.76	−11.80	−0.04
			2	−0.626	−0.625	−8.85	−8.84	+0.01
			5	−0.359	−0.357	−5.07	−5.05	+0.02
			10	−0.031	−0.029	−0.44	−0.41	+0.03
			20	+0.067	+0.066	+0.94	+0.93	−0.01
			30	+0.008	+0.008	+0.11	+0.11	0.00

curves, but rather whether the iso-K curves obtained from the quantum calculations (the "Q-i-K" curves) are unique (i.e., independent of B, for example). To investigate this point, a number of phase shift calculations were carried out with different B (and A); the range of B was from 62.5 to 375, with the range of K from 0.2 to 3.2. The results are presented in Table IV. The η_{calc}^* values refer to the directly calculated reduced phases, while the η_{est}^* values are taken from the data of Fig. 11 (with abscissa β'). The correspond-

ing phase shifts η are also listed. The average deviation $\eta_{est}-\eta_{calc}$ is ± 0.02 rad. Thus it appears that the present Q-i-K curves are very nearly unique, at least over the range of practical interest. Without a rigorous theoretical foundation, however, this result must be regarded as semi-empirical.

Figures 12 and 13 show the dependence of η^* upon K at various β'. Table V lists interpolated values of η^* vs β' and K to allow construction of graphs[17] similar to Figs. 11–13.

Thus, for any L-J (12, 6) system, the procedure for evaluating the scattering cross sections is as follows. From a given set of L-J parameters (σ, ϵ) one calculates B; knowing μ and v, one evaluates A and K. For each angular momentum quantum number l one calculates β', reads off the corresponding η^* from the Q-i-K curve and then calculates η_l. From the resulting table of phase shifts the computation of $d\sigma(\theta)/d\Omega[\equiv I(\theta)]$ is straightforward.

With the exception of the problem of the "bounded region" for cases when $K \leq 0.8$, Table V should suffice to enable estimation of the phase shifts without the necessity of carrying out the numerical integration of the wave equation.

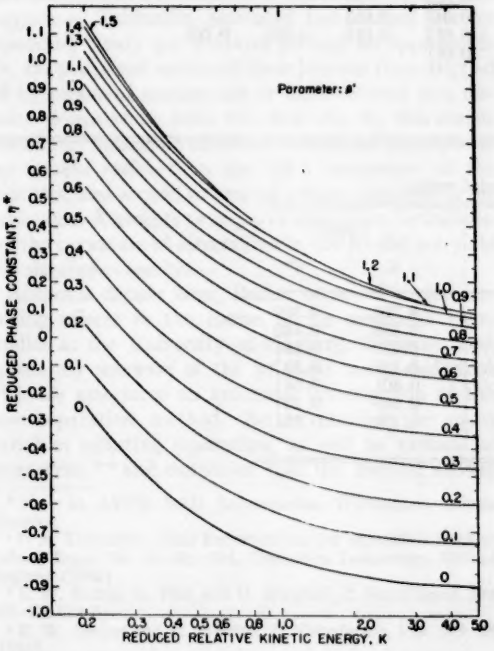

FIG. 12. Reduced phase constant vs reduced relative kinetic energy.

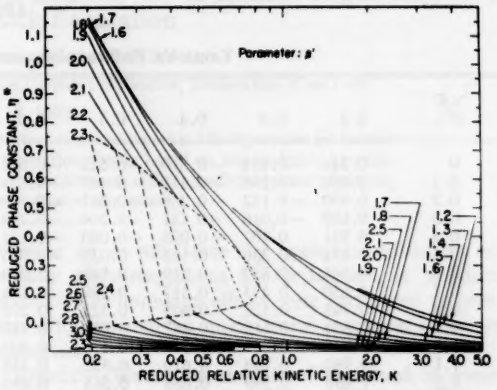

FIG. 13. Reduced phase constant vs reduced relative kinetic energy.

A preliminary study has been made of the errors introduced in the calculated cross sections due to (a) random errors [of the order of ± 0.02 to 0.05 in η_l] and (b) omission of the small higher-order phases. Random errors do not significantly affect the general shape of the scattering curve, but rather introduce strong changes locally in a few regions. The "wavelength" of the undulations in $d\sigma/d\Omega$ is governed primarily by $1/A$ (or λ) so that the positions of the maxima and minima are virtually unaffected. The error due to (b) is, however, more insidious; it affects the low angle scattering and thus may alter the total cross section Q by a significant degree. In addition, it is obvious that the accuracy of the numerical integration decreases (and the computing time increases) with increasing l, so that the integration technique is unsuitable for the precise calculation of the very high order phases (e.g., $l>60$). For improved accuracy in Q one should therefore use the Born approximation for the higher phases[18] and include in the calculation all phase shifts greater than about 0.005 rad. Further work in this direction with particular attention to the problem of the total cross section and its wavelength dependence is in progress.

ACKNOWLEDGMENTS

The author wishes to express his appreciation to Dr. Kenneth Smith of the Argonne National Laboratory for his advice and assistance with the prototype of the computer program for the wave function. In addition, many valuable discussions with Dr. H. U. Hostettler and Dr. R. S. Berry of this Department are gratefully acknowledged. The assistance of Mrs. H. Schumacher in plotting graphs and arranging tables is also appreciated.

[17] In the "bounded region" of Figs. 11–13, delineated in Table Vb, corresponding to the region of collision energies and angular momenta where orbiting or spiral scattering is possible, insufficient calculations of phase shifts were made to allow the precise location of the discontinuities in η^* vs β' at each value of K. Thus, for any individual case it would be necessary to make a few direct calculations of η in the neighborhood of the discontinuities.

[18] It may be shown that the Born approximation for the higher order phases yields $\eta = (3\pi/8)BA^4/l^6$. For $\eta \leq 0.5$ and $l \geq 2A$ this formula reproduces the directly calculated phases (cf. Table III) within ± 0.01.

APPENDIX

TABLE Va. Reduced phase constants (η^*) as a function of K and β'.

β' \ K	0.2	0.3	0.4	0.5	0.6	0.8	1.0	2.0	3.0	4.0	5.0
0	−0.244	−0.454	−0.570	−0.642	−0.692	−0.754	−0.790	−0.861	−0.883	−0.890	−0.896
0.1	−0.096	−0.298	−0.412	−0.487	−0.534	−0.597	−0.636	−0.711	−0.730	−0.738	−0.740
0.2	0.050	−0.152	−0.268	−0.341	−0.390	−0.453	−0.492	−0.571	−0.592	−0.599	−0.600
0.3	0.189	−0.016	−0.131	−0.206	−0.258	−0.324	−0.366	−0.438	−0.459	−0.468	−0.471
0.4	0.314	0.107	−0.008	−0.080	−0.131	−0.196	−0.237	−0.318	−0.340	−0.350	−0.356
0.5	0.435	0.230	0.112	0.038	−0.015	−0.082	−0.125	−0.209	−0.232	−0.245	−0.251
0.6	0.548	0.339	0.219	0.140	0.089	0.024	−0.020	−0.111	−0.138	−0.150	−0.158
0.7	0.650	0.433	0.317	0.239	0.184	0.115	0.071	−0.025	−0.057	−0.071	−0.081
0.8	0.748	0.528	0.405	0.325	0.270	0.200	0.153	0.048	0.012	−0.006	−0.018
0.9	0.834	0.615	0.487	0.403	0.347	0.271	0.220	0.108	0.070	0.050	0.036
1.0	0.912	0.687	0.557	0.470	0.409	0.330	0.276	0.153	0.110	0.086	0.070
1.1	0.980	0.746	0.610	0.521	0.458	0.376	0.318	0.186	0.131	0.102	0.087
1.2	1.038	0.799	0.658	0.563	0.496	0.406	0.348	0.199	0.137	0.103	0.082
1.3	1.088	0.834	0.690	0.594	0.523	0.424	0.356	0.190	0.120	0.086	0.063
1.4	1.128	0.868	0.711	0.609	0.531	0.424	0.350	0.154	0.088	0.061	0.047
1.5	1.151	0.885	0.713	0.606	0.521	0.399	0.304	0.102	0.057	0.040	0.030
1.6	1.166	0.872	0.700	0.586	0.490	0.344	0.237	0.068	0.039	0.030	0.025
1.7	1.164	0.859	0.663	0.522	0.418	0.225	0.128	0.048	0.029	0.020	0.017
1.8	1.145	0.816	0.619	0.481		0.115	0.082	0.033	0.021	0.016	0.012
1.9	1.105	0.755	0.553		0.128	0.074	0.054	0.023	0.015	0.010	0.007
2.0	1.013	0.691		0.117	0.084	0.053	0.038	0.019	0.011	0.007	0.004
2.1	0.910	0.645	0.101	0.073	0.058	0.040	0.031	0.012	0.008		
2.2	0.817		0.072	0.053	0.043	0.030	0.024				
2.3		0.090	0.052	0.040	0.032	0.023					
2.4		0.063	0.041	0.032	0.026	0.018	0.013				
2.5	0.077	0.045	0.032	0.026	0.021	0.014	0.010	0.006	0.004		
2.6	0.064	0.037	0.027	0.020	0.017	0.011					
2.7	0.050	0.030	0.021	0.017	0.012						
2.8	0.038	0.022	0.016								
3.0	0.025	0.013	0.012	0.009	0.008						
3.3	0.015	0.008	0.007	0.006	0.005						

TABLE Vb. Bounded region.

	Lower		Upper	
β'	K	η^*	K	η^*
1.7	0.800	0.225	0.704	0.319
1.8	0.707	0.160	0.538	0.440
1.9	0.574	0.144	0.422	0.524
2.0	0.468	0.131	0.353	0.590
2.1	0.378	0.120	0.301	0.643
2.2	0.333	0.110	0.249	0.700
2.3	0.287	0.100	0.200	0.755
2.4	0.240	0.090		

Separation of Gas Mixtures in a Supersonic Jet. II. Behavior of Helium-Argon Mixtures and Evidence of Shock Separation

S. ALEXANDER STERN, P. C. WATERMAN,* AND T. F. SINCLAIR

Research Laboratory, Linde Company, Division of Union Carbide Corporation, Tonawanda, New York

(Received April 15, 1960)

Further experimental evidence is presented for the separation of gas mixtures in the supersonic jet formed by a Laval nozzle. The results are in agreement with a separation theory based on free-molecule kinetics. In addition, anomalies are observed which can be attributed to pressure diffusion effects generated during passage through an oblique shock front located at the exit plane of the nozzle.

I. INTRODUCTION

THE possibility of separating gas mixtures in high-velocity jets appears to have been suggested first by Dirac during World War II, and demonstrated experimentally by Tahourdin at Oxford University.[1] This work was directed towards the separation of isotopic species, and rested on Dirac's idea that the separating action of a gas centrifuge could be secured without any moving parts in a high-velocity jet with lines of flow curving in an outward direction. The centrifugal field established across such a jet, the reasoning went, would affect the distribution of atoms and molecules differing in mass in a manner similar to that achieved in a conventional centrifuge. To test this suggestion, Tahourdin generated fast-moving jets by expanding binary gas mixtures through an appropriate slit; the peripheral section of these jets was then stripped off by means of another slit or baffle located at a distance downstream from the first slit. By this simple procedure, Tahourdin obtained in each case a peripheral gas stream enriched in the light component of the mixtures, and a core, or central stream enriched in the heavy one. Attempts to improve separation by increasing the curvature of streamlines in the jet did not yield any significant results.

Almost a decade later, Becker observed similar unmixing effects in the course of his molecular beam studies at the University of Marburg, Germany, and, apparently unaware of the previous work, undertook with his associates an extensive investigation of this new separation method. Becker studied the many variables affecting separation, as well as various jet geometries,[2-6] and concluded that the method showed promise as a substitute for gaseous diffusion, especially with respect to the separation of uranium isotopes. The unmixing effects were attributed to pressure diffusion, but no quantitative computations were presented.

Recently, Waterman and Stern[7] examined in somewhat more detail certain features of jet separation in a supersonic regime of flow. They found that the separation of molecules of different mass but having approximately the same collision cross section could be explained reasonably well by a mechanism based on the differences in thermal velocities of these molecules. Such a mechanism was originally suggested by Becker,[2] who later rejected it in favor of the pressure diffusion model. Waterman and Stern also studied the separation of molecules of equal mass but having different cross sections and were able to interpret the experimental results by means of a new diffusion process, which was called "size diffusion." Finally, they showed conclusively that the separation is "reversed" at higher pressure levels, the light components of the mixture tending to concentrate in the center of the jet and the heavy ones in the periphery.

The object of the present communication is to report the results of new separation experiments in supersonic jets involving mixtures of two gases which differ greatly in mass, namely helium and argon. The experiments were performed over a much wider range of pressures than heretofore, showing clearly the concentration reversal in the jet. Data on the effect of composition on separation factor are reported for the first time and are discussed in the light of the previously proposed theory. Finally, evidence is presented to show that the "reversed" separation may be caused by shock phenomena.

II. EXPERIMENTAL METHOD

The experimental method was similar to that employed by Tahourdin and by Becker. The supersonic jet was created by expanding a gas mixture of known composition through a Laval nozzle, and the periphery of the jet was separated from its core, or center, by means of a circular stripping baffle coaxial with the nozzle. The apparatus and procedure used have been described previously.[7] The Laval nozzle had a diameter

* Now at AVCO RAD Laboratories, Wilmington, Massachusetts.

[1] P. A. Tahourdin, Final Report on the Jet Separation Method, Oxford Rept. No. 36 Br. 694, Clarendon Laboratory, Oxford, England (1946).

[2] E. W. Becker, K. Bier, and H. Burghoff, Z. Naturforsch. **10a**, 565–572 (1955).

[3] E. W. Becker and R. Schütte, Z. Naturforsch. **11a**, 679–680 (1956).

[4] E. W. Becker, W. Beyrich, K. Bier, H. Burghoff, and F. Zigan, Z. Naturforsch. **12a**, 609–621 (1957).

[5] E. W. Becker, K. Bier, H. Burghoff, O. Hagena, P. Lohse, R. Schütte, P. Turowski, and F. Zigan, *Proceedings of the Symposium on Isotope Separation, Amsterdam, 1957* (Interscience Publishers, Inc., New York, 1958), pp. 560–578.

[6] E. W. Becker, K. Bier, H. Burghoff, O. Hagena, P. Lohse, R. Schütte, P. Turowski, and F. Zigan, *Proceedings of the Second United Nations International Conference on the Peaceful Uses of Atomic Energy* (United Nations, Geneva, 1958), A/Conf. 15/P/1002, Federal Republic of Germany.

[7] P. C. Waterman and S. A. Stern, J. Chem. Phys. **31**, 405–419 (1959).

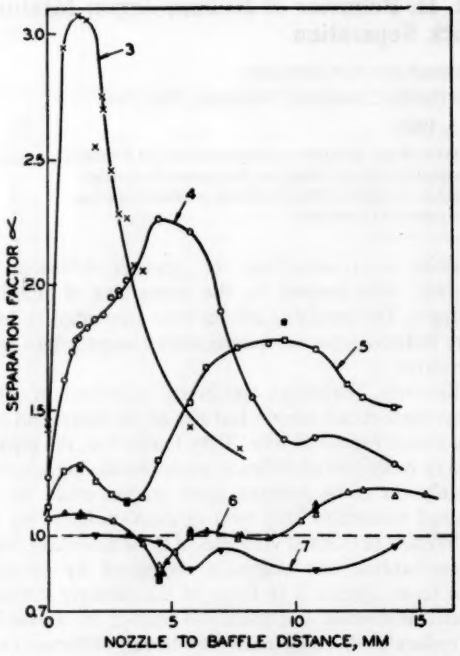

FIG. 1. Effect of pressure on the separation of a He–Ar mixture. Inlet composition: 53.6 mole % He–46.4 mole % Ar. Inlet and postnozzle pressures (in mm Hg): test 3: 9.5, 0.07_0; test 4: 45.0, 0.4_1; test 5: 75.0, 0.6_0; test 6: 150.0, 1.2_0; test 7: 680.0, 6.0_0. Data marked ×, ○, □, Δ were obtained by continuous analysis of the gas streams; ■, ▼, ▲ were determined by the sample bulb technique.

of 0.020 in. at its throat and 0.060 in. at the exit plane, while the inlet diameter of the baffle was 0.0292 in.

The analysis of the two gas streams, peripheral and central, emerging from the separator was performed in the early stages of the study by the same technique as before. Several sample bulbs were filled simultaneously with the gas mixture of interest and analyzed by means of a General Electric model G–5 mass spectrometer. This rather cumbersome procedure was greatly improved by modifying a Consolidated Electrodynamics model 21–620 mass spectrometer to permit the continuous analysis of gas streams at pressures as low as 20 μ Hg. For this purpose, it was necessary that the diameter of the gas lines to the spectrometer be made sufficiently large to maintain viscous flow and that back diffusion from the sample pump be reduced to a minimum. The pressure of the gas streams being analyzed was measured directly above the spectrometer "leak" by means of a tilting McLeod gauge. The agreement between the two methods was very satisfactory, as can be seen from Fig. 1. The accuracy of the composition measurements was 0.1% or better.

The inlet pressure was measured by means of a mercury manometer located at a distance of 8 in. upstream of the exit plane of the nozzle, while the postnozzle and postbaffle pressures were determined with Pirani gauges *outside* the gas jet. The accuracy of these measurements has been discussed.

Three helium-argon mixtures with the following composition, in mole %, were studied: (1) 92.1% He–7.9% Ar; (2) 53.6% He–46.4% Ar; and (3) 9.4%He–90.6% Ar. The helium was Grade A, stated by the Bureau of Mines to be at least 99.99% pure; the argon was a "Linde" gas with a purity of 99.995%.

III. EXPERIMENTAL RESULTS

There are two respects in which the helium-argon experiments differ from previous separation studies. First, the mass ratio of the components, $m_{Ar}/m_{He}=10$, is an order of magnitude larger than encountered with the mixtures investigated earlier (oxygen-nitrogen, argon-nitrogen, and nitrogen-ethylene). Second, and more important, is the fact that the ratio of specific heats for a helium-argon mixture, $\gamma_{mix}=\frac{5}{3}$, is considerably larger. As a consequence, the design pressure ratio[8] of the Laval nozzle employed was about 230, an increase of 50% or so above previous values. Because of the limited capacity of the exhaust pumps this pressure ratio could not be maintained, thus creating conditions favorable to the formation of standing shock waves.

The inlet and postnozzle pressures at which the various helium-argon separation experiments were performed are summarized in Table I. The postbaffle pressures were always equal to the postnozzle pressures. Experimental results are presented graphically in Figs. 1, 2, 7–10, where the separation factor and, in most cases, the compositions of the peripheral and central streams are plotted as a function of the distance between nozzle and stripping baffle for the pressures shown in Table I. The separation factor α, which measures the extent of the separation achieved under a given set of conditions, is defined as previously

$$\alpha=N_H{}^C N_L{}^P/N_L{}^C N_H{}^P, \qquad (1)$$

where N_H and N_L represent the mole fractions of the heavy and light components in the gas streams emerging from the jet separator, while the superscripts C and P refer to the central and peripheral streams, respectively. The data presented were obtained, as mentioned before, by continuously monitoring the composition of these streams by means of the Consolidated Electrodynamics mass spectrometer, with the exception of test 7 (see Table I) which required the exclusive use of the sample bulb technique due to the high pressure level employed.

Consider Fig. 1, which summarizes the results for an inlet composition of 53.6 mole % He and 46.4 mole % Ar. Test 3, performed at the lowest pressure *level*, is

[8] The design pressure ratio is by definition the ratio of inlet pressure to pressure in the jet at the exit plane of the nozzle. The operating pressure ratio is the ratio of inlet pressure to pressure in the postnozzle chamber.

TABLE I. Values of composition and pressure employed in the He–Ar experiments.

Test No.	Inlet composition (mole %)	Inlet pressure (mm Hg)	Postnozzle pressure (mm Hg)	Inlet-to-postnozzle pressure ratio
1	92.1% He–7.9% Ar	9.5	0.07_0	140
2	92.1% He–7.9% Ar	75.0	0.6_0	125
3	53.6% He–46.4% Ar	9.5	0.07_0	140
4	53.6% He–46.4% Ar	45.0	0.4_1	110
5	53.6% He–46.4% Ar	75.0	0.6_0	125
6	53.6% He–46.4% Ar	150.0	1.2_0	125
7	53.6% He–46.4% Ar	680.0	6.0_0	110
8	9.4% He–90.6% Ar	9.4	0.07_0	140
9	9.4% He–90.6% Ar	45.0	0.2_5	180
10	9.4% He–90.6% Ar	60.0	0.4_0	150
11	9.4% He–90.6% Ar	75.0	0.4_0	190
12	9.4% He–90.6% Ar	75.0	0.6_0	125

quite similar to the results obtained previously with other gas mixtures, and shows a nearly linearly rising portion with increasing nozzle-to-baffle distance, followed by a maximum and subsequent decay. As expected, the separation is normal, the helium being enriched in the peripheral stream and the argon in the central stream. Test 4, in which the pressure level has been increased by a factor of about five, shows a slight dip cutting into the rising portion. As the pressure level is further increased (curves 5–7) the dip becomes more pronounced, until finally in test 7 the separation is completely "reversed." This condition arises when the helium concentrates in the *center* of the jet and the argon in its *periphery*, and is characterized according to definition (1) by values of α of less than unity. The same trend is exhibited in the results for a composition of 9.4 mole % He–90.6 mole % Ar, shown in Fig. 2, and can be surmised also from the limited data available for the composition 92.1 mole % He–7.9 mole % Ar.

Referring again to Fig. 1, it is seen that the highest separation is obtained at the lowest pressure *level*. If the pressure level is increased while the inlet-to-postnozzle pressure *ratio* is maintained approximately constant, the maximum in the separation factor α decreases rapidly and moves towards larger nozzle-to-baffle distances. This behavior has been observed also with other gas mixtures.[7]

At the lowest pressures, the maximum separation is only slightly dependent on composition, as can be seen from Table II. It is interesting to note that the maximum occurs at about the same distance between nozzle and stripping baffle for all compositions studied. The separation can probably be increased above the values given in Table II by further lowering the pressure level and by raising the pressure ratio up to the design ratio of the nozzle. At higher pressures the separation depends strongly on composition, as shown in Fig. 2.

A variable which has proved useful for the interpretation of the above phenomena is the stripping ratio R, defined as the fraction of the inlet stream which forms the peripheral stream. R can be calculated from available composition data (see Appendix), and is presented in Figs. 7–10 as a function of the distance between nozzle and stripping baffle. At all distances except the smallest, R is larger than 0.8, i.e., the peripheral steam is much larger than the central stream. This uneven flow distribution is dictated by the geometry of the apparatus, since the opening of the stripping baffle is small compared to the exit plane of the nozzle. Another consequence of this distribution is that the composition of the peripheral stream differs only

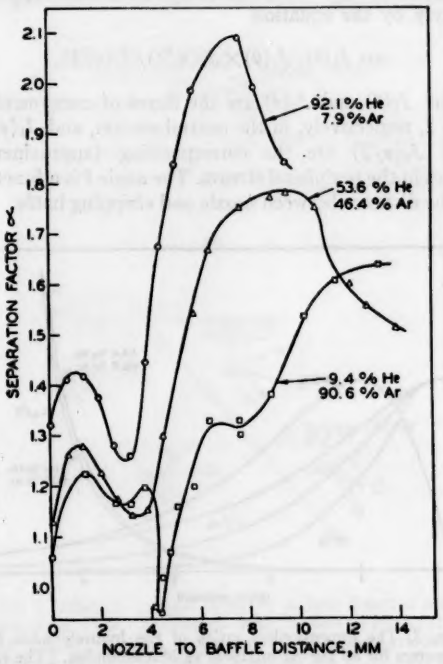

FIG. 2. Effect of composition of He–Ar mixtures on separation factor. Inlet compositions as indicated. Inlet pressure: 75.0 mm Hg. Postnozzle pressure: 0.6_0 mm Hg.

TABLE II. Effect of composition on maximum separation of helium-argon mixtures. Inlet pressure (for all compositions): 9.50 mm Hg, postnozzle and postbaffle pressures (for all compositions): 0.07_0 mm Hg.

Inlet Composition (mole-%)	Maximum separation factor	Nozzle-to-stripping baffle distance for maximum separation (mm)
9.4% He–90.6% Ar	2.7_4	0.8
53.4% He–46.6% Ar	3.0_8	1.2
92.1% He– 7.9% Ar	2.5_0	0.7

slightly from the inlet composition, as evident from Figs. 7–10.

III. DISCUSSION

It has been shown in a previous publication[7] that the unmixing of gases in a supersonic jet can be attributed to differences in thermal velocities if the gases differ in molecular weight, or to "size diffusion" if the gases are dissimilar only in collision cross section. Helium and argon differ in both these respects, but only separation due to disparity in mass needs to be considered since "size diffusion" is a relatively minor effect.

(1) In the case where the central stream is only a small fraction of the total, as in the present experiments, the separation factor can be expressed approximately by the equation

$$\alpha = J_1(\theta)/J_2(\theta) \times J_2(\pi/2)/J_1(\pi/2), \qquad (2)$$

where $J_1(\theta)$ and $J_2(\theta)$ are the fluxes of components 1 and 2, respectively, in the central stream, and $J_1(\pi/2)$ and $J_2(\pi/2)$ are the corresponding (approximate) fluxes in the peripheral stream. The angle θ is a function of the distance between nozzle and stripping baffle.

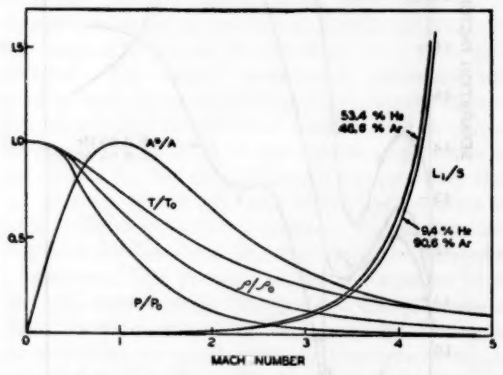

FIG. 3. The dimensionless ratios of the hydrodynamic flow parameters for all He–Ar mixtures vs Mach number. [The ratio L_1/S, shown for two He–Ar mixtures, is the reciprocal of the number of collisions suffered on the average by argon atoms between a given station (cross section) in the divergent section of the nozzle and its exit plane.]

$J_1(\theta)$ was shown to be given by the expression

$$J_1(\theta) = (K_1\sigma_1\pi^{\frac{1}{2}}/2\mu^2\beta_1^3) \times \{1 + \operatorname{erf}(\beta_1\mu) - \exp(-\beta_1^2\mu^2\sin^2\theta)[1 + \operatorname{erf}(\beta_1\mu\cos\theta)] + (2\beta_1\mu/\pi^{\frac{1}{2}})(\cos\theta - 1)\exp(-\beta_1^2\mu^2)\}, \qquad (3)$$

where K_1 is a normalizing constant, σ_1 is the collision cross section of component 1, and μ is the stream velocity parallel to the axis of the nozzle; further,

$$\beta_1\mu = (\gamma m_1 M^2/2\bar{m})^{\frac{1}{2}}, \qquad (4)$$

where γ is the ratio of the mean specific heats $(\bar{C}_p/\bar{C}_v)$, m_1 is the molecular weight of component 1, $\bar{m}$ is the average molecular weight of the mixture, and M is the Mach number of the flow. $J_2(\theta)$ is obtained from a similar expression.

In order to calculate the separation factor for helium-argon mixtures, it is necessary to evaluate $(\beta_1\mu)$ and $(\beta_2\mu)$ for the experimental conditions. As seen from Eq. (4), this requires in turn a knowledge of the velocity of the gas stream emerging from the nozzle in terms of the Mach number.

TABLE III. Cutoff parameters for helium–argon mixtures.[a]

Cutoff parameters	Composition (mole %) 9.4% He–90.6% Ar	53.4% He–46.6% Ar
L_1/S[b]	0.5	0.5
Mach number, M	3.94	3.86
A^*/A	0.180	0.188
S (mm)	0.51	0.56
$(\beta_{He}\mu)$	1.19	1.55
$(\beta_{Ar}\mu)$	3.77	4.89

[a] The distance S of the cutoff from the exit plane of the nozzle is given from geometrical considerations by the relation $(3.05\text{-}S)^2 = 4.82[(A/A^*)^{\frac{1}{2}} - 1] - 0.0640[(A/A^*)^{\frac{1}{2}} - 1]^2$, where S is in mm.

[b] Subscript (1) refers to argon. The use of a composition-averaged $\bar{L}/s$ would be preferable, but would not affect the results significantly.

The computational procedure has been described.[7] First, the flow parameters P/P_0, ζ/ζ_0, and T/T_0, where P, ζ, and T are the pressure, density, and temperature of the expanding gas mixture, respectively, and the subscript (0) refers to the stagnation conditions, are calculated for different stations (cross sections) in the nozzle. These parameters, obtained by means of the one-dimensional approximation for isentropic flow,[9] are shown in Fig. 3 as a function of the Mach number. The corresponding station in the nozzle is indicated by the cross-section ratio A^*/A, where A^* is the cross section at the throat of the nozzle. The flow parameters are independent of composition, since at low pressures the heat capacity ratio γ is $\frac{5}{3}$ for all helium-argon mixtures.

From a consideration of the pressure variation it is evident that the expanding gas undergoes a gradual transition from hydrodynamic flow to "free molecule"

[9] A. H. Shapiro, *The Dynamics and Thermodynamics of Compressible Fluid Flow* (Ronald Press, New York), Vol. 1, Chap. 4.

flow somewhere in the diverging section of the nozzle It is convenient to approximate the flow in this section by assuming that the transition occurs sharply at a specific station in the nozzle. The hydrodynamic flow is "cut off" at this station, downstream of which the effect of further collisions is neglected. The criterion for selecting the position of the cutoff was shown to be given by the ratio L_1/S, where L_1 is the *mean free stream path*, i.e., the distance between successive collisions in the direction of flow, and S is the distance from any station in the divergent section of the nozzle to its exit plane. L_1/S is, consequently, the reciprocal of the

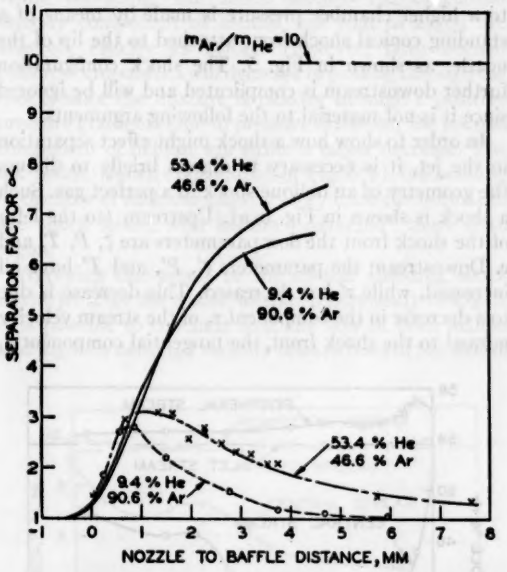

FIG. 4. Theoretical (solid curves) and experimental (dashed curves) results are shown for the separation factor α as a function of nozzle-to-baffle distance. (Agreement is seen to be satisfactory for the rising portion of the curves. Peaking and subsequent decay of the experimental separation factor is attributed to *ordinary* diffusion, an effect not included in the theory.)

number of collisions in the nozzle *after* the cutoff. This ratio has been computed as a function of the Mach number and is shown in Fig. 3 for two different helium-argon mixtures; in the computation, the collision diameters of helium and argon were taken as 2.18×10^{-8} cm and 3.64×10^{-8} cm, respectively,[10] and the stagnation density at the inlet of the nozzle was $n_0=3.05\times10^{17}$ cm^{-3}, corresponding to a temperature of 300°K and a pressure of 9.5 mm Hg.

Since L_1/S is a free parameter, its value has to be selected by trial and error so that calculated separation factors will best fit the experimental data. In past work with oxygen-nitrogen, argon-nitrogen, and nitrogen-ethylene mixtures it was found that a ratio of $L_1/S=$

[10] E. H. Kennard, *Kinetic Theory of Gases* (McGraw-Hill Book Company, Inc., New York, 1938), p. 149.

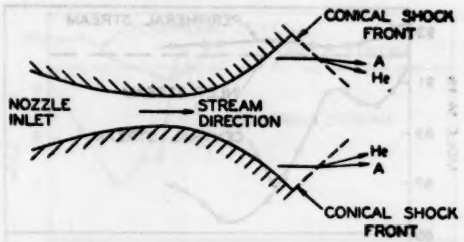

FIG. 5. Position of conical shock front developed at the lip of the nozzle at higher pressures. [The relative bending of the flow of He and Ar atoms due to pressure diffusion across the shock front is shown. The He atoms are more strongly "refracted" than the Ar atoms, causing a decrease in separation factor. In addition the shock causes an increase in the density of the central stream (evidenced by a lowering of the stripping ratio, R).]

0.5 provided satisfactory agreement between theory and experiment. This value establishes the cutoff at a distance of two mean free stream paths (on the average) from the exit plane of the nozzle. In the case of two of the helium-argon mixtures studied, the choice of $L_1/S=$ 0.5 yielded the cutoff parameters reported in Table III. By means of these values and of Eqs. (2) and (3), the separation factors for the two mixtures were calculated as a function of nozzle-to-baffle distance and the results are shown in Fig. 4. The separation factors approach asymptotically the value of $m_{Ar/He}=10$ which, according to theory, is the maximum separation obtainable at low pressures with the nozzle-baffle geometry under

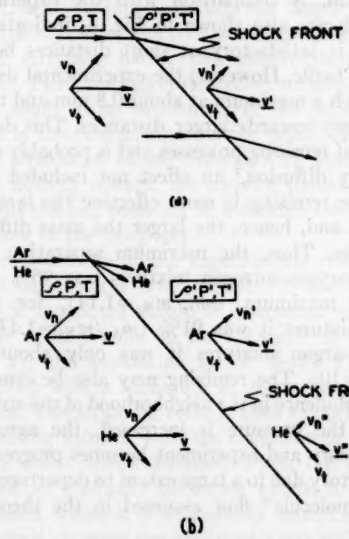

FIG. 6. Effect of pressure diffusion on flow direction across a planar shock front. (a) General case; (b) flow of He-Ar stream. (The density, pressure, temperature, and stream velocity, respectively, are ζ, P, T, and v upstream and ζ', P', T', and v' downstream of the shock front. v_n and v_t are the components of the stream velocity normal and tangential to the shock front, respectively.)

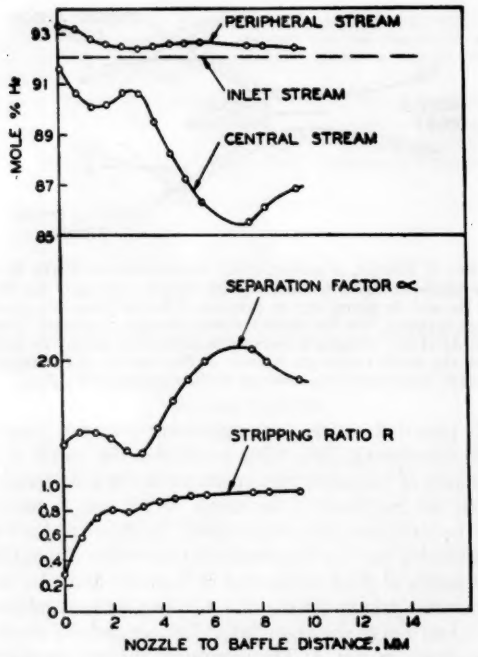

FIG. 7. Composition of separated gas streams, separation factor α, and stripping ratio R as a function of nozzle-to-baffle distance. Inlet composition: 92.1 mole % He–7.9 mole % Ar Inlet pressure: 75.0 mm Hg. Postnozzle pressure: 0.6_0 mm Hg.

consideration. A comparison with the experimental data, which are also shown in Fig. 4, indicates that agreement is satisfactory at short distances between nozzle and baffle. However, the experimental data are seen to reach a maximum at about 0.8 mm and then to fall off slowly towards larger distances. This decay is indicative of remixing processes and is probably caused by ordinary diffusion,[7] an effect not included in the theory. The remixing is more effective the larger the separation, and, hence, the larger the mass difference of the gases. Thus, the maximum separation factor found for oxygen-nitrogen mixtures was 96% of the theoretical maximum ($m_{O_2}/m_{N_2}=1.14$), for argon-nitrogen mixtures it was 91% ($m_{Ar}/m_{N_2}=1.43$), and for helium-argon mixtures it was only about 30% ($m_{Ar}/m_{He}=10$). The remixing may also be caused, in part, by turbulence in the neighborhood of the stripping baffle. As the pressure is increased, the agreement between theory and experiment becomes progressively less satisfactory due to a large extent to departures from the "free molecule" flow assumed in the theoretical model.

The theory also predicts that the effect of composition on separation should be small (Fig. 4). This prediction is certainly confirmed at short nozzle-to-baffle distances, where theory can be compared with experiment. The exact quantitative predictions of the theory cannot be confirmed since, as may be seen from the figure, the experimental results are indistinguishable in this region.

(2) The "reversal" of the jet separation at higher pressures deserves a separate discussion. There is strong evidence that this reversal is not due to any *ordinary* diffusion effects, since the latter are not capable of the required "overshooting." Instead, we suggest that the phenomenon is produced by pressure diffusion across oblique standing shock waves generated in the jet flow after the nozzle.

Since flow is supersonic in the diverging portion of the nozzle, high pressure levels in the postnozzle chamber cannot be felt upstream in the nozzle and adjustment to a higher chamber pressure is made by means of a standing conical shock front attached to the lip of the nozzle, as shown in Fig. 5. The shock configuration further downstream is complicated and will be ignored since it is not material to the following arguments.

In order to show how a shock might effect separation in the jet, it is necessary to digress briefly to discuss the geometry of an oblique shock in a perfect gas. Such a shock is shown in Fig. 6(a). Upstream (to the left) of the shock front the flow parameters are ζ, P, T, and v. Downstream the parameters ζ', P', and T' have all increased, while v' has decreased. This decrease is due to a decrease in the component v_n of the stream velocity normal to the shock front, the tangential component v_t

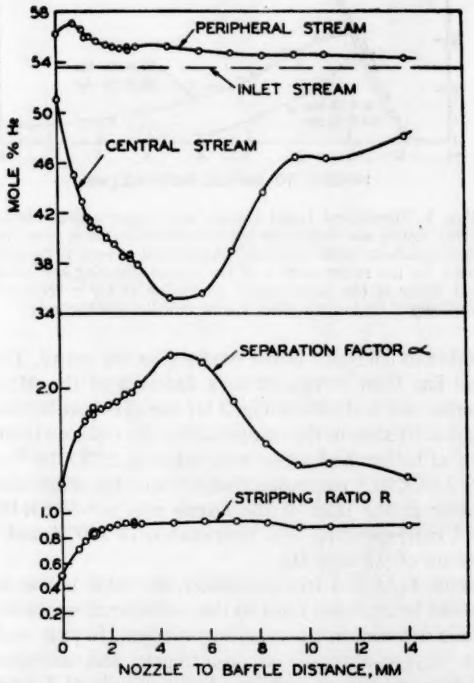

FIG. 8. Composition of separated gas streams, separation factor α, and stripping ratio R as a function of nozzle-to-baffle distance. Inlet composition: 53.6 mole % He–46.4 mole % Ar. Inlet pressure: 45.0 mm Hg. Postnozzle pressure: 0.4_1 mm Hg.

remaining unchanged as illustrated in the vector diagrams. The decrease is produced by deceleration through the pressure gradient across the shock front. Since the gradient of pressure has no component parallel to the shock, the tangential component of velocity is unaffected. The net result is a bending of the flow *away* from the shock front normal, analogous to the refraction phenomenon encountered in optics when light enters a medium of lower refraction index.

In the case of a helium-argon mixture it is assumed that upstream of the shock both gases have the same stream velocity v, so that no diffusion is occurring. While traversing the shock neither the tangential velocity component of helium, nor that of argon are affected, exactly as before. However, both normal velocity components will decrease in passing through the shock, since the mixture is passing through a positive pressure gradient. Due to pressure diffusion, the normal component of helium will suffer a larger decrease. The net result, shown exaggerated in Fig. 6(b), is a bending of the flow of each component away from the normal to the shock front, with helium "refracted" more than argon.

Applying this result to the conical standing shock in the jet after the nozzle, as shown previously in Fig. 5, it is possible to conclude that the flow of both helium and argon is deflected radially inward toward the axis of the jet, with helium suffering the larger deflection. Consequently, when the core of the gas jet is separated by the stripping baffle, two effects should be observable. First, the larger deflection suffered by helium should result in an enrichment of the helium concentration in the central stream and, hence, in a decrease in the separation factor. Second, with both gases deflected radially inward, the density should rise in the center of the jet, resulting in a smaller fraction of the total flow in the periphery.

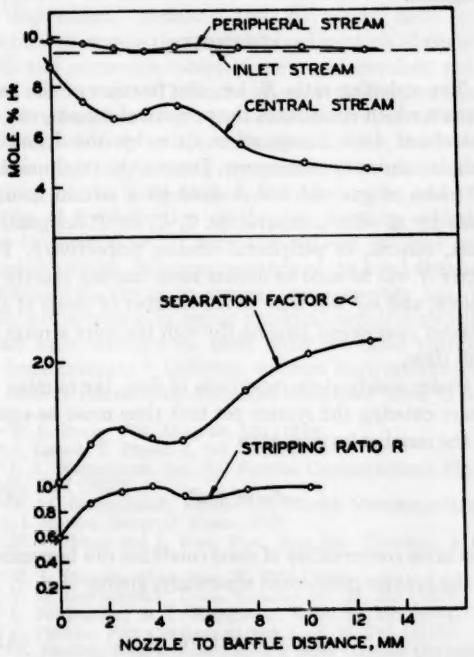

FIG. 9. Composition of separated gas streams, separation factor α, and stripping ratio R as a function of nozzle-to-baffle distance. Inlet composition: 9.4 mole % He–90.6 mole % Ar. Inlet pressure: 60.0 mm Hg. Postnozzle pressure: 0.4_0 mm Hg.

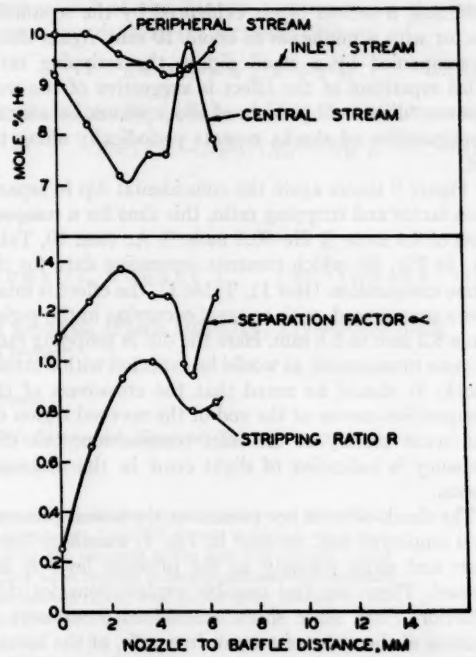

FIG. 10. Composition of separated gas streams, separation factor α, and stripping ratio R as a function of nozzle-to-baffle distance. Inlet composition: 9.4 mole % He–90.6 mole % Ar. Inlet pressure: 75.0 mm Hg. Postnozzle pressure: 0.4_0 mm Hg.

An examination of the experimental results reveals both of these effects to be present. For example, in Fig. 7, which shows the result of separation tests with a mixture of 92.1 mole % He–7.9 mole % Ar (test 2, Table I), the separation factor shows a moderately strong dip with a minimum at 3-mm nozzle to baffle distance. The stripping ratio R rises smoothly towards the limiting value 1, with the exception of a small dip also at about 3-mm distance. Thus, the jet may be pictured as gradually diverging except in the region mentioned, where it is temporarily turned inward.

Figure 8, showing the results of a test with a mixture of 53.6 mole % He–46.4 mole % Ar (test 4, Table I), is also of interest. Here there is a very slight break in the initial rising portion of the separation factor vs nozzle-to-baffle distance curve. Corresponding to this break is a just perceptibly flattened region in the stripping ratio, extending from approximately 1.5 mm to 3 mm. In

addition, a second dip is evidenced by the separation factor with a minimum at about 10 mm. Again this is accompanied by a small dip in the stripping ratio. This repetition of the effect is suggestive of the well-known "diamond" pattern of shock waves, in which a configuration of shocks repeats periodically along the jet.

Figure 9 shows again the coincidental dip in separation factor and stripping ratio, this time for a composition of 9.4 mole % He–90.6 mole % Ar (test 10, Table I). In Fig. 10, which presents separation data for the same composition (test 11, Table I), the effect is much more pronounced, with reversal occurring in the region from 5.1 mm to 5.6 mm. Here the dip in stripping ratio is more pronounced, as would be expected with a strong shock. It should be noted that the crossovers of the composition curves at the end of the reversal region do not occur exactly at the inlet composition; this discrepancy is indicative of slight error in the measurements.

The shock effect is not present at the lowest pressure level employed and, as seen in Fig. 1, manifests itself more and more strongly as the pressure level is increased. There are two possible explanations for this behavior. First, since shock transitions occur over a distance of the order of a mean free path, at the lowest pressure the shock front and hence its effects might be "blurred" to such a point that separation is no longer observable. At higher pressures the shock gains definition and separation effects begin to manifest themselves. A more likely explanation, however, is as follows. Since the gas mixture traversing the nozzle can expand only to the point where free-molecule kinetics begins to predominate, at a sufficiently low pressure it cannot overexpand relative to the chamber pressure and thus no shock front will form. As the inlet pressure is increased the nozzle expansion will proceed further, increasing the degree as overexpansion and thus generating stronger shocks with a consequent enhancement of the effect on the separation.

IV. CONCLUSIONS

In this paper data on the separation of helium-argon mixtures in a supersonic jet are reported, showing in detail the transition from "normal" to "reversed" separation. The "free molecule" theory proposed by the writers appears to predict again satisfactorily the dependence of the separation factor on nozzle-to-baffle distance, as well as on the composition of the mixtures. It is particularly gratifying that these results were obtained by using in the calculations a "cutoff" parameter L_1/S of 0.5, a value which gave also reasonable agreement with experiment for mixtures of oxygen-nitrogen, argon-nitrogen, and nitrogen-ethylene. On the other hand, it is unfortunate that the early peaking and decay of the separation factor, probably due to strong remixing effects, did not permit a check of the theory over larger nozzle-to-baffle distances. A study of these effects may well lead to a more efficient jet separator design.

The "reversed" separation occurring at the higher pressures has been attributed to differential pressure diffusion across a standing shock front. It is indeed difficult to conceive of any other mechanism that will produce the simultaneous minima in separation factor and stripping ratio, which were observed with all the helium-argon mixtures studied. The apparatus used is, however, not well suited for the study of gas separation processes involving shock waves. More sophisticated techniques are necessary to confirm the proposed mechanism and to provide a firmer basis for its quantitative description.

ACKNOWLEDGMENTS

The writers wish to express their thanks to Dr. P. H. Mohr for many helpful discussions and for his continued interest in the problem. Thanks are due to Dr. C. M. Birdsall for assistance in mass spectrometry problems, and to N. R. Mumbach and D. R. Acker for analyses of gas samples.

The writers are also grateful to Dr. N. Kurti for information on the work on jet separation performed at the Clarendon Laboratory, Oxford University, England.

APPENDIX

The stripping ratio R, i.e., the fraction of the inlet stream which constitutes the peripheral stream, can be calculated from composition data by the following simple continuity arguments. Denote the total number of moles of gas which flow through a stream in unit time by n, with a superscript 0, C, or P designating inlet, central, or peripheral stream, respectively. The letter N will be used to denote mole fraction exactly as before, and $n_H{}^0$ will refer to the number of moles of the heavier component passing through the inlet stream in unit time.

Under steady-state conditions of flow, the number of moles entering the system per unit time must be equal to the number leaving, thus

$$n^0 = n^C + n^P. \tag{A1}$$

The same conservation of mass condition can be applied to the heavier component separately, giving

$$n_H{}^0 = N_H{}^C n^C + N_H{}^P n^P, \tag{A2}$$

where the terms on the right are the number of moles of heavier component leaving the system per unit time

via the central and peripheral streams, respectively. Dividing this equation by n^0, and substituting the expression given by Eq. (A1) for n^C, we have

$$n_H{}^0/n^0 = N_H{}^C[(n^0-n^P)/n^0]+N_H{}^P(n^P/n^0). \quad \text{(A3)}$$

Noting that the left side of Eq. (A3) is just the mole fraction $N_H{}^0$ of the heavier component in the inlet stream, and defining the stripping ratio as

$$R = n^P/n^0 = n^P/(n^P+n^C), \quad \text{(A4)}$$

we obtain from Eqs. (A3) and (A4) the final expression

$$R = (N_H{}^C - N_H{}^0)/(N_H{}^C - N_H{}^P). \quad \text{(A5)}$$

THE JOURNAL OF CHEMICAL PHYSICS VOLUME 33, NUMBER 3 SEPTEMBER, 1960

Orbital Radii and the Dependence of Bond Length Upon Ionicity, Hybridization, and Bond Order

J. K. WILMSHURST

Parma Research Laboratory, Union Carbide Corporation, Cleveland, Ohio

(Received December 21, 1959)

Expressions for the dependence of hybrid orbital radii upon the constituent atomic orbitals and the ionicity of the bond to be formed are given. Using accurate bond-length data (±0.005 A) and a suitable expression for bond ionicity, atomic orbital radii have been obtained for the elements of the first four periods (other than transition metals). These radii can be used to calculate bond lengths in lone molecules, ionic crystals or metals or, alternatively, the experimental internuclear distance can be used in the same manner as the nuclear quadrupole coupling constant to describe the bond parameters in some detail.

FROM the time interatomic distances were first determined, chemists and physicists have attempted to express them as additive functions of atomic radii and numerous tables of ionic and covalent radii have been set up.[1–10] That the interatomic distance is an additive function of two well-defined covalent or ionic radii is, however, an approximation. Rather, the interatomic distance between two atoms depends on the ionicity of the bond formed, the bond order, and the degree of hybridization of the two bonding orbitals, and in some cases, it may also depend on lone-pair repulsion forces. This nonconstancy of the bond distance between two atoms in various environments has, in fact, led to its use in many empirical correlations with some such quantity as bond order,[10,11] bond energy[12] or force constant.[13] Different workers have endeavored to correct interatomic distances computed from tables of atomic radii, by taking into account one or more of the possible perturbations mentioned above, but in most cases these considerations applied to one element only, usually carbon. Thus, Stoicheff and Costain[14] and Bernstein[15] have noted the effects of neighbors on carbon-carbon single, double and triple bonds, while Cook[16] has discussed the interatomic distance between two sp_2 hybridized carbon atoms. Schomaker and Stevenson[17] have suggested a correction term for the effect of ionicity on more polar bonds, while Pauling,[10] and more recently Brown,[18] have noted the effects of hybridization on interatomic distance. Zachariasen[19] has given a set of atomic radii for atoms in sixfold coordination together with an empirical relation and empirical coefficients to allow an adjustment of these radii to any degree of coordination.

Since interatomic distances must depend on ionicity, bond order, and hybridization, then it should be possible to obtain estimates of one of these quantities from observed bond distances if some theoretical or empirical estimate of the other two quantities and their effects upon bond distance could be made. Alternatively nuclear quadrupole coupling constants, which can be

[1] W. L. Bragg, Phil. Mag. **40**, 169 (1920).
[2] A. Landé, Z. Physik **1**, 191 (1920).
[3] J. A. Wasastjerna, Soc. Sci. Fennica Commentaliones Phys.-Math. **38**, 1 (1923).
[4] V. M. Goldschmidt, Skrifter det Norske Videnskaps-Akad. Oslo I. Matern.-Naturvid Klasse, 1926.
[5] W. L. Bragg and J. West, Proc. Roy. Soc. (London) **A114**, 450 (1927).
[6] M. L. Huggins, Phys. Rev. **28**, 1086 (1926).
[7] V. M. Goldschmidt, Trans. Faraday Soc. **25**, 253 (1929).
[8] L. Pauling and M. L. Huggins, Z. Krist. **87**, 205 (1934).
[9] L. Pauling, Proc. Natl. Acad. Sci. U. S. **18**, 293 (1932).
[10] L. Pauling, *Nature of the Chemical Bond* (Oxford University Press, London, 1950).
[11] W. Gordy, J. Chem. Phys. **15**, 305 (1947).
[12] G. Glockler, J. Phys. Chem. **61**, 31 (1957); **62**, 1049 (1958).
[13] R. M. Badger, J. Chem. Phys. **2**, 128 (1934); **3**, 710 (1935).
[14] C. C. Costain and B. P. Stoicheff, J. Chem. Phys. **30**, 777 (1959).
[15] H. J. Bernstein, J. Phys. Chem. **63**, 565 (1959).
[16] D. Cook, J. Chem. Phys. **28**, 1001 (1958).
[17] V. Schomaker and D. P. Stevenson, J. Am. Chem. Soc. **63**, 37 (1941).
[18] M. G. Brown, Trans. Faraday Soc. **55**, 694 (1959).
[19] C. Kittel, *Introduction to Solid State Physics* (John Wiley & Sons, New York, 1956), p. 81.

TABLE I. Orbital hybridizations and bond lengths.

Element	Compound	Hybridization[a]	Bond length[b]
C	Diamond	sp_3	C—C 1.5445
	CH_4	sp_3	C—H 1.0936
	$H_2C{=}CH_2$	sp_2	C—H 1.086 C—C 1.337
	$HC{\equiv}CH$	sp	C—H 1.0597 C—C 1.205
N	Pyrrole	sp_2	N—H 0.990[d]
Li	Li_2	14.7% p[e]	2.6725
Cl	Cl_2	0% s	1.988
	HCl	28% s	1.2744
Si	Si (diamond structure)	sp_3	2.3517
	SiH_4	sp_3	1.4798
Na	Na_2	11.6% p[e]	3.0786
Br	Br_2	0% s	2.2836
	HBr	22% s	1.4144
Ge	Ge (diamond structure)	sp_3	2.4498
	GeH_4	sp_3	1.527
	GeH	0% s	1.591
K	K_2	~0% s	3.923
I	I_2	7% s	2.666
	HI	19% s	1.6165
Sn	Sn (diamond structure)	sp_3	2.8099
	SnH_4	sp_3	1.701[e]
	SnH	0% s	1.785

[a] The hybridization, unless obvious, was taken from nuclear-quadrupole coupling data [J. K. Wilmshurst, J. Chem. Phys. **30**, 561 (1959)].

[b] Bond lengths, unless otherwise stated, were taken from either G. Herzberg, *Diatomic Spectra* (D. Van Nostrand Company, Inc., New York, 1950) or *Tables of Interatomic Distances* (Special publication No. 11, The Chemical Society London, 1958). See also reference 14.

[c] J. K. Wilmshurst, J. Chem. Phys. **30**, 889 (1959).

[d] B. Bak, D. Christensen, L. Hansen, and J. R. Anderson, J. Chem. Phys. **24**, 720 (1956).

[e] G. R. Wilkinson and M. K. Wilson, J. Chem. Phys. **25**, 784 (1956).

interpreted in terms of the same three quantities,[20] could be combined with the interatomic distance and two, and sometimes all three, of the parameters determined. This latter approach could be applied to both molecules in the solid state, as well as in the vapor state, and hence estimates of these fundamental parameters could be made for both phases and compared.

In the present investigation expressions are suggested for the dependence of atomic hybrid orbital radii on the constituent orbitals as well as upon the ionicity of the bond which is about to be formed. Using molecules in which the interatomic distances are accurately known (±0.005 A) and for which the orbital hybridizations of the pair of atoms in the bond concerned are available, estimates of the s and p orbital radii for the elements of the first four periods have been made, together with estimates of ionic expansion and contraction factors. The decrease in bond length with π-bonding has also been considered. These results have then been used to calculate the degrees of hybridization of atoms in a number of molecules and the results are compared with hybridization parameters obtained from other sources. The table of radii set up here can be used to calculate bond lengths in molecules, ionic crystals or in pure metals if the bond properties are known, or alternatively, the observed radii can be used to describe the bond properties in some detail.

[20] C. H. Townes and B. P. Dailey, J. Chem. Phys. **17**, 782 (1949).

ATOMIC RADIUS AND IONICITY

It is well known that the atomic radius of an atom will depend upon the ionicity of the bond that the atom is about to form, becoming smaller if it is less electronegative than its bonding partner or expanding if it is more electronegative. If it is assumed that this change in radius with ionicity is a linear function of the ionicity, then the radius r_A of an atom A in a bond of ionicity, i, can be written as

$$r_A = r_A^{cov}(1 - i\Delta^{0|+}/r_A^{cov}), \tag{1}$$

if A is the least electronegative partner, or

$$r_A = r_A^{cov}(1 + i\Delta^{0|-}/r_A^{cov}), \tag{2}$$

if A is the more electronegative partner in the bond; where r_A^{cov} is the radius of the atom A in a pure covalent bond and $\Delta^{0|+}$ and $\Delta^{0|-}$ are the magnitudes of the differences in atomic radii between the covalent atom A and the ions A^+ and A^-, respectively. Combining Eqs. (1) and (2) and writing B for A in Eq. (2), the $A-B$ bond length is given as

$$d_{AB} = r_A^{cov} + r_B^{cov} - i(\Delta^{0|+} - \Delta^{0|-}), \tag{3}$$

which can be compared with Schomaker and Stevenson's[17] expression for the correction of the covalent bond distance for ionicity

$$d_{AB} = r_A^{cov} + r_B^{cov} - ik,$$

where

$$ik = 0.09\,|\,\chi_A + \chi_B\,|. \tag{4}$$

ATOMIC RADII AND ORBITAL RADII

If an atom A is about to form a bond using a hybrid orbital ψ derived from the atomic s and p orbitals as

$$\psi = (1-\lambda)^{\frac{1}{2}}\psi_s + \lambda^{\frac{1}{2}}\psi_p,$$

then we may write the radius r_h of this hybrid orbital approximately in terms of the radii r_s, r_p, of the constituent atomic orbitals as

$$r_h^2 = (1-\lambda)r_s^2 + \lambda r_p^2. \tag{5}$$

If now this atom is to form a bond of ionicity, i, in which it will be the least electronegative partner, then combining Eqs. (1) and (5) the hybrid orbital radius becomes

$$r_h^2 = (1-\lambda)\{r^{cov}(1 - i\Delta^{0|+}/r^{cov})\}_s^2 + \lambda\{r^{cov}(1 - i\Delta^{0|}/r^{cov})\}_p^2, \tag{6}$$

where subscripts s and p indicate that all terms within the brackets apply to the s and p orbitals, respectively. In order to reduce the number of unknowns it has been found necessary to make the assumption (but see

TABLE II. Atomic orbital radii and δ factors.

1st Period			2nd Period			3rd Period			4th Period		
$\delta^{0\|+}=0.2492$	$\delta^{0\|-}=0.4791$		$\delta^{0\|+}=0.1626$	$\delta^{0\|-}=0.5483$		$\delta^{0\|+}=0.1564$	$\delta^{0\|-}=0.5030$		$\delta^{0\|+}=0.1356$	$\delta^{0\|-}=0.4628$	
Element	r_s	r_p	Element	r_s	r_p	Element	r_s	r_p	Element	r_s	r_p
Li	1.3877	0.9979	Na	1.5499	1.4230	K	1.9615	(1.8270)	Rb	2.0209	...
Be	1.0820	0.9297	Mg	1.3783	1.3403	Ca	1.8038	(1.7553)	Sr	1.9008	...
B	0.8436	0.8661	Al	1.2254	1.2626	Ga	1.1034	1.3400	In	1.1935	1.5327
C	0.6577	0.8069	Si	1.0900	1.1893	Ge	1.0147	1.2874	Sn	1.1226	1.4872
N	0.5128	0.7517	P	0.9693	1.1203	As	0.9331	1.2369	Sb	1.0560	1.4430
O	0.3999	0.7003	S	0.8620	1.0553	Se	0.8581	1.1884	Te	0.9933	1.4002
F	0.3118	0.6524	Cl	0.7665	0.994	Br	0.7890	1.1418	I	0.9343	1.3586
$r_H^{cov}=0.3161$			$\delta^{0\|+}=1$			$\delta^{0\|-}=0.2485$					

later)

$$(\Delta^{0|+}/r^{cov})_s=(\Delta^{0|+}/r^{cov})_p=(\Delta^{0|+}/r^{cov})\text{hybrid}=\delta^{0|+}, \tag{7}$$

when Eq. (6) reduces to

$$r_A^2=(1-i\delta^{0|+})^2\{(1-\lambda)(r^{cov})_s^2+\lambda(r^{cov})_p^2\}$$
$$=(1-i\delta^{0|+})^2(r^{cov})_A^2. \tag{8}$$

Similar Eqs. to (6), (7) and (8) are obtained in the case that the atom is the more electronegative partner in the bond and in this case

$$r_A^2=(1+i\delta^{0|-})^2(r^{cov})_A^2. \tag{8a}$$

ORBITAL RADII AND δ VALUES

Both the effects of orbital hybridization and ionicity are in general very small and accordingly if any real meaning is to be ascribed to the final results only those bond lengths which have been determined with an accuracy of better than 0.005 A and without the need of any assumptions about the geometry of the system, must be used. Since the hybridization of the bonding orbitals in the bond under consideration must be known, and since this bond must be a σ-type bond with no π component, the amount of experimental data is very limited. The actual bond lengths and orbital hybridizations used in setting up the radii in the present work are given in Table I. We will assume that the hydrogen atom always forms a σ-type bond and that the energy of the higher levels is so great that no hybridization occurs. The proton H^+ will have zero radius and hence we can write

$$\delta_H^{0|+}=1.$$

The ionicity of a bond has been derived elsewhere[21] and is given in terms of the electronegativities[22] χ_A, χ_B of the two atoms A and B in the bond as

$$i=(\chi_A-\chi_B)/(\chi_A+\chi_B). \tag{9}$$

It should be noted that, where applicable, group electronegativities[23] must be used in Eq. (9).

Since the amount of experimental data available on accurate bond lengths as well as values of hybridization parameters are so limited, except perhaps for carbon, some assumptions within each row of the periodic table must be made if atoms other than carbon are to be considered. One theoretically acceptable assumption is that the screening constants of the s and p electrons in the atoms and their ions are the same and do not change as one progresses across any row of the periodic table, in agreement with Slater's rules.[24] It will be further assumed that the relative increase in size of the orbitals of any two atoms A and B within the same period is a function of the difference in effective nuclear charges of the two atoms only:

$$\frac{r_A-r_B}{r_A}=f(Z_{\text{eff}}{}^B-Z_{\text{eff}}{}^A), \tag{10}$$

and this immediately gives rise to the following important relations between the orbital radii:

$$\left(\frac{r_{Li}}{r_{Be}}\right)_s=\left(\frac{r_{Be}}{r_B}\right)_s=\left(\frac{r_B}{r_C}\right)_s=\cdots$$
$$\left(\frac{r_{Li}}{r_{Be}}\right)_p=\left(\frac{r_{Be}}{r_B}\right)_p=\left(\frac{r_B}{r_C}\right)_p=\cdots \tag{11}$$

with similar relations for the other rows of the periodic tables. These relations will be used later in setting up the tables of orbital radii.

Taking B as the ion A^+ and assuming that f is the same for both s and p electrons, Eq. (7) follows and

[21] J. K. Wilmshurst, J. Chem. Phys. **30**, 571 (1959).
[22] W. Gordy, Phys. Rev. **79**, 604 (1946).
[23] J. K. Wilmshurst, J. Chem. Phys. **27**, 1129 (1957); **28**, 733 (1958).
[24] J. C. Slater, Phys. Rev. **36**, 57 (1930).

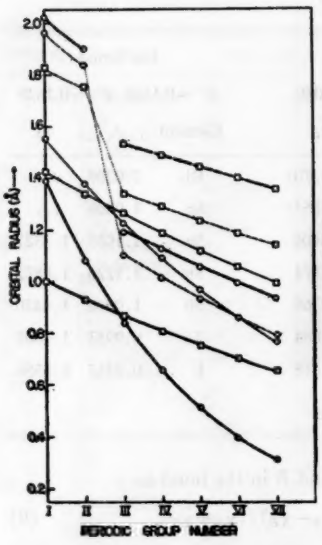

FIG. 1. The plot of the s and p orbital radii against periodic group number for the elements of the first four periods; ○ s-orbital radius; □ p-orbital radius; —— 1st period; —— 2nd period; - - - 3rd period; —— 4th period.

it is seen that $\delta^{0|-}$ and $\delta^{0|+}$ must be constant across any row of the periodic table.

First Short Period

Accurate bond lengths are known for the C—H bonds in methane, ethylene and acetylene and for the C—C bond in diamond, while the orbital hybridization of the carbon atom in methane and diamond is known to be strictly sp_3 and in the C—H bonds of ethylene and acetylene probably approximately sp_2 and sp, respectively. From the simultaneous solution of these four pieces of data, values of $(r_C^{cov})_s$, $(r_C^{cov})_p$, $\delta^{0|-}$ and r_H^{cov} can be obtained and these are given in Table II. To complete the first row elements two pieces of data were available; the accurate N—H bond length of sp_2 nitrogen in pyrrole and the Li—Li bond length in the diatomic molecule Li_2 for which the hybridization parameter is known from calculation[25] and valence state energies.[26] Using Eq. (11) the relation

$$(r_N^{cov})_{sp_2}^2=\frac{1}{3}\left(\frac{r_C^4}{r_{Li}}\right)_s^{\frac{1}{3}}+\frac{2}{3}\left(\frac{r_C^4}{r_{Li}}\right)_p^{\frac{1}{3}}$$

was obtained and solved simultaneously with the expression

$$\{\tfrac{1}{2}d_{Li-Li}\}^2=0.85(r_{Li})_s^2+0.15(r_{Li})_p^2.$$

Values of the other orbital radii were then determined from Eq. (11) and are given in Table II. The factor $\delta^{0|+}$ was derived from the ionic crystal LiF (see later).

Second Short Period

Using the accurate bond lengths for Cl_2 and HCl together with the hybridization parameters determined from the nuclear quadrupole coupling data[21] and the interatomic distance in crystalline LiCl, values of $\delta^{0|-}$, $(r_{Cl}^{cov})_s$ and $(r_{Cl}^{cov})_p$ were obtained and are given in Table II. Making use of the expression corresponding to Eq. (11) the covalent radius of sp_3 silicon obtained from the diamond structure can be related to the sodium orbital radii as

$$(\tfrac{1}{2}d_{Si-Si})^2=\tfrac{1}{4}(r_{Na}\cdot r_{Cl})_s+\tfrac{3}{4}(r_{Na}\cdot r_{Cl})_p,$$

and solved simultaneously with the expression

$$(\tfrac{1}{2}d_{Na-Na})^2=0.884(r_{Na})_s^2+0.116(r_{Na})_p^2$$

using the bond length determined for the Na_2 molecule and the orbital hybridization derived from valence state energies.[26] The remaining orbital radii can then be obtained (Table II) using the expression corresponding to Eq. (11) and $\delta^{0|+}$ can be calculated from the interatomic distance in crystalline NaCl (see later).

Combining the accurate bond length data for SiH_4 and solid silicon, having the diamond structure, the ionic expansion factor $\delta^{0|-}$ for H can be determined and this is given in Table II.

Third Period Elements

Using the bond lengths for Br_2 and HBr, together with the hybridization parameters determined from nuclear quadrupole coupling data[21] and the interatomic distance in crystalline NaBr, values of $\delta^{0|-}$, $(r_{Br}^{cov})_s$ and $(r_{Br}^{cov})_p$ were derived (Table II). From the internuclear distance in solid germanium (diamond structure) and the GeH bond length in germane, $\delta^{0|+}$

TABLE III. Orbital hybridizations derived from bond lengths.

	% s Character in the bonding orbital		
Hydride	From bond lengths	From bond angles[a]	From valence state energies[b]
H—F	17	...	...
H—O	19	...	15
H—N	17	...	...
H—C	6	...	7
H—B	0	...	...
H—Be	91	...	...
H—Li	98	...	93
H—S	23	...	...
H—P	3	...	...
H—Si	0	...	...
H—Al	0	...	...
H—Mg	100	...	100
H—Na	100	...	100
H_2O	23	20	...
H_2N	26	22	...
H_2S	32	5	...
H_2P	10	5.7	...
H_2Se	9	~2	...
H_2As	10	3.4	...
H_2Sb	11	2.5	...

[a] The degree of hybridization, α, is related to the bond angle θ as $\alpha=\cos\theta/(\cos\theta-1)$.

[b] Reference 26. Allowance is made for the contribution of electron-decoupling energy to the observed valence-state energy, using electron-decoupling-energy values obtained from atomic spectral data.

[25] L. Pauling, Proc. Roy. Soc. (London) **A196**, 343 (1949).
[26] J. K. Wilmshurst, J. Chem. Phys. **30**, 889 (1959).

was calculated. Assuming that germanium used a pure p-orbital for bonding in the diatomic molecule GeH, it was possible to calculate $(r_{Ge})_s$ and $(r_{Ge})_p$ and hence from the appropriate expression for Eq. (11) the orbital radii of the other B group elements were obtained. Valence state energy data[26] indicate that the p orbital hybridization in potassium in the diatomic molecule K_2 is only 3.7% and hence the s orbital radius for potassium was taken as one-half the internuclear distance in K_2. The s orbital radius for calcium was obtained from the expression corresponding to Eq. (11). The p orbital radii for calcium and potassium cannot be obtained. [However, an approximate estimate can be made by assuming the same functional dependence in Eq. (10) for both s and p orbitals and this is given in Table II in brackets.]

Fourth Period Elements

From a simultaneous solution of the three equations derived from the internuclear distances in I_2, HI, and the crystal LiI using the hybridization parameters determined from nuclear quadrupole coupling data,[21] $\delta^{0|-}$, $(r_I^{cov})_s$, and $(r_I^{cov})_p$, were obtained. Using the bond data for solid tin (diamond structure) and stannane, $\delta^{0|+}$ was computed, and assuming the tin orbital in the diatomic molecule *SnH* to be pure p, $(r_{Sn}^{cov})_s$ and $(r_{Sn}^{cov})_p$, and, hence from Eq. (11) all the orbital radii of the B subgroup were obtained (Table II). The s-orbital radius of rubidium was obtained from the interatomic distance in crystalline RbCl (see later).

It is very interesting to note that in every period, elements in Groups I and II have an s orbital radius larger than the p-orbital radius, while elements in Group III onwards have their p-orbital radii larger than their s orbital radii. This is illustrated graphically in Fig. 1.

A further point of interest concerns the δ values obtained in the present analysis. If, as has been assumed, the screening constants of the outer electrons are the same in the ion as in the atom, then the δ values in any one period can be related as

$$\delta^{0|-} = \delta^{0|+}/(1-\delta^{0|+}). \qquad (12)$$

The calculated δ values do not obey this relation, approaching it most favorably in the first period and departing more in the higher periods.

This suggests that either the δ values are not constant within any one period or, as is more likely, either the δ values for an s and a p electron are not the same or the screening constants of the electrons may change as one proceeds from the "covalent atom" to the ion. It is, of course, impossible to decide between the latter two possibilities as to which one is the main cause of the invalidity of Eq. (12), though both are probably effective. The $\delta^{0|+}$ values have been obtained mainly for an s electron, while the $\delta^{0|-}$ values have been derived predominantly for p electrons and if these values are not independent of orbital type, then Eq. (12) would not be expected to apply. In the case of hydrogen the low $\delta^{0|-}$ value is very surprising, an infinite value being predicted by Eq. (12) if the screening constant did not vary.

TABLE IV. Orbital hybridizations in the interhalogens.

Interhalogen		% s Character[a] From bond lengths	From nuclear-quadrupole data
Cl	F	9	...
	Br	6	13
	I	9	7
Br	F	17	...
	Cl	0	0
I	Cl	21	16

[a] Refers to the second atom in the interhalogen. The s hybridization for the first atom was taken from nuclear-quadrupole coupling data (reference 21).

It can be quickly seen that the atomic radii in Table II are consistent with Pauling's[10] well-known "averaged" single bond covalent radii and reproduce his radii nicely for the correct amount of "average" hybridization.

Another point of interest concerns Eq. (3) and its relation to the Schomaker-Stevenson[17] expression (4). It is seen from Table II that in all cases $\Delta^{0|-} > \Delta^{0|+}$ and this implies that as the ionicity of the bond increases, the bond length increases, exactly opposite to the Schomaker-Stevenson assumption.[27]

ESTIMATION OF HYBRIDIZATION PARAMETERS

Using the orbital radii in Table II together with Eqs. (5), (8) and (9), it is now possible to determine the orbital hybridization of an atom in a bond from the internuclear distance if the orbital hybridization of the other atom is known. In Table III percentage s orbital hybridizations are given for a number of atoms in diatomic and polyatomic hydrides and compared with values obtained from bond angles and valence state energies. In all cases the hybridization parameters determined from bond angles are smaller than those derived from the bond length indicating that the lone pair-bond repulsions are greater than bond-bond repulsions in agreement with stereochemical argu-

[27] The Schomaker-Stevenson expression applies quite well to bonds containing fluorine, but for many other bonds it does not seem to give correct results. If the expression is to apply to fluorine itself, the long covalent radius derived from F_2 must be used. However, this long radius for fluorine includes the extension due to lone-pair repulsions and the Schomaker-Stevenson expression, rather than correcting for ionicity in the fluoro derivatives, is actually correcting for lone-pair-repulsion effects which existed in F_2. For a discussion of the Schomaker-Stevenson relation and the best covalent radii to be used in applying this relation, see W. Gordy, W. V. Smith, and R. F. Trambarulo, *Microwave Spectroscopy* (John Wiley & Sons, Inc., New York, 1953), p. 313.

TABLE V. Hybridization in the alkali halides.

Alkali halide	Bond length	Ionicity	Alkali metal radius		Halide orbital radius		Minimum halide s character[a]	s Character from quadrupole coupling
			Pure s	Pure p	Pure s	Pure p		
NaCl	2.3606	0.539	1.4141	1.3284	0.9928	1.2874	88	97
NaBr	2.5020	0.497	1.4291	1.3426	0.9863	1.4274	65	85
NaI	2.7115	0.448	1.4370	1.3500	1.1279	1.6401	59	79

[a] Occurs for maximum p character in the alkali metal.

TABLE VI. Interatomic distances in the solid alkali halides[a] (NaCl- type structure).

	calc	obs	Pauling[b]		calc	obs	Pauling[b]		calc	obs	Pauling[b]		calc	obs	Pauling[b]
LiF	(2.009)	2.009	1.96	NaF	2.259	2.310	(2.31)	KF	2.619	2.664	2.69	RbF	2.710	2.82	2.84
LiCl	(2.565)	2.565	2.41	NaCl	(2.814)	2.814	2.76	KCl	3.177	3.138	(3.14)	RbCl	(3.267)	3.267	3.29
LiBr	2.738	2.745	2.55	NaBr	2.987	2.980	2.90	KBr	3.350	3.285	3.28	RbBr	3.431	3.418	(3.43)
LiI	(3.002)	3.002	2.76	NaI	3.250	3.231	3.11	KI	3.614	3.525	3.49	RbI	3.704	3.663	3.64

[a] The values in brackets have been used in setting up the tables of atomic radii.
[b] Calculated from Pauling's ionic radii (footnote reference 10).

ments.[28] For H_2S the orbital hybridization determined from the bond length is very much larger than that obtained from the bond angle. This is in agreement with the fact that the asymmetry parameter determined from nuclear quadrupole data is large[29] and would require a large s orbital contribution in the hybrid.

For the diatomic interhalogens, accurate bond lengths are known and the orbital hybridization of one atom can be obtained from nuclear quadrupole coupling data.[21] The orbital hybridization of the other halogen is then determined and compared with the orbital hybridization obtained from nuclear quadrupole data. The results are shown in Table IV.

It has been suggested previously[21] from the interpretation of nuclear quadrupole coupling constants that in the diatomic molecules NaCl, NaBr, and NaI, the bonding orbital of the halogen atom contained much more s character than had hitherto been considered likely. Since the bond lengths in these molecules are accurately known, a check can now be made on this suggestion and it is found in fact that to fit the observed bond lengths, the minimum amount of s character in the halogen orbital which occurs when the alkali orbital has a maximum amount of p character, must be still extremely large and that both the alkali and the halogen atom must be hybridized to a very considerable extent. Minimum per cent s characters are given in Table V. The high p character of the alkali atoms is in agreement with the large quadrupole coupling constants observed for the alkali atoms in the alkali halides.[30,31]

[28] R. J. Gillespie and L. S. Nyholm, Quart. Rev. **11**, 339 (1958).
[29] C. A. Burrus and W. Gordy, Phys. Rev. **92**, 274 (1953).

INTERATOMIC DISTANCES IN IONIC CRYSTALS

A bond AB having ionicity i has covalency $(1-i)$. If a molecule AB crystallizes in an ionic lattice of coordination number, n, then it can be assumed following Pauling[10] that the original $A-B$ bond now resonates over n positions such that the covalency of any $A-B$ bond in the lattice is $(1/n)(1-i)$, and hence the ionicity is given by

$$1-(1/n)(1-i). \qquad (13)$$

From Eqs. (13) and (3) it is easily seen that as n increases the interatomic distance should increase and as n decreases the interatomic distance should decrease, in complete agreement with experiment.

If it is assumed that in the alkali halides no s hybridization of the halogen or p hybridization of the alkali atom occurs, then the internuclear distances can be calculated for the ionic alkali halide crystals using Eqs. (1), (2), and (13) as

$$r_{AB}=r_A^{\text{cov}}(1-i\delta^{0|+})+r_B^{\text{cov}}(1+i\delta^{|-})\cdots, \qquad (14)$$

and these are given in Table VI together with the observed distances and distances calculated from Pauling's ionic radii.[10] The internuclear distances com-

[30] B. P. Fabricand, R. O. Carlson, C. A. Lee, and I. I. Rabi, Phys. Rev. **91**, 1403; **91**, 1395 (1953).
[31] A. Honig, M. Mandel, M. L. Stitch, and C. H. Townes, Phys. Rev. **96**, 629 (1954).

puted in this work agree with the experimental values to the same degree of accuracy as those computed from Pauling's radii. It should be noted, however, that these internuclear distances have effectively been calculated from a set of ionic radii similar to those of Pauling,[10] but derived assuming a fluoride ion radius of 0.965 A (obtained from the covalent radius for fluorine and $\delta^{0|-}$ from carbon) instead of a radius of 1.36 A as assumed by Pauling.[10] This arises from the fact that the δ factors, with the exception of $\delta^{0|-}$ for the first row and $\delta^{0|+}$ for the third row, were calculated from the internuclear distances in the ionic alkali halide crystals. The ionic radii calculated assuming a fluoride ion radius of 0.965 A are absurd (Table VII) and suggest that not only are the δ values dependent on orbital type, but that the screening constants must also change in going from the "covalent atom" to the ion.

INTERATOMIC DISTANCES IN METALS

The diatomic metal molecule M_2 is assumed to have a perfectly covalent bond. When this metal crystallizes into a lattice of coordination number n, then the original covalent bond will resonate over n positions and we can write, by analogy with the ionic crystal discussed before, an expression similar to Eq. (14) with $A=B=M$ for the internuclear distance in the metal as

$$r_{M-M}^{\text{metal}}=r_M^{\text{cov}}\{2+[1-(1/n)](\delta^{0|-}-\delta^{0|+})\}.$$

By using this equation bond distances in the alkali metals have been calculated, assuming pure s bonding, and compared with the experimental values (Table VIII). [It should be mentioned in passing that the derivation of the metal case from the ionic case by letting the two participating atoms become identical is the same as associating "no bond" character in the metal with "ionic" character in the ionic crystal.]

LONE PAIR REPULSIONS

If the two atoms forming the bond under consideration have lone pairs of electrons, then these lone pairs will repel one another with the consequence that the bond between the pair of atoms is lengthened. These repulsion effects can be approximately combined into one term varying as r^{-5} where r is the distance between the lone pairs. Thus, the extension τ of the bond due to the lone pair repulsion can be written as

$$\tau=K\cdot\sum_{ij}r_{ij}^{-5}, \tag{15}$$

the summation being carried out over all possible lone pair orbital interactions between atoms. For fluorine $\tau=0.113$ A and hence K can be calculated from Eq. (15) to be 0.0369. Using this value of K the bond extension in O_2^- due to lone pair repulsion is calculated to be 0.08 A in agreement with the observed value.

Since the bond extension due to lone pair effects decreases as r^{-5} it is only of significance for bonds between oxygen and fluorine. Thus, for chlorine the effects of lone pair interaction would make a difference of less than 0.005 A in the radii given in Table I. It should be mentioned in passing that bond-bond interaction could also lengthen the bond distance, e.g., in ethane. However, bond-bond repulsion is of much less consequence than lone pair-lone pair repulsions[27] and its effect on C—C bonds would not be expected to be greater than the present allowable experimental error.

TABLE VII. Radii of the alkali metal and halide ions.

Ion	This work[a]	Pauling[b]	Goldschmidt[c]	Huggins and Mayer[d]
Li^+	1.042	0.60	0.78	0.475
Na^+	1.298	0.95	0.98	0.875
K^+	1.655	1.33	1.33	1.185
Rb^+	1.747	1.48	1.49	1.320
F^-	0.965	1.36	1.33	1.110
Cl^-	1.539	1.81	1.81	1.475
Br^-	1.716	1.95	1.96	1.600
I^-	1.987	2.16	2.20	1.785

[a] See discussion in text.
[b] See reference 10.
[c] See reference 7.
[d] M. L. Huggins and J. E. Mayer, J. Chem. Phys. 1, 643 (1933).

TABLE VIII. Interatomic distances in the alkali metals.

Metal	Coordination Number	Interatomic distance Calc	Obs
Li	8	3.054	3.039
Na	8	3.623	3.715
K	8	4.518	4.554
Rb	8	4.620	4.860

MULTIPLE BONDING EFFECTS

The effect of π bonding superimposed on σ bonding is to shorten the bond length. This shortening, or π contraction, can be determined from the observed bond length if the number of π bonds and the σ bond length without π bonding are known. Thus for carbon the π_1 and π_2 contractions due to the first and second π bonds can be calculated from the expression

$$\tfrac{1}{2}r_{H_2C=CH_2}=(r_C^{\text{cov}})_{sp^2}-\pi_1$$

$$\tfrac{1}{2}r_{HC\equiv CH}=(r_C^{\text{cov}})_{sp}-\pi_1-\pi_2.$$

For other molecules (e.g., N_2, O_2), the π contraction factors can be determined from similar equations if the σ bond length without π bonding is known. This implies a knowledge of the orbital hybridization of the atom and in Table IX π contraction factors have been calculated for a number of atoms, assuming orbital hybridizations derived from valence state energies[26] were available.

These π contraction factors are useful in the determination of bond distances in multiple bonded molecules. Thus the length of the central double bond in butatriene is derived from the length of a $\sigma(sp-sp)$

TABLE IX. Atomic π contraction factors

Atom	Molecule	Hybridization[a] σ	Bond length	π_1	π_2
C	$H_2C{=}CH_2$	sp_2	1.5208	0.0919	
	$HC{\equiv}CH$	sp	1.4722		0.0417
N	$\phi{-}N{=}N{-}\phi$	sp_2	1.3630	0.0665	
	N_2	40% s	1.3330		0.0512
O	O_2	5% s	1.3700	0.0813	
P	P_2	5% s	2.2240	$\pi_1+\pi_2=0.1648$	
S	S_2	11% s	2.0680	0.0905	...
Se	Se_2	2% s	2.3636	0.106	...
Te	Te_2	p	2.8004	0.105	...

[a] From valence-state-energy data (reference 26).

bond less twice the π_1 contraction factor for carbon as 1.288 A (experimental value[14]=1.284 A). Similarly in ketene the C=C bond length can be obtained from the $\sigma(sp_2{-}sp)$ bond length less twice the π_1 contraction factor for carbon as 1.313 A (observed[14] 1.313 A). Alternatively the bond distances in such conjugated molecules can be used together with the π contraction factor to estimate bond orders. Thus in benzene the bond order is found to be 1.67 and for the single bond in butadiene it is 1.21. The molecular orbital theoretical[32] values are 1.67 and 1.44, respectively.

CONCLUSION

The lack of accurate bond length data (±0.005 A) and the poor knowledge of hybridization parameters makes any attempt at setting up a table of atomic orbital radii extremely difficult. In the present case some assumptions were necessary in order to extend the treatment past carbon and, even for carbon itself, the orbital hybridization of the carbon atom in the C—H bond in ethylene and acetylene may not be strictly sp_2 or sp as assumed. However, the assumptions introduced are not so unreasonable as to invalidate completely the orbital radii obtained here and, in fact, it is felt that the interpretation of bond lengths analytically in terms of the bond parameters, ionicity, hybridization, and bond order may be of considerable use in explaining semiquantitatively "unexpected" variations in bond length which have hitherto only been explained qualitatively (e.g., the C—Cl length in CH_3—Cl,[33] CCl_4 and CF_3Cl.[34] In particular the main use of this analytic breakdown of the bond length lies in the fact that there are now two types of accurate experimental data available, namely bond lengths and nuclear quadrupole coupling constants, both of which can be interpreted in terms of the same fundamental parameters to about the same extent of approximation and from which these fundamental parameters can be uniquely determined for both gas phase and solid phase molecules. Finally, estimates of orbital hybridization derived from bond angles are open to considerable doubt due to the effects of nonbonding forces upon the bond angle, and it is suggested that orbital hybridizations determined from bond length data as described here will in general be more reliable.

The present treatment could be improved by systematically removing the assumptions made as more data become available. However, since the δ factors appear dependent on orbital type and also vary as the screening constants of the electrons vary from the "covalent atom" to the ions, it would seem impossible to obtain good estimates of ionic radii from this treatment. For most molecules, however, the present treatment is probably adequate to interpret the rather small but significant variations that occur in observed bond lengths.

[32] C. A. Coulson, *Valence* (Oxford University Press, London, 1953).

[33] W. J. O. Thomas, J. T. Cox, and W. Gordy, J. Chem. Phys. **22**, 1718 (1954).

[34] L. S. Bartell and L. O. Brockway, J. Chem. Phys. **23**, 1860 (1955).

THE JOURNAL OF CHEMICAL PHYSICS VOLUME 33, NUMBER 3 SEPTEMBER, 1960

Threshold Law for the Probability of Excitation of Molecules by Photon Impact. A Study of the Photoionization Efficiencies of Br_2, I_2, HI, and CH_3I*

J. D. MORRISON,† H. HURZELER,‡ AND MARK G. INGHRAM, *Department of Physics, University of Chicago, Chicago, Illinois*

AND

H. E. STANTON, *Argonne National Laboratory, Lemont, Illinois*

(Received April 13, 1960)

A study is made of two types of excitation process in molecules, leading to either dissociation to an ion-pair, or to autoionization. The latter process, in the case of the iodine-containing molecules, clearly makes a very significant contribution to the total ionization. The threshold law for the probability of excitation by photon impact is shown to be approximated closely by a delta function of the excess energy. Energy values are measured for various states of the molecules, and are in good agreement with available spectroscopic data. The electron affinities of Br and I are found to be 3.53±0.12 and 3.13±0.12 ev, respectively.

INTRODUCTION

IT has been shown that the probability curves for excitation processes can be studied in ionization curves, and that, for the case of electron impact, the threshold law for such processes is one power of the excess energy less than that for direct single ionization.[1] If the theory of the factors which determine threshold laws is correct, the threshold law for excitation by photon impact should be one power less than that for excitation by electron impact. It has also been established by photoionization studies that the probability of a given electronic transition giving rise to direct single ionization, when induced by photon impact, can be approximated by a step function of the excess photon energy. A reasonable interpretation can be made on this basis of the photoionization efficiency curves for a number of simple molecules in terms of energy states, vibrational levels, etc.[2] The observation that the threshold law for direct single ionization by photon impact is a step function of the energy is also in accord with the theoretical suggestions made by Wannier[3] and Geltman.[4]

It is not possible, however, to account for all the features of photoionization efficiency curves in terms of a step-function threshold law. The curves obtained by Weissler *et al.*,[5] while not detailed, show pronounced peaks at certain energies. Similar peaks occur in the first derivative ionization efficiency curves obtained by electron impact, and these have been interpreted by Dorman, Morrison, and Nicholson[1] as being due to processes of autoionization, where the primary energy-dependent step is that of excitation, and that this is followed subsequently by an energy-independent step of ionization.

The present study of the photoionization efficiency curves for Br_2, I_2, HI, and CH_3I produces some direct evidence regarding the threshold law for excitation processes, and for the importance of autoionization. Fragment ions are observed in Br_2 and I_2, which arise in an ion-pair process, and this is reflected in the threshold law. The ionization efficiency curves for the parent ions for the iodine-containing molecules exhibit features which are quite inexplicable in terms of the step-function threshold law for direct single ionization, but which can be accounted for very satisfactorily in terms of autoionization processes. The data for the fragment ions, in combination with spectroscopic data, can be employed to give values for the electron affinities of the Br and I atoms.

EXPERIMENTAL RESULTS

The apparatus and the technique of measurement used are the same as those which have been described in an earlier paper.[2]

The photoionization efficiency curves for Br_2^+ and the Br^+ fragment ion are shown in Fig. 1. The curve for Br_2^+ is normal in shape, and its interpretation in terms of a step-function threshold law is straightforward. Apart from the curvature immediately at threshold, which is of the same magnitude as the photon energy spread, and is due to it, the curve is steepest at its foot. It is probable,[6] therefore, that the adiabatic ionization potential is being observed, and also that the adiabatic and vertical ionization potentials coincide at 10.53 ev. This suggests that the internuclear spacing in the ion is close to that in the neutral molecule, and that the electron ionized is a nonbonding one. This has been predicted on theoretical grounds.[7] A second threshold occurs at about 11.0 ev, but the data

* This work was supported jointly by the National Science Foundation, the Geophysics Research Directorate Air Force Cambridge Research Center, Air Research and Development Command and the U. S. Atomic Energy Commission.

† Commonwealth Fund Fellow 1956–1957, present address: Division of Chemical Physics, Commonwealth Scientific and Industrial Research Organization, Melbourne, Australia.

‡ Present address: C.I.B.A., Basle, Switzerland.

[1] F. H. Dorman, J. D. Morrison, and A. J. C. Nicholson, J. Chem. Phys. 32, 378 (1960).

[2] H. Hurzeler, M. G. Inghram, and J. D. Morrison, J. Chem. Phys. 28, 76 (1958).

[3] G. H. Wannier, Phys. Rev. 100, 1180 (1955).

[4] S. Geltman, Phys. Rev. 171, 102 (1956).

[5] G. L. Weissler, J. A. R. Samson, M. Ogawa, and G. R. Cook, J. Opt. Soc. Am. 29, 339 (1959).

[6] The reasons for this statement have been discussed in earlier papers, and will not be repeated here, cf. footnotes 1 and 2.

[7] R. S. Mulliken, Phys. Rev. 47, 413 (1935).

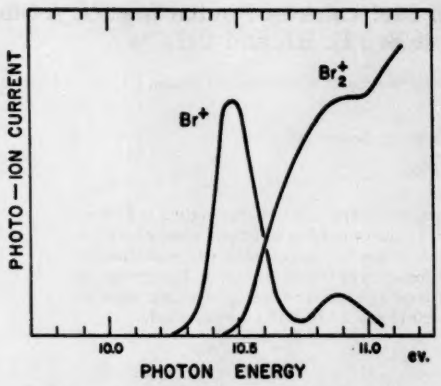

FIG. 1. Observed photoionization efficiency curves for Br_2^+ and $Br_{(Br_2)}^+$.

do not extend far enough to permit an accurate measurement of the vertical ionization potential for this state.

The curve for the Br^+ fragment ion is of interest, because its threshold occurs 0.2 ev below that of the parent ion. Clearly a measurement of the molecular ionization potential without a mass analyzer would have given an incorrect value. This possibility has been considered for this particular case by Watanabe,[8] following Price, from theoretical considerations. It does point out the need for care in accepting results obtained when mass analysis is not employed. The ionization efficiency for Br^+ rises to a maximum within 0.2 ev of threshold, and falls almost to zero again within the next 0.2 ev. It is followed by a second, smaller peak. The observed ionization efficiency curve is the product integral of three functions: the photon energy spread, which is a peak with a half-width in this case of about 0.04 ev; the function describing the threshold law appropriate to the process; and the electronic transition probability function. The last is given approximately by the reflection of the ground state eigenfunction in the potential curve for the upper state, and will be a peak which for bromine is unlikely to have a half-width in energy much less than 0.2 ev. It seems probable therefore that the threshold law for the process giving rise to the Br^+ ion can be approximated fairly closely by a delta function of the excess energy.

A delta-function threshold law would be expected for a process where there is one less degree of freedom for removal of the excess energy than that for direct single ionization by photon impact. This can occur only in a reaction of excitation, confirming that in this case the primary reaction is

$$Br_2 + h\nu \rightarrow Br_2^*.$$

The excited molecule subsequently dissociates to Br^+ and Br^-. Two possible potential curves might describe such an excited state of the molecule, and are shown as curves (a) and (b) in Fig. 2. The dissociation limit for this excited state can be obtained from the ionization efficiency data only if the Franck-Condon region intersects a curve of type (a) both above and below the dissociation limit, and this should be indicated by the profile of the observed peak. In the case of bromine it is not possible to make a definite decision. The peak, in Fig. 1, is slightly asymmetrical, but the threshold does not seem to be steep enough for its initial curvature to be due only to the photon energy spread. It is possible to measure the energy necessary for a vertical transition to this state, from the position of the peak maximum, as 10.48 ± 0.02 ev. It can be estimated from the curve that the dissociation limit is at least 0.2 ev less than this, i.e., ≤ 10.28 ev. Evidence that it is not less than 10.28 ev is obtained by the method of electron impact. Using a combination of a cylindrical electrostatic energy analyzer followed by sector type of mass analyzer a direct determination was made of the kinetic energy carried off by the Br^+ fragment ion. At an electron ionizing energy of 14 ev, the Br^+ ions possess a most probable kinetic energy of 0.15 ev, indicating a most probable total kinetic energy for the reaction of 0.3 ev with an error of about 0.1 ev. As the electron energy is reduced the most probable energy is decreased until at threshold, about 10.9 ev, the most probable energy is zero. Thus the Franck-Condon region does intersect the dissociation limit and the threshold for Br^+ appearance (shown in Fig. 1) can be taken as the dissociation limit.

The second peak in the Br^+ curve can be interpreted likewise as due to a second excitation-fragmentation process, with a vertical excitation potential of 10.88 ± 0.05 ev. This is 0.40 ev above the lower process, and is consistent with the energy difference (0.39 ev) between the $^3P_2$ and $^3P_1$ levels of the Br^+ ions.[9] The

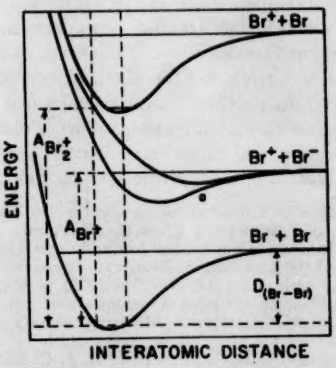

FIG. 2. Potential energy diagrams for the bromine molecule (schematic) based on its behavior under photon impact.

[8] K. Watanabe, J. Chem. Phys. 26, 542 (1956).

[9] C. E. Moore, "Atomic Energy Levels," Natl. Bur. Standards No. 67 (1952), p. 161.

TABLE I. The ionization and excitation potentials listed are the vertical values, i.e., they correspond to the energies at which the center of the Franck-Condon region intersects the upper state potential energy curves.

	Br_2	I_2	HI		CH_3I	
	This work	This work	This work	Spect.	This work	Spect.
Ionization potentials	10.53±0.03	9.3±0.1	10.4±0.1	10.39	9.55±0.1	9.54
	11.0±0.1	10.0±0.1		11.05	10.15±0.1	10.16
		10.9±0.1				
Excitation potentials of autoionizing states		9.39±0.02	10.50±0.02	10.45 10.49	9.62±0.02	9.61
		9.57±0.02	10.67±0.02	10.62 10.65	9.80±0.02	9.78
		9.68±0.02	10.80±0.05	10.78 10.82	9.90±0.02	9.90
Excitation potentials of ion-pair states	10.48±0.02	8.95±0.02				
	10.88±0.02	9.32±0.03				

electron affinity of bromine ($E_{(Br)}$) is given by the equation

$$-E_{(Br)}=10.28-I_{(Br)}-D_{(Br-Br)},$$

where $I_{(Br)}$ is the lowest ionization potential of the bromine atom, and $D_{(Br-Br)}$ is the dissociation energy of the bond in the ground state of Br_2. $I_{(Br)}$ and $D_{(Br-Br)}$ are known from spectroscopic data,[10] and give a value for $E_{(Br)}$ of 3.53 ev. This is in good agreement with the "best" value given by Pritchard[11] of 3.54 ev.

The data for the I_2^+ and I^+ ions from I_2, and for the parent ions from HI and CH_3I are shown in Fig. 3. The ionization efficiency curves for I_2^+, HI^+, and CH_3I^+ are closely similar, indicating clearly that the transitions involved in each are those of nonbonding $p\pi$ electron of the iodine atom. The curves are quite unlike that for the Br_2^+ ion, or that for any other molecule-ion formed by photon impact which has been studied so far in this detail. The curves have a well-defined threshold, rise to a sharp maximum within 0.1 ev, then decrease equally rapidly. The first maximum is followed by a second and a third, then by a region where the efficiency varies more slowly and in a more normal manner.

The theory of threshold laws for various ionization processes would again indicate that these sharp peaks are due to a process of excitation. The fact that a threshold curve for an excitation process is observed in a curve for ionization of a parent molecule can be accounted for only by assuming that a primary energy-dependent process of excitation is followed by an energy-independent step of autoionization. There must of course be a suitable ionized state present at a lower energy, so that the autoionization can occur into the energy continuum above it. At first sight it is not evident from the shape of the curves that such a state is present for the I-containing molecules. If the lowest ionized state and an excited state of the neutral molecule immediately above it are close together, the two different threshold laws would be difficult to distinguish. It is suggested that the observed curves are produced by the superposition of the sharp peaks due to the excitation-autoionization processes, on the normal type of threshold curve due to production of the molecular ions in their lowest states. The contribution due to this direct ionization may be obtained approximately by

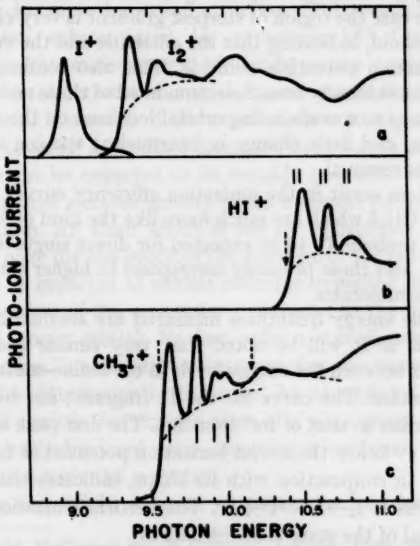

FIG. 3. Observed photoionization efficiency curves for (a) I_2^+ and $I_{(I)}^+$, (b) HI^+ and (c) CH_3I^+. The contribution due to direct ionization is shown by a broken line. Known ionization limits are indicated by arrows, and known Rydberg levels by short lines.

[10] G. Herzberg, *Spectra of Diatomic Molecules* (D. Van Nostrand Company, Inc., Princeton, New Jersey, 1950), 2nd ed.

[11] H. O. Pritchard; Chem. Revs. 52, 529 (1953).

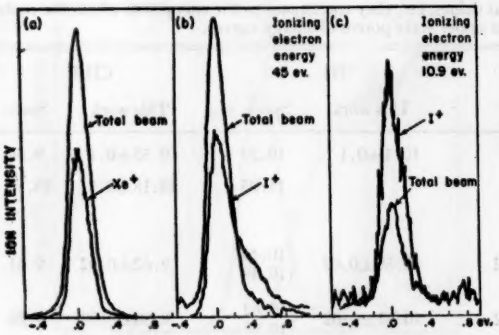

FIG. 4. Curves showing the distribution of kinetic energy for (a) Xe^+ ion used to calibrate the zero energy scale; (b) I^+ ion produced from I_2 by impact of 45 volt electrons; (c) I^+ ion produced from I_2 by impact of 10.9 volt electrons.

drawing smooth curves from the threshold through the successive minima of the observed curves. These are shown in Fig. 3 by broken lines.

A completely analogous phenomenon has been already observed in the ionization curves for N_2, O_2, and other molecules excited by electron impact.[1] In that case, because of the extra electron involved in the collision process, there is an additional degree of freedom, and the threshold laws for direct single ionization and autoionization are one power greater than those obtained by photon impact.

The ionization potentials of I_2, HI, and CH_3I are obtained from the maxima of the first derivatives of the dotted curves corresponding to direct ionization. In each case the region of steepest gradient is very close to threshold, indicating that the adiabatic and the vertical ionization potentials coincide. This also confirms that the most loosely bound electron in all of these molecules belongs to a nonbonding orbital localized on the iodine atom, and little change is internuclear spacing occurs on its removal.

Steps occur in the ionization efficiency curves for I_2 and CH_3I which are much more like the kind of ionization probability to be expected for direct single ionization, and these probably correspond to higher states of these molecules.

The energy quantities measured are summarized in Table I. It will be noted that very similar spacings occur between the energy levels in the iodine-containing molecules. The curve for the I^+ fragment ion from I_2 is similar to that of Br^+ from Br_2. The first peak occurs 0.35 ev below the lowest ionization potential of I_2, and this, in conjunction with its shape, indicates that the process is $I_2 \rightarrow I_2^* \rightarrow I^+ + I^-$. The vertical ionization potential of the state is 8.95 ± 0.02 ev.

The shape of the ionization efficiency curve for I^+ in (a), Fig. 3, leads to the conclusion that the actual threshold corresponding to the dissociation limit for the state may occur at an energy slightly less than the vertical ionization potential, at about 8.85 ± 0.1 ev. This would imply a most probable total kinetic energy of the fragments formed in the dissociation of 0.1 ev, so that the I^+ ions must carry off a most probable energy of 0.05 ev. A direct measurement was made of the kinetic energy of the I^+ ions, in a similar manner to that for the Br^+ ions. Typical results are shown in Fig. 4. At energies well above the threshold (b) Fig. 4, appreciable numbers of the I^+ ions have kinetic energies of the order of 0.4 ev. At energies of 10.9 ev down to 9.15 ev, i.e., 0.25 ev above threshold, the shape of the kinetic energy distribution (c) in Fig. 4 remains unchanged and similar to that for Xe^+ indicating that the average kinetic energy is zero within the experimental error, which is about ± 0.03 ev. Thus from the direct measurements, the most probable total kinetic energy might be as much as 0.06 ev, while from the profile of the photoionization curve it is estimated as 0.1 ev. The electron affinity for iodine may then be calculated as $E_{(I)} = 3.13 \pm 0.12$ ev. Pritchard's best value for $E_{(I)}$ is 3.23 ev. A second, less well-defined peak occurs at about 9.32 ± 0.03 ev which may be due to the production of I^+ and I^- from an excited state, corresponding to the similar feature in the Br^+ curve.

The structure in the curves for I_2 and the iodides is noticeably sharper than that for Br_2, being very little wider than the energy spread of the beam of ultraviolet radiation used in the experiments. This might be expected, in that the Franck-Condon region in the case of the iodine-containing molecules is appreciably narrower than it is for Br_2.

The interpretation of the structure as being due to autoionization receives strong support from spectroscopic work. Both CH_3I and HI have been studied in detail by Price.[12] In CH_3I, two Rydberg series are observed with limits at 9.54 and 10.16 ev, while in HI only one series tending to the upper ionization potential at 11.05 ev can be identified. In both molecules the Rydberg levels above the lower ionization potential show greatly enhanced absorption, and this is attributed by Price to autoionization. The energy values at which this strong absorption occurs are listed in Table I, and it will be seen that the agreement with the peaks in the ionization curve is excellent.

It may be stated, in conclusion, that the results on the iodides illustrate very clearly the importance in impact studies of using a beam of photons or electrons with a narrow energy spread. With an electron beam as usually used, the existence of the numerous autoionized levels is not even suspected.

[12] W. C. Price, J. Chem. Phys. 4, 539 (1936); Proc. Roy. Soc. (London) A167, 216 (1938).

Electron-Spin Resonance of Electrochemically Generated Free Radicals. Isomeric Dinitrobenzene Mononegative Ions*

AUGUST H. MAKI AND DAVID H. GESKE

Department of Chemistry, Harvard University, Cambridge, Massachusetts

(Received April 15, 1960)

The mononegative ions of *meta*-, *ortho*- and *para*-dinitrobenzene have been prepared in acetonitrile by controlled potential electrolysis within a microwave cavity and their electron spin resonance observed. The radical spectra exhibit hyperfine structure due to the isotropic magnetic interaction of the unpaired electron with the nitrogen and ring proton nuclear moments. Coupling constants were obtained with the aid of deuterium substitutions in the parent molecule. The nitrogen hyperfine coupling constants for the isomeric meta, ortho, and para anions were found to be 4.68, 3.22, and 1.74 gauss, respectively, and were identical for each of the two nitrogen nuclei of a given radical. Proton coupling constants range between 0.42 gauss and 4.19 gauss. The larger total hyperfine width of the *meta*-dinitrobenzene anion compared with the ortho and para isomers is ascribed to the existence of negative spin density in the π system of the first-mentioned radical and to the possibility of quinonoid resonance in the others which places considerable unpaired spin density in the oxygen nonbonding orbitals.

INTRODUCTION

(a) Electron-Spin Resonance of Free Radicals

THE study of nitrobenzene derivatives by electron-spin resonance (ESR) has been introduced by a report on the nitrobenzene mononegative ion.[1] This initial work, to be referred to as I, forms the basis for a second study of the three isomeric dinitrobenzene mononegative ions. These ions have been prepared by controlled potential reduction at a mercury pool electrode within a microwave cavity. The generated radicals are sufficiently stable that the ESR can be detected in the solution near the electrode surface.

ESR studies of solutions of aromatic free radicals[2] and singly charged ions[3] are already numerous. In general, dilute solutions of these free radicals exhibit complicated hyperfine structure; analysis of these structures leads to isotropic hyperfine coupling constants[4] of the unpaired electron with the various magnetic nuclei of the molecule. The hyperfine structure exhibited by aromatic hydrocarbon radicals must be assigned to protons, and since the interaction is not averaged out by molecular tumbling it must arise from the *s* character of the unpaired electron at the proton positions.[5]

A theoretical treatment of the problem by McConnell and Chestnut[6] has shown that a π-σ exchange interaction on aromatic carbon atoms causes a penetration of unpaired electron density into the σ system of the hydrocarbon. The magnitude of the coupling constant for a given proton, furthermore, is approximately proportional to the unpaired electron density in the π orbital of the contiguous carbon atom. For this reason proton hyperfine coupling constants are useful in "mapping" the unpaired electron distribution in the π system of the aromatic hydrocarbon radicals.

On the basis of this theory it is predicted that C^{13} and heteroatoms such as N^{14} and N^{15} should also give rise to isotropic hyperfine structure. This prediction has been substantiated by experiment.[1,7,8] Consequently, the measurement of the hyperfine coupling constants of heteroatom nuclei in aromatic radicals is also useful in a study of the unpaired electron distribution. For an sp^2 hybridized atom, the hyperfine interaction might be expected to be roughly proportional to the unpaired electron density in the π atomic orbital of that atom. An atom which is not sp^2 hybridized, but which none the less overlaps the π system of the radical, would be expected to exhibit isotropic hyperfine structure because of the zero order *s* character in the interacting atomic orbital. No first-order π-σ configuration interaction is necessary to account for the isotropic hyperfine interaction in this case. An example of this type of atom is the nitrogen atom of a nitro group that is sterically hindered from assuming a coplanar configuration with the π system.

The three dinitrobenzene mononegative ions form a

* Presented at the 1960 Annual Meeting of the American Physical Society, New York, New York, January 27, 1960.

[1] D. H. Geske and A. H. Maki, J. Am. Chem. Soc. **82**, 2671 (1960).

[2] C. A. Hutchison, Jr., R. C. Pastor, and A. Kowalsky, J. Chem. Phys. **20**, 534 (1952); H. S. Jarrett and C. J. Sloan, *ibid.* **22**, 1783 (1954); P. Sogo, M. Nakazaki, and M. Calvin, *ibid.* **26**, 1343 (1957); E. Müller, K. Ley, K. Schleffer, and K. Mayer, Chem. Ber. **91**, 2682 (1958).

[3] B. Venkataraman and G. K. Fraenkel, J. Am. Chem. Soc. **77**, 2797 (1955); J. Chem. Phys. **23**, 588 (1955); B. Venkataraman, B. G. Segal, and G. K. Fraenkel, *ibid.* **30**, 1006 (1959); D. Lipkin, D. E. Paul, J. Townsend, and S. I. Weissman, Science **117**, 534 (1953); D. E. Paul, D. Lipkin, and S. I. Weisman, J. Am. Chem. Soc. **78**, 116 (1956); E. de Boer and S. I. Weissman, *ibid.* **80** 4549 (1958); M. Adams, M. S. Blois, Jr., and R. H. Sands, J. Chem. Phys. **28**, 774 (1958).

[4] E. Fermi, Z. Physik **60**, 320 (1930).

[5] S. I. Weissman, J. Chem. Phys. **22**, 1378 (1954).

[6] H. M. McConnell and D. Chestnut, J. Chem. Phys. **28**, 107 (1958).

[7] T. R. Tuttle and S. I. Weissman, J. Chem. Phys. **25**, 189 (1956).

[8] R. L. Ward and M. P. Klein, J. Chem. Phys. **28**, 518 (1958); **29**, 678 (1958); R. L. Ward, *ibid.* **30**, 852 (1959).

natural series for study by ESR for the following reasons:

(i) They are all stable enough to be studied by the electrolytic method within the microwave cavity.[1,9]

(ii) Resonance theory[10] predicts widely different electronic structures for them and ESR hyperfine structure should reflect these differences.

(iii) They form a complete, isomeric set.

(b) Polarography and Free Radicals

The first paper on the subject of polarography was published in 1922.[11] Since then, chemical transformations occurring at the surface of a microelectrode have been the subject of extensive research. A potential is applied between a microelectrode and a large *reference electrode* and the resulting current through the cell is measured. A current-potential plot of this type is called a polarogram. An inert electrolyte, such as potassium nitrate, is also present to increase the conductivity of the solution and is called a *supporting electrolyte*. A less rudimentary description of this method is beyond the scope of this paper; the reader is referred to a standard text, such as Kolthoff and Lingane.[12]

The substance being investigated is dissolved in a suitable solvent, frequently water. Recent work with organic solvents substituted for water has greatly extended the usefulness of polarography in the study of organic systems. Work by Hoijtink *et al.*[13] has shown that in 96% dioxane the reduction of anthracene and other hydrocarbons at a mercury drop is represented by the sequence:

$$R+e^- \rightleftharpoons \cdot R^- \qquad (1)$$

$$\cdot R^- + e^- \rightleftharpoons R^{--}. \qquad (2)$$

Both reactions are reversible and (2) occurs at a more negative potential than (1). Addition of a proton donor such as water or hydrogen iodide to the solvent causes the substitution of the following irreversible sequence, which takes place at the potential of (1):

$$R+e^- \rightleftharpoons \cdot R^- \xrightarrow{H^+} \cdot RH \xrightarrow{e^-} :RH^- \xrightarrow{H^+} RH_2. \qquad (3)$$

Austin *et al.*[14] have used ESR to confirm the existence of free radicals in the controlled potential reduction of anthracene, benzophenone, and anthraquinone, using the aprotic solvent *N*,*N*-dimethylformamide. Samples were removed during electrolysis and frozen. The ESR was detected at liquid oxygen temperature.

Thus, it becomes apparent that, if controlled potential reduction were carried out at a potential at which (1) occurred but (2) did not occur, and in an aprotic solvent so that the sequence (3) were suppressed, the mononegative ions could be generated and their ESR observed. This is the basis of the method that is used here to generate the free radical ions. The electrode at a controlled potential is a versatile, selective reducing agent.

Preliminary polarography of a solution of *R* (which need not be a hydrocarbon) is done to verify that one-electron reduction occurs and is polarographically reversible. Subject to the condition that the mononegative ions is sufficiently stable, its study by ESR is possible.

Acetonitrile (CH_3CN) was chosen as the solvent in this study and tetra-*n*-propylammonium perchlorate as the supporting electrolyte. As in I, a small mercury pool was used as the polarizable electrode. The part of the electrolytic cell containing the mercury pool was placed inside the microwave cavity of the ESR spectrometer so that the portion of the solution immediately above the microelectrode was in the region of maximum r magnetic field. Radicals were then generated by applying a previously determined potential between the mercury pool and a saturated calomel reference electrode. As the negative ions were formed at the surface and diffused into the solution they were directly detected by the ESR spectrometer. Since the radicals were present in solution, the resonances were characterized by well-resolved hyperfine structure.

The advantages of this method of free radical generation in comparison with the conventional alkali metal reduction are threefold. Since these have been elaborated in I, they will only be outlined here.

(i) Alkali metal ions are eliminated from the solution of the radical anion.

(ii) Complicating effects of ion association are minimized by use of a relatively high dielectric constant solvent along with a bulky (tetra-*n*-propyl-ammonium) counter ion.

(iii) Since the potential of the microelectrode is controlled during electrolysis, we have reasonable assurance that no reaction other than the reversible one-electron transfer (indicated by polarographic criteria for reversibility) is taking place at the electrode.

It is necessary to mention a limitation in this method of radical study. Free radicals, as they are produced at the surface of the mercury pool, are in a region of relatively low filling factor and must diffuse upwards away from the metallic surface before they enter a region of reasonable sensitivity. Also, the electrolysis current is limited by the rate of diffusion of the parent molecules to the electrode surface. Both of these conditions limit the technique described in this paper to the study of relatively long-lived radicals. With our spectrometer we have found that radicals with lifetimes of five minutes could be conveniently studied by this method.

[9] A. H. Maki and D. H. Geske, J. Chem. Phys. **30**, 1356 (1959).
[10] L. Pauling, *The Nature of the Chemical Bond* (Cornell University Press, Ithaca, New York, 1960), 3rd ed.
[11] J. Heyrovsky, Chem. Listy **16**, 256 (1922).
[12] I. M. Kolthoff and J. J. Lingane, *Polarography* (Interscience Publishers, New York, 1952), 2nd ed.
[13] G. J. Hoijtink, J. van Schooten, E. deBoer, and W. J. J. Aalbersberg, Rec. trav. chim. **73**, 355 (1954).
[14] D. E. G. Austin, P. H. Given, D. J. E. Ingram, and M. F. Peover, Nature **182**, 1784 (1958).

We have made some preliminary investigations of electrolytic reduction of hydrocarbons including naphthalene, anthracene, acenapthene, diphenylene, triphenylene, and coronene within the microwave cavity. Preliminary polarography indicated that in each case the electrode reaction in acetronitrile was a reversible one-electron transfer. ESR has been observed in each case. All but the triphenylene and coronene negative ions exhibited a well-resolved hyperfine structure. Triphenylene and coronene negative ions gave broad resonances with little resolution. This result is in agreement with the findings of Townsend and Weissman,[15] who attribute this lack of resolution to a Jahn-Teller effect.

EXPERIMENTAL

(a) ESR Spectrometer

The ESR spectrometer is of conventional design and employs a cylindrical microwave reflection cavity operated in the TE_{011} mode. The resonant frequency of the cavity containing the electrolysis cell is about 9200 Mc. A proton resonance spectrometer locked to a BC-221 frequency meter is used to monitor the magnetic field, which is modulated at 280 cps and slowly swept through the ESR spectrum of the sample. The amplitude of the modulation is kept smaller than the line width of the resonances to obtain maximum resolution. The Varian, Inc. X-13 klystron is immersed in a bath of mineral oil for cooling and thermal stabilization. In addition, it is locked to the sample cavity frequency by a modified Pound stabilization circuit that operates at 100 kc.

(b) Electrolysis Cell

The electrolysis cell consists of a 3-mm o.d. Pyrex tube sealed over a platinum wire at the lower end. The microelectrode is a small mercury pool at the bottom of this tube and makes electrical contact with the platinum. The tube extends into the center of the cylindrical microwave cavity and is attached at the upper end to the main compartment of the cell; the whole is filled with the solution to be electrolyzed. The upper compartment contains a fritted tube through which prepurified nitrogen is bubbled to exclude atmospheric oxygen from the solution. A subcompartment is separated from the main compartment by a sintered disk. The solution in this compartment is connected by means of a salt bridge to the reference electrode, which is a large aqueous saturated calomel electrode (SCE). A potential is applied between the SCE and the mercury microelectrode by means of a simple potentiometer circuit. A microammeter is used to monitor the current through the cell.

[15] M. G. Townsend and S. I. Weissman, J. Chem. Phys. **32**, 309 (1960).

TABLE I. Polarographic data. 0.1 *M* tetra-*n*-propylammonium perchlorate supporting electrolyte in acetonitrile at 25.0°.

	$-E_{1/2}$, v vs SCE	$-(E_{3/4}-E_{1/4})$ mv	I_d[e]
meta-Dinitrobenzene[a]	0.90	61	4.19
	1.25	63	3.61
	2.01	d	10.24
ortho-Dinitrobenzene	0.81	52	4.17
	1.06	57	3.20
	2.54	d	19.3
para-Dinitrobenzene	0.69	53	4.99
	0.89	58	3.56
	ca 2.5	d	f
Nitrobenzene[b]	1.15	56	4.07
	1.9[c]	...	7.5

[a] These data contradict the report of L. Holleck, R. Schindler, and O. Löhr, Naturwissenschaften **46**, 625 (1959) that *meta*-dinitrobenzene has an irreversible wave at −1.200 v in acetonitrile.

[b] Data from I.

[c] Wave distorted by maximum.

[d] Wave was irreversibly drawn out.

[e] I_d represents the quantity $i_d/m^{2/3}t^{1/6}C$, where i_d is the maximum diffusion current in microamperes, m the drop-weight in mg sec^{-1}, t is the drop time in seconds, and C is the millimolar concentration of electroactive material. I_d is given for individual waves.

[f] Drawn-out wave did not have a diffusion current plateau.

(c) Electrolytic Radical Generation

In the case of each isomer the electrolysis within the microwave cavity was carried out at a potential just on the plateau of the first reduction wave, or at a potential about 100 mv more negative than the half-wave potential. The current-time behavior of the system was similar to that described for nitrobenzene in I. Good spectra were obtained after about fifteen minutes of electrolysis; after this the number of radicals in the cavity appeared to have become approximately constant. Successive tracings of spectra over the period of one to two hours showed no significant differences. During one run with a solution of *para*-dinitrobenzene, the electrolysis current was discontinued while the most prominent hyperfine component in the spectrum was observed. The ESR signal was observed to decay with a time constant of about five minutes. This is a much shorter time than would be required for a significant fraction of the radicals to diffuse out of the microwave cavity and is attributed to the decay of the radical. Since no new lines were observed in the spectrum, the decay must be products which do not exhibit ESR, probably diamagnetic products. This time interval (five minutes) is about the same as that associated with a color change from greenish yellow to red, which may be observed if the electrolysis is carried out outside of the cavity.

(d) Synthesis of Deuterium Substituted Compounds

1,3-Dinitrobenzene-5-d_1

3,5-Dinitroaniline, prepared according to the pro-

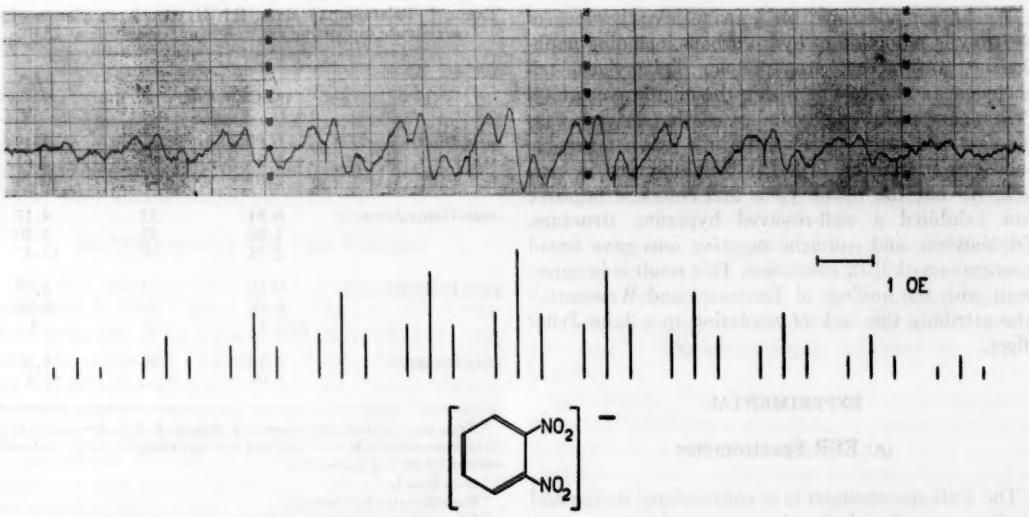

FIG. 1. Derivative of electron-spin resonance absorption spectrum vs magnetic field strength for *o*-dinitrobenzene anion in acetonitrile (upper portion); spectrum calculated using coupling constants of Table II shown to scale (lower portion).

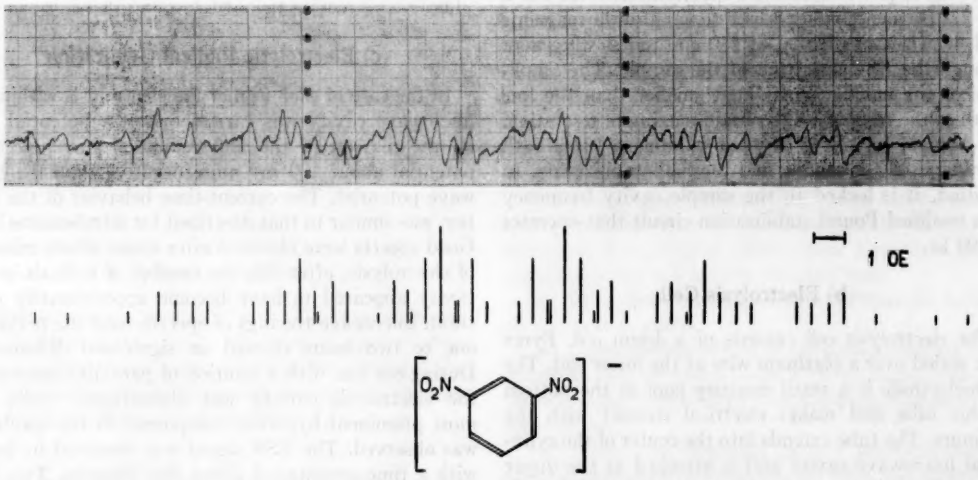

FIG. 2. Derivative of electron-spin resonance absorption spectrum vs magnetic field strength for *m*-dinitrobenzene anion in acetonitrile (upper portion); spectrum calculated using coupling constants of Table II shown to scale (lower portion).

cedure of Blanksma and Verberg,[16] was diazotized by dissolution in *deutero*nitrosylsulfuric acid[17] at 0°. *Deutero*hypophosphorous acid was added to reduce the diazonium compound to the dinitrobenzene. The reduction reaction was accelerated by diluting the reaction mixture with deuterium oxide. The solid material which precipitated had a melting point of 90.0° after one recrystallization from water. Mass spectral analysis showed 83% monodeuteration.

[16] J. J. Blanksma and G. Verberg, Rec. trav. chim. **53**, 988 (1934).
[17] L. Welsh, J. Am. Chem. Soc. **63**, 3276 (1941).

1,3-Dinitrobenzene-d_4

Benzene-d_6 (99.5% isotopic purity) obtained from Merck Company, Ltd., Montreal, Canada, was nitrated with potassium nitrate in concentrated *deutero*sulfuric acid. After recrystallization from an ethanol-water mixture the 1,3-dinitrobenzene-d_4 had a melting point of 90.0°.

1,2-Dinitrobenzene-3,5-d_2

2-Nitro-3-aminosulfonic acid was hydrolyzed to 2-

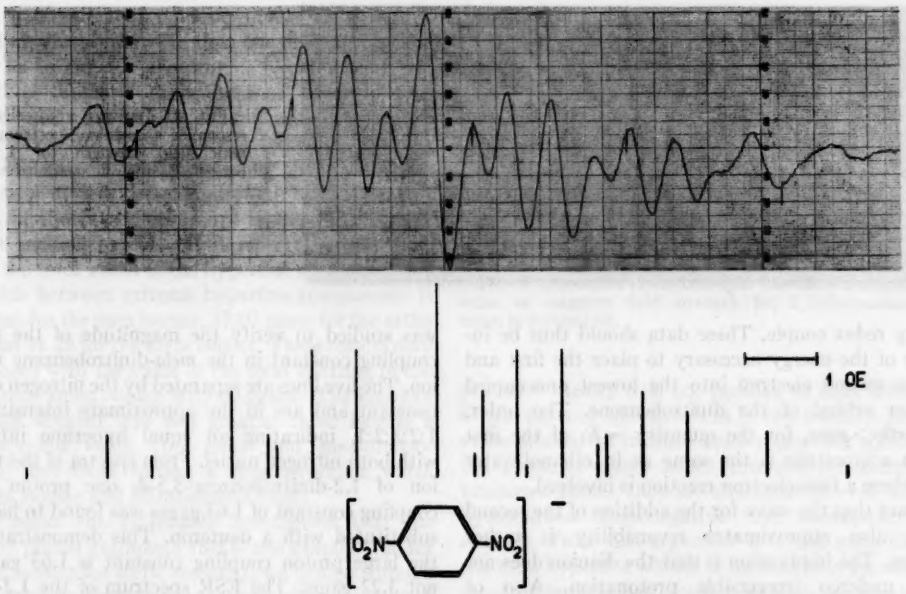

FIG. 3. Derivative of electron-spin resonance absorption spectrum vs magnetic field strength for *p*-dinitrobenzene anion in acetonitrile (upper portion); spectrum calculated using coupling constants of Table II shown to scale (lower portion).

nitroaniline-3, 5-d_2[18] by refluxing for 30 min in 56% *deutero*sulfuric acid in deuterium oxide. The nitroaniline was oxidized to 1,2-dinitrobenzene-3,5-d_2 (mp 115°) with trifluoroperoxyacetic acid.[19] Mass spectrometric analysis showed 94.9% dideuteration and 4.5% monodeuteration.

1,2-Dinitrobenzene-3-d_1

2,3-Dinitroaniline was prepared by nitration of *m*-nitroacetanilide[20] followed by hydrolysis in concentrated sulfuric acid.[20] The amine was diazotized with *deutero*nitrosylsulfuric acid in the presence of *deutero*phosphoric acid.[17] The reduction with *deutero*hypophosphorous acid was accelerated by dilution of the reaction mixture with deuterium oxide. After two recrystallizations from water the melting point was 116°. Mass spectrometric analysis showed 87.5% monodeuteration.

RESULTS

(a) Polarography

The polarography of the dinitrobenzenes has been studied in various ethanol-water mixtures.[21–23] Two reduction waves were observed for each isomer. The half-wave potentials are all dependent on the *p*H of the media. Pearson reports that the first wave represents the four-electron reduction of the dinitrobenzene to the corresponding monohydroxylamine. Polarographic data have also been obtained in concentrated sulfuric acid[24] and glacial acetic acid.[25] While a systematic polarographic study of reduction of the dinitrobenzenes in acetonitrile was beyond the scope of the present project, preliminary data (Table I) were obtained for a single concentration (*ca* one millimolar) of each isomer. For each isomer three waves were observed, the first two being approximately equal in magnitude and the third being significantly larger.[26]

One criterion for a reversible wave is that $E_{3/4} - E_{1/4} = -56$ mv for a one-electron reaction at 25°. Since this criterion is approximately fulfilled for both the first and second waves (Table I) the $E_{\frac{1}{2}}$ values are essentially equal to the standard reduction potential for the corre-

[18] While assignment of one deuterium to the 3-position is unequivocal because of the hydrolysis of the sulfonic acid group, the assignment of the second deuterium to the 5-position is based on assumed ring-activation of the 5-position. The electron spin resonance spectrum of the corresponding anion radical is consistent with this formulation.

[19] W. D. Emmons, J. Am. Chem. Soc. **76**, 3470 (1954).

[20] K. H. Pausacker and J. G. Scroggie, J. Chem. Soc. **1955**, 1897.

[21] J. Pearson, Trans. Faraday Soc. **44**, 683 (1948).

[22] S. F. Dennis, A. S. Powell, and M. J. Astle, J. Am. Chem. Soc. **71**, 1484 (1949).

[23] E. Gergely and T. Iredale, J. Chem. Soc. **1953**, 3226.

[24] J. C. James, Trans. Faraday Soc. **47**, 1240 (1951).

[25] I. Bergman and J. C. James, Trans. Faraday Soc. **48**, 956 (1952).

[26] The quantity I_d in Table I is approximately proportional to the number of electrons involved in the reactions. The fact that the I_d value for the second wave is somewhat smaller than the first remains unexplained. Similar behavior has been observed by S. Wawzonek, R. Berkey, E. W. Blaha, and M. E. Runner, J. Electrochem. Soc. **103**, 456 (1956), in the reduction of quinones in acetonitrile.

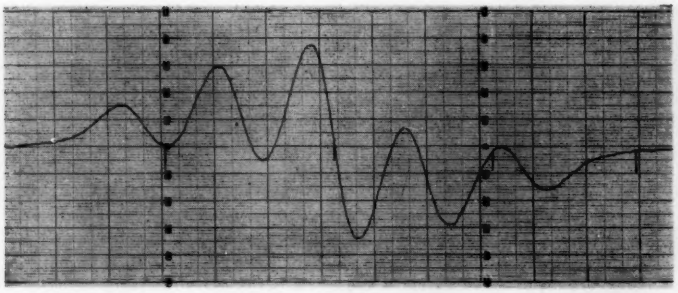

FIG. 4. Derivative of electron-spin resonance absorption spectrum vs magnetic field strength for 1,3-dinitrobenzene-d_4 anion in acetonitrile.

sponding redox couple. These data should thus be indicative of the energy necessary to place the first and then the second electron into the lowest unoccupied molecular orbital of the dinitrobenzene. The order, *meta*>*ortho*>*para*, for the quantity $-E_{\frac{1}{2}}$ of the first wave in acetonitrile is the same as in ethanol-water media where a four-electron reaction is involved.

The fact that the wave for the addition of the second electron also approximates reversibility is rather surprising. The implication is that the dianion does not rapidly undergo irreversible protonation. Also of interest is the observation that the difference between the half-wave potentials for the first and second waves varies for the three isomers. This probably reflects the difference in coulomb repulsion energy of two electrons in the lowest unoccupied molecular orbital of the three isomers, since it may be argued that the solvation energies of the ions are comparable.

(b) ESR

Derivatives of the ESR absorption spectra of the three isomeric dinitrobenzenes are displayed in Figs. 1–3. Directly below each spectrum is the calculated absorption spectrum based upon the coupling constants given in Table II. Only in the case of *p*-dinitrobenzene negative ion is the assignment of coupling constants to specific nuclei of the radical possible without isotopic substitution, and this is done on the basis of relative intensity considerations. In the other cases deuterium substituted molecules were prepared and the negative ions investigated.

The line widths are about 0.35 gauss between points of maximum slope for each of the undeuterated ions. Spectra of the deuterium substituted ions have broader lines when the deuterium hyperfine structure is not resolved and therefore contributes to the line width. In each case, the observed spectrum was compared with spectra calculated on the basis of the several possible coupling constants for the substituted proton(s). There was only one obvious assignment in each case. Spectra of the negative ion of 1,3-dinitrobenzene-5-d_1 were consistent with the assumption that the substituted proton has a coupling constant of 1.08 gauss and not 3.11 gauss The spectrum of the negative ion of 1,3-dinitrobenzene-d_4 is shown in Fig. 4. This ion was studied to verify the magnitude of the nitrogen coupling constant in the *meta*-dinitrobenzene negative ion. The five lines are separated by the nitrogen coupling constant and are in the approximate intensity ratios 1:2:3:2:1, indicating an equal hyperfine interaction with both nitrogen nuclei. From spectra of the negative ion of 1,2-dinitrobenzene-3,5-d_2 one proton with a coupling constant of 1.63 gauss was found to have been substituted with a deuteron. This demonstrated that the large proton coupling constant is 1.63 gauss and not 3.22 gauss. The ESR spectrum of the 1,2-dinitrobenzene-3-d_1 identified the substituted proton as one of the pair with the small 0.42 gauss coupling constant. In this case the doublet structure resulting from the remaining proton with 0.42 gauss coupling constant is clearly evident, since the deuterium nuclear moment produces no significant line broadening. The derivative spectrum of 1,2-dinitrobenzene-3-d_1 negative ion is shown in Fig. 5.

DISCUSSION OF RESULTS

The electron-spin resonance spectra presented in the last section are all consistent with the full molecular symmetry of the parent dinitrobenzene isomer. Protons and nitrogen nuclei that are interchanged by covering operations of the molecule are characterized by the same hyperfine coupling constant. Our results on the *meta*-dinitrobenzene negative ion are thus in disagreement with results recently reported by Ward,[27] who finds one dominant nitrogen coupling constant of 9.0 gauss in solutions of *meta*-dinitrobenzene in 1,2-dimethoxyethane which has been reduced with metallic potassium. We do not understand this result on the basis of a simple *meta*-dinitrobenzene negative ion. Possibly, ion pairing between metal and radical ions in 1,2-dimethoxyethane might sufficiently perturb the symmetry of the electron distribution of radicals to give the observed result, but it is also possible that reduction reaction might have proceeded beyond a simple electron transfer, in which case the identity of the radical remains to be determined. The large value of the single nitrogen coupling constant is characteristic of negative ions of aromatics containing but one nitro

[27] R. L. Ward, J. Chem. Phys. **32**, 410 (1960).

group in the ring.[28] One would expect a smaller value of the coupling constant if more than one nitro group were involved as an electron acceptor.

The three isomeric dinitrobenzene negative ions generated electrochemically exhibit widely divergent hyperfine structure. This behavior indicates that the unpaired electron distribution among the atoms comprising the π system depends strongly on the relative positions of the two nitro groups in the ring. One of the most striking aspects of the spectra is the large range of the total width of the hyperfine structure. This total width between extreme hyperfine components is 11.44 gauss for the para isomer, 17.00 gauss for the ortho isomer and 31.28 for the meta isomer. These results may be compared with the value of the total splitting in the nitrobenzene anion, which is 33.60 gauss.[1] The ions can be roughly divided into two groups: those having a small hyperfine width (the *ortho-* and *para*-dinitrobenzenes) and those having a large hyperfine width (the meta isomer and nitrobenzene itself).

If we make the reasonable assumption that the anions are planar (although this is not exactly true for the ortho isomer for steric reasons), we can go through the process of starring alternant atoms of the π system,[29] regardless of whether they are carbon atoms or heteroatoms. We do this in such a way that at least one nitrogen atom is starred. The nitrobenzene negative ion under the starring process is analogous to an odd alternant hydrocarbon radical. The *meta*-dinitrobenzene anion is similarly analogous even though it has an even number of atoms, because no covering operation of the molecule interchanges starred and unstarred atoms. It is then possible that negative spin density occurs in the p_z orbitals of the unstarred atoms of these two radicals. This is a result which is already familiar for hydrocarbon radicals[6,30] and which has recently been rigorously proved.[31] Clearly it is not possible to have alternation in the signs of spin densities in the isomeric para and ortho anions, for in these cases a covering operation of the molecule exists which interchanges starred and unstarred atoms; they are analogous to even alternant hydrocarbon mononegative and monopositive ion radicals. From this argument it is not surprising that the total hyperfine widths of the ions that are analogous to odd alternant hydrocarbon radicals are greater than the widths of those analogous to even alternant hydrocarbon ions. No attempt is made to make this argument on as quantitative a basis as it has been made for hydrocarbons. We lack knowledge of the spin densities on the oxygen atoms and do not have quantitative relationship between the spin distribution in the π system vicinal to the nitrogen atom and its hyperfine coupling constant.

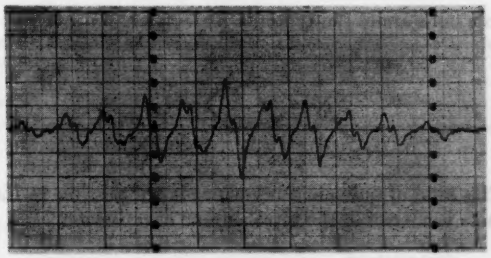

FIG. 5. Derivative of electron-spin resonance absorption spectrum vs magnetic field strength for 1,2-dinitrobenzene-3-d_1 anion in acetonitrile.

It is noteworthy that the ring proton coupling constants of both the nitrobenzene and *meta*-dinitrobenzene anions suggest the alternation of positive and negative spin densities since the proton interaction on unstarred carbon atoms is about $\frac{1}{3}$ to $\frac{1}{4}$ that on starred carbon atoms. For instance, this result may be compared with the perinapthenyl radical[32] for which this ratio is 0.30.

The nitrogen coupling constants might be expected to be about the same in the ortho and para anions. The larger nitrogen coupling constant in the ortho isomer can be explained on the basis of a steric effect. The nitro groups cannot be coplanar with the ring and consequently some *s* character is expected to occur in the π orbitals of the nitrogen atoms.[33]

Another effect which undoubtedly contributes to the smaller total hyperfine width of the *para* and *ortho* isomers is the possibility of quinonoid type resonance,[10] which would be expected to result in considerable unpaired electron density in the oxygen nonbonding orbitals of these isomers. The pertinent bond eigen-

TABLE II. Absolute values of nitrogen and proton hyperfine coupling constants.

	Hyperfine coupling constants (gauss)					
Anion	$\lvert A_N \rvert$	$\lvert A_2 \rvert$[c]	$\lvert A_3 \rvert$	$\lvert A_4 \rvert$	$\lvert A_5 \rvert$	$\lvert A_6 \rvert$
1,2-Dinitrobenzene	3.22[b]	...[d]	0.42	1.63	...	...
1,3-Dinitrobenzene	4.68[b]	3.11	...	4.19	1.08	...
1,4-Dinitrobenzene	1.74[b]	1.12	...	...	...	...
1-Nitrobenzene[a]	10.32	3.39	1.09	3.97	...	...

[a] Values from I.
[b] Both nitrogen nuclei interact equally.
[c] The proton which interacts with $\lvert A_i \rvert$ is the one bonded to the ith ring carbon atom. Carbon atoms are numbered cyclically.
[d] A position without an entry is either occupied by the second nitrogen atom, or the coupling constant is given by the position(s) related to it by the covering operation(s) of the ion.

[28] A. H. Maki and D. H. Geske, unpublished work on negative ions of various substituted nitrobenzenes.
[29] C. A. Coulson and G. S. Rushbrooke, Proc. Cambridge Phil. Soc. **36**, 193 (1940).
[30] P. Brovetto and S. Ferroni, Nuovo cimento **5**, 142 (1957).
[31] A. D. McLachlan, Mol. Phys. **2**, 223 (1959).
[32] P. B. Sogo, M. Nakazaki, and M. Calvin, J. Chem. Phys. **26**, 1343 (1957).
[33] S. I. Weissman, J. Chem. Phys. **25**, 890 (1956).

functions are of the type:

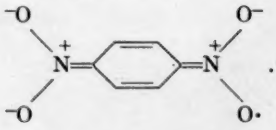

This kind of quinonoid resonance is not possible in the meta isomer or in the nitrobenzene negative ion.

ACKNOWLEDGMENTS

The mass-spectrographic analysis of the deuterated species was done by Professor Klaus Biemann of the Massachusetts Institue of Technology, to whom we are deeply grateful.

Financial support for this work has been provided by the National Institutes of Health and the National Science Foundation.

THE JOURNAL OF CHEMICAL PHYSICS VOLUME 33, NUMBER 3 SEPTEMBER, 1960

Diamagnetism as a Test of Wave Functions for Some Simple Molecules

K. E. BANYARD

Department of Physics, University of Leicester, Leicester, England

(Received April 18, 1960)

A theoretical study is made of the diamagnetism of some simple molecules in a gaseous form, attention being mainly devoted to the "neon-like" series Ne, H_2O, NH_3, and CH_4. In this way an attempt is made to gain insight into the way in which the radial electron density distribution within the molecules is influenced, firstly, by the allowance of exchange effects and secondly, by the inclusion of angular terms which must be accounted for in any "physically real" description of the electron density.

In general, it is found that exchange effects cause the radial density distribution to contract, while the inclusion of angular terms results in the subsequent radial electron density becoming more diffuse.

INTRODUCTION

IT has been demonstrated recently[1] that by adopting central-field wave functions it was possible to provide a very satisfactory theoretical interpretation of the x-ray scattering to be observed from the series of "neon-like" molecules Ne, H_2O, NH_3, and CH_4, all in gaseous form. Such an approach was amply justified by a detailed study of the water molecule.[2] Here it was shown that, for such a series, angular terms when included in the density made an almost negligible contribution to the resulting x-ray scattering factor, the major contribution arising from the radial or spherically symmetrical density term. Thus it was seen that, for this series of molecules, the use of central-field analytical wave functions of determinantal form does tend to provide a radial distribution of electrons which is a good first approximation to the true electron density within the molecule when averaged over angles.

Nevertheless, while the over-all radial density distribution may be accounted for quite satisfactorily by using a central-field method, it is only to be expected that the averaged density in the outer regions of the molecule may not be very adequately described in detail by such an approach. A physical quantity which is comparatively sensitive to the radial distribution of the outer electrons is the diamagnetic susceptibility. Recently Weltner[3] has provided, for this series of molecules, values for the subsidiary paramagnetic contribution to this quantity based on other experimental observations, thus rendering the determination of the total susceptibility a more tractable problem. The major contribution, or purely diamagnetic part, of the total susceptibility may then be determined from the electron density after averaging over angles.

Such calculations were performed using various approximate results for the electron density. Hence, by comparing the theoretical susceptibility with the observed value it is hoped to demonstrate how the radial density distribution (i.e., the electron density within the molecule when averaged over angles) is influenced not only by including exchange effects but also by making allowance for angular terms which must be accounted for in any realistic description of the density within polyatomic molecules.

CALCULATION OF THE DIAMAGNETIC SUSCEPTIBILITY

Van Vleck[4] has shown that the diamagnetic susceptibility χ for a molecule may be expressed as

$$\chi=\chi_r+\chi_{hf}, \quad (1)$$

[1] K. E. Banyard and N. H. March, Acta Cryst. **9**, 385 (1956).
[2] K. E. Banyard and N. H. March, J. Chem. Phys. **26**, 1416 (1957).
[3] W. Weltner, J. Chem. Phys. **28**, 478 (1958).
[4] J. H. Van Vleck, *Theory of Electric and Magnetic Susceptibilities* (Oxford University Press, London, 1932).

TABLE I.[11] Results for the neon-like molecules.

	Bond length in a.u.	χ^a (Pascal)	Experimental χ	Experimental χ_{hf}	Experimental χ_r	Theoretical χ_r	Comment
Ne	...	...	-6.75^d	...	-6.75^d	-5.8	Using analytical central-field wave functions with exchange
H_2O	1.81[b]	-10.5	-13.0^e	1.46^e	-14.46	-12.5	
NH_3	1.91[b]	-14.4	-18.7^e	4.3^e	-23.0	-18.8	
CH_4	1.975[c]	-17.7	-12.2^f / -16^g	9.3^e	-21.5 / -25.3	-26.3	
NH_4^+	1.836[c]	...	-13.3^h / -14.5^i	6.1	-19.4 / -20.6	-17.0	

[a] See footnote reference 10.
[b] See footnote reference 1.
[c] See footnote reference 9.
[d] P. W. Selwood, *Magnetochemistry* (Interscience Publishers, Inc., New York, 1943), p. 34.
[e] See footnote reference 3.
[f] See footnote reference 12.
[g] See footnote reference 13.
[h] See footnote reference 19.
[i] See footnote reference 20.

where χ_r represents a purely diamagnetic contribution arising from the Larmor precessional effect. On the other hand, χ_{hf} is a temperature-independent paramagnetic term which vanishes for the case of atoms as a result of their spherically symmetrical nuclear field. This "high-frequency" contribution to χ is extremely difficult to calculate since it basically involves a knowledge of all excited electronic states within the molecule. However, Eshbach and Strandberg[5] have shown that χ_{hf} may be determined from a knowledge of the experimental molecular rotational magnetic moment. Using this approach, Weltner[3] has given χ_{hf} for various molecules, the results for H_2O, NH_3, and CH_4 being reproduced in Table I. For NH_4^+, with an experimental bond length N–H of 1.937 atomic units,[6] the value of χ_{hf} was estimated in a manner similar to that outlined by Weltner for CH_4.

The term χ_r can be written as

$$\chi_r = -0.7923 \int_0^\infty 4\pi r^2 \rho(r) \cdot r^2 \cdot dr, \qquad (2)$$

where $4\pi r^2\rho(r)$ is the radial density distribution within the molecule such that if N is the total number of electrons then

$$\int_0^\infty 4\pi r^2 \rho(r) dr = N.$$

Equation (2) is expressed in atomic units[7] which were used throughout this work. Since the values of χ_{hf} given by Weltner are referred to the center of mass of the molecule as origin, it was found more convenient to express χ_r with respect to this point. It is perhaps worth adding that the change in χ_r for H_2O and NH_3 due to this shift in origin away from the "central" atom was fairly small. Thus all values given in Table I refer to the center of mass as origin.

Since the values of χ_{hf} are essentially based upon experimental observations it was decided to compare our theoretical χ_r with the "experimental" value derived from the observed total suceptibility χ and χ_{hf}. The results of the calculations for Ne, H_2O, NH_3, CH_4 and NH_4^+ using central-field wave functions of determinantal form are given in Table I. For Ne we used the wave functions of Coulson and Duncanson,[8] for H_2O and NH_3 use was made of the wave functions of Banyard and March[1] and for CH_4 and NH_4^+ the functions of Bernal[9] were employed. For comparison, Table I also contains the values of χ determined from Pascal's rules.[10]

DISCUSSION OF RESULTS

It is seen from Table I that the theoretical values of χ_r for Ne, H_2O, NH_3, and NH_4^+ are all less than the corresponding "experimental" χ_r. This would seem to indicate that such an application of a central-field approach yields a radial density which is somewhat too concentrated.

[5] J. R. Eshbach and M. W. P. Strandberg, Phys. Rev. **85**, 24 (1952).
[6] H. S. Gutowsky, G. B. Kistiakowsky, G. E. Pake and E. M. Purcell, J. Chem. Phys. **17**, 972 (1949).
[7] G. W. C. Kaye and T. H. Laby, *Tables of Physical and Chemical Constants* (1958).
[8] C. A. Coulson and W. E. Duncanson, Proc. Roy. Soc. (Edinburgh) **62A**, 37 (1944).
[9] M. J. M. Bernal, Proc. Phys. Soc. (London) **66A**, 514 (1953).
[10] A. Weissberger, *Physical Methods of Organic Chemistry* (Interscience Publishers, Inc., New York, 1945), Vol. 1, 2455.

TABLE II.[11] Results for CH_4.

Bond Length in a.u.	"Experimental" χ_r	Theoretical χ_r	Comment
1.975	-21.5 / -25.3	-26.3	From Table I.
2.0	-21.5 / -25.3	-26.6[a]	Molecular orbital approach. Ionicity but no exchange effects allowed.
2.0	-21.5 / -25.3	-27.7[a]	Heitler-London approach. Exchange effects but no ionicity allowed.
2.0	-21.5 / -25.3	-33.2[b]	Hartree S.C.F. wave functions. No exchange effects.
2.06	-21.5 / -25.3	-21.11[c]	Heitler-London approach with the introduction of ionicity.
2.0	-21.5 / -25.3	-28.4	Using the Hartree-Fock central-field electron density.[d]
2.0	-21.5 / -25.3	-29.0	'Modified' Hartree-Fock density due to angular term allowance.[d]

[a] See footnote reference 14.
[b] See footnote reference 17.
[c] See footnote reference 15.
[d] See footnote reference 16.

For CH_4 however, we see that using the experimental value for χ of -12.2[11,12] results in a corresponding value of -21.5 for the "experimental" χ_r. The use of a later suggested value[13] for χ of -16 still only yields an "experimental" χ_r of -25.3. Thus χ_r for CH_4, as determined by our central-field approach, does not appear to follow the general trend shown by the other molecules but exceeds both the suggested "experimental" values. For this reason it was decided to study the results for CH_4 in greater detail.

CH_4

In Table II we compare our result with the values determined earlier by Coulson.[14] He evaluated the ground-state wave function, and hence χ_r, for CH_4 by using two different methods. Firstly, he used the molecular orbital method which allowed for ionicity but not exchange effects and secondly, Coulson applied the Heitler-London approximation which allowed for exchange effects but not ionicity. As can be seen the agreement among the three values is quite good. Venkatachalam and Kabadi[15] attempted to improve the Heitler-London approach of Coulson by allowing for ionicity. In this way they obtained a value of -21.11 which agrees extremely well with the "experimental" χ_r based on the observed susceptibility due to Bitter.

Another useful comparison is given by using the wave functions of Mills[16] who performed a complete Hartree-Fock study of CH_4 within the central-field approximation. Using his radial density distribution we obtained a value of -28.4 for χ_r. Comparing this result with that obtained using analytical central-field functions indicates how the use of the more flexible wave functions of Mills allows the radial density to become rather more diffuse. Further, a comparison with the χ_r of -33.2 for CH_4 determined by Buckingham, Massey, and Tibbs,[17] using their Hartree self-consistent field wave functions, indicates the way in which the radial density becomes more diffuse, and hence χ_r larger, when exchange effects are neglected.

Mills attempted to modify his Hartree-Fock wave functions by taking into account the first angular term with the symmetry of the molecule. In this way Mills was able to obtain a density expression [see Eq. (9) of footnote reference 16] which contained angular terms which expressed as a series expansion in spherical harmonics. At this point it is perhaps worth mentioning

[11] All values of χ, χ_r, and χ_{hf} are in units of 10^{-6} emu/mole.
[12] F. Bitter, Phys. Rev. **33**, 388 (1929).
[13] C. M. French and V. C. G. Trew, Trans. Faraday Soc. **41**, 439 (1945).
[14] C. A. Coulson, Proc. Roy. Soc. (London) **54**, 51 (1942).
[15] K. A. Venkatachalam and M. B. Kabadi, J. Phys. Chem. **59**, 740 (1955).
[16] I. M. Mills, Mol. Phys. **1**, 99 (1958).
[17] R. A. Buckingham, H. S. W. Massey, and S. R. Tibbs, Proc. Roy. Soc. (London) **A178**, 124 (1941).

TABLE III.[11] Results for NH_4^+.

Bond Length in a.u.	"Experimental" χ_r	Theoretical χ_r	Comment
1.836[a]	$\frac{-19.4}{-20.6}$	−17.0	From Table I.
1.937[b]	$\frac{-19.4}{-20.6}$	−18.9	Approximate central-field value after use of a simple scaling factor.
1.889	$\frac{-19.4}{-20.6}$	−24.89[c]	Heitler-London approach. Exchange effects but no ionicity allowed.
1.889	$\frac{-19.4}{-20.6}$	−13.4[c]	Heitler-London approach with the introduction of ionicity.

[a] See footnote reference 9.
[b] See footnote reference 6.
[c] See footnote reference 15.

that we feel that his Eq. (9) represents only a first approximation to the density which one would obtain using the wave function given in Eq. (7) of footnote reference 16. Even so, it is felt that the radial electron density distribution obtained from Eq. (9) will reflect qualitatively the change brought about by including angular terms in any wave-mechanical description of the electron density. The corresponding χ_r was found to be −29.0. This is suggestive of the interpretation that as allowance is made for angular terms the resulting electron density, when averaged over all orientations, will tend to become, on the whole, slightly more diffuse.

It is worth observing that, owing to symmetry properties, CH_4 and NH_4^+ are essentially different from the molecules H_2O and NH_3. Due to the tetrahedral symmetry of the former molecules the first angular term in the expansion of the "physically real" density, expressed as a series in spherical harmonics, is an f term. For H_2O and NH_3 however, the existence of a dipole moment indicates the occurrence of a p term in the density expansion. Thus, the influence on the s term, or radial density distribution, due to the inclusion of angular components in any theoretical description of the electron density is expected to be a good deal larger for molecules like H_2O and NH_3, which possess a dipole moment, than for the molecules CH_4 and NH_4^+ which exhibit a tetrahedral symmetry.

NH_4^+ [18]

In Table III a comparison of χ_r for NH_4^+ is made with the "experimental" value. For the observed susceptibility χ we use the value of −13.3 given by Trew[19] (invoked in footnote reference 15) along with a later value of −14.5 suggested by Bedwell, Spencer, and Trew.[20]

Since the theoretical N—H distance of 1.836 obtained by Bernal using a central-field approach is rather less than the experimental value of 1.937, a rough approximation to the radial density distribution corresponding to the experimental N—H value was obtained by applying a simple scaling-factor method which correlated the theoretical and experimental bond lengths, normalization, of course, being preserved. Using this modified central-field electron density, the resulting value for χ_r of −18.9 shows a pleasing degree of improvement, especially when compared with the "experimental" χ_r of −19.4. Included in Table III are the results of the two Heitler-London calculations of Venkatachalam and Kabadi[15] for NH_4^+. Thus, if the "experimental" values for χ_r are a reasonable estimate, this would indicate that the effect of ionicity introduced into their Heitler-London treatment has perhaps been over-compensated. If that is so, it may offer a partial explanation for the close agreement between the χ_r for CH_4 of −21.11 and the "experimental" value based on the observed susceptibility of Bitter, which we feel may be rather too low.

H_2O and CO_2

For H_2O, Ellison and Shull[21] performed a complete Roothaan treatment in which the mutual interactions of all ten electrons were considered. Using the corresponding radial density distribution (see footnote reference 2) the value of χ_r was found to be −15.2.[22] Although this result is suggestive of a slight over-diffuseness of the electron density the agreement with the "experimental" χ_r shows a considerable improvement over that pro-

[18] In connection with recent experimental results using x rays a more detailed analysis of the radial electron density for NH_4^+ is now under investigation. This will be reported shortly elsewhere.
[19] V. C. G. Trew, Trans. Faraday Soc. 37, 477 (1941).
[20] M. E. Bedwell, J. F. Spencer, and V. C. G. Trew, Trans. Faraday Soc. 45, 217 (1949).
[21] F. O. Ellison and H. Shull, J. Chem. Phys. 21, 1420 (1953).
[22] The center of mass is taken as the origin.

vided by a central-field approximation. This indicates that the move away from a central-field approach by including angular terms in the density should, in general, influence the radial distribution such that χ_r will become numerically larger, hence resulting in better agreement with experiment. This, it is felt, lends support to the conclusions concerning CH_4.

Since a Roothaan treatment of H_2O gave a fairly satisfactory agreement for χ_r with "experiment" (see also Das and Ghose[23] in this connection) it was decided to determine χ_r for CO_2 for which a similar calculation had been performed by Mulligan.[24] The choice of CO_2 was appropriate since we possessed, in connection with another investigation, the corresponding radial distribution of electrons derived from Mulligan's ground-state wave function. A χ_r of -79 was obtained, which, combined with the observed susceptibility χ of -18.6[25] for CO_2, indicates that χ_{hf} may be of the order of 60.

The nature of the agreement of χ_r with subsequent "experimental" values is rather uncertain for Mulligan, in his Roothaan approach, did not allow for inner-outer-shell electron mixing. The influence on the radial density distribution of such an approximation, while expected to be small, does cause our value of χ_r for CO_2 to be rather tentative.

CONCLUSION

For the above molecules[26] it is felt that a central-field approach which neglects exchange will cause the resulting radial density to be too diffuse, whereas when exchange effects are accounted for by using a central-field analytical wave function of determinantal form then the corresponding density appears to be somewhat too highly concentrated. Greater flexibility in the molecular wave functions and the inclusion of angular terms in the theoretical discussion of the molecules do seem to influence the subsequent electron density (when averaged over angles) such that it becomes more diffuse than that due to a central-field approach.

It should be noted that the use of analytical determinantal wave functions and Hartree-Fock functions neglects correlation effects between electrons with antiparallel spins. The over-all effect on the radial density distribution due to such an omission is, at present, rather difficult to anticipate. However, it is thought that a complete Roothaan treatment of a molecule involving all electrons should, in general, yield a fairly satisfactory value of χ_r when compared with "experiment."

Finally, from the above discussion, it would appear that a redetermination of the diamagnetic susceptibility for CH_4 might perhaps be worthwhile in view of the appreciable discrepancy between the two existing values, and the theoretical value.

ADDITIONAL NOTE

As a result of the subsequent analysis[27] for NH_4^+, mentioned in footnote reference 18, it was realized that for an N—H separation of 1.836 atomic units a Hartree self-consistent field calculation had been performed by Bernal and Massey.[28] The radial electron density distribution resulting from this central-field calculation was found to give a χ_r of -21.0. By a modification of the Hartree density, using the simple scaling factor method as before, an approximate value for χ_r corresponding to the experimental N—H distance of 1.937 atomic units was found to be -23.4.

Reference to Tables II and III reveals that the above results for NH_4^+ are in general agreement with the nature of the findings obtained for the tetrahedral molecule CH_4, thus tending to substantiate the conclusions drawn for that case.

[23] T. P. Das and T. Ghose, J. Chem. Phys. **31**, 42 (1959).
[24] J. F. Mulligan, J. Chem. Phys. **19**, 347 (1951).
[25] *Handbook of Chemistry and Physics* (Chemical Rubber Publishing Company, Cleveland, 1958–1959), 40th Edition.
[26] CO_2 excepted.
[27] K. E. Banyard and N. H. March (to be published).
[28] M. J. M. Bernal and H. S. W. Massey, Monthly Notices Roy. Astron. Soc. **114**, 172 (1954).

THE JOURNAL OF CHEMICAL PHYSICS VOLUME 33, NUMBER 3 SEPTEMBER, 1960

Thermal Expansion of Delta and Epsilon Zirconium Hydrides

CHARLES P. KEMPTER, REED O. ELLIOTT, AND KARL A. GSCHNEIDNER, JR.

Los Alamos Scientific Laboratory, University of California, Los Alamos, New Mexico

(Received April 14, 1960)

The thermal expansion characteristics of polycrystalline delta (face-centered-cubic) zirconium hydride and epsilon (body-centered-tetragonal) zirconium hydride were determined between room temperature and 362°C and 300°C, respectively, by means of x-ray diffraction techniques. The average linear thermal expansion coefficient for the delta phase is 2.98×10^{-6}/°C for the range 24° to 362°C. For the epsilon phase, the average coefficients for the range 24° to 300°C are -1.4×10^{-6}/°C and 30.6×10^{-6}/°C for the *a* and *c* directions, respectively, and 9.3×10^{-6}/°C for the randomly oriented polycrystalline material.

INTRODUCTION

THE dilatometric thermal expansion of "zirconium hydride" has been studied by Rentschler[1] and by Custer.[2] Rentschler[1] measured the expansion of specimens containing 1.80×10^{22}, 2.46×10^{22}, and 3.62×10^{22} atoms of hydrogen per cc ($N_H=1.80$, 2.46, and 3.62) from 75° to 925°, 850°, and 825°F, respectively. He found that the thermal expansion increased with increasing hydrogen content. Custer[2] measured the expansion of specimens having N_H values of 1.67, 1.73, 1.74, 2.33, 2.34, 3.36, and 3.70 from 75° to 1300°F. The correlation of thermal expansion with hydrogen content varied with the temperature range selected.

The dilatometric method is well suited to the determination of the thermal expansion of multiphase materials for engineering applications. However, when one considers the complexity of the zirconium-hydrogen phase diagram, it is not surprising that the correlation of empirical formulas with dilatometric thermal expansion results is difficult. The authors have found that "zirconium hydride" specimens usually consist of several phases such as alpha-zirconium, delta-zirconium hydride, epsilon-zirconium hydride, and gamma-prime zirconium hydride in varying proportions. One must also consider the possibility of finding a metastable beta-zirconium or the gamma-zirconium hydride reported by Hägg.[3] Filer, Rau, and Tholke[4] have confirmed the existence of this hexagonal gamma phase, isomorphous with α-Zr. The crystallography of the Zr-H system has been recently reviewed by Pearson.[5] Espagno, Azou, and Bastien[6–8] have used the dilatometric method for the study of the Zr-H phase diagram, but have not published thermal dilatometric data; these investigators[9] have very recently published plots of lattice constants vs hydrogen content for the delta and epsilon phases.

No investigations could be found in the literature on the thermal expansion of delta phase zirconium hydride.

The x-ray thermal expansion of epsilon zirconium hydride was first reported by Yakel,[10] who published his results in the form of a figure showing the lattice parameters, axial ratio, and the cube root of the volume of the unit cell of $ZrH_{1.92}$ as a function of temperature from ~80° to ~780°K. For the interval 300° to 700°K (27° to 427°C), he reported an average linear thermal expansion coefficient of approximately 9.03×10^{-6}/°K. Also, Goon and Malgiolio[11] reported on the x-ray thermal expansion of $ZrH_{1.95}$ from "room temperature" to 626°C. In all cases, the calculated lattice parameters were slightly lower than those obtained by Yakel.[10] The results of both of these investigations are discussed in comparison with the results reported later in this paper.

Vaughan and Bridge[12] made a high temperature x-ray diffraction investigation of the Zr-H system, but did not measure the thermal expansion of the phases. However, they did tabulate approximate interplanar spacings for several phases at 400°C and 600°C, and presented a plot of axial ratio vs temperature from room temperature to approximately 650°C for $ZrH_{1.86}$. Soffna, Azarkh, and Orlova[13] also carried out a structural x-ray analysis of the Zr-H system, but did not present thermal expansion data. A second x-ray struc-

[1] R. R. Rentschler, M. S. thesis, Air Force Institute of Technology (1957).
[2] B. C. Custer, M. S. thesis, Air Force Institute of Technology (1958).
[3] G. Hägg, Z. physik. Chem. **11B**, 433 (1930).
[4] E. W. Filer, R. C. Rau, and W. H. Tholke, General Electric Report APEX-444 (December 31, 1958).
[5] W. B. Pearson, *A Handbook of Lattice Spacings and Structures of Metals and Alloys* (Pergamon Press, New York, 1958).
[6] L. Espagno, P. Azou, and P. Bastien, Compt. rend. **247**, 83 (1958).
[7] L. Espagno, P. Azou, and P. Bastien, Compt. rend. **247**, 1199 (1958).
[8] L. Espagno, P. Azou, and P. Bastien, Compt. rend. **248**, 2003 (1959).
[9] L. Espagno, P. Azou, and P. Bastien, Compt. rend. **249**, 1105 (1959).
[10] H. L. Yakel, Jr., Acta Cryst. **11**, 46 (1958).
[11] E. J. Goon and J. Malgiolio, U. S. Atomic Energy Commission Report NYO-7547 (1958).
[12] D. A. Vaughan and J. R. Bridge, Trans. Am. Inst. Mining Met. Engrs. **206**, 528 (1956).
[13] V. V. Soffna, Z. M. Azarkh, and N. N. Orlova, Kristallografiya **3**, 539 (1958).

TABLE I. Spectrographic analysis results (ppm).

	Epsilon phase	Delta phase
Major	Zr	Zr
5000		Si
1000		Fe
500	Fe	
300		Al
200	Ni	
100	Al, Ba, Hf	Mg, Ca, V, Cr
<100	Si, Ca, Ti, V, Co, Zn, Mo, Pb	Ti, Co, Ni, Zn, Mo, Pb
40		Hf
30	Mg	B
<30	Na, K, Sr, Cd, Sn, Bi	Na, K, Sr, Cd, Sn, Bi
10		Mn, Ag, Ba
<10	Li, Be, B, Cr, Mn, Cu, Ag	Li, Be, Cu

tural investigation which is not included in Pearson's[5] review was carried out by Trzebiatowski and Stalínski.[14]

EXPERIMENTAL

The two hydride samples, which had been prepared by hydriding zirconium metal, were obtained from John D. Rogers of this laboratory. All operations with these materials were carried out in a helium atmosphere dry box. Both samples were pulverized in a Plattner mortar and −325 mesh specimens sealed in evacuated silica capillaries for x-ray diffraction.

The delta zirconium hydride specimen was mixed with a small amount of powdered silver (for use as a standard) prior to sealing. The high-temperature camera (Unicam, Cambridge, England) used had a diameter of 19 cm. The temperatures were determined from Owen and Roberts[15] silver calibration curves, and the lattice constants were determined from the (440), (531), and (600) Cu$K\alpha$ doublets using the method of Vogel and Kempter,[16] and assuming $\Delta a_0/a_0$ directly proportional to $\phi \tan\phi$, where a_0 is the lattice constant and ϕ is the complement of the Bragg angle. The silver lattice constants were determined from the (511) and (422) Cu$K\alpha_1$, lines.

The epsilon zirconium hydride specimen was examined in a 114.59-mm diameter camera (Central Research Laboratories, Inc., Red Wing, Minnesota). The temperatures above 20°C were determined from a power vs chromel-alumel thermocouple temperature calibration curve. The lattice constants of the face-centered tetragonal pseudo cell were determined from the (531), (404), (513), and (424) Cu$K\alpha$ doublets using the method described above.

TABLE II. Epsilon phase lattice constants versus temperature.

t, °C	a_0, A	c_0, A	c_0/a_0
24	4.97565±0.00066	4.45095±0.00045	0.894
95	4.97583±0.00096	4.45804±0.00066	0.896
196	4.97538±0.00138	4.47264±0.00094	0.899
300	4.97138±0.00642	4.49058±0.00285	0.903

[14] W. Trzebiatowski and B. Stalínski, Roczniki Chem. **30**, 691 (1956).
[15] E. A. Owen and E. W. Roberts, Phil. Mag. **27**, 294 (1939).

RESULTS AND DISCUSSION

A combustion analysis of the delta phase material gave 98.31% Zr. Hydrogen analyses of the epsilon and delta phase zirconium hydrides yielded 2.12 wt % and 1.59 wt % H, respectively; the corresponding empirical formulas are $ZrH_{1.96}$ and $ZrH_{1.46}$. Examination by x-ray powder diffraction revealed body-centered tetragonal epsilon phase in the first case, and face-centered cubic delta phase (with a secondary phase of epsilon and a minor phase of alpha) in the second case. Spectrographic analyses (based on the samples as ZrO_2) are presented in Table I.

TABLE III. Delta phase lattice constants versus temperature.

No.	t, °C	Lattice constant, A
1	28	4.77887±0.00029
2	110	4.77980±0.00043
3	215	4.78027±0.00049
4	301	4.78210±0.00023
5	362	4.78382±0.00040
6	251	4.78085±0.00020
7	166	4.78020±0.00036
8	24	4.77844±0.00029

The lattice constants of the epsilon phase are presented in Table II as a function of temperature. For ease of comparison with previously published work, the lattice constants are not corrected for refraction in Cu$K\alpha$ radiation. The precision is expressed as the standard deviation of the parameter.

The lattice constants of the delta phase are presented in Table III as a function of temperature. The constants were corrected for refraction in Cu$K\alpha$ radiation by adding 0.00017 A, and are tabulated in the same order that the runs were made.

[16] R. E. Vogel and C. P. Kempter, Los Alamos Scientific Laboratory Report LA-2317 (1959).

The data from Table II are shown in Fig. 1 in comparison with the data of Yakel[10,17] and Goon and Malgiolio,[11] all run with Cu$K\alpha$ radiation. Yakel sealed his samples in the presence of approximately one-third atmosphere of hydrogen, whereas the latter investigators used one atmosphere of hydrogen. From reference to Fig. 1, it can be seen that dissociation of the epsilon phase is not a problem to at least 300°C. Since Gulbransen and Andrew[18] have shown that the delta phase is more thermally stable than the epsilon phase, the dissociation of the delta phase should also be negligible for the temperature range shown.

It should be noted that Goon and Malgiolio[11] tabulated interplanar spacings for the epsilon phase at "room temperature" (which we have assumed to be 25°C in Fig. 1). The (511) and (224) reflections of the face-centered pseudo lattice were not indexed, and the (333) and (115) reflections were incorrectly indexed as (304) and (441), respectively. The (602) reflection was not tabulated. If one carries out a transformation of axes and face indices from the face-centered pseudo lattice to the body-centered lattice, the transformation matrix is

$$\begin{vmatrix} 1/2 & 1/2 & 0 \\ -1/2 & 1/2 & 0 \\ 0 & 0 & 1 \end{vmatrix}$$

and therefore

$$H=(h+k)/2$$

$$K=(h-k)/2,$$

and

$$L=l,$$

where H, K, L are the Miller indices of the new lattice and h, k, l are those of the old lattice. The determinant of the matrix (the modulus of the transformation) is equal to $-\frac{1}{2}$; therefore, the new cell volume is one-half the old cell volume. If proper indexing has been carried out for the pseudo lattice, the new indices will obey conditions limiting possible reflections for space group D_{4h}^{17}—$I4/mmm$. If the same transformation matrix is applied to the face-centered-tetragonal indices of the gamma-prime phase first reported by Gulbransen and Andrew,[18] the new indices also are consistent with the above space group. Therefore, it would appear that all reported face-centered phases in the Zr-H system are based on a fluorite lattice with varying degrees of tetragonality, where the axial ratios for the gamma prime, delta, and epsilon phases are >1, unity, and <1, respectively. The conclusion was first made on the basis of experimental results by Vaughan and Bridge.[12] The confirmation of this would await complete neutron diffraction investigations of the gamma prime and delta phases.

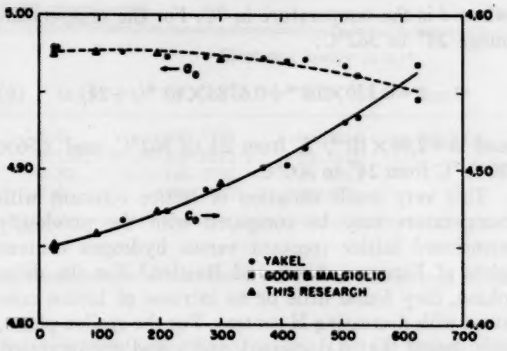

FIG. 1. The lattice constants of episilon ZrH_2 as a function of temperature.

The curves shown in Fig. 1 are the IBM 704 least squares fits of the data from all three investigations on epsilon ZrH_2. The equations are

$$a_0=4.9752+2.7458\times10^{-5}t-1.0566\times10^{-7}t^2, \quad (1)$$

$$c_0=4.4481+8.4948\times10^{-5}t+1.5835\times10^{-7}t^2, \quad (2)$$

where t is the temperature in °C for the range 24° to 626°C. The average linear thermal expansion coefficients from 24° to t°C are

$$\bar{\alpha}_a=5.518\times10^{-6}-2.124\times10^{-8}(t+24), \quad (3)$$

$$\bar{\alpha}_c=19.088\times10^{-6}+3.558\times10^{-8}(t+24). \quad (4)$$

The derivation of equations of this type has been previously discussed by Kempter and Elliott.[19] It should be noted that Eq. (1) has a maximum at 130°C which is about 0.001 A higher than the room temperature a values. This difference is of the same magnitude as the standard deviations of the a values in this range; therefore, this maximum may not be real. A cubic IBM 704 least squares fit was also tried, but it gave an inflection between room temperature and 95°C. The average linear thermal expansion coefficients of epsilon ZrH_2 are -1.4×10^{-6}/°C and 30.6×10^{-6}/°C for the a and c directions, respectively, for the range 24°–300°C. Taking the cube roots of the calculated volumes of the unit cells at 24°C and 300°C, the average coefficient for randomly oriented polycrystalline epsilon ZrH_2 is 9.3×10^{-6}/°C from 24° to 300°C.

For the delta phase (see Table III), the IBM 704 least squares fit is

$$a_0=4.77872+1.716\times10^{-6}t+3.24\times10^{-8}t^2, \quad (5)$$

[17] H. L. Yakel, Jr. (personal communication).

[18] E. A. Gulbransen and K. F. Andrew, J. Electrochem. Soc. **101**, 474 (1954).

[19] C. P. Kempter and R. O. Elliott, J. Chem. Phys. **30**, 1524 (1959).

where t is the temperature in °C. For the temperature range 24° to 362°C:

$$\bar{\alpha}=0.359\times10^{-6}+0.6783\times10^{-8}(t+24) \quad (6)$$

and $\bar{\alpha}=2.98\times10^{-6}$/°C from 24 to 362°C, and 2.56×10^{-6}/°C from 24° to 300°C.

This very small variation of lattice constant with temperature may be compared with the previously mentioned lattice constant versus hydrogen content plots of Espagno, Azou, and Bastien.[9] For the delta phase, they found little or no increase of lattice constant with decreasing H content. For the epsilon phase, they found that a decreased, and c and c/a increased with decreasing H content. These results are analogous to the lattice constant versus temperature results shown in Tables II and III.

It is concluded that the concept of a single *face-centered* Zr-H phase which varies in degree of tetragonality is a useful tool for x-ray diffraction studies, but that the concept cannot be extended to the assumption of a uniform variation in physical properties.

ACKNOWLEDGMENTS

The authors wish to thank Dr. E. Van Kooten and G. C. Heasley for the chemical analyses, J. A. Mariner for the spectrographic analyses, and Miss Dorothy L. Cooper for the IBM 704 least squares fits.

THE JOURNAL OF CHEMICAL PHYSICS VOLUME 33, NUMBER 3 SEPTEMBER, 1960

Some Intra-Atomic Correlation Correction Studies

M. KRAUSS, *National Bureau of Standards, Washington 25, D. C.*
AND
B. J. RANSIL,* *Laboratory of Molecular Structure and Spectra, Department of Physics, University of Chicago, Chicago 37, Illinois*

(Received February 15, 1960)

The applicability of the "intra-atomic correlation correction" (ICC) formulation of Hurley is discussed. It is shown that accurate bond energies cannot be obtained with the usual restricted basis set without employing another empirical procedure, although it may be possible to obtain accurate excitation energies.

I. INTRODUCTION

THERE has been considerable interest in the "atoms-in-molecule" (AIM) procedure for the quantitative calculation of molecular energies introduced by Moffitt[1] and later modified by Hurley[2] and Arai.[3] We shall be concerned with results and comments based exclusively on the Hurley formulation. Hurley[4] has shown that accurate results may be obtained for excitation energies of the first-row hydrides and the agreement of experimental and calculated dissociation energies is considerably improved over that of *ab initio* orbital calculations. This was supported by similar calculations by Krauss and Wehner.[5] As the AIM procedure considered here is based on a partly empirical Hamiltonian, it may be possible to obtain accurate total energies without using good wave functions. Hurley has suggested that more reliable results would be obtained if more flexible and accurate atomic functions were used. The correction, or empirical portion of the Hamiltonian, is reduced in this manner. It is the purpose of this paper to introduce evidence indicating the necessity of such an improvement, especially if we are interested in the total energy or dissociation energy. The calculation of accurate excitation energies, however, should be possible without such improvements.

II. APPLICATIONS

The basic equations in the ICC theory are given by Hurley[6] as

$$E=\Gamma^{+}H\Gamma \quad (1)$$

and

$$H=\tilde{H}+\tfrac{1}{2}[\tilde{M}(W-W')+(W-W')\tilde{M}], \quad (2)$$

where the molecular wave function is expressed as a linear combination of approximate composite functions (ACF).[1] The expression in brackets in Eq. (2) is the correction term, for which $\tilde{M}$ is the overlap matrix of the ACF's and $W-W'$ is the diagonal matrix of the atomic energy differences. We have applied these equations to HF using LCAO-MO-SCF wave functions with sets of effective nuclear charges ζ, corresponding to (1) Slater orbitals; (2) best atom (BA) orbitals[7];

* Consultant, Heat Division, National Bureau of Standards, Washington 25, D. C.

[1] W. Moffitt, Proc. Roy. Soc. (London) **A210**, 245 (1951).
[2] A. C. Hurley, Proc. Phys. Soc. (London) **A69**, 49 (1956).
[3] T. Arai, J. Chem. Phys. **26**, 435 (1957).
[4] A. C. Hurley, Proc. Roy. Soc. (London) **A249**, 402 (1959).
[5] M. Krauss and F. Wehner, J. Chem. Phys. **29**, 1287 (1958).
[6] A. C. Hurley, J. Chem. Phys. **28**, 532 (1958).
[7] C. C. J. Roothaan, Tech. Rept. 1955, Laboratory of Molecular Structure and Spectra, University of Chicago.

TABLE I. Total energies of HF ground state.

Orbital	ξ_{1s}	ξ_{2s}	$\xi_{2p\sigma}=\xi_{2p\pi}$	ξ_H	Electronic energy (a.u.)[a] ICC	SCF	Exptl.[c]
Best atom	8.6501	2.5639	2.54985	1.0	−100.5352	−99.4915	−100.5278
	8.6501	2.5639	2.54985	1.15815	−100.5612	−99.5216	
	8.65	2.56	2.5	1.32	−100.5865	−99.5292	
Slater	8.68	2.6	2.6	1.0	−100.5097[b]	−99.475	

[a] 1 a.u. = 27.210 ev.
[b] A. C. Hurley, Proc. Roy. Soc. (London) A248, 119 (1958).
[c] Internuclear distance is 1.733 a.u. Experimental total energy, including zero-point energy, quoted from A. M. Karo and L. C. Allen, J. Chem. Phys. 31, 968 (1959).

and (3) a selected intermediate choice. It is necessary to use the transformation from the ACF basis to the molecular orbital (MO) basis[6] in the manner used by Krauss and Wehner.[5] We should note that the latter were not correct in neglecting ACF's where the inner 1*s* shell is singly occupied in the determination of the correction matrix in the MO basis. However, all the errors arising from the failure of the basis functions to span the same function space do not seem to amount to more than 0.1 ev, as seen from the agreement of the results of Hurley and of Krauss and Wehner. Similar calculations were performed for OH, OH^-, and HF^+ using Slater orbitals. The linear symmetrical configuration of H_3 was also minimized with respect to R using the functions described by Griffing, Jackson, and Ransil[8] In the latter case the MO and ACF bases span the same space.

III. RESULTS AND DISCUSSION

The ICC calculations on HF summarized in Table I yield molecular energies lower than the experimental value by rather large amounts. Hurley has observed that the correction as applied generally is not a pure correlation correction, since Hartree-Fock orbitals are not used to calculate the atomic energies. For the ground-state F atom approximately 11 ev of the W-W' matrix element may be related to the inadequacy of the Slater function.

It is possible to completely separate the functional and correlation components of the correction matrix elements, provided the atomic orbitals used to construct the ACF's are flexible enough to afford a good approximation to the Hartree-Fock function for the atoms in the molecular composite function, and provided also there is no intra-atomic CI among the asymptotic composite functions. Such flexible atomic orbitals would, presumably, permit the calculation of a molecular energy reasonably close to the Hartree-Fock value. However, the ACF basis does not allow for a separation of the molecular energy as it does for the atoms. Presumably, most of the molecular correlation energy is accounted for by the ICC correction, given as the weighted sum of the correlation energies of the adiabatically separated atomic states. The CI among the ACF is then assumed to account quantitatively for the Hartree-Fock energy plus any additional molecular correlation energy associated with couplings between the prepared atom states of an ACF in accordance with the requirements of molecular symmetry and complete antisymmetry of the total wave function. It is possible that this assumption may not be realized and a total energy lower or higher than the experimental value may be calculated. It must be noted that in practice Eq. (2) must be considered purely heuristically. Only in a few cases involving the hydrogen atom do the composite functions satisfy conditions for a purely theoretical AIM approach, i.e., the atomic functions are eigenfunctions of the "atomic" part of the Hamiltonian. If additional composite functions are considered then we should have to consider intra-atomic CI, and the correlation correction would be obtained nonempirically. The correction matrix would then go to zero as the basis is extended, if the relativistic correction is considered.

If our atomic orbitals are relatively simple, then the accuracy of the calculations for such a basis set requires cancellation of the functional errors in the molecular and atomic calculations. For HF the basis set used here is evidently better for computing the energy of the molecule than it is for the atoms if the effective nuclear charges are allowed to vary for the molecular case as well as in the atomic one. *For severely restricted basis sets it is not to be expected that such sets would be as accurate for related molecular and atomic calculations.* We note that an additional empirical

TABLE II. Binding energy of H_3[a,b]

R(a.u.)	CI-MO[c]	ICC
1.75	65.4	84.8
1.80	67.0	86.4
1.85	68.0	87.3
1.90	68.3	87.6
1.95	68.2	87.5
2.00	66.3	85.8

[a] All values in kcal/mole. Calculated with respect to the energy of 3 H atoms at infinity: −1.5 a.u.
[b] Experimental: 103 kcal/mole.
[c] See footnote reference 8.

[8] V. Griffing, J. L. Jackson, and B. J. Ransil, J. Chem. Phys. 30, 1066 (1959).

TABLE III. Total energies of the OH and OH^- ground states.

	Electronic energy (a.u.)			
	OH		OH^-	
R(a.u.)	ICC	SCF	ICC	SCF
1.6	−75.7311	−75.0101	−75.8227	−74.8189
1.8	−75.7589	−75.0586	−75.8389	−74.8729
1.8342	−75.764	−75.062	−75.8395	−74.8785
2.0	−75.7605	−75.0746	−75.8329	−74.8956
2.2	−75.7486	−75.0719	−75.8168	−74.9012
2.4	−75.7302	−75.0583	−75.7972	−74.8973

TABLE IV. Detachment potentials.[a]

	Calculated		Experimental
	ICC	SCF	
HF	16.5_2	12.75	15.77,[b] 16.0[c]
OH^-	2.0_5	−2.25	1.8[d]

[a] All values in ev.
[b] D. C. Frost and C. A. McDowell, Can. J. Chem. **36**, 39 (1958).
[c] R. Thorburn, Proc. Phys. Soc. (London) **73**, 122 (1959).
[d] S. J. Smith and L. M. Branscomb, Phys. Rev. **99**, 1657 (A) (1955).

element could be introduced by determining rules for the choice of parameters by comparing calculated results in a series of related molecules with known experimental values. It is conceivable that very poor functions could yield accurate results in this manner.

The successful calculations[2,9] for H_2 and HeH^+ are probably to be attributed to the relatively accurate functions for both the atoms and molecules. For the H_3 case we would expect that the molecular function, composed as it is only 1s functions, is a relatively poorer one than the corresponding atomic functions. The total energy (ICC) is about 16 kcal (0.6 ev) above the experimental value.[10] This compares very favorably with the results Hurley obtained for H_2 using only 1s functions. Boys and Shavitt,[11] using a configuration interaction (CI) treatment with an "open-shell" basis set of six 1s orbitals, obtained an improvement of approximately 8 kcal (0.3 ev) with respect to the value calculated for the closed-shell CI case without the correlation correction. By comparing our results in Table II with the analogous values calculated by Hurley for H_2, we obtain an activation energy of 14.3 kcal/mole for the reaction of H with H_2. Shavitt reports an activation energy of 15.4 kcal/mole.

The accurate excitation energies obtained by Hurley[9] for a number of the first-row hydrides encouraged us to extend such calculations to the determination of the electron affinity of OH and the ionization potential of HF. The results are given in Tables III and IV. A practical difficulty in considering ions involves the choice of atomic screening factors for the molecular calculation. Previous calculations indicate that Slater's rules are adequate. There is, however, some ambiguity in the choice due to the uncertainties of the charge distribution in the ions OH^- and HF^+. We have assumed that all of the charge is associated with the O atom and chose screening constants accordingly. For HF^+ it was assumed that neutral screening factors would be adequate as we were interested only in an approximate check on the analogous OH calculations. Presumably a more suitable choice of screening constants would improve the agreement with experiment for HF, but the results as they stand represent a great improvement over the SCF result.

For the OH^- calculation it is also necessary to have an estimate of the energy of the O^{--} ion. An experimental value is unobtainable. The correlation correction for O^{--} was equated to that obtained for F^- after correcting for the difference in the relativistic correction[12] between O^{--} and F^-. This choice is based on the assumptions that the correlation energy in an isoelectronic sequence is invariant with variation[12] in Z, and that the deviation from the Hartree-Fock energy is approximately the same for the two ions. The calculated electron affinity may be in error by ±0.5 ev due to uncertainties in the O^{--} correction.

The agreement with experiment can be considered quite good, but such agreement must be viewed in the light of the results for HF and with regard to the sensitivity of a calculated observable to the accuracy of a wave function. Although energy differences would seem to be amenable to less exacting calculations than accurate total energies would require, it is necessary to investigate many analogous cases in order to establish rules indicating the dependability of the results for application to less well-known situations. It may prove far less tedious to extend the basis, at least for relatively small systems, as recommended by Hurley, and improve, in that way, the reliability and accuracy of this technique.

ACKNOWLEDGMENT

We are indebted to Dr. A. C. Hurley for his critical review of our results and his stimulating comments and suggestions.

[9] A. C. Hurley, Proc. Phys. Soc. (London) **A69**, 868 (1956).
[10] A. Farkas and L. Farkas, Proc. Roy. Soc. (London) **A152**, 124 (1935).
[11] S. F. Boys and I. Shavitt, Nature **178**, 1207 (1956); I. Shavitt, J. Chem. Phys. **31**, 1359 (1959).
[12] A. Fröman, Phys. Rev. **112**, 870 (1958); T. Arai and T. Onishi, J. Chem. Phys. **26**, 70 (1957).

Electron Coupling of Nuclear Spins. IV. Temperature Dependence in Substituted Ethanes*

JOHN C. SCHUG,† PAUL E. MCMAHON, AND H. S. GUTOWSKY

Noyes Chemical Laboratory, University of Illinois, Urbana, Illinois

(Received April 27, 1960)

The proton-proton coupling constant, $A_{HH'}$, in H—C—C'—H' groups is known to depend upon the dihedral angle, ϕ. Previous valence-bond calculations by Karplus have given the result that

$$A_{HH'} \cong A_0 \cos^2\phi + B.$$

This relation is used to estimate the effects upon the average coupling constant of torsional vibrations and reorientations about the C—C' bond. For substituted ethanes, it is found that torsional vibrations produce a modest temperature dependence, of opposite sign for the *trans* and *gauche* coupling. However, for molecules in which the potential function, $V(\phi)$, has threefold symmetry, rotational averaging leads to a cancellation of the vibrational effects, giving a temperature independent value, $\langle A_{HH'} \rangle$, for the average coupling. This prediction has been verified in experiments on ethyl nitrate for which $\langle A_{HH'} \rangle$ was found to have a constant value of 6.92 cps over a 100° temperature range.

When there is an energy difference, ΔE, between *trans* and *gauche* forms, ΔE determines the sign and magnitude of the temperature dependence of $\langle A_{HH'} \rangle$; however, corrections for the vibrational effects appear desirable if accurate values of ΔE are to be obtained from such experiments. The temperature dependence of $\langle A_{HH'} \rangle$ could not be calculated analytically for any but the simplest potential functions and simplest approximations to the torsional motions. However, it was found that the detailed form of $V(\phi)$ has but a slight effect on the results. $\langle A_{HH'} \rangle$ is, of course, more sensitive to the functional form of $A(\phi)$.

I. INTRODUCTION

HIGH resolution nuclear magnetic resonance spectra depend on the relative chemical shifts and the electron coupling of the magnetic nuclei involved.[1] Both of these quantities can be calculated from the molecular wave function and considerable work of this nature has been done. Neither quantity has an intrinsic temperature dependence[2] but such effects can and do result indirectly from changes in the molecular electronic structure with temperature. The latter may be grouped into four classes: (a) reversible changes in molecular conformation, as in the equilibrium between chair and boat forms of cyclohexane; (b) molecular interactions, such as hydrogen bonding; (c) thermal excitation to higher electronic states; (d) molecular vibrations.[3]

Of these possibilities, numerous examples of (a) and (b) are known,[1] while electronic excitation energies are ordinarily so great that (c) is unimportant. On the other hand, the amplitudes of molecular vibrations are sufficiently dependent upon temperature that small but observable effects could result, particularly for protons where the amplitudes are relatively large. Evidence for the existence of detectable vibrational effects is provided by studies which demonstrate the dependence of chemical shifts upon isotopic species.[4] A major difficulty in experimentally detecting vibrational effects, and this applies to chemical shifts as well as to the coupling constants, is their separation from conformational changes and molecular interactions. In any event, some recent calculations of Karplus[5] led us to consider the effects upon the proton-proton coupling in H—C—C'—H' groups of torsional vibrations and reorientations about the C—C' bond.

By means of a valence bond theory,[6] and with the assumption that the carbon hybrid orbitals are tetrahedral (sp^3) in the H—C—C'—H' fragment, it was found[5] that the proton-proton coupling constant may be approximately fitted by a curve of the form

$$A_{HH'} = A_0 \cos^2\phi + B, \qquad (1)$$

where $A_{HH'}$ is the coupling constant in cps, ϕ is the dihedral angle between the two carbon-hydrogen bonds, and A_0 and B are constants. This relation predicts experimentally observed trends, although the magnitudes observed tend to be larger than those predicted.

In a molecule, the angle ϕ is time-dependent because of torsional oscillations and reorientations about the C—C' bond. Therefore, the apparent value of $A_{HH'}$ is an average, $\langle A_{HH'} \rangle$, over those dynamic processes which have correlation times, τ_c, satisfying the condition[7] $\tau_c \gtrsim 1/A_{HH'}$. If there are different states of the

* Acknowledgment is made to the donors of The Petroleum Research Fund, administered by the American Chemical Society, for partial support of this research. Support was also received from the Office of Naval Research.

† General Electric Company Predoctoral Fellow.

[1] J. A. Pople, W. G. Schneider, and H. J. Bernstein, *High-Resolution Nuclear Magnetic Resonance* (McGraw-Hill Book Company, Inc., New York, 1959).

[2] N. F. Ramsey, Phys. Rev. **78**, 699 (1950); **86**, 243 (1952); **91**, 303 (1953).

[3] It is assumed that the angular dependences are averaged out by the random molecular rotations in a fluid state; see reference 2 for details.

[4] H. S. Gutowsky, J. Chem. Phys. **31**, 1683 (1959) and prior work cited there, particularly that of G. V. D. Tiers.

[5] M. Karplus, J. Chem. Phys. **30**, 11 (1959).

[6] M. Karplus, D. H. Anderson, T. C. Farrar, and H. S. Gutowsky, J. Chem. Phys. **27**, 597 (1957); M. Karplus and D. H. Anderson, *ibid.* **30**, 6 (1959).

[7] H. S. Gutowsky, D. W. McCall, and C. P. Slichter, J. Chem. Phys. **21**, 279 (1953); H. S. Gutowsky and C. H. Holm, *ibid.* **25**, 1228 (1956).

molecule whose lifetimes exceed this condition, separate spectra are obtained from them, each with its own $\langle A_{HH'}\rangle$. The torsional frequencies and other vibrations as well as the lifetimes of excited vibrational states have $\tau_c \geqq 10^{-10}$ sec so that $A_{HH'}$ is always averaged over such motions and states. However, τ_c for the hindered internal rotation about the C—C′ bond, may or may not be short enough for it to produce averaging.

Three aspects of Eq. (1) and of the averaging are considered. Equation (1) provides a basis for estimating the magnitude of vibrational effects and their sensitivity to the shape of the potential function inhibiting internal reorientation. The validity of Eq. (1) can be examined by using it in calculating a temperature dependence of $\langle A_{HH'}\rangle$, and seeing if the calculated dependence agrees with experiment. Also, if Eq. (1) is indeed a good approximation, then it can be used to analyze the temperature dependence of $\langle A_{HH'}\rangle$ in those molecules where the different rotational forms have different energies, and thereby estimate the energy differences. In this paper, these calculations are described and they are compared with the experimental results obtained thus far.

Throughout this work, it must be borne in mind that the basic relation, Eq. (1), was calculated for tetrahedral carbon orbitals. This is an approximation which will affect the comparisons with experiment. As will be seen, the case of ethane itself is rather unexciting because $\langle A_{HH'}\rangle$ is predicted to be virtually independent of temperature. On the other hand, substituted ethanes, which are likely to possess a temperature-dependent $\langle A_{HH'}\rangle$, are not likely to have tetrahedral carbon orbitals. However, it is our feeling that if the constants, A_0 and B, in Eq. (1) are allowed some freedom, reality might still be approached. Here, we are really assuming that the coupling constant may be expressed as

$$A_{HH'}=A_0(\theta,\theta')\cos^2\phi+B(\theta,\theta'), \qquad (2)$$

where we have written A_0 and B as functions of θ and θ', the H—C—C′ bond angles. To consider the temperature dependence, then, we will examine the variation of the quantity

$$(\langle A_{HH'}\rangle-B)/A_0=\langle\cos^2\phi\rangle. \qquad (3)$$

II. MATHEMATICAL METHODS

The calculations may be approached either classically or quantum-mechanically. In either case, the first step is to adopt an expression for the barrier to internal rotation, $V(\phi)$, because the calculation is just that of averaging $\cos^2\phi$ over the torsional oscillations and internal rotation. Molecular vibrations other than the torsional oscillations are neglected because of their much smaller amplitudes in the cases studied.

Quantum-mechanically, one would use the wave function for the system[8] to calculate $\langle\cos^2\phi\rangle$. This procedure is difficult, and it is our feeling that such a complete calculation is not yet justified. We have made approximate quantum-mechanical calculations, for the case of a barrier with threefold symmetry (ethane), in the harmonic oscillator approximation. The results, as described in the next section, are the same as in the classical calculation, and the hope is that this will be very nearly true in general.

Classically, one must carry out the integrations in the following version of Eq. (3),

$$\langle\cos^2\phi\rangle=\int_0^{2\pi}\cos^2\phi e^{-V(\phi)/RT}d\phi \Big/ \int_0^{2\pi}e^{-V(\phi)/RT}d\phi. \qquad (4)$$

This equation includes the approximation that if a torsional oscillator has a *total* amount of energy equal to $V(\phi)$, it spends all of its time at the value of ϕ for which the *potential* energy is $V(\phi)$. The resulting average is thus weighted more heavily at the ends of the classical oscillation than it should be; however, it is still useful as a limiting case inasmuch as the quantum-mechanical calculation weights the values of ϕ near the potential minima more heavily than would the precise calculation for the classical oscillator.

In any event, even with the simplified "classical" probability distribution assumed for ϕ in Eq. (4), the calculation proves to be rather difficult; and we have not been able to accomplish it analytically for any but the simplest potential functions $V(\phi)$. For barriers with less than threefold symmetry, we have calculated the temperature dependence for various oversimplified barrier shapes with the hope of then being able to generalize to a certain extent regarding the actual situation.

In most ethane derivatives of the types considered here, the internal barriers are of the order of a few kcal mole^{-1} and thus small enough that rotational averaging occurs as well as vibrational. Therefore, most of our calculations treat the combined effects. The size of the barrier below which rotational averaging occurs may be estimated in the following manner. We assume the internal rotation to be thermally activated and write the frequency of rotation, ν, as

$$\nu=\nu_0\exp(-E_a/RT), \qquad (5)$$

where ν_0 is a frequency factor and E_a is the barrier height. Rotational averaging occurs when the frequency of internal rotation exceeds the dependence upon ϕ of the chemical shift and of the coupling constant, in cps.[7] For the ϕ dependence of the chemical shift and of $A_{HH'}$, we choose 10 cps.[1,5] With the further approximation that the frequency factor ν_0 is given by $\nu_0=kT/h$, the condition for rotational averaging

[8] C. C. Lin and J. D. Swalen, Revs. Modern Phys. **31**, 841 (1959).

TABLE I. The dependence upon vibrational state n and temperature, of $\langle A_{HH'}\rangle$ for the H—C—C′—H′ fragment in ethane obtained from a quantum-mechanical calculation for a torsional harmonic oscillator with $\nu_0=208.6$ cm^{-1}.

n	$\langle A_{HH'}{}^{trans}\rangle_n$	$\langle A_{HH'}{}^{gauche}\rangle_n$	T °K	$\langle A_{HH'}{}^{trans}\rangle_v$	$\langle A_{HH'}{}^{gauche}\rangle_v$	$\langle A_{HH'}\rangle_{v,r}$
0	8.21	2.26	200	7.95	2.38	4.24
1	7.24	2.74	300	7.76	2.48	4.24
2	6.67	3.11	400	7.63	2.56	4.25
3	6.01	3.42				

becomes

$$(kT/h)\exp(-E_a/RT)\gtrsim 10, \qquad (6)$$

which requires that $E_a\gtrsim 13$ kcal mole^{-1}, at room temperature. If the ϕ dependence of the chemical shift and of $A_{HH'}$ differ greatly in magnitude, it is, of course, possible for one to be averaged and not the other.

III. CALCULATIONS AND RESULTS

A. Molecules Having Barriers with Threefold Symmetry

Ethane and 1-substituted derivatives such as CH_3CH_2X and CH_3CHXY have rotational isomers which are indistinguishable. Therefore, the potential barrier has threefold symmetry about the C—C′ bond, the populations of the three rotational forms are equal, and even though rotational averaging occurs, any temperature dependence of $\langle A_{HH'}\rangle$ has its primary origin in the increase of the torsional amplitudes with temperature. To do the classical calculation, we chose a barrier of the form[9]

$$V(\phi)=(V_0/2)(1+\cos 3\phi). \qquad (7)$$

The integrations in Eq. (4) may then be conveniently done by means of a transformation to complex variables, $z=e^{i\phi}$, and use of the theory of residues.[10] This results in identical infinite series for the numerator and the denominator, the final result being independent of temperature,

$$(\langle A\rangle-B)/A_0=\tfrac{1}{2}, \qquad (8)$$

where for simplicity of notation the subscripts on A have been dropped.

The approximate quantum-mechanical calculation was made by assuming that each of the three equivalent potential wells was parabolic, with the relative populations of the harmonic oscillator energy levels being determined by the Boltzmann factor. The calculation then involves averaging $\cos^2\phi$ over the appropriate Hermite polynomials.[11] The necessary integrations were done graphically. The results are summarized in Table I. Individual values of $\langle A_{HH'}\rangle$ for the *trans* and *gauche* configurations of the H—C—C′—H′ fragment are given for the ground and first three excited torsional states. The calculations are for a fundamental torsional frequency of 208.6 cm^{-1} (i.e., $V_0\cong 3$ kcal mole^{-1})[9] and for a moment of inertia equal to that of the CH_3 group about its symmetry axis. The values of A_0 and B, used in Eq. (3) to obtain $\langle A_{HH'}\rangle$ from $\langle\cos^2\phi\rangle$, are the averages of those obtained by Karplus,[5] namely 9.0 and 0.28 cps.

It is seen that the dependence upon torsional level is relatively large for both $\langle A_{HH'}{}^{trans}\rangle$ and $\langle A_{HH'}{}^{gauche}\rangle$ but that the averaging over the various levels gives only moderate temperature dependences. Moreover, the sign of the temperature dependence is opposite for the *trans* and *gauche* coupling, there being, respectively, a decrease of 0.32 cps and an increase of 0.18 cps upon increasing the temperature from 200° to 400°. In fact, the two effects cancel when the averaging process is extended over the internal rotations. Because of the symmetry assumed, the final average, $\langle A_{HH'}\rangle_{v,r}$, is $(1/3)\langle A_{HH'}{}^{trans}\rangle_v+(2/3)\langle A_{HH'}{}^{gauche}\rangle_v$, which has the constant value of 4.25 cps over the 200° temperature interval for which calculations were made. Not only does the constancy predicted by the quantum-mechanical calculation agree with the classical result, but also the numerical value is virtually the same as the classical average, 4.22 cps, which in turn is identical with the average obtained over the rotation alone, neglecting the torsional oscillations.

B. Other Symmetric Molecules

As used here, the term "symmetric" is meant to imply any molecule in which both *gauche* forms are equivalent, e.g., 1,1,2,2-tetrachloroethane. In other words, this section is concerned with substituted ethanes for which the barrier to internal rotation is symmetric relative to $\phi=\pi$. The calculations were made along the "classical" lines of Eq. (4).

The general procedure was to write the integrals from 0 to 2π as a sum of integrals over the ranges 0 to $2\pi/3$, $2\pi/3$ to $4\pi/3$, and $4\pi/3$ to 2π. The potential function used for ethane, Eq. (7), was extended to these molecules by writing separate expressions for each of the three ranges, of the form

$$V(\phi)=V_1+V_2\cos 3\phi. \qquad (9)$$

[9] S. Mizushima, *The Structure of Molecules and Internal Rotation* (Academic Press, Inc., New York, 1954).
[10] R. V. Churchill, *Introduction to Complex Variables* (McGraw-Hill Book Company, Inc., New York, 1948).
[11] L. Pauling and E. B. Wilson, Jr., *Introduction to Quantum Mechanics* (McGraw-Hill Book Company, Inc., New York, 1935), p. 80.

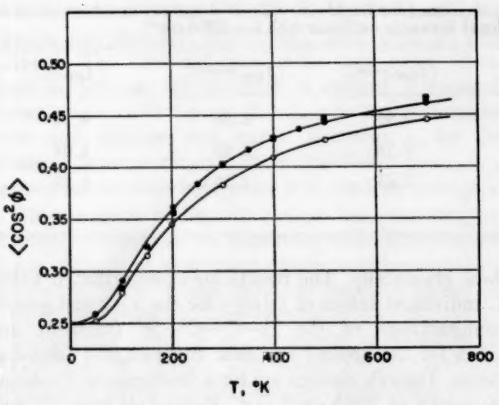

FIG. 1. Plots of $\langle\cos^2\phi\rangle$ for the H—C—C′—H′ fragment, calculated as a function of temperature for several potential functions in which the *trans* configuration is 0.5 kcal mole^{-1} less stable than the *gauche*, i.e. $\Delta E=E_t-E_g=0.5$. The open circles are for delta function potential wells with rotational but no vibrational averaging. The solid circles and squares are for parabolic and V-shaped wells, respectively, each potential function having three maxima 5 kcal above E_g.

V_1 and V_2 may be adjusted in each of the three ranges to make the entire barrier continuous and to make either the *gauche* or *trans* form favored, as desired. The resulting integrals cannot be evaluated as simply as before, however, because one runs into the problem of "trisecting an angle." The integrals in the denominator are expressible in terms of Bessel functions of complex argument and zero order,[12] but we have not found a convenient way of expressing the integrals in the numerator. Expansion of the exponentials in a power series is not expected to give reasonable results at

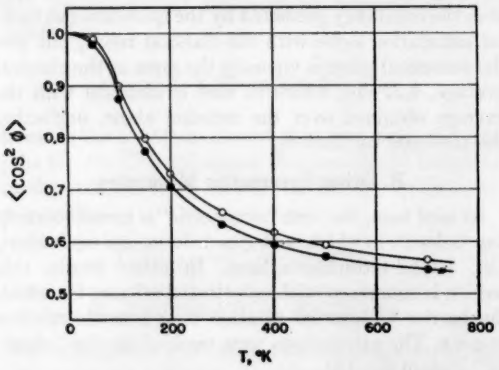

FIG. 2. Plots of $\langle\cos^2\phi\rangle$ for the H—C—C′—H′ fragment calculated as a function of temperature for two potential functions in which the *trans* configuration is 0.5 kcal mole^{-1} more stable than the *gauche*, the reverse of the situation in Fig. 1. The open circles are for delta function potential wells with rotational but no vibrational averaging, the solid, for parabolic wells having three maxima 5 kcal above E_g.

[12] G. N. Watson, *Theory of Bessel Functions* (Cambridge University Press, London, 1922).

moderate temperatures, due to the relatively large values of E_a/RT which must be considered.

For these reasons, it was decided that the best approach would be to consider a number of different barriers for which the necessary integrations could be performed analytically, and to see how much effect the shape of the barrier actually has.

Delta Function Potential Wells with No Vibrational Averaging

The crudest barrier that one may consider is one which is large everywhere except at $\phi=\pi/3$, π, and $5\pi/3$, i.e., the two *gauche* and the *trans* positions. In this case, there is effectively no torsional oscillation, the temperature dependence reflects solely the changing

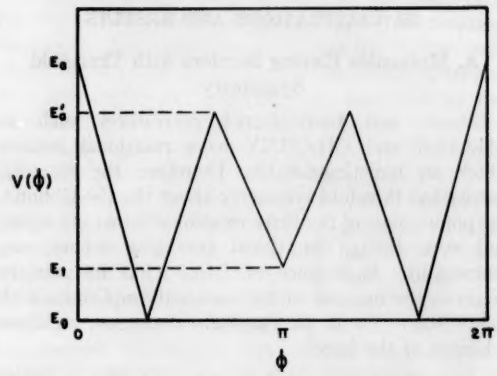

FIG. 3. Potential function with V-shaped wells used in calculating effect of barrier shape upon temperature dependence of $\langle A_{HH'}\rangle_{\nu,r}$ in the H—C—C′—H′ fragment.

relative populations of the *trans* and *gauche* forms, and Eq. (4) reduces to

$$(\langle A\rangle-B)/A_0 = [1+(\tfrac{1}{2})\exp(\Delta E/RT)]/[1+2\exp(\Delta E/RT)], \quad (10)$$

where ΔE is the difference in energy between *trans* and *gauche* forms, i.e. (E_t-E_g). Equation (10) is plotted for $\Delta E=\frac{1}{2}$ kcal mole^{-1} in Fig. 1 and for $\Delta E=-\frac{1}{2}$ kcal mole^{-1} in Fig. 2. When ΔE is positive, this means that the *gauche* configuration is favored, and ΔE negative, the *trans* form.

A Linear Potential Function with V-Shaped Wells

The next approximation is to take $V(\phi)$ as a combination of linear functions of ϕ in the various ranges such that the potential wells are V-shaped, as in Fig. 3. The resulting integrations may all be performed via the

standard forms

$$\int e^{ax}dx=(1/a)e^{ax},$$

$$\int e^{ax}\cos^2 x dx=e^{ax}[\cos x(2\sin x+a\cos x)+2/a]/(4+a^2). \tag{11}$$

The resulting expression is rather cumbersome, and is not reproduced here, but the results, for $E_a=E_a'=5$ kcal mole^{-1} and $\Delta E=\frac{1}{2}$ kcal mole^{-1}, are plotted in Fig. 1. E_a is the potential barrier between the two *gauche* forms and E_a' that on going from *gauche* to *trans*, as shown in Fig. 3.

It may be seen in Fig. 1 that the shape of this curve for $\langle\cos^2\phi\rangle$ is quite similar to but systematically displaced from that obtained for the delta function potential wells for which there is no vibrational averaging. This displacement represents the imbalance in the opposing effects of the vibrational averaging upon $\langle A_{HH',gauche}\rangle_v$ and $\langle A_{HH',trans}\rangle_v$, produced by having $\Delta E\neq 0$.

Parabolic Potential Wells

The next approximation, and probably the best one that can be conveniently treated, is that of three parabolic wells. That is, in each of the three ranges, i, the potential barrier is written in the form

$$V_i(\phi)=V_{1i}+V_{2i}(\phi-\delta)^2. \tag{12}$$

Here, δ is a phase factor, equal to $\pi/3$, π, and $5\pi/3$, for the respective regions and V_{1i} and V_{2i} are adjusted to move the wells up or down and to make two adjacent wells meet at a common point. Making a substitution, $x=\phi-\delta$ and proceeding in the manner outlined in the Appendix, one obtains the following final expression for Eq. (4),

$$(\langle A\rangle-B)/A_0=\frac{[2I(x_0)+\exp(-\Delta E/RT)I'(x_{01})]}{[2K'(x_0)+\exp(-\Delta E/RT)K'(x_{01})]}. \tag{13}$$

Here, $x_0=9E_a/\pi^2RT$, $x_{01}=9(E_a-\Delta E)/\pi^2RT$, $I(x)=\frac{1}{6}(\pi/x)^{\frac{1}{2}}[2-e^{-1/x}]P[\pi(x^{\frac{1}{2}})/3]$, $I'(x)=\frac{1}{2}(\pi/x)^{\frac{1}{2}}[1+e^{-1/x}]P[\pi(x^{\frac{1}{2}})/3]$, $K'(x)=(\pi/x)^{\frac{1}{2}}P[\pi(x^{\frac{1}{2}})/3]$, and $P(x)$ is the probability integral.[13] The other symbols are as defined in Eq. (3), $\Delta E=E_t-E_g$, and, for simplicity it has been assumed as before that $E_a=E_a'$. Considering the approximation made in the derivation one concludes that the relation holds up to a temperature of about 700°K.

Equation (13), for $E_a=5$ kcal mole^{-1} is plotted as a function of temperature in Fig. 1 for $\Delta E=0.5$ kcal and

[13] B. O. Pierce, *A Short Table of Integrals* (Ginn and Company, New York, 1929).

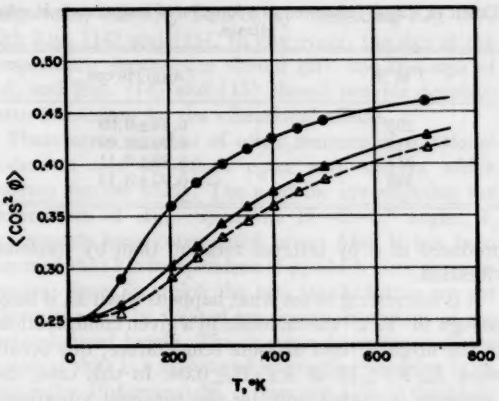

FIG. 4. Plots of $\langle\cos^2\phi\rangle$ for the H—C—C′—H′ fragment calculated as a function of temperature for parabolic potential wells. The solid circles are for $\Delta E=0.5$ kcal and $E_a=5$ kcal while the solid and open triangles are for $\Delta E=1$ kcal, and $E_a=5$ and 10 kcal, respectively. In all cases it is assumed that the three potential maxima have the same value, $E_a=E_a'$.

in Fig. 2 for $\Delta E=-0.5$ kcal. In Fig. 1, it is seen that there is little difference between the results for the parabolic and V-shaped potential wells. For the latter, $\langle\cos^2\phi\rangle$ is only very slightly smaller at low temperatures and slightly larger at high temperatures than for the parabolic case. However, as mentioned in connection with the V-shaped wells, the averaging by the torsional vibrations does produce discernible effects when $\Delta E\neq 0$. This is shown in both Figs. 1 and 2 by the sizeable shifts between the curves for the delta function and the parabolic potential wells having the same E_a and ΔE. Moreover, a comparison of Figs. 1 and 2 shows that the direction of this shift depends upon the sign of ΔE; it is determined by whether the *gauche* or *trans* form is favored, as one would predict from the opposite temperature dependences of $\langle A_{HH',trans}\rangle_v$ and $\langle A_{HH',gauche}\rangle_v$ in Table I.

Effects of E_a and ΔE upon the Temperature Dependence

Assuming that the final approximation considered, that of parabolic potential wells, comes closest to reality, we have plotted in Fig. 4 the temperature dependence calculated for several combinations of E_a and ΔE. Changing the barrier height, E_a, by a factor of two produces the relatively small difference between the two lower curves in the figure. This difference results from the smaller average amplitude of the torsional vibrations for the larger barrier. However, a similar twofold change in the energy difference between the *gauche* and *trans* wells has a relatively large effect.

The upper curve in Fig. 4, for $\Delta E=0.5$ kcal and $E_a=5$ kcal, is displaced from the two lower curves, for $\Delta E=1$ kcal and $E_a=5$ and 10 kcal, by several times the separation of the latter. This is certainly expected in view of the angular dependence of $A_{HH'}$ and the larger changes

TABLE II. $\langle A_{HH'}\rangle$ observed as a function of temperature in ethyl nitrate.

T in °K	$\langle A_{HH'}\rangle$ in cps
295	6.94±0.09
313	6.93±0.09
357	6.88±0.11
398	6.92±0.13

produced in ϕ by internal rotation than by torsional vibration.

It is interesting to see what happens when E_a is large enough to "lock" the molecule in a given configuration. In the neighborhood of room temperature, this occurs when $E_a/RT \lesssim 25$ or $RT/E_a \gtrsim 0.04$. In this case, the averaging is caused only by the torsional vibrations, and the results for $E_a=3$ kcal have been given in Table I for the quantum-mechanical calculation. However, by using a parabolic potential well and taking the classical average of $\cos^2\phi$ over the one range of interest, more general expressions can be obtained. For the *gauche* form stable, we find

$$(\langle A\rangle - B)/A_0 = \tfrac{1}{4}\{2 - \exp[-(\pi^2/9)(RT/E_a)\} \cong \tfrac{1}{4}[1+(\pi^2/9)(RT/E_a), \quad (14)$$

and for the *trans* form stable,

$$(\langle A\rangle - B)/A_0 = \tfrac{1}{2}\{1 + \exp[-(\pi^2/9)(RT/E_a)\} \cong \tfrac{1}{2}[2-(\pi^2/9)(RT/E_a)]. \quad (15)$$

The entire temperature dependence should then be only of the order of a few percent, that is a few tenths of a cps. Moreover, because of the nature of the approximations in the physical model used to derive Eqs. (14) and (15), they most likely predict too large a vibrational effect.

C. Dependence of $\langle A_{HH'}\rangle$ upon the Functional Form of $A(\phi)$

Our considerations thus far have been restricted to Eq. (1), the angular dependence of $A_{HH'}$ obtained by Karplus[5] in the valence bond analysis of the H—C—C′—H′ fragment. A matter of interest is the sensitivity of $\langle A_{HH'}\rangle$ to the functional form of $A(\phi)$. Exploration of this question is simplified to some degree by the condition imposed upon $A(\phi)$ that $A_{HH'}$ be symmetrical about ϕ values of 0 and π because of the molecular symmetry assumed in the cases considered. Therefore, we have examined the temperature dependence of $\langle A\rangle$ for several different $A(\phi)$ functions. Even so, the results are instructive rather than conclusive in nature.

It is appropriate to note that throughout these calculations it has been assumed that the constants A_0 and B each have but one value over the entire range of ϕ. This is not entirely the case, however. Karplus[5] indicated that one set of constants was to be used in the ranges $0<\phi<\pi/2$ and $3\pi/2<\phi<2\pi$, and a different set in the range $\pi/2<\phi<3\pi/2$, namely $A_0=8.5$ and $B=-0.28$ cps in the first two ranges, and $A_0=9.5$ and $B=-0.28$ cps in the third range. The correction for this "asymmetry" has been calculated and was found to be very small. The correction to ${}_NA_{HH'B}$ is about +0.1 cps at 200°K and +0.2 at 700°K when the *gauche* form is favored by 0.5 kcal. When the *trans* form is favored, the correction is larger at the lower temperature.

$$A(\phi) = A_0 \sin^2\phi + B$$

This relation is the reverse of Eq. (1) in that for given values of A_0 and B it interchanges the relative values and temperature dependences for $A_{HH'}{}^{trans}$ and $A_{HH'}{}^{gauche}$. However, for molecules having threefold symmetry in $V(\phi)$, the changes compensate one another so that the classical calculation of $\langle \sin^2\phi\rangle$ gives the same temperature independent value as for $\langle \cos^2\phi\rangle$, namely $\frac{1}{2}$. Of course, if the potential function does not have threefold symmetry, the temperature dependence of $\langle \sin^2\phi\rangle$ differs from that of $\langle \cos^2\phi\rangle$. In particular, for the case of two equivalent *gauche* forms, the curves of $\langle \sin^2\phi\rangle$ versus T are similar to those in Figs. 1 and 2 except that they are reflected in the plane defined by $\langle \cos^2\phi\rangle=\frac{1}{2}$. Thus, for the *trans* form stabler than the *gauche*, $\langle \sin^2\phi\rangle$ starts at 0 for low temperatures and approaches $\frac{1}{2}$ at high temperatures, while for the *gauche* form stabler, the corresponding range is 0.75 to 0.5.

$$A(\phi) = C - A_0 \cos\phi$$

This function gives results very similar to those for Eq. (1). $\langle A_{HH'}{}^{trans}\rangle_v$ decreases with increasing temperature, while the *gauche* coupling increases. For molecules with threefold symmetry in $V(\phi)$, the effects cancel, giving a temperature independent coupling constant, $\langle A\rangle = C$. The results for molecules with less than threefold symmetry are qualitatively very similar to those calculated using Eq. (1).

Linear Functions for $A(\phi)$

The symmetry necessary for $A(\phi)$ can be constructed from any function which is single-valued in the range $0\leqslant\phi\leqslant\pi$, by reflecting it in the plane defined by $\phi=\pi$. The simplest example consists of two linear portions, $A(\phi)=A_0\phi+B$ for $0\leqslant\phi\leqslant\pi$ and $A(\phi)=A_0(2\pi-\phi)+B$ for $\pi\leqslant\phi\leqslant 2\pi$. For this type of function, $\langle A_{HH'}{}^{gauche}\rangle_v$ is not affected by changing the temperature while $\langle A_{HH'}{}^{trans}\rangle_v$ either decreases or increases depending on whether A_0 is positive or negative. The constancy of the *gauche* coupling results in a temperature dependence of $\langle A\rangle$ which follows that of the *trans* coupling, at least in molecules having an internal barrier with threefold symmetry.

However, in molecules with less symmetry, the temperature dependence is more nearly that obtained

for Eq. (1). That is, $\langle A \rangle$ as a function of temperature extends between the same low and high-temperature limits, and the shape of the curve is very similar. The small systematic differences present are mainly a consequence of the differences in the effects of the torsional vibrarions. If monotonic but nonlinear functions are used for $A(\phi)$ in the regions 0 to π and π to 2π, the several results are qualitatively the same as those for linear functions.

IV. EXPERIMENTAL RESULTS AND DISCUSSION

Of the various calculations given above, that lending itself most readily to experimental check is the temperature dependence of $\langle A_{HH'} \rangle$ in a 1-substituted ethane. This has been done for ethyl nitrate, using apparatus and methods described previously.[14] The results are summarized in Table II. It is seen that to well within an experimental error of about 1% the observed coupling constant is independent of temperature over the 100° range investigated. This is consistent with the form of $A(\phi)$ given in Eq. (1) but, as shown in the preceding section, it is by no means conclusive support.

Additional experiments are in progress on the temperature dependence of $\langle A_{HH'} \rangle$ in various substituted ethanes, particularly those for which $E_g \neq E_t$. If one uses 9.0 and 0.28 cps for A_0 and B in Eq. (1), one finds that the change in $\langle A_{HH'} \rangle$ over the entire temperature range should be about 2 to 3 cps for a molecule in which the *gauche* form is favored and about 4 to 5 cps when the *trans* form is favored. In the temperature range accessible for measurements of $\langle A_{HH'} \rangle$ and for typical values of ΔE, perhaps one-third of the total change may be expected. This is rather small. However, the estimate should be increased by a factor between 1.5 and 2, because several observations support larger values for A_0 and B than those calculated.[5] For example the quantum-mechanical results for $\langle A_{HH'} \rangle_{v,r}$ in Table I is only 4.24 cps compared with the experimental value of 6.92 cps for ethyl nitrate. There are also the recent experimental studies by Sheppard and Turner[15] of 1,2-polysubstituted ethanes at room temperature which give approximate values for the *gauche* and *trans* coupling constants nearly double those from the valence bond calculation for the H—C—C′—H′ fragment.[5]

The main factor that determines the temperature dependence of $\langle A_{HH'} \rangle$ is ΔE, the difference in energy between the *trans* and *gauche* forms. The temperature dependence predicted for $\Delta E \neq 0$ is not too large but it should be observable in many cases and provide useful information. However, the effects of the torsional vibrations cannot be neglected if one wishes to analyze a set of experimental data and obtain an accurate value for ΔE. Moreover, the relative importance of the vibrations increases as E_a and E_a' approach ΔE in magnitude; this may be seen by comparing Eq. (10) with Eqs. (14) and (15). In any event, the sign of the temperature dependence should give one the sign of ΔE, and Eqs. (14) and (15) should provide approximate corrections for the vibrational effects.

There are a number of other features of rotational isomerism and its effect upon nmr spectra which warrant further study. The need for investigating the dependence of $A_{HH'}$ upon the H—C—C′ angles, θ, has already been commented upon. Also, it has been assumed that θ is independent of ϕ, which is an approximation. Cases in which the two *gauche* forms are not equivalent can be treated by simple extensions of the methods used herein. The angular dependence of the chemical shift is a major and interesting question in its own right. Unfortunately, it does not appear too likely that the angular dependence of the chemical shifts can be described by as simple and general a function as that for $A_{HH'}$. However, studies of the temperature dependence of the chemical shifts as well as of the coupling constants in the same system are attractive in principle.

APPENDIX

The evaluation of $\langle \cos^2\phi \rangle$, using the "classical" approach of Eq. (4), and assuming that $V(\phi)$ is comprised of parabolic potential wells, leads to integrals of the form

$$K(a) = \int_0^{\pi/3} \exp(-ax^2)\,dx \tag{16}$$

in the denominator. These integrals are the so-called probability integrals, which Pierce[13] tabulates as

$$P(x) = (2/\pi^{\frac{1}{2}}) \int_0^x \exp(-x^2)\,dx.$$

Hence, we obtain

$$K(a) = (\tfrac{1}{2})(\pi/a)^{\frac{1}{2}} P[\pi(a^{\frac{1}{2}})/3]. \tag{17}$$

The numerator yields integrals of the form

$$I(a) = \int_{-\pi/3}^{\pi/3} \exp(-ax^2)\, \cos^2(x+\delta)\,dx. \tag{18}$$

By using the trigonometric identities

$$\cos(x+\delta) = \cos\delta \cos x - \sin\delta \sin x,$$

$$\cos^2 x = (\tfrac{1}{2})(1 + \cos 2x),$$

$$\sin^2 x = (\tfrac{1}{2})(1 - \cos 2x), \tag{19}$$

the $I(a)$ may be written in terms of $K(a)$ and $J(a)$, where

$$J(a) = \int_0^{\pi/3} \exp(-ax^2)\, \cos(bx)\,dx, \tag{20}$$

and $b = 2$.

[14] H. S. Gutowsky and C. H. Holm, J. Chem. Phys. **25**, 1228 (1956), and references cited therein.

[15] N. Sheppard and J. J. Turner, Proc. Roy. Soc. (London) **A252**, 506 (1959).

$J(a)$ may be evaluated approximately by Liebnitz's rule,[16]

$$dJ/db=\int_0^{\pi/3}\exp(-ax^2)(-x\sin bx)\,dx$$
$$=(\tfrac{1}{2}a)\left[\exp(-ax^2)\sin bx\right]_0^{\pi/3}$$
$$-(b/2a)\int_0^{\pi/3}\exp(-ax^2)\cos(bx)\,dx$$
$$=(\tfrac{1}{2}a)\exp(-a\pi^2/9)\sin b(\pi/3)-(b/2a)J. \quad (21)$$

[16] W. Kaplan, *Advanced Calculus* (Addison-Wesley Publishing Company, Reading, Massachusetts, 1953), p. 219.

Assuming that we can neglect the first term on the right relative to the second term, we have

$$dJ/db=-(b/2a)J,$$

which gives, on integration, and setting $b=2$,

$$J(a)=K(a)e^{-1/a}. \quad (22)$$

Using this expression, one is able to justify neglecting the first term on the right of Eq. (21) for large values of a. When a is as small as three, the first term is still two orders of magnitude smaller than the second. Substitution into Eq. (4) of these results for $I(a)$, $J(a)$, and $K(a)$ leads to the relation given in Eq. (13).

THE JOURNAL OF CHEMICAL PHYSICS VOLUME 33, NUMBER 3 SEPTEMBER, 1960

Dissociation of Methyl Bromide by Nuclear Isomeric Transition of 4.4-hr Br^{80m} *

S. WEXLER AND G. R. ANDERSON†

Argonne National Laboratory, Lemont, Illinois

(Received April 11, 1960)

The pattern of positively charged fragments from methyl bromide as a result of isomeric transition of 4.4-hr Br^{80m} has been measured by mass spectrometric techniques. A peaked distribution of charge states of atomic bromine ranging from Br^{+1} to Br^{+13} was observed, the most probable being Br^{+7}. The finding of singly, doubly, and triply charged carbon-containing fragments gives evidence that the CH_3Br^{80} daughter ion breaks apart by Coulombic repulsion of redistributed charges following internal conversion and subsequent Auger electron transitions. Multiply charged polyatomic species produced by the nuclear transition are unstable.

I. INTRODUCTION

SEVERAL researches[1–5] have been devoted to the breakup of molecules by nuclear isomeric transition of bound 4.4-hr Br^{80m}. The efficiency with which the 18-min Br^{80} daughter splits out of the parent molecule is found to vary over a wide range, depending on the chemical composition and physical state of the parent. In gaseous CH_3Br^{80m}, for example, less than 1% of the radioactive daughters are observed to remain attached after the nuclear transition,[1,3] while for solid $(NH_4)_2PtBr_6$ the value is 100%.[4] The chemical behavior of the energetic radioactive daughter which has broken free of the parent molecule has been the subject of many studies.[3,6–12] The 18-min Br^{80} is observed to undergo hydrogen and halogen displacement reactions, and it has been proposed[3] that this unique chemical behavior is due to a positive charge residing on the bromine.

Although the carbon-bromine bond has been shown to be ruptured in a high fraction of the decays of Br^{80m} attached to organic molecules in the gas phase, little is known about the nature of the fragments which arise from the original tagged molecule. The internal conversions of the nuclear transformation of Br^{80m} and subsequent vacancy cascades (Auger effect) should be expected to leave the molecule with a very high positive

* Work performed under the auspices of the U. S. Atomic Energy Commission.

† Resident Research Associate (summer). Present address: State University of Iowa, Iowa City.

[1] W. H. Hamill and J. A. Young, J. Chem. Phys. **20**, 888 (1952).

[2] R. S. H. Chiang and J. E. Willard, J. Am. Chem. Soc. **74**, 6213 (1952).

[3] A. A. Gordus and J. E. Willard, J. Am. Chem. Soc. **79**, 4609 (1957).

[4] A. W. Adamson and J. M. Grunland, J. Am. Chem. Soc. **73**, 5508 (1951).

[5] R. H. Luebbe, Jr., and J. E. Willard, J. Chem. Phys. **29**, 124 (1958).

[6] Marjorie L. Hunt, Ph.D. Thesis (University of Chicago, 1954).

[7] G. Gavoret and N. Ivanoff, Bull. Soc. Chim. France 166 (1952).

[8] E. G. Bohlmann and J. E. Willard, J. Am. Chem. Soc. **64**, 1342 (1942).

[9] J. E. Willard, J. Phys. Chem. **52**, 585 (1948).

[10] S. Goldhaber, N. S. H. Chiang, and J. E. Willard, J. Am. Chem. Soc. **73**, 2271 (1951).

[11] J. F. Horning and J. E. Willard, J. Am. Chem. Soc. **75**, 461 (1953).

[12] C. C. Coffin and W. D. Jamieson, J. Chem. Phys. **20**, 1324 (1952).

charge.[13–16] The average charge which forms on $C_2H_5Br^{80}$ by these processes has been measured to be 10 ± 2 electron units.[17] Similar experiments on rare gas atoms have shown the mean positive charge of the daughters from internal conversion to be high: $(8.5\pm0.3)e$ for Xe^{131},[18] and $(7.7\pm0.4)e$ for Kr^{83}.[17] The distribution of daughters with regard to positive charge has been determined mass spectrometrically[19,20] for Xe^{131m} and Xe^{133}. For both nuclides a peaked distribution ranging up to about $+22e$ was found, with the most probable charge being about $+9e$. A molecule possessing such a high charge would probably break apart by Coulombic repulsion if the charge distributed itself over the molecule before the C—Br bond dissolved from loss of bonding electrons.[21,22] Molecular dissociation may also be caused by electron excitation from the "shaking" accompanying the vacancy cascades,[23] and, in gases at higher pressures or in condensed phases, from charge neutralization and collisions with neighboring molecules.

In this paper we describe the application of the mass spectrometric techniques, previously used in beta-decay studies,[24–28] to the study of the fragmentation of isolated CH_3Br^{80m} molecules which undergo isomeric transition. Of interest in this experiment is the elucidation of the charge states of the positively charged fragments from the nuclear decay, of the mechanism by which the molecule dissociates, and of the extent of internal charge transfer in methyl bromide before disruption. An added incentive is the possibility of correlating information obtained in these very low-pressure experiments with data derived from studies on gases at high pressures—for example, the completeness of rupture of the C—Br bond in this nuclear event.

II. EXPERIMENTAL

The mass spectrometer for radioactive gases at this laboratory has been extensively modified; a profile sketch of the improved apparatus appears in Fig. 1.

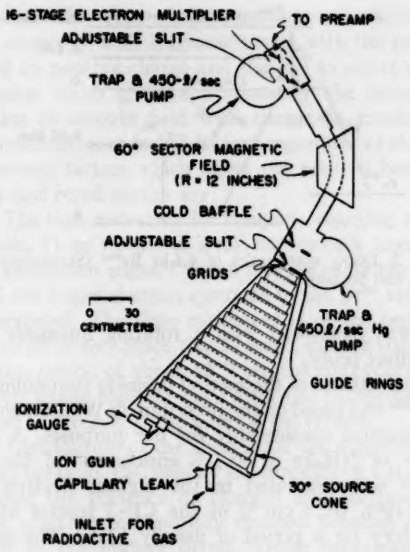

FIG. 1. Mass spectrometer for radioactive gases.

The CH_3Br^{80m} with high specific activity was introduced from a ballast volume through a capillary leak into the large source volume and allowed to decay there at total pressures ranging from 2×10^{-6} to 1.5×10^{-5} mm, as measured with an ionization gauge. In general, an appropriate aliquot of the active gas was let into the ballast line behind the leak so as to result in an initial source pressure of $1\text{–}2\times10^{-5}$ mm. As the gas was depleted the pressure in the cone decreased slowly, so that a study of pressure effects on the relative yields of the fragments could be made. The positively charged fragments from the nuclear decays were swept toward the apex of the source cone by an axial electric field produced by applying, through a voltage divider, the proper voltages to a ring system within the conical housing. At the source slit the ions were accelerated to high energies as they passed between two grids which obstructed only a small fraction of the opening. The ratio of the voltage between the grids to that impressed across the entire ring system was held at 12:1 so as to ensure symmetrical shapes of ion peaks so that the mass pattern would not be affected by the different total energies of ions originating at different points in the source volume. The voltage between the grids was 6000 v. The fragments were sorted out by a 60° sector magnetic field of 12-in. radius of curvature and detected by a 16-stage electron multiplier. Counting techniques were employed. Counting rates above background varied between about 10 counts/min to about 1500 counts/min depending on the fragment, pressure, and time after activation of the Br^{80m}. The electron multiplier detected virtually every ion of all fragments which hit the first dynode. The magnetic

[13] E. P. Cooper, Phys. Rev. **61**, 1 (1942).
[14] D. C. DeVault and W. F. Libby, J. Am. Chem. Soc. **63**, 3216 (1941).
[15] J. L. Magee and E. F. Gurnee, J. Chem. Phys. **20**, 894 (1952).
[16] R. L. Platzman, *Symposium on Radiobiology* (John Wiley & Sons, Inc., New York, 1952), Chap. 7.
[17] S. Wexler, Phys. Rev. **93**, 182 (1954).
[18] M. L. Perlman and J. A. Miskel, Phys. Rev. **91**, 899 (1953).
[19] F. Pleasonton and A. H. Snell, Proc. Roy. Soc. (London) **A241**, 141 (1957).
[20] A. H. Snell and F. Pleasonton, Phys. Rev. **111**, 1338 (1958).
[21] E. Segrè and A. C. Helmholtz, Revs. Modern Phys. **21**, 271 (1949).
[22] F. L. Mohler, V. H. Dibeler, and R. M. Reese, J. Chem. Phys. **22**, 394 (1954).
[23] M. Wolfsberg and M. L. Perlman, Phys. Rev. **99**, 1833 (1955).
[24] S. Wexler and D. C. Hess, J. Phys. Chem. **62**, 1382 (1958).
[25] S. Wexler, J. Inorg. Nuclear Chem. **10**, 8 (1959).
[26] S. Wexler, G. R. Anderson, and L. A. Singer, J. Chem. Phys. **32**, 417 (1960).
[27] A. H. Snell and F. Pleasonton, J. Phys. Chem. **62**, 1377 (1958).
[28] T. H. Carlson, J. Chem. Phys. **32**, 1234 (1960).

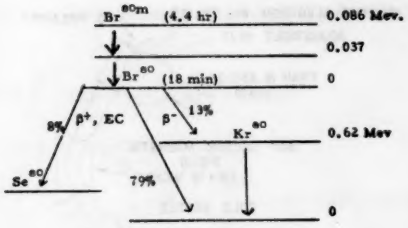

FIG. 2. Decay systematics of 4.4-hr Br^{80m} (Strominger, Hollander, and Seaborg[30]).

field was monitored with a rotating fluxmeter or a Hall-effect probe.

The synthesis of the methyl bromide containing 4.4-hr Br^{80m} was based on the procedure of Winteringham,[29] but modified considerably for our purposes. A 6-mg sample of NH_4Br of 95.1% enrichment of the Br^{79} isotope was irradiated in the highest neutron flux ($\approx 2\times10^{13}$n sec^{-1} cm^{-2}) of the CP-5 reactor at this laboratory for a period of usually 12 hr. The quartz tube containing the irradiated sample was transferred to a close fitting tube, 50 μl of a solution containing H_2O, H_2SO_4, and CH_3OH in the proportions 7:6:5 added, the outer tube immediately attached to a vacuum line, and the mixture frozen out in liquid N_2. The tube was evacuated, shut off from the system, warmed to 80–100°C and refluxed at these temperatures for 15 min. The contents were again frozen in liquid N_2 and outgassed. The mixture was then allowed to warm up, and the vapors passed through a spiral cooled in a dry ice-acetone bath and condensed in a transfer bulb at −195°C. The time required for transfer of the CH_3Br^{80m} from the reaction tube to the transfer bulb could be measured by a radiation meter. Because of the intensely radioactive sample, shielding and some remote control techniques were used. A mass spectrometric analysis of one of the preparations indicated that 83% was methyl bromide; the remaining components were NO, CH_3OH, and H_2O. Less than 0.2% of the gaseous preparation consisted of HBr or higher organic bromides. Since the compounds associated with the methyl bromide in these preparations are not radioactive, they should not contribute to the mass patterns observed.

In order to be certain that the fragments observed in these experiments originate in the nuclear decay process, four effects which could contribute to the mass patterns were considered. To study possible ionization by field emission, current leakages, etc., in the source volume, we introduced inactive CH_3Br into the cone and measured the intensities of the various fragments over the same pressure region as that used when active methyl bromide was present. Only CH_3^+ and CH_3Br^+ ions were found, their intensities (which varied roughly linearly with the pressure) each being about 10% of those observed with CH_3Br^{80m} present at the same pressure. The yields reported in Sec. IV have been corrected for this spurious effect.

A second possible contribution to the fragmentation pattern is the spectra of ions from β-γ decay of 35.9-hr Br^{82}. This radioactive nuclide is produced by neutron activation of Br^{81}, which comprises 4.9% of the bromine in the enriched NH_4Br irradiated in the reactor. The extent of the ion pattern from Br^{82} decay was appraised by determining relative abundances of fragments from active CH_3Br about four hours after the end of the neutron activation, allowing the active gas to stand about 48 hours, and again measuring the ion intensities. During the 2-day cooling period, the disintegration rate of 4.4-hr Br^{80m} will have decreased to 2×10^{-3} of its original value while that of 35.9-hr Br^{82} will have dropped only to 40% of the earlier decay rate. On the basis of this experiment, 5 to 10% of the CH_3^+ intensity could be attributed to Br^{82} decay, but no other ions observed about four hours after irradiation were due to Br^{82}. This result is expected on the basis of a calculation of the relative disintegration rates for Br^{80m} and Br^{82}, taking into account the isotopic enrichment of the NH_4Br, the length of the neutron irradiation, the cooling times prior to the measurements, and the fact that CH_3^+ would probably be the predominant fragment from Br^{82} decay.[24]

The daughter of the 4.4-hr Br^{80m} is also radioactive (Fig. 2)[30] and so there is the possibility that the ion pattern may be distorted by products from the decay of this 18-min activity. However, Gordus and Willard[3] have observed the isomeric transition of CH_3Br^{80m} in the gas phase to result in molecular disruption in more than 99% of the decays, and that the 18-min lower isomer deposits on the walls of the container. In our experiment this deposition results in virtually pure CH_3Br^{80m} entering the source volume through the capillary leak. Many experiments at this laboratory have shown HBr at low pressures to be virtually completely adsorbed on glass or metal surfaces, and atomic Br probably would show the same behavior. Decay of the upper isomer in the source should also result in a deposit of the 18-min daughter on the internal structure of the cone. But, fortunately, the recoils from transformation of beta radioactive nuclides deposited on ordinary surfaces are not charged because the ionization potentials of the recoils usually exceed the work function of the substrate.[31] Further evidence that the Br^{80} decay does not affect the fragmentation pattern is the observation that the net ion intensities decrease to zero within several minutes on pumping out the ballast line. Finally, even if there is a slight nonrupture of the gaseous CH_3Br^{80} in the isomeric transition, disruption of the molecule by decay of the 18-min

[29] F. P. W. Winteringham, J. Chem. Soc. **1949**, Suppl. Issue 2, 416.

[30] D. Strominger, J. M. Hollander, and G. T. Seaborg, Revs. Modern Phys. **30**, Pt. II, 649 (1958).

[31] C. W. Sherwin, Phys. Rev. **75**, 1799 (1948); **82**, 52 (1951).

isomer should give rise predominantly to the CH_3^+ fragment with no $(CH_3Br^{80})^+$ or multiply charged ions.[24]

The radiations from Br^{80m} may of course ionize the bulk CH_3Br in the source volume. Intensities of fragments produced by these self-radiation processes will increase with the square of the pressure of radioactive gas in the cone, while intensities of fragments from the nuclear event will vary directly with the pressure. Accordingly, this disturbing effect may be studied by measuring the variation of the relative intensities of fragments with source pressure. Within the precision of the experiment, the relative intensities of the various charged species were found to be independent of the source pressure over the range from 2×10^{-6} to 1×10^{-5} mm. This observation indicates that ionization by electrons and radiation from the nuclear decay is of little or no consequence at these pressures.

III. CONSIDERATIONS ON RELATIVE TRANSMISSION EFFICIENCIES OF FRAGMENTS

Of primary importance in quantitative mass spectrometric measurements of decomposition spectra is the establishment of experimental conditions which assure detection of all fragments with the same efficiency. This is particularly necessary for radioactive polyatomic gases since recoil energies may be appreciable and may vary with the fragment, since there is considerable discrimination by mass spectrometers against fragments with initial kinetic energies.[22] In order that all ionic fragments be transmitted through the spectrometer with the same efficiency, it is necessary that the relation

$$\dot{E}ne/(\text{K.E.})_0 = \text{constant} \qquad (1)$$

hold for all ions entering the electrical field in the same direction from a common point of origin.[23] Here $\dot{E}$ is the electric field acting on the ion of charge ne with initial kinetic energy $(\text{K.E.})_0$, and the constant must be the same for all such fragments. The electric field is proportional to voltages between rings and grids in the source volume, but the kinetic energy of the ionic fragment at the moment of formation is determined in these studies by the mechanism of the bond rupture in the original molecule. Since the initial kinetic energies of the several fragments from disruption of CH_3Br^{80} were not known, exact presetting of the collecting and focussing fields to assure the same experimental sensitivity for all ions was not possible. Because of this difficulty, the results reported here are only of a qualitative nature. But they do, as will be seen, give an insight into the fragmentation of highly charged molecular ions. Many factors, the magnitude of which can only be roughly estimated, make the recoil energies different for different ions. So it has only been possible to deduce the approximate manner in which the initial energy of a Br fragment varies with the magnitude of its positive charge and thereby to arrive at an expression which gives approximately the necessary variation of electric field with charge to ensure the same transmittance for all Br ions regardless of charge. The several factors which affect the relation between charge and recoil energy are:

(a) The time necessary for complete charging of the molecule. From widths of x-ray fluorescence lines and x-ray absorption edges,[34–37] one may estimate the time for all the Auger electron ejections in the Br^{80} atom to be completed. The time calculated is of the order of 10^{-15} to 10^{-16} sec. Since this is much shorter than the vibration period of about 10^{-14} sec, the methyl bromide molecule hangs together until after the charge has developed as a result of the internal conversion.

(b) Distribution of the charges on the molecule just prior to breakup. Preliminary experiments on CH_3Br^{80m} indicated the presence of charged hydrocarbon ions plus a spectrum of multiply charged bromine atoms formed in the nuclear decay. These data suggested that there must be internal transfer of electrons from the CH_3 to the Br prior to fragmentation and that the molecule breaks up by Coulombic repulsion of the redistributed charges. We have assumed that the function governing the range of positive charges on the methyl after these electronic transfers has a character somewhere between independence of and direct proportionality to the charge on the Br.

(c) The interionic distance at the instant the Coulomb forces are exerted. Since the charging of the molecule and the internal electron transfers occur in times very short relative to vibrational periods, the nuclei remain essentially fixed during the electron transitions. Thus the interionic length should be fairly independent of the charge on the molecule. Separation of the charges[22] combined with reduction of the ionic radius of the bromine as the charge increases[38] will tend to decrease the interionic distance somewhat. We approximate these conditions by assuming that the interionic distance is the same for all charge states which the molecule may attain. Actually though, there will be a distribution of interionic distances because the charging process will be occurring while the methyl bromide molecule is at different places on its hypersurface of energy. From the above arguments we take these distributions to be the same for all charges.

As a result of the Coulomb repulsion between charged methyl and bromine, the molecule must break up, and

[22] C. E. Berry, Phys. Rev. **78**, 597 (1950).

[23] P. A. Sturrock, *Static and Dynamic Electron Optics* (Cambridge University Press, New York, 1955), p. 8. Equation (1.3.8) of this reference, when generalized for multiply charged ions, shows that the forces on the ions must be proportional to their initial kinetic energies if they are to have the same trajectory.

[34] E. H. S. Burhop, *The Auger Effect* (Cambridge University Press, New York, 1952), pp. 87, 88.

[35] F. K. Richtmyer, S. W. Barnes, and E. Ramberg, Phys. Rev. **46**, 843 (1934).

[36] E. Ramberg and F. Richtmyer, Phys. Rev. **51**, 913 (1937).

[37] A. H. Compton and S. K. Allison, *X-Rays in Theory and Experiment* (D. Van Nostrand Co., Inc., Princeton, New Jersey, 1935), 2nd ed., pp. 745, 747.

[38] L. Pauling, *The Nature of the Chemical Bond* (Cornell University Press, Ithaca, New York, 1944), 2nd ed., p. 350.

TABLE I. Distribution of positively charged fragments from isomeric transition of CH_3Br^{80m}.

Fragment	Relative abundance
Br^{+1}	0.54±0.02
Br^{+2}	0.66±0.02
Br^{+3}	0.54±0.03
Br^{+4}	0.51±0.03
Br^{+5}	1.00
Br^{+6}	1.33±0.10
Br^{+7}	1.46±0.08
Br^{+8}	1.35±0.04
Br^{+9}	0.95±0.03
Br^{+10}	0.70±0.05
Br^{+11}	0.31±0.07
Br^{+12}	0.09±0.02
Br^{+13}	0.06±0.02
CH_3Br^+	0.99±0.10
CH_3^+	1.84±0.14
CH_2^+	0.16±0.01
CH_1^+	0.21±0.03
C^+	0.26±0.02
H_2^+	0.10±0.01
H^+	0.17±0.03
CH_3Br^{+2}	<0.02
CH_3^{+2}	<0.01
C^{+2}	0.15±0.02
CH_3Br^{+3}	<0.02
CH_3^{+3}	<0.03
C^{+3}	0.065±0.006
C^{+4}	<0.01

the initial kinetic energy attained by the bromine of charge ne is

$$(\text{K.E.})_0=[(ne)(me)/r][M_2/(M_1+M_2)], \quad (2)$$

where me is the charge residing on the CH_3 group, r the interionic distance, and M_1 and M_2 are the masses of the Br and CH_3, respectively. Combining relations (1) and (2), and using the approximations discussed under (b) and (c) above, one obtains

$$\bar{E}=\text{constant} \quad (3)$$

and

$$\bar{E}/n=\text{constant} \quad (4)$$

as the limiting conditions depending respectively on the assumptions that the charge on the methyl group is independent of or proportional to the charge of the Br. Thus for all bromine ions to be detected with the same efficiency, regardless of their charge, the relation between the electric fields (and hence the potentials) and the charge on the Br must be somewhere between independence and direct proportionality.

The situation in Br^{80m}, however, is further complicated by internal conversion of a 37-kev transition, which follows the 49-kev step in 55% of the events. (Fig. 2.) A theoretical estimate[39] of the lifetime for the second decay is 10^{-11} sec, but this may be too short by several orders of magnitude.[40] After the bromine ion is ejected by the Coulomb forces resulting from the 49-kev transition, it will travel some hundreds of angstroms or more from its bonding partner before its charge is increased by vacancy cascades initiated by the 37-kev transition. Accordingly, the further charging will take place in a free Br atom. Therefore, the electric field $\bar{E}$ will be acting on an ion of positive charge greater than ne while the energy of the ion will have been determined by the initial charges ne and me of the Br and CH_3, respectively [Eq. (2)]. For the 55% of the ions that are the result of two internal conversions, the limiting expressions which give the relation between the electric fields and the state of ionization of the bromine become

$$\bar{E}n'/n=\text{constant} \quad (5)$$

and

$$\bar{E}n'/n^2=\text{constant}, \quad (6)$$

where n' is the final charge on the Br after both internal conversions and n is the charge after the 49-kev step. These relations are derived by combining Eqs. (1) and (2) and noting that the electric field acts on Br of charge $n'e$ and that after the first nuclear transition the charge me on the methyl group is taken to be first independent of the charge on the bromine [for Eq. (5)] and then proportional to it [for Eq. (6)]. Thus $\bar{E}$ should be varied as some function between n/n' and n^2/n' to assure constant sensitivity for all bromines, the choice depending on the function taken to account for internal charge transfer. But n is unknown for these cases; it may vary from 1 to $(n'-1)$. Accordingly, Eq. (5) may vary from $\bar{E}n'=\text{constant}$ to approximately $\bar{E}=\text{constant}$; while Eq. (6) may go from $\bar{E}n'=\text{constant}$ to $\bar{E}/n'=\text{constant}$. The charge spectrum of bromines actually observed will be a summation of the distribu-

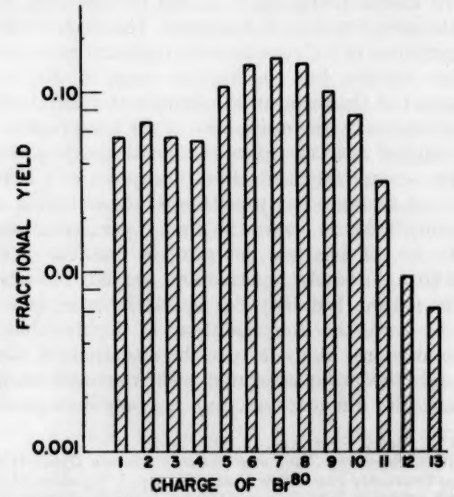

FIG. 3. Ion yields of charged bromine atoms from nuclear isomeric transition of Br^{80m}.

[39] V. F. Weisskopf, Phys. Rev. 83, 1073 (1951).
[40] M. Goldhaber and A. W. Sunyar, *Beta- and Gamma-Ray Spectroscopy*, edited by K. Siegbahn (Interscience Publishers, Inc., New York, 1955), pp. 463, 464.

tions from the 45% and 55% of the transitions which have undergone one and two internal conversions, respectively. Note that for 45% of the bromines the limits of the required variation of the potential with magnitude of charge is from a fixed field to one which increases linearly with the charge, while for the remaining Br ions the limits are from an electric field which is varied inversely with the charge of the bromine to a field condition which is proportional to the charge. Thus the most reasonable approximation for this admittedly complex situation is to hold the electric fields the same for all the bromine ions in order to have the sensitivity of the spectrometer remain approximately independent of the charge state. Because of these difficulties, the results on the distribution of charge states reported here are only semiquantitative. For an exact experiment it will be necessary to know the initial recoil energy of each of the observed fragments.

In the present state of this type of experiment it is not possible to select voltage conditions to ensure that the fraction of ionic organic fragments transmitted through the spectrometer is the same as that of the bromines, because the same hydrocarbon fragments are the dissociation partners of all the bromines in the spectrum of charged Br ions and thus their initial energies will be a complicated function of the charge distribution. Secondly, the intensities measured for the hydrocarbon fragments include an undetermined fraction originating in dissociation of excited singly charged CH_3Br^{80}. Therefore, we have had to be content with measurements on the hydrocarbon fragments under field conditions which provided the highest possible sensitivity for these ions, and their relative abundances are in no direct way related to the intensities of the bromine ions. They are used only to arrive at a qualitative picture of fragmentation of methyl bromide by nuclear isomeric transition of Br^{80m}.

IV. RESULTS

Table I contains the relative abundances of the positively charged fragments from isomeric transition of CH_3Br^{80m}. The errors listed are probable errors based on the scatter of results from many runs taken over a period of four months. The abundances are arbitrarily determined relative to that of Br^{+5}. In Fig. 3 the relative intensities of the monoatomic bromine species are plotted in histogram form, the ordinate being the fractional yield of all atomic bromine ions. The distribution is slightly peaked, with the most probable charge being $+7e$. From this distribution the average charge on the atomic bromine fragments is $+6.4e$. If it is assumed that the CH_3Br^+ ion, which is the result of nuclear transitions in which only one electron is lost (by internal conversion), is transmitted with the same efficiency as the charged Br ions, and that only one electron is transferred from methyl to Br prior to bond rupture, the average charge developed on the CH_3Br^{80} molecule as a result of internal conversion and vacancy cascades is calculated to be $+6.8e$. This average should be a lower limit because in small fractions of the transitions two and three electrons appear to be transferred internally (Table I). There appears to be a dip in the region Br^{+3} and Br^{+4}, and the yields of ions drop off markedly above a charge of $+10$. But the distribution is not symmetrical, in contrast to the fair symmetry in the Xe^{131} spectrum,[19] the lower charged ions being much enhanced. The relatively high yields of Br^{+1} and Br^{+2} make the spectra appear nearly flat.

In the previous discussion (Sec. III) it was pointed out that the lack of information on the recoil energies of the hydrocarbon fragments make it impossible to preset conditions to ensure the same collection efficiency for them as for the bromines. Consequently, the ion yields of the hydrocarbons tabulated in Table I have no quantitative relation to that of the Br spectrum. They do, however, indicate certain characteristics of the molecular effects of the nuclear isomeric transition of 4.4-hr Br^{80m}. The presence of $(CH_3Br^{80})^+$ in the fragmentation pattern suggests that on ejection of only the conversion electron, the molecular-ion may remain bound, but the absence of $(CH_3Br)^{+2}$ and $(CH_3Br)^{+3}$ imply that multiply charged methyl bromide ions dissociate. The CH_3^+ is the major fragment in the mass pattern and its presence suggests that Coulombic repulsion after an internal transfer of a single electron is the principal mechanism by which a multiply charged CH_3Br ion breaks up. In smaller fractions of the nuclear transitions two or three electrons move from the CH_3 to the highly charged Br prior to the molecular decomposition, as shown by the detection of C^{+2} and C^{+3}. It appears that CH_3Br molecules and CH_3 fragments which have lost more than one electron are unstable, as seen in the absence of $(CH_3Br)^{n+}$ and CH_3^{n+} where $n>1$. They apparently have shorter lifetimes than their transit times in the source (10^{-5} to 10^{-4} sec). Excited methyl fragments may lose hydrogens as evidenced by the presence of CH_2^+, CH^+, and C^+.

V. DISCUSSION

The isomeric decay of 4.4-hr Br^{80m} to its 18-min daughter proceeds by two successive transitions, as shown in Fig. 2.[30] The 49-kev step is completely converted while the second 37-kev jump is 55% converted.[41] The internal conversions in the K (84% and 87% for the first and second transition, respectively) and L (16% and 13%, respectively) shells of Br^{80} result in deep-lying shell vacancies which are filled by subsequent Auger and radiative electron transitions, with numerous concomitant electron ejections. The end product of the many vacancy cascades is a bromine ion of rather high positive charge. Considering the most probable Auger transitions except those of the Coster-Kronig type, Cooper[13] has calculated an average of $+4.7e$ for a Br atom which has undergone internal conversion in its K

[41] P. Rothwell and D. West, Proc. Phys. Soc. (London) **A63**, 539 (1950).

TABLE II. Estimated distribution of charge states of Br^{80} from isomeric transition.

Charge state	Estimated relative abundance
+2	0.03
+4	0.27
+6	0.05
+7	0.34
+8	0.14
+9	0.11
+11	0.06

shell. Because of the myriad paths by which the vacancy cascades may proceed, a spectrum of charge states will result. The shape of the charge spectrum from internal conversion in Br^{80m} will be determined by the conversion coefficients for the two transitions, the probabilities of conversion of each γ ray in the various electron shells, the fluorescence yield characteristic of each level, and the relative probabilities of the numerous energetically possible radiationless and x-ray transitions. States of low charge will result when the original deep-lying vacancies are filled principally by x-ray transitions, or by conversion in the outer shells, while the states of high charge will be produced when each of the two internal conversions is followed mainly by radiationless (Auger) transitions. If the Br^{80m} is attached in a molecule, such as CH_3Br, molecular effects such as internal charge transfer will modify the charge pattern. The complexity of the charging effects and lack of information on the relative probabilities of the many x-ray and Auger transitions prevent an exact calculation of the expected charge spectrum for comparison with the observed one. Nevertheless, we have used Cooper's procedure to make an admittedly crude estimation of the charge pattern of Br^{80}, but have taken into account the fact that two successive transitions are involved and have used only the known conversion coefficients,[30] the K/L conversion ratios and the fluorescence yields[37] associated with the inner shells of bromine. It was assumed (a) that all electron transitions following conversion of the 49-kev nuclear jump are completed before the 37-kev decay occurs; (b) the only Auger transitions are $K \rightarrow LL$, $L \rightarrow MM$, $M \rightarrow NN$, i.e., subshell effects and Coster-Kronig transitions are ignored; and (c) the only x-ray transitions are $K \rightarrow L$, $L \rightarrow M$, and $M \rightarrow N$. Table II contains the charge distribution estimated by this method. The average charge derived from this pattern is $+6.8e$. Despite the crudeness of the calculation, the predicted spectrum (except for the discontinuity at charge +6) is peaked and is in the same region of charges as that observed in this experiment (Fig. 3). Further, the average charge derived from the calculated charge distribution agrees exactly (and fortuitously!) with the mean computed from the experimental data.

Now let us consider the electronic and molecular consequences of the isomeric transition when the Br^{80m} is attached in a molecule such as methyl bromide. From the breadths of x-ray absorption edges and emission lines,[34-37] it is possible to make a rough estimate of the time necessary for completion of the charging process initiated by the nuclear internal conversion. This length of time comes to 10^{-15} to 10^{-16} sec. Consequently, the entire charging process takes less time than the period of one vibration of each of the bonds (10^{-13} to 10^{-14} sec), so the atoms in the methyl bromide molecule remain roughly fixed in their relative positions until after the molecule receives a high, but variable, charge. The vacancy cascades probably occur only in the bromine atom and not in other atoms of the molecule because of the nearness of the electrons in the former.[42] In those nuclear transitions in which only the 49-kev step is converted and this process is followed only by x-ray and γ-ray emission, the CH_3Br^{80} will end up with a single positive charge. This ion may remain bound or, because it may also be excited, dissociate partially into charged hydrocarbon and bromine ions and neutral fragments, as when CH_3Br is ionized by electron impact. Since the recoil the $(CH_3Br^{80})^+$ receives is nearly all from ejection of a 37-kev electron, its initial kinetic energy will be very low (0.2 ev), and it will therefore be transmitted through the mass spectrometer with higher efficiency than ions formed in more complicated processes. If the charge that builds up in the valence shell of the Br^{80} atom is greater than one, a redistribution of charges on the methyl bromide becomes probable because the ionization potential of the CH_3 radical (9.96 ev) is always less than that of singly or multiply charged bromine (first ionization potential = 11.84 ev). From the data of Table I, it appears that the internal transfer of a single electron is most probable, as shown by the appearance of singly charged hydrocarbon fragments in the mass pattern, but two and three electron transfers are also possible. The rearrangement of charges on the CH_3Br^{80} molecule will then cause the bromine and hydrocarbon parts to fly apart with kinetic energies determined by Coulombic repulsion. In those cases in which many electrons leave the molecule, the bond holding the bromine and carbon together is probably broken simply by disappearance of the bonding electrons. But the kinetic energies of the fragments are the result of Coulomb repulsion of the separated charges. Taking the separation of charges to be equal to the carbon-bromine bond length (1.9 A),[43] we find that the total energy of Coulombic repulsion between the CH_3^+ and the bromine ion varies from 7.6 ev for Br^{+1} to 99 ev for Br^{+13}. This energy range is higher when more than one charge is on the hydrocarbon fragment. The energies calculated are clearly in excess

[42] See footnote reference 34, pp. 11–14.
[43] See footnote reference 38, p. 167.

of the energy of the C—Br bond (2.3 ev).[44] Consequently, only singly charged CH_3Br^{80} has a chance of remaining bound. Gordus and Willard[3] have found that less than 1% of the methyl bromides tagged with Br^{80m} fail to undergo carbon-bromine bond rupture in the isomeric transition. This percentage may be compared with the relative abundance of 9.5 to 10.0% found for $(CH_3Br^{80})^+$ in the experiments reported in this paper, the assumption being that this molecular-ion is transmitted through the spectrometer with the same efficiency as the bromines and that the other ions observed are not produced by dissociation of CH_3Br^+. The higher apparent nonrupture observed in the mass spectrometric measurements is probably due to the higher transmission of the bound ion relative to the bromines and the possibility of dissociation by neutralizing collisions in the earlier high-pressure experiments. In addition, the relative yield of the bound methyl bromide ion found here would be somewhat lower if part of the hydrocarbon intensities were the result of dissociation of excited $(CH_3Br^{80})^+$.

In concluding from the results that the CH_3Br molecule breaks apart by Coulombic repulsion of separated charges, we have assumed that the charged bromines and carbon-containing fragments observed come off in the same modes of dissociation. It is very unlikely that the charged carbon species are formed in those dissociative processes which give neutral Br. Studies on charge exchange demonstrate that under nonresonant conditions electron transfer is not complete.[45–47]

From the distribution of monoatomic bromine ions and the abundance of the $(CH_3Br^{80})^+$ ion, the lower limit on the average number of electrons (conversion and Auger) which leave the methyl bromide molecule in the isomeric transition is calculated to be 6.8. In this calculation the relative yield of $(CH_3Br^{80})^+$ ion was taken to indicate the fraction of nuclear transitions in which only one electron left the molecule, the yield of $(Br^{80})^{+1}$ the fraction of decays wherein two electrons were lost, etc. We assumed that the fraction of CH_3Br^{80} ions transmitted through the spectrometer was the same as that of each of the charged bromines, and that there is a transfer of only one electron from methyl to bromine prior to separation of the ionic fragments. The value is lower than the average of 10 ± 2 electrons ejected from $C_2H_5Br^{80m}$ in the isomeric transition process, as determined by direct measurements of the currents of ionic fragments.[17] Although it is possible that the difference in molecules may play a role, it is more likely that the lower average derived from the mass spectrometric experiments may be accounted for partly by limitations in sensitivity of the apparatus, which precluded measurements beyond Br^{+13}, but mainly by the approximations involved in arriving at the proper conditions of the electric field. The appearance of C^{+2} and C^{+3} in the fragmentation pattern (Table I), though in low abundance, indicates that on occasion there may be intramolecular transfers of more than one electron, and in these events therefore the bromines are associated with higher charge states of the molecule. Also, because the kinetic energies of the bromines from breakup of these molecular ions are higher than when they are repulsion partners of CH_3^+, they are collected in lower fraction. Furthermore, it is not clear from this experiment whether the H^+ fragments (Table I) are the result of internal electron transfer in the CH_3Br molecule or of the decomposition of singly-charged polyatomic species. If their presence in the mass pattern is due to the former process, the internal charge transfer in the methyl bromide prior to disruption may be as much as six electrons going from methyl to bromine. Proper corrections for these effects as well as the probably excessive relative transmission of the $(CH_3Br^{80})^+$ would undoubtedly move the observed distributions to higher charges and thereby increase the average derived.

It is of interest to note that isolated multiply charged molecular fragments are unstable; their lifetimes are shorter than the transit times in the source volume (10^{-4} to 10^{-5} sec). For example, $(CH_3Br^{80})^{+2}$, $(CH_3Br^{80})^{+3}$, $(CH_3)^{+2}$, and $(CH_3)^{+3}$ are absent from the breakup pattern (Table I), but C^{+2} and C^{+3} are found. It is probable that multiply charged polyatomic species are also unstable in condensed media or in gases at relatively high pressure. Consequently, molecular species formed by replacement reactions of multiply charged bromine ions with organic compounds[3,6–12] must be stabilized by charge neutralization within a very short time. Alternately, the replacement reactions may be due to singly charged or neutral Br atoms after nearly complete or total neutralization of the positive charge developed as a result of the isomeric transition.

ACKNOWLEDGMENT

The authors wish to thank Dr. Lee Teng for several informative discussions on ion optics.

[44] See footnote reference 38, p. 53.
[45] C. W. Sherwin, Phys. Rev. **57**, 814 (1940).
[46] A. Wolf, Ann. Physik. **34**, II, 341 (1939).
[47] F. L. Arnot and W. D. Hart, Proc. Roy. Soc. (London) **A171**, 383 (1939).

Mass Spectra of Aluminum(III) Halides and the Heats of Dissociation of $Al_2F_6(g)$ and $LiF \cdot AlF_3(g)$*

RICHARD F. PORTER† AND ERNEST E. ZELLER

Department of Chemistry, Cornell University, Ithaca, New York

(Received March 24, 1960)

Mass spectra of gaseous aluminum(III) chloride and bromide have been obtained and interpreted quantitatively in terms of the degree of association in the vapor phase. Ion currents indicative of a molecular trimer of $AlCl_3$ have been observed. Mass spectra of the vapors effusing from a Knudsen cell containing AlF_3 have been obtained and the stability of the molecular dimer of $AlF_3(g)$ has been determined quantitatively. Mass spectra of vapors from LiF–AlF_3 mixtures indicate the existence of a stable $LiF \cdot AlF_3(g)$ molecule. Ion current data have been obtained as a function of condensed phase composition. A second complex molecular species which appears to be either $(LiF)_2 \cdot AlF_3(g)$ or $(LiF \cdot AlF_3)_2(g)$ has been observed. For the reaction $Al_2F_6(g) = 2AlF_3(g)$, $\Delta H°_{1000} = 48.0 \pm 4.0$ kcal/mole dimer, and for $LiF \cdot AlF_3(g) = LiF(g) + AlF_3(g)$, $\Delta H°_{1000} = 73 \pm 4$ kcal/mole.

INTRODUCTION

THE degree of dimerization of $AlCl_3(g)$, $AlBr_3(g)$, and $AlI_3(g)$ has been determined from vapor density measurements.[1] These results indicate that for the chloride, bromide, and iodide salts of aluminum, the species evaporating from the condensed halide phase is primarily the dimeric molecule, Al_2X_6. The degree of dimerization of $AlF_3(g)$ has not been determined although several investigators[2] have measured the volatility of $AlF_3(s)$. Vapor density experiments with AlF_3 would involve some experimental difficulties, since the volatility of $AlF_3(s)$ is considerably less than that of the other aluminum halides. Treatments[2,3] of existing vapor pressure data indicate that the dimer of $AlF_3(g)$ is not a major vapor species.

In the present experiments a combination of mass spectrometric and Knudsen effusion techniques have been employed to study the vaporization behavior of AlF_3 and LiF–AlF_3 mixtures. Mass spectra of aluminum chloride and aluminum bromide vapors have also been obtained.

EXPERIMENTAL

Descriptions of the mass spectrometer and furnace assembly have been given earlier.[4] A beam of gaseous molecules effusing through a small opening in a Knudsen cell is ionized by electron bombardment with electrons of energy between 5 and 150 volts. The ions thus formed are analyzed in a 12-in., 60°, direction-focusing mass spectrometer. A shutter located between the ion source and the Knudsen cell may be operated externally. This allows one to determine the intensity of ions formed by electron impact of molecules leaving the cell in the presence of background ions appearing at the same mass positions. For experiments with pure AlF_3, the Knudsen cell was constructed of graphite. This was set into a heavy Inconel base to which a Pt–Pt, 10% Rh thermocouple was securely fastened. For experiments with LiF–AlF_3 mixtures, graphite and molybdenum cells were used. Cells were heated by the combined radiative and high-voltage electron bombardment power from two surrounding tungsten filaments.

For experiments with $AlCl_3$ and $AlBr_3$ the sample was also introduced into the mass spectrometer from a small effusion cell located within the furnace assembly. Due to the extreme volatility of the chloride and bromide, the method of introducing the gas sample resembles the conventional leak procedure, except that the pressure control was achieved by heating the cell. "Shutter effects" were not obtained since the vapor leaving the cell does not condense on the shutter plates, which are slightly above room temperature, or collimating plates in the ion source. Under these conditions the mass spectra are not necessarily representative of the equilibrium vapor composition at the cell temperature, since there is the possibility that dissociation processes could occur in the ion source, which is heated by the filament used for obtaining the ionization current. The operating temperatures of the cells were usually between 50°C and 80°C.

Anhydrous aluminum halides were obtained through commercial sources. The $AlCl_3$ was distilled prior to use. Rapid transfer of the anhydrous $AlCl_3$ and $AlBr_3$ was essential to minimize the hydrolysis problem. Hydrolysis was not prevented entirely as was evidenced by the appearance of HCl^+ and HBr^+ in the mass spectrometer.

* This research was supported by the United States Air Force through the Air Force Office of Scientific Research of the Air Research and Development Command.

† Alfred P. Sloan research fellow.

[1] W. Fischer and O. Rahlfs, Z. anorg. u. allgem. Chem. **205**, 1 (1932); A. Smits and J. L. Meijering, Z. physik. Chem. (Leipzig) **B41**, 98 (1938).

[2] W. P. Witt and R. F. Barrow, Trans. Faraday Soc. **55**, 730 (1959) and references quoted therein.

[3] T. B. Douglas, A. C. Victor, and A. R. Beaudoin, Natl. Bur. Standards U. S. Rept. 6484, 62 (July, 1959).

[4] R. F. Porter and R. C. Schoonmaker, J. Chem. Phys. **29**, 1070 (1958).

RESULTS

AlF_3

A typical mass spectrum of AlF_3 vapor is given in Table I. The ion species indicated had well defined shutter effects and the ion intensities are therefore proportional to the effusion cell pressure of the molecular species from which the ions originate. The mass spectrum is consistent with that expected for conditions where $AlF_3(g)$ is the major vapor species. The high intensity of AlF_2^+ is not surprising since fragmentation processes with the loss of one halogen atom appear to be common to many metal halide systems. The mass spectrum of AlF_3 resembles that of $BF_3(g)$[5] where the ratio of parent ion to fragment ion, BF_3^+/BF_2^+, is about 20 for electron energies of 75 v. The only polymeric ion of significant intensity was $Al_2F_5^+$. The $AlF_2^+/Al_2F_5^+$ ratio was generally between 50 and 100. The formation of polymeric ions by ion-molecule interactions subsequent to ionization is unlikely because of the geometrical arrangements of the ion source and high drawing-out potentials employed. Further, on the basis of observations of ion-molecule reactions, a reaction involving AlF_2^+ and $AlF_3(g)$ would be expected to favor two fragments each with mass less than that of $Al_2F_5^+$. The $Al_2F_5^+$ ion is thus assumed to be formed primarily by fragmentation of the molecular dimer of AlF_3. Subsequent observations with $AlCl_3$ and $AlBr_3$ lend support to this assumption.

TABLE I. Mass spectra of AlF_3, vapor ($T=1025°K$, ionizing electron energy = 100 v).

I_{Al^+}	I_{AlF^+}	$I_{AlF_2^+}$	$I_{AlF_3^+}$	$I_{Al_2F_5^+}$
0.9	0.7	100.0	5.7	2.5

$AlCl_3$

Relative intensities for ions produced by electron impact of $AlCl_3$ vapor are given in Table II. The highest masses were identified by calibration with a field meter and were confirmed by comparing the relative intensities of isotopic ions due to Cl^{35} and Cl^{37} with those calculated statistically from the known abundances of the two isotopes. A few extraneous masses with small intensities were also observed. These were later identified as $Al_2Cl_4F^+$ and $Al_2Cl_3F_2^+$, and may originate from molecular species formed by the reaction of the chloride molecules with traces of AlF_3 deposited in the ion source. Since the intensities of these ions were at least two orders of magnitude lower than that of $Al_2Cl_5^+$, the contribution these species make to the $Al_2Cl_5^+$ peak is assumed to be negligible. The high intensity of polymeric ions is consistent with the large degree of association in the vapor phase. It is interesting to note that species containing three Al atoms were also found. Ion species containing four Al atoms were not observed. In Table II we have classified the ion species as originating from monomeric, dimeric, and trimeric molecular species. A simple linear proportionality between the monomeric and dimeric ions as a function of gas pressure was not observed, and it is thus assumed that the number of monomeric ions formed in fragmentation processes involving the dimer, relative to that formed from $AlCl_3(g)$, is small. It should be emphasized that Al_2Cl_6 molecules, after leaving the effusion cell, may undergo partial dissociation in the ion source region of the mass spectrometer. The increase in the $AlCl_2^+/Al_2Cl_5^+$ ratio with pump-out time also indicates this behavior.

TABLE II. Mass spectra of $AlCl_3$ vapor.

Molecular species	Ion (X^+)	X^+ intensity[a] (relative units)	$A(X^+)$[b] volts
Monomer	Al^+	16.1	22.1±0.5
	$AlCl^+$	26.1	19.7±0.5
	$AlCl_2^+$	100.0	13.4±0.5
	$AlCl_3^+$	43.5	12.8±0.5
Dimer	$Al_2Cl_5^+$	187	13.1±0.5
	$Al_2Cl_6^+$	1.0	
Trimer	$Al_3Cl_7^+$	0.28	
	$Al_3Cl_8^+$	0.52	
	$Al_3Cl_9^+$	0.06	

[a] Ionizing electron energy = 100 volts; total intensities of all isotopic species are given; relative intensities of monomer/dimer/trimer are not necessarily of quantitative significance since they are time dependent and may vary with ion source conditions.
[b] Calibrated against $A(HCl^+)=13.8$ v.

The trimer spectrum is qualitatively similar to monomer and dimer spectra in which the major ion observed is $Al_nCl_{3n-1}^+$. Speculation that the trimeric ions are formed by ion-molecule reactions seems unwarranted since the most conceivable reactions (i.e., $Al_2Cl_5^+ + AlCl_3$ or $AlCl_2^+ + Al_2Cl_6$) are expected to lead to fragments smaller than $Al_3Cl_5^+$. A small intensity of parent ion, $Al_3Cl_9^+$, was also observed.

Appearance potentials for Al^+, $AlCl^+$, and $AlCl_2^+$ which are attributed to fragmentation of $AlCl_3(g)$ were

TABLE III. Mass spectra of $AlBr_3$ vapor.

Molecular species	Ion (X^+)	X^+ intensity[a] (relative units)	$A(X^+)$[b] volts
Monomer	Al^+	40	18.3±0.5
	$AlBr^+$	18	17.7±0.5
	$AlBr_2^+$	100	13.3±0.5
	$AlBr_3^+$	71	12.2±0.5
Dimer	$Al_2Br_5^+$	28	12.3±0.5
	$Al_2Br_6^+$	0.2	

[a] Ionizing electron energy = 100 v.
[b] Calibrated against $A(HBr^+)=13.2$ v.

[5] See, for example, J. Marriott and J. D. Craggs, J. Electronics 3, 194 (1957).

TABLE IV. Thermochemical data for the reaction $(AlF_3)_2(g) = 2AlF_3(g)$.

Cell temp., °K	I_d/I_m	$P(AlF_3)$ (atmos.)	K_{eq}	ΔF_T^0 kcal/mole dimer	ΔH_T° kcal/mole dimer
965	0.014	1.1×10^{-6}	1.1×10^{-4}	17.50	48.40
965	0.017	1.1×10^{-6}	8.7×10^{-5}	17.95	48.84
1022	0.023	1.1×10^{-6}	6.3×10^{-4}	15.00	47.74
1065	0.015	4.2×10^{-6}	3.7×10^{-3}	11.85	45.95
995	0.023	4.2×10^{-6}	2.4×10^{-4}	16.45	48.25
1025	0.025	1.2×10^{-6}	6.4×10^{-4}	15.00	47.80
1014	0.016	8.1×10^{-6}	6.6×10^{-4}	14.75	47.25

TABLE V. Ion intensities for LiF-AlF_3 vapors as a function of condensed phase composition (ionizing electron energy = 100 v).

Initial molar ratio LiF:AlF_3	Cell temp., °K	I_{Li^+}	I_{LiF^+}	$I_{Li_2F^+}$	$I_{AlF_2^+}$	$I_{LiAlF_3^+}$	$I_{Li_2AlF_4^+}$
8:1	1067	100.0	8.0	48	7.4	3.7	...
2:1	1029	100.0	2.4	14.2	8.9	2.4	...
1:1	991	100.0	...	...	8.6	5.1	1.5
1:2	1079	100.0	...	...	32.3	5.4	Small
1:5	969	100.0	...	...	22.7	6.1	2.9

higher than that for $AlCl_3^+$. These values show a trend similar to that found for BCl_3.[5] The very high appearance potential for Al^+ suggests a process: $AlCl_3(g) + \bar{e} \rightarrow Al^+ + 3Cl + 2\bar{e}$.

$AlBr_3$

Mass spectra for $AlBr_3$ vapor are presented in Table III. No attempt was made to search for polymeric species higher than $Al_2Br_6^+$. Impurity peaks containing Cl atoms were also found. The species $Al_2Br_4Cl^+$ was the largest of these. A small contribution to the $Al_2Br_5^+$ peak may therefore arise from fragmentation processes involving the molecule Al_2Br_5Cl. The bromide spectrum is qualitatively very similar to that of the chloride. In general appearance potentials for the bromide species were lower, however. The lower value for $A(Al^+)$ from $AlBr_3$ is presumably an implication that the average Al–X bond strength in $AlBr_3$ is less than that in $AlCl_3$.

HEAT OF DIMERIZATION OF $AlF_3(g)$

By a procedure similar to that used previously[4] we may calculate ΔH° for the reaction:

$$2AlF_3(g) = Al_2F_6(g)$$

with aid of the intensity ratio of monomeric to dimeric ions. We have the relationship

$$P_d/P_m = (\sigma_m/\sigma_d)(S_m/S_d)[\Sigma I(x^+)_d/\Sigma I(x^+)_m].$$

In this case $\Sigma I(x^+)_d = I_{Al_2F_5^+}$ and $\Sigma I(x^+)_m \approx I_{AlF_2^+} + I_{AlF_3^+}$ and P_d/P_m is the ratio of the partial pressures of Al_2F_6 and AlF_3 in the effusion cell. The quantities σ_m/σ_d and S_m/S_d are relative cross section and detection efficiency terms, respectively. For σ_m/σ_d we use an estimated value of 0.5. The S_m/S_d term is calculated to be about 1.5. Free energy increments for the dimerization reaction were then computed from values of P_d/P_m and the vapor pressure data of Witt and Barrow,[2] which are applicable to the conditions employed in these experiments where the vapor phase is primarily monomeric AlF_3. Values of ΔF° thus obtained were combined with ΔS° to yield the enthalpy change for the reaction. A value of $\Delta S^\circ = -32 \pm 3$ entropy units for the dimerization reaction was used. This value was estimated from considerations of the entropy of dimerization of the alkali halides and the other aluminum halides.[1,3] These calculations are summarized in Table IV. For the dimerization reaction we obtain a value of $\Delta H^\circ_{1000} = -48.0 \pm 4.0$ kcal/mole dimer.

LiF-AlF_3 Mixtures

Mass spectra of the vapors in equilibrium with mixtures of LiF and AlF_3 were obtained for a range of condensed phase composition. The ion species observed on electron impact had normal shutter effects indicating that they were formed in processes involving molecular species leaving the effusion cell. The relative abundances of most ions changed markedly with condensed phase composition. This effect is indicated in Table V. Under all conditions, Li^+ was initially the ion of greatest intensity. At low LiF/AlF_3 ratios LiF^+ and Li_2F^+ were low in abundance. In mixtures rich in AlF_3, the Li^+ and other ions with Li atoms dropped abruptly relative to AlF_2^+, after the cell had been heated for several minutes, indicating that a volatile lithium species had vaporized. For the condition where LiF/$AlF_3 \approx 1$ the relative ion intensities changed very little even after the cell had been heated for several hours and a large fraction of the sample had evaporated. As indicated in Table V, the $Li^+/LiAlF_3^+$ ratio was found to be nearly constant for most conditions, except when the molar ratio LiF/AlF_3 was large. The

above observations are taken as evidence that Li^+ and $LiAlF_3^+$ are formed from the same molecular precursor which logically appears to be $LiF \cdot AlF_3(g)$ when $LiF/AlF_3 \approx 1$. The appearance potential curve (Fig. 1) for Li^+, taken with $LiF/AlF_3 \approx 1$, shows that the ion is formed by one or more high-energy processes and cannot be formed primarily from $LiF(g)$.[6] At high LiF/AlF_3 ratios LiF^+ and Li_2F^+ appeared, indicating that $LiF(g)$ and $Li_2F_2(g)$ were becoming important vapor species. Under these conditions, $Li^+/LiAlF_3^+$ is larger than that observed at lower LiF mole fractions. This effect is to be anticipated since the Li^+ ion then may be formed from $LiF \cdot AlF_3(g)$ and $LiF(g)$. The $Li_2AlF_4^+$ ion which appears under certain conditions is presumed to be formed from either $(LiF)_2 \cdot AlF_3(g)$ or $(LiF \cdot AlF_3)_2(g)$.

A summary of the proposed ion-precursor relationships, based on the observations of ion current ratio as a function of condensed phase composition, is presented in Table VI.

HEAT OF DISSOCIATION OF $LiF \cdot AlF_3(g)$

To evaluate $\Delta H°$ for the reaction

$$LiF \cdot AlF_3(g) = LiF(g) + AlF_3(g),$$

we consider the thermodynamic cycle involving the reactions:

$$Li_2F_2(g) + AlF_3(g) = LiF(g) + LiF \cdot AlF_3(g) \qquad (1)\ \Delta H_1°$$

and

$$2LiF(g) = Li_2F_2(g). \qquad (2)\ \Delta H_2°$$

The $\Delta H°$ of interest is $-(\Delta H_1° + \Delta H_2°)$. For reaction (2) $\Delta H°$ has been determined previously.[4] For reaction (1) we have the expression

$$K_{eq} = \frac{(P_{LiF})(P_{LiF \cdot AlF_3})}{(P_{Li_2F_2})(P_{AlF_3})}.$$

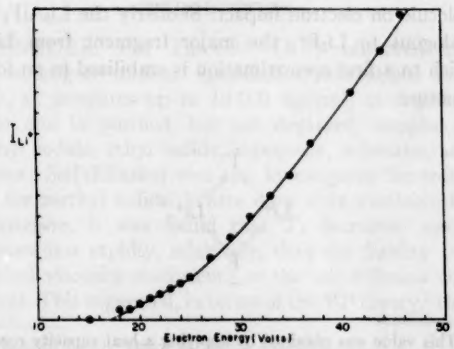

FIG. 1. Appearance potential curve from Li^+ formed by electron impact of vapors from a 1:1 molar mixture of $LiF:AlF_3$.

[6] The appearance potential of Li^+ observed here is several volts higher than that required to form Li^+ from $LiF(g)$.

TABLE VI. Proposed ion-molecule precursor relationships for LiF-AlF_3 system.

Condensed phase composition in molar units	Ion	Molecular species
$LiF = AlF_3$	Li^+	$LiF \cdot AlF_3$
	AlF_2^+	AlF_3
	$LiAlF_3^+$	$LiF \cdot AlF_3$
	$Li_2AlF_4^+$	$(LiF)_2 \cdot AlF_3$ or $(LiF \cdot AlF_3)_2$
$LiF > AlF_3$	Li^+	LiF and $LiF \cdot AlF_3$
	LiF^+	LiF
	Li_2F^+	Li_2F_2
	AlF_2^+	AlF_3
	$LiAlF_3^+$	$LiF \cdot AlF_3$
$LiF < AlF_3$	Li^+	$LiF \cdot AlF_3$
	AlF_2^+	AlF_3
	$LiAlF_3^+$	$LiF \cdot AlF_3$
	$Li_2AlF_4^+$	$(LiF)_2 \cdot AlF_3$ or $(LiF \cdot AlF_3)_2$

In this type of reaction we may approximate K_{eq} by the relationship

$$K_{eq} \approx K' = \frac{[(I_{Li^+} + I_{LiF^+})_{LiF}][(I_{Li^+} + I_{LiAlF_3^+})_{LiF \cdot AlF_3}]}{[(I_{Li_2F^+})_{Li_2F_2}][(I_{AlF_2^+} + I_{AlF_3^+})_{AlF_3}]},$$

where the terms in brackets refer to the total ion current that is proportional to the partial pressure of the molecular species in the effusion cell. This approximation can be reasonably justified since the ionization cross section, detection efficiency, and sensitivity factors should very nearly cancel in the exact expression. To evaluate K', ion current data were obtained from experiments where the molar ratio of LiF to AlF_3 was large since only under these conditions are $LiF(g)$ and $Li_2F_2(g)$ in appreciable concentration in the vapor phase. In order to proceed we must first resolve the Li^+ ion current into the fractions coming from $LiF(g)$ and $LiF \cdot AlF_3(g)$. This may be accomplished either by calculating the Li^+ contributions from the observed intensity of $LiAlF_3^+$ and the $Li^+/LiAlF_3^+$ ratio obtained with high AlF_3 mole fractions or by computing the Li^+ contribution from $LiF(g)$ with the aid of the LiF^+ intensity and the Li^+/LiF^+ ratio obtained with pure LiF.[4] The latter procedure was considered to be the more reliable since with the appropriate experimental conditions, the $LiAlF_3^+$ peak was small relative to LiF^+ and could not be measured as accurately.

Values of K' were obtained from experiments where the initial LiF/AlF_3 ratio in the condensed phase was approximately 8. In the temperature range 1000–1100°K measurements of K' were made as the composition changed due to distillation of the sample. From twelve series of ion current measurements we obtained $K' = 9.0$ with maximum fluctuations of about $\pm 30\%$. Values of K' were found to be quite insensitive to temperature changes and the observed fluctuations were too large to establish the trend in K' with temperature. Ion current ratios of Li_2F^+/Li^+ and Li^+/AlF_2^+,

however, varied by factors of 2 or more during the course of the experiment. These effects may be attributed to changes in cell temperature and changes in composition as $LiF \cdot AlF_3(g)$ is lost by evaporation.

For reaction (1) we have $\Delta F^\circ_{1000} = -RT \ln K' = -4.4$ kcal/mole. The standard entropy change for reaction (1) was determined by combining separate translational, vibrational and rotational contributions. To obtain ΔS°(vib) we assume total cancellation of all but one vibrational degree of freedom contributed by $LiF \cdot AlF_3(g)$. Assuming this to lie between 200 cm^{-1} and 600 cm^{-1} we find ΔS°_{1000} (vib) $= +3.4 \pm 1.0$ units. For calculations of the rotational contribution a planar, rhombic model for Li_2F_2 and a planar, symmetrical model for AlF_3 were assumed. For Li_2F_2, Li–F and F–F distances of 1.80 A and 2.78 A, respectively were used. These were obtained by averaging the theoretical values calculated by Milne and Cubicciotti[7] and by Berkowitz.[8] An Al–F distance of 1.69 A was used for $AlF_3(g)$.[2] For $LiF \cdot AlF_3(g)$ the model was one in which Al is tetrahedrally coordinated by fluorine atoms and the Li atom is located in a F–Al axis below the three fluorine atoms at the base of the tetrahedron. There are thus three equal short Li–F distances and one longer Li–F distance. A short Li–F distance of 1.85 A and an Al–F distance of 1.75 A were estimated. A value of $r_{Li\text{-}F} = 1.70$ A was used for LiF(g). These calculations lead to ΔS°_{1000} (trans. and rot. including symmetry) $= -8.0$ entropy units. Use of an alternative structure for $LiF \cdot AlF_3$ in which the Li atom is extended from only one fluorine atom results in a change in this quantity of only 0.8 entropy units. Summing entropy terms then leads to ΔS°_{1000} (total) $= -4.6 \pm 2.0$ entropy units. The computed value of ΔS° was combined with the experimental ΔF° to give $\Delta H^\circ_{1000} = -9.0 \pm 2.0$ kcal/mole for reaction (1). For reaction (2) we have $\Delta H^\circ_{1073} = -64.1 \pm 3$ kcal/mole of dimer.[4] The enthalpy change for the dissociation of $LiF \cdot AlF_3(g)$ into LiF(g) and $AlF_3(g)$ is then calculated to be $\Delta H^\circ_{1000} = 73$ kcal/mole, with a probable uncertainty of about ± 4 kcal/mole.

DISCUSSION

The magnitude of ion currents attributed to ionization processes involving the trimer of $AlCl_3$ indicates that at the leak pressures suitable for these mass spectrometric studies, the amount of trimer present is quite small. This species, however, may become relatively more important at saturation pressures in condensed-vapor equilibria. Vapor density experiments[1] with $AlCl_3$ pertain to conditions where the gas is below saturation values and where the trimer/dimer ratio is likely to be small. A reasonable structure for $(AlCl_3)_3$ is one in which Al atoms are joined by chlorine bridges to form a six-membered ring. With this structure tetrahedral coordination of chlorine atoms about aluminum can probably be preserved.

The absolute value for ΔH° of dimerization of $AlF_3(g)$ as determined in these experiments is about 20 kcal/mole of dimer larger than values obtained for $AlCl_3$, $AlBr_3$, and AlI_3, which apparently differ from each other by small increments. Combining ΔH° of dimerization of $AlF_3(g)$ with a value[9] of $\Delta H^\circ_{1000} = 69.2$ kcal/mole for the heat of sublimation of $AlF_3(g)$, we obtain for the reaction $2AlF_3(s) = Al_2F_6(g)$, $\Delta H^\circ_{1000} = 90 \pm 4$ kcal/mole of dimer. Comparison of the heats of sublimation of monomer and dimer shows that the dimer/monomer ratio in the saturated vapor increases with increase in temperature. A rough extrapolation of the vapor pressure data for monomer and dimer indicates that at the sublimation temperature (about 1560°K) the dimer/monomer ratio is between about 0.3 and 0.4.

As indicated in Table V, $LiF \cdot AlF_3(g)$ is observed to be a major species evaporating from $LiF–AlF_3$ mixtures with mole fractions of LiF at least as high as 0.9 and as low as 0.2 in the temperature range of these experiments. With mixtures quite rich in LiF, $Li_2F_2(g)$ and LiF(g) also become important species. With condensed phase compositions of LiF/AlF_3 equal to unity the vapor phase consists almost exclusively of $LiF–AlF_3(g)$. Evidence for the existence of complex gaseous species formed in alkali-halide—aluminum-halide systems has been obtained from other sources. From vapor pressure measurements Dewing[10] has proposed that a molecule $NaCl \cdot AlCl_3$ evaporates from $NaCl–AlCl_3$ mixtures. Howard[11] has observed that the condensate of vapors from $NaF–AlF_3$ mixtures have compositions of NaF to AlF_3 in a molar ratio of 1:1. This may be interpreted in terms of a volatile $NaF \cdot AlF_3$ species.

Features of the mass spectrum of $LiF \cdot AlF_3(g)$ are in a sense similar to those for LiF(g) where there is a high probability of splitting off the anion portion of the molecule on electron impact. Similarly the $Li_2AlF_4^+$ is analogous to Li_2F^+, the major fragment from Li_2F_2 which to a first approximation is stabilized in an ionic structure

[7] T. A. Milne and D. Cubicciotti, J. Chem. Phys. **29**, 846 (1958).
[8] J. Berkowitz, J. Chem. Phys. **29**, 1386 (1958).
[9] This value was obtained by applying a heat capacity correction to ΔH_{298}° of sublimation given by Witt and Barrow (reference 2). This value is in close agreement with that evaluated in reference 3.
[10] E. W. Dewing, J. Am. Chem. Soc. **77**, 2639 (1955).
[11] E. H. Howard, J. Am. Chem. Soc. **76**, 2041 (1955).

A species such as

would then be expected to fragment either to $Li^+-\overline{F}-Li^+$ or $Li^+-\overline{AlF_4}-Li^+$. A dimer of $LiF\cdot AlF_3$ with structure

would presumably also fragment to the stable $Li_2AlF_4^+$ ion. Hence only on the basis of the appearance of the $Li_2AlF_4^+$ peak, it is not possible *per se* to decide between $(LiF)_2\cdot AlF_3$ or $(LiF\cdot AlF_3)_2$ as the molecular precursor. The variation in relative ion intensities of $Li_2AlF_4^+$, Li^+ (from $LiF\cdot AlF_3$) and AlF_2^+ (from AlF_3) as a function of condensed phase composition, as observed here, is not sensitive enough to decide the issue on thermodynamic grounds. On structural grounds the $(LiF)_2\cdot AlF_3$ species seems somewhat more acceptable since in this structure there would presumably be a more favorable coordination of Li by fluorine atoms than in a structure involving the interactions of two AlF_4^- groups with relatively small Li^+ ions.

THE JOURNAL OF CHEMICAL PHYSICS VOLUME 33, NUMBER 3 SEPTEMBER, 1960

Effects of Pressure on Proton Spin-Lattice Relaxation in Several Degassed Organic Liquids*

A. W. NOLLE AND P. P. MAHENDROO

Department of Physics, The University of Texas, Austin, Texas

(Received August 17, 1959)

The hydrogen nuclear magnetic relaxation time (T_1) for degassed samples of several organic liquids has been measured, by a transient method, at pressures up to 1400 kg/cm², primarily for comparison with results obtained without degassing. Certain of the liquids were investigated, without degassing, by Benedek and Purcell, who concluded that T_1 decreases under pressure less rapidly than the rates of translational processes (fluidity and diffusion). The present results confirm this for degassed methyl iodide and *n*-heptane, in both of which the effect of degassing is to increase T_1 less than 20%. For benzene and toluene, degassing causes T_1 to increase by several hundred percent, and the preceding conclusion ceases to apply, but instead, in the degassed samples, the relative rate of decrease of T_1 under pressure is comparable to that of the fluidity; in benzene, at low pressures, it is greater. Additional pressure studies are reported for purified cyclohexane, for purified 1,1,1-trichloroethane, and for chloroform, which was not successfully purified.

INTRODUCTION

BENEDEK and Purcell[1,2] (BP) observed the hydrogen nuclear spin-lattice relaxation time (T_1), at pressures up to 10 000 kg/cm², in degassed water and in purified, but not degassed, samples of methyl iodide, ethyl iodide, *n*-pentane, *n*-hexane, and toluene. Self-diffusion was also investigated for water and for methyl iodide. Where data were available for comparison, it was found that T_1 decreased under pressure less rapidly, relatively, than the fluidity (reciprocal viscosity coefficient) or the self-diffusion coefficient. This suggested, in terms of the BP theory,[3] that molecular rotation is slowed much less with increasing pressure than are the translational jump processes.

It was shown later by Chiarotti, Cristiani, and Giulotto[4] (CCG) and by Nederbragt and Reilly[5] that T_1 for various liquids (particularly, aromatic compounds) increases markedly with removal of dissolved oxygen. In these cases, T_1 in the presence of dissolved oxygen is controlled by the correlation time for magnetic interactions between the hydrogen nuclei and O_2, rather than by the correlation time for hydrogen spin-spin interactions. It is therefore of interest to observe the effect of degassing on the T_1 vs pressure functions for such liquids. Here we report observations of this kind for toluene and benzene, as well as for several liquids in which the effect is smaller.

* Assisted by the Office of Naval Research.

[1] G. B. Benedek, "Nuclear magnetic resonance in liquids under high pressure" (unpublished thesis, Harvard University, 1953).

[2] G. B. Benedek and E. M. Purcell, J. Chem. Phys. **22**, 2003 (1954).

[3] N. Bloembergen, E. M. Purcell, and R. V. Pound, Phys. Rev. **73**, 679 (1948).

[4] G. Chiarotti, G. Cristiani, and L. Giulotto, Nuovo cimento **1**, 863 (1955).

[5] G. W. Nederbragt and C. A. Reilly, J. Chem. Phys. **24**, 1110 (1956).

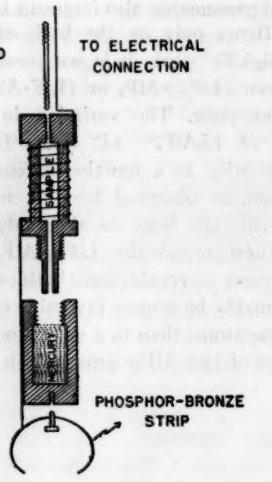

FIG. 1. Section of parts of sample cartridge (not to scale).

EXPERIMENTAL

The sample was contained in a cartridge of Kel-F plastic, as shown in Fig. 1. The coil wound on the cartridge was tuned to the NMR frequency, 28.7 Mc, by an external capacitor. The mercury seal was provided to accommodate to changes in sample volume under pressure. A silicon bronze ("Everdur 1014") pressure cylinder, having inside and outside diameters of 0.390 and 0.875 in., contained the sample cartridge, and was in turn contained within a bronze jacket which permitted circulation of temperature control fluid. This entire assembly fitted within the 1.25-in. gap of a permanent magnet with 6-in. diam pole faces. The pressure transmitting fluid was Kel-F No. 10 liquid, which gave no observable NMR signal. Maximum experimental pressures were 1400 kg/cm², the limit being set by the strength of a pair of stainless steel vessels which were connected as a mercury-filled trap, to isolate the Kel-F fluid from the pump oil. Pressures were read from a dial gauge, calibrated to ±15 kg/cm². No residue

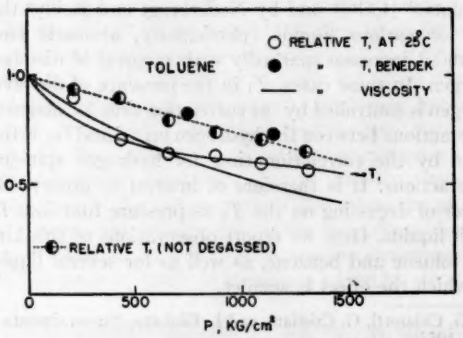

FIG. 2. Normalized T_1 data for toluene, compared with BP data for T_1 and with the reciprocal viscosity behavior.

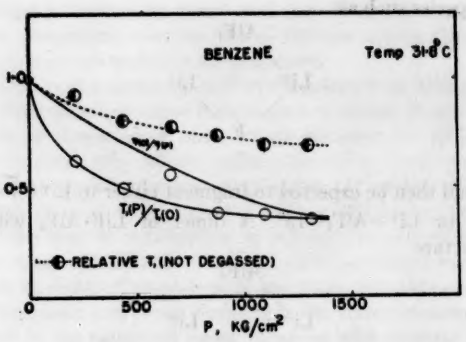

FIG. 3. Normalized T_1 data for benzene, compared with the reciprocal viscosity behavior.

of Kel-F fluid was found in a sample which was removed and evaporated after a complete pressure cycle.

The relaxation time T_1 was found by observing the magnetic recovery of the sample from saturation. The amplitude of the free induction signal following a 90° pulse[6] was used as a measure of the magnetization. Initial saturation was produced by a series of 90° pulses in rapid succession, usually 60/sec. T_1 was determined with an uncertainty of 5 to 10% varying with hydrogen concentration.

Degassing was done with a mechanical vacuum pump and a trap at liquid air temperature. During a 15-min evacuation period, the sample was kept frozen by a solid CO_2 bath or, where lower temperatures were needed, by a bath of melting ethyl bromide at −119°C. The cycle was repeated after thawing. In some cases, improved results were obtained by continued pumping during the thawing period, with some loss of sample. All parts of the sample cartridge, including the mercury, were kept submerged in the test liquid during degassing and subsequent assembly.

A gradual decrease of T_1 occurred for as long as 10

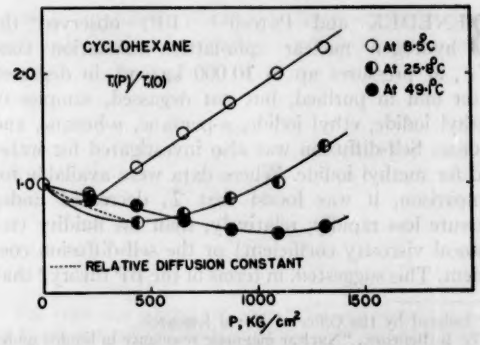

FIG. 4. Normalized T_1 data for cyclohexane, compared with the relative self-diffusion coefficient. Each T_1 curve is carried through the freezing point.

[6] E. L. Hahn, Phys. Rev. **80**, 580 (1950).

hr after completion of the foregoing procedure. This apparently results from release of oxygen from the mercury, although the effect was not entirely eliminated through use of vacuum distilled mercury. The rate of deterioration increased with increasing pressure. It was necessary to complete each pressure cycle before undue contamination occurred. Results were discarded when there was a discrepancy of more than 10% in T_1 at atmospheric pressure before and after a pressure cycle. The data to be given for cyclohexane and benzene were obtained for samples to which magnesium filings were added, the runs being made after a wait of one or more days, during which T_1 increased.

The cyclohexane was Eastman spectroscopic grade. The toluene and the benzene were distilled in a multiple-plate column before degassing. Other samples were commercial reagent-grade preparations and were degassed without further purification.

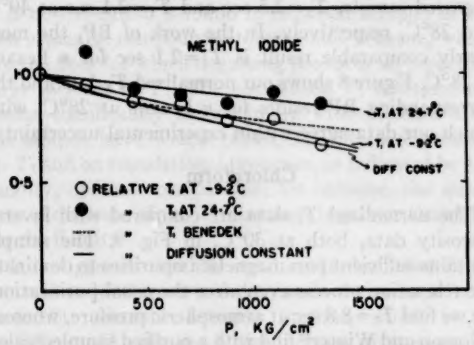

FIG. 5. Normalized T_1 for methyl iodide, compared with data from BP for T_1 and for the diffusion coefficient at 29°C.

RESULTS

All quantities plotted (reciprocal viscosity, T_1, and self-diffusion coefficient) are normalized with respect to atmospheric pressure. The data for the viscosity coefficient (η) vs pressure are due to Bridgman.[7] Since the present experiments are confined to a small portion of the pressure range of his data, interpolation has been made, for want of a better basis, on the assumption that $d\log\eta/dp$ is independent of pressure. McCall *et al.*[8,9] find for a variety of liquids that the closely related self-diffusion coefficient behaves in this fashion, with few exceptions, on the basis of measurements to 700 atm.

Most of the present measurements were made at various ambient temperatures as indicated, without regulation. Where the sample purity was adequate for a sufficient time, additional temperatures were included.

[7] P. W. Bridgman, Proc. Natl. Acad. Sci. U. S. **11**, 603 (1925).
[8] D. W. McCall, D. C. Douglass, and E. W. Anderson, Phys. Fluids **2**, 87 (1959).
[9] D. W. McCall, D. C. Douglass, and E. W. Anderson, J. Chem. Phys. **31**, 1555 (1959).

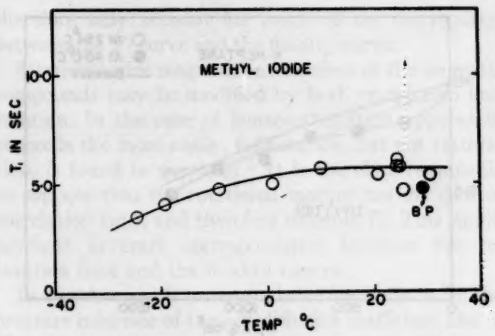

FIG. 6. T_1 as a function of temperature at atmospheric pressure, and point determined by BP.

Difficulties from sample deterioration generally increased when the temperature was raised.

Toluene

Figure 2 shows the present T_1 results, those obtained earlier by BP, and the viscosity data. The absolute value of T_1 obtained at atmospheric pressure was 10.0 sec, compared with 2.4 sec reported by BP and 12.5 sec by CCG. An additional run at 43°C, not shown, gave an initial value of 13 sec and a more rapid fall under pressure.

The values of T_1 found for purified toluene depend to some extent upon the portion of the magnetic recovery curve observed, because this liquid has two relaxation times,[5] corresponding to protons on the ring and to those in the methyl group. The two values were resolvable in pulse measurements of T_1 for a degassed sample in a larger rf coil in air, but the signal-to-noise ratio in the pressure experiments was insufficient for such resolution. For a sample not degassed, the normalized T_1 vs pressure curve (Fig. 2) agrees with the BP results.

Benzene

The normalized data are shown in Fig. 3. The absolute

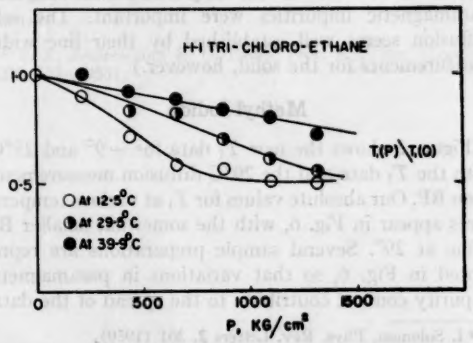

FIG. 7. Normalized T_1 for 1,1,1-trichloroethane.

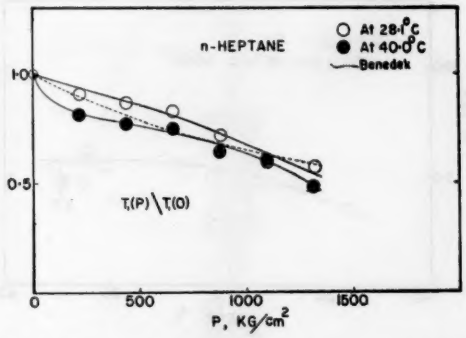

FIG. 8. Normalized T_1 for *n*-heptane, compared with BP data for *n*-hexane.

value found for T_1 at atmospheric pressure was 18.4 sec (or, after the pressure cycle, 17.4 sec), obtained with a magnesium treated sample, six days after assembly. The value immediately after assembly was 10 sec, some air having been admitted with the magnesium. Nederbragt and Reilly[5] reported $T_1=19.3$ sec. Solomon[10] has found $T_2=19.6\pm1.5$ sec for purified benzene. As this liquid was not used in the BP experiments, a T_1 curve for a sample not degassed was also determined, and is shown in Fig. 3. At atmospheric pressure, T_1 for this sample was 4.2 sec.

Cyclohexane

Relative T_1 values for 8.5°, 26°, and 49°C are shown in Fig. 4, as well as diffusion data.[9] The absolute initial values of T_1 were 4.1, 6.1, and 8.1 sec, respectively. The minima evidently indicate solidification. The values of T_1 at the minima are much greater than the minimum possible T_1 for this compound,[11] and there is little or no discontinuity. A similar situation obtains at the freezing point under atmospheric pressure, which has been explained by Andrew and Eades on the basis that molecular reorientation and diffusion, in the region of the freezing point, occur in both phases. (Note: This comparison has the flaw that Andrew and Eades found at 8°C a T_1 value of only 2 sec, indicating that paramagnetic impurities were important. The self-diffusion seems well established by their line width measurements for the solid, however.)

Methyl Iodide

Figure 5 shows the new T_1 data for $-9°$ and 25°C, with the T_1 data and the 29°C diffusion measurements from BP. Our absolute values for T_1 at various temperatures appear in Fig. 6, with the somewhat smaller BP value at 29°. Several sample preparations are represented in Fig. 6, so that variations in paramagnetic impurity content contribute to the spread of the data.

[10] I. Solomon, Phys. Rev. Letters **2**, 301 (1959).

[11] E. R. Andrew and R. G. Eades, Proc. Roy. Soc. (London) **A216**, 398 (1953).

1,1,1-Trichloroethane

Although viscosity data are not available for this liquid, the T_1 results are reported in Fig. 7 for comparison with those for methyl iodide. The substitution of the group CCl_3 for the iodine atom of methyl iodide renders the molecule more elongated, so that increased sensitivity of T_1 to pressure is expected, according to arguments of BP, and is in fact observed. The absolute initial values for 12.5°, 29.5°, and 40°C, respectively, are 4.2, 5.6, and 4.7 sec, the small size of the latter suggesting contamination by O_2. The shape of the 12.5° curve suggests freezing.

n Heptane

This liquid is an example of one in which T_1 is little affected by atmospheric oxygen. We obtained, for a degassed sample, $T_1=2.5$ sec and $T_1=2.1$ sec at 40°C and 28°C, respectively. In the work of BP, the most nearly comparable result is $T_1=2.1$ sec for *n* hexane at 28°C. Figure 8 shows our normalized T_1 data and the corresponding BP results for *n* hexane at 28°C, with which our data agree within experimental uncertainty.

Chloroform

The normalized T_1 data are compared with inverse viscosity data, both at 30°C, in Fig. 9. The sample contains sufficient paramagnetic impurities to dominate the relaxation process even after the usual purification, for we find $T_1=8.8$ sec at atmospheric pressure, whereas Solomon and Winter[12] find with a purified sample, sealed in glass, that it is possible for a limited time to observe T_1 not less than 42 sec, and $T_2\approx10$ sec.

DISCUSSION

The absolute values of T_1 found here for degassed samples of methyl iodide and for *n* heptane differ by less than 20% from those given by Benedek and Purcell for samples of methyl iodide and *n* hexane which were not degassed. Moreover, the normalized T_1 vs pressure

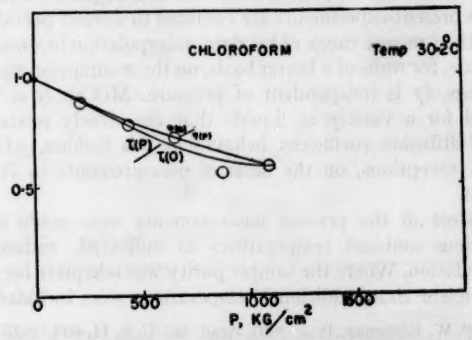

FIG. 9. Normalized T_1 and reciprocal viscosity for chloroform.

[12] I. Solomon and J. Winter, Commissariat énergie atomique (SACLAY), France, private communication.

functions correspond closely in the degassed and the not-degassed cases. There is not a sufficient change in these functions to affect the conclusion drawn by Benedek and Purcell from them, that the jump rate for the translations occurring in flow and diffusion is reduced more under pressure than the one controlling T_1, which is ascribed to rotation.

In principle, it is possible for the correlation time for one process (for example, rotation) to govern T_1 at low pressure and for the correlation time for a different process to do so at high pressure. Since contributions to $1/T_1$ increase with pressure, the more pressure-sensitive of two mechanisms dominates at the higher pressures. A corresponding increase in $|d \log T_1/dp|$ might be found. This has not been observed in experiments thus far, except possibly in the BP results for water.

A new situation is found in degassed samples of the two aromatic compounds, toluene and benzene, which are the ones for which degassing produces an especially large increase in T_1. The normalized T_1 functions decrease significantly more rapidly with pressure after the samples have been degassed. The effects of pressure on T_1 and on translational processes, as indicated by the fluidity, are now comparable; for benzene, the initial rate of decrease of the T_1 functions is greater than that for the fluidity.

It is suggested that the rapid initial decline of T_1 for benzene is due in part to reduction in the average intermolecular distance between protons, which is especially rapid with the initial increase in pressure. In support of this, the data of Nederbragt and Reilly[5] on the hydrogen T_1 in aromatic compounds and their solutions indicates that the major contribution to relaxation in degassed samples is intermolecular, for ring protons. An accurate method for calculating the change in this intermolecular contribution, from the compressibility, is not available. To estimate roughly what the effect might be for benzene at 1000 kg/cm^2, we note that the corresponding decrease in volume is of the order of 5%. If the protons were at the centers of the molecules, the corresponding reduction in T_1 would be 10%, on the basis of the inverse sixth power law. Since the protons are actually peripheral, the effect may be much greater, depending upon the manner in which the packing of the molecules varies with pressure, and therefore may account for much of the discrepancy between the T_1 curve and the fluidity curve.

Intermolecular magnetic interactions of the aromatic compounds may be modified by both translation and rotation. In the case of benzene, rotation apparently proceeds the more easily, for rotation, but not translation, is found in the solid.[13] It is therefore reasonable to suppose that the rotational motion has the shorter correlation time, and therefore controls T_1. This would preclude accurate correspondence between the relaxation time and the fluidity curves.

In Fig. 4, a rough correspondence is seen between the pressure behavior of the self-diffusion coefficient and of T_1 for cyclohexane, near room temperature. The pressure range before solidification is too small to permit accurate comparison. The comparison here is between processes dependent on translation and processes dependent on both translation and rotation, the distance between neighboring protons in the molecule being sufficiently small that both inter- and intramolecular contributions to magnetic relaxation are important.

Since the T_1 for our chloroform sample was apparently controlled by dissolved oxygen, as pointed out earlier, the close agreement of the T_1 and the fluidity curves in Fig. 9 indicates that the effect of pressure on the diffusion of O_2 in chloroform is nearly the same as that on translation of the solvent molecules. This is understandable in view of the comparable size of the molecules.

The original T_1 curve of BP for toluene, and the new T_1 curve for benzene not degassed, when compared with the corresponding fluidity curves, indicate that under pressure the diffusion rate of dissolved O_2 is reduced less, relatively, than the rotational and translational jump rates of the aromatic molecules.

We have attempted no theoretical calculations of the effects of pressure on T_1 or on diffusion processes, inasmuch as available liquid theories give only rough agreement with experiment.[3,4,8,9]

ACKNOWLEDGMENT

We acknowledge the kind assistance of Miss Joye Murphy, who performed the distillations of certain samples.

[13] E. R. Andrew and R. G. Eades, Proc. Roy. Soc. (London) **A218**, 537 (1953).

Organic Semiconductors. II.* The Electrical Resistivity of Organic Molecular Complexes

MORTIMER M. LABES, ROBERT SEHR, AND MONISHA BOSE†

The Franklin Institute, Laboratories for Research and Development, Philadelphia 3, Pennsylvania

(Received April 19, 1960)

Thirty molecular complexes involving quinones, halogens, polynitroaromatics, or tetracyanoethylene as electron acceptors and aromatic hydrocarbons or substituted aromatics as electron donors have been prepared and the room temperature electrical resistivities measured on compressed microcrystalline material. A lowering of electrical resistivity is generally associated with complex formation. The results are discussed in terms of crystal structure and charge transfer complex theory.

I. INTRODUCTION

MOLECULAR complexes can be formed from the interaction of a wide variety of molecules, primarily aromatics which can behave as electron donors (D) with electron acceptors (A) such as quinones, halogens, and nitro-compounds.[1] The present concept of the nature of these complexes, based on the charge transfer or donor acceptor interaction theory, was developed by Mulliken.[2] This theory has recently been reviewed by McGlynn[1b]; briefly, the ground state of a 1:1 complex can be described by a wave function ψ_n, given by

$$\psi_n(D, A) = a\psi_0(D, A) + b\psi_1(D^+A^-). \quad (1)$$

ψ_0 designates a no-bond wave function; ψ_1 represents a "dative bond" wave function, corresponding to a transfer of an electron from D to A. The excited state wave function ψ_E is given by

$$\psi_E(D, A) = a^*\psi_1(D^+A^-) - b^*\psi_0(D, A). \quad (2)$$

For weak molecular complexes $a \gg b$, $|a| \cong 1$, $|b| \cong 0$, so that ψ_n has essentially no bond character and ψ_E has essentially ionic character. For primarily ionic complexes, the ground state wave function is given by Eq. (1), with $b > a$.

A few of these molecular complexes have been observed to have resistivities many decades lower than conventional organic materials. Our investigation has concerned itself with examining the generality of this observation, a thorough study of several semiconductor parameters on some typical representatives, and a contribution to an understanding of the mechanism of semiconduction in organic molecular solids. This paper concerns itself with the first of these questions.

II. EXPERIMENTAL

Apparatus

The apparatus employed in performing the electrical measurements has already been described[3]; the most convenient sample holder which we have devised is pictured in Fig. 1.

Materials

The following materials were purified by simple recrystallizations to constant melting point; hexamethylbenzene, dimethoxybenzene, *p*-anisidine, *p*-phenylenediamine, quinhydrone, chloranil, 1,3,5-trinitrobenzene, picric acid, 2,4,7-trinitrofluorenone. Tetracyanoethylene was kindly supplied by E. I. Dupont de Nemours & Company. 1,5-Diaminonaph-

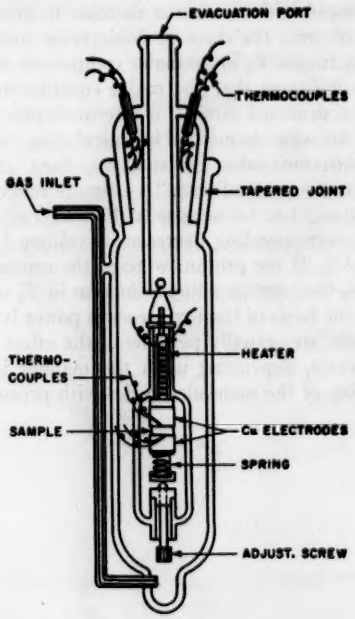

FIG. 1. Sample holder.

* These results were presented at the Princeton University Conference on Semiconduction in Molecular Solids, February 16–17, 1960.

† Visiting Research Associate from the Department of Chemistry, University of Calcutta, India.

[1] For recent reviews see (a) L. J. Andrews, Chem. Revs. **54**, 713 (1954); (b) S. P. McGlynn, *ibid.* **58**, 1113 (1958).

[2] R. S. Mulliken, Rec. trav. chim. **75**, 845 (1956), and earlier papers cited therein.

[3] M. M. Labes, R. Sehr, and M. Bose, J. Chem. Phys. **32**, 1570 (1960).

TABLE I. Literature data on electrical resistivity of molecular complexes.

Compound (A-B)	Molar ratio A:B	dc Room temp. resistivity ohm cm	Temp. range °C	E^a ev	Compounding conditions	Reference
Perylene-Br_2	1:2.2	7.8	−20 to −170	0.13	g	13
Pyranthrene-Br_2	1:1.7	220	−20 to −170	0.20	g	13
Violanthrene-Br_2	1:2.3	66	−20 to −170	0.20	g	13
Violanthrene-I_2	1:2	45	−20 to −170	0.15	g	13
Violanthrene-I_2	1:2	45	10 to 60	0.14	g	13
Pyrene-I_2	1:2	75	...	0.22	g	14a
Perylene-I_2	2:3	8	...	0.03	g	14a
Dimethylaniline-chloranil	...	10^9	...	0.45[b]	...	f
Dimethylaniline-bromanil	...	10^9	...	0.45[b]	...	f
Dimethylaniline-iodanil	...	10^8	...	0.45[b]	...	f
p-Phenylenediamine-chloranil	...	10^{8c}	−10 to 20	0.50	...	12
p-Phenylenediamine-chloranil	3:2 5:3	10^7	−25 to 55	1.15	h	3
Li Anthracene[d]	1.16:1	10^{11}	25 to 50	1.34	i	11a
K-anthracene[d]	1.18:1	10^{11}	25 to 50	1.12	i	11a
Na-anthracene[d]	2.12:1	10^8	25 to 50	0.63	i	11a, 11b
Na-3:4 benzoquinoline[e]	1.5:1	10^{10}	...	0.35	j	11e
3:4-benzoquinoline-Br_2[e]	1:2.8	10^8	...	0.37	j	11e

[a] Calculated from $\rho=\rho_0 \exp(E/2kT)$.
[b] This value given in a private communication cited in footnote 12.
[c] Resistivity at 0°.
[d] Reference gives data at other metal concentrations and also for Na—anthracene which retains ether.
[e] Reference gives data on other benzoquinoline isomers and complex compositions.
[f] D. D. Eley and H. Inokuchi, *Proceedings of the Third Conference on Carbon* (Pergamon Press, New York, 1959), p. 91.
[g] Compressed at 200 kg/cm² using silver coated metallic cap electrodes.
[h] Compressed at 42 000 psi (3000 kg/cm²) using Cu or Pt foil electrodes.
[i] Compressed at 20 kg/cm² using Cu or stainless steel electrodes.
[j] Compressed at 8-12 kg/cm² using Cu electrodes fitted with Pt caps.

thalene, 1,8-diaminonaphthalene, *p*-aminodiphenylamine, and acridine were obtained from Aldrich Chemical Company and used without purification. Iodine was Merck reagent grade; iodine monochloride was Eastman practical. *N,N*-dimethylamine was freshly distilled *in vacuo* immediately prior to use. Pyrene, perylene, and coronene were purified by the continuous adsorption purification technique of Sangster and Irvine.[4] *N,N,N',N'*-tetramethyl-*p*-phenylenediamine was obtained as the dihydrochloride from B.D.H; the free base was liberated with ammonia and the washed solid dissolved in benzene. The benzene solution was dried, filtered, and used immediately in complex formation.

3,8- and 3,10-diaminopyrene were prepared by the procedure of Vollman *et al.*[5] 3,8-Diaminopyrene was crystallized 3 times from xylene, mp 226–27°; 3,10-diaminopyrene was crystallized 3 times from xylene, and 2 times from toluene, mp 160–62°.

Bromanil and iodanil were prepared according to the procedure described by Jackson and Bolton.[6] Bromanil was recrystallized twice from benzene, mp 299–299.5°. Iodanil was recrystallized twice from ethyl acetate, mp 265–268°. Octoiodo-*p*-benzoquinhydrone was also prepared by Jackson and Bolton's method.[6]

The complexes were then prepared by mixing the ingredients separately dissolved in solvent, usually benzene; *s*-tetrachloroethane was a convenient solvent for the iodine complexes of coronene and perylene. The complexes formed immediately from cold solutions, or upon cooling in the cases where hot solvents were used, and were obtained as microcrystalline solids. Occasionally, slow cooling would yield crystals of reasonable size to attempt single crystal measurements (see Table II), but these results are not as yet considered reliable. The complexes were not routinely submitted for analyses except in those cases where detailed study of the temperature dependence of resistivity and other semi-

[4] R. C. Sangster and J. W. Irvine, Jr., J. Chem. Phys. **24**, 670 (1956).
[5] H. Vollman, H. Becker, M. Corell, H. Streeck, and G. Langbein, Ann. **531**, 1 (1937).
[6] C. L. Jackson and E. K. Bolton, J. Am. Chem. Soc. **36**, 301 (1914).

TABLE II. Room temperature electrical resistivities of molecular complexes.

Acceptor	Donor	Resistivity ohm-cm
Tetracyanoethylene	Pyrene	10^{9a}, 10^{10}
Tetracyanoethylene	Perylene	10^{9a}, 10^{11}
Tetracyanoethylene	Hexamethylbenzene	10^{11}
Tetracyanoethylene	Dimethoxybenzene	10^{11}
Chloranil	Pyrene	10^{11}
Chloranil	Perylene	10^{8}
Chloranil	Hexamethylbenzene	10^{11}
Chloranil	*N,N*-Dimethylaniline	10^{10}
Chloranil	*p*-Phenylenediamine	10^{7}
Chloranil	1,5-Diaminonaphthalene	10^{11}
Chloranil	1,8-Diaminopaphthalene	10^{11}
Chloranil	*p*-Aminodiphenylamine	10^{10}
Chloranil	*N,N,N',N'*-Tetramethyl-*p*-phenylenediamine	10^{9}
Chloranil	3,8-Diaminopyrene	10^{4}
Chloranil	3,10-Diaminopyrene	10^{8}
Chloranil	*p*-Anisidine	10^{11}
Bromanil	*p*-Phenylenediamine	10^{10}
Bromanil	3,8-Diaminopyrene	10^{3}
Iodanil	*p*-Phenylenediamine	10^{11}
Iodanil	3,8-Diaminopyrene	10^{2}
Iodine	Coronene	10^{9}
Iodine	Perylene	10
Iodine	Acridine	10^{13}
Iodine monochloride	Acridine	10^{12}
1,3,5-Trinitrobenzene	*N,N*-Dimethylaniline	10^{9a}, 10^{11}
1,3,5-Trinitrobenzene	Coronene	10^{13}
Picric acid	Coronene	10^{12}
2,4,7-Trinitrofluorenone	Coronene	10^{12}
Quinhydrone		10^{11}
Octoiodo-*p*-benzquinhydrone		10^{11}

[a] Initial attempts at single crystal measurements; we do not as yet consider these values reliable.

conductor properties were undertaken. Hence the values should be considered and are given as order of magnitude values.

RESULTS AND DISCUSSION

The literature concerned with measurements of electrical resistivity for molecular complexes is summarized in Table I. Some of the reports do not give details of measuring apparatus, condition of compression, or electrode materials, making comparison of results rather difficult. Table II lists 30 complexes we have studied. Our values agree within an order of magnitude with the literature values for the three compounds we have reinvestigated: perylene-I_2, dimethylaniline-chloranil, *p*-phenylenediamine-chloranil. It can be seen that a lowering of electrical resistivity is generally associated with complex formation. We have not been able to find any new donor-acceptor systems with resistivities as low as the aromatic amine-tetrahalogen-*p*-benzoquinone or aromatic hydrocarbon-halogen systems, and most of our work involved the preparation and screening of a series of amino substituted hydrocarbons complexed with the tetrahalogen-*p*-benzoquinones. In addition to having low resistivities, these complexes appear to be more stable than the tetracyanoethylene or halogen complexes.

It is important to consider whether there are any changes in the molecular crystal of an aromatic charge transfer complex as compared with the parent hydrocarbon. In hydrocarbons like coronene and ovalene, the perpendicular distance between successive molecular planes is very close to the interplanar distance found in graphite, 3.4 A, the normal van der Waals approach. This also applies to other large molecules with aromatic character such as the phthalocyanines. In the case of smaller aromatic molecules, the distances are a little greater, varying from about 3.5 to 3.7 A.[7]

A good possibility is that the basic structural feature which differentiates a molecular complex crystal having resistivities lower than conventional organic materials from a pure hydrocarbon crystal is a chain-like structure with large regions of parallel positioning of molecular planes, and an alternation of sites with donor (positive) and acceptor (negative) character. There is not a significant decrease in interatomic distances between molecular planes in general but the molecular planes are much closer to having a common chief axis. In the complexes which exhibit the lowest resistivities, there may, however, be some decrease in distance between planes. We still consider two types of complexes which seem to have a chain-like structure; aromatic hydrocarbon-halogen complexes, and an aromatic hydrocarbon-quinone complex.

[7] J. M. Robertson, *Organic Crystals and Molecules* (Cornell University Press, Ithaca, New York, 1953).

Hassel[8a] has succeeded in determining the crystal structure of the 1:1 benzene-bromine charge transfer complex at −40° to 50°C. Here the bromine atoms are symmetrically situated on the common chief axis of two neighboring benzene rings. The crystal is built up of chains consisting of alternating benzene and bromine molecules. No change in the Br—Br distance (2.36 A) is found. The distance to the center of the nearest benzene ring is 3.36 A. Each bromine atom is symmetrically situated with respect to all C—C bonds. A steep fall in x-ray intensities at increasing reflection angles is observed indicating the weakness of the bond. The benzene-chlorine complex[8b] has a similar structure, the Cl—Cl distance being 1.99 A, and the distance from one particular chlorine atom to the nearest benzene plane (3.28 A) a little shorter than the corresponding bromine compound.

According to Harding and Wallwork,[9f] in the chloranil-hexamethylbenzene complex, it is impossible for a pair of hexamethylbenzene molecules, one on either side, both to approach close enough for π orbital overlap to occur over the whole of the area of the C_6 rings. A compromise is made; one-half of the chloranil molecule interacts strongly with the molecule above it; one-half interacts strongly with the molecule below leading to a zig-zag arrangement. The perpendicular spacing between the molecules is about 3.5 A. Thus the component rings of molecular complexes, although parallel, do not necessarily have coaxial orientations. This picture has, however, been seriously criticized[10] as to structural detail, so that the only clear case of chain-like structure is that of the aromatic hydrocarbon-halogen complexes.

Theoretical evidence shows that the structure with perfect coaxial orientation is not the most favored for the hypothetical benzene-benzene complex.[2] The more favored structures can be obtained by sliding one ring parallel to the other for a distance of approximately an angstrom. In practice each case must be examined separately since a compromise between polarization bonding and steric repulsion is reached, which may then be further modified by specific interactions such as hydrogen bonding.[9d]

There are, of course, many complexes in which parallel stacking does not occur or deviations from parallel stacking occur either as a result of steric repulsion or specific interactions. In the *aza*-aromatic-halogen or amine-halogen complexes ("*n*-type" or "onium" complexes), the charge transfer interaction is localized, leading to primarily an ionic bond between tertiary nitrogen-halogen. X-ray studies[8] show a very short distance from tertiary nitrogen to directly bonded halogen atoms which is not much longer than an ordinary covalent bond, and the arrangement donor atom-halogen-halogen is linear.

Although the complexes of diaminonaphthalene had higher resistivities than those of *p*-phenylenediamine, diaminopyrene complexes have been found to have quite low resistivities. Thus the fact that one might expect larger aromatic ring systems to interact to give lower resistivity complexes can easily be obscured by possible structural and composition differences. The two isomeric diaminopyrenes, for example, form complexes of quite different composition and have quite different resistivities. Further work on complexes of this type is in progress.

It was our observation that complexes which are primarily ionic in nature and that would be expected to have the linear arrangement of *N*-halogen-halogen atoms discussed above had very high resistivities. This is in disagreement with the results of Ubbelohde *et al.*[11e]

We also found that complexes involving the polynitroaromatics had, typically, high resistivities. There is evidence that there is deviation from parallel plane stacking with the anthracene-1,3,5-trinitrobenzene complex.[9g] However, the observation which points out most clearly the difficulties in making generalizations regarding correlations of chemical structure and electrical properties is our study of the coronene-iodine complex. The fact that the resistivity of this halogen-hydrocarbon complex is 7 orders of magnitude higher than halogen complexes of hydrocarbons both smaller and larger than coronene is puzzling. In light of this observation, other results involving measurements of very few compounds with a given electron acceptor must not be considered as necessarily describing that class of complexes. It is clear that crystal structure is of great importance and may profoundly influence the electrical properties.[11f]

The aromatic amine-tetrahalogen-*p*-benzoquinone complexes have been called biradical molecular compounds, because of their paramagnetism. Bijl, Kainer, and Rose-Innes[12] consider this a case of complexing in which the ionic state is the lowest state because *A* and

[8] (a) O. Hassel, J. Mol. Phys. **1**, 241 (1958); (b) O. Hassel and H. Stromme, Acta Chem. Scand. **13**, 1781 (1959).

[9] (a) J. S. Anderson, Nature **140**, 583 (1937); (b) K. Nakamoto, J. Am. Chem. Soc. **74**, 1739 (1952); (c) H. M. Powell and G. Huse, Nature **144**, 77 (1939); J. Chem. Soc. **1943**, 435; (d) H. M. Powell, G. Huse, and P. W. Cooke, *ibid.* **1943**, 153; (e) S. C. Wallwork and T. T. Harding, Nature **171**, 40 (1953); (f) T. T. Harding and S. C. Wallwork, Acta Cryst. **8**, 787 (1955); (g) S. C. Wallwork, *ibid.* **7**, 648 (1954).

[10] J. Donohue and K. N. Trueblood, Acta Cryst. **9**, 960 (1956).

[11] (a) W. A. Holmes-Walker and A. R. Ubbelohde, J. Chem. Soc. **1954**, 720; (b) J. P. V. Gracey and A. R. Ubbelohde, *ibid.* **1955**, 4089; (c) W. Slough and A. R. Ubbelohde, *ibid.* **1957**, 911; (d) **1957**, 918; (e) **1957**, 982.

[11] (f) *Note added in proof*: Preliminary results of a study of the structure of the coronene-iodine complex (R. Pepinsky, private communication) indicate that the crystal does not have alternate coronene and iodine molecules in a stack, but rather may have alternate stacks of coronene and iodine molecules. This would explain the relatively high resistivity. Another paper which also discusses semiconductivity and crystal structure in these complexes has just appeared. See D. D. Eley, H. Inokuchi, and M. R. Willis, Disc. Faraday Soc. **28**, 54 (1960).

[12] D. Bijl, H. Kainer, and A. C. Rose-Innes, J. Chem. Phys. **30**, 765 (1959).

D have such greatly different electron affinities. Paramagnetism has also been observed in the aromatic hydrocarbon-iodine complexes.[13e,d,14] A later paper will present measurements of Seebeck coefficient and resistivity as a function of temperature and spin density determinations for several complexes selected from the above screening program.

[13] (a) H. Akamatu, H. Inokuchi, and Y. Matsunaga, Bull. Chem. Soc. Japan **29**, 213 (1956); (b) H. Akamatu, Y. Matsunaga, and H. Kuroda, *ibid.* **30**, 618 (1957); (c) Y. Matsunaga, *ibid.* **28**, 475 (1955); (d) Y. Matsunaga, J. Chem. Phys. **30**, 855 (1959).

[14] (a) J. Kommandeur and F. R. Hall, Bull. Am. Phys. Soc. **4**, 421 (1959); (b) L. S. Singer and J. Kommandeur, Bull. Am. Phys. Soc. **4**, 421 (1959).

IV. ACKNOWLEDGMENTS

We wish to acknowledge gratefully technical assistance by P. J. Hackett and Mrs. F. R. Taylor.

THE JOURNAL OF CHEMICAL PHYSICS VOLUME 33, NUMBER 3 SEPTEMBER, 1960

Electronic Spectra of Dimers: Derivation of the Fundamental Vibronic Equation*

ANDRZEJ WITKOWSKI† AND WILLIAM MOFFITT

Chemistry Department, Harvard University, Cambridge 38, Massachusetts

(Received February 1, 1960)

The Hamiltonian describing the vibronic states of a dimer formed by two identical molecules is derived. The monomeric units are assumed to couple by resonance forces only and to have different equilibrium positions in the ground and excited states. The competition of these two effects is formulated mathematically. The strong coupling case occurs when the resonance forces dominate; the weak coupling case arises when the effect of the change of equilibrium positions dominates.

INTRODUCTION

IT has been recognized for some time that the electronic spectra of molecular crystals must be analyzed with some care. For, whereas two molecules which are electronically unexcited attract each other by the familiar dispersion forces of asymptotic dependence R^{-6}, these same forces result in a greater attraction of asymptotic dependence R^{-3} between two identical molecules, only one of which is electronically excited. This so-called resonance coupling has been adduced to explain the long-range transfer of energy between molecules in solution[1]; in crystals, it splits the individual molecular energy levels into "exciton" bands but, nevertheless, gives rise to spectra that are often sharp, owing to stringent selection rules.[2]

Two limiting forms of behavior have been characterized, both empirically and theoretically; in the one case, the resonance coupling is strong and the pattern of vibronic levels is determined in the first place, by electronic considerations;[2,3] in the other, the resonance coupling is rather weak, and the spectral effects are limited to details in the vibrational structure of band systems.[4] Recently, both Simpson and Peterson[5] and McClure[6] have investigated the criteria for strong and weak resonance coupling, giving qualitative arguments to cover the treatment of intermediate cases. These authors paid particular attention to the example of a single pair of chromophores, namely that of a dimeric molecule.

We have also been interested in this problem insofar as it involves a coupling between low-frequency electronic motions and nuclear modes, not unlike that encountered in the dynamics of Jahn-Teller instability.[7] Since our approach is perhaps somewhat different from that of other authors, we are encouraged to report it in the present note. We pay particular attention to a rather idealized dimer in the hope of illustrating as clearly as possible the factors involved in the intermediate coupling case.

GENERAL CONSIDERATIONS

In this section, we derive the basic equations describing the vibronic states of a simple dimer. To avoid complicating the argument unnecessarily, we set up a model which contains the most important features of

* This paper is the first and major part of a preliminary manuscript covering this joint work which was drafted by Professor Moffitt. His death prevented him from putting it in final form.

† Present address: Department of Theoretical Chemistry, Jagellonian University, Kraków, Poland.

[1] Th. Förster, Ann. Physik **2**, 55 (1948); A. Gołębiewski and A. Witkowski, Roczniki. Chem. **33**, 1443 (1959).

[2] A. S. Davydov, Zhur. Eksptl. i Teoret. Fiz. **18**, 210 (1948).

[3] D. P. Craig and P. C. Hobbins, J. Chem. Soc. **1955**, 539.

[4] D. P. Craig, J. Chem. Soc. **1955**, 2302; W. A. Bingel, Can. J. Phys. **37**, 680, (1959).

[5] W. T. Simpson and D. L. Peterson, J. Chem. Phys. **26**, 588 (1957).

[6] D. S. McClure, Can. J. Chem. **36**, 59 (1958).

[7] H. A. Jahn and E. Teller, Proc. Roy. Soc. (London) **A161**, 220 (1937).

the vibronic coupling, but which neglects others that play a subordinate role. No great effort will be made to justify the omission of unimportant factors, since the modifications which must be made in applying our results to particular physical situations are reasonably obvious. We begin by describing our notation as this applies to a single chromophore, and only then by constructing our model for the dimer.

A. Monomer

Suppose we have a molecule whose electronic and vibrational coordinates are symbolized by q_A and Q_A, respectively; we ignore rotational degrees of freedom. The molecular Hamiltonian may be written

$$H_A = V_A + T_A, \tag{1}$$

where V_A, which contains the Q_A parametrically, governs the electronic motion in the field of the stationary nuclei and T_A represents the kinetic energy of the nuclei. In the adiabatic approximation, we write the eigenfunctions of H_A in the form

$$\Psi_{Mm}(q_A, Q_A) = \psi_M(q_A, Q_A)\chi_m{}^M(Q_A), \tag{2}$$

where the electronic factor ψ_M satisfies

$$V_A\psi_M(q_A, Q_A) = V_M(Q_A)\psi_M(q_A, Q_A) \tag{3}$$

and the characteristic value $V_M(Q_A)$ provides the potential energy surface for the nuclear motions

$$[T_A + V_M(Q_A)]\chi_m{}^M(Q_A) = E_{Mm}\chi_m{}^M(Q_A). \tag{4}$$

The index M refers to a particular electronic state, m to a vibrational level of this state and, by definition, a "vibronic" state is specified by the pair of indices (M, m). (It is tacitly supposed that the electronic state M is nondegenerate and that, for ordinary vibrational amplitudes, the surface $V_M(Q_A)$ is separated from neighboring surfaces $V_{M'}(Q_A)$ by an energy appreciably larger than the vibrational spacing on either; under these circumstances, the omission of $[T_A, \psi_M(q_A, Q_A]$ which is made in passing from (2) and (3) to (4), may be justified.)

In what follows, we shall be concerned with the chromophoric properties of the molecule. To this end, we shall always confine our attention to one and the same pair of states, namely the ground electronic state N and a particular excited state M. Moreover, we shall suppose that we are dealing with low-temperature absorption spectra, so that N is vibrationally unexcited $(n=0)$ and there is no appreciable population of any vibronic level (M, m). The intensity of the vibronic transition $(M, m)\leftarrow(N, 0)$ is proportional to the squared magnitude of the electric moment vector

$$\mu_A{}^{m,0} = (\Psi_{N0}, \mu_A\Psi_{Mm}). \tag{5}$$

It will be assumed that the transition is electronically allowed and that, over normal vibrational amplitudes, the vector

$$\mu_A{}^0 = (\psi_N, \mu_A\psi_M) \tag{6}$$

is sensibly constant; then

$$\mu_A{}^{m,0} = \mu_A{}^0(\chi_0{}^N, \chi_m{}^M). \tag{7}$$

Throughout, we use the "scalar product" symbol $(\ ,\ )$ to indicate integrations over that space or subspace spanned by the enclosed "vectors": thus, in (5), these extend over both q_A and Q_A; in (6), over q_A alone; in (7) over Q_A alone.

The relative intensity of two different vibronic transitions, $(M, m)\leftarrow(N, 0)$ and $(M, m')\leftarrow(N, 0)$, say, is determined by the Franck-Condon principle, as is the over-all width of the entire $M\leftarrow N$ band system. It is convenient to characterize this spectrum by means of the dipole strength D_0 and its successive moments D_1, D_2, defined by

$$\begin{aligned} D_0 &= \sum_m |\ \mu_A{}^{m,0}\ |^2 = |\ \mu_A{}^0\ |^2 \\ D_1 &= (D_0)^{-1}\sum_m |\ \mu_A{}^{m,0}\ |^2(E_{Mm} - E_{N0}), \\ D_2 &= (D_0)^{-1}\sum_m |\ \mu_A{}^{m,0}\ |^2(E_{Mm} - E_{N0})^2. \end{aligned} \tag{8}$$

Thus D_0 gauges the total intensity of the system,

$$\omega_0 = D_1/\hbar \tag{9}$$

locates its center of gravity on an angular frequency scale and, correspondingly,

$$\Delta\omega = [D_2 - (D_1)^2]^{\frac{1}{2}}/\hbar \tag{10}$$

is a convenient measure of its width. It is easy to show that D_1 and D_2 are determined by the relations

$$D_1 = \langle V_M - V_N\rangle, \qquad D_2 = \langle (V_M - V_N)^2\rangle, \tag{11}$$

where the angular brackets denote, respectively, the expectation values of $[V_M(Q_A) - V_N(Q_A)]$, and of its square, taken over the ground state $\chi_0{}^N(Q_A)$. For instance, if A is a diatomic molecule and Q_A represents displacements from equilibrium in its ground electronic state, we may write, approximately

$$V_N = \tfrac{1}{2}KQ_A^2, \qquad V_M = V_0 + lQ_A + \tfrac{1}{2}K'Q_A^2, \tag{12}$$

where, in addition to the "vertical" electronic excitation energy V_0, we have allowed for a different equilibrium distance and a different force constant in the excited state. In this case,

$$D_1 = V_0 + \tfrac{1}{2}(K' - K)\langle Q_A^2\rangle \tag{13}$$

$$D_2 - (D_1)^2 = l^2\langle Q_A^2\rangle + \tfrac{1}{4}(K' - K)^2[\langle Q_A^4\rangle - \langle Q_A^2\rangle^2]. \tag{14}$$

Unless the zero-point amplitudes are unusually large, the second term on the right-hand side of (14) will be very small: other things being equal, the bandwidth is determined more by differences in equilibrium distances for states M and N, than by differences in force constants.

B. Dimer

Now suppose we have two identical molecules or radicals, A and B, say, whose relative orientation is fixed. The relative motion of their centers of gravity is confined to a single degree of freedom, namely, the variable distance L_0+L, L_0 constant, between them. Thus we may envisage a stable dimer, whose constituents are held together by van der Waals forces, or a single molecule, such as 2:2:1-bicycloheptadiene, containing two identical chromophores which are linked by primary chemical bonds. We further suppose that L_0+L is always sufficiently large that electron exchange between the moieties is excluded; in so doing, we leave out of consideration so-called charge-transfer spectra, which require a somewhat modified treatment.

Motions of the dimer—or rather those motions which, in our model, we chose to separate for special attention—are governed by the Hamiltonian

$$H=H_A+H_B+V_{AB}+T_L. \tag{15}$$

Here H_A and H_B, as defined by (1) refer to the internal coordinates of the respective fragments, V_{AB} represents their mutual potential energy, and T_L is the kinetic energy associated with their relative motion L. Since the relative orientation of the molecules is held fixed, it is a good approximation to regard V_{AB} as a function of the electronic coordinates q_A, q_B and of the intermolecular parameters L_0, L alone:

$$V_{AB}=V_{AB}(q_A, q_B;\quad L, L_0). \tag{16}$$

We suppose that the correlative part of the interaction V_{AB} is small with respect to the separation of two different potential energy surfaces $V_M(Q)$ in any one chromophore. It is then meaningful to prescribe the electronic state of the dimer in terms of the degree of excitation of its components: we may adopt a representation in which V_A and V_B are separately diagonal, treating V_{AB} as a perturbation of the electronic motions. The lowest electronic state of the dimer has both its constituent chromophores unexcited and is represented, in zeroth order, by the simple product function

$$\pi_0=\psi_N(q_A, Q_A)\psi_N(q_B, Q_B). \tag{17}$$

Since electron exchange is negligible, we need not trouble to antisymmetrize this and similar functions. However, when only one of the two chromophores is excited, the zeroth-order functions take the more general form

$$\alpha\pi_A+\beta\pi_B, \tag{18}$$

where α, β remain undetermined and

$$\pi_A=\psi_M(q_A, Q_A)\psi_N(q_B, Q_B)$$
$$\pi_B=\psi_N(q_A, Q_A)\psi_M(q_B, Q_B) \tag{19}$$

in π_A, it is A which carries the excitation, whereas the moiety B is excited in π_B. For simplicity, we shall disregard high-frequency terms in the electronic motions, induced by V_{AB}, and replace the accurate electronic functions by their zeroth-order approximations, such as (17) and (18). Although the neglected terms are responsible for dispersion forces, which may account for the stability of the dimer, their omission is of secondary importance in the present context.

We now look for solutions to the eigenvalue problem

$$(H-W)\Omega(q_A, q_B, Q_A, Q_B, L)=0 \tag{20}$$

first when the dimer is in its lowest electronic state. Under these circumstances, we may write solutions in the form

$$\Omega_\nu=\pi_0\gamma_\nu(Q_A, Q_B, L), \tag{21}$$

where the subscript ν serves to identify stationary states associated with the vibrational degrees of freedom, but also associates these specifically with the ground electronic level; different vibrational states of the same electronic level would be indexed ν', $\nu''\cdots$. The function γ_ν is now determined by the equation

$$(h_A+h_B+h_L-W_\nu)\gamma_\nu=(h-W_\nu)\gamma_\nu=0 \tag{22}$$

where

$$h_A=T_A+V_N(Q_A), \qquad h_B=T_B+V_N(Q_B)$$
$$h_L=T_L+V_0(L), \qquad V_0(L)=(\pi_0, V_{AB}\pi_0). \tag{23}$$

We see that the system is separable in the respective coordinates, namely the set Q_A, the set Q_B, and L. If each chromophore is effectively diatomic and therefore has but a single internal vibrational mode, we may adopt the harmonic approximation to write the potential energy surface in the form

$$V_N(Q_A)=\tfrac{1}{2}KQ_A^2$$
$$V_N(Q_B)=\tfrac{1}{2}KQ_B^2$$
$$V_0(L)=\tfrac{1}{2}KL^2, \tag{24}$$

where the origin for the energy has been chosen to coincide with the minimum on this surface, for which $Q_A=Q_B=L=0$. With each of the three modes, we may associate a quantum number, n_A, n_B, or n_L, all of which are subsumed in ν. There is a systematic degeneracy in the pattern of vibrational levels, arising from our neglect of the Q_A, Q_B dependence in V_{AB} of (16): thus the states $(n_A=n', n_B=n'', n_L)$ and $(n_A=n'', n_B=n', n_L)$ have the same energy. This degeneracy is removed in a higher approximation. When the moieties are exchangeable by a symmetry operation, this is best accomplished by a transition to normal coordinates

$$q_1=2^{-\frac{1}{2}}(Q_A+Q_B)$$
$$q_2=2^{-\frac{1}{2}}(Q_A-Q_B) \tag{25}$$

in a familiar fashion.

We next look for solutions to (20) in which one chromophore is excited and the other is in its ground

electronic state. These take the general form

$$\Omega_\mu=\pi_A\alpha_\mu(Q_A, Q_B, L)+\pi_B\beta_\mu(Q_A, Q_B, L) \quad (26)$$

where, with neglect of terms like $[T_A, \psi(Q_A)]$ as before, we find that α_μ, β_μ satisfy the coupled equations

$$(h_A'+h_B+h_L^{AA}-W_\mu)\alpha_\mu+h_L^{AB}\beta_\mu=0$$
$$h_L^{BA}\alpha_\mu+(h_A+h_B'+h_L^{BB}-W_\mu)\beta_\mu=0. \quad (27)$$

Augmenting (23), we have here set

$$h_A'=T_A+V_M(Q_A), \qquad h_B'=T_B+V_M(Q_B)$$
$$h_L^{CC'}=T_L\delta_{CC'}+(\pi_C, V_{AB}\pi_{C'}), \qquad (C, C'=A, B). \quad (28)$$

When the two chromophores are equivalent, in the sense that they may be interchanged by a symmetry operation of the dimer, it is easy to see that

$$h_L^{AA}=h_L'(L)=h_L^{BB}. \quad (29)$$

By the Hermitian property

$$h_L^{AB}=v(L)=h_L^{BA} \quad (30)$$

whenever the functions π_A, π_B are real, as, without loss of generality, we may always suppose.

Equations (27) are fundamental to the problem and, in their respective limiting cases, lead to the "strong and weak" couplings that have been recognized. Their structure is most conveniently displayed by considering α_μ, β_μ to be the elements of a column vector

$$\phi=\begin{pmatrix}\alpha_\mu\\ \beta_\mu\end{pmatrix}. \quad (31)$$

Making use of the symmetry relations (29), (30), our system (27) now takes the succinct form

$$(\bar{h}-W_\mu)\phi=0 \quad (32)$$

where $\bar{h}$ is the matrix operator

$$\bar{h}=\tfrac{1}{2}(h_A'+h_A+h_B'+h_B)+h_L'$$
$$+\tfrac{1}{2}(h_A'-h_A-h_B'+h_B)\sigma_3+v\sigma_1; \quad (33)$$

where σ_1 and σ_3 are the familiar Pauli matrices. The complicating feature of the coupled equations is easily seen to arise from the noncommutativity of σ_1, and σ_3. Since the coefficient of σ_3 is just

$$\Delta V=\tfrac{1}{2}[V_M(Q_A)-V_N(Q_A)-V_M(Q_B)+V_N(Q_B)] \quad (34)$$

by the definitions (23) and (28), and the coefficient of σ_1, namely $v(L)$, the resonance coupling parameter, depends only on L, we see that the system is separable when either coefficient is negligible.

This observation enables us to distinguish, immediately, between two limiting forms of behavior, which are investigated more specifically below. The concomitant criteria are best formulated with respect to the spectroscopic properties of the dimer, in which two different types of spectra have already been distinguished.[3-6] By the Franck-Condon principle, the coefficients of σ_1 and σ_3 are then to be compared over the zero-point amplitude in the ground electronic state. We note that $v(L)$ may be written

$$v(L)=v_0+v_1L+\tfrac{1}{2}v_2L^2 \quad (35)$$

to good approximation, and that $|v_0|$ will be by far the most important term in this expansion. Thus, when

$$|v_0|^2\gg\langle(\Delta V)^2\rangle \quad (36)$$

we speak of "strong" coupling and may treat the σ_3 term of (33) as a small perturbation, and when

$$|v_0|^2\ll\langle(\Delta V)^2\rangle \quad (37)$$

we speak of "weak" coupling, regarding the σ_1 term of $\bar{h}$ as small. As before, the angular brackets are used to denote expectation values taken over the vibrationally unexcited ground state N. Making use of (11) we see that

$$\langle(\Delta V)^2\rangle=\tfrac{1}{2}[D_2-(D_1)^2]=\tfrac{1}{2}(\hbar\Delta\omega)^2 \quad (38)$$

so that our inequalities become

$$|v_0|\gg\hbar\Delta\omega, \qquad \text{strong coupling} \quad (39)$$
$$|v_0|\ll\hbar\Delta\omega, \qquad \text{weak coupling.} \quad (40)$$

We recover the results of Simpson and Peterson,[7] whose arguments were both more general and more qualitative, being based on time-dependent perturbation theory: when the resonance coupling parameter $|v|$ is much greater than the width of the band system in an isolated chromophore, strong coupling results.

Mean Square Length of a Hindered Alkane Chain

RICHARD P. SMITH

Department of Chemistry, University of Utah, Salt Lake City, Utah

(Received January 27, 1960)

An exact formula, valid for any number of links and any constant angle between links, is derived for the mean square end-end length of a chain, subject to the following conditions. Any three successive bonds must be in a *trans* configuration or one of two *gauche* configurations. The energy of a *trans* configuration is lower by E (per mole) than the energy of a *gauche* configuration. The excluded volume problem is ignored.

RECENTLY, Tobolsky[1] has obtained a formula for the mean square of the end-end length of a tetrahedral alkane chain of n links of length l_0 each, treating the problem as a Markoff chain problem in probability. Each successive bond was required to go in one of the three directions determined by having every atom coincide with one of the points of a diamond lattice, so that the two sets of three bonds (including C—H bonds) attached to the ends of any C—C bond are staggered. The energy of a *trans* arrangement of three successive C—C bonds was taken to be lower by energy E (per mole) than the energy of a *gauche* configuration.

We wish to consider the same model, but with the angle (acute) between two successive links generalized to θ. A formula valid for any n will be obtained, and Tobolsky's formula will be confirmed. The method used will be substantially the same as that introduced by Eyring[2] when he made the first calculation of the mean square length of an aliphatic chain in the free rotation limit.

We use bond vectors, bond coordinate systems, and transformation matrices as assigned by Eyring.[2] The square of the resultant vector was found by Eyring to be the sum of the squares of the bond vectors, plus twice all scalar products of all bond vectors after one bond vector is transformed by consecutive transformations through the connecting bonds to the coordinate system of the other bond vector. Taking the magnitude of every bond vector to be l_0, the resultant square end-end length is therefore

$$L^2=nl_0^2+2l_0^2\sum_{j=1}^{n}\sum_{s<j}\mathbf{e}_{xs}\cdot(\mathbf{A}_{s+1}\cdot\mathbf{A}_{s+2}\cdots\mathbf{A}_j\cdot\mathbf{e}_{xj}). \quad (1)$$

This is Eyring's Eq. (3) after a minor transposition.[3] Here $\mathbf{e}_{xj}$ is a unit vector along the x_j direction of bond j and the $\mathbf{A}_j$ are the transformations

$$\mathbf{A}_j=\begin{bmatrix}\cos\theta_j & -\sin\theta_j & 0\\ \cos\phi_j\sin\theta_j & \cos\phi_j\cos\theta_j & -\sin\phi_j\\ \sin\phi_j\sin\theta_j & \sin\phi_j\cos\theta_j & \cos\phi_j\end{bmatrix}$$

used for transforming a vector from the coordinate system[4] for bond j to the coordinate system for bond $j-1$. We require all $\theta_j=\theta=$constant. The averaging of Eq. (1) over configurations may be carried out on the elements of each matrix before multiplying the matrices, when, as in our case, the energy is a sum of terms, each one involving only one ϕ_j. Following Tobolsky's notation, let

$$a=1/[1+2\exp(-E/RT)] \quad (2)$$

be the probability of going *trans*; $\frac{1}{2}(1-a)$ will then be the probability of going to a given *gauche* position. Then the averages of $\cos\phi_j$ and $\sin\phi_j$ for any index j are

$$\langle\cos\phi_j\rangle=a\cos180°+\tfrac{1}{2}(1-a)(\cos60°+\cos300°)=\alpha$$

$$\langle\sin\phi_j\rangle=a\sin180°+\tfrac{1}{2}(1-a)(\sin60°+\sin300°)=0,$$

where

$$\alpha=\tfrac{1}{2}(1-3a), \quad (3)$$

and therefore

$$\langle\mathbf{A}_j\rangle=\langle\mathbf{A}\rangle=\begin{bmatrix}\cos\theta & -\sin\theta & 0\\ \alpha\sin\theta & \alpha\cos\theta & 0\\ 0 & 0 & \alpha\end{bmatrix}. \quad (4)$$

Note that for $a=\frac{1}{3}$, $\alpha=0$ (i.e., no trans stabilization) Eq. (4) reduces to the same result that Eyring found for free rotation. Therefore the final result for $\langle L^2\rangle$ in the $\alpha=0$ case will be the same as the free rotation result. The free-rotation formula for $\langle L^2\rangle$ will hold in the more general case of any periodic barrier (such as a sine curve) which superimposes on itself when shifted 120°, for $\alpha=0$, for $\cos\phi_j$ and $\sin\phi_j$ will average to zero even in this more general case. The latter statement follows from the identity

$$\cos(180°+x)+\cos(60°+x)+\cos(300°+x)=0,$$

and a similar identity for the sine function.

The quantity which is summed in Eq. (1) now be-

[1] A. V. Tobolsky, J. Chem. Phys. **31**, 387 (1959).
[2] H. Eyring, Phys. Rev. **39**, 746 (1932).
[3] A typographical subscript error in the original equation is corrected here.
[4] See R. P. Smith and E. M. Mortensen, J. Chem. Phys. **32**, 502 (1960) for a detailed description, with figure, of Eyring's coordinate system.

comes, after averaging over configurations,

$$\mathbf{e}_{xs}\cdot(\langle\mathbf{A}\rangle)^{j-s}\cdot\mathbf{e}_{xj}$$

$$=\begin{bmatrix}1 & 0 & 0\end{bmatrix}\begin{bmatrix}\delta_{j-s} & xx & 0\\ \epsilon_{j-s} & xx & 0\\ 0 & 0 & xx\end{bmatrix}\begin{bmatrix}1\\0\\0\end{bmatrix}=\delta_{j-s}. \quad (5)$$

Here xx represents quantities which need not concern us. The following recursion formulas hold for δ_m and ϵ_m

$$\delta_{m+1}=(\cos\theta)\,\delta_m-(\sin\theta)\,\epsilon_m \quad (6)$$

$$\epsilon_{m+1}=(\alpha\sin\theta)\,\delta_m+(\alpha\cos\theta)\,\epsilon_m. \quad (7)$$

The first of these quantities are, of course,

$$\delta_1=\cos\theta, \qquad \epsilon_1=\alpha\sin\theta. \quad (8)$$

Substituting Eq. (5) in Eq. (1) after averaging the latter over configurations,

$$\langle L^2\rangle=nl_0^2+2l_0^2F, \quad (9)$$

where

$$F=(n-1)\delta_1+(n-2)\delta_2+\cdots+\delta_{n-1}. \quad (10)$$

For $\alpha=0$, $\delta_m=\cos^m\theta$, and Eq. (9) reduces to Eyring's final equation.

We now must find an explicit expression for δ_m in the general case. Solving Eq. (6) for ϵ_m and substituting in Eq. (7),

$$\delta_{m+2}-A\delta_{m+1}+\alpha\delta_m=0,$$

where

$$A=(1+\alpha)\cos\theta. \quad (11)$$

The solution of this difference equation is easily found to be[5]

$$\delta_m=c_1r_1^m+c_2r_2^m, \quad (12)$$

where

$$r_1=\tfrac{1}{2}(A+\sigma), \qquad r_2=\tfrac{1}{2}(A-\sigma) \quad (13)$$

$$\sigma=(A^2-4\alpha)^{\frac{1}{2}}. \quad (14)$$

The constants c_1 and c_2 are determined by fitting Eq. (12) to the special cases δ_1 (Eq. 8) and $\delta_0=1$ [found by combining Eqs. (6–8)]. The results are

$$c_i=\tfrac{1}{2}\pm[(1-\alpha)\cos\theta/(2\sigma)]\,(+,c_1;-,c_2). \quad (15)$$

In view of Eq. (12), the quantity F [Eq. (10)] may be written

$$F=n(\delta_1+\delta_2+\cdots+\delta_{n-1})-[\delta_1+2\delta_2+\cdots+(n-1)\delta_{n-1}]$$

$$=c_1\left[n(r_1+r_1^2+\cdots+r_1^{n-1})-r_1(d/dr_1)(r_1+r_1^2+\cdots+r_1^{n-1})\right]+\text{similar } r_2 \text{ term}$$

$$=c_1\left[n\frac{r_1^n-r_1}{r_1-1}-r_1\frac{d}{dr_1}\left(\frac{r_1^n-r_1}{r_1-1}\right)\right]+r_2 \text{ term}$$

$$=c_1\frac{r_1}{r_1-1}\left[\frac{r_1^n-1}{r_1-1}-n\right]+r_2 \text{ term}. \quad (16)$$

[5] C. Jordan, *Calculus of Finite Differences* (Chelsea Publishing Co., New York, 1947), 2nd ed., paragraph 165.

Using Eqs. (11) and (13)–(15),

$$c_1\frac{r_1}{r_1-1}+c_2\frac{r_2}{r_2-1}=\frac{\alpha-\cos\theta}{(1+\alpha)(1-\cos\theta)} \quad (17)$$

$$c_1\frac{r_1}{(r_1-1)^2}+c_2\frac{r_2}{(r_2-1)^2}=\frac{(1+\alpha^2)\cos\theta-2\alpha}{(1+\alpha)^2(1-\cos\theta)^2} \quad (18)$$

$$c_1\frac{r_1^{n+1}}{(r_1-1)^2}+c_2\frac{r_2^{n+1}}{(r_2-1)^2}=\frac{G}{2(1+\alpha)^2(1-\cos\theta)^2}. \quad (19)$$

Here

$$G=(\alpha-r_1)^2\left[1+\left(\frac{1-\alpha}{1+\alpha}\right)\frac{A}{\sigma}\right]r_1^{n-1}+(\alpha-r_2)^2\left[1-\left(\frac{1-\alpha}{1+\alpha}\right)\frac{A}{\sigma}\right]r_2^{n-1}. \quad (20)$$

Upon substituting Eqs. (17)–(19) in Eq. (16), we find, using Eq. (9),

$$\langle L^2\rangle=nl_0^2\left[\frac{(1+\cos\theta)(1-\alpha)}{(1-\cos\theta)(1+\alpha)}+\frac{1}{n}\frac{4\alpha-2(1+\alpha^2)\cos\theta+G}{(1-\cos\theta)^2(1+\alpha)^2}\right]. \quad (21)$$

If $\alpha=0$ (no extra stabilization of *trans* configurations) then $G=2\cos^{n+1}\theta$ and Eq. (21) agrees with Eyring's formula for free rotation in the rearranged form given by Wall.[6]

A tedious algebraic comparison confirms the necessary equivalence of the foregoing equation in the tetrahedral ($\cos\theta=\frac{1}{3}$) case and Eq. (15) of Tobolsky's paper.[7]

Since $\frac{1}{3}\leq a\leq 1$ [cf. Eq. (2)], it follows that neither r_1 nor r_2 can ever exceed unity. Therefore $G\to 0$ for large n, and the limiting form for long chains is

$$\langle L^2\rangle=nl_0^2\left(\frac{1+\cos\theta}{1-\cos\theta}\right)\left(\frac{1-\alpha}{1+\alpha}\right)-2l_0^2\left[\frac{(1+\alpha^2)\cos\theta-2\alpha}{(1-\cos\theta)^2(1+\alpha)^2}\right]. \quad (22)$$

For a tetrahedral chain, $\cos\theta=\frac{1}{3}$, and, using Eq. (3), this reduces to

$$\langle L^2\rangle=\frac{(2+6a)nl_0^2}{3(1-a)}-\left[\tfrac{3}{2}+\frac{8(3a-1)}{3(1-a)^2}\right]l_0^2. \quad (23)$$

For large values of n, the n independent terms in the above equations will be negligible. Then Eq. (23) will agree with Tobolsky's Eq. (16).

Various other authors have treated chain lengths using the approach represented by Eq. (1),[8] usually

[6] F. T. Wall, J. Chem. Phys. **11**, 67 (1943). Note that Wall's $\cos\Theta$ differs in sign from ours.

[7] The power *2* in Tobolsky's final term is a misprint; it should be *3*.

[8] W. J. Taylor, J. Chem. Phys. **32**, 146 (1960), and references cited in that article.

obtaining formulas valid only for $n\to\infty$, and always employing mathematical techniques which differ from our difference equation method. Taylor[9] derived, for long chains, the first of the two terms of our Eq. (21), with a general $\langle\cos\phi\rangle$ in place of our α. Wolkenstein and Ptitsyn[10] have derived a more general formula, valid for any n, using a matrix diagonalization technique for reducing our Eq. (1). This diagonalization technique has been used a number of times[8] and appears to us to be considerably more cumbersome than our approach. Generalizing α of our Eq. (21) to $\langle\cos\phi\rangle$, and noting that this quantity is $-\eta$ of the paper by Wolkenstein and Ptitsyn, it is easy to show that Eq. (21) of the latter paper is the same as our Eq. (21).

The accuracy of the approximate Eqs. (22) and (23) may be tested for $E=0.8$ kcal, a reasonable choice for hydrocarbon chains,[11] and 25°C. Here the exact formula, Eq. (21), gives 109.6 and 277.8 for $\langle L^2\rangle$ in diamond lattice units ($l_0=\sqrt{3}$) for $n=10$ and $n=20$, respectively; Eq. (23) gives 102.8 and 277.2, respectively. For larger n, the agreement will, of course, be even closer. The n independent part of Eq. (23) is equal to 71.5 in this case, so that the results will be too high by this amount if the constant part is dropped.

It does not seem possible to rigorously incorporate excluded volume considerations into the foregoing formulas in a simple way.

ACKNOWLEDGMENTS

The author is indebted to Mr. Leon L. Jones and Mr. Francis H. Ree for helpful discussions of this work, and to Dr. Earl M. Mortensen for discussions and aid with the calculations.

[9] W. J. Taylor, J. Chem. Phys. **15**, 412 (1947). Note that Taylor's ϕ differs from ours by 180°.
[10] M. W. Wolkenstein and O. B. Ptitsyn, J. Phys. Chem. (U.S.S.R.) **26**, 1061 (1952).
[11] S. Mizushima, *Structure of Molecules and Internal Rotation* (Academic Press Inc., New York, 1954), p. 98.

THE JOURNAL OF CHEMICAL PHYSICS VOLUME 33, NUMBER 3 SEPTEMBER, 1960

Electronic Structure and Hyperfine Structure Constants of NO Molecule*

CHUN C. LIN, KATSUNORI HIJIKATA, AND MICHIKO SAKAMOTO

Department of Physics, University of Oklahoma, Norman, Oklahoma

(Received April 18, 1960)

The coupling constants of the magnetic hyperfine, electric quadrupole, and spin-orbit interaction have been calculated from the self-consistent field molecular orbitals formed by linear combination of atomic orbitals. The calculated values of the electron spin-orbit, nuclear spin-orbit, and nuclear-electronic spin-spin interaction constants agree reasonably well with experiment. The results for the nuclear quadrupole coupling constant and the Fermi contact term are less satisfactory, although the latter can be improved by configuration mixing. The relations of these coupling parameters to the electronic structure of the molecule are discussed.

I. INTRODUCTION

BECAUSE of the presence of an unpaired electron, the nitric oxide molecule exhibits very complicated hyperfine structure in its rotational spectrum due to the interaction between the nuclear spin, nuclear quadrupole moment, electron spin, electron orbital angular momentum, and molecular rotation. From the microwave spectrum the coupling constants of the various angular momentum vectors have been determined by several authors.[1–5] Dousmanis[6] has given an account of the interpretation of the magnetic coupling parameters in terms of the valence-bond description of the electronic structure of the molecule. Recently the self-consistent field molecular orbitals have been determined by the approximation of linear combination of atomic orbitals.[7] In this paper we shall calculate these hyperfine coupling constants from the SCF LCAO MO and discuss the relations of such constants to the electronic structure of the molecule.

II. MAGNETIC HYPERFINE STRUCTURE CONSTANTS

From the experimentally determined coupling constants of the hyperfine interactions in the NO molecules,

* Supported by the Air Force Cambridge Research Center, Air Research and Development Command, USAF.
[1] C. A. Burrus and W. Gordy, Phys. Rev. **92**, 1437 (1953).
[2] J. J. Gallagher and C. M. Johnson, Phys. Rev. **103**, 1727 (1956).
[3] M. Mizushima, Phys. Rev. **94**, 569 (1954).
[4] C. C. Lin and M. Mizushima, Phys. Rev. **100**, 1726 (1955).
[5] P. G. Favero, A. M. Mirri, and W. Gordy, Phys. Rev. **114**, 1534 (1959).
[6] G. C. Dousmanis, Phys. Rev. **97**, 967 (1955).
[7] H. Brion, C. Moser, and M. Yamazaki, J. Chem. Phys. **30**, 673 (1959).

it has been found that[6,8]

$$(1/r^3)_{Av}=14.9\times10^{24}\ \text{cm}^{-3},$$

$$(\sin^2\chi/r^3)_{Av}=13.4\times10^{24}\ \text{cm}^{-3},$$

$$-[(3\cos^2\chi-1)/r^3]_{Av}$$

$$+(16\pi/3)\,|\psi(0)\,|^2=24.7\times10^{24}\ \text{cm}^{-3}, \quad (1)$$

where r is the distance from the "unpaired" electron to the nitrogen nucleus, χ is the angle between the radius vector $\mathbf{r}$ and the internuclear axis (z axis), and $|\psi(0)|^2$ is the density of the electron spin at the nitrogen nucleus. The first expression is to be averaged over the distribution of the orbital angular momentum, while the last two refer to the spin distribution. For the ground configuration[9] $(1\sigma)^2(2\sigma)^2(3\sigma)^2(4\sigma)^2(5\sigma)^2(1\pi)^4(2\pi)$ of NO, the averaging processes for all the three molecular parameters are identical; they apply only to the 2π electron. Within the ground-configuration approximation, we obtain $\psi(0)$ from Eqs. (1) as

$$|\psi(0)\,|^2=0.85\times10^{24}\ \text{cm}^{-3}. \quad (2)$$

However, for the excited configurations such as $(1\sigma)^2(2\sigma)^2(3\sigma)^2(4\sigma)^2(5\sigma)^2(1\pi^+)(1\pi^-)(2\pi^+)^2(2\pi^-)$, the spin-average is not the same as the average over the orbital angular momentum distribution and Eq. (2) is no longer valid.

Using the SCF LCAO MO given in the Table VI (Third Calculation) of footnote 7, we have computed the various coupling parameters listed in Eqs. (1). For the ground configuration these constants are simply

$$(\sin^2\chi/r^3)_{Av}=\int\phi_{2\pi}^*(\sin^2\chi/r^3)\phi_{2\pi}d\tau,$$

$$(1/r^3)_{Av}=\int\phi_{2\pi}^*(1/r^3)\phi_{2\pi}d\tau,$$

$$\psi(0)=\phi_{2\pi}\ (\text{nitrogen nucleus}), \quad (3)$$

where

$$\phi_{2\pi}=0.8781(2p\pi_n)-0.6936(2p\pi_0).$$

These integrals can be decomposed into integrals involving only atomic orbitals of nitrogen and oxygen as

$$(2p\pi_n\,|\,(\sin^2\chi/r^3)\,|\,2p\pi_n), \quad (2p\pi_n\,|\,(\sin^2\chi/r^3)\,|\,2p\pi_0),$$

$$(2p\pi_0\,|\,(\sin^2\chi/r^3)\,|\,2p\pi_0), \quad \text{etc.} \quad (4)$$

The first integral can be evaluated by straightforward integrations, while the last two have been tabulated by Hijikata.[10] By applying logarithmic interpolation to Hijikata's table, we obtained

$$(\sin^2\chi/r^3)_{Av}=9.33\times10^{24}\ \text{cm}^{-3},$$

$$(1/r^3)_{Av}=11.6\times10^{24}\ \text{cm}^{-3}.$$

Both of these calculated values are smaller than the corresponding experimental ones. Our calculations show that integrals of the first type in (4) constitute the major part of $(\sin^2\chi/r^3)_{Av}$ and $(1/r^3)_{Av}$, the contributions from the last two integrals being about 10% or less. This is quite understandable since only the portion of electron cloud near the nitrogen atom contributes significantly to $(1/r^3)$. In order to improve our calculation we used Hartree-Fock wave functions instead of the Slater orbitals to evaluate the atomic integrals

$$(2p\pi_n\,|\,(\sin^2\chi/r^3)\,|\,2p\pi_n), \qquad (2p\pi_n\,|\,(1/r^3)\,|\,2p\pi_n).$$

For the integrals involving the oxygen orbitals such as $(2p\pi_n\,|\,1/r^3\,|\,2p\pi_0)$ and $(2p\pi_0\,|\,1/r^3\,|\,2p\pi_0)$ the Slater functions are retained. Furthermore, the coefficients of $2p\pi_n$ and $2p\pi_0$ in the SCF LCAO MO of the 2π state are assumed to be unaffected by the introduction of the Hartree-Fock functions. This procedure is justifiable for our purpose since $(1/r^3)_{Av}$ is rather insensitive to a minor change in the electron distribution around the oxygen atom. While the Hartree-Fock functions are not entirely satisfactory for computing atomic quantities such as $(1/r^3)_{Av}$, the two coupling parameters calculated by this modified procedure do become closer to the experimental results (see the second row of Table I).

TABLE I. Magnetic hyperfine coupling constants calculated by SCF LCAO MO (in units of 10^{24} cm^{-3}).

	$(\sin^2\chi/r^3)_{Av}$	$(1/r^3)_{Av}$	$[(3\cos^2\chi-1)/r^3]_{Av}$
Slater orbital for $2p\pi_N$	9.33	11.6	−4.71
Hartree-Fock function for $2p\pi_N$	10.3	12.6	−5.72
Experimental	13.4	14.9	−10.4

If we restrict ourselves to the approximation of using SCF MO of the 2π state which are linear combinations of the first and second quantum atomic orbitals, we might expect with about 90% accuracy that

$$(1/r^3)_{Av}:(\sin^2\chi/r^3)_{Av}\cong(2p\pi_n\,|\,1/r^3\,|\,2p\pi_n):$$

$$(2p\pi_n\,|\,\sin^2\chi/r^3\,|\,2p\pi_n)=1.20,$$

independent of the relative weighting of the $2p\pi_n$ and $2p\pi_0$ orbitals in the 2π function. Although this seems to compare favorably with the ratio 1.11 found in experiment, this small difference is rather critical to the determination of $\langle(3\cos^2\chi-1)/r^3\rangle_{Av}$ which we shall discuss in the following paragraph.

From $(1/r^3)_{Av}$ and $(\sin^2\chi/r^3)_{Av}$ we may determine another coupling parameter $\langle(3\cos^2\chi-1)/r^3\rangle_{Av}$ which

[8] C. H. Townes, G. C. Dousmanis, R. L. White, and R. F. Schwarz, Discussions Faraday Soc. No. 19 (1955).

[9] The notations for the molecular orbitals used here are chosen in accordance with those of reference 7.

[10] K. Hijikata (to be published).

occurs in the dipole-dipole interaction. The calculated value for this quantity is -4.71×10^{24} cm^{-3} in contrast with -10.4×10^{24} cm^{-3} from experiment. This discrepancy is rather difficult to explain. At first thought one might hope to increase the calculated value by mixing some of the excited configurations to the ground-state wave function. However, this does not seem promising since among all the SCF LCAO MO given in footnote 7, the 2π state has the largest negative value of $\langle(3\cos^2\chi-1)/r^3\rangle_{Av}$. Inclusion of the excited configurations (within the manifold of $1s$, $2s$, $2p$ atomic orbitals) in the wave function would not increase the absolute value of $\langle(3\cos^2\chi-1)/r^3\rangle_{Av}$. Of course, the states containing two unpaired 2π orbitals may have larger absolute values of $\langle(3\cos^2\chi-1)/r^3\rangle_{Av}$, but the amount of mixing of these excited configurations in the ground state should be quite negligible. The result of the calculation using Hartree-Fock atomic orbitals, as we described above, (Table I) improves this value somewhat. The discrepancy from the experimental data is, however, still quite large. In their calculation of the electronic structure of O_2, Kotani *et al.*[11] found that the theoretical values of $\langle(3\cos^2\chi-1)/r^3\rangle_{Av}$ are -11.49×10^{24} cm^{-3} and -11.60×10^{24} cm^{-3} for the ground configuration and for the wave function containing fifteen configurations, respectively. These are to be compared with the experimental value of -17.83×10^{24} cm^{-3}. If we use the Hartree-Fock atomic orbital in the same manner as before, we obtain -13.63×10^{24} cm^{-3}. The discrepancy in the case of O_2 is, therefore, not as large as ours and the error is comparable to that of $(1/r^3)_{Av}$ and $(\sin^2\chi/r^3)_{Av}$ of NO. The values of $\langle(3\cos^2\chi-1)/r^3\rangle_{Av}$ and $|\psi(0)|^2$ of O_2 were obtained from the nuclear-electronic spin-spin coupling, while in NO these were determined through the measurement of the hyperfine structure and Λ-type doubling in the $^2\Pi_{\frac{1}{2}}$ and $^2\Pi_{\frac{3}{2}}$ states. As we can easily see, a small change in $(1/r^3)_{Av}$ or $(\sin^2\chi/r^3)_{Av}$ may cause an appreciable variation in the value of $\langle(3\cos^2\chi-1)/r^3\rangle_{Av}$.

For the ground configuration of the molecule $\psi(0)$ vanishes. However, in the excited configurations in which some of the σ orbitals are occupied by unpaired electrons, the contact term is no longer equal to zero. The values of $\psi(0)$ for the various SCF σ orbitals of footnote 7 are 0.0056 for 1σ, 9.7484 for 2σ, -1.2020 for 3σ, -1.8558 for 4σ, -0.9003 for 5σ, -1.0091 for 6σ (in atomic units). In order to obtain a nonvanishing $\psi(0)$ one must recourse to configuration interactions. Using the wave function,[7,12]

$$\Psi=0.9693\psi_0-0.1335\psi_3-0.1234\psi_4+0.0935\psi_{4'}-0.0700\psi_5+0.0709\psi_{5'}+0.0327\psi_6-0.0699\psi_{6'}-0.0533\psi_7, \quad (5)$$

we obtain 0.00047 a.u. for $|\Psi(0)|^2$. However, if the configurations which have unpaired electrons in (2π) (6σ) (5σ), (2π) (6σ) (4σ), and (2π) (6σ) (3σ) are included in the ground state wave function, $|\Psi(0)|^2$ is increased to about 0.119 a.u. or 0.804×10^{-24} cm^{-3} by a simple perturbation-type calculation. This value becomes smaller when an exact configuration interaction calculation is performed. A detailed account of this work will be published in a forthcoming paper.

III. NUCLEAR QUADRUPOLE COUPLING CONSTANT

A. Calculation by the Method of Townes and Dailey

The nuclear quadrupole coupling constant of NO molecule has been determined as[5]

$$eQq=-2\text{ Mc/sec}$$

from the microwave spectrum. Here Q is the nuclear quadrupole moment, and q is defined as

$$q=\sum_i e_i[(3\cos^2\chi-1)/r^3]_i, \quad (6)$$

where the summation extends to all the charged particles of charge e_i (including the nuclei) outside the nitrogen nucleus.

In terms of the valence-bond theory nitric oxide may be regarded to have two main resonance structures[13]

$$\underset{\text{(I)}}{:\dot{N}::\ddot{O}:} \qquad \underset{\text{(II)}}{\ddot{N}::\dot{O}:}.$$

In the theory of Townes and Dailey[14] only the valence electrons associated with the nitrogen atom are considered for the calculation of q. The four atomic orbitals (nitrogen) available for these electrons are $2p\pi_x$, $2p\pi_y$, and two hybridized orbitals formed by $2s$ and $2p\sigma$ (same as $2p_z$) which may be expressed as

$$\psi_{2\sigma_1}=\xi_1\psi_{2s}+\xi_2\psi_{2p\sigma},$$
$$\psi_{2\sigma_2}=\xi_2\psi_{2s}-\xi_1\psi_{2p\sigma}. \quad (7)$$

The valence electrons of nitrogen in the two structures may be assigned, respectively, to the configurations

$$(2p\pi_x)(2p\pi_y)(2\sigma_1)(2\sigma_2)^2$$

and

$$(2p\pi_x)^2(2p\pi_y)(2\sigma_1)(2\sigma_2)^2.$$

If we adopt the self-consistent field type approximation for the atomic orbitals of the nitrogen atom, the average of $(3\cos^2\chi-1)/r^3$ for $2p\sigma$ is twice that for $2p\pi_x$ (or $2p\pi_y$) with an opposite sign. Thus the values of q for the two structures are

$$q_{\text{I}}=\xi_1^2 q_{2p\sigma}, \qquad q_{\text{II}}=(\xi_1^2-\tfrac{1}{2})q_{2p\sigma}, \quad (8)$$

[11] M. Kotani, Y. Mizuno, K. Kayama, and E. Ishiguro, J. Phys. Soc. Japan **12**, 707 (1957).

[12] This wave function differs somewhat from that obtained by Brion, Moser, and Yamazaki. We have independently made an analysis of the configuration interactions and our results will be reported in a forthcoming paper.

[13] L. Pauling, *The Nature of Chemical Bond* (Cornell University Press, Ithaca, New York, 1960), 3rd ed., p. 343.

[14] C. H. Townes and B. P. Dailey, J. Chem. Phys. **17**, 782 (1949).

TABLE II. Values of eQq calculated by the method of Townes and Dailey (in Mc/sec).

	Structure I	Structure II	65% I 35% II	50% I 50% II
$\xi_1=1/2$	−6	4.8	−2.2	−0.6
$eQq_{2p\sigma}=-24$				
$\xi_1=1/\sqrt{2}$	−5	0	−3.3	−2.5
$eQq_{2p\sigma}=-10$				

where

$$q_{2p\sigma}=-|e|\int\psi_{2p\sigma}^{*}[(3\cos^2\chi-1)/r^3]\psi_{2p\sigma}d\tau. \quad (9)$$

While it is difficult to determine the hybridization coefficient ξ_1 and the integral $q_{2p\sigma}$, Townes and Dailey[14] have given two semiempirical methods for estimating these quantities. In the first method ξ_1 and $eQq_{2p\sigma}$ are taken, respectively, as $\frac{1}{2}$ and -24 Mc/sec; and in the second, $1/\sqrt{2}$ and -10 Mc/sec. For the case of structure II because of the negative formal charge in the nitrogen atom, the q value is decreased by a factor of 1.25.[15] Alternatively, $eQq_{2p\sigma}$ may be estimated in the following manner. The nuclear quadrupole moment of nitrogen has recently been determined[16] as 1.6×10^{-26} cm^2. The average of $(3\cos^2\chi-1)/r^3$ for a $2p\sigma$ electron in a nitrogen atom may be calculated approximately from the Hartree type wave function or Slater atomic orbital. The former procedure[6] yields 18.0×10^{24} cm^{-3} and the latter, 13.4×10^{24} cm^{-3}. These correspond to $eQq_{2p\sigma}=-10$ Mc/sec and -7.5 Mc/sec, respectively. These results agree quite well with the second value of $eQq_{2p\sigma}$ (-10 Mc/sec) chosen by Townes and Dailey.[14]

Finally it is necessary to ascertain the relative weighting of the two resonance structures of NO. Various methods are available for estimating this ratio though none of these can be expected to be absolutely reliable. Pauling[13] suggests approximately equal mixing of the two structures while Dousmanis[6] obtained 65% N=O and 35% N≡O$^+$ from the magnetic hyperfine structure constants. Table II shows the values of eQq calculated by assuming these two sets of the weighting ratio of structures I and II. The coupling constants calculated by these different ways, though all in reasonable agreement with the experimental results, do show a considerable variation from one electronic structure to another.

B. Calculation by SCF LCAO MO

The average values of $(3\cos^2\chi-1)/r^3$ for the various SCF MO of the nitric oxide molecule given in footnote 7 have been calculated by the use of Hijikata's table[10] with the following results

$$(1\sigma\,|\,1\sigma)=0.1950,$$
$$(2\sigma\,|\,2\sigma)=-0.001126,$$
$$(3\sigma\,|\,3\sigma)=0.3006,$$
$$(4\sigma\,|\,4\sigma)=0.02057,$$
$$(5\sigma\,|\,5\sigma)=0.9299,$$
$$(6\sigma\,|\,6\sigma)=1.638,$$
$$(1\pi\,|\,1\pi)=-0.2025,$$
$$(2\pi\,|\,2\pi)=-0.6982,$$

expressed in atomic units (reciprocal of the third power of Bohr radius). Upon summing over all fifteen electrons one finds

$$q_{\text{electrons}}=\sum_{\text{all electrons}}e_i[(3\cos^2\chi-1)/r^3]_i=-1.382 \text{ a.u.}$$

To this we must add the contribution to q from the oxygen nucleus which amounts to $16\,|\,e\,|\,/R^3$ or 1.56 a.u., where R is the internuclear distance (1.15 A). Using $Q=0.016\times10^{-24}$ cm^2 we obtain the quadrupole coupling constant as 0.68 Mc/sec. When the molecular eigenfunction[7] which includes the interactions of a few excited configurations is used, eQq becomes 0.79 Mc/sec. It may be noticed that the contribution to eQq due to the electrons almost cancels that from the oxygen nucleus, and this results in a small coupling constant. A minor variation in the electron distribution may cause a substantial fractional change in eQq. Thus it is difficult to expect much accuracy in the calculation of the nuclear quadrupole coupling constant.

IV. SPIN-ORBIT COUPLING CONSTANT

For the ground configuration of the NO molecule only the unpaired 2π electron contributes to the spin-orbit interaction. The Hamiltonian associated with this effect has been treated extensively in the literature.[17] When configuration mixing is neglected, the spin-orbit term takes the form of

$$g_s\mu_0^2[(Z_0/r_0^3)+(Z_N/r_N^3)]_{\text{av}}(\Lambda\cdot S), \quad (10)$$

where r_O and r_N are the distances from the odd electron to the oxygen and nitrogen atoms, respectively, μ_0 is the Bohr magneton and g_s is the Landé factor of electron spin. Using the SCF LCAO MO given in footnote 7 for the ground configuration we obtain the spin-orbit coupling constant (the coefficient of the $\Lambda\cdot S$ term in (10)) as 146 cm^{-1} which agrees well with the experimental value[5] of 122.094 cm^{-1}.

[15] C. H. Townes and A. L. Schawlow, *Microwave Spectroscopy* (McGraw-Hill Book Company, Inc., New York, 1955), p. 239.
[16] C. C. Lin, Phys. Rev. (to be published).
[17] J. H. Van Vleck, Revs. Modern Phys. 23, 213 (1951).

Molecular Rotation in Crystals of N_2 and CO*

BARBARA C. KOHIN†

Department of Physics, University of Maryland, College Park, Maryland

(Received May 6, 1960)

Molecular rotation in low-temperature crystals of nitrogen and carbon monoxide is investigated. The following contributions to the crystal field hindering free rotation are taken into account: (a) the interaction of the molecular quadrupoles; (b) the effect of the anisotropic molecular polarizabilities; and (c) the short-range repulsive forces. The results of a theoretical calculation of the minimum-energy configuration at 0°K support the generally accepted structure; it is shown that the crystal field in this structure is axially symmetric at each lattice site. The Schrödinger equation for a rigid rotor in the crystal field is solved for the lowest rotational states of N_2 and CO. It is found that a classical treatment of the rotation is not justified for these crystals due to the large separations of the lowest eigenvalues. The zero-point energy of rotation is found to be about half as large as the zero-point vibrational energy for these crystals.

I. INTRODUCTION

THE first quantitative treatment of molecular rotation in solids was carried out by Pauling,[1] who suggested that the transitions in crystals of CH_4, N_2, O_2, CO, and the hydrogen halides are due to the change from oscillation to free rotation of the molecules. He approximated the effect of the crystal field on a diatomic molecule by a potential of the form

$$V(\theta)=V_0(1-\cos 2\theta), \tag{1}$$

where θ is the angle by which a molecular axis deviates from its equilibrium position.

Pauling's model was extended by Fowler,[2] who suggested that the dependence of the dielectric constants of some liquids and solids on temperature is linked to the onset of free rotation. The treatment of molecular rotation as a cooperative phenomenon, introduced by Fowler, was extended by Chang,[3] who treated the problem of the rotational specific heats in dipole lattices with a method closely allied to Bethe's method for order-disorder transitions in alloys.[4] The potential chosen by Chang to represent the interaction of nearest neighbors is of the form

$$V_{ij}=-V_0\cos\theta_{ij}, \tag{2}$$

where θ_{ij} is the angle between the length axes of two adjacent molecules. The crystal was treated as an assembly of rigid rotors, and a critical temperature for the transition from hindered to free rotation was obtained by requiring that the distribution of molecular orientations be consistent with the crystal field.

Treatments essentially equivalent to that of Chang were subsequently applied to various types of dipole lattices.[5] The limiting approximation in all of these is the choice of the potential [Eq. (2)]. This form is a rather poor representation of the dipole interaction which actually depends not only on the relative orientation of the two dipoles, but on the direction of the vector separating their centers.

Apart from the inapplicability of early theories to nonpolar substances, the results failed to explain the existence of multiple transitions, such as those which take place in the hydrogen halides. Krieger and James[6] have proposed a model of a crystal which can exhibit more than one phase transition. They assume rigid rotors coupled by a nearest-neighbor potential of the form

$$V(\theta_{ij})=A\cos\theta_{ij}+B\cos^2\theta_{ij}. \tag{3}$$

Depending on the relative values of A and B, this model shows a single first-order transition, a single second-order transition, two first-order transitions, or a second-order transition followed by a first-order transition as the temperature is raised. Although Krieger and James did not attempt to obtain quantitative agreement with observed transition temperatures, their model does show some qualitative features resembling the behavior of the hydrogen halides, and the model is the first to exhibit multiple transitions.

The most thorough and realistic classical treatment of rotation and transitions in molecular crystals is that of James and Keenan[7] for solid CD_4. They have assumed nearest neighbors orientationally coupled by octupole forces, and have succeeded in explaining the existence of three solid phases. A single parameter, the octupole moment of CD_4, was fitted to the temperature of the

* Based on a thesis submitted to the Faculty of the Graduate School of the University of Maryland in partial fulfillment of the requirements for the degree of Doctor of Philosophy. Research supported by the U. S. Air Force through the Air Force Office of Scientific Research of the Air Research and Development Command.

† Present address: Department of Chemistry, The Catholic University of America, Washington 17, D. C.

[1] L. Pauling, Phys. Rev. **36**, 430 (1930).
[2] R. H. Fowler, Proc. Roy. Soc. (London) **A149**, 1 (1935).
[3] T. S. Chang, Proc. Cambridge Phil. Soc. **33**, 524 (1937).
[4] H. A. Bethe, Proc. Roy. Soc. (London) **A150**, 522 (1935).
[5] J. G. Kirkwood, J. Chem. Phys. **8**, 205 (1940); Y. Kakiuchi, J. Phys. Soc. Japan **6**, 313 (1951); R. Kikuchi, Phys. Rev. **81**, 988 (1951); T. Oguchi and Y. Takagi, J. Phys. Soc. Japan **7**, 145 (1952); T. Nakamura, *ibid.* **7**, 264 (1952).
[6] T. J. Krieger and H. M. James, J. Chem. Phys. **22**, 796 (1954).
[7] H. M. James and T. A. Keenan, J. Chem. Phys. **31**, 12 (1959). (I am indebted to Professor James for a copy of this paper prior to its publication.)

upper transition, and predictions of the theory are in satisfactory agreement with the lower transition temperature, the latent heats, and the optical properties of the phases.

It is the purpose of the work reported here to derive a realistic form for the orientational field in a crystal of nonpolar diatomic molecules and to investigate the effects of this field on the rotation of the molecules. The results will be applied to N_2 and CO crystals at low temperatures.

II. CRYSTAL FIELD

Intermolecular Potential

The interaction of a pair of diatomic molecules can be separated into two parts: a spherically symmetric interaction which includes a short-range repulsion and a longer-range attraction; and an anisotropic or directional interaction arising from the nonspherical symmetry of the molecules. The latter term is a function of the orientations of the molecular axes.

The spherical interaction potential has no effect on the orientations of the molecules in the crystal, and thus need not be considered here. The most important terms in the directional interaction potential for nonpolar diatomic molecules are:

(a) a term due to the interaction of the quadrupole moments of the molecules;

(b) a directional correction to the attractive dispersion forces due to the anisotropic polarizabilities of the molecules; and

(c) a directional correction to the repulsive forces. The dipole moment of CO makes such a small contribution to the potential that it will be neglected in this treatment.

The quadrupole interaction of two *axially symmetric* charge distributions can be written[8]

$$E_q(1,2)=\tfrac{3}{4}Q_1Q_2R^{-5}[1-5(\hat{n}_1\cdot\hat{r}_{12})^2-5(\hat{n}_2\cdot\hat{r}_{12})^2+35(\hat{n}_1\cdot\hat{r}_{12})^2(\hat{n}_2\cdot\hat{r}_{12})^2+2(\hat{n}_1\cdot\hat{n}_2)^2-20(\hat{n}_1\cdot\hat{n}_2)(\hat{n}_1\cdot\hat{r}_{12})(\hat{n}_2\cdot\hat{r}_{12})]. \quad (4)$$

In this relation $\hat{n}$ is a unit vector along the axis of a charge distribution and $Q=(q_{zz}-q_{xx})$ is the scalar quadrupole moment. The quantity $\hat{r}_{12}$ is a unit vector along **R**, the separation of the centers of the two charge distributions.

The principal attractive forces between spherical atoms or molecules at distances large compared with bond lengths are the dispersion forces first derived by London.[9] The nonspherical correction to the dispersion forces between two identical diatomic molecules is

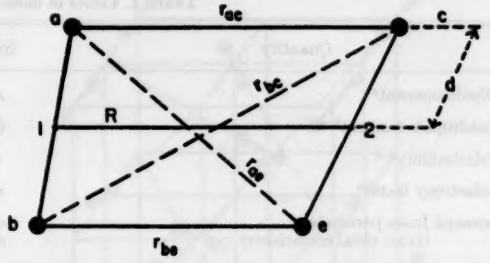

FIG. 1. Internuclear distances appearing in the repulsive interaction potential for two diatomic molecules [Eq. (7)].

well represented by a potential of the form[10]

$$E_\alpha(1,2)=4\epsilon\sigma^6R^{-6}\{\kappa[1-\tfrac{3}{2}(\hat{n}_1\cdot\hat{r}_{12})^2-\tfrac{3}{2}(\hat{n}_2\cdot\hat{r}_{12})^2]+\kappa^2[\tfrac{3}{2}(\hat{n}_1\cdot\hat{r}_{12})^2+\tfrac{3}{2}(\hat{n}_2\cdot\hat{r}_{12})^2-13.5(\hat{n}_1\cdot\hat{r}_{12})^2(\hat{n}_2\cdot\hat{r}_{12})^2+9(\hat{n}_1\cdot\hat{r}_{12})(\hat{n}_2\cdot\hat{r}_{12})(\hat{n}_1\cdot\hat{n}_2)-\tfrac{3}{2}(\hat{n}_1\cdot\hat{n}_2)^2]\}, \quad (5)$$

in which κ is the factor expressing the anisotropy of the polarizability α:

$$\kappa=(\alpha_{zz}-\alpha_{xx})/3\langle\alpha\rangle,$$
$$\langle\alpha\rangle=\tfrac{1}{3}(\alpha_{xx}+\alpha_{yy}+\alpha_{zz}). \quad (6)$$

The quantities ϵ and σ are the usual parameters occurring in the Lennard-Jones molecular interaction potential[8] [Eq. (9)]. The unit vectors $\hat{n}_1$, $\hat{n}_2$, and $\hat{r}_{12}$ are the same as those appearing in Eq. (4).

The short-range repulsive forces between molecules, which arise from exchange and overlap and are often represented by an empirical potential of the form A/R^{12}, are asymmetric for diatomic molecules; the deviation of these forces from spherical symmetry gives an important contribution to the orientational forces between N_2 or CO molecules separated by crystal distances. To obtain the directional dependence of these forces for diatomic molecules it is usual to sum the pairwise interactions between atoms of neighboring molecules.[10,11] The interaction potential for the pair of homonuclear diatomic molecules (see Fig. 1) is then given by

$$E_r(1,2)=B(r_{ac}^{-12}+r_{ae}^{-12}+r_{bc}^{-12}+r_{be}^{-12}). \quad (7)$$

If Eq. (7) is expanded in powers of d/R (where d is $\frac{1}{2}$ the nuclear separation within a molecule), the result is

$$E_r(1,2)=4BR^{-12}\{1+6d^2R^{-2}[14(\hat{n}_1\cdot\hat{r}_{12})^2+14(\hat{n}_2\cdot\hat{r}_{12})^2-2]+42d^4R^{-4}[1-16(\hat{n}_1\cdot\hat{r}_{12})^2-16(\hat{n}_2\cdot\hat{r}_{12})^2+288(\hat{n}_1\cdot\hat{r}_{12})^2(\hat{n}_2\cdot\hat{r}_{12})^2+2(\hat{n}_1\cdot\hat{n}_2)^2-64(\hat{n}_1\cdot\hat{r}_{12})(\hat{n}_2\cdot\hat{r}_{12})(\hat{n}_1\cdot\hat{n}_2)]+\text{higher-order terms}\}. \quad (8)$$

In this expression the unit vectors are those defined before. Equation (8) will be employed for CO as well as

[8] See, for example, J. Hirschfelder, C. F. Curtiss, and R. B. Bird, *The Molecular Theory of Gases and Liquids* (John Wiley & Sons, Inc., New York, 1954).

[9] F. London, Trans. Faraday Soc. **33**, 8 (1937).

[10] J. de Boer, Physica **9**, 363 (1942).

[11] I. Amdur, E. A. Mason, and J. E. Jordan, J. Chem. Phys. **27**, 527 (1957).

TABLE I. Values of molecular parameters for CO and N_2.

Quantity	Symbol	N_2 value	CO value
Dipole moment[a]	μ	...	0.117×10^{-18} esu
Quadrupole moment[b,c]	Q	1.29×10^{-26} esu	1.62×10^{-26} esu
Polarizability[a,d]	$\langle\alpha\rangle$	1.741 A^3	1.844 A^3
Anisotropy factor[e]	κ	0.189	0.168
Lennard-Jones parameters[f] (from virial coefficients)	ϵ σ	1.313×10^{-14} erg 3.708 A	1.382×10^{-14} erg 3.769 A
Nearest-neighbor distance[f]	R_0	4.00 A	3.98 A
Nuclear separation[g,h]	$2d$	1.104 A	1.128 A
Moment of inertia (calculated)	A	1.417×10^{-39} g cm^2	1.479×10^{-39} g cm^2
Repulsive potential parameter[i] (from viscosity data)	B	4.565×10^{-6} erg A^{12}	3.787×10^{-6} erg A^{12}
α-β transition temperature[j,k]	T_{tr}	35.61°K	61.57°K
Latent heat of transition[j,k]	ΔH_{tr}	54.71 cal/mole	151.3 cal/mole
α crystal structure[l]		$Pa3$	$Pa3$
β crystal structure[l]		$P6_3/mmc$	$P6_3/mmc$
α lattice constant[l]	a	5.667 A	5.64 A
α crystal field constant (calculated)	C/k	−520°K	−673°K

[a] A. van Itterbeek and K. de Clippelier, Physica **14**, 349 (1948).
[b] W. V. Smith and R. Howard, Phys. Rev. **79**, 132 (1950).
[c] R. M. Hill and W. V. Smith, Phys. Rev. **82**, 451 (1951).
[d] A. Michels, H. Wouters, and J. de Boer, Physica **1**, 587 (1934).
[e] K. G. Denbigh, Trans. Faraday Soc. **36**, 936 (1940).
[f] See footnote reference 15.
[g] M. E. Boyd, National Bureau of Standards (private communication).
[h] G. Herzberg, *Spectra of Diatomic Molecules* (McGraw-Hill Book Company, Inc., New York, 1950).
[i] See footnote reference 8, p. 1111.
[j] J. O. Clayton and W. F. Giauque, J. Am. Chem. Soc. **54**, 2610 (1932).
[k] W. F. Giauque and J. O. Clayton, J. Am. Chem. Soc. **55**, 4875 (1933).
[l] J. D. H. Donnay and W. Nowacki, *Crystal Data* (Geological Society of America, New York, 1954).

N_2 interactions since in the former case the dipolar asymmetry is very small.

Potential Parameters

The parameters occurring in Eqs. (4), (5), and (8) for the directional interaction potentials can be determined from experimental data for CO and N_2. The molecular quadrupole moments are obtained from pressure broadening of microwave lines.[12] The quantities ϵ and σ occurring in the anisotropic dispersion potential [Eq. (5)] are obtained by fitting the second virial coefficients of the gases[13] to a potential of the form

$$\phi(1,2)=4\epsilon[(\sigma/R)^{12}-(\sigma/R)^6]. \quad (9)$$

The anisotropy factor κ is obtained from measurements of refractive index and Kerr effect.

Since the virial coefficients are rather insensitive to the short-range terms in the interaction potential, the coefficient B occurring in the expression for the repulsion is obtained from viscosity data[14] instead of virial data. The average repulsive energy for a pair of diatomic molecules is given by

$$\langle E_r(1,2)\rangle_{Av}=\langle B(r_{ac}^{-12}+r_{ae}^{-12}+r_{bc}^{-12}+r_{be}^{-12})\rangle_{Av}. \quad (10)$$

Here the r's are the separations of nuclei on neighboring molecules (Fig. 1). For two molecules separated by R the averaging over orientations yields[11]

$$\langle E_r(1,2)\rangle_{Av}=4BR^{-12}\{(R^2/360d^2)[(1-2d/R)^{-9}+(1+2d/R)^{-9}+2]\}. \quad (11)$$

By comparing Eq. (11) with the average of the lowest-order terms retained in Eq. (8), one can obtain an estimate of the magnitude of the terms neglected. This calculation shows that the higher-order terms contribute only about 2% of the repulsive energy, and are therefore negligible. The average of E_r from Eq. (11) is equated to the experimental value of the repulsive potential obtained from viscosity measurements to obtain B.

[12] Footnote reference 8, p. 1025 ff.
[13] Footnote reference 8, p. 162 ff.
[14] Footnote reference 8, p. 562 ff.

A summary of the values of the potential parameters used in this paper is given in Table I.

As a check on the accuracy of these potentials to represent the interaction of N_2 and CO molecules in crystals and to show the relative contributions of the various components of the field to the crystal energy, the total energy at 0°K has been calculated for these crystals. The results of this calculation are shown in Table II. The only significant terms omitted from Table II are (a) the deviation from pairwise additivity of the potentials (estimated at about −30 cal/mole by Lupton[15]), and (b) the zero-point rotational energy due to hindered rotations of the molecules. The latter term will be discussed in Sec. IV.

Structure of N_2 and CO Crystals

The structure of crystals of carbon monoxide and nitrogen has been studied by Vegard,[16] Ruhemann,[17] and Boltz *et al.*[18] The form stable at lowest temperatures is known as the α form; at higher temperatures the β form exists. The crystal structure of the α form is $Pa3$ and there are four molecules per unit cell. The centers of the molecules are located at the lattice points of a face-centered cubic array, and at very low temperatures the molecular axes are directed toward the centers of the edges of the cube. This configuration is shown in Fig. 2.

In the β-phase crystals stable at higher temperatures the molecular centers are located at hexagonal close-packed lattice sites. The orientations of the molecular axes have not been ascertained; some degree of molecular rotation is evident.

Orientational Field

The forces tending to orient the axes of diatomic molecules in α-form crystals arise from the nonspherically symmetric interactions discussed at the beginning of this section. If the α structure is assumed to contain four molecules per unit cell and the centers of these molecules are assumed fixed on a face-centered cubic lattice in accord with the evidence of x-ray diffraction measurements, then the contribution of the directional interactions to the potential energy of the crystal at 0°K can be written as a function of the orientations of four molecules. If the expression for the energy, which is a function of the coordinates specifying these orientations, is differentiated with respect to these variables, the results show that the assumed configuration of the α-form structure (Fig. 2) corresponds to a minimum in the orientational energy.

TABLE II. Crystal energy at 0°K.[a]

Quantity	N_2	CO
Spherical dispersion	−3465 cal/mole	−4146 cal/mole
Spherical repulsion	+1991	+2476
Zero-point lattice vibration	+213	+225
Anisotropic dispersion	+88	+86
Anisotropic repulsion	−362	−356
Quadrupole interaction	−251	−406
Total	−1786 cal/mole	−2121 cal/mole
Experimental sublimation energy[b]	−1652 cal/mole	−1987 cal/mole

[a] Some of these terms were calculated by Lupton.[15]
[b] K. K. Kelley, Bull. 383, U. S. Dept. of the Interior, Bureau of Mines (1935).

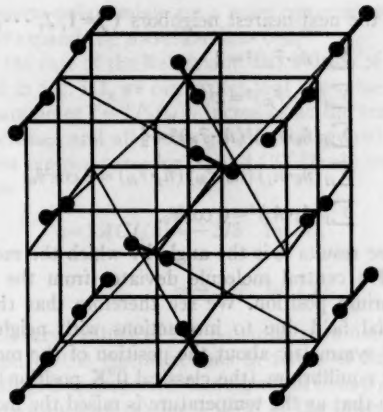

FIG. 2. Alpha-form crystal structure for N_2 and CO.

Axial Symmetry of the Field; Average Pair Interaction Energy

The energy with which a diatomic molecule in an α-form crystal interacts with its neighbors has been calculated as a function of its orientation. All molecules except one are assumed fixed in the equilibrium positions shown in Fig. 2. The directionally dependent terms in the interaction potentials [Eqs. (4), (5), and (8)] are then determined as functions of the orientation of the single molecule. The results are as follows.

For 12 nearest neighbors ($i=1, 2, \cdots, 12$) about a central molecule parallel to $\hat{n}_0$:

$$\sum_i(\hat{n}_0\cdot\hat{r}_{i0})^2=4$$

$$\sum_i(\hat{n}_i\cdot\hat{r}_{i0})^2=4$$

$$\sum_i(\hat{n}_0\cdot\hat{r}_{i0})^2(\hat{n}_i\cdot\hat{r}_{i0})^2=2\sin^2\theta_0$$

$$\sum_i(\hat{n}_0\cdot\hat{n}_i)(\hat{n}_0\cdot\hat{r}_{i0})(\hat{n}_i\cdot\hat{r}_{i0})=2\sin^2\theta_0$$

$$\sum_i(\hat{n}_0\cdot\hat{n}_i)^2=\tfrac{4}{3}+4\sin^2\theta_0. \qquad (12)$$

[15] J. M. Lupton, thesis, University of Amsterdam, 1954.
[16] L. Vegard, Z. Physik **58**, 497 (1929); **61**, 185 (1930); **79**, 471 (1932); **88**, 235 (1934).
[17] M. Ruhemann, Z. Physik **76**, 368 (1932).
[18] L. H. Boltz, M. E. Boyd, F. A. Mauer, and H. S. Peiser, Acta Cryst. **12**, 247 (1959).

For the next-nearest neighbors ($j=1, 2, \cdots, 6$):

$$\sum_j(\hat{n}_0\cdot\hat{r}_{j0})^2=2$$
$$\sum_j(\hat{n}_j\cdot\hat{r}_{j0})^2=2$$
$$\sum_j(\hat{n}_0\cdot\hat{r}_{j0})^2(\hat{n}_j\cdot\hat{r}_{j0})^2=\tfrac{2}{3}$$
$$\sum_j(\hat{n}_0\cdot\hat{n}_j)(\hat{n}_0\cdot\hat{r}_{j0})(\hat{n}_j\cdot\hat{r}_{j0})=2\cos^2\theta_0$$
$$\sum_j(\hat{n}_0\cdot\hat{n}_j)^2=6\cos^2\theta_0.$$

In these results θ_0 is the angle by which the molecular axis of a central molecule deviates from the α-form equilibrium position. We see therefore that the total potential field due to interactions with neighbors is axially symmetric about the position of the molecular axis at equilibrium (the classical 0°K position). If we assume that as the temperature is raised the molecules tend to rotate classically about their equilibrium positions in this axially symmetric field then we can assume as an approximation that this axial symmetry is preserved. The large number of neighbors in a close-packed crystal appears to justify this approximation.

The axial symmetry simplifies the calculation of the crystal field. We can transform the pair interaction represented by Eqs. (4), (5), and (8) to a coordinate system in which the z axes at the two lattice sites lie along the symmetry axes through the sites. We can then average the interaction over the angles in the planes perpendicular to these two z axes. If we then sum this average pair interaction for two shells of neighbors about a central molecule, we obtain for the average potential energy of a diatomic molecule in an α-form crystal:

$$V=CIP_2(\cos\theta), \tag{13}$$

in which θ is the angle between the molecular axis and the symmetry axis at the lattice site and $P_2(\cos\theta)=-\frac{1}{2}+\frac{3}{2}\cos^2\theta$. The quantity I is the average value of $P_2(\cos\theta_i)$ for the neighbors. C is a function of the molecular parameters and the lattice constants, as follows:

$$C=-21.47Q^2R_0^{-5}+46\epsilon\sigma^6\kappa^2R_0^{-6}-51037Bd^4R_0^{-16}, \tag{14}$$

in which R_0 is the nearest-neighbor distance. The value of C for N_2 and CO is given in Table I.

III. CLASSICAL ROTATIONAL DISTRIBUTION

Order Parameter

The parameter I in the expression for the crystal field [Eq. (13)] is a measure of the rotational order of the crystal. If zero-point rotation is negligible then all molecular axes will approach coincidence with the α-form symmetry axes as $T\to0$°K, and therefore $\theta_i\to0$ and $I\to1$. For a rotationally disordered crystal $\langle\cos^2\theta_i\rangle=\frac{1}{3}$ and $I=0$.

In order to calculate the value of the order parameter I as a function of temperature we employ the *internal field approximation*, which is equivalent to the following assumptions:

(a) each molecule orients itself independently in the average field of its neighbors; and

(b) the probability distribution for molecular orientation is the same for each lattice site.

If we then require the rotational distribution to be consistent with the crystal field, we obtain a consistency equation relating the temperature and the order parameter.

Consistency Relation

If an assembly of classical rigid rotors with fixed centers is taken as a model for a crystal of diatomic molecules, then the normalized rotational distribution function will have the form

$$f(\theta,\phi)=\exp[-V(\theta,\phi)/kT]\Big/\int\exp[-V(\theta,\phi)/kT]d\omega, \tag{15}$$

where $f(\theta,\phi)d\omega$ is the probability that the axis of a molecule lies in the solid angle $d\omega$ about (θ,ϕ). $V(\theta,\phi)$ is the orienting potential due to the crystal field. In the case of α-form crystals we have found $V(\theta)=CIP_2(\cos\theta)$, in which I is the assembly average of $P_2(\cos\theta)$. The classical consistency relation for $I(T)$ therefore becomes

$$I(T)=\frac{\int P_2(\theta)\exp[-CIP_2(\theta)/kT]d\omega}{\int\exp[-CIP_2(\theta)/kT]d\omega}. \tag{16}$$

There are two solutions of Eq. (16). One solution corresponds to rotational disorder: $I(T)=0$ for all T. The other solution, corresponding to an ordered array, has an extremum at $I=0.312$ corresponding to a maximum in the temperature. The value of this temperature maximum is given by

$$T_{\max}=-0.217C/k. \tag{17}$$

Since x-ray diffraction data indicate that the molecular axes are ordered over the entire range of stability of α-form crystals of CO and N_2, the values of $T_{\max}$ are theoretical upper bounds for the $\alpha-\beta$ phase transition temperatures for these crystals. Using this classical model Jansen and de Wette[19] obtained values of $T_{\max}$ which are in close agreement with the observed $\alpha-\beta$ transition temperatures. However, the directional anisotropy in the intermolecular repulsive forces was not included in their calculation of the field constant C. When this component of the field is included the derived maxima are much higher than the experimental transition temperatures. Furthermore, as

[19] L. Jansen and F. W. de Wette, Physica **21**, 83 (1955); F. W. de Wette, *ibid.* **22**, 644 (1956).

will be shown in Sec. IV, the classical treatment is not applicable to the cases of N_2 and CO.

IV. QUANTUM-MECHANICAL TREATMENT OF MOLECULAR ROTATION

Schrödinger Equation for the Rotational States

We have found that the average directional interaction of a diatomic molecule at a lattice site in an α-form crystal with its neighbors can be represented by

$$V=CIP_2(\cos\theta), \tag{18}$$

where I is the average of $P_2(\cos\theta)$ for the assembly of molecules, and C is a function of the lattice dimensions, the molecular properties, and the orientations of the symmetry axes of the field at the lattice sites.

The potential (18) represents the field in which a diatomic molecule rotates. If a diatomic molecule is treated as a rigid rotor, the Schrödinger equation for the rotational motion is

$$\frac{-\hbar^2}{2A\sin\theta}\left[\frac{\partial}{\partial\theta}\left(\sin\theta\frac{\partial\Psi}{\partial\theta}\right)+\frac{1}{\sin\theta}\frac{\partial^2\Psi}{\partial\phi^2}\right]+CIP_2(\cos\theta)=E\Psi. \tag{19}$$

Here A is the moment of inertia for the rigid rotor.

The separation of Eq. (19) yields

$$\Psi(\theta,\phi)=Q(\theta)\Phi(\phi)$$

$$(1/\Phi)(d^2\Phi/d\phi^2)=-m^2;$$

$$\Phi=(2\pi)^{-1}\exp(im\phi) \tag{20}$$

and

$$(d/d\omega)[(1-\omega^2)(dQ/d\omega)]+Q[\mu-\eta\omega^2-m^2(1-\omega^2)^{-1}]=0, \tag{21}$$

where

$$\omega=\cos\theta,$$

$$\mu=ACI/\hbar^2+2AE/\hbar^2, \tag{22}$$

and

$$\eta=3ACI/\hbar^2.$$

The quantity η is negative for α-N_2 and α-CO. Equation (21) is a spheroidal wave equation and the eigensolutions $Q_{lm}(\eta,\omega)$ are oblate spheroidal wave functions.

Application to CO and N_2

The eigenfunctions Q_{lm} for a hindered rotor which are solutions of the Schrödinger equation are characterized by two integral quantum numbers l and m ($l\geq 0$, $|m|\leq l$). For relatively small values of the potential parameter η, these eigenfunctions have been determined by Stratton *et al.*[20] as linear combinations of associated Legendre polynomials. In the limit of large η the Laguerre polynomials are a more convenient set in which to expand the wavefunctions Q_{lm}.[21]

As in the case of the Boltzmann distribution of rotors assumed in Sec. III, we can expect that the value of the order parameter $I=\langle P_2(\omega)\rangle$ increases as the temperature decreases and all rotors go into the ground state. At lowest temperatures for N_2 and CO ($I\sim 1$) we have therefore

$$\eta=3ACI/\hbar^2\approx -275 \quad \text{for } N_2,$$

and

$$\approx -370 \quad \text{for CO.} \tag{23}$$

For such large values of the potential parameter η an expansion of the eigenfunctions in terms of Laguerre polynomials is appropriate. The eigenfunctions $Q_{lm}(\eta,\omega)$ and eigenvalues $\mu_{lm}(\eta)$ for several of the lowest rotational states have been calculated using the method of Flammer.[21] The eigenfunctions are either even or odd with respect to inversion of the rotor, and for the appropriate range of η the lowest eigenvalues coalesce in pairs, with one even and one odd eigenfunction corresponding to each eigenvalue.

Validity of the Classical Approximation

The eigenvalues for the rotational states obtained from the solution of the Schrödinger equation can be used to assess the validity of the assumption of a classical Boltzmann distribution which was employed in Sec. III. The condition that the Boltzmann distribution be a good approximation requires that the distance adjacent energy levels be small in comparison to kT. For CO and N_2 at low temperatures, the separation of the two lowest levels is found to be (setting $I=1$)

$$\Delta E/k\sim 93^\circ\text{K} \quad \text{for } N_2,$$

$$\sim 104^\circ\text{K} \quad \text{for CO.} \tag{24}$$

In order to determine whether the Boltzmann distribution is a valid approximation at higher temperatures it is necessary to determine I as a function of temperature by a self-consistent method analogous to that of Sec. III, using now the partition function for the rotational states in place of the Boltzmann distribution. As the temperature of an assembly of rotors increases, the expectation value of $P_2(\cos\theta)$ for the assembly will decrease and therefore the potential parameter η will also decrease.

The procedure for calculating I vs T is as follows.

(a) Choose I; $\eta=3ACI/\hbar^2$.

(b) Determine the wave functions Q_{lm} and eigenvalues μ_{lm} for several of the lowest eigenstates; calculate the expectation values $i_{ml}=\langle P_2(\omega)\rangle_{ml}$ for each of these states.

[20] J. A. Stratton, P. M. Morse, L. J. Chu, D. C. Little, and F. J. Corbató, *Spheroidal Wave Functions* (The Technology Press of Massachusetts Institute of Technology, Cambridge, Massachusetts and John Wiley & Sons, Inc., New York, 1956).

[21] C. Flammer, *Spheroidal Wave Functions* (Stanford University Press, Stanford, California, 1957).

TABLE III. Results of the quantum-mechanical calculations.

	T	Order parameter I	Ground-state energy E_0/k	Separation of two lowest states $\Delta E/k$
For N_2	0°K	0.9068	−396°K	88°K
	17.5	0.9046	−393	88
	33	0.8874	−386	87
	42	0.8761	−381	87
For CO	0°K	0.9176	−538°K	100°K
	26.5	0.9127	−534	99
	37	0.9028	−529	99
	57	0.8734	−510	97
	110	0.8096	−467	93

(c) Calculate the partition function

$$\sum_j \gamma_j \exp(-E_j/kT),$$

in which γ_j is the degeneracy of the jth state and

$$E_j = (\hbar^2/2A)(\mu_j - CI/2). \tag{25}$$

The consistency equation,

$$I = \sum_j i_j \gamma_j \exp(-E_j/kT) / \sum_j \gamma_j \exp(-E_j/kT), \tag{26}$$

which is the quantum-mechanical analog of Eq. (16), then yields T as a function of I.

This procedure was carried out for several values of I and the results are shown in Table III. It is evident from the table that the assumption of a Boltzmann distribution for the rotational states is completely unjustified for all temperatures below the melting point. The hindering potential in α-phase crystals of N_2 and CO is so strong that the energy levels are appreciably separated. On the basis of this model the molecules would be expected to remain almost completely in the rotational ground state over the entire range of stability of α-form crystals.

In this model no account is taken of the thermal expansion of the lattice, which would be expected to weaken the field as the temperature rises. However, available data on thermal expansion of N_2 crystals indicate that this effect is very small. For example, in the range 4.2° to 20°K the average coefficient of linear expansion for solid N_2 is 2×10^{-4} per deg.[18] This expansion leads to an increase of less than 0.5% in the potential for a 20° rise in temperature.

Rotational Zero-Point Energy

The results of the quantum-mechanical treatment yield the following values for the zero-point rotational energy in α-form crystals:

for N_2, $E_{zpr} = 123$ cal/mole;

for CO, $E_{zpr} = 134$ cal/mole.

The zero-point energy due to hindered rotation is therefore somewhat smaller than the vibrational zero-point energy of the lattice for these crystals. The inclusion of this term improves the agreement between the calculated and experimental values of the sublimation energies at 0°K (Table II).

V. CONCLUSIONS

Although the results of the previous section indicate that a classical assembly of rigid rotors is a poor model for N_2 and CO crystals, a classical treatment may be applicable to crystals of molecules having weaker directional interactions, or at higher temperatures. In general, however, these molecules with small directional interactions also have small moments of inertia, and there is therefore an appreciable separation of rotational eigenstates even in the absence of a crystal field.

The calculations in which the directional energy of the crystal field is minimized to determine the most favorable orientations of the molecules provide a theoretical confirmation of the observed structures for α-CO and α-N_2. Such a method is unfortunately applicable only to configurations at very low temperatures since the molecules must be assumed stationary. It has therefore been impossible to treat β-form crystals of N_2 and CO in a similar fashion since the observed structure appears to correspond to a configuration which is orientationally unstable at 0°K.

Although no allowance has been made in any of these calculations for the thermal expansion of the crystals, available data on the thermal expansion of N_2 indicate that this effect is very small.

Probably the most serious defect of the present treatment is the neglect of direct correlations between neighbors. This omission is inherent in the internal field approximation and is justified somewhat by the high coordination numbers in close-packed crystals. However, in view of the large directional forces between neighbors it is quite possible that some direct coupling of the motions of adjacent molecules could result in a lower crystal energy. Such a phenomenon has actually been observed in benzene crystals, in which adjacent molecules appear to rotate together like meshed gears.[22] Such coupled motions may provide an explanation for the stability of β-form crystals, which cannot be treated with the internal field approximation. The effect of such coupled motions would be the enhancement of the contribution of nonspherical molecular symmetry to the crystal field, and an increase in the separation of the lowest rotational states.

In spite of the neglect of possible direct correlations, the values obtained for the contributions of hindered rotations to the zero-point energies are of some interest, indicating that the zero-point rotational energy is more

[22] E. G. Cox, Revs. Modern Phys. 30, 159 (1958).

than half as large as the vibrational zero-point energy for crystals of CO and N_2.

The large separation of the lowest rotational eigenvalues leads to the conclusion that most of the molecules in α-form crystals of CO and N_2 will exist in the rotational ground state, which is not in disagreement with experimental evidence. There should be very little contribution of rotation to the crystalline specific heat.

VI. ACKNOWLEDGMENTS

I am thankful for the helpful advice of Dr. A. A. Maradudin, under whose guidance this work was completed, and I am indebted to Dr. J. L. Jackson, Dr. E. A. Mason, and Dr. G. Weiss for illuminating comments and discussion. The research was undertaken at the suggestion of Dr. Laurens Jansen, whose contribution is gratefully acknowledged.

THE JOURNAL OF CHEMICAL PHYSICS VOLUME 33, NUMBER 3 SEPTEMBER, 1960

Identification of Colloidal Sodium in Sodium Azide

BRIAN S. MILLER

Basic Research Group, U. S. Army Engineer Research and Development Laboratories, Fort Belvoir, Virginia

(Received April 11, 1960)

Under treatment with ultraviolet radiation and heat, sodium azide develops an optical absorption band centered at 520 mμ. The centers responsible for this band have been identified by the dual techniques of electron spin resonance and cryoabsorption spectroscopy as colloidal sodium.

INTRODUCTION

THE apparent similarity of azides and halides, as regards color center formation, has been noted by several workers. Rosenwasser, Dreyfus, and Levy[1] studied coloring of sodium azide by gamma rays, fast and slow neutrons, and detected several optical absorption bands by reflection techniques. Tompkins and Young[2] used low-temperature spectrophotometry to investigate the effect of ultraviolet radiation on potassium azide, and by analogy with potassium chloride were able to tentatively identify several types of color centers. Cunningham and Tompkins[3] used both ultraviolet and x rays to color sodium azide at liquid-nitrogen temperature and found centers corresponding to both *F* and *V* centers. On warming their samples, an absorption band was found which they ascribed to selective photoemission from excess metallic sodium into the conduction band of the salt.

In the present work, it has been found possible to produce excess metal by photolysis and subsequently thermally aggregate this excess metal to form colloidal particles, and to detect them by both electron spin resonance and optical absorption.

EXPERIMENTAL

Sodium azide crystals were prepared by triple recrystallization at room temperature from aqueous solution of Matheson, Coleman, & Bell reagent grade sodium azide. Platelets of fair optical quality were obtained by this method. All spectra were run with samples mounted in a metal Dewar constructed to fit the sample compartment of the Beckman DK-2 ratio recording spectrophotometer (Fig. 1).

Thin plates of the azide were clamped over an opening in the brass finger, the temperature of which was monitored by a copper-constantan thermocouple. The Dewar employed enabled measurements to be made at temperatures approaching liquid helium, although no attempt was made to measure temperature in this region. Less than one liter of liquid helium in the inner chamber would last approximately two hours. The entire Dewar assembly could be lifted out of the sample compartment of the spectrophotometer by means of two jacks to allow irradiation through the quartz windows.

Temperatures above room temperature were obtained by means of an auxiliary heater lowered through the helium fill tube to engage a stud in the bottom of the helium finger.

OPTICAL RESULTS

Untreated sodium azide crystals showed no absorption bands between 270 mμ and 1000 mμ at liquid-helium temperature.

Curve A of Fig. 2 shows the result of two hours of irradiation with the unfiltered output of a 100-w Hanovia type S-100 mercury vapor lamp at 298°K. The crystal appears pale greenish-brown after the irradiation. The peak at 3.6 ev is identified with photo-

[1] H. Rosenwasser, R. W. Dreyfus, and P. W. Levy, J. Chem. Phys. **24**, 184 (1956).
[2] F. C. Tompkins and D. A. Young, Proc. Roy. Soc. (London) **236**, 10 (1956).
[3] J. Cunningham and F. C. Tompkins, Proc. Roy. Soc. (London) **251**, 27 (1959).

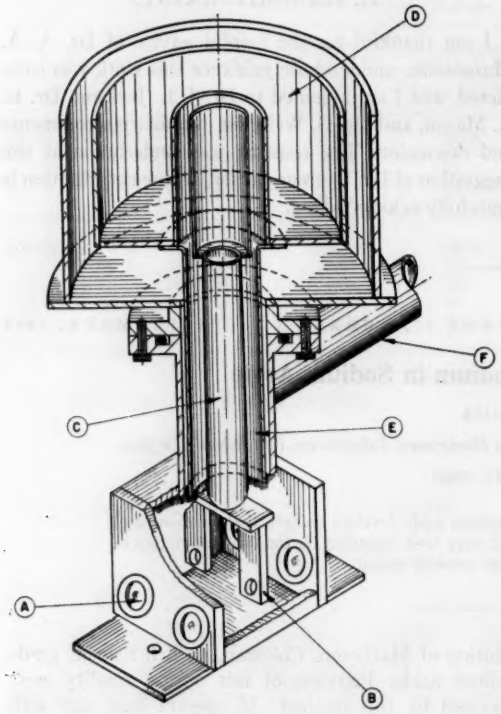

FIG. 1. Cut away drawing of lower portion of helium Dewar for Beckman DK-2 spectrophotometer. (*A*) quartz windows; (*B*) sample finger; (*C*) liquid-helium chamber; (*D*) liquid air; (*E*) radiation shield; (*F*) pumping line.

emission from the sodium left in the crystal as a result of photolysis.[3] The shoulder at 4.7 ev can be identified with perturbation of the absorption edge (i.e., an "alpha" band).[3]

Curve B of Fig. 2 was obtained after heating this crystal to 600°K at which it becomes dark red, almost purple in color. The plot shown is a "difference" curve, the bands at 3.6 and 4.7 ev still being present. Further heating results in an increase in optical density. We attribute this band to colloidal sodium.[4-6]

The curves in Fig. 2 were run at 90°K, but no significant difference in bandwidth or position was noted when the experiments were performed at room temperature or liquid helium temperature.

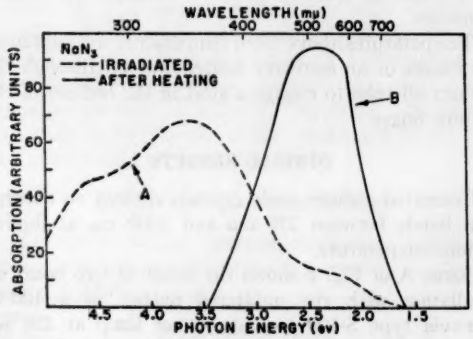

FIG. 2. Production of colloid band in sodium azide by ultraviolet radiation and heat.

ESR RESULTS

The crystal used to obtain the curves in Fig. 2 was removed from the Dewar, fragmented, and sealed in a low-loss glass tube which was inserted through the side of a cavity operating at 8.9 kMcs. A Lorentzian resonance peak was obtained at $g=2.0018\pm0.0002$ with a width of 8.8 gauss (peak to peak on derivative curve). This g value agrees with the experimental value for an ultrasonic dispersion of sodium obtained by Feher and Kip[7] and theoretical values given by Brooks[8] and Yafet.[9] The line shape shown in Fig. 3 was obtained on powdered samples sealed in quartz tubes and treated with high intensity ultraviolet light and heating.[10]

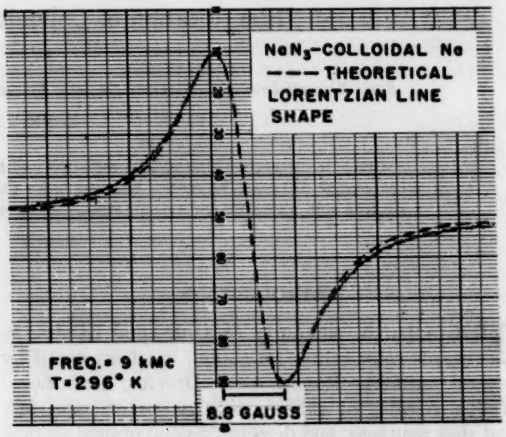

FIG. 3. Electron spin resonance absorption in sodium azide containing colloidal sodium.

DISCUSSION

The mechanism of formation of the colloidal particles is attributed to photochemical reduction by irradiation in the region of the ultraviolet absorption edge of the azide, leaving an excess of sodium in the lattice which forms clusters during thermal diffusion.

[4] W. D. Compton, Phys. Rev. **107**, 1271 (1957).
[5] A. B. Scott, W. A. Smith, and M. A. Thompson, J. Phys. Chem. **57**, 757 (1953).
[6] A. B. Scott and W. A. Smith, Phys. Rev. **83**, 982 (1951).
[7] G. Feher and A. F. Kip, Phys. Rev. **78**, 337 (1955).
[8] H. Brooks, Phys. Rev. **94**, 1411(A) (1954).
[9] Y. Yafet, Phys. Rev. **85**, 478 (1952).
[10] G. J. King, B. S. Miller, F. F. Carlson, and R. C. McMillan, J. Chem. Phys. **32**, 940 (1960).

The only products obtained by decomposition of the salt are sodium and nitrogen[11] by the following reaction:

$$2\,NaN_3 \rightarrow 2\,Na + 3\,N_2.$$

Raising the temperature allows aggregation of the excess metal, probably by vacancy or electron diffusion. The mechanism is, no doubt, quite similar to the print-out effect in photographic processes. Crystals of sodium azide irradiated briefly (no visible change) with ultraviolet light and stored in the dark show evidence of colloidal aggregation on heating even after two months of storage. From this experiment it is evident that a latent image can be formed in sodium azide by irradiation.

Crystals irradiated with x rays (35 kv, Cu) at room temperature and then heated to 450°K show the same characteristic colloid coloring as the crystals exposed to ultraviolet and subsequently heated to 600°K for the same period of time. However, the coloring of the x-ray treated crystal is observed throughout the crystal while the ultraviolet irradiated crystal displays its coloring on the surface only.

On using the formula from footnote reference 13 for the maximum optical absorption, we should obtain a peak at

$$\lambda_0 = (1+2n_0^2)^{\frac{1}{2}}\lambda_c, \qquad (1)$$

where λ_c is the critical wavelength for ultraviolet transparency of the alkali metal and n_0 is the index of refraction (1.37 for NaN_3)[12] of the host crystal.

Equation (1) predicts the maximum absorption at 4580 A in not too unreasonable agreement with the observed peak at 5200 A. As shown in Table I, the error is in the same direction and of the same magnitude as found in NaCl.[13] Apparently the discrepancy between the theoretical and observed peaks is not peculiar to the alkali halides.

TABLE I. Colloid band position: comparison of observed and calculated values (in A) for NaN_3 and NaCl.[a]

	Obs	Calc [Eq. (1)]	C−O
NaCl	5650	5040	0.27 ev
NaN_3	5200	4580	0.33 ev

[a] See footnote reference 13.

One can estimate the particle size from the bandwidth of the optical absorption.[13] With a half-width of 1.0 ev, the particle diameter would be about 15 A.

The narrow width and high symmetry of the ESR line is attributed to the small and homogeneous particle size.

CONCLUSION

The identification of the colloid centers in sodium azide is based on two criteria:

(1) Establishment of the presence of finely divided metallic sodium by the characteristic electron spin resonance absorption for sodium. The g value, line width, and shape agree with experimental and theoretical determinations. Relaxation time, as indicated by low temperature measurement, is of the proper magnitude.

(2) Detection of a temperature insensitive optical absorption band. Neither half-width nor peak position of this band are appreciably affected by changing the temperature from 300° to 90°K or below. This criterion has been used to indicate the presence of colloids produced in NaCl by ionizing radiation.[4]

ACKNOWLEDGMENTS

The author wishes to express thanks to M. D. Kemp and O. F. Kezer for preparation of crystals used in this work. Thanks are due to G. J. King, F. F. Carlson, and R. C. McMillan of the ESR team for assistance with ESR measurements.

[11] W. E. Garner, D. J. B. Marke, J. Chem. Soc. **1936**, 657.
[12] Private communication from O. F. Kezer, Basic Research Group.
[13] W. T. Doyle, Phys. Rev. **111**, 1067 (1958).

Spectral Solvent Shift. I. Paraffin Hydrocarbon Solvent Interactions with Polynuclear Aromatic Hydrocarbons*

O. E. Weigang, Jr.

Chemistry Department, Texas Lutheran College, Seguin, Texas

(Received August 3, 1959)

The electronic shifts for 11 ultraviolet transitions of the chromophores naphthalene, phenanthrene and the polar aromatic hydrocarbon, azulene, have been observed in a series of 17 paraffin hydrocarbon solvents from isopentane to *n*-tridecane. The contribution to the shift of branching and cyclization of solvent molecules has been observed by including the five structural isomers of hexane, 2,2,4-trimethylpentane and 2,2,5-trimethylhexane together with the cyclo- and methylcyclopentanes and hexanes.

The statistical approach is used to interpret the electronic shifts in terms of interbond potentials and the solvent radial distribution function and is compared to the McRae extension of the Bayliss solvent shift theory. Dispersive type potentials suffice to account for the frequency shifts of transitions, except the ^1L_b transition of azulene which shifts to the blue from the vapor to hydrocarbon solutions. The behavior can be accounted for by a change in the static dipole moment of azulene on excitation, a phenomenon predicted by quantum mechanical calculations on the molecule.

INTRODUCTION

THE immersion of a light absorbing material in a liquid solvent shifts the electronic spectrum associated with the pure light absorber in the vapor state. Figure 1, for example, shows the paraffin hydrocarbon solution spectrum of azulene superimposed on its vapor spectrum. Such effects may be attributed to the difference in energy of interaction with the surrounding solvent molecules between the excited state and ground state chromophore and several theories have been proposed to account for the phenomenon.[1–5]

Recent studies have been made of this phenomenon by pressurizing the solvent-chromophore solution so that continuous effects may be observed.[4,6] However, for this work the spectral solvent shift is studied by varying the solvent without additional external pressure. The effect is observed for a group of nonpolar hydrocarbon solvents, including observations on the effect of branching or cyclization of the hydrocarbon chain. While the shifts from solvent to solvent are not as large as might be obtained with a polar solvent series, the effect is more amenable to interpretation since the environment of the chromophore is varied quite gradually and regularly. In addition, drastic reshaping and loss of structural detail in the spectra, occurring typically with polar solvents, are held to a minimum in hydrocarbon solvents, if they occur at all.

Aromatic polynuclear hydrocarbons form a convenient set of chromophores since each contains several electronic transitions in the near ultraviolet with widely varying oscillator strengths, and the nature of their transitions is fairly well understood with regard to polarization and other details.[7–9] For these reasons they have been used in several other investigations of solvent effects.[4,10]

THEORETICAL

Statistical Theory

The statistical theory interprets a spectral shift as due to the unequal perturbation of a light absorber in its ground and its excited state when surrounded by a particular configuration of solvent molecules. The intensity at each frequency is taken to be proportional to the probability of occurrence of a given configuration, and different configurations generally produce various degrees of interaction that lead to solvent broadening.[11]

Within the approximation of additivity of intermolecular potentials, the interaction with the solvent or solvation energy per mole of chromophore in a given state may be expressed as

$$E_{AB}=4\pi N n_0 \int V_{AB}(R)\, g_{AB}(R)\, R^2 dR, \qquad (1)$$

where n_0 is the mean number density in the system (for dilute solutions the density of the solvent), R is the chromophore to solvent intermolecular distance, $V_{AB}(R)$ is the intermolecular potential between chromophore (A) and solvent (B), $g_{AB}(R)$ is the radial distribution (rd) function for the solvent about the chromophore.

* Presented at the 137th meeting of the American Chemical Society, Division of Physical Chemistry, Cleveland, Ohio (April, 1960).

[1] N. S. Bayliss, J. Chem. Phys. **18**, 292 (1950).

[2] Y. J. Ooshika, Phys. Soc. (Japan) **9**, 594 (1954).

[3] H. C. Longuet-Higgins and J. A. Pople, J. Chem. Phys. **27**, 192 (1957).

[4] W. W. Robertson, O. E. Weigang, Jr., and F. A. Matsen, J. Mol. Spectroscopy **1**, 1 (1957).

[5] E. G. McRae, J. Phys. Chem. **61**, 562 (1957).

[6] W. W. Robertson, S. E. Babb, Jr., and F. A. Matsen, J. Chem. Phys. **26**, 367 (1957).

[7] H. B. Klevens and J. R. Platt, J. Chem. Phys. **17**, 470 (1949).

[8] D. E. Mann, J. R. Platt, and H. B. Klevens, J. Chem. Phys. **17**, 264 (1949).

[9] R. Pariser, J. Chem. Phys. **25**, 1112 (1956).

[10] N. D. Coggeshall and A. Pozefsky, J. Chem. Phys. **19**, 980 (1951).

[11] S. Ch'en and M. Takeo, Revs. Modern Phys. **29**, 20 (1957).

The shift arises from the difference between an excited state term and a ground state term, a change occurring in the potential term $V_{AB}(R)$. According to the Franck-Condon principle, the rd function $g_{AB}(R)$, or more precisely, any one of the momentary configurations which go into the average, will remain constant during the brief light absorption process. Accordingly, the shift from the vapor may be written

$$hc\Delta\nu = E_{AB}{}^{X} - E_{AB}{}^{G}$$

$$= 4\pi N n_0 \int [V_{AB}{}^{X}(R) - V_{AB}{}^{G}(R)] g_{AB}(R) R^2 dR, \quad (2)$$

where $V_{AB}{}^{X}$ and $V_{AB}{}^{G}$ represent the potentials between solvent and excited and ground state chromophores, respectively. In Eqs. (1) and (2) the variety of solvent configurations have been replaced by a single most probable or average distribution, as might be determined from x-ray diffraction, and thus the shift may be measured from the band maximum. Solvent broadening of single vibration bands in ultraviolet spectra are observed to be quite symmetrical,[12] indicating that the most probable is very nearly identical to the mean solvent distribution.

Dispersive Interactions Between Hydrocarbons

For dispersive type interactions, the intermolecular potentials, $V_{AB}(R)$, may be developed on the basis of bond-bond interactions according to Haugh and Hirschfelder's extension of London's treatment by transition multipoles in extended molecules.[13,14] The perturbation treatment involves the interaction of these transition multipoles in a fashion formally identical to the interactions of electrostatic distributions. The transition moments of carbon-hydrogen and carbon-carbon sigma bond electrons are adequately treated by the point dipole approximation, while for pi electron transition moments, the multipoles are treated as distributions of monopoles each of which is a point transition polarization, all the same sign in a given region j of the molecule, of magnitude

$$g_{0k}{}^{A}(j) = \int_j \psi_0{}^{A} \psi_k{}^{A} dv_a, \quad (3)$$

where $\psi_0{}^{A}$ and $\psi_k{}^{A}$ are the wave functions of the chromophore in the 0 and k states, the monopoles being centered at

$$R_{0k}{}^{A}(j) = \int_j \mathbf{r}_a \psi_0{}^{A} \psi_k{}^{A} dv_a / g_{0k}{}^{A}(j). \quad (4)$$

For transitions between pi electron states of the chromophore in paraffin solvents, the potential difference $(V_{AB}{}^{X} - V_{AB}{}^{G})$ reduces to interactions between the solvent sigma bond transition dipoles and the excited and ground state transition monopoles of the chromophore, other terms cancelling in the difference. Then the interaction *with each solvent bond* is

$$(V_{AB}{}^{X} - V_{AB}{}^{G})_{\text{disp}}$$

$$= \alpha_B \left\{ \sum_{k\neq 0} \sum_j \frac{[g_{0k}{}^{A}(j)]^2/2[1 + E_k{}^{A}/I_B]}{R_j{}^{A}{}_B} - \sum_{k\neq i} \sum_j \frac{[g_{ik}{}^{A}(j)]^2/2[1 + (E_k{}^{A} - E_i{}^{A})/I_B]}{R_j{}^{A}{}_B} \right\}$$

$$\cong \alpha_B (K_A{}^{G} - K_A{}^{X})/R^4. \quad (5)$$

The summations are over the j monopoles of each kth chromophore state. α_B is the polarizability of the solvent sigma bond, I_B the ionization energy of the solvent sigma bond, $g_{ik}{}^{A}(j)$ is the jth monopole of the chromophore $i-k$ transition, $E_k{}^{A}$ the energy of the chromophore k state relative to its ground state, and R_{jB} is the monopole to solvent bond distance. Haugh and Hirschfelder's equation has been partially reduced here by the approximations used in the more common polarizability dispersion expression.[15,4]

The transition dependence is virtually separated from the solvent dependence since the solvent bond ionization energy is nearly constant and since the solvent sigma bond to chromophore monopole distance R_{jB} should not vary greatly for the various transition polarizations with a given solvent configuration. Here $K_A{}^{G}$ and $K_A{}^{X}$ are terms which correspond to energy terms and the ground state and excited state polarizabilities of the chromophore in the usual point dipole development of dispersion forces, the greater polarizability of the excited state leading to red (negative) frequency shifts.

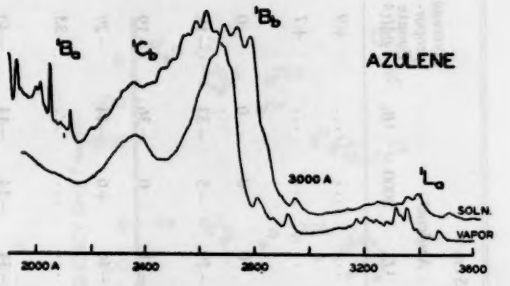

FIG. 1. The near-ultraviolet electronic transitions of azulene in the vapor state and in 2,2,4-trimethylpentane solution. One may note the transition dependence of the spectral shift. The ^1B_b transition moves at such a rate as to partially cover a much less solvent sensitive and weaker transition to the red side of it on going from vapor to solution.

[12] O. E. Weigang, Jr. and W. W. Robertson, J. Chem. Phys. **30**, 1413 (1959).
[13] E. F. Haugh and J. O. Hirschfelder, J. Chem. Phys. **23**, 1778 (1955).
[14] See also, J. N. Murrell and H. C. Longuet-Higgins, J. Chem. Soc. **1955**, 2552; Proc. Phys. Soc. (London) **A68**, 601 (1955).
[15] S. E. Babb, Jr., J. M. Robinson, and W. W. Robertson, J. Chem. Phys. **30**, 427 (1959).

TABLE I. Solvent parameters and spectral shifts.

Solvent	Mole bond density[a] n_b (cm^{-3})	$\Delta w/N^2$	Bayliss parameter $\frac{n^2-1}{2n^2+1}$	Surface tension[a] (dyne$^{1/4}$·$cm^{-1/4}$)	Relative spectral frequency shifts. Average deviation about ±5 cm^{-1}											Average proportionate shift[d]
					Naphthalene			Phenanthrene				Azulene[c]				
					^1L_b	^1L_a	^1B_b	^1L_b	^1L_a	^1B_b	^1C_b	^1L_b	^1L_a	3000	^1B_b	
Isopentane	0.1374	0.0800	0.1785	1.951	0	+5	+37	+10	−10	+14	+17	...	...	...	...	+9
2,2-Dimethylbutane	0.1433	0.1944	0.1840	1.994	−3	+1	+16	+2	+20	+9	+23	...	...	...	...	+7
n-Pentane	0.1389	...	0.1796	1.984	0	0	0	0	0	0	0	0	0	0	0	0
2,3-Dimethylbutane	0.1459	0.1667	0.1863	2.027	−17	−16	−39	+5	−19	...	...	+3	−29	−5	−33	−18
2-Methylpentane	0.1440	0.0833	0.1851	2.027	−11	−17	...	+2	−18	−50	...	−16	−31	0	−36	−19
3-Methylpentane	0.1463	0.1111	0.1869	2.048	−17	−28	−58	−4	−35	−61	−20	+6	−46	+6	−44	−29
2,2,4-Trimethylpentane	0.1515	0.2812	0.1923	2.069	−19	−22	−54	−20	−48	−60	−27	...	...	...	...	−33
n-Hexane	0.1455	...	0.1863	2.056	−30	−42	−68	−9	−51	−88	−55	+7	−34	−14	−44	−40
2,2,5-Trimethylhexane	0.1543	0.2716	0.1947	2.104	−37	−36	...	−15	−63	−103	...	...	...	...	...	−48
n-Heptane	0.1503	...	0.1909	2.105	−29	−47	−124	−26	−81	−133	−88	+1	−69	−5	−79	−65
Methylcyclopentane	0.1604	...	0.1985	2.16[b]	−27	−65	...	−30	−112	−165	...	+27	−76	−31	−109	−78
Cyclopentane	0.1593	...	0.1972	2.19[b]	−38	−80	−220	−40	−127	−193	−138	+31	−49	−33	−136	−95
n-Nonane	0.1568	...	0.1970	2.175	−64	−81	−201	−35	−135	−203	−117	−3	−82	−13	−127	−100
Cyclohexane	0.1661	...	0.2041	2.222	−38	−84	−238	−38	−139	−233	−148	+33	−90	−25	−157	−108
Methylcyclohexane	0.1646	...	0.2022	2.194	−44	−86	−234	−37	−148	−272	−164	+6	−62	−29	−157	−109
n-Undecane	0.1612	...	0.2005	2.218	−59	−125	...	−57	−160	...	...	...	−81	−44	...	−125
n-Tridecane	0.1644	...	0.2030	2.248	−71	−134	...	−52	−196	...	...	...	−87	−51	−197	−138

[a] Taken or calculated from A.P.I. Project 44, Selected Values of Properties of Hydrocarbons and Related Compounds. Petroleum Research Laboratory, Carnegie Institute of Technology, Pittsburgh, Pennsylvania.
[b] Surface tension determined in this laboratory by the ring method with correction factor.
[c] The ^1C_b azulene band is too broad for accurate wavelength determination.
[d] *n*-Pentane to *n*-Nonane shifts taken to be 100. Azulene ^1L_b and 3000 A not included in the average.

Thus, for a given chromophore transition observed in a series of paraffin solvents, Eq. (2) together with Eq. (5) would predict that the solvent shift would depend on: (1) the density of solvent bonds, conveniently measured in moles of bonds per cc, n_b, the mole density times the number of bonds per molecule; (2) the rd of solvent bonds about a chromophore; and (3) the solvent bond ionization energy and bond polarizability. The linear density dependence has been observed previously with the pressurization of *n*-pentene solutions of the same chromophores.[4]

Chromophore-Dipole Solvent-Induced-Dipole Interactions

If a chromophore dipole moment should change on excitation, additional contributions to the potential difference must be considered. For qualitative considerations one may use the point-dipole induced-dipole potential[16] which leads to the potential difference term

$$(V_{AB}{}^{X}-V_{AB}{}^{G})_{\text{dip-ind}} = \alpha_B[(\mu_A{}^{G})^2-(\mu_A{}^{X})^2]/R^6, \quad (6)$$

where $\mu_A{}^{G}$ and $\mu_A{}^{X}$ are the magnitudes of the chromophore dipole moments in the ground and excited state, respectively. Red (negative) or blue (positive) contributions may arise depending on whether the excited dipole is larger or smaller in magnitude, respectively. It should be noted that the actual direction of dipole moment is immaterial for nonpolar solvents since the induced dipole presumably follows the direction of the inducing static dipole.

McRae Solvent Shift Theory

McRae has applied second-order perturbation theory to the solvent-chromophore interaction and expresses the potential fields of the solvents in terms of their macroscopic properties.[5] The complete theory includes the effect of polarity of the solvent as well as the chromophore and has received considerable attention in the literature.[17,18] Considering only dispersive contributions and chromophore-dipole. solvent-induced-dipole interactions, the McRae theory reduces to

$$hc\Delta\nu=(AL_0+B)[(n^2-1)/(2n^2+1)]. \quad (7)$$

The solvent refractive index parameter was first proposed by Bayliss.[1] A and B are constants of the chromophore, L_0 is the "weighted mean wavelength" of the solvent.

EXPERIMENTAL

Measurements were made with a Beckman DK-1 recording spectrophotometer. Various techniques were devised for maintaining maximum wavelength accuracy, the most recent and successful consisting of superimposing on the spectrogram a mercury emission line of known wavelength near the region under investigation. This is accomplished without interrupting the synchronized movements of the wavelength and recorder drives. Thus errors which involve failure to match the wavelength scroll to the strip recorder calibrations and errors from temperature change are minimized or eliminated. The data do not show any significant variations in *relative* wavelength shifts for the different correction methods used. The data are the average of at least two and usually three determinations. Usually the first reasonably intense vibration band maximum of a transition was measured. The relative precision is estimated to be about one-half A, ranging possibly to one A in some instances, band broadness most often being the limiting factor.

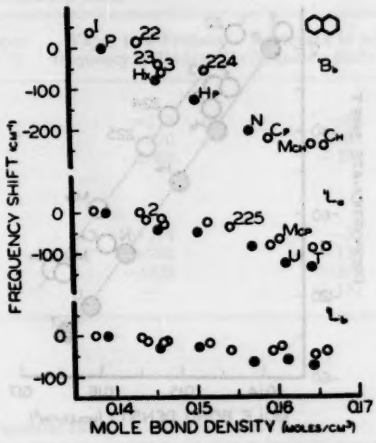

FIG. 2. Spectral frequency shifts of the transitions ^1B_b, ^1L_a and ^1L_b of naphthalene. The circles approximate the average deviation from experimental error. See Fig. 3 for the solvents.

Most of the hydrocarbon solvents were Phillips "Pure Grade," 99 mole % minimum purity. Cyclohexane, methylcyclohexane, and 2,2,4-trimethylpentane were spectrograde solvents obtained from Distillation Products Industries. The solvents were used as received except for Phillips cyclopentane which was distilled over sulfuric acid and collected in a narrow temperature range near 49°C. This treatment decreased the cutoff wavelength from 2850 to 2200 A. Also, 2,3-dimethylbutane was distilled immediately before use to remove an antioxidant (du Pont No. 6 inhibitor).

The chromophores naphthalene, azulene, and phenanthrene were the best grades from J. T. Baker Chemical Co., Terra Chemicals, Inc., and Distillation Products Industries, respectively. No further purifications were carried out since the spectrograms obtained with them compared favorably in every detail without

[16] J. O. Hirschfelder, C. F. Curtiss, and R. B. Bird, *Molecular Theory of Gases and Liquids* (John Wiley & Sons, Inc., New York, 1954) p. 29.
[17] O. Popovych and L. B. Rogers, J. Am. Chem. Soc. **81**, 4469 (1959).
[18] E. G. McRae, Spectrochim. Acta **12**, 192 (1958).

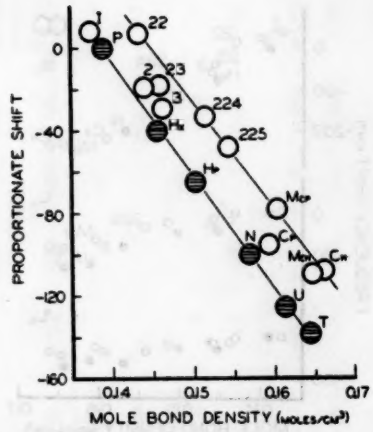

FIG. 3. Proportionate spectral shift (*n*-pentane 0, *n*-nonane 100) averaged over transitions vs the mole bond density of the solvent. Reference lines are drawn through the normal hydrocarbon solvent points (filled circles) and through the most highly branched solvents. The circles approximate the average deviation from experimental error. The solvents are: *P*—*n*-pentane, *Hx*—*n*-hexane, *Hp*—*n*-heptane, *N*—*n*-nonane, *U*—*n*-undecane, *T*—*n*-tridecane, *I*—isopentane, 2—2-methylpentane, 3—3-methylpentane, 22—2,2-dimethylbutane, 23—2,3-dimethylbutane, 224—2,2,4-trimethylpentane, 225—2,2,5-trimethylhexane, *Cp*—cyclopentane, *Mcp*—methylcyclopentane, *Ch*—cyclohexane, *Mch*—methylcyclohexane.

spurious bands to those given in API Ultraviolet Spectrograms,[19] Klevens and Platt,[7] or Mann, Platt, and Klevens.[8]

Stock solutions appropriate for the weakest transition (concentrations 0.004 molar or less) were freshly mixed, diluted for the stronger transitions and compared to the solvent as reference. One centimeter matched silica cells were used. Isopentane solutions were cooled to prevent excessive evaporation and the density was probably somewhat greater than indicated in Table I and Figs. (2) and (3). Vapor spectra were obtained by heating the cell compartment and using a ten-centimeter cell with quartz windows compared to air as reference.

RESULTS AND DISCUSSION

General

Table I shows that the frequency shift of maxima relative to their position in *n*-pentane solution varies with the transition for given solvents, and for a given transition varies from solvent to solvent well outside of experimental error. Figure 1 shows the vapor to 2,2,4-trimethylpentane solvent spectral shift for four of the five transitions of azulene observed in this investigation. Here the transition dependence is particularly apparent as the ^1B_b transition shifts at a rate to partially cover the less sensitive 3000 A transition in solution.

[19] A.P.I. Project 44, Ultraviolet Spectral Data, Petroleum Research Laboratory, Carnegie Institute of Technology, Pittsburgh, Pennsylvania.

Tables II and III show that while the relative shift observed for two solvents is some measure of vapor to *n*-pentane shift, the behavior is not regular enough to give vapor frequency predictions of any great accuracy. The rather capricious agreement between extrapolations and experimental vapor values has been observed before.[1,4,5] While some cases may be due to incorrect assignments of corresponding vapor and solution bands, most discrepencies are undoubtedly real and quite marked.

Red (negative) shifts from vapor to hydrocarbon solutions are observed in every case with the exception of ^1L_b transition of azulene which displays a relatively small, but distinct shift to the blue.

Nonpolar Chromophores—Naphthalene and Phenanthrene

Table II shows that the *n*-pentane to *n*-nonane red shift increases with the oscillator strength of the transition. A similar behavior has been observed for the same chromophores in pressurized *n*-pentane solutions where the rate of frequency shift with density was found to have a high correlation with the oscillator strength of transitions of a large number of catacondensed hydrocarbon chromophores.[4] While Eq. (5) (or consideration of charge-transfer complexing between solute and solvent) might suggest a dependence on transition energies, it apparently plays a minor role on consideration of the ^1C_b transition of phenanthrene, where the lower shift goes with the reduced intensity of the higher energy transition. Furthermore, the rates of frequency shift with density of two pyrene transitions of similar intensity have been observed to be nearly equal even though they were quite widely separated in frequency.[4]

While the extent of spectral frequency shift produced by a hydrocarbon solvent clearly depends on the chromophore transition, the same proportionate frequency shift, independent of the transition, is obtained for a given solvent nearly within experimental error, in agreement with the separation of solvent and chromophore contributions proposed for Eq. (5). This enables the construction of a relative proportionate shift scale, arbitrarily taking *n*-pentane and *n*-nonane to produce 0 and 100 relative units of shift respectively for each transition, other solvents being assigned proportionate values accordingly. The proportionate shift produced by each of the solvents averaged over the transitions is given in Table I. The general features of plots using proportionate shifts are the same as those of plots of shifts of individual transitions as shown by Fig. 2 compared to Fig. 3.

Averages taken only over transitions with small shifts (due to solvent cutoff) show larger deviations from the average proportionate shift due to the experimental error of wavelength determinations becoming quite large on the proportionate scale. However, the cyclics, especially methylcyclohexane, cyclopentane,

TABLE II. Nonpolar chromophores and spectral shifts.

Transition	Oscillator strengths[a]	Experimental vapor frequencies (cm^{-1})	Vapor to n-Pentane frequency shifts (cm^{-1})	n-Pentane to n-Nonane frequency shifts (cm^{-1})
Naphthalene				
^1L_b	0.002	32456[b]	−258	−64
^1L_a	0.18	35919[b]	−870	−81
^1B_b	1.70	47481[c]	−2068	−201
Phenanthrene				
^1L_b	0.003	29163[b]	−214	−35
^1L_a	0.18	35260[b]	−986	−135
^1B_b	1.09	41314[c]	−1328	−203
^1C_b	0.60	—	—	−117

[a] Taken from footnote reference 7.
[b] W. E. Deal, Jr., Doctoral Dissertation, The University of Texas (1951).
[c] Determined in this laboratory.

TABLE III. Polar chromophore and spectral shifts.

Transition	Oscillator strengths[a]	$(\mu_A{}^O)^2-(\mu_A{}^X)_b{}^2$ (D^2)	Experimental vapor frequencies (cm^{-1})	Vapor to n-Pentane frequency shifts (cm^{-1})	n-Pentane to n-Nonane frequency shifts (cm^{-1})
Azulene					
^1L_b	0.009	1.68	14270[c]	+53	−3
^1L_a	0.08	−3.76	29760[d]	−366	−82
3000	0.1	1.95	34164[d]	−368	−13
^1B_b	1.10	0.22	37382[c]	−1607	−127

[a] Experimental values from footnote reference 8, except 3000 A, calculated by Pariser, footnote reference 9.
[b] Calculated from theoretical values, footnote reference 9.
[c] Determined in this laboratory.
[d] E. Heilbrenner and K. Wieland, Helv. Chim. Acta 30, 947 (1947).

and cyclohexane in that order, show average deviations nearly twice as large as comparable solvents even though their spectral purity allowed observation of all the transitions.

Figure 3 shows a plot of the relative proportionate shift versus the mole bond density n_b of the solvents used. One may note that (1) the normal hydrocarbon solvents (filled circles) give a remarkably linear shift with solvent bond density, (2) the noncyclic hydrocarbons isomers with one, two and three methyl branches, in that order, produce less shift than would normal hydrocarbon solvents of equal bond density, and (3) the cyclic hydrocarbons also produce less shift than would normal hydrocarbons solvents of equal bond density.

Such dependence on structure appears in the physical properties of the hydrocarbons and has been correlated with a remarkable degree of accuracy to Platt's f, p, w structural parameters, where f is the sum of first C—C bond neighbors of every C—C bond in the molecule, p is the number of carbon atoms three bonds apart, and w, the Wiener number, is the sum of the number of bonds between all pairs of carbon atoms in the molecule.[20] Attempts to fit the shift data to correlations of the type used by Platt were not as successful however as the following, suggested by the large coefficients that were obtained for the w parameter. The relative proportionate shift for normal and branched hydrocarbons (except isopentane for the reason mentioned) may be given by

$$\text{rel prop shift}=776-5.59\times10^3 n_b$$
$$+131\Delta w/N^2\pm2\ (6\ \text{max dev}), \quad (8)$$

where Δw is the change in the Wiener number from branched to normal isomer, and N is the number of carbon atoms in the skeleton.

Platt interpreted the w/N^2 term as a measure of the mean external contact area of the molecule (except for steric hindrance). Greenshields and Rossini observed that the similar (for correlations) term, $2w/N(N-1)$ was the average distance between pairs of carbon atoms measured in bond lengths,[21] i.e., a measure of the linear extension of the molecule and a qualitative index of the solvent radial distribution function arising from intramolecular distribution.

Direct measurements of the rd of constituent atoms of solvents may be made by observing x-ray scattering by the liquids. By graphically integrating the Zernicke-Prins scattering equation, Warren has shown that the

[20] J. R. Platt, J. Chem. Phys. 17, 484 (1949).

[21] J. B. Greenshields and F. D. Rossini, J. Phys. Chem. 62, 271 (1958).

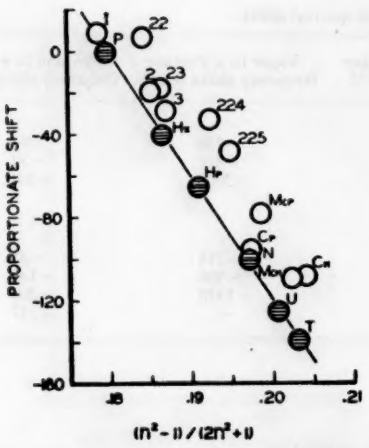

FIG. 4. Proportionate spectral shift versus the Bayliss-McRae spectral shift parameter. See Fig. 3 for the solvents.

single intense scattering peak in long chain hydrocarbons is due to a main concentration of scattering matter at a distance determinable from the corresponding scattering angle.[22] Stewart's measurements of the positions of these peaks shows that this concentration of matter (maximum of the rd function) is at the same radial distance in all the normal hydrocarbons from *n*-pentane to *n*-pentadecane.[23] Further measurements on branched hydrocarbons show that this distance increases with branching[24] and also with cyclization,[25] although the interpretation of the scattering may be somewhat different in the latter case. If $g_{AB}(R)$ of Eq. (2) at least follows the rd of the pure solvents, an attractive potential gives qualitative agreement between these simple rd analyses and the relative position of the data points in Fig. 3, and furthermore, supports the interpretations of the Wiener parameter.

No meaningful method of assigning Wiener numbers to the cyclic hydrocarbons by summing over neighbors, etc., has been proposed and extensive scattering measurements of the substituted cyclics seem not to have been made. However recent conformational studies of the cyclohexanes, cyclopentanes and their derivatives draws speculation as to whether the shifts follow their conformations. Cyclic shapes certainly reduce the external contact area of the molecule and would lead to less interaction than normals of the same n_b as is observed. Furthermore, the preferred equatorial position of the methyl group in the methylcyclohexane changes very little the over-all planar shape of the molecule,[26] while one of the preferred configurations of methylcyclopentane thrusts the methyl group back toward the ring to resemble a highly branched noncyclic, as opposed to the nearly planar cyclopentane molecule.[27]

Figure 4 shows the average proportionate shift versus the Bayliss-McRae parameter, giving a plot which is indistinguishable from the bond density plot. If the refractive index dispersion constant is a good measure of the variation of weighted mean wavelength L_0, as suggested by McRae, then the variation in L_0 for hydrocarbons does not satisfactorily account for the smaller shift of both branched-chain and cyclic hydrocarbons. The work of Lauer shows that the former has a dispersion constant higher and the latter a dispersion constant lower than the straight chain hydrocarbons.[28]

The use of solvent refractive indices at 250 mu, calculated from Lauer, which should measure bond polarizabilities at frequencies near the absorptions of the chromophores, gives a plot which differs by little more than 0.01 units in the relative positions of branched and cyclics to the normal solvent line, effecting no significant change in the plot. No regular variation can be detected in the ratio of branched to straight chain solvent shift on going from short wavelength to long wavelength transitions. It would seem from these tests of the data that solvent bond energies or polarizabilities do not vary to an extent that produce observable effects in the paraffin solvents.

Since the McRae derivation of the reaction field from which the refractive index term arises makes the assumption of a continuous homogeneous dielectric about the spherical chromophore cavity, it is plausible to assume that here also the modified shifts arise from neglect of short range order in the liquid state, i.e., is due to solvent molecular conformation.

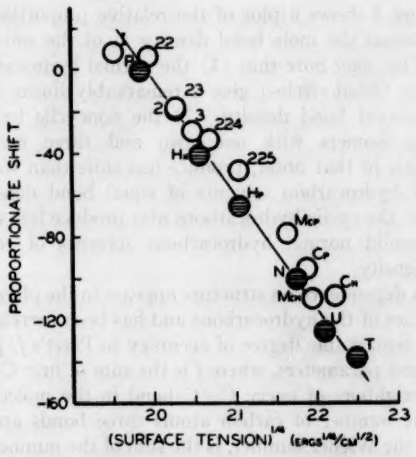

FIG. 5. Proportionate spectral shift versus the fourth root of the solvent surface tension. See Fig. 3 for the solvents.

[22] B. E. Warren, Phys. Rev. **44**, 969 (1933).
[23] G. W. Stewart, Phys. Rev. **31**, 174 (1928).
[24] G. W. Stewart, Phys. Rev. **32**, 153 (1928).
[25] S. Katzoff, J. Phys. Chem. **2**, 841 (1934).
[26] C. W. Beckett, K. S. Pitzer, and R. Spitzer, J. Am. Chem. Soc. **69**, 2488 (1947).
[27] K. S. Pitzer and W. E. Donath, J. Am. Chem. Soc. **81**, 3213 (1959).
[28] J. L. Lauer, J. Chem. Phys. **16**, 612 (1948).

Attempts to find solvent properties which implicitly include the structural effects and give high correlations with the shift have led to examination of solvent boiling point, heat of vaporization, surface tension and others. None is as successful as Eq. (8) and most show gross inversions of the shift versus the parameter. The most successful is found to be the fourth root of the surface tension, shown in Fig. 5 which can be derived from Eqs. (2) and (5) by assigning a constant parachor contribution per hydrocarbon bond.[29] The average deviation is about ±4 proportionate shift units.

Polar Chromophore—Azulene

Table III gives the transition oscillator strengths of azulene, which should be some measure of the red shift contribution from dispersive potentials, and the difference of the squares of static dipole moments in ground and excited states, which gives a qualitative estimate of the sign and magnitude of induced dipole contributions according to Eq. (6). The dipole moments were calculated by Pariser using Huckel MO's with configuration interaction.[9]

Accordingly, static dipoles should lead to a red (negative) shift contribution for the ^1L_a and nearly zero contribution for the ^1B_b transition from the ground state in addition to the dispersive red shift, agreeing with the behavior observed.

The ^1L_b transition should have a rather large blue induced dipole contribution with the weakest red dispersive contribution. Experimentally, a small blue shift is observed from the vapor that can also be detected in pressurized hydrocarbon solutions.[30] The 3000 A band should have a slightly larger blue contribution, but the greater dispersive red shift to be expected from the oscillator strength of the transition seems to predominate to give the smallest red shift observed, much smaller than shifts of comparable intensity transitions in nonpolar chromophores of this type.

The two latter solvent shifts were omitted from the average of the proportionate shift scale since they are barely outside of experimental error. However the other transitions of azulene followed and were included in the scale since the discussion of solvent dependence for nonpolar chromophores should apply equally well to polar azulene.

[29] J. O. Hirschfelder, C. F. Curtis, and R. B. Bird, see footnote 16, pp. 352, 354.

[30] W. W. Robertson, O. E. Weigang, Jr., and A. D. King, Jr., Ohio State Symposium on Molecule Structure and Spectroscopy, Ohio State University (1959).

SUMMARY

It would seem that the statistical approach to the problem of spectral solvent shifts may be applied with some success to liquid systems of this type, and there is no distinguishable difference between a simple bond density interpretation and the McRae extension of the Bayliss solvent shift theory for these systems. Solvent structural variations give rise to modified shifts which might be laid to varying solvent bond polarizabilities or energy levels with branching. However no relation between such variables and the modified shift can be observed. Rather there is evidence that the modified shifts arise from the change in physical conformation of the molecules and the resultant opportunity for close contact or interaction with the chromophore, i.e., from varying short range order in the liquid state as disclosed by the radial distribution function. This is in keeping with other evidence that "anomolous" properties of other than straight chain hydrocarbons can be accounted for in the main by considering conformations and nearest neighbor interactions without recourse to different potentials for different bond types.[27,31–34]

However, discrepancies from the average in the individual behavior of transitions, in the influence of certain solvents, and the absence of at least a regular behavior in vapor to hydrocarbon solution shifts point up to the complexities of the phenomenon. Quite possibly only complete quantum mechanical treatments of the interactions, both attractive and repulsive together with detailed knowledge about liquid state solutions can fully explain these details.

ACKNOWLEDGMENTS

This research was supported in part by a grant from the Petroleum Research Fund administered by the American Chemical Society. Grateful acknowledgment is hereby made to the donors of said fund.

This research was also supported by a grant from the National Science Foundation, whose support is gratefully acknowledged.

Many helpful discussions with Professors F. A. Matsen and W. W. Robertson are gratefully acknowledged together with the capable help of research assistants A. J. Dahl and H. K. Loeffler.

[31] T. L. Allen, J. Chem. Phys. **29**, 951 (1958).

[32] William Weltner, Jr., J. Chem. Phys. **31**, 264 (1959).

[33] Linus Pauling, Proc. Natl. Acad. Sci. U. S. **44**, 211 (1958).

[34] L. S. Bartell, J. Chem. Phys. **32**, 827 (1960).

Infrared Absorption Spectra of Alkali Metal Nitrates and Nitrites above and below the Melting Point

J. GREENBERG AND LEANDER J. HALLGREN

Minneapolis-Honeywell Research Center, Hopkins, Minnesota

(Received March 14, 1960)

The infrared absorption spectra of $LiNO_3$, $NaNO_2$, KNO_3, $RbNO_3$, $CsNO_3$, $NaNO_3$, and KNO_2 above and below the melting point have been obtained by supporting the salts in the interstices of a fine mesh platinum screen. The frequencies observed have been assigned values according to the symmetry classification. The effects of temperature and cation size have also been noted.

THE infrared absorption spectra of inorganic salts have been relatively neglected.[1] Although some Raman shifts have ben observed for fused salts there is very little information available concerning the infrared absorption of such systems. Recently two techniques have been developed which make these measurements possible.[2] The data presented here were obtained by supporting the fused salt in the interstices of a fine mesh platinum screen. By allowing the molten salt to freeze on the screen, the absorption spectra below the melting point were obtained.

Reagent grade chemicals were further purified by being melted, agitated with dry nitrogen gas, and filtered through Pyrex glass wool. The system was then evacuated and the infrared absorption measured. Comparison of the spectra obtained under these conditions with the spectra of reagent grade chemicals taken from newly opened bottles and measured in air showed no differences. It was then decided to make these measurements in air for convenience. The apparatus used is shown in Fig. 1. The platinum screen was 32 mesh, 0.15 mm thick, 2.5 cm wide, and 4.0 cm long. There was no apparent deterioration of the screen due to reaction with the salts and the data were reproducible to within $\pm 0.025\ \mu$. All measurements were made using the Perkin Elmer model 21 double-beam spectrophotometer. When a single platinum screen cell was introduced into the sample beam, the beam reaching the detector was attenuated by approximately 50%. Under these conditions, the reference beam had to be attenuated when the sample was introduced into the cell and consequently our results are reported as relative transmission. The reference beam was masked off using the Perkin-Elmer attenuator attachment. The amount of masking necessary in each of the cases was approximately the same and as a result, the direct comparison of the intensities obtained is somewhat valid. The placement of a matched, heated screen in the reference beam did not improve the resolution and consequently all measurements were made using a single platinum screen in the sample beam. Our measurements of relative transmission were obtained by subtracting the readings obtained with the shutter closed on the sample beam from the readings obtained with the sample beam shutter open. With the sample beam shutter closed the detector is activated by thermal radiation from the cell and salt plus the specific emission of the salt at those wavelengths at which there is also maximum absorption. The fact that there are relatively high specific emissions from the fused salts is

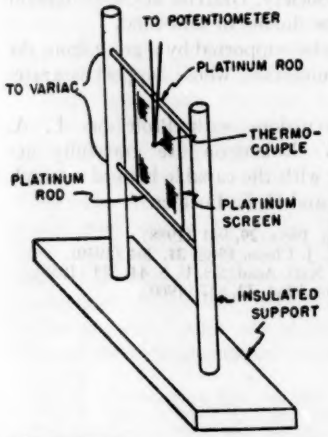

FIG. 1. Platinum screen apparatus for measuring the infrared salts.

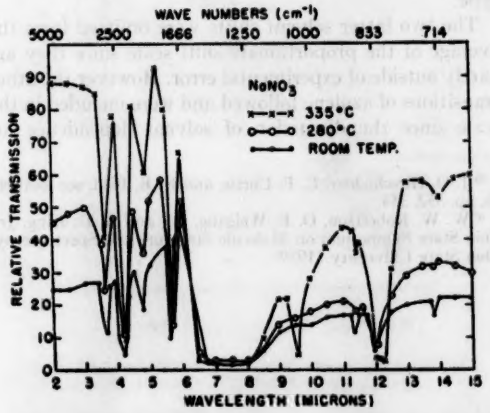

FIG. 2. Infrared absorption spectra of $NaNO_3$ above and below the melting point.

[1] F. A. Miller and C. H. Wilkins, Anal. Chem. **24**, 1253 (1952).
[2] J. Greenberg and L. J. Hallgren, Rev. Sci. Instr. **31**, 444 (1960).

TABLE I. Alkali nitrate frequencies (ν cm^{-1}).

		$2\nu_3$	$\nu_1+\nu_3$	$2\nu_1$	$\nu_1+\nu_4$	$2\nu_2$	$2\nu_4$	ν_3	ν_1	ν_2	ν_4	Point group
$LiNO_3$	mp+25°C	2817	2439	2083	1770	1640[a]	1450[b]	1390[c]	1053	816	741	D_3h
	mp−25°C	2777	2410	2062	1786	Broad band			...	833	733	
	RT	2740	2410	2083	1786				...	840	733	
$NaNO_3$	mp+25°C	2777	2381	2062	1770				1047	816	714	D_3h
	mp−25°C	2777	2381	2083	1770	Broad band			...	830	722	
	RT	2740	2381	2083	1786				...	833	725	
KNO_3	mp+25°C	2740	2353	2062	1754				1042	826	714	D_3h
	mp−25°C	2740	2353	2062	1770	Broad band			1042	830	714	
	RT	2740	2353	2062	1770				1042	833	714	
$RnNO_3$	mp+25°C	2703	2353	2041	1754				1042	823	707	D_3h
	mp−25°C	2703	2381	2041	1770	Broad band			...	833	714	
	RT	2740	2381	2062	1754				1053	833	719	
$CsNO_3$	mp+25°C	2597	2439	2041	1754				1036	833	704	D_3h
	mp−25°C	2703	2410	2041	1739	Broad band			1042	833	...	
	RT	2703	2381	2041	1754				1047	833	714	

[a] F. Vratny, *Infrared Spectra of Metal Nitrates*, Purdue University, Lafayette, Indiana, (Publication Bureau 137469) August, 1958.
[b] J. Hibben, *The Raman Effect and Its Chemical Applications* (Reinhold Publishing Corporation, New York, 1939).
[c] G. Herzberg, *Molecular Spectra and Molecular Structure* (D. Van Nostrand Company, Inc., Princeton, New Jersey, 1945), Vol. II.

TABLE II. Alkali nitrite frequencies (ν cm^{-1}).

		$\nu_1+\nu_3$	$\nu_2+\nu_3$	ν_1	ν_3	ν_2	Point group
$NaNO_2$	mp+25°C	2564	2041	1331	1220[a]	813	C_{2v}
	mp−25°C	2564	2041	...	Broad	820	
	RT	2564	2062	1325	band	826	
KNO_2	mp+25°C	2532	2041	1333	1220[a]	806	C_{2v}
	mp−25°C	2532	2041	Broad band		806	
	RT	2532	2041			800	
						(833)	

[a] D. Williams, J. Am. Chem. Soc. **61**, 2987 (1939).

to be expected since $h\nu$ is of the same order of magnitude as kt. In order to reduce the thermal radiation as much as possible and thereby increase our resolution, only the screen was heated. This was done by passing current directly through it. The resistance across the platinum was about $\frac{1}{4}$ ohm and currents as high as 15 amp could be passed without any complicating effects.

The thermocouple used was platinum-platinum (90%) rhodium (10%) and the temperature was plotted as a function of time by a Brown recorder. With proper shielding the temperature of the screen could be maintained to within ±2°C of the desired temperature by adjustment of the Variac.

Measurements were made at approximately 25°C above the melting point, 25°C below the melting point, and at room temperature for purposes of comparison.

The spectra of the alkali metal nitrates consist almost exlusively of the frequencies to be associated with the NO_3 group and are not materially altered in going from the solid to liquid state. The nitrate ion as it exists in these salts may be represented[3] as follows:

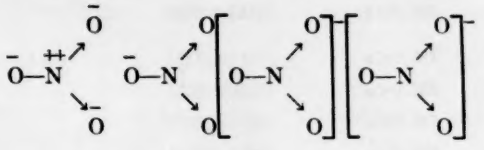

The configuration of the nitrate ion is a plane equilateral

[3] J. H. Hibben, *The Raman Effect and Its Chemical Applications* (Reinhold Publishing Corporation, New York, 1939).

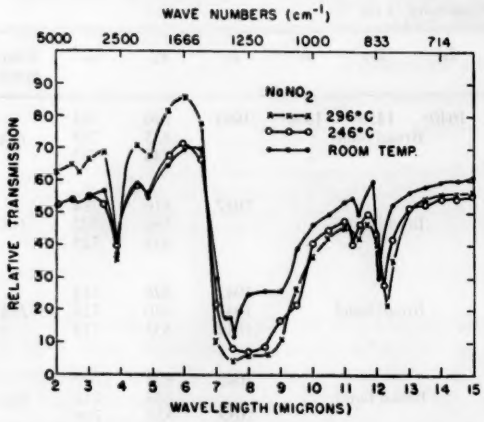

FIG. 3. Infrared absorption spectra of $NaNO_2$ above and below the melting point.

triangle having the symmetry D_{3h} with a nitrogen atom in the center.[3] Although the group has six fundamental frequencies $(3N-6)$, because two of these frequencies are doubly degenerate, only four are observed. The absorption spectra of $NaNO_3$ are shown in Fig. 2 and the assigned frequencies for the alkali nitrates are given in Table I.

The frequencies observed do not all change in the same manner as a result of increasing cation size. The ν_4, ν_1, and $2\nu_3$ frequencies show a general shift to lower values with increasing cation size while ν_2 moves to higher frequencies and $\nu_1+\nu_3$ values show a minimum for KNO_3.

The variation of frequency with state of aggregation has been the subject of several investigations. It has been reported that there is a shift to lower frequencies in going from the crystal to the melt to solution. The generalization that has been made is that if there are weaker binding forces, there will be lower frequencies of oscillation.[3,4] We have observed that, in general, the fundamental frequencies shift to lower energies as the temperature is raised. No uniform change with temperature was detected for the combination and overtone bands.

The nitrite ion may be represented as an isosceles triangle having C_{2v} symmetry with an apex angle of 90°. The spectra of $NaNO_2$ are shown in Fig. 3 and the assigned frequencies for $NaNO_2$ and KNO_2 are given in Table II. The ν_2 frequency shows a shift to lower energies when Na^+ is replaced with K^+ and with increasing temperatures. It is interesting to note that this frequency shows a double peak for KNO_2 at room temperature.

At 2μ where there is relatively little absorption in the melt due to the particular species present, there is usually a decrease in the percent transmission upon freezing. This is primarily due to the formation of dendrites, cracks and other scattering centers in the solid. Investigation of this portion of the spectrum can be of interest in determining the structure of the solid.

ACKNOWLEDGMENTS

The authors wish to acknowledge the assistance of Stanley Bruckenstein, Douglas A. Olsen, and C.F.F.

[4] D. Williams and L. Dechard, J. Am. Chem. Soc. **61**, 1382 (1939).

Interatomic Distances in FeS_2, CoS_2, and NiS_2*

NORMAN ELLIOTT

Department of Chemistry, Brookhaven National Laboratory, Upton, New York

(Received April 15, 1960)

The crystal structures of FeS_2, CoS_2, and NiS_2 have been re-examined. The sulfur-sulfur distances are found to vary, depending on the number of antibonding electrons shared with the metal ions.

THE structural and magnetic properties of FeS_2, CoS_2, and NiS_2 have been interpreted by Pauling[1] on the basis of a covalent bond structure. More recently Néel[2] proposed a $^3\Sigma$ configuration for the S_2 group in NiS_2, analogous to that of the O_2 molecule, to explain the magnetism. Transfer of one and two electrons from S_2 to the metal atoms in CoS_2 and FeS_2, respectively, accounted also for the observed magnetic properties of these compounds.

An examination of the interatomic distances found in these substances might be expected to give information bearing on the correctness of models proposed for the pyrite structures.

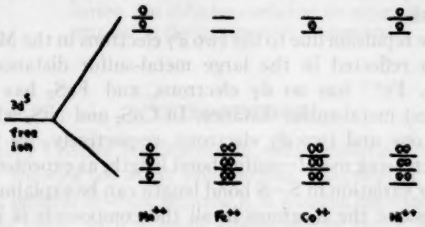

FIG. 1. $3d$ electronic structures.

Published x-ray data for compounds with the pyrite structure are incomplete[3-6] and in some disagreement. A reinvestigation was, therefore, carried out in this laboratory on carefully prepared powder specimens, all having the correct stoichiometry within the accuracy of experimental analysis.

X-ray powder patterns were obtained with copper, iron, and chromium radiation, using a camera with a circumference of 360 mm. Intensities were measured from densitometer records, and films were calibrated with a sodium chloride standard. No extraneous reflections were observed.

The use of several wavelengths allowed a comparison of line intensities to be made on groups of reflections for which the Lorentz and polarization factor was nearly constant.

Compounds with the pyrite structure belong to the space group T_h^6 ($Pa3$). The atomic positions are M:(000; $0\frac{1}{2}\frac{1}{2}$; ↷) and S:$\pm(uuu;\ \frac{1}{2}+u,\ \frac{1}{2}-u,\ u;$ ↷). Intensities were calculated with the formula

$$I\sim[(1+\cos^2\theta)/(\cos\theta\sin^2\theta)]hF^2.$$

The form factors are

$$F=4f_M+8f_S\cos2\pi hu\cos2\pi ku\cos2\pi lu$$

for hkl all even or all odd,

and

$$F=8f_S\cos2\pi hu\sin2\pi ku\sin2\pi lu$$

for hk odd and l even or hk even and l odd.

Fermi-Thomas atomic scattering factors were used, to which it was found necessary to apply a dispersion correction in accounting for intensities.

Qualitative intensity comparisons limited the range of values for the parameter u. These are given in Table I.

TABLE I. Qualitative intensity comparisons.

Compound	Observation	Parameter
FeS_2	[422]>[421]	$u>0.383$
	[422]>[152]	$u>0.382$
	[023]>[421]	$u>0.380$
	[331]>[332]	$u>0.381$
	[421]>[331]	$u<0.390$
	[420]>[331]	$u<0.387$
	[222]>[331]	$u<0.389$
	[420]>[222]	$u<0.386$
CoS_2	[331]>[421]	$u>0.387$
	[331]>[042]	$u>0.388$
	[220]>[112]	$u>0.387$
	[021]>[220]	$u<0.393$
NiS_2	[331]>[224]	$u>0.394$

* Research performed under the auspices of the U. S. Atomic Energy Commission.

[1] L. Pauling, *Nature of the Chemical Bond* (Cornell University Press, Ithaca, New York, 1945), p. 181.
[2] L. Néel, Compt. rend. **7**, 444 (1953).
[3] W. L. Bragg, Phil. Mag. **40**, 169 (1920).
[4] H. M. Parker and W. J. Whitehouse, Phil. Mag. **14**, 939 (1932).
[5] W. F. de Jong and H. W. V. Willems, Z. anorg. Chem. **160**, 185 (1927).
[6] D. Lundquist and A. Westgren, Z. anorg. Chem. **239**, 85 (1938).

TABLE II. Quantitative intensity comparisons.

hkl	FeS_2 I_{obs}	FeS_2 I_{calc}	CoS_2 I_{obs}	CoS_2 I_{calc}	NiS_2 I_{obs}	NiS_2 I_{calc}
111	200	202	210	223	215	208
200	540	588	700	800	720	850
021	380	401	445	444	345	310
112	320	320	380	380	340	285
220	250	280	390	390	400	360
003, 221	Not obs.	5	Not obs	14	25	19
310	Not obs.	0	Not obs.	0	Not obs.	0
311	575	577	675	633	650	705
222	85	86	105	107	140	131
023	130	126	145	143	175	166
132	175	165	180	180	215	199
400	Not obs.	5	Not obs.	2	Not obs.	0
041, 223	Not obs.	5	Not obs.	2	30	40
114, 330	Not obs.	3	Not obs.	1	20	20
133	61	69	105	109	160	153
204	85	86	100	101	105	106
241	105	106	95	97	70	77
332	50	42	40	34	30	28
224	125	116	140	142	160	150
005, 043	Not obs.	5	Not obs.	14	30	42
150, 134	Not obs.	3	Not obs.	19	40	48
115, 333	365	364	380	430	530	660
025, 243	210	174	180	181	200	230
152	150	111	110	103	135	144
440	290	275	285	300	460	550
114, 225	Not obs.	4				
350, 334	Obs.	27				
135	Not obs.	11				
600, 244	215	214				
061	Obs.	46				
352, 116	185	184				

The intensities of about thirty reflections were calculated for a reasonable range of parameter values and compared with the observed intensities. Parameters giving the best agreement were found to be 0.384 ± 0.001, 0.389 ± 0.001, and 0.395 ± 0.002 for FeS_2, CoS_2, and NiS_2, respectively. A comparison of calculated and observed intensities is given in Table II.

A comparison of the interatomic distances found in these compounds together with those found by Offner[7] for MnS_2 is given in Table III. It is of interest to note in this table that the S—S bond length is not constant in these compounds, although it is very nearly the same in MnS_2 and NiS_2. Also there is a discontinuity in the metal—sulfur distance in going from MnS_2 to FeS_2, the Fe–S distance being the shortest in the series. The metal—sulfur distance increases and the sulfur—sulfur distance decreases in the order FeS_2, CoS_2, NiS_2. This takes place in such a way, however, that the sum of the two bond lengths, M—S, and S—S, is nearly constant.

These observations are in good agreement with ligand-field theory. In the pyrite structure the metal atoms are octahedrally surrounded by the sulfur atoms of six S_2 groups, and the d orbitals split into a triply degenerate $d\epsilon$ group and a higher lying $d\gamma$ group, doubly degenerate. The grouping of the electrons in these orbitals is shown for the metal ions of the series in Fig. 1.

In the case of Mn^{++} the splitting is not sufficient to overcome the stability of a half-filled shell and produce a low-spin state. For Fe^{++}, however, a low-spin state is formed, and all six electrons of Fe^{++} are paired in $d\epsilon$ orbitals.

The repulsion due to the two $d\gamma$ electrons in the Mn^{++} ion is reflected in the large metal-sulfur distance in MnS_2. Fe^{++} has no $d\gamma$ electrons, and FeS_2 has the shortest metal-sulfur distance. In CoS_2 and NiS_2 which have one and two $d\gamma$ electrons, respectively, we find an increasing metal—sulfur bond length, as expected.

The variation in S—S bond length can be explained if we assume the S_2 group in all the compounds is in a singlet state, either as a neutral molecule or a doubly-charged negative ion. Using molecular-orbital notation for the S_2^{2-} ion, the configuration is

$$S_2^{2-}[(\sigma 3s)^2(\sigma^* 3s)^2(\sigma 3p)^2(\pi_y 3p)^2(\pi_z 3p)^2 \times (\pi_y^* 3p)^2(\pi_z^* 3p)^2].$$

Now it is the antibonding $\pi^* 3p$ electrons, which come from the $4s$ orbitals of the metal ions, that cause the S—S distance to be larger in the pyrite structures than

TABLE III. Unit cell dimensions and interatomic distances.

Compound	a_0 (A)	u	S—S (A)	M—S (A)
MnS_2	6.097	0.4012	2.086	2.59
FeS_2	5.404	0.384	2.171	2.259
CoS_2	5.523	0.389	2.124	2.315
NiS_2	5.677	0.395	2.065	2.396

[7] F. Offner, Z. Krist. **89**, 182 (1934).

it is in the sulfur molecule.[8] And it is the sharing of these electrons with the metal atoms that gives rise to variations in the S—S bond. It is a reasonable assumption, and in agreement with the observations, that the shorter the metal-sulfur distance is, the greater is the concentration of antibonding electrons in the π^*3p orbitals.

[8] G. Herzberg, *Spectra of Diatomic Molecules* (D. Van Nostrand Company, Inc., Princeton, New Jersey, 1950), p. 566.

ACKNOWLEDGMENTS

I wish to thank Dr. William Clinton and Dr. Max Wolfsberg of this laboratory for much helpful discussion on this problem.

THE JOURNAL OF CHEMICAL PHYSICS VOLUME 33, NUMBER 3 SEPTEMBER, 1960

Oxygen Diffusion in Periclase Crystals

Y. OISHI AND W. D. KINGERY

Ceramics Division, Department of Metallurgy, Massachusetts Institute of Technology, Cambridge, Massachusetts

(Received February 25, 1960)

Oxygen self-diffusion coefficients have been determined for MgO crystals over the temperature range 1300–1750°C. Results can be represented by the equation $D=2.5\times10^{-6}\exp(-62\,400/RT)$. By comparison with data for alkali halides and previous measurements for aluminum oxide, diffusion is probably extrinsic in nature. The diffusion coefficient for oxygen in this material is about two orders of magnitude less than that reported in the literature for magnesium.

I. INTRODUCTION

DIFFUSION coefficients in oxide materials are of interest for many applications. Magnesium oxide is of general interest because it is a stable high-melting-point oxide with a small stoichiometry range having the sodium chloride structure. Consequently, it is an oxide that can be directly compared with halides for which considerable data are available. Diffusion data for magnesium in MgO have been reported by Lindner and Parfitt.[1]

II. EXPERIMENTAL

Oxygen diffusion coefficients were determined by measuring the rate of exchange between a limited volume gas phase (oxygen gas at 150 mm pressure) enriched with the stable isotope O^{18} and MgO grain. The solid particles (200–230 mesh and 60–65 mesh grain) were all obtained from one single crystal of selected clear periclase. Spectrographic analysis indicated the presence of the following impurities: Si~0.01%, K≤0.01%, Fe≤0.01%, Ca≤0.01%, Al<0.01%, Ag<0.01%, Cr<0.01%, Cu<0.01. That is, the sample was not of exceptionally high purity. Diffusion coefficients were determined with the apparatus and techniques previously employed for aluminum oxide and already described in detail.[2]

III. RESULTS AND DISCUSSION

The rate of exchange between the gas phase and solid periclase was found to be controlled by volume diffusion with a diffusion coefficient independent of the amount of material exchange, as indicated by the straight line through the origin in Fig. 1.

Experimental values for the diffusion coefficient of oxygen are given in Fig. 2. Results are satisfactorily represented by the relation

$$D=2.5\times10^{-6}\exp(-62\,400/RT), \quad (1)$$

and the maximum possible estimation of activation energy (from the three high-temperature points) is 83 400 cal/mole although the standard error is ±6 kcal/mole. Results are compared with the Lindner and Parfitt[1] data for magnesium in Fig. 2. The absolute value of the oxygen diffusion coefficient is about 2 orders of magnitude less than that for magnesium. This is similar to results for alkali halides[3] and is not unexpected for magnesium oxide which has the sodium chloride structure. Of those alkali halides that have been measured, the ionic radius ratio, $r_{O^{2-}}/r_{Mg^{2+}}=2.16$, is most similar to that of sodium chloride, $r(Cl^-)/r(Na^+)=1.91$. In the intrinsic diffusion region, the ratio of activation energies for Cl^- and Na^+ diffusion in sodium chloride is $Q(Cl^-)/Q(Na^+)=51.4/37.0=1.39$. Since the anion/cation radius ratio is larger for MgO than for NaCl, we would expect that the ratio of activation energies for intrinsic diffusion of oxygen ion and magnesium ion in MgO would also be greater than 1.39. The ratio of activation energies found here, however,

[1] R. Lindner and G. D. Parfitt, J. Chem. Phys. **26**, 182 (1957).
[2] Y. Oishi and W. D. Kingery, J. Chem. Phys. (to be published).
[3] J. F. Laurent and J. Benard, J. Phys. Chem. Solids **3**, 7–19 (1957).

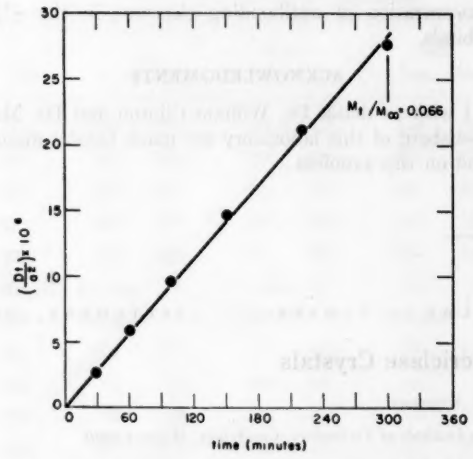

FIG. 1. Plot of nondimensional Dt/a^2 as a function of time for oxygen exchange with MgO.

is $Q(O^{2-})/Q(Mg^{2+})=62.4/79.0=0.79$, considerably less than in NaCl. (A maximum estimation would be $83.4/79.0=1.05$, still less than the ratio for NaCl.)

The anion structure in magnesium oxide is face-centered-cubic with an oxygen-oxygen separation of 2.97 A. This is similar to aluminum oxide which has an hexagonal-close-packed oxygen ion structure with an oxygen-oxygen separation of 2.94 A. In MgO all the available octahedral interstices are filled with Mg^{2+}, while in Al_2O_3, two-thirds of the available octahedral sites are filled with Al^{3+}. In alumina the oxygen ion diffusion coefficient in the impurity-controlled or structure-sensitive range was given for one set of samples by

$$D_{Al_2O_3}(O^{2-})=6.3\times10^{-8}\exp(-57\,600/RT). \quad (2)$$

This result is typical, but different samples gave variable results. The similarity of the activation energy and pre-exponential term with those found for magnesia is apparent. By contrast, the activation energy for intrinsic oxygen diffusion in alumina is 152 000 cal/mole, and $D_0=1.9\times10^3$ cm²/sec.

By comparison with NaCl and also with Al_2O_3, it seems probable that the results reported here correspond to impurity-controlled or structure-sensitive diffusion, and the activation energy refers to oxygen ion mobility. For the Eyring equation,

$$D=\lambda^2(kT/h)\exp(\Delta S^*/R)\exp(-\Delta H^*/RT) \quad (3)$$

for a jump distance of 2.97 A we calculate $\Delta S^*=-6.5$ cal/kg and $\Delta H^*=80$ kcal/mole. The negative entropy of activation was also found for impurity-controlled or structure sensitive diffusion in aluminum oxide[2] and has also been found for some alkali halides.[3]

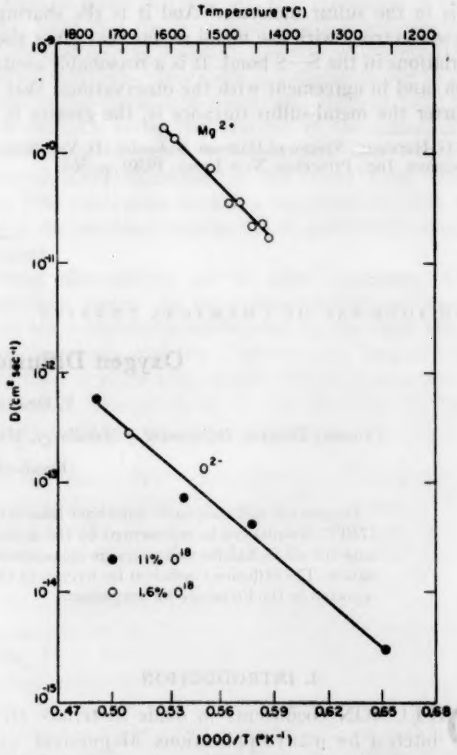

FIG. 2. Oxygen diffusion coefficients measured in single crystal MgO. Upper curve is Lindner and Parfitt result for magnesium diffusion.

IV. SUMMARY

The self-diffusion coefficient for oxygen in single crystals of magnesium oxide has been determined in the temperature range 1300–1750°C. Data can be represented by the equation

$$D=2.5\times10^{-6}\exp(-62\,400/RT). \quad (4)$$

By comparison with data for alkali halides and previous results for aluminum oxide, this diffusion is believed to correspond to an impurity-controlled or structure-sensitive process, and the activation energy corresponds to ion mobility.

Oxygen diffusion coefficients in magnesium oxide are about two orders of magnitude smaller than magnesium diffusion coefficients.

ACKNOWLEDGMENTS

This research was carried out at the Massachusetts Institute of Technology with support of U. S. Atomic Energy Commission. During a portion of the study Dr. Oishi was on leave of absence from the Osaka Industrial Research Institute, Osaka, Japan.

Microwave Spectrum, Structure, Dipole Moment, and Internal Rotation of Trimethyl Silane*

LOUIS PIERCE AND D. H. PETERSEN

Department of Chemistry, University of Notre Dame, Notre Dame, Indiana

(Received April 15, 1960)

The microwave spectra of eleven isotopic species of trimethyl silane have been measured and assigned. From the observed ground state rotational constants the structural parameters of trimethyl silane are calculated to be

CH 1.095 A	SiH 1.489 A
HCH 107°56′	SiC 1.868 A
	CSiC 110°10′

The equilibrium conformation is found to be the one in which each methyl group staggers the SiH and adjacent SiC bond axes. Stark effect measurements yield a dipole moment of 0.525 debye. Relative intensities of torsional satellites of $(CD_3)_2CH_3SiH$ have been measured and analyzed to provide information about the barrier to internal rotation in trimethyl silane. Structural changes which accompany methylation and fluorination of methyl silane are discussed.

I. INTRODUCTION

PRECISE values of bond distances and interbond angles for several fluoro- and methyl-fluorosilanes have recently been determined from their microwave spectra.[1] The microwave studies of these two series of molecules have revealed certain interesting structural trends. Thus in both series the SiF distances decrease markedly with progressive fluorination, while in the methyl fluorosilanes there is also a decrease of the SiC distance with each substitution of fluorine for hydrogen on silicon. These trends are especially interesting because in the analogous carbon compounds progressive fluorination shortens the CF bond, while fluorination apparently has no appreciable effect on the CC distance.[2] Bond and Brockway[3] have reported another interesting structural trend in the methyl silanes. From electron diffraction measurements they conclude that the SiC distance increases smoothly from 1.857 A in methyl silane to 1.888 A in tetramethyl silane. Thus according to their work, insofar as the SiC distance is concerned, methylation of methyl silane has the opposite effect of fluorination. It is interesting to note that in the carbon analogs of the methyl silanes the CC distance is essentially constant.

The present work is concerned with the investigation of the microwave spectra of several isotopic species of trimethyl silane. The work was primarily undertaken to complete an independent determination, by microwave spectroscopy, of structural trends in the methyl silanes. The complete structure of methyl silane as determined by microwave spectroscopy has already been reported.[4] Partial results for dimethyl silane have also been reported.[5] Structural calculations for dimethyl silane are now completed and details will be given in a separate paper. However, structural data for mono-, and di- as well as trimethyl silane are tabulated here.

Also considered in the present work is the problem of internal rotation in trimethyl silane. The results of the study of isobutane by Lide and Mann[6] suggest that the independent top approximation is a reasonably good one. Since the methyl groups are somewhat farther apart in trimethyl silane than they are in isobutane, it seems reasonable to expect that the independent top model will be an excellent approximation for trimethyl silane. We have analyzed the relative intensities of two torsional satellites of $(CD_3)_2(CH_3)SiH$ in an effort to determine the extent to which top-top interactions are important in this molecule.

II. EXPERIMENTAL

A. Preparation of Samples

Samples of $(CH_3)_3SiH$ and $(CH_3)_3SiD$ were prepared by reduction of $(CH_3)_3SiCl$ with $LiAlH_4$ and $LiAlD_4$ respectively in *n*-butyl ether at 0°C. Samples of $(CH_3)_3SiH$ (16%)-$(CH_3)_2(C^{13}H_3)SiH$ (48%)-$(C^{13}H_3)_2(CH_3)SiH$ (36%)—(a mixture), and $(CD_3)_2(CH_3)SiH$ were prepared by reacting $C^{13}H_3MgI$

* This research was made possible by a grant from the National Science Foundation.

[1] A summary of results and complete references are given by L. C. Krisher and L. Pierce, J. Chem. Phys. **32**, 1619 (1960).

[2] B. Bak and co-workers have recently determined the complete structure of ethyl fluoride from microwave data. They find a CC distance of 1.533 A. We are grateful to Professor Bak for a preprint of this work. The most recent high resolution infrared study of ethane, H. C. Allen, Jr., and E. K. Plyler, J. Chem. Phys. **31**, 1062 (1959), yields a CC distance of 1.534 A.

[3] A. C. Bond and L. O. Brockway, J. Am. Chem. Soc. **76**, 3312 (1954).

[4] R. W. Kilb and L. Pierce, J. Chem. Phys. **27**, 108 (1957).

[5] L. Pierce, J. Chem. Phys. **31**, 547 (1959), and a forthcoming publication.

[6] D. R. Lide, Jr. and D. E. Mann, J. Chem. Phys. **29**, 914 (1958).

TABLE I. Observed rotational transitions of symmetric top species of trimethyl silane (Mc).

	$(CH_3)_2SiH$	$(CH_3)_3SiD$
1←0		
Si^{28} [a]	10 690.34	10 319.40
2←1		
Si^{28} [a]	21 380.58	20 638.87
Si^{29} [b]	21 351.36	20 615.49
Si^{30} [b]	21 323.35	20 592.50

[a] ±0.10 Mc.
[b] ±0.20 Mc. Observed in natural abundance.

(60% C^{13}) and CD_3MgI respectively with CH_3SiHCl_2 in *n*-butyl ether at 0°C. Reduction of $(CH_2Cl)(CH_3)_2SiCl$ and $(CHCl_2)(CH_3)_2SiCl$ with LiD in *n*-butyl ether at 45°C provided samples of $(CH_2D)(CH_3)_2SiD$ and $(CHD_2)(CH_3)_2SiD$. Simple bulb to bulb distillations (dry ice to liquid nitrogen) of the reaction mixtures in general gave trimethyl silane of roughly 90% purity or better. In certain cases samples were further purified by the gas chromatography technique.

B. Spectra

The *C*-type 1←0 and/or 2←1 transitions of eleven isotopic species of trimethyl silane were observed with a conventional Hughes-Wilson spectrograph[7] employing 100-kc Stark modulation and coherent detection. Absorption frequencies were measured using a crystal controlled microwave frequency standard monitored by the 10-Mc WWV signal; oscilloscope presentation was employed for measurement of lines of enriched isotopic species (±0.10 Mc), while the weaker absorptions due to Si^{29} and Si^{30} isotopic species in natural abundance were measured (±0.20 Mc) with narrow system bandwidth (1 cps) on a recording potentiometer. Relative intensities [$(CD_3)_2CH_3SiH$ only] were measured on a recording potentiometer under a variety of conditions and are believed to be accurate to within about 10 to 15%.

The observed absorption frequencies for six symmetric top species of trimethyl silane are listed in Table I. As expected, *K* splitting due to centrifugal distortion was too small to be observed. Similarly, tunnel effect splittings arising from coupling of internal and over-all rotation were not resolvable for rotational transitions from the ground torsional state. However, a weak and complex multiplet pattern roughly centered 15 Mc lower than the ground state 2←1 line was observed in the spectra of both $(CH_3)_3Si^{28}H$ and $(CH_3)_3Si^{28}D$. The multiplets very probably are the result of rotational transitions from excited torsional states of trimethyl silane. Analysis of these multiplet patterns would be a fairly formidable task, since tunnel effect splittings and *l*-type doubling effects are probably equally important for excited torsional states of trimethyl silane. Furthermore, the importance of tunnel effect splittings, in the excited torsional states of $(CH_3)_3SiH$ and $(CH_3)_3SiD$, rules out the possibility of an internal rotation study of the type used by Lide and Mann.[6,8]

Observed transition frequencies for five asymmetric top species of trimethyl silane are given in Tables II and VI. Transitions were in all cases identified by their characteristic Stark patterns. Unfortunately, the asymmetry corrections to the 2_{20}←1_{10} transitions are too small to yield reliable values for the *C* rotational constants.

The excited state spectrum of $(CD_3)_2(CH_3)SiH$ is of special interest. Assuming that the only internal degrees of freedom are torsional motions, there are then three torsional modes of oscillation. Two of these belong to the *A''* species of the point group C_s, and may to a good approximation be described as CH_3 group torsion (ω_1), and antisymmetric CD_3 group torsion (ω_2—both CD_3 groups moving in phase). The third mode, symmetric CD_3 group torsion (ω_3–CD_3 groups moving with opposite phase), belongs to the *A'* species of C_s. An unsuccessful attempt was made to assign rotational transitions from the $v_1=1$ state. It was expected that these transitions would show tunnel effect splittings, and that analysis of these splittings by means of simple one-top theory[9] would provide precise information about the height of the barrier hindering internal rotation. A promising looking doublet pattern was found (see Table II), but these transitions were much too intense to assign them to $v_1=1$. Assuming a barrier height in the range 1400 to 2000 cal/mole,[10] the observed intensities more nearly correspond to those expected for the $v_2=1$ and $v_3=1$ satellites. Furthermore the doublet splittings were analyzed and found to be completely inconsistent with an assignment to $v_1=1$. Consequently, we have assigned the observed satellites to $v_2=1$, and $v_3=1$, and have used their intensities relative to the ground-state transitions to determine internal barrier parameters for trimethyl silane. In making the internal barrier calculations we have in essence used the method employed by Lide and Mann in their studies of three-top molecules such as $(CH_3)_3N$.[8] The details of our calculations (see Sec. IV) of course differ from theirs, since $(CD_3)_2(CH_3)SiH$ and $(CH_3)_3N$ do not belong to the same point group.

[7] K. B. McAfee, Jr., R. H. Hughes, and E. B. Wilson, Jr., Rev. Sci. Instr. 20, 821 (1949).

[8] D. R. Lide, Jr. and D. E. Mann, J. Chem. Phys. 28, 572 (1958).

[9] (a) R. W. Kilb, C. C. Lin, and E. B. Wilson, Jr., J. Chem. Phys. 26, 1695 (1957); (b) J. D. Swalen and D. R. Herschbach, *ibid.* 27, 100 (1957); (c) D. R. Herschbach, *ibid.* 31, 91 (1959).

[10] The assumed range of 1400 to 2000 cal/mole for the barrier of trimethyl silane seemed to us reasonable in view of the fact that the barriers for methyl and dimethyl silane are 1660 and 1670 cal/mole, respectively.

TABLE II. Observed rotational transitions[a] of asymmetric top species of trimethyl silane.

	$1_{10}\leftarrow 0_{00}$	$2_{11}\leftarrow 1_{01}$	$2_{20}\leftarrow 1_{10}$	$2_{21}\leftarrow 1_{11}$
$(C^{13}H_3)(CH_3)_2SiH$	10 514.75	20 860.02	21 039.24	21 199.01
$(CH_3)(C^{13}H_3)_2SiH$		20 512.02	20 690.03	20 848.06
$(CD_3)_2(CH_3)SiH$	8 941.09	17 374.08	17 987.14	18 390.30
$v_2=1$[b]		17 358.67	17 974.66	18 378.75
$v_3=1$[b]		17 346.60	17 966.81	18 372.55

[a] ±0.1 Mc unless otherwise stated. See Table VI for observed transitions of $(CH_2D)(CH_3)_2SiD$ and $(CHD_2)(CH_3)_2SiD$.
[b] Torsional satellites of $(CD_3)_2CH_3SiH$ corresponding to torsional frequencies $\omega_2=104$ cm^{-1} and $\omega_3=141$ cm^{-1} as determined from relative intensity measurements at 200°K. Estimated accuracy of the rotational frequencies is ±0.20 Mc.

C. Stark Effect

In order to determine the dipole moment of trimethyl silane, Stark displacements of the four lobes of the 2←1 transition of $(CH_3)_3Si^{28}H$ were measured. The apparatus was calibrated with OCS before and after making measurements on trimethyl silane. The Stark coefficients are listed in Table III, and from them the dipole moment was calculated to be 0.525±0.005 debye.

III. STRUCTURE AND EQUILIBRIUM CONFORMATION

The measurements described above yield a total of twenty ground-state rotational constants which are listed in Table IV. Since all positions have been isotopically substituted, it is possible to locate all atoms in principal axes of $(C^{12}H_3)_3Si^{28}H$ using only differences in moments of inertia. If use is made of the symmetry (C_3 at least) of $(CH_3)_3SiH$, as well as the relation

$$\Delta I_c=\Delta I_b-\Delta I_a \qquad (1)$$

then there are sufficient data to determine all atom coordinates, except those for two hydrogens on each methyl group, by means of Kraitchman's equations.[11] Because data are available for several multiply substituted isotopic species, many of the coordinates can be calculated in more than one way from differences of moments of inertia, though of course Kraitchman's equations are not applicable in every case. Except for the methyl hydrogens, the agreement between different determinations of each coordinate is well within the estimated experimental accuracy. The average experimental value of each atom coordinate was used in calculating the structure of trimethyl silane.

Because accurate C moments were not experimentally obtained, it was necessary to make at least one assumption in calculating the methyl group parameters. We made two assumptions—the usual ones, i.e., each methyl group is symmetrical and its symmetry axis coincides with the CSi bond axis. With these assumptions it was found that the parameters CH=1.095 A and ∠HCH=107°58′ gave the best fit of the differences in moments of inertia. For the five isotopic pairs [$(C^{12}H_3)_3Si^{28}H$ in each pair] which involve deuterium substitution (methyl), these methyl group parameters give ten ΔI's which agree on the average to within ±0.011 Amu-A^2 with observed ΔI's. The worst disagreement between observed and calculated ΔI's is 0.028 amu-A^2. Deviations of this order of magnitude are quite typical for deuterium substitution.

The structural parameters of trimethyl silane are listed in Table V. Note that the quoted uncertainties represent only the effect of estimated experimental uncertainties in the ΔI's. Since all atoms in the molecule have been located by using only differences in moments of inertia, two independent checks of the structure are available; the calculated B moment of inertia of $(C^{12}H_3)_3Si^{28}H$ may be compared with the observed moment, and the sum $\sum m_i c_i$ may be compared with the theoretical value of zero which is required for equilibrium values of the c_i (m_i is the mass and c_i the c coordinate of the ith atom). The difference of 0.24 amu-A^2 between observed and calculated values of I_b is quite typical of the method of structural analysis used here. The absolute value of 0.07 amu-A for $\sum m_i c_i$ is slightly larger than typical, but errors of about 0.002 A in either the silicon or carbon c coordinates would account for the greater part of the 0.07 amu-A discrepancy.

TABLE III. Stark coefficients for the 2←1 transition of $(C^{12}H_3)_3Si^{28}H$.[a]

First-order lobes	
$(\Delta\nu/E)$ (Mc/volt-cm^{-1})$_{obs}$	μ_{calc} (debye)
+0.0882±0.007	0.527
−0.0876±0.007	0.523
Second-order lobes	
$(\Delta\nu/E^2)$ (Mc/kv^2-cm^{-2})$_{obs}$	μ_{calc} (debye)
−1.011±0.015	0.529
+0.798±0.010	0.522
$\mu_{Av}=0.525$ debye	

[a] Apparatus calibrated with COS taking $\mu_{COS}=0.7124D$ as determined by S. A. Marshall and J. Weber, Phys. Rev. **105**, 1502 (1957).

[11] J. Kraitchman, Am. J. Phys. **21**, 17 (1953).

TABLE IV. Ground state rotational constants (Mc).

	B	C[a]
Symmetric top species		
$(CH_3)_2Si^{29}H$	5 345.15	3 166
$(CH_3)_2Si^{30}H$	5 337.84	
$(CH_3)_2Si^{30}H$	5 330.84	
$(CH_3)_2Si^{28}D$	5 159.71	
$(CH_3)_2Si^{29}D$	5 153.87	
$(CH_3)_2Si^{30}D$	5 148.13	
Asymmetric top species		
	A	B	C[a]
$(C^{13}H_3)(CH_3)_2SiH$	5 342.14	5 172.63	3 105
$(C^{13}H_3)_2(CH_3)SiH$	5 254.02	5 086.00	3 135
$(CD_3)_2(CH_3)SiH$	4 724.61	4 216.49	2 656
s-$(CH_2D)(CH_3)_2SiD$[b]	5 070.23	4 905.69	3 101
a-$(CH_2D)(CH_3)_2SiD$[c]	5 157.86	4 859.67	3 050
s-$(CD_2H)(CH_3)_2SiD$[b]	5 076.72	4 662.40	2 945
a-$(CD_2H)(CH_3)_2SiD$[c]	5 052.74	4 650.07	2 992

[a] Calculated from the structural parameters of Table V.
[b] *sym* form.
[c] *asym* form.

Of the possible conformations of trimethyl silane, the most probable ones are (1) each methyl group staggered with respect to the SiH bond and adjacent SiC bonds (C_{3v}); (2) each methyl group eclipsed with respect to the SiH bond and adjacent SiC bonds (C_{3v}); (3) each methyl group rotated slightly from the staggered position (C_3); (4) each methyl group rotated slightly from the eclipsed position (C_3); (5) one methyl group in the eclipsed position and two in the staggered position or vice versa (C_s).

Table VI compares the observed spectra of $(CH_2D)(CH_3)_2SiD$ and $(CHD_2)(CH_3)_2SiD$ with the calculated spectra for the staggered (1) and eclipsed (2) conformations. The comparison shows clearly that conformations (2), (4), and (5) are definitely ruled out. The choice between (1) and (3) can be made by using simple physical arguments. The data of Table VI, show that if the methyl groups *are* rotated from the staggered position, then the extent of this rotation must certainly be small, probably no more than 2 to 4 degrees. A barrier separating two such closely spaced potential minima must certainly be very small, so that the only reasonable conclusion is that the proper symmetry group for trimethyl silane is C_{3v} and not C_3.

TABLE V. Structure of trimethyl silane.[a]

CSi	1.868±0.002 A
SiH	1.489±0.001 A
CH	1.095±0.002 A
<CSiC	110°10′±12′
<HCH	107°56′±14′
$(C^{13}H_3)_2Si^{29}H$	
I_B (calc) = 94.337 amu-A^2	
I_B (obs) − I_B (calc) = 0.241 amu-A^2	
$\Sigma m_i z_i$ = 0.074 amu-A	

[a] Errors represent only the effect of uncertainties in measured frequencies, see footnotes to Table I and II. The atomic masses were taken from C. H. Townes and A. L. Shawlow, *Microwave Spectroscopy* (McGraw-Hill Book Company, Inc., New York, 1955), Appendix VII. The conversion factor 5.05531×10^5 amu-A^2 Mc was used.

TABLE VI. Comparison of calculated spectra for two conformations of trimethyl silane with observed spectra of $(CH_2D)(CH_3)_2SiD$ and $(CHD_2)(CH_3)_2SiD$.

Isotopic species	Calculated frequencies (2←1) Eclipsed conformation[b]	Staggered conformation[b]	Observed frequencies[a]
sym-$(CH_2D)(CH_3)_2SiD$	19 676 Mc	19 785	19 787.30
	20 011	19 960	19 962.62
	20 276	20 115	20 116.38
asym-$(CH_2D)(CH_3)_2SiD$	19 798	19 737	19 736.85
	20 045	20 071	20 068.81
	20 250	20 337	20 333.25
sym-$(CD_2H)(CH_3)_2SiD$	19 168	19 067	19 063.92
	19 527	19 547	19 544.30
	19 754	19 895	19 892.55
asym-$(CD_2H)(CH_3)_2SiD$	18 968	19 001	19 002.95
	19 481	19 470	19 470.41
	19 865	19 809	19 808.32

[a] ±0.10 Mc.
[b] C_{3v} symmetry.

IV. INTERNAL ROTATION

In order to make use of the measured relative intensities of the $v_2=1$ and $v_3=1$ satellites of $(CD_3)_2(CH_3)SiH$, it is necessary to perform a normal coordinate calculation. Following the treatment of Lide and Mann,[5] internal degrees of freedom other than torsional are suppressed and the potential energy in the harmonic oscillator approximation is taken to be

$$2V = K\sum_{k=1}^{3}\alpha_k^2 + 2L\sum_{k>k'}\alpha_k\alpha_{k'}, \qquad (2)$$

TABLE VII. Molecular parameters of the methyl silanes.

	SiH_4	CH_3SiH_3[a]	$(CH_3)_2SiH_2$[b]	$(CH_3)_3SiH$[c]	$(CH_3)_4Si$
SiH		1.484 A	1.483 A	1.489 A	...
HCH	...	108°0′	108°0′	107°56′	
CSi	...	1.867 A	1.867 A	1.868 A	
CH	...	1.092 A	1.095 A	1.095 A	
HSiH	109°28′	108°44′	107°50′	...	
CSiH	...	110°12′	109°29′	108°46′	...
CSiC	...	...	110°59′	110°10′	109°28′
Dipole moment	0	0.73 D	0.75 D	0.525 D	0
Barrier to internal rotation (cal/mole)	...	1670	1660	1830	

[a] References 4 and 9(c), and D. R. Lide and D. K. Coles, Phys. Rev. **80**, 911 (1950). This structure differs slightly from the one reported in reference 4. We have recomputed the structure using only differences in moments of inertia.
[b] Reference 5.
[c] This work.

where

$$K=(9/2)(V_1+2V_2+V_3)$$
$$L=(9/2)(V_4+V_5).$$

The parameter V_1 represents the potential barrier for methyl group rotation in the absence of coupling between methyl groups. The parameters V_2 to V_5 represent barrier terms resulting from interactions between methyl groups.

Herschbach[9c] has recently derived a convenient expression for the kinetic energy for internal and over-all rotation in molecules containing several internal tops. In the present calculation we are assuming that the barrier to internal rotation is sufficiently high for the harmonic oscillator approximation to hold. In the limit of this approximation we can neglect terms coupling internal and over-all rotation and write the purely torsional kinetic energy as

$$T=\sum_{k,k'}F_{kk'}p_kp_{k'};\qquad k,k'=1,2,3 \tag{3}$$

where p_k is the momentum conjugate to α_k, and $F_{kk'}$ are the inverse reduced moments for internal rotation defined by Herschbach.[9c]

If α_1 is taken to be the torsion angle for the CH_3 group, and α_2, α_3 the torsion angles for the CD_3 groups, then the appropriate symmetry coordinates for the present problem are

$$X_1=\alpha_1$$
$$X_2=(1/\sqrt{2})(\alpha_3+\alpha_2)$$
$$X_3=(1/\sqrt{2})(\alpha_3-\alpha_2), \tag{4}$$

and their conjugate momenta are

$$P_1=p_1$$
$$P_2=(1/\sqrt{2})(p_3+p_2)$$
$$P_3=(1/\sqrt{2})(p_3-p_2). \tag{5}$$

In terms of the symmetry coordinates the secular equation consists of a quadratic factor (ω_1 and ω_2 modes), and a linear factor (ω_3 mode). The exact expression for ω_3 is

$$\omega_3=[2(F_{33}-F_{23})(K-L)]^{\frac{1}{2}}. \tag{6}$$

The cumbersome exact expression for ω_1 and ω_2 will not be given. However, for small L and F_{12} the following approximate equations may be used:

$$\omega_1\approx[2(F_{11}K+2F_{12}L)]^{\frac{1}{2}}$$
$$\omega_2\approx[2(F_{22}+F_{23})(K+L)+4F_{12}L)]^{\frac{1}{2}}. \tag{7}$$

From the observed satellite intensities the CD_3 torsional frequencies are calculated to be 104 cm^{-1} and 141 cm^{-1}. From the present observations alone it is not possible to determine which of the two possible assignments to ω_2 and ω_3 is correct. However, Lide and Mann[6,8] in their studies of three-top molecules, have found L always to be negative. Assuming L to be negative for trimethyl silane also, we must conclude then that $\omega_3=141$ cm^{-1} and $\omega_2=104$ cm^{-1}. In support of this assignment we note the 141 cm^{-1} satellites are lower in frequency than the 104 cm^{-1} satellites, and that Lide and Mann in all cases observed the $v_3=1$ satellites to occur at a lower frequency than the $v_2=1$ satellites.

With the above assignments the values of K and L are calculated to be

$$K=2870\pm600\ cm^{-1}$$
$$L=-550\pm200\ cm^{-1},$$

[the approximate formulas (7) do note quite hold in this case]. Lide and Mann found similar results, i.e., $L\ll K$, and they have reasoned that the smallness of L suggests the approximation $K\approx(9/2)V_1$ to be a good one. Applied to the present case this approximation leads to a value of 1830±400 cal/mole for V_1. Thus to within

a rather large experimental error, V_1 for trimethyl silane is identical with the barrier to internal rotation in methyl silane (1670±20 cal/mole)[4,9e].

V. DISCUSSION

Table VII summarizes structural parameters, dipole moments, and internal barrier of the methyl silanes as determined from microwave spectra. For completeness, those parameters of silane and tetramethyl silane determined by symmetry alone (tetrahedral) are also included in the table.

Uncertainties resulting from estimated experimental errors are ±0.002 A or less for bond distances and ±20′ or less for bond angles in this series of molecules. Uncertainties due to neglect of zero-point contributions to differences of moments of inertia cannot at present be reliably estimated. However, very general considerations lead to the conclusion that the method of structural analysis employed here greatly minimizes zero-point effects, especially for coordinates of these atoms which are far removed from the principal axes of the molecule.[12,13] According to these considerations, the methyl silanes are particularly suitable subjects for structural study by microwave spectroscopy. There are no near-axis heavy atoms in this series; the smallest carbon coordinate is 0.24 A while the smallest silicon coordinate is 0.36 A. It is interesting to note that the center of mass condition is much more nearly fulfilled by methyl silane ($\sum m_i a_i = 0.02$ amu-A) and dimethyl silane ($\sum m_i b_i = 0.01$ amu-A) than it is for trimethyl silane ($\sum m_i c_i = 0.07$ amu-A), and that both of the above mentioned small heavy atom coordinates occur in trimethyl silane. Except for two of the hydrogen atoms on each methyl group of di- and trimethyl silane, all hydrogens lie 0.88 A or farther from any principal axis. The imposition of the reasonable requirement of methyl group symmetry bypassed the necessity of using small isotope shifts associated with the near-axis hydrogen atoms.

To within the experimental uncertainty of ±0.002 A the three SiC distances given in Table VII are identical. Thus according to the microwave data, methylation of methyl silane has no detectable effect on the SiC distance. This result is not actually in serious disagreement with the electron diffraction result, since the average uncertainty reported (excluding tetramethyl silane) for the electron diffraction SiC distance is ±0.006 A. Sheehan and Schomaker[14] report the SiC distance in tetramethyl silane as 1.888±0.020 A.

Besides constancy of the SiC distance, certain other structural regularities are apparent in the methyl silanes. Thus the CH distances and HCH angles are essentially invariant. Variations in the HSiH, CSiH, and CSiC angles exceeding experimental uncertainties are observed, but these variations are strikingly regular. Each substitution of methyl for H on Si decreases each of these angles by 46′±8′ on the average.

It is interesting to compare the dipole moments of the methyl silanes with those of the fluorosilanes. In the former series no large structural trends are observed, yet the trends in the dipole moments are not at all consistent with the bond moment model. In contrast to this, each additional fluorine lowers the SiF distance by 0.014 A in the fluorosilane series, yet the dipole moments are quite consistent with the requirements of the bond moment model.[15]

Another interesting fact is that the Schomaker-Stevenson[16] rule gives an SiC distance of 1.88 A which is in good agreement with the observed values for the methyl silanes. In contrast to this, the same rule predicts an SiF distance of 1.69 A compared to the observed value of 1.593 A (SiH_3F). Pitzer[17] has suggested that bonds between first and second row elements should be shorter than the sum of the appropriate covalent radii because of differences in inner shell repulsions for the two rows. If Pitzer's hypothesis is accepted and the observed SiF distance regarded as "normal," then the 1.867 A SiC distance must be considered abnormally "long."

A possible alternative explanation of the "short" SiF bond is that the bond has a considerable amount of double bond character. The energetically most favorable double bond structure makes use of the 3*d* orbitals of silicon:

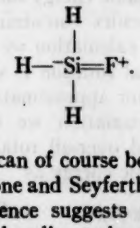

A similar structure can of course be written for methyl silane. However, Stone and Seyferth[18] have pointed out that chemical evidence suggests the role of the 3*d* orbitals of silicon in bonding to be especially important when silicon is bonded to a highly electronegative element such as F, N, or O. (Rather naive theoretical considerations support the chemical evidence: under the electrostatic influence of a nearby electronegative atom the 3*d* orbitals are less effectively screened and are thus lowered in energy.) If this is true then the structure

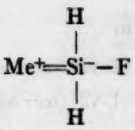

[12] C. C. Costain, J. Chem. Phys. **29**, 864 (1958).
[13] L. Pierce, J. Mol. Spectroscopy **3**, 575 (1959).
[14] W. F. Sheehan, Jr., and V. Schomaker, J. Am. Chem. Soc. **74**, 3956 (1952).
[15] V. W. Laurie, J. Chem. Phys. **26**, 1359 (1957).
[16] V. Schomaker and D. P. Stevenson, J. Am. Chem. Soc. **63**, 37 (1941).
[17] K. S. Pitzer, J. Am. Chem. Soc. **70**, 2140 (1948).
[18] F. G. A. Stone and D. Seyferth, J. Inorg. Nuclear Chem. **1**, 112 (1955).

would certainly be more important to CH_3SiH_2F than the corresponding structure for CH_3SiH_3. Perhaps this is a partial explanation for the fact that fluorination of the silyl group of methyl silane is accompanied by a decrease in the SiC distance. It is interesting to note that this type of double bond structure is very unfavorable in CH_3CH_2F since the $3d$ orbitals of carbon are so high in energy, and that the CC distance[2] in this molecule is essentially the same as that in ethane.

THE JOURNAL OF CHEMICAL PHYSICS VOLUME 33, NUMBER 3 SEPTEMBER, 1960

Thickness of Shock Fronts in Argon

K. HANSEN* AND D. F. HORNIG

Frick Chemical Laboratory, Princeton University, Princeton, New Jersey

(Received April 11, 1960)

The accuracy and sensitivity of the optical reflectivity method for determining the thickness of shock fronts have been improved. The thicknesses of shock fronts in argon have been measured up to $M=2.38$. Most of the effort was concentrated at $M=2.38$ where the reciprocal thickness in mean free paths, $l_0/L_0=0.234\pm0.007$. At $M=2.38$ the front is about twenty percent thicker than calculated from the Navier-Stokes equations but the thickness agrees very closely with that calculated by Muckenfuss using a bimodal distribution function.

PERHAPS the greatest value in the experimental study of the shock front transition is the check it provides on the validity of equations of gas flow when the gradients are very large and the velocity distribution certainly deviates from that at equilibrium. The theoretical description based on the Navier-Stokes equations is essentially complete in the absence of gas imperfections or relaxation effects.[1] Descriptions including higher order kinetic theory terms have also been given.[2-5]

All of the preceding agree for sufficiently weak shocks but begin to diverge by $M=1.5$ and become very different in the region above $M=2$. A very different kinetic theory approach, based on a bimodal distribution function, has been adopted by Mott-Smith[6] and developed for a variety of intermolecular force laws by C. Muckenfuss.[7] This approach cannot be exact for very weak shocks but ought to retain some validity even for very strong shocks when the methods of footnotes 1–5 must certainly fail.

Reasonably reliable experimental measurements on shock fronts in argon have been obtained by the reflectivity method at shock strengths up to $M=1.55$.[8]

Talbot and Sherman[5,9] have employed energy transfer to very fine wires to study not only the thickness but also the profiles of shock fronts in highly rarefied flows at shock strengths up to $M=1.85$ and have made a careful comparison of the available experiments and existing theories. Within this range the experimental thicknesses are slightly greater than predicted from the Navier-Stokes equations, definitely thinner than predicted from the Zoller or Burnett (footnote 5) equations and decidedly thinner than predicted by the 13 moment equations of Grad.[3]

It seemed worthwhile, therefore, to check the earlier measurements and to extend the reflectivity measurements to stronger shocks where a more sensitive test of the adequacy of various theoretical approaches might be obtained. Emphasis was placed on getting a single point reliably at the highest measurable shock strength, $M=2.4$.

EXPERIMENTAL

The general directions in which the experiment needed to be modified to achieve this goal were fairly

* Present address: University of Frankfurt, Physikalisch-Chemisches Institut, Frankfurt/Main, Germany.

[1] D. Gilberg and D. Paolucci, J. Rational Mech. 2, 617 (1953).

[2] C. S. Wang Chang, Report CM-503, Appl. Phys. Lab., The Johns Hopkins University (August, 1948.)

[3] H. Grad, Communs Pure and Appl. Math. V, No. 3, 257-300 (August, 1952).

[4] K. Zoller, Z. Physik 130, 1 (1951).

[5] L. Talbot and F. S. Sherman, NASA Memorandum 12-14-58 W (January, 1959).

[6] H. M. Mott-Smith, Phys. Rev. 82, 885 (1951).

[7] C. Muckenfuss (private communication).

[8] G. R. Cowan and D. F. Hornig, J. Chem. Phys. 18, 1008 (1950); E. F. Greene, G. R. Cowan, and D. F. Hornig, *ibid.* 19, 427 (1951); E. F. Greene and D. F. Hornig, *ibid.* 21, 617 (1953); W. H. Anderson and D. F. Hornig, J. Mol. Phys. 2, 49 (1959).

[9] L. Talbot and F. S. Sherman, Report No. HE-150-137, Institute of Engineering Research, University of California Berkeley (May, 1956).

TABLE I. Distance at which rarefaction overtakes shock (units, multiples of high-pressure chamber length).

M	1.34	1.55	1.84	2.24	2.86
$H_2 \rightarrow A$	2.89	2.56	2.63	2.9	3.62
$He \rightarrow A$	...	4.14($M=1.5$)	3.76	4.18($M=2$)	...
$A \rightarrow A$	16.3	17.4	22.2	...	...

apparent: First, the most convenient way to increase the shock strength was to lower the initial pressure, p_1. However, this would decrease the sensitivity of the method since the reflectivity of a shock wave is of the form[8]

$$R=(dn/d\rho)^2(1+\tan^4\theta)\,(\Delta\rho_0)^2 p_1^2 R'(p_1\lambda/L_0\cos\theta), \quad (1)$$

where n is the index of refraction, ρ the density, $\Delta\rho_0$ the density change when p_1 is one atmosphere and R' the square of the Fourier transform of dn/dx. The reflectivity declines as p_1^2 so the sensitivity of the experiment needed to be increased. Second, since $R' \rightarrow 1$ as $y=p_1\lambda/L_0\cos\theta \rightarrow \infty$, and dR'/dL_0 increases rapidly as y decreases, the accuracy of measuring L_0 could be improved by working at smaller y. This could be done conveniently by lowering p_1, which was consistent with the first objective, as well as by decreasing θ. However, a decrease in y entailed a still further loss in reflectivity. Third, it had been felt that the tilt of the shock wave from perpendicularity to the tube axis was a major source of the scatter in previous measurements. If present, this effect could be minimized by minimizing θ since both $\tan^4\theta$ and $\cos\theta$ become less sensitive to θ as θ is decreased from 90°. This change was also compatible with the previous ones. Finally, in order to obtain enough light in the earlier experiments the wavelength range included in a reflectivity measurement was very great, being defined either by Wratten filters or by the sensitivity curve of the photomultiplier tube and the source emissivity. In order to obtain more precise measurements it was felt necessary to define λ more carefully, at a still further cost in sensitivity.

The central experimental problem was therefore to increase the sensitivity of the reflectivity measurement. Consequently, the biggest change in the apparatus was to replace the tungsten source with a high-pressure mercury arc lamp. It not only emitted more usable radiation but a major portion of its output was in the line spectrum so that workable amounts of light could be obtained by isolating the 4358-A line with an interference filter. The GE AH-6 high-pressure lamp proved satisfactory but the Osram HBO 109 was much more so and was finally used. Its total output was much lower than that of the AH-6 but since its emissivity was higher more light could be put into the carefully collimated beam. It was also more convenient because it could be operated at low voltage from storage batteries (with resulting increased stability) and because it was air rather than water cooled.

Another effective factor of three was obtained by increasing the angle of divergence in the collimated beam from ±1° to ±3°. This was possible because the angle of reflection was decreased from 82° to 73°. The combined effect of these changes, together with a general elimination of scattered light in the optical system, was to make measurements possible at higher M, smaller y and very well-defined λ.

Barium titanate pressure transducers (Atlantic Research Corporation), placed approximately symmetrically on each side of the point at which reflectivity was measured, started and stopped a Berkeley timer, giving a measurement of the velocity of each shock. The rise time of the pulse from the transducers was about 15 μsec but since the pair was reasonably well matched the time was probably accurate to 2 or 3 μsec. Since the total time to traverse the 62 cm between gauges was about 800 μsec this was sufficiently precise for our purpose. The pressure was also measured with the transducers, giving us an independent measurement of the shock strength, p_2/p_1.

The shock tube was identical with that used earlier, consisting of a $2\frac{3}{4}$-in. i.d. stainless steel tube with a 60-cm long high-pressure section and 193-cm long low-pressure section. In picking the measuring point it was necessary to compromise between allowing enough distance for the formation of a stable shock front and risking catch up by the rarefaction wave. The catch up distance (in units of high pressure chamber length) for various gas combinations and shock strengths is given in Table I.

In the arrangement used in this and the earlier work one therefore expected the rarefaction to overtake the shock after approximately 1.5 meters for a $M=1.55$ shock in argon with hydrogen driver. This distance was greater than that to the point of reflectivity measurement, 1.10 meters, so at first sight this appeared satisfactory. Nevertheless, if the diaphragm bursting time amounted to as much as 500 μsec, serious trouble might arise and it seems likely in retrospect that this is what may have occurred in the $M=2.1$ shocks of Greene and Hornig.[5] To avoid this problem He was used as a driver gas in the present work.

During early tests on shocks with hydrogen as a driver, the shocks apparently were accelerating through the velocity measuring interval. This was determined by using the reflectivity pulse as a third time measurement. In some of these runs the reflectivity observed was greater than the expected limiting value, an impossible result for stable shocks. Even with He driver,

TABLE II. The thickness of shock fronts in argon.

M	No. runs	No. cal.	p_1 (atmos)	R'	σ_{L_0}	$L_0\times10^5$ cm	l_0/L_0
1.26	4	10	3	0.382	3.0%	8.37±0.41	0.0824±0.004
1.33	1	5	2	0.235	4.0%	6.95±0.45	0.0994±0.006
1.51	3	5	2	0.448	4.5%	5.06±0.36	0.137±0.010
2.38	43	50	1	0.341	2.02%	2.95±0.10	0.234±0.007

systematic differences appeared for $M=2.4$ shocks produced with the different diaphragm materials which were used. These included 0.062-in. aluminum, 0.0065-in. brass, and 0.015-in. Mylar; both scored and unscored diaphragms were used.

All of these evidences pointed to shock formation problems. In this connection it should be mentioned that a number of reflectivity pictures were obtained which showed small pulses ahead of the main one as well as others in which small pulses followed the main one. Similar phenomena appeared in the pressure transducer records. As a result the tube was lengthened and the measuring station removed another 1.37 meters (total= 2.47 meters) from the diaphragm. At this distance these phenomena disappeared and the scatter in reflectivity values was much reduced. The systematic difference between the reflectivities of shocks produced with brass and aluminum diaphragms vanished although Mylar diaphragms still yielded low reflectivities. The shocks actually used for measurement were normal in the following senses: (1) there was no evidence for acceleration or attenuation; they passed the midpoint of the velocity interval within 10 μsec of the expected time, (2) the pressure ratio, p_{21}, calculated from the velocity was more than 80% of the value calculated from the diaphragm pressure ratio, p_{41}, when ideal bursting was assumed, and (3) p_{21} calculated from the velocity agreed to better than 5% with p_{21} determined from the pressure transducers.

Except for the changes noted previously the optical system was identical with that used in earlier work. To avoid wall effects only the central portion of the shock wave, ca 1 cm high×3 cm wide, was illuminated. A Tektronix 535 oscilloscope was used to record the reflected pulses. The time constant of the photomultiplier circuit was fast compared to the rise time of the reflected pulses, about 2 μsec, so that no corrections were necessary.

EXPERIMENTAL RESULTS

At a constant angle of reflection, θ, the height of the reflected pulse on the oscilloscope trace is given for rare gases by

$$D=Kp_1^2[(M^2-1)/(M^2+3)]R'(p_1\lambda/L_0\cos\theta), \quad (2)$$

where K is a constant of the apparatus. The constant K was evaluated by measuring the reflectivity of weak shocks in the range $M=1.3$ to $M=1.6$. Ideally, this should be done for the so-called limiting case where $p_1\lambda/L_0\cos\theta\geqslant 20$ and $R'=1$, since the calibration is then independent of L. Most of the calibration shocks did not satisfy this condition but were taken at values of $p_1\lambda/L_0\cos\theta$ where R' ranged from 0.80 to 0.95 so the extrapolations were not great. The thicknesses, L_0, used to calculate R' in the calibrations were taken from Gilbarg and Paolucci,[1] using the μ proportional to $T^{1.0}$ curve which gives a good empirical fit to shock front thickness measurements in the range $M=1$ to $M=1.6$. It should be noted that because of the small extrapolation the calibration was quite insensitive to the thickness used.

In order to take account of possible drift in the intensity of the illuminating lamp, calibration shots were interspersed and usually alternated with actual measurements. In this way a mean apparatus constant $\bar{K}$ was determined for each group of measurements. The measured reflectivities were then fitted to the theoretical reflectivity

$$R'=\left(\frac{\pi^2L_0\cos\theta}{p_1\lambda}\right)^2\Big/\sinh^2\left(\frac{\pi^2L_0\cos\theta}{p_1\lambda}\right)$$

for the assumed density profile

$$\rho=\rho_0+\Delta\rho[1+\exp(-4x/L)]^{-1}$$

to find the best value of the parameter L_0. The results are summarized in Table II, where l_0 is the mean free path of the hard sphere gas having the same viscosity (0.69×10^{-5} cm at NTP).

In calculating these results we have used $\lambda=436$ mμ and $\theta_{\text{eff}}=73.5°$. The latter results from the divergence of the beam. To a good approximation

$$1+\tan^4\theta_{\text{eff}}=(2\Delta\theta)^{-1}\int_{\theta-\Delta\theta}^{\theta+\Delta\theta}(1+\tan^4\theta)\,d\theta$$
$$=(2\Delta\theta)^{-1}(\tan^3\theta/3-\tan\theta+2\theta]_{\theta-\Delta\theta}^{\theta+\Delta\theta}.$$

Since $\theta=73°$ and $\Delta\theta=3°$ (0.0524 radian), $\theta_{\text{eff}}=73.5°$.

The quantity σ_{L_0} is the estimated standard deviation for the quoted value of L_0. The estimate was based on the following considerations. All of the calibration runs behaved as members of a single population with a σ for the determination of individual values of K of 9.2%. The runs at $M=1.26$, 1.33 and 1.51 behaved as members of the same population. The standard deviation ($\sigma_{R'}$) for individual determinations of the reflectivity at $M=2.38$ was much greater, 26.5%. It

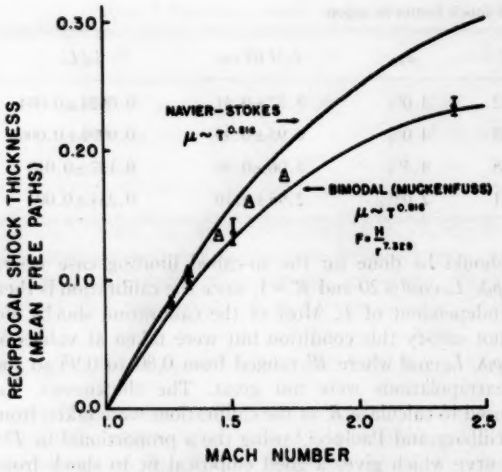

FIG. 1. Reciprocal of the thickness of shock fronts in argon, measured in mean free paths. ● Present results. △ Talbot and Sherman. Error flags represent 90% confidence levels.

then follows that the standard deviation for the determination of the average L_0 was

$$\sigma_{L_0} = (d \ln L_0/d \ln R')[(\sigma_K^2/n_K) + (\sigma_{R'}^2/n_{R'})]^{\frac{1}{2}},$$

where n_K and $n_{R'}$ are the number of calibrations and runs, respectively, included in the average. The quantity $d \ln L_0/d \ln R'$ was equal to 0.562, 0.388, 0.662, and 0.508 at $M = 1.26$, 1.33, 1.51, and 2.38. The limits given in the last two columns are the 90% confidence level. The present data together with those of footnote 5 are plotted in Fig. 1. For comparison the curves of Gilbarg and Paolucci for $\mu \sim T^{0.816}$ and the theoretical curve of Muckenfuss,[7] using an intermolecular potential which gives the correct temperature dependence of the viscosity, are also given.

DISCUSSION

It is apparent from Fig. 1 that the theoretical curve of Muckenfuss,[7] based on a bimodal distribution function, almost exactly reproduces the experimental point at $M = 2.38$ whereas the appropriate Navier-Stokes solution predicts a much thinner shock. The Zoller calculation[4] and the Burnett calculation of Sherman[5] were not included in Fig. 1 because they were carried out for the case $\mu \sim T^{1.0}$ which implies an incorrect intermolecular force law for argon. However, if it is assumed that the Burnett or Zoller corrections to the Navier-Stokes equations are about the same for $\mu \sim T^{0.816}$ as for $\mu \sim T$, they would reproduce the experimental point almost as well. Alternatively, it might be noted that at $M = 2.0$ the Burnett solution of Sherman and the bimodal solution for $\mu \sim T$ are nearly identical. These arguments can be summarized with the values of l_0/L_0 at M = 2.

Navier-Stokes[1]	$\mu \sim T^{0.816}$	0.248
Navier-Stokes[1]	$\mu \sim T$	0.224
Burnett	$\mu \sim T^{0.816}$	0.216 (estimated)
Bimodal[7]	$\mu \sim T^{0.816}$	0.203
Zoller	$\mu \sim T^{0.816}$	0.197 (estimated)
Burnett[5]	$\mu \sim T$	0.192
Bimodal[7]	$\mu \sim T$	0.191
Zoller[4]	$\mu \sim T$	0.173.

One further point which should be recognized is that Zoller found that his numerical integration diverged above $M = 2.36$ and Sherman found his solutions unstable above about $M = 3.0$, whereas bimodal solutions can be obtained over the entire range of shock strengths.

It may therefore be concluded that the Navier-Stokes equations are inadequate for shocks as strong as $M = 2.38$, but that solutions based on bimodal distribution functions are satisfactory in this region.

ACKNOWLEDGMENT

We should like to acknowledge the support given to this work by the Office of Naval Research and by a grant from the California Research Corporation.

Sublimation of Small Sodium Chloride Spheres into Argon*

D. H. WHITMORE AND J. B. MOSER

Department of Metallurgy and Materials Science, Northwestern University, Evanston, Illinois

(Received April 27, 1960)

The rate of vaporization of sodium chloride into an argon atmosphere was investigated over the temperature range 726° to 770°C using a hot-stage method to follow the change of radius of a small, subliming sodium chloride sphere. In general, the pressure and temperature behavior of the empirical rate data is consistent with the kinetic law derived by Langmuir on the basis of a model which assumes that the vaporization rate is controlled by molecular diffusion of sodium chloride vapor away from the surface of the sphere undergoing sublimation.

I. INTRODUCTION

IT was first noticed by Sresnewsky[1] that the mass rate of vaporization of a spherical droplet into still air is directly proportional to its radius and not to its surface area, a result which was subsequently confirmed by Morse[2] using solid spheres of iodine subliming from the pan of a microbalance. Langmuir[3] provided a theoretical interpretation for these observations by arguing that vaporization from a small spherical liquid droplet or solid particle into a still, inert gas atmosphere is controlled by the diffusion of vapor away from the surface analogous to the loss of heat from bodies of the same shape.

Topley and Whytlaw-Gray[4] extended Morse's experiments and derived a rate equation for this vaporization process, similar to that found by Langmuir, directly from Stefan's theory[5] for diffusion in gases. However, both Topley and Whytlaw-Gray's and Langmuir's expressions for the vaporization rate per unit area predict an infinite rate as a limiting case when either the radius of the spherical particle is progressively diminished at a constant inert gas pressure or the pressure of the inert gas within the containing vessel is diminished keeping the initial particle size fixed. Fuchs,[6] recognizing the shortcomings of the aforementioned treatments, demonstrated that these rate expressions simply represent a special case of a more general rate law which tends to the vacuum vaporization rate as the radius of the volatilizing sphere approaches the mean-free-path distance in the gas phase. There is mounting experimental evidence[7–11] supporting the correctness of the Fuchs rate equation for this condition and some attempts[12,13] have been made to extend and refine his theory by eliminating the vagueness of the model upon which it is based and defining the limits of its validity.

The principal objective of this investigation was to ascertain whether a direct observational method utilizing a hot-stage had general applicability in the study of high-temperature kinetics of the sublimation of solids. To this end, sublimation of sodium chloride into an ambient argon atmosphere was observed over a range of temperatures and argon pressures using a hot-stage technique. For the relatively large sphere sizes and ambient argon pressures (short mean free paths) encountered in the present research, significant departures from the simple Langmuir rate law should not be expected, and it is unnecessary to invoke kinetics based on more sophisticated models which incorporate the concept of diffusion boundary layers. Accordingly, the results of this study have been interpreted in the light of Langmuir's integrated rate expression[3] for the isothermal vaporization rate of a spherical particle under a constant ambient gas pressure

$$r_0^2 - r^2 = (2DMp_s/\rho RT)t,$$

where D is the diffusion coefficient of the subliming vapor in the ambient gas atmosphere, ρ is the density of the solid particle, R the gas constant, T the absolute temperature, M the molecular weight of the diffusing vapor species, p_s the equilibrium partial pressure of that species above the surface of the sphere, r_0 the initial radius of the sphere and r is its radius at any time t.

II. EXPERIMENTAL

The material used in the present investigation for the preparation of spheres was A.C.S. reagent grade sodium chloride in the form of cubic grains. These grains were crushed in an agate mortar, sized with the aid of a set of standard sieves and fused into spheres ranging from 238 to 287 μ in diameter by feeding the fractions between sieve sizes no. 60 and 45 into the three-phase carbon arc of an electric fusion furnace similar to that

* This work was partially supported by the Air Force Office of Scientific Research.

[1] B. Sresnewsky, Beibl. Ann. Physik **7**, 888 (1883).
[2] H. W. Morse, Proc. Am. Acad. Arts Sci. **45**, 363 (1910).
[3] I. Langmuir, Phys. Rev. **12**, 368 (1918).
[4] B. Topley and R. Whytlaw-Gray, Phil. Mag. **4**, 873 (1927).
[5] J. Stefan, Sitzber. Akad. Wiss. Wein, Math. natur-w. Kl. Abt. IIb. **65**, 323 (1872).
[6] N. Fuchs, Physik Z. Sowjetunion **6**, 224 (1934).
[7] R. S. Bradley, M. G. Evans, and R. Whytlaw-Gray, Proc. Roy. Soc. (London) **A186**, 368 (1946).
[8] R. S. Bradley, J. Colloid Sci. **10**, 571 (1955).
[9] J. Birks and R. S. Bradley, Proc. Roy. Soc. (London) **A198**, 226 (1949).
[10] R. S. Bradley and A. D. Shellard, Proc. Roy. Soc. (London) **A198**, 239 (1949).
[11] R. S. Bradley, Proc. Roy. Soc. (London) **A205**, 553 (1951).
[12] L. Monchick and H. Reiss, J. Chem. Phys. **22**, 831 (1954).
[13] H. L. Frisch and F. C. Collins, J. Chem. Phys. **20**, 1797 (1952).

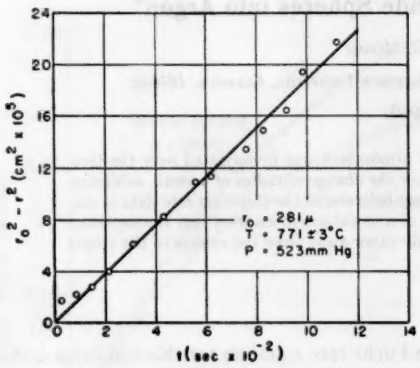

FIG. 1. Variation of $(r_0^2-r^2)$ with time for a typical sublimation run.

described by Kingery and Berg.[14] A slow stream of purified argon gas was continuously passed through the furnace chamber during the spheroidizing operation. The spheres were then hand checked for sphericity and only the most perfect specimens were selected for sublimation runs.

A high-temperature microstage furnace[14,15] was constructed to facilitate observation of the radius of the sphere of sodium chloride *in situ* during the course of the sublimation experiment. The electrical heating element of the hot stage was fabricated from a platinum-40% rhodium rod, 3 mm in diameter, so as to have a central groove about 2 mm deep and 1.5 mm wide. Compared with the diameter of the sodium chloride sphere, the heater groove was relatively deep and functioned as a "spoiler" for natural convection currents within the gas phase in the vicinity of the sublimation specimen. The absence of such convection currents permitted the assumption that the vaporization rate is controlled by molecular diffusion of sodium chloride vapor away from the surface of the subliming sphere. The heater was supported by two heavy copper electrode posts and a fine-wire, platinum-10% rhodium thermocouple was placed at each end of the heater groove, one serving as a monitoring couple and the other as a control couple. Power to the heater was supplied from a voltage stabilizer and an autotransformer, and a saturable reactor temperature controller operating in conjunction with the control thermocouple kept the temperature of the sample within ±3°C of the control temperature during a sublimation run.

The microstage furnace chamber was connected directly to a pumping system, capable of maintaining pressures of about 10^{-5} mm Hg, which consisted of a 2-in. oil diffusion pump backed by a mechanical vacuum pump. Purified argon gas could be introduced into the heating chamber at any desired pressure up to 2 atm, to serve as a static atmosphere during the sublimation experiment. Pressure readings of the argon atmosphere were taken to the nearest millimeter with the aid of an open-tube, mercury manometer. The specimen temperature was measured by means of a potentiometer and the monitoring thermocouple positioned within the heater groove; this thermocouple was initially calibrated by noting the emf corresponding to the observed melting point of several pure materials on the hot-stage heater and was likewise calibrated against the melting point of sodium chloride at the completion of each run.

The radius of the subliming sphere was measured with a vertically-mounted metallurgical microscope, equipped with a Filar eyepiece, which was focused on the specimen through the quartz window of the hot-stage. An internal shutter, operated through an O-ring seal by means of an external handle, served to prevent the fogging of the hot-stage window with condensed sodium chloride by being positioned directly below the window except at the actual times of observation. The usual magnification employed was 160× and this was periodically calibrated with the aid of a stage micrometer. It was estimated that the theoretical resolution of this optical system is somewhat less than 1 μ.

TABLE I. Values of the diffusion coefficient for sodium chloride vapor in argon computed from experimental data.

Temperature, °K	Gas pressure dynes/cm^2×10^{-6}	Slope, $\Delta(r_0^2-r^2)/\Delta t$ cm^2/sec×10^6	Diffusion coeff., D cm^2/sec
999±3	0.224	16.45	3.53
	0.224	16.73	3.59
	0.267	14.13	3.03
	0.267	15.58	3.34
	0.341	12.93	2.78
	0.356	12.06	2.59
	0.446	10.00	2.15
	0.446	9.74	2.09
	0.669	6.34	1.36
	0.687	6.70	1.44
	1.320	3.94	0.85
	1.330	4.35	0.93
1020±3	0.268	27.70	3.64
	0.283	22.70	2.98
	0.352	20.80	2.73
	0.358	19.77	2.59
	0.440	16.41	2.15
	0.440	15.10	1.98
	0.440	14.20	1.86
	0.675	12.18	1.60
	0.675	11.71	1.54
	1.335	5.10	0.67
	1.340	7.70	1.01
	1.340	5.75	0.76
1043±3	0.207	56.60	4.05
	0.430	26.40	1.88
	0.698	19.20	1.37
	0.830	13.69	0.98
	1.015	8.89	0.64
	1.274	8.16	0.58
	2.120	4.17	0.30

[14] W. D. Kingery and M. Berg, J. Appl. Phys. **26**, 1205 (1955).
[15] J. B. Moser and D. H. Whitmore, J. Appl. Phys. **31**, 488 (1960).

Following placement of the sodium chloride sphere on the heater, the stage was closed, evacuated, flushed with argon, re-evacuated and then filled with purified argon to some desired pressure. The specimen was heated in a matter of seconds to the sublimation temperature, maintained at that temperature by the controller, and microscopic measurements of its radius were made at frequent intervals over a total time period dictated by the experimental conditions (pressure and temperature) employed. To gain confidence in the experimental procedure described above, some preliminary measurements of the vacuum rate of sublimation of potassium chloride were made which compared favorably with those determined by Bradley and Volans[16] using a quartz microbalance technique.

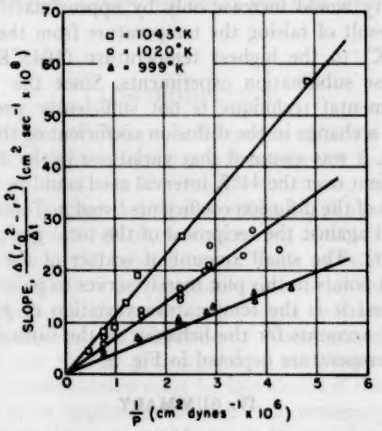

FIG. 2. Dependence of the slope values on the reciprocal of the total gas pressure for three sets of isothermal data.

When a solid particle undergoes sublimation, the latent heat of vaporization is lost by the specimen and the volatilizing particle self-cools, thereby lowering its sublimation rate. In the steady state, heat is transferred to the subliming particle from its environment at a rate which exactly balances the rate heat is lost by sublimation. Because of inherent difficulties associated with any calculation of the rate at which heat is transferred from its surroundings to a particle resting on the heater of a hot-stage at an elevated temperature, only a crude estimate of the effect of self-cooling on the sublimation rate was attempted here. Following the method outlined by Birks and Bradley[9] for calculating the self-cooling correction, estimates of the magnitude of this correction indicate that even the largest values (for lowest gas pressures) would decrease the observed sublimation rates by negligible amounts.

III. RESULTS AND DISCUSSION

It is apparent from the aforementioned Langmuir integrated rate expression, relating the radius of a subliming particle to time, that a plot of $(r_0^2 - r^2)$ against t should result in a straight line of slope equal to $2DMp_s/\rho RT$.[17] When the data from a typical subli-

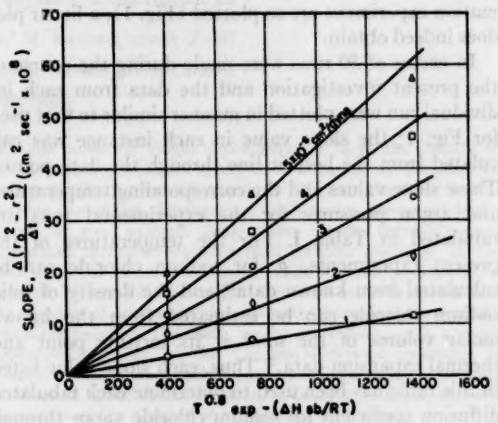

FIG. 3. Temperature dependence of the isobaric slope values. The appropriate reciprocal pressure value is indicated on each curve.

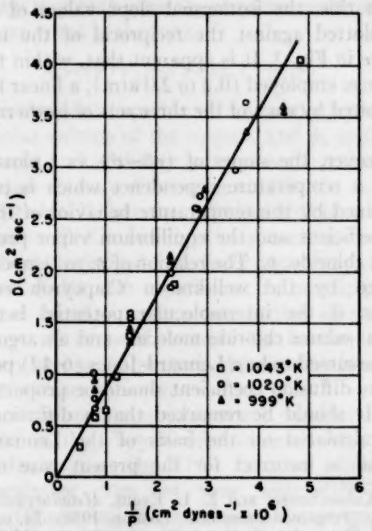

FIG. 4. Variation of the diffusion coefficient of sodium chloride vapor in argon with the reciprocal of the pressure.

[16] R. S. Bradley and P. Volans, Proc. Roy. Soc. (London) **A217**, 508 (1953).

[17] Since it has been well established that polymeric species (~36% dimers) are present in the sodium chloride vapor in equilibrium with the solid phase,[18,19] there is some uncertainty concerning the selection of a value for M, the molecular weight of the diffusing vapor species. Since in the present investigation the sodium chloride vapor is highly diluted with argon, collisions between sodium chloride molecules are extremely rare events, so that it seems reasonable to assume that the monomeric species is predominant and a value for M of 58.454 was accordingly selected.

[18] J. Berkowitz and W. A. Chupka, J. Chem. Phys. **29**, 653 (1958).

[19] R. C. Miller and P. Kusch, J. Chem. Phys. **25**, 860 (1956).

mation experiment are so plotted (Fig. 1), a linear plot does indeed obtain.

In excess of 30 runs were made during the course of the present investigation and the data from each individual run were plotted in manner similar to that used for Fig. 1; the slope value in each instance was calculated from the best-fit line through the data points. These slope values and the corresponding temperatures and argon pressures for the experimental runs are tabulated in Table I. For the temperatures of the present experiments, p_s for sodium chloride can be calculated from known data[20] and the density of solid sodium chloride can be estimated from the known molar volume of the solid at its melting point and thermal expansion data.[21] Thus, each slope value listed in this table has been used to determine each tabulated diffusion coefficient for sodium chloride vapor through argon at the specified temperature and pressure.

Since the diffusion coefficient for sodium chloride vapor appears in the numerator of the slope expression for $(r_0^2-r^2)$ vs t plots and is the only strongly pressure dependent quantity therein, the slope values listed in Table I should be inversely proportional to the total gas pressure because the diffusion coefficient is known to be inversely related to the total gas pressure.[22] To confirm this, the isothermal slope values of Table I were plotted against the reciprocal of the total gas pressure in Fig. 2. It is apparent that, within the pressure range employed (0.2 to 2.0 atm), a linear behavior is exhibited by each of the three sets of isothermal data plotted.

Moreover, the slopes of $(r_0^2-r^2)$ vs t plots should exhibit a temperature dependence which is primarily determined by the temperature behavior of the diffusion coefficient and the equilibrium vapor pressure of sodium chloride, p_s. The relation of p_s to temperature is provided by the well-known Clapeyron equation; whereas, if the intermolecular potential between a gaseous sodium chloride molecule and an argon molecule is assumed to be a Lennard-Jones (6–12) potential, then the diffusion coefficient should be proportional to $T^{1.8}$.[23] It should be remarked that a diffusion coefficient calculated on the basis of the Lennard-Jones potential is incorrect for the present case of polar molecules (NaCl) diffusing in a nonpolar gas (A); rather, these coefficients should be calculated on the basis of the Stockmayer potential.[24] Nevertheless, a diffusion coefficient computed using a Stockmayer intermolecular potential would also be related to $T^{1.8}$.[25] Thus, taking into account the factor T in the denominator of the slope expression, the Clapeyron relation between the saturation vapor pressure and temperature and the $T^{1.8}$ dependence of the diffusion coefficient, the slope of $(r_0^2-r^2)$ vs t plots should be proportional to $T^{0.8}\exp-(\Delta H_{sb}/RT)$ where ΔH_{sb} is the heat of sublimation of sodium chloride. The linearity of these plots provides further support for the essential correctness of the sublimation model employed here.

Using the aforementioned temperature dependence for the diffusion coefficient, it may be shown that this quantity would increase only by approximately 6.7% as a result of raising the temperature from the lowest (999°K) to the highest temperature (1043°K) used in these sublimation experiments. Since the present experimental technique is not sufficiently precise to detect a change in the diffusion coefficient of this magnitude, it was assumed that variations in the diffusion coefficient over the 44°K interval used could be ignored and all of the diffusion coefficients listed in Table I were plotted against the reciprocal of the total gas pressure (Fig. 4). The small amount of scatter of the experimental points in this plot merely serves to point up the fact that it is the temperature variation of p_s which largely accounts for the behavior of the isobaric slope with temperature depicted in Fig. 3.

IV. SUMMARY

Through a study of the sublimation of sodium chloride in the presence of argon gas, the present investigation has demonstrated the feasibility of utilizing a direct observational, hot-stage technique for kinetic studies of high-temperature sublimation phenomena. For the relatively large sphere sizes and ambient argon pressures employed, deviations from the Langmuir kinetic law which neglects diffusion boundary layer effects should be negligible, an expectation which was largely substantiated by the observed rate data of this study. Values of the diffusion coefficient of sodium chloride vapor into argon calculated from the empirical rate data with the aid of the Langmuir parabolic rate equation are of the correct magnitude for the temperatures and pressures encountered.

[20] O. Kubaschewski and E. L. Evans, *Metallurgical Thermochemistry* (Pergamon Press Ltd., London, 1956), 2d. ed.

[21] J. C. Slater, *Introduction to Chemical Physics* (McGraw-Hill Book Company, Inc., New York, 1939).

[22] S. Chapman and T. G. Cowling, *The Mathematical Theory of Non-Uniform Gases* (Cambridge University Press, Cambridge, 1952), 2d. ed.

[23] R. B. Bird, W. E. Steward, and E. N. Lightfoot, *Notes on Transport Phenomena* (John Wiley & Sons, Inc., New York, 1958).

[24] W. H. Stockmayer, J. Chem. Phys. **9**, 398 (1941).

[25] J. O. Hirschfelder, C. F. Curtiss, and R. B. Bird, *Molecular Theory of Gases and Liquids* (John Wiley & Sons, Inc., New York, 1954).

Theory of Dilute High Polymer Solutions. II

W. R. KRIGBAUM, D. K. CARPENTER,* M. KANEKO, AND A. ROIG†

Department of Chemistry, Duke University, Durham, North Carolina

(Received July 20, 1959)

The second virial coefficient is calculated according to the smoothed distribution method. Our treatment differs from those of Flory-Krigbaum and Isihara-Koyama through inclusion of the numerous short-range intramolecular contacts arising by virtue of the connected nature of the chain. The result is to replace the previous $F(X)$ by $F(X, \rho)$, where the parameter ρ depends upon the ratio of the total number of intramolecular contacts to the number of long-range contacts counted using a radial segment distribution. The number of intermolecular contacts created when two molecules overlap is estimated by the use of an additional smoothed radial segment distribution which is assumed to be uniformly expanded by intramolecular excluded volume effects.

Comparison with experiment reveals that both the temperature and molecular weight dependences of A_2 in the vicinity of the theta temperature are described in a reasonably quantitative fashion by the present treatment. In this case there are no adjustable parameters. Furthermore, satisfactory agreement is observed for good solvents using values for the thermodynamic interaction parameter deduced from intrinsic viscosity. In the limit $\rho=1$ the present treatment yields a result equivalent to those of *FK* and *IK*. We conclude that the latter underestimate the number of intramolecular contacts through neglect of the connected nature of the chain. In the other limit, $\rho=0$, a result approximating that of the Casassa-Markovitz treatment is obtained. We believe that their assumption of a spherical segment distribution about the initial point of contact results in an overestimation of the number of intermolecular contacts.

I. INTRODUCTION

TWO approaches have been employed in the treatment of dilute polymer solutions.[1] One of these, the method of molecular distribution functions, was first applied to polymer solutions by Zimm.[2] The result of this calculation is an alternating series, of which Zimm obtained only the second term. Much more recently Albrecht[3] obtained an approximate form for the third term, which was subsequently improved by the calculations of Kurata and Yamakawa.[4] Unfortunately, the series is not rapidly convergent, so that some rather drastic simplifications must be introduced if the treatment is to be applicable to other than extremely weak interactions. Casassa and Markovitz[5] have investigated the latter possibility by replacing the distribution function for the x segments by products of independent pair distribution functions. After some further simplifications they were able to obtain an expression for the second virial coefficient in closed form.

A second approach involves the treatment of a smoothed segment distribution. Here the approximations are introduced at the outset, and the mathematical operations can be carried out rigorously to yield the final result in closed form. The success of such a treatment will depend upon the degree to which the smoothed distribution represents the actual number of segment-segment contacts. This procedure was first investigated by Flory,[6] who took as his model a sphere of uniform segment density. Somewhat later Flory and Krigbaum[7,8] treated a smoothed segment distribution of Gaussian form, and still more recently Isihara and Koyama[9] performed the calculation using the exact radial distribution for a random flight chain.

The results of both general procedures outlined above may be expressed in the form:

$$A_2=(\bar{v}^2/V_1)\psi_1(1-\Theta/T)F(X), \qquad (1)$$

where $\bar{v}$ is the partial specific volume of the polymer, V_1 is the molar volume of the solvent, and ψ_1 and $\psi_1\Theta/T$ are entropy and enthalpy parameters,[10] respectively. The treatments may differ somewhat in the definition of the variable X, but the principal difference occurs in the factor $F(X)$. Ideally, the success of each procedure should be judged by a direct confrontation of the theoretical $F(X)$ with experiment. In practice, such a comparison usually involves some further assumptions, because in all cases of interest the interactions are sufficiently strong to perturb the distribution of the segments within a molecule.

Even when such reservations are considered, comparison[11,12] of the Flory-Krigbaum result with experiment indicates that the $F(X)$ function arising from their treatment does not vary sufficiently rapidly with X. Isihara and Koyama's treatment[9] employing the correct radial distribution function yields essentially the same $F(X)$ function as that deduced by Flory and Krigbaum. On the other hand, the $F(X)$ function deduced by Casassa and Markovitz[5] varies

* Present address: Department of Chemistry, Georgia Institute of Technology, Atlanta, Georgia.

† Present address: Department of Chemistry, Massachusetts Institute of Technology, Cambridge, Massachusetts.

[1] For the preceding paper of this series, see D. K. Carpenter and W. R. Krigbaum, J. Chem. Phys. **28**, 513 (1958).

[2] B. H. Zimm, J. Chem. Phys. **14**, 164 (1946).

[3] A. C. Albrecht, J. Chem. Phys. **26**, 1002 (1957).

[4] M. Kurata and H. Yamakawa, J. Chem. Phys. **29**, 311 (1958).

[5] E. F. Casassa and H. Markovitz, J. Chem. Phys. **29**, 493 (1958).

[6] P. J. Flory, J. Chem. Phys. **13**, 453 (1945).

[7] P. J. Flory, J. Chem. Phys. **17**, 1347 (1949).

[8] P. J. Flory and W. R. Krigbaum, J. Chem. Phys. **18**, 1086 (1950).

[9] A. Isihara and R. Koyama, J. Chem. Phys. **25**, 712 (1956).

[10] P. J. Flory and W. R. Krigbaum, Ann. Rev. Phys. Chem. **2**, 383 (1951).

[11] W. R. Krigbaum and P. J. Flory, J. Am. Chem. Soc. **75**, 5254 (1953).

[12] W. R. Krigbaum, J. Am. Chem. Soc. **76**, 3758 (1954).

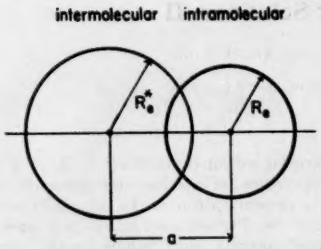

FIG. 1. Schematic diagram of the two equivalent spheres used to compute the excluded volume.

much more strongly with X than those mentioned above and, in fact, when compared with experiment in the same manner, it appears to decrease too rapidly with X. This treatment has subsequently been modified in two respects. Casassa[13] effected some improvement by introducing a correction for intermolecular excluded volume effects, but this did not suffice to bring about agreement with experiment. The most satisfactory result yet obtained by the molecular distribution function approach is due to Ptitsyn and Eizner,[14] who modified the Casassa-Markovitz treatment of intramolecular excluded volume effects.

In the preceding paper of this series,[1] a further examination of the equivalent sphere model demonstrated that the function $F(X)$ is quite insensitive to the particular form of the radial distribution function chosen to represent the smoothed segment distribution. The same conclusion was reached by Casassa and Markovitz[5] through a comparison of the results of the *F-K* and *I-K* treatments. This observation implies that the principal factor responsible for the discrepancy between observation and the theoretical $F(X)$ deduced by *F-K* and *I-K* is their use of a *spherically symmetrical* distribution about the center of gravity of the molecule. Due to its failure to consider the connected nature of the chain, such a function leads to an unrealistically small number of intramolecular contacts. In this paper we repeat the smoothed distribution treatment using a model which permits the inclusion of intramolecular contacts of short range.

II. EXCLUDED VOLUME

The volume, u, excluded to a pair of molecules is

$$u=\int_0^\infty [1-\exp(-\Delta F_a/kT)]4\pi a^2 da, \qquad (2)$$

where ΔF_a is the free energy change involved when the two molecules approach one another until their centers are separated by a distance a. The evaluation of ΔF_a requires a knowledge of the increase in the average number of segment-segment contacts on overlap.

The counting of intramolecular contacts can be performed in two ways. If all of the sites in the molecular domain are sampled, as in the treatments of *FK* and *IK*, the computed density of occupied sites will be relatively low. Thus the expected number of segment-segment contacts, N_{22}^*, will be relatively small. On the other hand, if only the sites in the immediate vicinity of the chain segments are sampled, the average segment density is considerably larger, resulting in a larger number of intramolecular contacts, N_{22}. This difference arises from the inclusion of the numerous "short-range" contacts in the latter procedure. An asterisk will be used throughout this paper to indicate that the first type of counting process, involving only long-range contacts, has been used. In counting the increase in the number of contacts when two molecules overlap we may again sample the nearest-neighbor sites of one of the chains, say α. However, in this case we know only the distance of the test volume from the center of gravity of the second molecule, β. Since the test volume moves over an arbitrary portion of the domain of molecule β, we may expect to encounter an average density of β segments which corresponds more closely to that obtained by the first of the two counting procedures described above. Thus, we propose to include short-range contacts when counting intramolecular contacts for both molecules, but to consider only long-range intermolecular contacts.

To perform this calculation we examine a volume element, δV, consisting of nearest-neighbor sites of chain α. If the effective volume fraction of α segments in this region is ϕ_α, then the number of α segments within the volume element will be $\delta V(\mathbf{N}/V_1)\phi_\alpha$, where V_1 is the molar volume of the solvent (or the polymer segments) and $\mathbf{N}$ is Avogadro's number. Now let molecule β approach to within a distance a, and represent the effective volume fraction of β segments in δV by ϕ_β^*. The number of new (intermolecular) contacts created will be $\delta V(\mathbf{N}/V_1)\phi_\alpha\phi_\beta^*$. We may replace each of the two distributions used to count intra- and intermolecular contacts by an equivalent sphere having a uniform segment probability, ϕ or ϕ^*, appropriately chosen to give the correct number of contacts for a chain of x segments, i.e., $\phi=(2/\gamma)(N_{22}/x)$ and $\phi^*=(2/\gamma)(N_{22}^*/x)$, where γ is the average number of nearest neighbors about a segment. Since x is fixed, the radius of the equivalent sphere, R_s or R_s^*, is adjusted to give the desired segment probability, e.g.

$$\phi=(\bar{v}M/\mathbf{N})/(4\pi R_s^3/3), \qquad (3)$$

where $\bar{v}$ is the partial specific volume of the polymer and M is its molecular weight. The problem thus reduces to the overlapping of two spheres of different size, as shown schematically in Fig. 1. The result for the volume element δV can now be summed over the entire volume, V_J, jointly occupied by the two spheres when their centers are separated by a distance a. The

[13] E. F. Casassa, J. Chem. Phys. **31**, 800 (1959).
[14] O. B. Ptitsyn and Yu. E. Eizner, Vysokomolekulyarnye Soedineniya **1**, 1200 (1959).

TABLE I. Values of $F(X, \rho)$.

X \ ρ	1.0	0.9	0.8	0.6	0.5	0.4	0.3	0.2	0.1
−1	1.18973	1.22565	1.26638	1.36081	...	1.46986	1.52880	1.59011	1.65333
0.5	0.92445	0.91348	0.90157	0.87542	0.86141	0.84695	0.83214	0.81720	0.80196
1	...	...	0.81994	0.77597	0.75275	0.72897	0.70482	0.68049	0.65616
2	...	...	0.69298	0.62905	0.59611	0.56289	0.52965	0.49663	0.46409
3	...	...	0.59962	0.52742	0.49101	0.45475	0.41894	0.38383	0.34966
4	...	...	0.52853	0.45383	0.41685	0.38037	0.34478	0.31027	0.27705
5	...	...	0.47278	0.39841	0.36210	0.32675	0.29246	0.25956	0.22825
6	...	...	...	0.35529	0.32026	0.28639	0.25387	0.22289	0.19368
7	...	...	...	0.32083	0.28728	0.25506	0.22435	0.19528	0.16801

number of intermolecular contacts is then given by $(N V_J/V_1)\phi\phi^*$, hence

$$\Delta F_e = 2kT\psi_1(1-\Theta/T)(N V_J/V_1)\phi\phi^*. \quad (4)$$

For spheres of unequal size separated by the distance a, the joint volume, V_J, may be expressed in terms of the parameter $y=a/2R_e^*$ as follows:

$$V_J = (4\pi R_e^{*3}/3)\Upsilon\rho^3, \quad (5)$$

where

$$\Upsilon = (1/4\rho^3)[2y^3-3(1+\rho^2)y+2(1+\rho^3)-3(1-\rho^2)^2/8y], \quad (6)$$

and

$$\rho = R_e/R_e^* = (N_{22}^*/N_{22})^{1/3}. \quad (7)$$

This definition of Υ makes comparison with the earlier treatments convenient, since

$$\Delta F_e/kT = X\Upsilon, \quad (8)$$

where X is the variable used previously[1,7,8]

$$X = (2\bar{v}M/V_1)\psi_1(1-\Theta/T)\phi^*. \quad (9)$$

From Eqs. (2) and (8) there is obtained, after transformation to the variable $y=a/2R_e^*$,

$$u = (4\pi R_e^{*3}/3)\int_0^{(1+\rho)/2} 24(1-e^{-X\Upsilon})y^2dy.$$

In the present case it is advantageous to consider separately the range of y values from zero to $(1-\rho)/2$ and from $(1-\rho)/2$ to $(1+\rho)/2$. Within the former interval the smaller sphere is completely overlapped, so that $V_J=\rho^3(4\pi R_e^{*3}/3)$ and $\Upsilon=1$

$$u = (4\pi R_e^{*3}/3)\left\{\int_0^{(1-\rho)/2} 24(1-e^{-X})y^2dy + \int_{(1-\rho)/2}^{(1+\rho)/2} 24(1-e^{-X\Upsilon})y^2dy\right\}.$$

Evaluation of the first integral gives $(1-\rho)^3(1-e^{-X})$. Upon integrating the second integral by parts, the first term exactly cancels the contribution from the first integral, and we have as a remainder

$$u = -(4\pi R_e^{*3}/3)(6X/\rho^3)\int_{(1-\rho)/2}^{(1+\rho)/2} e^{-X\Upsilon} \times[2y^5-(1+\rho^2)y^3+(1-\rho^2)^2y/8]dy.$$

The second virial coefficient, A_2, which is given by $Nu/2M^2$, therefore becomes

$$A_2 = (\bar{v}^2/V_1)\psi_1(1-\Theta/T)F(X,\rho), \quad (10)$$

where

$$F(X,\rho) = -(6/\rho^3)\int_{(1-\rho)/2}^{(1+\rho)/2} e^{-X\Upsilon} \times[2y^5-(1+\rho^2)y^3+(1-\rho^2)^2y/8]dy. \quad (11)$$

When $\rho=1$ this reduces to the expression which we have previously examined[1] and shown to be indistinguishable from the $F(X)$ function appearing in the FK treatment. The integral appearing in Eq. (11) was evaluated numerically for other values of ρ using an IBM 650.[15] For each summation the range was divided into 80 equal intervals. Values of $F(X, \rho)$ so obtained appear in Table I. We observe that as ρ decreases from unity, due to the inclusion of short range intramolecular contacts, the dependence of $F(X, \rho)$ upon X becomes more pronounced.

III. THE NUMBER OF INTRAMOLECULAR CONTACTS

As indicated above, the number of intramolecular contacts can be counted in two ways. In the preceding paper[1] we showed that for a segment distribution having radial symmetry the effective segment density, ϕ_0^*, could be calculated as follows:

$$\phi_0^* = \left(\frac{4\pi x V_1}{N}\right)\int_0^\infty [W(R)R]^2dR. \quad (12)$$

In this and the following equations the subscript zero denotes reference to a random flight chain without excluded volume effects. Upon representing the dis-

[15] The authors are indebted to Professor T. M. Gallie of the Duke University Computing Laboratory for his assistance with the programing of the numerical computations.

TABLE II. The ratio $(N_{22})_0/(N_{22}^*)_0$.

x	$(N_{22})_0/(N_{22}^*)_0$	x	$(N_{22})_0/(N_{22}^*)_0$
2	0.00000	20	1.4475
3	0.0786	30	2.0324
4	0.1731	50	2.9826
5	0.2703	100	4.7577
10	0.7221	1000	18.116[a]

[a] Evaluated according to Eq. (20).

tribution of the x segments having mean-square length b^2 by a simple Gaussian function normalized to yield the correct mean-square radius of gyration, $\langle R_0^2\rangle_{Av}=xb^2/6$, i.e.,

$$W_0(R)=[3/2\pi\langle R_0^2\rangle_{Av}]^{\frac{3}{2}}\exp[-3R^2/2\langle R_0^2\rangle_{Av}], \quad (13)$$

the number of intramolecular contacts is found to be

$$(N_{22}^*)_0=(\gamma V_1/2\mathrm{N})(9/2\pi b^2)^{\frac{3}{2}}x^{\frac{3}{2}}, \quad (14)$$

where γ is the number of nearest neighbors about a segment. If this counting procedure is used for both intra- and intermolecular contacts, then $\rho=1$ and Eq. (11) reduces to

$$F(X)=12\int_0^1\exp[-X(y^3-3y+2)/2](1-y^2)y^3dy, \quad (15)$$

which is equivalent to the FK result. In the IK treatment, Eq. (13) is replaced by the exact radial distribution function for a random flight chain; however, this only increases $(N_{22}^*)_0$ by the relatively trivial factor 1.22. It is evident that both of these counting procedures omit the short range intramolecular contacts, since the connected nature of the chain is lost when the segment distribution is represented by $W_0(R)$.

The second procedure starts with the probability that segments j and k will be separated by a distance $\mathbf{r}_{jk}$[16]:

$$W(\mathbf{r}_{jk})=(3/2\pi tb^2)^{\frac{3}{2}}\exp(-3\mid\mathbf{r}_{jk}\mid^2/2tb^2) \quad (16)$$

where $t=\mid j-k\mid$. The probability that links j and k overlap may then be calculated through use of the three-dimensional Dirac delta function, or it may be obtained directly from Eq. (16) upon setting $\mathbf{r}_{jk}=0$

$$P_{jk}=(3/2\pi tb^2)^{\frac{3}{2}}. \quad (17)$$

The number of intramolecular contacts may then be obtained as follows

$$(N_{22})_0=(\gamma V_1/2\mathrm{N})\sum_{j=1}^{N-2}\sum_{k=3}^{N}P_{jk}. \quad j\neq k \quad (18)$$

We expect this result to be larger than that given by Eq. (14), which omitted short-range contacts. The ratio of these two numbers is

$$(N_{22})_0/(N_{22}^*)_0=(2/3^{\frac{3}{2}})\{x^{\frac{3}{2}}\sum_{t=2}^{x-1}t^{-\frac{3}{2}}-x^{-\frac{3}{2}}\sum_{t=2}^{x-1}t^{-\frac{1}{2}}\}. \quad (19)$$

The two series were directly summed through $x=100$ with the results given in Table II. An asymptotic form for x large, obtained upon summing through $x=99$ and approximating the remainders by integrals from 99.5 to $x-0.5$, is as follows:

$$(N_{22})_0/(N_{22}^*)_0=0.621x^{\frac{1}{2}}-1.540. \quad (20)$$

In Fig. 2 the asymptotic relation is compared with the values obtained by direct summation. Evidently the convergence to the asymptotic form is quite rapid, so that Eq. (20) will be applicable in all cases of practical interest.

In the foregoing we have taken as our model an unperturbed random flight chain, but now we must introduce some assumption concerning the perturbation of the segment distribution due to the thermodynamic interactions. Since N_{22}^* consists exclusively of long-range interactions, it should depend strongly upon the average molecular dimensions. If we introduce the simplest assumption, that the spherically symmetrical distribution is uniformly expanded in each dimension by a factor α as a result of interactions, then the number of contacts for the perturbed spherically symmetrical distribution becomes

$$N_{22}^*=(N_{22}^*)_0/\alpha^3, \quad (21)$$

where $(N_{22}^*)_0$ is given by Eq. (14). Recalling that $\phi^*=(2/\gamma)(N_{22}^*/x)$, we obtain from Eqs. (14) and (21)

$$\phi^*=(\bar{v}/\mathrm{N}M^{\frac{1}{2}})(9M/2\pi\langle L_0^2\rangle_{Av})^{\frac{3}{2}}(1/\alpha^3), \quad (22)$$

where $\langle L_0^2\rangle_{Av}=xb^2$ is the unperturbed mean-square displacement length of the chain. We now may demonstrate that X as defined by Eq. (9) is the same variable appearing in the FK treatment by combining Eqs.

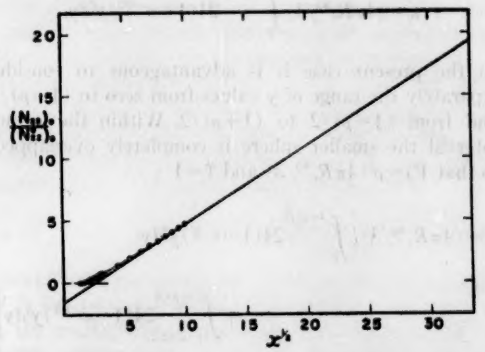

FIG. 2. The ratio of the number of intramolecular contacts for the distribution with correlations and for a spherically symmetrical segment distribution vs the square root of the number of chain links.

[16] S. Chandrasekhar, Revs. Modern Phys. 15, 1 (1943).

(9) and (22) to obtain

$$X=(2/\alpha^3)(\bar{v}^2/\mathrm{N}V_1)(9M/2\pi\langle L_0^2\rangle_{\mathrm{av}})^{\frac{1}{2}}\psi_1(1-\Theta/T)M^{\frac{1}{2}}. \tag{23}$$

Turning to the effect of a perturbation of the mean molecular dimensions on the number of intramolecular contacts, we recall that these are predominantly short-range interactions. Thus, it seems reasonable to suppose that N_{22} will not be greatly affected by excluded volume effects. If we take as an upper limit $N_{22}=(N_{22})_0$, then from Eq. (7) and Table II $\rho=0.381/\alpha$ for $x=10^3$. A much less probable lower limit is obtained upon setting $N_{22}=(N_{22})_0/\alpha$, so that $\rho=0.381$ for $x=10^3$. Fortunately, as will be shown in the next section, the $F(X,\rho)$ function is not very sensitive to this choice.

IV. COMPARISON WITH EXPERIMENT

A successful treatment of the second virial coefficient should be capable of representing both the observed temperature and molecular weight dependence of A_2. Since all of the results may be cast in the same form, we need only compare the diverse F functions. The quantities needed for this comparison are $[\langle L_0^2\rangle_{\mathrm{av}}/M]$, which is characteristic of the polymer under consideration, the thermodynamic parameters ψ_1 and Θ characteristic of the polymer-solvent system, and the values of M and α^2 pertaining to the particular sample investigated. In principle, all of these parameters could

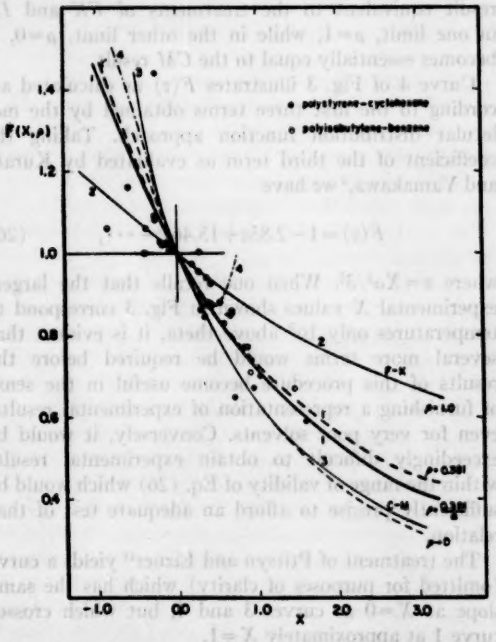

FIG. 3. A comparison of the experimental temperature dependence of $F(X)$ near the theta temperature with the predictions of several theoretical treatments (see text).

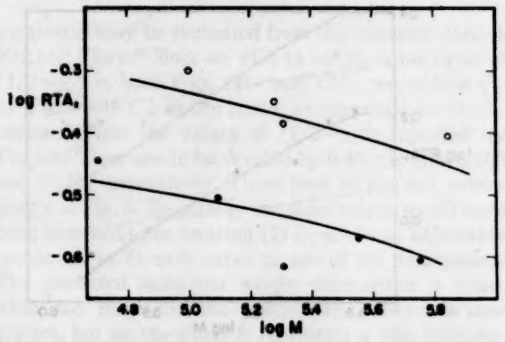

FIG. 4. The theoretical molecular weight dependence of A_2 compared with that observed for polyisobutylene-benzene at 40° (○), and for polystyrene-cyclohexane at 50° (●).

be evaluated by light scattering measurements performed at several temperatures near theta. Since most of the A_2 values we shall use were determined osmotically, we must refer to other data for the values of $[\langle L_0^2\rangle_{\mathrm{av}}/M]$ and α. We shall take the former from light scattering data, and for the latter we will employ the values calculated according to the Fox-Flory[17] treatment of intrinsic viscosity. Thus, we assume that $\alpha^3=[\eta]/[\eta]_\Theta$, and that the molecular weight dependence of α can be represented with sufficient precision by

$$\alpha^5-\alpha^3=2C_M\psi_1^{\eta}(1-\Theta/T)M^{\frac{1}{2}}, \tag{24}$$

where ψ_1^{η} is the value deduced from viscosity data. Our use of ψ_1^{η} and C_M in this calculation corresponds, in effect, to the utilization of the viscosity data of Fox and Flory, and says nothing about the relative merits of the value of the constant, C_M, appearing in the Fox-Flory treatment or the modified value, C_M' suggested by Stockmayer.[18] Indeed, if we wished to calculate α using the values of ψ_1 and Θ deduced osmotically, then for the two systems we shall examine the latter would be a better choice, as Stockmayer has already pointed out.[18]

Our first test concerns the temperature dependence of A_2 near theta as determined for the polyisobutylene-benzene system through osmotic measurements,[11] and for the polystyrene-cyclohexane system by osmotic pressure[12] and light-scattering data.[19] For a given temperature, $F(X,\rho)$ will depend upon molecular weight through both factors, X and ρ. The latter is relatively minor, and in the interests of simplicity we will suppress this dependence by assuming an average value, $x=10^3$, for the calculation of ρ. A comparison of the experimental and theoretical $F(X)$ functions

[17] P. J. Flory and T. G. Fox, Jr., J. Am. Chem. Soc. 73, 1904 (1951).

[18] W. H. Stockmayer, J. Polymer Sci. 15, 595 (1955).

[19] W. R. Krigbaum and D. K. Carpenter, J. Phys. Chem. 59, 1166 (1955).

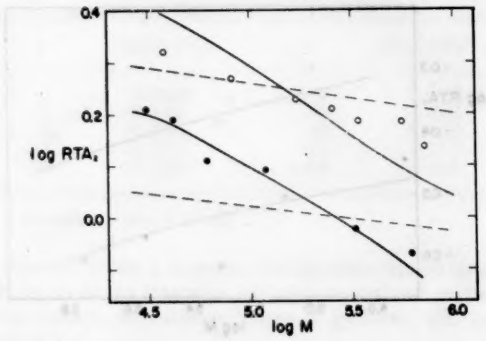

FIG. 5. Comparison of the molecular weight dependence of A_2 observed at 30° for polyisobutylene-cyclohexane (○) and polystyrene-toluene (●) with that predicted by the present treatment (full curves) and by the Flory-Krigbaum treatment (dashed lines).

appears in Fig. 3. The experimental points were obtained from the observed A_2 values in accordance with Eqs. (10) and (23), making use of the ψ_1 and Θ values determined osmotically and the α values calculated as described above. Full curve 1 represents the theoretical $F(X, \rho)$ values calculated for the case $\rho = 0.381/\alpha$ through use of Table I. The agreement with experiment is quite satisfactory for positive values of the argument, but somewhat less so for the negative X values. Since the onset of phase separation limits the range of negative X values accessible to measurement, the behavior of $F(X)$ cannot be as well defined by observation in this region. An alternative assumption concerning the effect of interactions is that both of the distributions described above are uniformly expanded by a factor α, so that $\rho = 0.381$. This leads to dashed curve 1′ in Fig. 3, which does not differ greatly from curve 1 for positive values of X. As discussed above, we believe the full curve is preferable.

Upon setting $\rho = 1$, which corresponds to the use of a Gaussian distribution about the center of gravity for the counting of both intra- and intermolecular contacts, Eq. (11) reduces to Eq. (15). This is represented by curve 2 in Fig. 3. In the preceding paper[1] we demonstrated that this was essentially the same function as that appearing in the *FK* treatment. Furthermore, since the $F(X)$ function of Isihara and Koyama is very nearly the same, curve 2 offers a reasonable representation of their results as well. The very considerable difference between curves 1 and 2 arises from the neglect of the numerous short-range intramolecular contacts when the segment distribution is expressed in terms of a single variable giving the distance from the center of gravity of the molecule.

Curve 3 of Fig. 3 represents the behavior predicted by the treatment of Casassa and Markovitz[5] as subsequently modified by Casassa.[13] The $F(\psi)$ values were calculated according to their approximate relation

$$F(\psi) = [1 - \exp(-1.420\psi)]/1.420\psi, \qquad (25)$$

where ψ (not to be confused with the thermodynamic parameter ψ_1) has been given the revised value: $\psi = (4/3^{\frac{1}{2}})(\alpha^3/\alpha_2^3)X$. Here α_2 is the expansion factor for a cruciform molecule taken as a representation of the two interacting molecules, and is to be calculated by an equation analogous to Eq. (24), but with C_M replaced by 0.93 C_M and ψ_1^{ν} replaced by the osmotic value, ψ_1. Their treatment assumes that after the first intermolecular contact has been formed, one can employ Eq. (16) to count both intramolecular contacts *and* the remainder of the intermolecular contacts. Comparison with the experimental data indicates that, even in the modified form, this procedure has yielded too many intermolecular contacts. It is not difficult to see why this should be the case. The application of Eq. (16) to the enumeration of intermolecular contacts involves the assumption that the $2x$ segments are distributed symmetrically about the initial point of contact, whereas this can only be strictly true when the two molecules are completely overlapped. It is interesting that we may approximate their result rather well by including short-range intermolecular contacts. Thus the product $\phi\phi^*$ in Eq. (4) becomes ϕ^2, which yields for ρ the exceedingly small value $(N_{22}^*/N_{22})^{2/3}$. We show in Fig. 3 a dashed curve for $\rho = 0$ which may be compared with their result. Hence Eq. (11) yields a result equivalent to the treatments of *FK* and *IK* in one limit, $\rho = 1$, while in the other limit, $\rho = 0$, it becomes essentially equal to the *CM* result.

Curve 4 of Fig. 3 illustrates $F(z)$ as calculated according to the first three terms obtained by the molecular distribution function approach. Taking the coefficient of the third term as evaluated by Kurata and Yamakawa,[4] we have

$$F(z) = 1 - 2.85z + 15.46z^2 - \cdots, \qquad (26)$$

where $z = X\alpha^3/3^{\frac{1}{2}}$. When one recalls that the largest experimental X values shown in Fig. 3 correspond to temperatures only 16° above theta, it is evident that several more terms would be required before the results of this procedure become useful in the sense of furnishing a representation of experimental results, even for very poor solvents. Conversely, it would be exceedingly difficult to obtain experimental results within the range of validity of Eq. (26) which would be sufficiently precise to afford an adequate test of that relation.

The treatment of Ptitsyn and Eizner[14] yields a curve (omitted for purposes of clarity) which has the same slope at $X = 0$ as curves 3 and 4, but which crosses curve 1 at approximately $X = 1$.

Next, we turn to a comparison of the predicted molecular weight dependence of A_2 with observation.

In our opinion the data obtained at the highest temperature for the two systems discussed above constitute the best test. Although the variation with molecular weight is more rapid for thermodynamically good solvents, and the available data in the latter category cover a more extended molecular weight range, our choice has the distinct advantage that there are no adjustable parameters, since ψ_1 and Θ may be evaluated from the osmotic data. Figure 4 shows the experimental data for polyisobutylene in benzene at 40° and for polystyrene in cyclohexane at 50° plotted as $\log RTA_2$ vs $\log M$. The full curves were calculated as before from Eq. (10) and Table I, except that here the small molecular weight dependence of ρ which enters through the N_{22}/N_{22}^* ratio has been included by application of Eq. (7). The fit obtained for the polystyrene data is excellent, while the theoretical curve for polyisobutylene appears to be 5 to 10% low. This agreement may also be considered satisfactory, since this difference is well within the limits of error in the determination of ψ_1.

For completeness, we show in Fig. 5 the molecular weight dependence typical of thermodynamically good solvents. The two systems are polyisobutylene-cyclohexane and polystyrene-toluene.[20] These measurements were performed at a fixed temperature, hence $\psi_1(1-\Theta/T)$ may be replaced by $(1/2-\chi_1)$. This parameter may be evaluated from the viscosity data of Fox and Flory.[17] Since we wish to use the same value of $(1/2-\chi_1)$ in both Figs. (10) and (24), we replace C_M by $C_M'=0.49\ C_M$ in the latter, as suggested by Stockmayer.[18] Thus the values of $(1/2-\chi_1^s)$ reported by Fox and Flory are to be divided by 0.49, yielding 0.165 and 0.118, respectively. These lead to the full curves shown in Fig. 5. Essentially the same values would have been obtained upon treating $(1/2-\chi_1)$ as an adjustable parameter to fit each curve to one of the data points. The predicted molecular weight dependence is somewhat too large for the polyisobutylene-cyclohexane system, but on the whole it represents a vast improvement over that deduced from the Flory-Krigbaum treatment (dashed lines).

[20] W. R. Krigbaum and P. J. Flory, J. Am. Chem. Soc. 75, 1775 (1953).

ACKNOWLEDGMENTS

W.R.K. wishes to express his gratitude to the Alfred P. Sloan Foundation for a Research Fellowship which made this work possible. A.R. of the Institute of Physical Chemistry, Madrid, Spain, gratefully acknowledges an appointment supported by the International Cooperation Administration under the Visiting Research Scientists Program administered by the National Academy of Sciences, U.S.A. Financial support for the machine calculations was provided by the Sloan Foundation and by the Allegany Ballistics Laboratory, an establishment owned by the United States Navy and operated by Hercules Powder Company.

Gamma Radiolysis of Propane

B. F. BIRDWELL AND GEORGE W. CRAWFORD

Texas Petroleum Research Committee, The University of Texas, Austin, Texas

(Received September 28, 1959)

Propane gas has been irradiated with cobalt-60 gamma rays. The primary products formed by the decomposition of 0.9–3.2% of the original propane have been identified. Based on hydrogen yield, the relative yields of the products are: hydrogen (1.00), hexanes (0.70), ethane (0.32), methane (0.27), butanes (0.17), and pentanes (0.08).

INTRODUCTION

THE investigation reported here was initiated as a part of a study concerning the effects of gamma radiation on petroleum natural gas made by the Texas Petroleum Research Committee at the University of Texas. At the time of initiation, there were available in the literature no reports on the decomposition of propane gas by exposure to gamma radiation and very few on propane radiolysis by other types of high energy radiation.

In 1926, Lind and Bardwell[1] reported the formation of products as heavy as pentanes in the gas phase, as well as the formation of a liquid phase during the bombardment of propane gas with 6-Mev alpha particles from radon gas. They actually irradiated the propane gas until it formed a liquid and then a solid, but analyzed samples were drawn off the gas phase during the stages of low decomposition. In 1952, Gevantman and Williams[2] made a study of the free radicals and their relative production in the radiolysis of propane with x rays and electrons, but did not report a complete product distribution. Yang and Manno[3] in 1959 reported the identification of ten different products, ranging from hydrogen to pentanes,[3a] formed during the gamma irradiation of propane contained in a Pyrex glass vessel. After irradiation by gamma rays from spent fuel elements (150 days cool), the products were analyzed by gas chromatography.

The purpose of the present work was to determine the primary products and their relative distribution in the gamma radiolysis of propane gas at comparatively low irradiation doses.

EXPERIMENTAL

The joint radiation facility of the Radiobiological Laboratory of the University of Texas and the U.S. Air Force[4] at the Balcones Research Center, Austin, Texas, was used for the irradiation work. This facility consists of a shielded cobalt-60 source of approximately 1 kC. Original dosimetry included the use of standard sources of 10 mC radium and 100 mC cobalt-60, an ionization chamber-rate meter combination, a Victoreen condenser *r*-meter, ferrous sulfate dosimeters, and a dyechloroform dosimeter. Recent dosimetry has included the above methods, plus comparison with kilocurie cobalt-60 sources at Los Alamos and Oak Ridge.

Special sample cells[5] were made from high pressure stainless steel valves. The gamma rays entered the $1\frac{1}{2}\times\frac{3}{4}\times\frac{3}{8}$ in. sample chamber after passing through the $\frac{1}{8}$-in. thick wall of the chamber. The sampling system was also constructed from stainless steel to satisfy the pressure requirements. For each sample, the sample cell was evacuated, flushed with the propane and then filled with 99.9+mole % pure propane at a pressure of about 75 psia and a temperature of 20–25°C to give a sample density of 0.009 g/cc. No impurities were detected in the source propane using a CEC 21-102 mass spectrometer.

The loaded sample cells were irradiated by the Balcones Research Center personnel, who insured that the radiation passed through the same cell face during all irradiations. Although a continuous period of irradiation would have been more desirable, availability of the radiation facility only on nights and weekends for this work required that an intermittent schedule of irradiation be used in order to obtain the total doses desired at the comparatively low dose rate available with this facility. Total doses (at the outer face of the cell) ranging from $0.88-2.98\times10^7$ r were applied to the samples at a dose rate of 1768 r/min (±5%). Control of the temperature surrounding the sample exposure slot was not possible with this facility. Due to the heavy shielding, however, the temperature remained fairly constant and did not vary more than ±5° from 25°C for any of the samples irradiated. After irradiation, both the irradiated sample cells and the original propane cylinder were sent to the Petroleum Analytical Research Corporation, Houston, Texas, and analyzed on a CEC 21-102 mass spectrometer. The resulting charts were returned to the authors and interpretations were made with the aid of PAR's calibration

[1] S. C. Lind and D. C. Bardwell, J. Am. Chem. Soc. **48**, 2335 (1926).

[2] L. H. Gevantman and R. R. Williams, Jr., J. Phys. Chem. **56**, 569 (1952).

[3] K. P. Yang and Peter Manno, Jr., J. Am. Chem. Soc. **81**, 3507 (1959); (a) Tables in paper show $i-C_5H_{10}$, but text refers to pentanes formation rather than pentenes.

[4] John A. Auxier, U. S. Air Force School of Aviation Medicine, Randolph Field, Texas, Rept. No. 55-40 (June, 1955).

[5] B. F. Birdwell, M.S. thesis, The University of Texas, Austin (1959), 28.

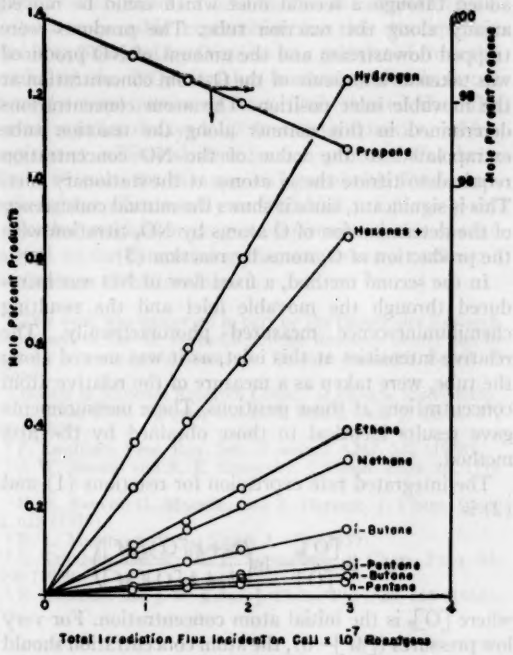

FIG. 1. Distribution of hydrocarbons in the gaseous mixture resulting from gamma irradiation of propane gas as a function of total radiation flux incident on the cell.

data. The remaining gas in the irradiated cells was analyzed using a Beckman GC-2 gas chromatograph. The hydrogen, methane, and ethane were identified using a 4-ft silica gel column at 40°C with a helium flow rate of 33 cc/min. The heavier components were identified using a 6 ft silicone-550 column at 40°C with helium flow rates of either 33 cc/min or 80 cc/min. Identification of the major products and the measurement of their relative amounts were made using both the mass spectrometer and the gas chromatograph.

RESULTS

The major products formed in the irradiation of the propane samples were in every case hydrogen, hexanes, ethane, methane, isobutane, isopentane, *n*-butane, and *n*-pentane, in the order listed. The hexanes fraction was composed primarily of 2,3-dimethyl butane and 2-methyl pentane, with slightly less *n*-hexane and a small amount of 2,2-dimethyl butane. The formation of 3-methyl pentane was not indicated.

In addition to the normal and iso-paraffins listed as the major products, trace amounts of certain alkenes and alkynes were detected. Isohexenes, isopentenes, butenes, propylene, ethylene, and mixed lower acetylenes were also indicated in the mass spectra of the irradiated propane samples. These products were formed in amounts too small for identification by the gas chromatograph but were indicated to be present in trace amounts by the mass spectrometer.

TABLE I. Product distributions from propane decomposition by high energy radiation.

Type radiation	Gamma radiation	Gamma radiation	Alpha radiation
Investigators	Birdwell and Crawford	Yang and Manno	Lind and Bardwell
	Product distribution, relative to hydrogen yield		
Hydrogen	1.00	1.00	1.00
Methane	0.27	0.25	0.27
Ethylene	trace	0.04	...
Ethane	0.32	0.34	0.16
Propylene	trace	0.04	...
Butane	0.17	0.15	0.19
Pentanes	0.08	0.07	0.14
Hexanes	0.70	...	...
Pressure, cm Hg	388	60	76
Temperature, °C	approx 25	22.5	25

The relative amounts of each of the components present in the gaseous mixtures found in the cells after irradiation are plotted in Fig. 1 vs the total irradiation flux incident on the sample cell. Decomposition of the propane is shown to be linear with total radiation dose from $0.88-2.98\times10^{7}$ r (0.9—3.2% decomposition). The relative abundances of the different products in the mixtures after irradiation (excluding undecomposed propane) remained constant over this decomposition range.

Table I shows a comparison of the decomposition product distribution obtained in this work with those of Yang and Manno and of Lind and Bardwell. Agreement of the two gamma irradiations is close, even though pressure, dose rates, and the wall material of the sample containers differed. It is believed that hexanes were also present in Yang and Manno's products, but that analysis for them was not made.[6]

ACKNOWLEDGMENTS

Appreciation is expressed to the Texas Petroleum Research Committee for permission to publish these results. The authors are indebted to Captain L. C. Logie, U.S. Air Force, and Jimmie Davis of the Radiobiological Laboratory, Balcones Research Center, The University of Texas, for the gamma irradiation of the samples.

[6] L. O. Morgan, University of Texas, Department of Chemistry (private communication).

Letters to the Editor

THE Letters to the Editor section is subdivided into three parts entitled Communications, Comments and Errata, and Notes. These three sections are all subject to the same limitations on length. The textual material of each Letter is limited to a number of words equal to 950 minus the following: (a) 200 words for each average-sized figure; (b) 50 words for each displayed equation; (c) 7 words for each line of table including headings and horizontal rulings. No proof will be sent to the authors of "Communications" and "Comments and Errata." Proof will be sent to the authors of "Notes." The publication charge for Letters is $30 per page, with a minimum of $30 per Letter. If honored, the Institution will be entitled to 100 reprints without covers. See issues of May–September, 1957, for descriptions of categories.

Communications

Recombination of Oxygen Atoms in the Absence of O_2*

J. E. MORGAN,† L. ELIAS, AND H. I. SCHIFF

Department of Chemistry, McGill University, Montreal, Canada

(Received July 7, 1960)

THE gas phase recombination of oxygen atoms in systems containing more than 90% O_2 occurs largely through the intermediate formation of ozone.[1–3] It is therefore difficult in such systems to study the direct atom recombination

$$O+O+M\rightarrow O_2+M. \quad (1)$$

Although several authors have measured the rate constant for this reaction in the presence of O_2,[4–6] it seemed desirable to determine this quantity in an O_2-free system. Under these conditions, atom recombination can occur only by reaction (1) and on the wall

$$O+W\rightarrow\tfrac{1}{2}O_2+W. \quad (2)$$

Oxygen atoms were generated by the reaction

$$N+NO\rightarrow N_2+O. \quad (3)$$

The nitrogen atoms were produced by subjecting N_2 to a microwave discharge. NO was added through an inlet to the gas stream in a manner described previously.[1] Excess of either reactant results in chemiluminescence—yellow with excess NO, blue with excess N atoms. An intermediate "dark" condition can then be obtained, which corresponds to equimolar amounts of both reactants. Under these conditions the gas stream contains only O atoms and N_2. Furthermore the concentration of O atoms formed can be accurately deduced from the flow rate of NO required to titrate the N atoms.

The O atom concentration was measured as a function of distance (or time) from the NO inlet by two methods. In the first method an excess of NO_2 was added through a second inlet which could be moved axially along the reaction tube. The products were trapped downstream and the amount of NO produced was taken as a measure of the O-atom concentration at the movable inlet position. The atom concentrations determined in this manner along the reaction tube extrapolated to the value of the NO concentration required to titrate the N atoms at the stationary inlet. This is significant, since it shows the mutual consistency of the determination of O atoms by NO_2 titration with the production of O atoms by reaction (3).

In the second method, a fixed flow of NO was introduced through the movable inlet and the resulting chemiluminescence measured photometrically. The relative intensities at this inlet, as it was moved along the tube, were taken as a measure of the relative atom concentrations at those positions. These measurements gave results identical to those obtained by the first method.

The integrated rate expression for reactions (1) and (2) is

$$k_2 t=\ln\frac{[O]_0}{[O]}-\ln\left(\frac{k_2+k_1[O]_0[M]}{k_2+k_1[O][M]}\right),$$

where $[O]_0$ is the initial atom concentration. For very low pressures ($[M]\rightarrow 0$), the atom concentration should follow a pseudo first-order behavior, an observation which can be used to calculate k_2 in the following manner. Plots of $\ln[O]$ vs time yielded curves which were approximately linear for the experimental conditions used. The average slopes of these curves of course depend on $[M]$. However, when these slopes are plotted as a function of $[M]$, they must extrapolate to a true value of k_2 at zero pressure. For this apparatus k_2 was found to be 0.40 sec^{-1}, which corresponds to a recombination coefficient $\gamma=1.6_5\times10^{-5}$. Once the value of k_2 is obtained, the integrated rate equation can be rearranged to permit an evaluation of k_1 for each experiment. The results of the work to date are summarized in Table I; the average value of $k_1=3.2_3\times10^{15}$ $mole^{-2}$ cm^6 sec^{-1}.

The measurement of $[O]$ by isothermal calorimetry has been used previously in this laboratory[1] to study discharged O_2. When used in the present system, this technique gave much higher atom concentrations, as well as a faster recombination rate, than did the methods outlined above. The presence of some additional

TABLE I.

Pressure (mm)	$10^9[O]_0$ (mole cm^{-3})	$10^9[O]$ (mole cm^{-3})	t (msec)	$10^{-15}k_1$ ($mole^{-2}$ cm^6 sec^{-1})
2.30	1.18_5	0.97_5	218	3.6_4
2.50	1.03_5	0.87_2	198	3.7_6
3.15	1.44_8	1.18_0	242	2.7_8
3.90	1.45_0	1.16_5	153	3.8_8
4.55	1.73_0	1.36_5	148	3.0_9
4.80	1.42_5	1.01_0	278	2.6_3

species which liberates heat to the calorimeter seems to be a reasonable explanation for this discrepancy. The heat liberated by O atoms was calculated from the results of the NO_2 titration method and subtracted from the total measured heat. This showed that the second species decayed by first-order kinetics, which suggests a collisional deactivation process. The half-life of 50 msec for this species agrees with Kaufman's estimate for vibrationally excited N_2.[7]

Further work is in progress for studying this species as well as for determining the temperature coefficient for O-atom recombination.

* This work was supported in part by the Geophysics Research Directorate of the Air Force Cambridge Research Center and in part by a grant-in-aid from the Defence Research Board of Canada.

† Holder of National Research Council of Canada Studentship.

[1] L. Elias, E. A. Ogryzlo, and H. I. Schiff, Can. J. Chem. **37**, 1680 (1959).
[2] F. Kaufman, Proc. Roy. Soc. (London) **A247**, 123 (1958).
[3] S. W. Benson and A. E. Axworthy, J. Chem. Phys. **26**, 1718 (1957).
[4] R. R. Reeves, G. Manella, and P. Harteck, J. Chem. Phys. **32**, 632 (1959).
[5] D. L. Matthews, Phys. Fluids **2**, 170 (1959).
[6] S. Krongelb and M. W. P. Strandberg, J. Chem. Phys. **31**, 1196 (1959).
[7] F. Kaufman and J. R. Kelso, J. Chem. Phys. **28**, 510 (1958).

The $^1\Sigma^+$ Excited States of Carbon Monoxide*

H. LEFEBVRE-BRION AND C. M. MOSER

Centre de Mecanique Ondulatoire Appliquée, Paris 15°, France

AND

R. K. NESBET

R.I.A.S., Baltimore 12, Maryland and Department of Physics, Boston University, Boston 15, Massachusetts

(Received June 27, 1960)

IF the ultraviolet spectra of diatomic molecules made up of atoms of the first row are calculated using the LCAO–MO–SCF orbitals calculated for the ground state using $1s$, $2s$, and $2p$ atomic basis functions, some of the lower excited states seem to be well represented by single electron excitations from occupied to virtual orbitals. The states which lie near the ionization potential are, on the contrary, poorly represented by single excitations and are often predicted to lie far higher than the ionization energy.[1–3] Configuration interaction in this limited basis does not appear to improve matters for these high-lying states.

Although we are using computer programs for the present calculations which make it possible to undertake more complicated work than has been customary, it still is a matter of great important to find the simplest calculation that will give useful results. Any unnecessary increase in the number of basis orbitals in these calculations greatly increases the over-all computer time required. For this reason it has seemed worthwhile to evaluate the effect of two different and, to a certain extent, complementary modifications to the set of atomic basis orbitals: (1) use of several L-shell orbitals with different exponents; (2) use of M-shell orbitals.

To test these effects we have recently recalculated the vertical excitation energies of the $B^1\Sigma^+$, $C^1\Sigma^+$, and $E^1\Sigma^+$ states of CO. Experimentally these are found about 11 ev above the ground state with equilibrium internuclear distances approximately the same as that of the ground state.

TABLE I. Exponents of orbitals in double L-shell calculation.

For C:	$1s$, 5.673, $2s$, 2.4, $2s'$, 1.2, $2p\sigma$, 2.4, $2p\sigma'$, 1.2, $2p\pi$, 2.4, $2p\pi'$, 1.2
For O:	$1s$, 7.658, $2s$, 3.37, $2s'$, 1.685, $2p\sigma$, 3.37, $2p\sigma'$, 1.685, $2p\pi$, 3.37, $2p\pi'$, 1.685

Herzberg and Hugo[4] have attributed these states to $\pi\rightarrow\pi$ and $\sigma\rightarrow\sigma$ single electron excitations, respectively. The LCAO–MO–SCF orbitals calculated with the usual $1s$, $2s$, and $2p$ atomic functions gave predicted energies more than twice too high.[1,2]

We have calculated the SCF orbitals for CO with two exponents for each of the functions in the L shell. These exponents are given in Table I. The lowest $\sigma\rightarrow\sigma$ excitation is at about 21 ev and the lowest $\pi\rightarrow\pi$ excitation is also at about 2 ev. Here, as in the earlier calculation,[1] configuration interaction does not make a marked difference.

TABLE II. $^1\Sigma^+$ states of CO.

State	Exp. Vert. excitation energy (ev)[a]	$3s$–$3p$ Calculation (ev) after first-order CI		Double L shell (ev) after first order CI	Single L shell (ev)
$X^1\Sigma^+$	0	0	Excitation	0 Excitation	0 Excitation
$B^1\Sigma^+$	10.78	11.12	mostly σ–σ	18.01 σ–σ	23.14 π–π
$C^1\Sigma^+$	11.40	11.78	mostly σ–σ	23.99 π–π	27.37 σ–σ
$E^1\Sigma^+$	11.52	13.32	mostly σ–σ		

[a] Y. Tanaka, A. S. Jursa, and F. Le Blanc, J. Chem. Phys. **26**, 862 (1957).

Using a basis-set made up of $1s$, $2s$, $2p$, $3s$, and $3p$ atomic functions with exponents given by Slater's rules, it is found that the energies of the virtual orbitals are markedly lowered as compared with those found in the double exponent calculation and are rather close together. Since this is a case of near degeneracy, configuration interaction is important here, although a very small effect in the other calculations. From a six-term CI function (containing both $\sigma\rightarrow\sigma$ and $\pi\rightarrow\pi$ excitations), it is found that the two lowest states both correspond largely to $\sigma\rightarrow\sigma$ excitations and the calculated

energies are in satisfactory agreement with experiment. These results are collected in Table II.

Both SCF calculations were carried out on the IBM 704 machine using automatic programs due to one of us (RKN). The necessary integrals were evaluated by methods developed by P. Merryman (unpublished).

While the exponents we have used in both calculations are not likely to be the "best," it seems improbable that the energies of the excited states are greatly dependent on the particular values chosen.

These results indicate that addition of functions from the M shell improves the correspondence between theory and experiment for the ultraviolet spectrum of CO much more than does doubling the number of L-shell functions, although doubling the L shell gives a significantly greater improvement to the total energy of the ground state (about 6 ev).

We are grateful to the Martin Company of Baltimore for the use of their IBM 704 computer. Several of the programs used for the SCF calculations were coded at the National Bureau of Standards by A. Beam, P. Walsh, and J. D. Waggoner under the supervision of Dr. E. Haynesworth.

* This work has been supported in part by the Ordnance Corps, U. S. Department of the Army, the National Science Foundation, and the Martin Company.

[1] H. Brion and C. M. Moser, J. Chem. Phys. **32**, 1194 (1960).
[2] P. Merryman, C. M. Moser, and R. K. Nesbet, J. Chem. Phys. **32**, 631 (1960).
[3] C. W. Scherr, J. Chem. Phys. **23**, 569 (1955).
[4] H. Herzberg and T. Hugo, Can. J. Phys. **33**, 757 (1955).

A Vibrational Effect on the Polarization of Molecular Crystal Fluorescence

E. G. McRae

Division of Chemical Physics,
C.S.I.R.O. Chemical Research Laboratories, Melbourne, Australia

(Received June 27, 1960)

THE theory of the electronically excited states of molecular crystals has been developed mainly for the model in which the atomic nuclei are considered to be fixed in their equilibrium positions.[1] On the basis of this model, the polarization ratio in the fluorescence of a molecular crystal is expected to vary with temperature in accordance with the Boltzmann distribution of electronic energies among the upper states of the Davydov components in absorption.

A more realistic model of a molecular crystal is an array of molecules whose positions and orientations are fixed, but which execute intramolecular vibrations. The theory for this model furnishes a prediction of vibrational structure in fluorescence spectra. The following result may be derived in the case of weak intermolecular interaction in the upper state: *in that part of the fluorescence spectrum starting one ground-state vibrational interval from the onset of emission, the polarization ratio should be independent of temperature and equal to the polarization ratio in the corresponding absorption band.* For the highest-frequency vibronic band, however, the theoretical prediction is the same as for the simple model. In this note, we derive the above result for the anthracene crystal, which has two molecules per unit cell. It will be evident that a similar derivation can be given for a crystal of any structure.

Let ϕ_g denote the electronic ground-state wave function for the anthracene molecule, and ϕ_e the lowest-energy singlet excited-state function. Let χ_{gp} and χ_{ep}, respectively, denote ground and excited-state vibrational wave functions corresponding to the excitation of p vibrational quanta in an active mode of vibration. The nonvibrating ground state of the crystal may be represented by the product function $\Psi_{g0}=\Pi m\phi_g{}^{(m)}\chi_{g0}{}^{(m)}$ where the superscripts designate individual molecules ($m=1, 2, \cdots, N$). The N lowest-energy excited states of the crystal may be represented approximately by the linear combinations

$$\Psi_{e0}(\mathbf{k})=N^{-\frac{1}{2}}\Sigma n \exp i\mathbf{k}\cdot\mathbf{r}^{(n)}\Psi_{g0}(\phi_e{}^{(n)}\chi_{e0}{}^{(n)}/\phi_g{}^{(n)}\chi_{g0}{}^{(n)})\cdots, \tag{1}$$

where $\mathbf{k}$ denotes an electronic wave vector and $\mathbf{r}^{(n)}$ denotes the position vector of the nth molecule. The relevant vibrational substrates of the electronic ground-state wave function may be represented in a similar way by the linear combinations

$$\Psi_{gp}(\mathbf{l})=N^{-\frac{1}{2}}\Sigma n \exp i\mathbf{l}\cdot\mathbf{r}^{(n)}\Psi_{g0}(\chi_{gp}{}^{(n)}/\chi_{g0}{}^{(n)})\cdots, \tag{2}$$

where $\mathbf{l}$ denotes a vibrational wave vector analogous to $\mathbf{k}$. In the absence of intermolecular vibrational coupling, the corresponding energy levels are degenerate, and lie p ground-state vibrational intervals above the zero-point level of the crystal.

The transition $\Psi_{e0}(\mathbf{k})\rightarrow\Psi_{g0}$ is forbidden unless $\mathbf{k}=0$ or $\mathbf{k}=\pi\boldsymbol{\varrho}$, where $\boldsymbol{\varrho}$ denotes the reciprocal lattice translation corresponding to a primitive translation along either the a axis or the b axis in the direct lattice.[2] With the usual choice of phase factors, the higher-frequency of the two allowed transitions is designated as $\Psi_{e0}(0)\rightarrow\Psi_{g0}$. This transition is a-polarized,[3] and we denote by $Q_a\mathbf{a}_0$ the electronic transition moment exclusive of the vibrational overlap factor. Here $\mathbf{a}_0$ denotes a unit vector in the direction of the a axis. The other allowed transition is b-polarized, and with a similar notation we denote the transition moment by $Q_b\mathbf{b}_0$. On the basis of the oriented gas model of the crystal, and making use of Eqs. (1) and (2), we obtain the following expression for the electronic transition moment of the transition $\Psi_{e0}(\mathbf{k})\rightarrow\Psi_{gp}(\mathbf{l})$:

$$N^{-\frac{1}{2}}(\delta_{\mathbf{k}-\mathbf{l},0}Q_a\mathbf{a}_0+\delta_{\mathbf{k}-\mathbf{l},\pi\boldsymbol{\varrho}}Q_b\mathbf{b}_0)\cdots. \tag{3}$$

Here δ denotes the Kronecker delta.

For $p=0$, the polarization ratio (a:b) should lie between the low-temperature limit, zero, and the high-temperature limit $|Q_a|^2/|Q_b|^2$ From Eq. (3), for $p\geq 1$, the polarization ratio should be equal to $|Q_a|^2/|Q_b|^2$ at all temperatures. The ratio

$$|Q_a|^2/|Q_b|^2$$

may be identified with the polarization ratio in absorption, whose experimental value is (1:3).[3] The theoretical and observed[4] polarization ratios for each of the first three vibronic bands in anthracene fluorescence are compared in Table I. The agreement between

TABLE I. Theoretical and observed polarization ratios in anthracene crystal fluorescence.

p	Polarization ratio (a:b) Theoret[a]	Obs[b]
0	0	0.07
1	0.33	0.28
2	0.33	0.31

[a] Temperature $T=0$°K.
[b] Average from Figs. 3(a) and 3(b), footnote reference 4. Thick crystals ($\sim 3\mu$). $T=4$°K.

theory and experiment is thought to indicate that intramolecular vibrations play an important part in the determination of fluorescence polarization.

The result derived in this note was obtained in the course of a more comprehensive study of intramolecular vibrations in molecular aggregates, which will later be published in the *Australian Journal of Chemistry*. The writer is glad to thank Dr. J. Ferguson for some very helpful discussions.

[1] D. S. McClure, *Solid-State Physics*, edited by F. Seitz and D. Turnbull (Academic Press, Inc., New York, 1959), Vol. 8, p. 1.
[2] A. S. Davydov, J. Exptl. Theoret. Phys. (U.S.S.R.) **18**, 210 (1948).
[3] A. V. Bree and L. E. Lyons, J. Chem. Soc. **1956**, 2662.
[4] J. Ferguson and W. G. Schneider, Can. J. Chem. **36**, 1070 (1958).

Proton Magnetic Resonance Studies of Nonstoichiometric Titanium Hydride*

B. STALINSKI,† C. K. COOGAN,‡ AND H. S. GUTOWSKY
Noyes Chemical Laboratory, University of Illinois, Urbana, Illinois

(Received July 13, 1960)

PROTON magnetic resonance experiments have been carried out on titanium hydride ranging in composition from $TiH_{1.61}$ to $TiH_{1.97}$. Results of remarkable simplicity have emerged from the temperature dependence of the line shape, which shows that the hydrogen diffusion takes place by a vacancy mechanism at a rate linearly dependent on the concentration of vacancies. This affords a very clear-cut case of diffusion by vacancies, as the tenfold range of vacancy concentration is accurately defined by the sample composition; there are no complications such as defect associations introduced by vacancy inducing additives. In addition the proton resonances of all samples exhibit a large negative Knight shift,[1] of the order of -3×10^{-4}. It is proposed that these shifts, as well as similar ones reported previously for vanadium hydride[2] result from an electron exchange interaction which pairs the spins of electrons in the conduction band with the spins of electrons centered on protons.

The observations were made with a spectrometer operating at 26.92 Mc/sec.[3] The six samples used were finely powdered with a grain size less than 10^{-3} cm. The compositions studied are from a homogeneous phase in which the crystals are cubic at room temperature, but undergo a second-order phase transition just below room temperature and become slightly tetragonal.[4-6]

The second moments of the absorption observed at -196°C range from 22.0 to 25.8 gauss^2, increasing with the hydrogen content. The observed values agree quite well with those calculated[7] for the rigid lattice in which the hydrogen atoms are distributed randomly among the tetrahedral lattice sites. However, the observed values are systematically about 4% higher than those computed. This is just outside the experimental error, so the effect may be real; if so, there are several possible explanations of the discrepancy, none of which is very significant.

At higher temperatures diffusional narrowing occurs. The linewidth change is centered at a temperature which increases with hydrogen content, being 66°C for $TiH_{1.607}$, 130°C for $TiH_{1.923}$, and about 230°C for $TiH_{1.969}$. The temperature dependence of the correlation frequency ν_c for the proton diffusion was obtained from the linewidths by using a slightly modified form of the BPP equation.[8] Arrhenius plots of the results for five samples give activation energies E_a for diffusion, increasing with hydrogen content from 9.4 kcal/mole for $TiH_{1.607}$ to 10.2 for $TiH_{1.923}$. Moreover, ν_c satisfies the equation

$$\nu_c=\nu_0(\delta-\delta_0)\exp(-E_a/RT), \qquad (1)$$

where ν_0 is a frequency factor, $\sim 2\times10^{12}$ sec^{-1}; δ is the stoichiometric defect as defined by the sample composition, $TiH_{2-\delta}$; and δ_0 is a small constant, about 0.02.

Equation (1) gives a good fit of the results for all the samples and temperatures for which ν_c was determinable from the observed linewidths. The tetrahedral vacancy concentration is directly proportional to δ; therefore, the linear dependence of the diffusion rate upon δ provides an exceptionally simple example of the vacancy mechanism. The quantity δ_0 is the same for all the samples and we suggest that it represents the "inaccessible vacancies." The latter can exist in the compressed region near edge dislocations. On this basis,

if there were 10^{12} dislocations/cm^2, a δ_0 of 0.02 corresponds to about 20 inaccessible vacancies per atom-plane per dislocation.

The proton resonance shift was measured at room temperature for all specimens and from -95°C to $+190$°C for the two extreme compositions. The shifts lay in the range -0.01% for $TiH_{1.607}$ to about -0.032% for $TiH_{1.969}$. In these two extreme specimens the shift showed a similar dependence upon temperature to that of the bulk susceptibility,[4] the shifts for $TiH_{1.969}$ exhibiting an anomaly at about 13°C as does the bulk susceptibility. The Ti resonance has not been reported for the metal nor the hydride. However, in $VH_{0.66}$ the V^{51} resonance has a normal Knight shift of $+0.17\%$ while the protons have a negative shift, -0.0095%.[2] Negative proton shifts, such as are found in titanium and vanadium hydrides, could be produced by an electron exchange interaction which polarizes the electron spin density at the proton opposite to that of the nearest conduction-band electron. In π-electron free radicals such an interaction does occur between unpaired electrons in the π-orbital and the electrons in the σ bonds.[9] This model leads to the following modification of the expression Eq. (20.1) used by Knight[1] to estimate the resonance shifts in alloys,

$$(\Delta H/H) = -[J_H a(s)_H \chi_p \xi_H M]/2g_{IH}\mu_B, \qquad (2)$$

where J_H represents the *net efficiency* with which the exchange interaction transmits the polarization of the conduction electrons to the electrons centered on the protons.

With the appropriate constants, observed quantities, and other parameters,[1] Eq. (2) yields an approximate value of 0.2 for J_H in titanium hydride. In the case of $VH_{0.66}$, the ratio of the vanadium and proton shifts leads to a value for J_H of 0.35 ξ_V/ξ_H, where ξ_V/ξ_H is known only to be of the order unity. These results for J_H seem reasonable, within the approximations involved. Moreover, the model predicts that the shifts will be small for highly ionic hydrides. This we found to be so in room temperature experiments on CaH_2 which gave $|\Delta H/H| < 0.001\%$.

We will present the details of our studies of titanium hydride in a forthcoming publication.

* Supported in part by the Office of Naval Research.

† On leave from the Institute of Technology and the Institute of Physical Chemistry of the Polish Academy of Sciences, Wroclaw, Poland; Visiting Senior Research Scholar of the Institute of International Education.

‡ On leave of absence from the Division of Chemical Physics, C.S.I.R.O., Melbourne, Australia; appointment supported by the International Cooperation Administration under the Visiting Scientist Program administered by the National Academy of Sciences of the United States of America.

[1] W. D. Knight, *Solid-State Physics*, edited by F. Seitz and D. Turnbull (Academic Press, Inc., New York), Vol. 2, p. 93.
[2] R. A. Oriani, E. McCliment, and J. F. Youngblood, J. Chem. Phys. **27**, 330 (1957).
[3] H. S. Gutowsky, L. H. Meyer, and D. E. Woessner, Rev. Sci. Instr. **24**, 644 (1953).
[4] B. Stalinski, Zeszyty Nauk. Politech. Wroclaw. Chem. **4**, 25 (1957).
[5] B. Stalinski and B. Idziak (unpublished work).
[6] H. L. Yakel, Acta Cryst. **11**, 76 (1958).
[7] J. H. Van Vleck, Phys. Rev. **74**, 1168 (1948).
[8] N. Bloembergen, E. M. Purcell, and R. V. Pound, Phys. Rev. **73**, 679 (1948).
[9] H. M. McConnell and D. B. Chesnut, J. Chem. Phys. **28**, 107 (1958); and prior work cited there.

Phosphorescence Lifetime of Benzene. An Intermolecular Heavy-Atom Effect, a Deuterium Effect, and a Temperature Effect*

M. R. Wright, R. P. Frosch, and G. W. Robinson

Gates and Crellin Laboratories of Chemistry,† California Institute of Technology, Pasadena, California

(Received June 20, 1960)

THE $^1B_{2u} \leftrightarrow {}^1A_{1g}$ absorption and emission spectra and the $^3B_{1u} \rightarrow {}^1A_{1g}$ phosphorescence spectrum and lifetime of benzene in solid CH_4, Ar, Kr, and Xe at 4.2°K are presently being studied. The results concerning the phosphorescence are of particular interest and seem worth reporting at this time.

Measurements of the lifetime, $\tau = (t_2 - t_1)/\ln I_1/I_2$, carried out in a standard manner[1] yield 16 sec, 16 sec, 1 sec, and 0.07 sec for C_6H_6 in CH_4, Ar, Kr, and Xe, respectively. For C_6D_6 in CH_4, Ar, Kr, and Xe the lifetimes are 22 sec, 26 sec, 1 sec, and 0.07 sec, respectively. The lifetimes in the low molecular weight "solvents" are 2–3 times longer than any previously reported but are reasonably consistent with the 21 sec upper-limit to the lifetime estimated through quantum yield measurements at 77°K.[2] Many of the present experiments were performed with an interference filter which transmitted a single phosphorescence band (common to C_6D_6 and C_6H_6 in all solids) near 3650 A. Phosphorescence ($\tau \approx 2$ sec) caused by impurities in the quartz was further minimized by this method after being largely removed by using high purity material. Slight nonexponential decay caused by nonuniform benzene environment could be substantially lessened by using molar concentrations of 10^{-4} rather than the 10^{-2} usually employed, but residual nonexponential decay probably causes a 5–10% error in all the measurements.

The phosphorescence spectra of C_6H_6 and C_6D_6 in Kr and Xe show a very strong band near 29 500 cm^{-1}, the probable O—O band. This band is very weak or missing in the spectra of C_6H_6 and C_6D_6 in the lower molecular weight "solvents"; in addition, many other major intensity differences between light and heavy solvents occur. The quantum ratio of fluorescence (all short-lived) to phosphorescence is greater than 1.0 in the methane matrix but is essentially zero in Ar, Kr, and Xe.

The experiments thus show a slight deuterium effect on the phosphorescence lifetime in low molecular

weight solvents at 4.2°K and a striking effect on the lifetime caused by the intermolecular[3] spin-orbit perturbation in this case where the intramolecular perturbation is weak. The extramolecular perturbation appears to be relatively small for CH_4 and Ar but dominates the intramolecular one for Kr and Xe "solvents"; it shows no deuterium effect; and it results in a different vibrational intensity distribution than does the intramolecular perturbation. The suspected effect[2] on the lifetime caused by nonradiative transisitions from the triplet state at 77°K has been verified. An experiment performed at 1.8°K (C_6H_6-argon) showed no further increase in lifetime below 4.2°K. The $^1B_{2u}\rightarrow{}^3B_{1u}$ radiationless process is shown to be extremely efficient at 4.2°K in all the solvents used except methane. Since argon acts like a low molecular weight "solvent" with respect to the spin-orbit perturbation, it is probable that the intersystem crossover, while requiring spin-orbit mixing, depends heavily on the existence of low-frequency lattice vibrations in the environment such as exist to a greater extent in argon than in methane.

In view of the behavior of the O—O band it appears likely, as suggested previously,[4,5] that the intramolecular phosphorescence mechanism is strongly vibrationally induced. Since the first strong band in the vibrationally induced spectrum (Ar or CH_4 "solvents") involves the 1600 cm^{-1} Fermi doublet of e_{2g} symmetry, it is possible that: (1) the $^3B_{1u}$ state mixes with the $^1B_{2u}$ state through the z component of the spin-orbit interaction, and (2) the transition between the $^1A_{1g}$ ground state and the "$^1B_{2u}$ part" of the $^3B_{1u}$ state is induced by e_{2g} vibrations as in the 2600 A $^1B_{2u}\leftrightarrow{}^1A_{1g}$ transition ($f=0.0014$).[6] This mechanism is consistent with the low oscillator strength, $f\approx10^{-10}$, for the $^3B_{1u}-{}^1A_{1g}$ transition. Combinations of the 1600 cm^{-1} frequency and totally symmetric carbon-stretching vibrations at 992 cm^{-1} comprise the major part of the vibrationally induced spectrum. The 992 cm^{-1} vibration also forms a prominent part of the solvent-induced spectrum. The one puzzling aspect is the absence of one-quantum excitation of the 606 cm^{-1} e_{2g} vibration in the vibrationally induced spectrum, since this is strong in the $^1B_{2u}-{}^1A_{1g}$ system.[7]

The fact that the O—O band is very weak in the absence of external perturbations is consistent with the results of Evans[8] and of Craig, Hollas, and King.[9] The latter authors state that "[29 410 cm^{-1}] was the limit attainable because of scattering and other losses and absorption by the long-wave tail of the 2600 A singlet system." It is probable that the major part of the absorption intensity of the $^3B_{1u}\leftarrow{}^1A_{1g}$ transition, consistent with the 16–26 sec lifetime, lies to the high-frequency side of their limit.

If radiationless processes were present at 77°K in naphthalene, as suggested by the work here and more directly by the work of Gilmore, Gibson, and McClure,[2] it could account for much if not all of the large deuterium effect on the lifetime reported by Hutchison and Mangum[10] for that molecule.[11] It is definitely possible that all of the residual deuterium effect in benzene at 4.2°K in low molecular weight solvents is a consequence of nonradiative processes from the zero-point vibrational state and thus has nothing to do with the intramolecular phosphorescence mechanism.

We thank H. M. McConnell and H. Sternlicht for many discussions which helped kindle our interest in certain aspects of this problem.

* Supported in part by NSF and OOR.
† Contribution No. 2598.

[1] For example, D. S. McClure, J. Chem. Phys. **17**, 905 (1949).
[2] E. H. Gilmore, G. E. Gibson, and D. S. McClure, J. Chem. Phys. **23**, 399 (1955).
[3] This effect was first reported by M. Kasha, J. Chem. Phys. **20**, 71 (1952).
[4] H. Shull, J. Chem. Phys. **17**, 295 (1949).
[5] D. P. Craig, J. Chem. Phys. **18**, 236 (1950).
[6] J. N. Murrell and J. A. Pople, Proc. Phys. Soc. (London) **A69**, 245 (1956).
[7] This aspect would not be puzzling if the $^3B_{2u}$, instead of the $^3B_{1u}$, state were taken as the phosphorescing state. In this case the spin-orbit interaction would cause the transition to have $^1B_{1u}-{}^1A_{1g}$ character and the different vibrational intensity distribution would not be surprising (see, for example, footnote reference 6.)
[8] D. F. Evans, J. Chem. Soc. **1957**, 1351, 3885.
[9] D. P. Craig, J. M. Hollas, and G. W. King, J. Chem. Phys. **29**, 974 (1958).
[10] C. A. Hutchison, Jr., and B. W. Mangum, J. Chem. Phys. **32**, 1261 (1960).
[11] Our preliminary measurements show a negligible temperature effect for $C_{10}H_8$, however.

EPR Observation of Steady-State Ethyl Radical Concentration in Radiolysis of Liquid Ethane

RICHARD W. FESSENDEN AND ROBERT H. SCHULER

Radiation Research Laboratories, Mellon Institute, Pittsburgh, Pennsylvania

(Received June 16, 1960)

FROM radical scavenging studies it is known that radicals are produced with a G of 5 in the radiolysis of liquid hydrocarbons. If one assumes that these radicals disappear at the maximum rate expected for bimolecular processes ($10^{11}[R]^2$ mole liter^{-1} sec^{-1}) then the steady-state concentration should be 4×10^{-8} M at an absorbed dose rate of 10^8 rad/hr (2×10^{18} ev g^{-1} sec^{-1}). Presently available paramagnetic resonance methods are sufficiently sensitive to permit direct observation of radicals at this concentration. EPR observations of the radicals produced during photolysis[1] and radiolysis[2] have been reported but in these experiments the second-order rate constants were considerably less than the above value. In the present study attention has been focused on the steady-state concentration of *reactive* radicals produced in *liquid* systems.

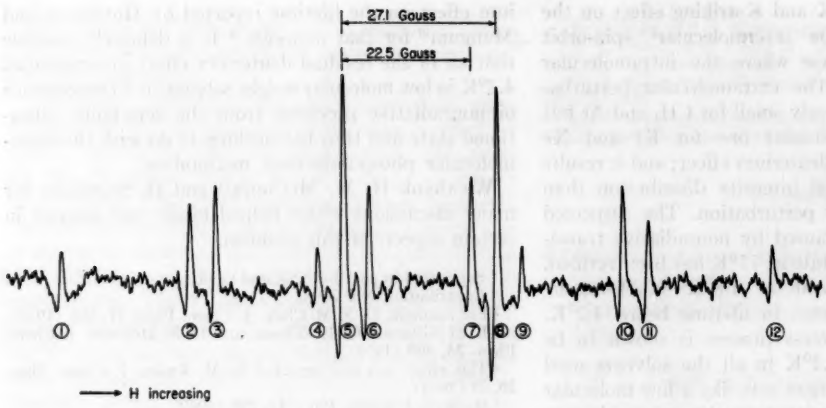

FIG. 1. EPR Spectrum of ethyl radicals observed during the radiolysis of liquid ethane at 135°K. Electron beam density was 0.5 μa/cm^2 at 2.5 Mev corresponding to an absorbed dose rate of 4×10^9 rad/hr.

The EPR spectrum of liquid ethane was examined with a Varian V-4500 spectrometer *during irradiation of the sample* with 2.5-Mev electrons from a Van de Graaff accelerator. Irradiations were carried out directly inside a specially constructed vacuum-tight microwave cavity with the electron beam entering the magnetic field through an axial hole in a six-inch magnet. The ethane samples were handled on a vacuum line and air rigorously excluded from the system. The second derivative of the absorption, determined by simultaneous modulation at 100 000 and at 200 cps, was recorded and is illustrated in Fig. 1. Lines 1–12 in the figure are due without question to ethyl radicals. The spacing and intensity of the lines indicate that the electron is coupled to one group of two equivalent protons and a second group of three equivalent protons. The resultant spectrum consists of four triplets: lines 1, 2, and 4; 3, 5, and 7; 6, 8, and 10; and 9, 11, and 12 in Fig. 1. The eight spacings within these sets (and the nine between sets) are internally consistant within a standard deviation of 0.1 gauss. The ratios of peak heights of lines 1 through 12 are 0.8: 2.2: 2.9: 1.1: 6.0: 2.9: 3.2: 5.7: 1.1: 2.8: 2.1: 1.1 in excellent agreement with the expected values of 1: 2: 3: 1: 6: 3: 3: 6: 1: 3: 2: 1. A similar interpretation has been given by Smaller and Matheson for the long-lived radical species observed in irradiated solid ethane.[3] In the present study the lines are narrow (0.8 gauss) as expected for liquid systems. The (isotropic) hyperfine coupling constants are for the $-CH_2\cdot$ protons 22.5±0.2 gauss (63.0 Mc) and for the CH_3-protons 27.1±0.2 gauss (75.9 Mc). The first hyperfine constant is exactly that expected for a proton in a (substituted) methyl radical.[4] The second value represents the electron interaction with a proton in an adjacent methyl group under conditions where this methyl group is expected to be freely rotating.

Two very minor peaks occur between lines 5 and 6, and 7 and 8. These are attributed to the central lines in the methyl radical spectrum and are more apparent on slower scans. From their intensity the methyl radical concentration is estimated to be 4% that of the ethyl radical. It is interesting that additional absorptions due to hydrogen atoms, radical ions, or species other than those described above, appear to be absent.

By comparison of the observed signals with those from known samples the radical concentration in the irradiation zone is estimated as 7×10^{-8} molar (4×10^{13} radicals) at a current of 0.1 μa. Because of uncertainties inherent in making a comparison appropriate to the conditions of irradiation this estimate may be inaccurate by a factor of two. The observed concentration was porportional to the 0.47 power of the electron current from 0.001 to 0.5 μa in essential agreement with the expected square-root dependence. Reasonable assumptions for the radiation chemical yield of ethyl radicals and for the deposition of energy within the sample taken with the above concentration give a radical lifetime of 0.25 msec. The absolute second-order rate constant for the recombination of ethyl radicals in liquid ethane is estimated as 4×10^9 liters mole^{-1} sec^{-1}. This rate constant is an order of magnitude less than the recombination rate observed for methyl radicals in rotating sector experiments.[5] The difference presumably is due to the presence of the rate-controlling diffusion process in the liquid system and is consistent with an activation energy for diffusion of 0.5 to 1 kcal. There is no indication that any appreciable activation energy is involved in the radical combination reactions.

* Supported in part by the U. S. Atomic Energy Commission.

[1] L. H. Piette and W. C. Landgraf, J. Chem. Phys. **32**, 1107 (1960).

[2] N. Ya. Buben, V. V. Voevodskii, A. T. Koritskii, Yu. N. Molin, I. I. Chkheidze, and V. N. Shamshev, Optika i Spektroskopia **6**, 799 (1959).

[3] B. Smaller and M. J. Matheson, J. Chem. Phys. **28**, 1169 (1958).

[4] See H. M. McConnell, C. Heller, T. Cole, and R. W. Fessenden, J. Am. Chem. Soc. **82**, 766 (1960) for further references.

[5] R. Gomer and G. B. Kistiakowsky, J. Chem. Phys. **19**, 85 (1951).

On the Assignment of the Lowest Triplet State in Benzene*

ANDREAS C. ALBRECHT

Department of Chemistry, Cornell University, Ithaca, New York

(Received July 11, 1960)

THERE appears to be general theoretical agreement concerning the assignment of the lowest triplet state of benzene: a recent comparison[1] of predictions shows that the lowest triplet state is uniformly found to be $^3B_{1u}$. Seemingly, experiment to date has not been able to confirm this assignment. Vibrational analyses of the phosphorescence of benzene by Shull[2] and by Dikun and Sveshnikov[3] clearly point to a transition which is symmetry-forbidden (as well as spin-forbidden) and of a "B_{1u}" type. The O—O band is very weak and believed to be environment induced. The active vibrations are of the species e_{2g} (specifically ν_8 and ν_9) and b_{2g} (ν_4). The presence of the latter, though very weak, serves to distinguish B_{1u} from B_{2u}. More recent theoretical considerations strongly reinforce this interpretation. All vibronic theories without exception[4,5] predict that of the two e_{2g} carbon modes (ν_6 and ν_8) ν_8 should be distinctly more active in mixing B_{1u} and E_{1u} states. With less unanimity, ν_6 is predicted to be the most active in mixing B_{2u} and E_{1u} states (as has been observed in the first singlet transition). Furthermore a recent calculation[5] suggests that ν_9, a hydrogen mode, might be somewhat active in $B_{1u}-E_{1u}$ mixing but not in $B_{2u}-E_{1u}$ mixing. Evidence for a "B_{1u}" type transition in the phosphorescence has been taken to indicate the presence of $^1B_{1u}$ character in the lowest triplet state; and McClure,[6] in outlining the spin-orbit coupling selection rules, shows that in benzene a triplet state which contains $^1B_{1u}$ character through spin-orbit coupling must be $^3B_{2u}$. This stands in contradiction to the $^3B_{1u}$ theoretical assignment. The purpose of this communication is to emphasize an alternative scheme for removing the double forbiddenness which eliminates this contradiction and anticipates, qualitatively, preliminary observations made in our laboratory of polarized phosphorescence in benzene and a benzene derivative.

It is suggested here that the major part of the electric-dipole allowedness in the phosphorescence is achieved by vibronic mixing of $^3B_{1u}$ and $^3E_{1u}$ states which, theoretically at least,[1] appear to be close lying. That is, the $^1A_{1g}-^3B_{1u}$ intensity is "stolen" from the $^1A_{1g}-^3E_{1u}$ intensity which is actually $^1A_{1g}-^1E_{1u}$, $^1A_{2u}$ intensity through spin-orbit coupling. One way to formally achieve this is to employ vibronic theory which uses zeroth-order functions in which spin states are mixed. Mizushima and Koide,[7] whose work may by implication anticipate this particular approach, have considered the $^3E_{1u}-^1A_{2u}$ mixing in which relatively favorable matrix elements can be found. On the other hand, McClure[8] has shown that spin-orbit interaction among π-electronic states tends to be unusually weak. Thus the contribution of the intense accessible $^1A_{1g}-^1E_{1u}$ system (in plane) may not necessarily outweigh the $^1A_{1g}-^1A_{2u}$ (out-of-plane) contribution. Preliminary measurements of polarized phosphorescence in benzene in a rigid glass (−195°C) show that the out-of-plane component represents about $\frac{1}{3}$ of the visible intensity. More careful but still preliminary photometric observations of polarized phosphorescence in *p*-dimethoxybenzene[9] show that at least $\frac{1}{2}$ of the intensity is out-of-plane. Measurable out-of-plane intensity would not be compatible with the original scheme, for the amount of b_{2g} intensity (out-of-plane vibronic intensity) is negligible. On the other hand, the present route leads one to predict in-plane and out-of-plane intensity according to the relative contributions of $^1A_{1g}-^1E_{1u}$ and $^1A_{1g}-^1A_{2u}$ intensities and here measurable out-of-plane intensity would not seem surprising. Thus a $^3B_{1u}$ phosphorescing state is predicted on the basis of the vibrational analysis alone, and at the same time there is a probability for both out-of-plane and in-plane polarization through spin-orbit-coupling.

A more quantitative and complete discussion of the problem, with a critical study of other possible routes, shall await the completion of our polarization studies where oxygen effects shall receive careful attention.[10]

* This work was supported in part by the NSF.

[1] D. P. Craig, Revs. Pure and Appl. Chem. (Australia) **3**, 207 (1953).
[2] H. Shull, J. Chem. Phys. **17**, 295 (1949).
[3] P. P. Dikun and B. Ya. Sveshnikov, Zhur. Eksptl. i. Teoret. Fiz. **19**, 1000 (1949).
[4] For a comparison of theories see A. D. Liehr, Can. J. Phys. **35**, 1123 (1957); **36**, 1588 (1958).
[5] A. C. Albrecht, J. Chem. Phys. **33**, 169 (1960).
[6] D. S. McClure, J. Chem. Phys. **17**, 665 (1949).
[7] M. Mizushima and S. Koide, J. Chem. Phys. **20**, 765 (1952).
[8] D. S. McClure, J. Chem. Phys. **20**, 682 (1952).
[9] P. Russell and A. C. Albrecht (unpublished work).
[10] The preliminary data reported here have been taken without concern for oxygen effects.

Metastable States of Acridine Orange in Solution

G. BLAUER* AND H. LINSCHITZ

Department of Chemistry, Brandeis University, Waltham, Massachusetts

(Received July 1, 1960)

FLASH-EXCITATION has proved in recent years to be a powerful tool for the formation and analysis of metastable states in solution.[1] In the present work, a photoelectric flash-illumination apparatus of very short flash-duration was used,[2] which permitted measurement in solution of the absorption spectra and decay kinetics of the dye investigated. By this technique the decay of the metastable states of both ionized and unionized forms of 3,6-bisdimethyl-aminoacridine (acri-

dine orange) was recorded and analyzed. Measurements were performed at room temperature at different dye concentrations and in various solvents degassed in high vacuum. The spectral range covered was 3500–10 000 A. Previously the absorption spectrum of the metastable state of the acridine orange cation has been determined at 183°C.[3]

In acetic acid, water, and pyridine containing aqueous hydrochloric acid, the absorption band of the acridine orange cation around 5000 A diminished on flashing. In other spectral regions, where the ground state does not absorb, the metastable state showed measurable absorption. In acetic acid, this absorption was found to increase above 9000 A. On the other hand, absorption of the metastable state of the undissociated dye in triethylamine (TEA) solutions was higher than that of the ground state at most wavelengths between 3500 and 8000 A. The main peak was shifted from 4200 to 4100 A, and a small and broad absorption band appeared near 5500 A. Unlike the cation, the metastable state of the undissociated form did not absorb in the region 8000–10 000 A. Similar results were obtained with solutions of the dye in ethanol containing sodium methylate and in pyridine and toluene containing TEA.

The decay curves obtained in the region of the main absorption peaks indicated the existence of two metastable states of different lifetimes. In 10^{-6} *M* TEA solutions of the dye, and at room temperature, the two half-lives were of the order 0.1 and 1 msec, respectively, while in acetic acid, at comparable conditions, the half-lives were of the order 0.5 and 5–10 msec. Kinetic analysis of the decay curves obtained for the short-lived state in TEA indicated a reaction order close to two, together with some first-order contribution. The rate constant for the second-order reaction between two metastable molecules was found to be not less than 4×10^{9} 1 mole^{-1} sec^{-1}, while the first-order decay constant was 4×10^{8} sec^{-1}. The absorption of the long-lived state was too small to permit, under the experimental conditions used, determination of decay order and of rate constants. In acetic acid, the second-order constant for the decay of the short-lived state was smaller by a factor of about 6. In water, the spectra of both the ground state and the metastable state of the dye were similar to those obtained in acetic acid, but their difference in optical density was considerably smaller. It is therefore difficult to prove the existence of more than one metastable state in this solvent.

In pyridine containing TEA and in the presence of cobaltous acetate hydrate as a quenching agent, the lifetime of the short-lived state was reduced, with a quenching rate constant of 2×10^{7} 1 mole^{-1} sec^{-1}. The long-lived state could not be observed under the experimental conditions used. *p*-Toluene thiol in TEA caused the lifetime of the short-lived state to decrease but the flash excitation of the dye was accompanied by irreversible phenomena. 10^{-4}—10^{-5} mm of air in the space over a degassed TEA solution of acridine orange caused irreversible bleaching of the dye on flashing the solution. On repeated flash-excitation of acridine orange in different degassed solvents, various degrees of stability were observed. The most stable solutions were in pyridine containing cobaltous acetate, and in pure acetic acid.

It seems plausible to identify the short-lived state observed in flash-excitation of acridine orange with a triplet state. The long-lived metastable state could either be another triplet or a free radical of the semiquinone type formed by hydrogen abstraction from the solvent.

A detailed account of the present investigation will be published elsewhere.

This work was assisted by a grant from the U.S. Atomic Energy Commission.

* Weizmann Institute of Science, Rehovoth, Israel.

[1] G. Porter, Proc. Chem. Soc. (London) **1959**, 291; J. P. Simons, Quart. Revs. **13**, 3 (1959).
[2] H. Linschitz and K. Sarkanen, J. Am. Chem. Soc. **80**, 4826 (1958).
[3] V. Zanker and E. Miethke, Z. physik. Chem. (Frankfurt) **12**, 13 (1957).

Comments and Errata

Mechanism of Ozone Decomposition

H. J. SCHUMACHER

Instituto de Investigaciones de la Facultad de Química y Farmacia de la Universidad de La Plata, La Plata, Argentina

(Received May 27, 1960)

IN some papers dealing with the mechanism of zone decomposition,[1,2] Benson states that there is no evidence which proves the existence of energy chains during the course of this reaction.

I think that there is such evidence. Schumacher[3] using hitherto unpublished experimental data of Kistiakowsky for the photochemical decomposition of ozone by red light ($\lambda\simeq6400$ A) and Schumacher and Beretta, investigating the same reaction in the uv ($\lambda=3130$ A), found under certain experimental conditions quantum efficiencies much higher than 2. These results were explained assuming energy chains initiated by energy-rich oxygen molecules produced by the highly exothermic reaction

$$O+O_3\rightarrow2O_2^*.$$

The quantum efficiencies found in the red and in the uv (3130 A) region were quite similar and could be calculated in a satisfactory manner using the same reaction scheme and the same velocity constants for

its secondary reactions. No difference has been observed in the rate of reaction (2) whether the oxygen atoms were in the ground state (^3P) produced in the photochemical decomposition of ozone by red light, or were in the (^1D) state produced by absorption of uv light (3130 A).

L. J. Heidt[5] working at 3130 A obtained results similar to Beretta and Schumacher.

Benson, in his paper, does not discuss the high quantum efficiencies of the photochemical decomposition of ozone in red light. He is only referring to the results of the decomposition in the uv and proposes, disregarding the mechanism he gave in his first paper[1] which obviously cannot account for the high velocity experimentally established, the following reaction scheme:

$$O_3 + h\nu \rightarrow O_2^* + (^1D)O, \quad (1)$$

$$(^1D)O + O_3 \rightarrow (^2\Sigma_g^-)O_2 + (^3\Sigma_u^-)O_2, \quad (2)$$

$$(^3\Sigma_u^-)O_2 \rightarrow (^3\Sigma_g^-)O_2 + h\nu(2000\text{ A}), \quad (3)$$

$$h\nu + O_3 \rightarrow O_2^* + (^1D)O. \quad (4)$$

This mechanism, naturally, can not be applied to the experiments with red light. Considering the experiments done with uv light, the mechanism is theoretically possible, but there are several reasons which make its occurrence highly improbable.

(a) Reaction (2) is, as Benson has mentioned, endothermic by 4 kcal. Calculating with a steric factor of 0,1 and with the most favorable value for the heat of activation, it has to be postulated that the excited (^1D) oxygen atoms survive at least ten thousand collisions with other molecules without loosing their energy.

(b) In reaction (2) the energy of the electronic excitation of the (^1D) oxygen atom and the whole energy of reaction have to be transferred to one of the reaction products and transformed in electronic energy to form an oxygen molecule in the ($^3\Sigma_u^-$) state. There is no reason to believe that the (^1D) oxygen atoms will not react in a more simple way with the ozone molecules.

Assuming that the experimental data of the photochemical experiments are correct there is, in the author's opinion, no reason to doubt the existence of energy chains in the decomposition of ozone.[6]

[1] S. W. Benson and A. E. Axworthy, Jr., J. Chem. Phys. **26**, 1718 (1957).
[2] S. W. Benson, J. Chem. Phys. **26**, 1351 (1957).
[3] H. J. Schumacher, Z. physik. Chem. **B17**, 405 (1932).
[4] H. J. Schumacher and U. Beretta, Z. physik. Chem. **B17**, 417 (1932).
[5] L. J. Heidt, J. Am. Chem. Soc. **56**, 1671 (1934). The quotation in Benson's paper[2] that the quantum efficiencies of 3,5 found by Heidt for $\lambda = 3130$ A are twice as high as the ones found by Beretta and Schumacher is not correct.
[6] See also: W. D. McGrath and R. G. W. Norrish, Proc. Roy. Soc. (London) **A242**, 265 (1957); Z. physik. Chem. **15**, 245 (1958).

On the Existence of Energy Chains in Ozone Decomposition*

SIDNEY W. BENSON

Chemistry Department, University of Southern California Los Angeles 7, California

(Received June 20, 1960)

THE thermal decomposition of O_3 has been examined in extensive detail[1-3] and shown to fit a modified Jahn mechanism over the range 5°C to 254°C with no evidence for an energy chain. The studies are difficult because of the extreme sensitivity of the system to trace catalysis.[1] In addition, there are effects due to thermal self-heating at very fast reaction rates and a small acceleration by added H_2O.

Applied to the photolysis, this mechanism yields $1/\phi = k_2(M)(O_2)/2k_3(O_3) + 0.5$ for the quantum yield ϕ. Thus, k_2 comes from $O_2 + O + M \rightarrow O_3 + M$ while k_3 is for $O + O_3 \rightarrow 2O_2$. The data of Kistiakowsky[4] at 6200 A fit this relation very well.[1] However the slope is 2.2 greater than that predicted by the thermal results while the intercept is about 0.4 ± 0.1 rather than 0.5 and some results gave ϕ as high as 2.8. The precision of ϕ[5] was however only $\pm 30\%$ and in addition there was a very high dark rate attributed to stopcock grease so that these discrepancies are not serious. The effect of H_2O was also minor as in the thermal decomposition. The high quantums yields were obtained only at very low pressures where the precision was poorest. All of these findings lead me to conclude that the photolysis in the red does not support the existence of energy chains.

Heidt[6] has shown that the results of B and S[7] at 3130 fit the expression of the above type with an intercept of about 0.33 ± 0.05. However his ϕ are about twofold greater than those of B and S under comparable conditions. His dark rates agree very well with the thermal data. However, both authors find ϕ can exceed 2 (3130 A) and be as large as 3.5. At shorter λ, Heidt gets ϕ up to 6 which if we can neglect the known effects of impurities and H_2O[8] would seem to indicate short chains.

The only possible way to reconcile all of these findings is to attribute them to processes unique to wave lengths below 3200 A. Two mechanisms for this have already been presented[2,3] involving $[^1D]O + O_3 \rightarrow (^3\Sigma_u^-)O_2 + O_2$. Although this reaction is endothermic by 4 kcal, the O atoms produced at short λ can have excess translational energies of from 14 kcal (3100 A) to about 46 kcal (2100 A). 75% of this excess is available for inelastic processes in collisions with O_3. The average collision with O_2 will dissipate only $\frac{1}{8}$ of this energy and O_3 only $\frac{1}{48}$. The production of excited O_2 can thus be quite fast at high O_3 concentrations. The argument that $(^1D)O$ atoms cannot survive many collisions is not well founded.[9]

If any of this excess energy survives, it is possible to produce vibrationally excited $(^3\Sigma_u^-)O_2$ which can then

decompose rapidly (<0.1 sec) to reproduce (^1D)O or else radiate to initiate a photon chain.[10]

ϕ<4 are accountable by the reaction of O_3 with translationally excited (^3P)O to form the very weakly bound states of $O_2(^1\Sigma_\mu^-$, $^3\Sigma_\mu^+$ or $^3\Delta_\mu)$[11] which can dissociate in less than 0.01 sec at 25°C.

There is a good deal of evidence for excited O atoms in O_3 photolysis (<3100 A) which there is not space to discuss here.[12] Energy chains, if they do exist, cannot in my judgment be attributed to vibrationally excited O_2 but only to excited O. The problem can only be resolved by some new and careful experimental work.

* This work has been supported by a grant from the Office of Ordnance Research, U. S. Army.

[1] A. E. Axworthy, Jr., thesis, University of Southern California January, 1959.

[2] A. E. Axworthy, Jr., and S. W. Benson, Am. Chem. Soc. **1959**, 388, 398.

[3] A. E. Axworthy, Jr. and S. W. Benson, J. Chem. Phys. **26**, 1718 (1957).

[4] H. J. Schumacher, J. Am. Chem. Soc. **52**, 2377 (1930).

[5] G. B. Kistiakowsky, Z. physik. Chem. **117**, 348 (1925). The reproducibility of these experiments is about ±40%. The dark rate was as high as 60%.

[6] L. J. Heidt, J. Am. Chem. Soc. **57**, 1710 (1935).

[7] U. Beretta and H. J. Schumacher, Z. physik. Chem. **B17**, 417 (1932).

[8] G. S. Forbes and L. J. Heidt, J. Am. Chem. Soc. **56**, 1671 (1934), have obtained ϕ=120 with H_2O present and find $\phi \alpha (H_2O)^{\frac{1}{2}}$. At H_2O=0.01 mm this can still give ϕ=4.

[9] J. F. Noxon, thesis, Harvard University, 1957, finds that the less stable (^1S)O can survive 10^8 collisions.

[10] At 3000 A and 0.1 atm O_3, the photon mean-free-path is 0.6 cm (3 cm at 3100 A). Shorter wavelengths are also possible.

[11] J. T. Vanderslice *et al.*, J. Chem. Phys. **32**, 515 (1960); B. G. Reuben and J. W. Linnett, Trans. Faraday Soc. **55**, 1543 (1959) have presented evidence for the possible importance of translationally excited (^3P)O in N_2O pyrolysis.

[12] The very rapid decomposition of O_3 observed by W. D. McGrath and R. G. W. Norrish, Proc. Roy. Soc. (London) **A242**, 265 (1957) in flash photolysis is only compatible with such excitation.

Electrical Conduction in Magnesium Oxide

HERMANN SCHMALZRIED

Max-Planck-Institut für physikalische Chemie, Göttingen, Germany

(Received June 9, 1960)

MITOFF[1] has recently measured the electrical conductivity of single crystals of MgO as a function of oxygen partial pressure and temperature between 800 and 1400°C and has concluded that electronic conduction prevails.

To test this conclusion, the emf of the cell

$$\text{Pt} \mid \text{Fe, FeO} \mid \text{MgO} \mid \text{Ni, NiO} \mid \text{Pt} \qquad \text{(I)}$$

in thoroughly purified nitrogen has been measured. The setup of the cell was the same as that used recently for the determination of the free energy of formation of spinels.[2] Single crystals of MgO of optical quality with iron contents of 8, 100, and 1300 ppm in form of flat disks about 0.6 cm in diameter and 0.1 cm high were obtained from Mitoff.

If MgO were an electronic conductor, the emf of cell I would be equal to zero. Actually, the emf of cell I at 1100°C was found to be 0.285±0.010 v for each of the three MgO samples. Steady-state values were reached after about one hour with the sample containing 1300 ppm Fe, and after about three hours with the purer samples. After the measurements, the interior of the samples was completely clear. Next to the Fe–FeO mixture there was a very thin brownish zone presumably due to the formation of a MgO–FeO solid solution.

The observed value of 0.285 v is close to the value of 0.295 v which Kiukkola and Wagner[3] found for the cell

$$\text{Pt} \mid \text{Fe, FeO} \mid \text{ZrO}_2(+\text{CaO}) \mid \text{Ni, NiO} \mid \text{Pt}, \qquad \text{(II)}$$

in which ZrO_2(+CaO) is an ionic conductor with oxygen ions migrating via anion vacancies. Accordingly, on passing two faradays across cell II, the virtual cell reaction is

$$\text{NiO} + \text{Fe} = \text{FeO} + \text{Ni}. \qquad (1)$$

Hence the emf E of cell II is determined by the standard free energy change of reaction (1).

Since the emf values of cells I and II are nearly equal, it must be concluded that both cells involve the same virtual cell reaction, i.e., MgO is predominantly an ionic conductor at 1100°C, and oxygen partial pressure lies between the dissociation pressures of FeO and NiO. The ratio of electronic to ionic conductivity, however, may change at higher or lower chemical potentials of the nonmetallic constituent as has been shown, e.g., for AgBr.[4] No decision is possible as to whether cation or anion conduction in MgO prevails.

Similarly, emf values obtained on cells of type

$$\text{Pt, } H_2, H_2O \mid \text{slag(1)} \mid \text{MgO(s)} \mid \text{slag(1)} \mid \text{Pt, } H_2, H_2O, \qquad \text{(III)}$$

with slags of the system CaO–Al_2O_3–SiO_2, and on cells involving iron bearing slags,[5,6] indicate that MgO also exhibits predominantly ionic conduction above 1100°C.

The author is indebted to Dr. S. P. Mitoff for obtaining single crystals of MgO used in this investigation and to Professor C. Wagner for his valuable advice.

[1] S. P. Mitoff, J. Chem. Phys. **31**, 1261 (1959).

[2] H. Schmalzried, Z. physik. Chem. N.F. (to be published).

[3] K. Kiukkola and C. Wagner, J. Electrochem. Soc. **104**, 379 (1957).

[4] C. Wagner, Z. Elektrochem. **63**, 1027 (1959).

[5] J. Esin *et al.*, Izvest. Akad. Nauk S.S.S.R. Otokl. Tekh. Nauk. **9**, 114 (1957).

[6] K. Sanbongi and Y. Omori, Rept. Invest. of Tohuko Imp. Univ. **A11**, 244 (1959).

Comments on Dr. Schmalzried's Letter

S. P. MITOFF

Metallurgy and Ceramics Research Department, General Electric Research Laboratory, Schenectady, New York

(Received June 17, 1960)

DR. Ralph Carter and the author have duplicated Dr. Schmalzried's experiment using Norton single crystals of MgO (about 100 ppm iron) in contact with Fe, FeO, and Ni, NiO pellets. The nitrogen atmosphere was purified by causing it to flow past iron wire in the hot zone of the furnace. We obtained a lower potential than Dr. Schmalzried. At 1100°C we find an equilibrium potential of 0.235 v, whereas we obtain 0.285 v using ZrO_2 (with 18 mole percent CaO) in place of the MgO.

We conclude from these results that Dr. Schmalzried is correct in stating that the conduction MgO is predominantly ionic under the test conditions. However, the lower voltage indicates that a smaller portion (about 17%) of the current is simultaneously carried by an electronic mechanism.

The detection of an ionic conduction mechanism in MgO leaves many of the conductivity results reported in the original paper difficult to explain, especially the reversible changes in conductivity with changing oxygen pressure. For this reason, we are at present undertaking a more extensive program to study the fraction of ionic conductivity in MgO.

I would like to thank Dr. Schmalzried for his interest and for his contribution to our knowledge of MgO.

"Average Energy Approximation" in Spin-Coupling Calculations

MARTIN KARPLUS*

Noyes Chemical Laboratory, University of Illinois, Urbana, Illinois

(Received June 27, 1960)

IN a recent note, McLachlan[1] has pointed out that the "average energy approximation" can lead to false conclusions when applied indiscriminately to simplify second-order perturbation theory calculations. With a perturbation operator $\mathcal{H}'$, the second-order energy $E^{(2)}$ is given by the expression

$$E^{(2)}=\sum_n{}^1[\langle 0\,|\,\mathcal{H}'\,|\,n\rangle\langle n\,|\,\mathcal{H}'\,|\,0\rangle/(E_n-E_0)]. \quad (1)$$

Since $\langle 0\,|\,\mathcal{H}'\,|\,n\rangle\langle n\,|\,\mathcal{H}'\,|\,0\rangle=|\,\langle 0\,|\,\mathcal{H}'\,|\,n\rangle\,|^2$ is positive for all n, a replacement of the differences (E_n-E_0) by a *necessarily positive* energy denominator Δ is always possible and leads to the simple result

$$E^{(2)}=(1/\Delta)[\langle 0\,|\,(\mathcal{H}')^2\,|\,0\rangle-(\langle 0\,|\,\mathcal{H}'\,|\,0\rangle)^2]. \quad (2)$$

In applications of a corresponding procedure to magnetic resonance phenomena, the perturbation operator is written conveniently as the sum of two terms ($\mathcal{H}'=\mathcal{H}_A+\mathcal{H}_B$) with the significant part of the second-order energy arising from matrix elements of the form $\langle 0\,|\,\mathcal{H}_A\,|\,n\rangle\langle n\,|\,\mathcal{H}_B\,|\,0\rangle$. [For the spin-coupling problem,

$$\mathcal{H}_A=\xi\sum_k\delta(\mathbf{r}_{kA})\mathbf{S}_k$$

and

$$\mathcal{H}_B=\xi\sum_k\delta(\mathbf{r}_{kB})\mathbf{S}_k,$$

where A and B are the coupled nuclei.] Since these cross terms may vary in sign as a function of the state n, in contrast to the product of the matrix elements of the complete Hamiltonian $\mathcal{H}'$ appearing in Eq. (1), the energy denominator Δ may not be simply related to the excitation energies; in fact, Δ can have a negative value.

Although McLachlan has directed his criticism of the average energy approximation particularly toward its application to the spin-coupling problem, we wish to show that the use of Eq. (2) can be justified in certain of the calculations that have been reported.[2,3] The spin-coupling operators $\mathcal{H}_A$ and $\mathcal{H}_B$ have nonzero matrix elements between the singlet ground state and triplet excited states. In all of the molecules considered, the singlet and triplet eigenfunctions of interest can be represented in terms of a localized bond description; that is, in the valence-bond approach the only structure that contributes significantly[4] to the ground state is the perfect-pairing structure. Correspondingly, the triplet states can be expressed as functions which differ from the perfect-pairing structure only by having the spins of one electron pair coupled to a triplet instead of a singlet bond function. For such systems it can be demonstrated by a simple extension of the theory developed for the pi-electron contribution[5] that the proton coupling constant $A_{HH'}$ has the form

$$A_{HH'}=K\sum_T[a_H(T)a_{H'}(T)/\Delta(T)], \quad (3)$$

where the sum is over the localized triplet states that contribute to $A_{HH'}$, $\Delta(T)$ is the singlet to triplet excitation energy, and K is a positive constant.[6] The quantities $a_H(T)$ and $a_{H'}(T)$ are the hyperfine constants for the radical fragments associated with the triplet state T. In the case of the pi-electron terms,[5] $a_H(T)$ and $a_{H'}(T)$ can be related to data obtained in ESR measurements. Although for the sigma-electron contributions in the molecules of interest here such a direct

evaluation is not always possible, we can determine the interactions that are important. If the triplet T involves a bond between H and H′ in the perfect-pairing structure (i.e., H_2), $a_H(T)$ and $a_{H'}(T)$ are approximately equal to the hyperfine constants for the hydrogen atom. For protons not bonded in the perfect-pairing structure, the triplets that are important involve one or the other of the proton bonds. The quantity $a_H(T)$, say, is still equal to the hydrogen atom constant, but a $a_{H'}(T)$ would be zero except for deviations from perfect pairing. These can be introduced into the wave function by perturbation theory with an operator of the form

$$-\sum_{\sigma,\sigma'}(e^2/r_{\sigma\sigma'})P_{\sigma\sigma'},$$

where $P_{\sigma\sigma'}$ is the transposition operator for electrons in the bonds σ and σ'. Triplets that do not involve the bond of H or H′ can be neglected.

With this formulation of the coupling constant, we can consider the validity of the average energy approximation for the molecules to which it has been applied. In the directly-bonded case (H_2) only the lowest triplet contributes significantly and Eq. (3) reduces directly to an expression of the form given in Eq. (2) with Δ equal to $\Delta(T)$. In the nonbonded cases (HCH′ and HCC′H′), only the two triplets T and T' involving, respectively, the HC and the H′C′ bonds are important. Since their excitation energies are the same in the localized approximation [also $a_H(T)=a_{H'}(T')$ and $a_{H'}(T)=a_H(T')$] again Δ is a positive quantity simply related to $\Delta(T)$. Thus, for these localized-bond systems, the average energy approximation is applicable to the coupling constant calculation.[7] The sign of $A_{HH'}$ is determined by the numerators in both Eqs. (2) and (3) with Δ and $\Delta(T)$ positive. For more complicated molecules, particularly those in which delocalization is significant (e.g., aromatic molecules), considerable care is necessary in the use of the average energy approximation.[1]

* Alfred P. Sloan Foundation Fellow. Present address: Columbia University, New York, New York.

[1] A. D. McLachlan, J. Chem. Phys. **32**, 1263 (1960).

[2] N. F. Ramsey, Phys. Rev. **91**, 303 (1953).

[3] M. Karplus and D. H. Anderson, J. Chem. Phys. **30**, 6 (1959); M. Karplus, J. Chem. Phys. **30**, 11 (1959).

[4] The word "significantly" refers to the over-all energy and the form of the wave function; that is,

$$\psi=\psi_1+\sum_{i>1}c_i\psi_i,$$

with ψ_1 the perfect pairing structure and $c_i(i>1)\ll 1$. For the coupling terms ψ_i are, of course, important. See footnote reference 3.

[5] M. Karplus, J. Chem. Phys. **33**, 316 (1960).

[6] For $A_{HH'}$, $a_H(T)$, $a_{H'}(T)$ in cps and $\Delta(T)$ in ev, K is on the order of 2×10^{-15}, its exact value depending on the form of localized bond function.

[7] Dr. A. D. McLachlan has informed me that he is in complete agreement with this conclusion.

Erratum: Some Observations on Atomic Exchange in NO

[J. Chem. Phys. **32**, 1579 (1960)]

W. Spindel and Marvin J. Stern

Department of Chemistry, Rutgers, The State University, Newark 2, New Jersey

(Received July 13, 1960)

REFERENCE to the work of Dulmage, Meyers, and Lipscomb[1] regarding the structure of the NO dimer in the solid state erroneously implied that their studies indicated a square structure for this compound. Actually, their data allowed for several structures which averaged out to a rectangular planar model with a short edge of 1.12 A and a long edge of 2.4 A. Such a structure is consistent with the absence of exchange after freezing and revaporization.

[1] W. J. Dulmage, E. A. Meyers, and W. N. Lipscomb, Acta Cryst. **7**, 760 (1953).

Errata: "Contributions of Bound, Metastable, and Free Molecules to the Second Virial Coefficient and Some Properties of Double Molecules" and "Initial Pressure Dependence of Thermal Conductivity and Viscosity"

[J. Chem. Phys. **31**, 1531, 1545 (1959)]

Daniel E. Stogryn and Joseph O. Hirschfelder

Theoretical Chemistry Laboratory, University of Wisconsin, Madison 5, Wisconsin

(Received July 11, 1960)

THE authors wish to correct the errors in their work arising from the omission of a factor of two on the right side of Eq. (14) in their paper on double molecules and the corresponding equations given in footnote 5 of that paper. We wish to thank Mr. James T. O'Toole and Dr. John S. Dahler for calling our attention to this omission of the factor of two, which was due to not including integrations over negative values of the radial momentum.

The following changes should be made in the paper on double molecules: The right side of Eqs. (14), (35), (43), (45), (55), (57), (65), and (67) should be multiplied by two. The columns labeled B_m^* in Tables I, II, and III should be labeled $\frac{1}{2}B_m^*$ and the columns labeled B_f^* should be labeled $B_f^*-\frac{1}{2}B_m^*$. In Figs. 6, 7, and 8, the curves labeled B_m^* and B_f^* should be labeled $\frac{1}{2}B_m^*$ and $(B_f^*-\frac{1}{2}B_m^*)$, respectively. Finally, in Table

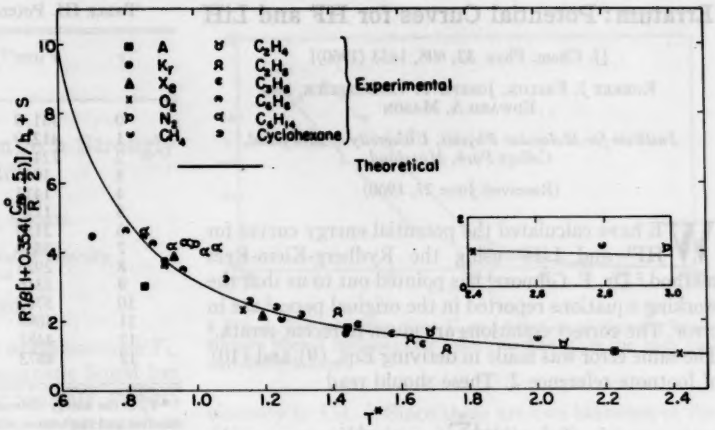

FIG. 3. A comparison of theoretical and experimental values of $RT\beta\{1+0.354[(C_{pA}^{\circ}/R)-\frac{5}{2}]\}/b_0+S$ for the Lennard-Jones (6-12) potential. The theoretical curve and experimental points are calculated on the basis $\epsilon_{A_2A}/\epsilon_{AA}=1.32$ and $\sigma_{A_2A}/\sigma_{AA}=1.04$.

IV, the rows labeled x_{2m}/b_0 and x_{2m} should be labeled $\frac{1}{2}x_{2m}/b_0$ and $\frac{1}{2}x_{2m}$, respectively.

In the paper "Pressure Dependence of Thermal Conductivity and Viscosity," the equations, except for Eq. (53), remain unchanged but the tables must be altered because some of the quantities listed depend on the numerical values of B_m* and its derivatives as well as on the parameter $\sigma_{A_2A}/\sigma_{AA}$ given in Eq. (53). Using the correct values for B_m*, we find empirically, by comparing calculated and experimental values of $RT\beta/b_0$ for the noble gases, that a good value for $\sigma_{A_2A}/\sigma_{AA}$ is $\sigma_{A_2A}/\sigma_{AA}=1.04$. Thus, Table I should read:

TABLE I.

T	$\Delta H/RT$	$\mathfrak{A}$	$\mathfrak{B}$*	$\mathfrak{C}$*	$\mathfrak{D}$
0.5	−3.02079	9.53052	0.156	16.5	4.717
0.6	−2.87798	8.56102	0.125	9.74	2.904
0.7	−2.79012	7.98657	0.102	6.57	2.040
0.8	−2.73190	7.61603	0.076	4.85	1.564
0.9	−2.69113	7.36164	0.058	3.81	1.275
1.0	−2.66130	7.17852	0.042	3.13	1.087
1.25	−2.61381	6.89245	0.011	2.20	0.8261
1.50	−2.58649	6.73145	−0.0023	1.72	0.6976
1.75	−2.56907	6.63037	−0.011	1.43	0.6236
2.0	−2.55713	6.56196	−0.015	1.25	0.5762
2.5	−2.54203	6.47656	−0.018	1.01	0.5192
3.0	−2.53300	6.42620	−0.017	0.863	0.4857
4.0	−2.52286	6.37049	−0.015	0.699	0.4467
5.0	−2.51739	6.34085	−0.012	0.607	0.4232
10.0	−2.50780	6.28995	−0.0050	0.433	0.3661

* These values are obtained by taking $\epsilon_{A_2A}/\epsilon_{AA}=1.32$ and $\sigma_{A_2A}/\sigma_{AA}=1.04$.

In Table II, the values of S (computed with $\sigma_{A_2A}/\sigma_{AA}=1.04$) should be 0, 0, 0; 0, 0, 0; 0, 0; +0.023, −0.018; +0.042, −0.017; +0.012, −0.023, −0.042; −0.030, −0.068; +0.006, −0.037, −0.057; −0.016, −0.056, −0.086; 0.71, 0.68, 0.66, 0.62, 0.56; 1.14, 0.97, 0.89, 0.76, 0.69, 0.38, 0.30, 0.20, 0.13; 0.19, 0.14, 0.12, 0.090; 0.34, 0.31. The values of $RT\alpha/b_0$ in Table III should be ($\sigma_{A_2A}/\sigma_{AA}=1.04$) 0.770, 0.375, 0.218, 0.169, 0.150, 0.149, 0.171, 0.181, 0.189, 0.192, 0.189, 0.181, 0.166, 0.154, 0.123, and in Table IV the values of $RT\alpha_{calc}/b_c$ should be 0.12; 0.192, 0.190; 0.182; 0.173; 0.187, 0.185; 0.178, 0.176; 0.182.

Figures 3 and 4 should appear as given in this erratum. The minimum in the computed curve in Fig. 4 may very likely be due to the approximations in the theory. If the parameter $\sigma_{A_2A}/\sigma_{AA}$ is chosen to be 1.033 or less, the computed values of $RT\alpha/b_0$ are greater than when $\sigma_{A_2A}/\sigma_{AA}=1.04$, and a minimum in the computed curve does not occur. However, with $\sigma_{A_2A}/\sigma_{AA}=1.033$ the agreement with experimental thermal conductivity data is slightly less good. Since the experimental values of $\beta=[(1/\lambda)(\partial\lambda/\partial p)]_{p=0}$ are more reliable than the experimental values of $\alpha=[(1/\eta)(\partial\eta/\partial p)]_{p=0}$, we have chosen $\sigma_{A_2A}/\sigma_{AA}=1.04$ as the best estimate of this parameter.

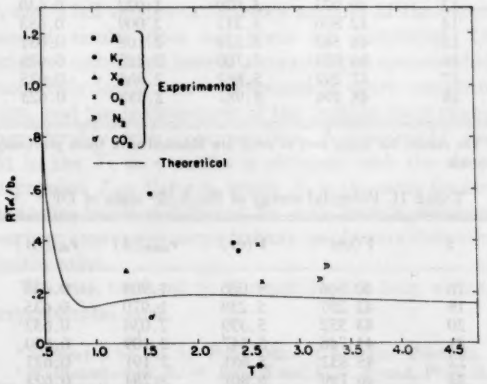

FIG. 4 A comparison of theoretical and experimental values of $RT\alpha/b_0$. The theoretical curve is calculated on the basis $\epsilon_{A_2A}/\epsilon_{AA}=1.32$ and $\sigma_{A_2A}/\sigma_{AA}=1.04$.

Erratum: Potential Curves for HF and LiH

[J. Chem. Phys. **32**, 698, 1453 (1960)]

ROBERT J. FALLON, JOSEPH T. VANDERSLICE, AND EDWARD A. MASON

Institute for Molecular Physics, University of Maryland, College Park, Maryland

(Received June 27, 1960)

WE have calculated the potential energy curves for HF[1] and LiH[2] using the Rydberg-Klein-Rees method.[3] Dr. F. Gilmore[4] has pointed out to us that the working equations reported in the original paper[3] are in error. The correct equations are given in recent errata.[5] The same error was made in deriving Eqs. (9) and (10) of footnote reference 2. These should read

$$f=(8\pi^2\mu c/h)^{\frac{1}{2}}\sum_{i=1}^{n}(-\omega x)_i^{-\frac{1}{2}}Y_i \qquad (1)$$

$$g=(8\pi^2\mu c/h)^{\frac{1}{2}}\sum_{i=1}^{n}\{\alpha_i(-\omega x)_i^{-1}\times[(U_n-U_i)^{\frac{1}{2}}-(U_n-U_{i-1})^{\frac{1}{2}}]+(-\omega x)_i^{-\frac{1}{2}}[B_i+\alpha_i\omega_i(-2\omega x_i)^{-1}]Y_i\}, \qquad (2)$$

where

$$Y_i=\arcsin\frac{[1+4U_i(-\omega x)_i\omega_i^{-2}]^{\frac{1}{2}}}{[1+4U_n(-\omega x)_i\omega_i^{-2}]^{\frac{1}{2}}}-\arcsin\frac{[1+4U_{i-1}(-\omega x)_i\omega_i^{-2}]^{\frac{1}{2}}}{[1+4U_n(-\omega x)_i\omega_i^{-2}]^{\frac{1}{2}}}.$$

We have recalculated the curves for the reported states of HF and LiH using these corrected equations, and have found that only the $X\,^1\Sigma^+$ states of HF and DF and the $A\,^1\Sigma^+$ states of LiH and LiD are changed. In the former case only the upper levels are affected. The new results for these states are listed in Tables I to IV. The maximum correction is about two percent for the uppermost levels. The results for the $A\,^1\Sigma^+$ state of LiH are now in better agreement with the results obtained graphically by Rosenbaum.[2,6] None of the other conclusions drawn are affected by the new results.

TABLE I. Potential energy of the $X\,^1\Sigma^+$ state of HF.[a]

v	$V(\text{cm}^{-1})$	$V(\text{ev})$	$r_{\max}(A)$	$r_{\min}(A)$
13	40 973	5.079	1.922	0.639
14	42 850	5.312	2.009	0.635
15	44 543	5.522	2.108	0.631
16	46 031	5.706	2.223	0.628
17	47 292	5.862	2.364	0.625
18	48 294	5.987	2.555	0.623

[a] The results for levels $v=0$ to $v=12$ are identical with those previously reported.

TABLE II. Potential energy of the $X\,^1\Sigma^+$ state of DF.[a]

v	$V(\text{cm}^{-1})$	$V(\text{ev})$	$r_{\max}(A)$	$r_{\min}(A)$
18	40 866	5.066	1.908	0.638
19	42 257	5.238	1.970	0.635
20	43 552	5.399	2.036	0.632
21	44 746	5.547	2.109	0.630
22	45 832	5.681	2.191	0.627
23	46 799	5.801	2.284	0.625

[a] The results for levels $v=0$ to $v=17$ are identical with those previously reported.

TABLE III. Potential energy of the $A\,^1\Sigma^+$ state of LiH.

v	$V(\text{cm}^{-1})$	$V(\text{ev})$	$r_{\max}(A)$	$r_{\min}(A)$	$T_e+V(\text{ev})$[a]
0	131.0	0.0162	3.010	2.246	3.3021
1	412.0	0.0511	3.292	2.030	3.3380
2	724.9	0.0899	3.475	1.911	3.3768
3	1061	0.1315	3.625	1.827	3.4184
4	1413	0.1752	3.757	1.761	3.4621
5	1779	0.2206	3.877	1.706	3.5075
6	2155	0.2671	3.991	1.660	3.5540
7	2538	0.3146	4.100	1.620	3.6015
8	2925	0.3626	4.207	1.585	3.6495
9	3316	0.4109	4.310	1.549	3.6978
10	3707	0.4593	4.417	1.525	3.7462
11	4098	0.5080	4.521	1.500	3.7949
12	4487	0.5563	4.627	1.476	3.8432
13	4873	0.6041	4.735	1.455	3.8910

[a] T_e is the energy difference between the bottom of the potential curve in question and the bottom of the curve for the $X\,^1\Sigma^+$ state.

TABLE IV. Potential energy of the $A\,^1\Sigma^+$ state of LiD.[a]

v	$V(\text{cm}^{-1})$	$V(\text{ev})$	$r_{\max}(A)$	$r_{\min}(A)$	$T_e+V(\text{ev})$
0	94.6	0.0117	2.942	2.277	3.2986
1	300.6	0.0373	3.195	2.086	3.3242
2	525.2	0.0651	3.360	1.976	3.3520
3	765.2	0.0949	3.491	1.897	3.3818
4	1017	0.1261	3.604	1.834	3.4130
5	1279	0.1586	3.706	1.782	3.4455
6	1550	0.1921	3.800	1.737	3.4790
7	1826	0.2264	3.890	1.699	3.5133
8	2108	0.2614	3.975	1.664	3.5483
9	2394	0.2969	4.058	1.633	3.5838
10	2684	0.3327	4.139	1.605	3.6196
11	2975	0.3689	4.219	1.578	3.6558
12	3268	0.4052	4.296	1.552	3.6921
13	3562	0.4416	(4.379)	(1.536)	3.7285
14	3856	0.4781	(4.461)	(1.521)	3.7650
15	4149	0.5144	(4.537)	(1.499)	3.8013
16	4442	0.5506	(4.614)	(1.481)	3.8375
17	4732	0.5867	(4.693)	(1.461)	3.8736

[a] Numbers in parentheses are less accurate than the number of figures reported because of loss of significant figures in the calculation.

[1] R. J. Fallon, J. T. Vanderslice, and E. A. Mason, J. Chem. Phys. **32**, 698 (1960).
[2] R. J. Fallon, J. T. Vanderslice, and E. A. Mason, J. Chem. Phys. **32**, 1453 (1960).
[3] J. T. Vanderslice, E. A. Mason, W. G. Maisch, and E. R. Lippincott, J. Mol. Spectroscopy **3**, 17 (1959).
[4] Address: Rand Corporation, Santa Monica, California.
[5] J. T. Vanderslice, E. A. Mason, W. G. Maisch, and E. R. Lippincott, J. Chem. Phys. **33**, 614 (1960).
[6] E. J. Rosenbaum, J. Chem. Phys. **6**, 16 (1938).

Notes

Nuclear Magnetic Relaxation in a Strongly Associated Liquid*

C. R. K. MURTHY AND R. D. SPENCE

Department of Physics, Michigan State University, East Lansing, Michigan

(Received May 27, 1960)

THE relation between the nuclear relaxation time T_1, and the viscosity η of nonparamagnetic liquid has been studied by making use of the viscosity changes produced by changes in temperature[1] or pressure[2] or by varying the concentration of one of the components of a mixture of two liquids. We have examined the variation of T_1 with viscosity in the mixture phenyl isothiocyanate+diethyamine. The viscosity of this mixture shows a sharp maximum at equimolecular proportions, rising to a value 26 000 times that of its most viscous component. The fact that the mixing is accompanied by a liberation of heat and a volume contraction shows that the system exhibits a high degree of association. The values of T_1 as a function of concentration were obtained with conventional pulse apparatus operating at 5 Mc. The results shown in Fig. 1 clearly reflect the viscosity maximum at 50 mole %. The values of T_1 are shown as a function of the viscosity in Fig. 2. Since there are two branches of the curve for mole fractions c greater than and less than 0.5, it is clear that there is no unique relation between T_1 and η which is valid for all concentrations. If one attempts to fit the separate branches with an expression involving a single correlation time τ_c such as

$$1/T_1=(K/\omega)\{[\omega\tau_c/1+(\omega\tau_c)^2]+[2\omega\tau_c/1+(2\omega\tau_c)^2]\}, \quad (1)$$

one must require $\omega\tau_c\leq 2^{-1}$ since it appears from Fig. 2 that T_1 approaches but does not pass through a minimum as η increases. If τ_c is assumed to vary linearly with viscosity, then for the branch $c<0.5$ τ_c would vary by a factor of 26 000. According to Eq. (1), the minimum variation in T_1 consistent with such a variation in τ_c and the condition $\omega\tau_c\leq 2^{-1}$ amounts to a factor of 11 600 as compared with an experimentally observed variation of T_1 by a factor of 267. The branch $c>0.5$ shows a corresponding disagreement with Eq. (1). Assigning different coefficients to the first and second terms in Eq. (1) does not improve the agreement.

The fact that expressions of the form of Eq. (1) coupled with an assumption of a linear relation between τ_c and η fail to give satisfactory account of the experimental results does not seem too surprising. The mixture considered here is a complicated system which essentially forms a new compound at every concentration, and the environment of the protons must change considerably with concentration. A reasonably good fit to the T_1 vs η curves is obtained with the simple expression $T_1=T_0+a/\eta$, where T_0 is the same for both branches but a is different for each branch. However, such an expression seems to have no obvious theoretical justification.

We wish to thank S. Kirmani for his help with the experimental work.

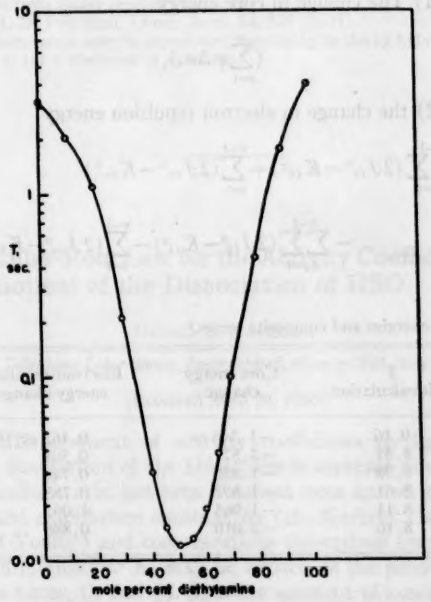

FIG. 1. The relaxation time T_1 as a function of mole percent diethylamine in the mixture phenyl isothiocynate+diethylamine.

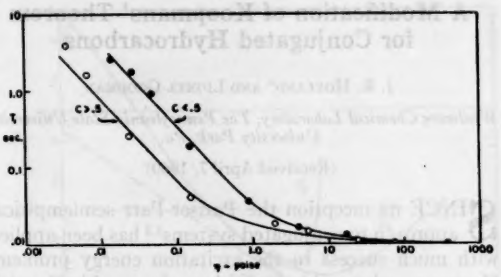

FIG. 2. The relaxation time T_1 as a function of viscosity in the mixture phenyl isothiocynate+diethylamine. C is the mole percent diethylamine.

* Supported by the Air Force Office of Scientific Research.

[1] N. Bloembergen, E. M. Purcell and R. V. Pound, Phys. Rev. **73**, 679 (1948).

[2] G. B. Benedek and E. M. Purcell, J. Chem. Phys. **22**, 2003 (1954).

[3] N. Kurnakov and S. Zemchuzny, Z. physik. Chem. **83**, 481 (1913).

A Modification of Koopmans' Theorem for Conjugated Hydrocarbons

J. R. HOYLAND* AND LIONEL GOODMAN

Whitmore Chemical Laboratory, The Pennsylvania State University, University Park, Pa.

(Received April 7, 1960)

SINCE its inception the Pariser-Parr semiempirical approach to conjugated systems[1,2] has been applied with much success to the excitation energy problem. However, when this procedure is combined with Roothaan's SCF formulation,[3] poorer results are obtained for the ionization energies of such systems if Koopmans' theorem[3a] is applied. This theorem states that for a closed-shell configuration, the ionization potential should be approximately given by $I=-\epsilon_n$, where ϵ_n is the Hartree-Fock energy of the highest filled shell.

This communication represents an interim report on ionization energy calculations which attempt to include those effects neglected in the application of Koopmans' theorem to conjugated hydrocarbons:

(1) The effect of π-electron ionization on the σ framework.

(2) Changes in the $C2p_z$ basis functions upon ionization.

(3) Changes in the π–MO's through construction of a new Hartree-Fock Hamiltonian for the ionized state.

In this note calculations including only factors (1) and (2) will be summarized. As a framework, a strict Goeppert-Mayer-Sklar core formulation[4] with neglect of penetration integrals is adhered to, rather than the procedure used by Pople.[5]

Factor 1 is accounted for by assuming $E\sigma_\mu \sim -bZ_\mu^2(\sigma)$, where Z_{eff} for a σ electron is given by

$$Z_\mu(\sigma)=Z_\mu^0(\sigma)+k'\Delta q_\mu^{(\pi)},$$

$\Delta q_\mu^{(\pi)}$ being the change in π-electron density at carbon atom μ, Z_μ^0 being Z_{eff} for π-electron density = unity. Then

$$\Delta E_\sigma=-\sum_\mu 2bZ_\mu^0(\sigma)k'\Delta q_\mu^{(\pi)} \qquad (1)$$

Inasmuch as $\sum_\mu \Delta q_\mu^{(\pi)}=1$ upon ionization, for any hydrocarbon the change in σ-bond energy, ΔE_σ, should be a constant (k).[6]

Changing the $2p_z$ basis functions will effect the π-MO energy levels by changing both I_c and $(pp|qq)$ through $Z_\mu(\pi)$. It was assumed that $I_{c_\mu}=I_{c_\mu}^0+c\Delta q_\mu^{(\pi)}$ and that $(pp|qq)=(pp|qq)^0+c'\Delta\bar{q}_{pq}^{(\pi)}$. The one-center repulsion integral $(pp|pp)^0$, given in the Pariser-Parr formulation as I_c-A_c, was taken to be 11.54−0.46=11.08 ev.[8]

Values for k, c, and a were obtained by equating the ionization energies of benzene, ethylene, and acetylene[9] to the expression

$$I=E^+-E_G=2\sum_{i=1}^{n-1}H_i^+ + H_n^+ + \sum_{i,j=1}^{n-1}\sum(2J_{ij}^+-K_{ij}^+) + \sum_{i=1}^{n-1}(2J_{in}^+-K_{in}^+)+k-2\sum_{i=1}^{n}H_i^0 - \sum_{i,j=1}^{n}\sum(2J_{ij}^0-K_{ij}^0), \qquad (2)$$

where H_i^+, J_{ij}^+, and K_{ij}^+ were written in terms of c and a. The three simultaneous equation for k, c, and a were then solved giving $k=-.816$ ev, $c=1.078$ ev, and $a=2.619$ ev. These constants were then utilized to compute the ionization energy via Eq. (2) for the series of conjugated hydrocarbons in Table I, utilizing ground-state SCF orbitals. As can be seen from Table I, considerable improvement is brought about in the results. This improvement is broken into three terms:

(1) The change in core energy

$$(\sum_{i=1}^{n}q_i\Delta\alpha_i),$$

(2) the change in electron repulsion energy

$$(\sum_{i,j=1}^{n-1}\sum(2J_{ij}^+-K_{ij}^+)+\sum_{i=1}^{n-1}(2J_{in}^+-K_{in}^+) - \sum_{i,j=1}^{n-1}\sum(2J_{ij}^0-K_{ij}^0)-\sum_{i=1}^{n-1}(2J_{in}^0-K_{in}^0)),$$

TABLE I. Computed and observed ionization energies and composite terms.[e]

Compound	I Experimental	I Koopmans' Theorem	I This calculation	Core energy change	Electron-repulsion energy change
Trans-butadiene	9.18 ev[a]	10.86	9.16	−1.346 ev	0.462 ev
Trans-hexatriene	8.23[b]	10.37	8.57	−1.577	0.594
Styrene	8.86[c]	10.87	8.98	−1.820	0.744
Naphthalene	8.26[d]	10.53	8.61	−1.892	0.788
Anthracene	7.55[d]	9.80	8.11	−1.965	1.092
Phenanthrene	8.03[d]	10.10	8.16	−2.010	0.886

[a] J. Collin and F. P. Lossing, J. Am. Chem. Soc. **79**, 5848 (1957).
[b] Price and Walsh, Proc. Roy. Soc. (London) **A185**, 182 (1946).
[c] J. D. Morrison and L. C. Nicholson, J. Chem. Phys. **20**, 1021 (1952).
[d] M. E. Wacks and V. H. Dibeler, J. Chem. Phys. **31**, 1557 (1959).
[e] The calculated change in σ-bond energy term is −0.816 ev for all cases considered here.

(3) the change in σ-bond energy (k). The sum of these three factors represents the difference between the energy of the ionized state when the modifications listed above are considered and that given by Koopmans' theorem.

Although considerable improvement is brought about by adjustment of the σ framework and the p_z basis functions, the results are still in error by an appreciable amount for some of the compounds. This, in all probability, is due to the neglect of factor (3). Reminimization of the ionized state yields sizable changes in the individual MO's and thus in the MO electron-repulsion integrals (both J_{ij} and K_{ij}) and in the core energy.

Particular attention is called to the calculated σ-bond energy change (0.8 ev). The σ bonds would seem far from insensitive to their π-electron environment. Of course, this is indirectly tied up with the change in basis functions which yield an average improvement in ionization energy of over 1 ev.

* National Science Foundation Pre-Doctoral Fellow 1959–1960.
[1] R. Pariser and R. G. Parr, J. Chem. Phys. **21**, 466 (1953).
[2] R. Pariser and R. G. Parr, J. Chem. Phys. **21**, 767 (1953).
[3] C. C. J. Roothaan, Revs. Modern Phys. **23**, 69 (1951).
[3a] T. Koopmans, Physica **1**, 104 (1934).
[4] M. Goeppert-Mayer and A. L. Sklar, J. Chem. Phys. **6**, 645 (1938).
[5] J. A. Pople, Trans. Faraday Soc. **49**, 1375 (1953); N. S. Hush and J. A. Pople, *ibid.* **51**, 600 (1955).
[6] Ignored here are σ-bond reorganization effects such as discussed for formaldehyde by Parks and Parr, J. M. Parks and R. G. Parr, J. Chem. Phys. **32**, 1657 (1960).
[7] For $(p_p|p_p)$ $c'\equiv a$. For $(p_p|q_q)$ nearest neighbors, $\Delta\bar{J}_{pq}^{(\sigma)}=[\Delta q_p^{(\sigma)}+\Delta q_q^{(\sigma)}]/2$, and the constant c is assumed to be proportional to a with the proportionality factor theoretically computed from Slater orbitals.
[8] H. D. Pritchard, Chem. Revs. **52**, 529 (1955).
[9] Some error may be introduced here owing to the sp hybridization of the σ electrons in acetylene.

A Cube-Root Law for the Activity Coefficient Quotient of the Dissociation of HSO_4^- Ion

GEORGE E. WALRAFEN

Bell Telephone Laboratories, Incorporated, Murray Hill, New Jersey

(Received April 29, 1960)

THE quotient of activity coefficients Q_f for the dissociation of the HSO_4^- ion in aqueous solutions of sulfuric acid has been obtained from known values of the equilibrium constant K_2 (cf., Kerker,[1] Hamer,[2] and Young[3]) and concentrations determined from Raman intensities.[4] K_2 may be written as the product of two terms, Q_c and Q_f. Q_c is the quotient of concentrations and Q_f the quotient of activity coefficients. Q_c has been determined by Raman methods for various compositions of sulfuric acid at 25°C.[4] From these data and the knowledge of K_2 values of Q_f are obtained. For the dissociation of HSO_4^- ion Q_f takes the form

$$Q_f=f_+f_-/f_-. \tag{1}$$

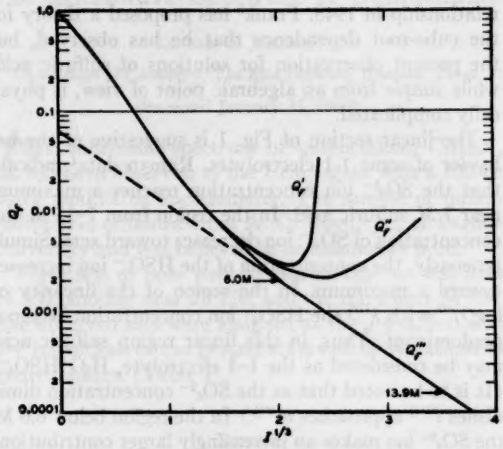

FIG. 1. Activity coefficient quotient dependence for HSO_4^- dissociation. Q_f' molar basis. Q_f'', Q_f''' molal basis, but Q_f''' corrected for solvation of H^+ by H_2O. I corresponds in each case. From Debye-Huckel limiting law $d\log Q_f/dI^{1/3}=0$ at $I^{1/3}=0$. All data from footnote reference 4 are for 25°C.

Q_c may be expressed in various units. For molarity and molality units Q_c has been designated as Q_c' and Q_c'', respectively.[4] If allowance is made for the increased molality produced by the solvation of H^+ by H_2O the symbol Q_c''' is employed. The units of Q_c must correspond to those of the ionic strength I. I' and I'' correspond to molarity and molality units, respectively. If the molality has been corrected for solvation of H^+ by H_2O, the symbol I''' is employed.

Young, Maranville, and Smith[4] have compared $\log(\gamma_\pm)^3$ of Na_2SO_4 with $\log Q_f'$, Q_f'', Q_f'''. The close correspondence obtained provides support for the magnitudes of Q_f obtained from Raman data. Minima observed in $\log Q_f'$, Q_f'' were removed by considering H^+ solvated with H_2O.

Young's plot of $\log Q_f'''$ against $I'''^{\frac{1}{3}}$ shows considerable curvature. A plot of $\log Q_f'''$ against $I'''^{\frac{1}{3}}$ is shown in Fig. 1. The region from 6.0–13.9 M is remarkably linear. Linearity is not obtained from Q_f' and Q_f''.

Frank[5] has found linearity of $\log f_\pm$ with $c^{\frac{1}{3}}$ for electrolytes of the 1-1 type in moderately dilute solutions. Glueckauf[6] has found linearity of $\log\gamma_\pm$ with $m^{\frac{1}{3}}$ for more concentrated solutions, e.g., to ~6 molal for CsCl. In this work linearity of the logarithm of the activity coefficient quotient Q_f''' with $I'''^{\frac{1}{3}}$ has been observed to ~14 molar sulfuric acid. Linearity of $\log\gamma_\pm$ with $m^{\frac{1}{3}}$ was first suggested by Bjerrum[7] in 1918. Robinson and Stokes[8] again drew attention to this

relationship in 1948. Frank[6] has proposed a theory for the cube-root dependence that he has observed, but the present observation for solutions of sulfuric acid, while simple from an algebraic point of view, is physically complicated.

The linear section of Fig. 1 is suggestive of the behavior of some 1-1 electrolytes. Raman data[4] indicate that the SO_4^{2-} ion concentration reaches a maximum near 7 M sulfuric acid. In the region from 7–15 M the concentration of SO_4^{2-} ion decreases toward zero. Simultaneously, the concentration of the HSO_4^- ion increases toward a maximum. In the region of the linearity of $\log Q_f'''$ with $I'''^{\frac{1}{3}}$ the HSO_4^- ion concentration becomes predominant. Thus, in this linear region sulfuric acid may be considered as the 1–1 electrolyte, $H_3O^+HSO_4^-$. (It is to be noted that as the SO_4^{2-} concentration diminishes $I'''^{\frac{1}{3}}$ approaches $m'''^{\frac{1}{3}}$.) In the region below 6.0 M the SO_4^{2-} ion makes an increasingly larger contribution. Accordingly, $\log Q_f'''$ deviates more from the extrapolated (dotted) line of Fig. 1.

It is interesting to note that linearity with $I'''^{\frac{1}{3}}$ is obtained for a quotient of activity coefficients. The linearities observed by Glueckauf[6] and Frank[5] referred to mean activity coefficients. The linearity of $\log f_+''' + \log f_-''' - \log f_-'''$ with $I'''^{\frac{1}{3}}$ suggests that $\log f_i'''$ (where f_i''' refers to f''' of ion i) may be linear with $I'''^{\frac{1}{3}}$ (in the region from 6.0 to 13.9 M). The concentrations of the ions HSO_4^-, SO_4^{2-} and H_3O^+ change considerably in the 6.0–13.9 M region, and those concentrations are not linear with $I'''^{\frac{1}{3}}$.

It is improbable that the corresponding changes in $\log f_i'''$ should exactly compensate to provide precise linearity in $I'''^{\frac{1}{3}}$. Further, there is no basis to equate $\log f_-'''$ with zero. (While the concentration of SO_4^{2-} is approaching zero near 13.9 M the ionic strength is increasing in this region.) Thus, linearity of $\log f_i'''$ with $I'''^{\frac{1}{3}}$ seems the most probable possibility. (It must be remembered, however, that the quantity f_i''' may not be determined by thermodynamic measurements.)

The dotted line of Fig. 1 deviates from Q_f as the solution deviates from 1-1 type. The intercept is not significant, since the cube-root linearity is proposed only for concentrated solutions.

[1] M. Kerker, J. Am. Chem. Soc. **79**, 3664 (1957).
[2] W. J. Hamer, J. Am. Chem. Soc. **56**, 860 (1934).
[3] T. F. Young, I. M. Klotz, and C. R. Singleterry, based on dissertations of the latter two, University of Chicago, 1940.
[4] T. F. Young, L. F. Maranville, and H. M. Smith, *The Structure of Electrolytic Solutions* (John Wiley & Sons, Inc., New York, 1959), Chap. 4, edited by W. J. Hamer.
[5] H. S. Frank and P. T. Thompson, *The Structure of Electrolytic Solutions*, edited by W. J. Hamer (John Wiley & Sons, Inc., New York, 1959), Chap. 4.
[6] E. Glueckauf, see footnote reference 5, Chap. 7.
[7] N. Bjerrum, Z. Elektrochem. **24**, 321 (1918).
[8] R. A. Robinson and R. H. Stokes, *Electrolyte Solutions* (Butterworths Scientific Publications, Ltd., London, 1955).

Recombination Kinetics of Atomic Oxygen at Room Temperature*

C. B. Kretschmer and H. L. Petersen
Aerojet-General Corporation, Azusa, California

(Received May 9, 1960)

Molecular oxygen, confined in a 300-cm³ spherical Pyrex reaction vessel at pressures of 2 mm Hg or less, was partially dissociated in a 2450-Mc electrodeless discharge. The rate of recombination after the discharge was interrupted was observed by monitoring the intensity of the afterglow produced by the reaction of oxygen atoms with nitric oxide,[1] formed in the discharge from a trace of added nitrogen. When oxygen atoms are present in excess, nitric oxide is regenerated by the rapid reaction between nitrogen dioxide and atomic oxygen, and the afterglow intensity is directly proportional to the oxygen atom concentration. An observable afterglow is produced by as little as 0.01% nitric oxide. At this concentration its effect on the rate of disappearance of oxygen atoms is negligible. The mole fraction of atomic oxygen when the discharge was running was measured with a Wrede gauge attached directly to the reaction vessel, and was between 0.1 and 0.2. It can be shown that the gas temperature, which may have been as high as 600°K when the discharge was on, fell nearly to the temperature of the wall (350°K) within about 0.01 sec after the discharge was stopped. Since this interval is much smaller than the characteristic time for decay of the afterglow, the observed recombination was a process taking place at a constant temperature of 350°K.

A priori, two homogeneous mechanisms are available for recombination of oxygen atoms. These are three-body recombination, (1) $O+O+M \rightarrow O_2+M$, and the ozone mechanism, (2) $O+O_2+M \rightarrow O_3+M$; (3) $O+O_3 \rightarrow 2O_2$. The rate of decay of the afterglow intensity is

$$-(d\ln I/dt) = -[d\ln(O)/dt]$$
$$= 2(M)\{k_1(O)+k_2(O_2)\}+k_w.$$

The surface recombination rate constant, k_w, was made very small by coating the vessel with phosphoric acid. Since the initial degree of dissociation was less than 10% (O_2) and (M) may be taken equal to the stoichiometric concentration of oxygen confined in the reaction vessel.

The object of this investigation was to obtain the value of k_1. It is evident that this is equivalent to determining the curvature of plots of $\ln I$ vs t. In the course of the work, numerous experiments gave curved plots. However, values of k_1 calculated from these plots varied widely, and seemed to be correlated with the amount of water in the gas. After the oxygen and the apparatus were rigorously dried, linear plots were obtained. An upper limit of 2×10^{14} cc²/mole² sec can be assigned to

k_1 for $M=O_2$ on the basis that any larger value would have produced noticeable curvature in experiments from which linear plots were actually obtained. The value $k_2=1.1\times10^{14}$ cc²/mole² sec for $M=O_2$ was obtained from the slope of a plot of $-d\ln I/dt$ against (O_3) (M) for experiments at different pressures.

The upper limit for k_1 found here is compatible with the value 3×10^{14} cc²/mole² sec found by Golden and Myerson[2] in somewhat similar experiments, when it is realized that part of their observed decay must have been due to the ozone mechanism. The value found for k_2 is in reasonable agreement with the value 7×10^{13} cc²/mole² sec found by Benson and Axworthy[3] from the rate of thermal decomposition of ozone. Since recent shock-tube investigations[4,5] have given values of 4×10^{14} and 8×10^{14} cc²/mole² sec for k_1 at 3500°K (for $M=O_2$), it appears that k_1 increases very slowly with temperature instead of varying as $T^{-\frac{1}{2}}$, as has often been assumed.

The effect of dissociated water vapor on oxygen atom recombination was investigated in flow experiments. Oxygen containing known amounts of water vapor was passed through a discharge, and the afterglow intensity was measured as a function of distance along the flow tube. The rate of decay of the afterglow in oxygen containing dissociation products from 0.45% of added water was several times as large as the rate in dry oxygen at the same pressure. This effect can be understood in terms of the mechanism suggested by Kaufman,[1] (4) $O+OH\rightarrow O_2+H$; (5) $H+O_2+M\rightarrow HO_2+M$; (6) $O+HO_2\rightarrow OH+O_2$. Since $-d\ln(O)/dt$ was constant during the decay, Reaction (5) is not the rate-determining step. If it is assumed that the water vapor was completely dissociated in the discharge, the observed rates give a value at 300°K of 5×10^9 cc/mole sec for the smaller of the two rate contants k_4 and k_6. This is smaller by two orders of magnitude than the room-temperature value of k_4 which can be extrapolated from the results of high-temperature work[6] on the hydrogen-oxygen reaction. Therefore it is concluded that the rate-determining step in the recombination catalyzed by dissociated water is reaction (6), with $k_6=5\times10^9$ cc/mole sec at 300°K.

The occurrence of curved plots of $\ln I$ vs t in static experiments when water vapor was not rigorously excluded can be explained by reactions (4) to (6) with the addition of a chain-termination step such as $OH+OH+M\rightarrow H_2O_2+M$.

* This work was supported by the United States Air Force through the Air Force Office of Scientific Research of the Air Research and Development Command.

[1] F. Kaufman, Proc. Roy. Soc. (London) **A247**, 123 (1958).
[2] J. A. Golden and A. L. Myerson, J. Chem. Phys. **28**, 978 (1958).
[3] S. W. Benson and A. E. Axworthy, Jr., J. Chem. Phys. **26**, 1718 (1957).
[4] S. R. Byron, J. Chem. Phys. **30**, 1380 (1959).
[5] D. L. Matthews, Phys. Fluids **2**, 170 (1959).
[6] G. L. Schott and J. L. Kinsey, J. Chem. Phys. **29**, 1177 (1958).

The Microwave Spectrum of Quinuclidine

LAUREN G. JOHNSON*
Department of Chemistry, The Rice Institute, Houston, Texas

(Received January 25, 1960)

THE rotational spectrum of quinuclidine, $C_7H_{13}N$, has been observed in the 1 cm region with a 100-kc Stark modulated spectrometer. The sample of quinuclidine was obtained from A. C. Boyd, Jr., of Purdue University and was believed to be reasonably pure.

Three sets of lines were measured. One set was near 24 300, another near 29 150, and the third near 34 050. The observed sets were assigned as the J 4–5, 5–6, and 6–7 transitions of the ground state and of vibrationally excited states. (Table I).

TABLE I.

J 4–5	5–6	6–7
24 311.5	29 121.0	34 019.9
(ground state)	29 160.6	34 033.7
24 325.7	29 173.5	(ground state)
24 349.6	(ground state)	34 048.2
24 391.4	29 187.6	34 072.4
	29 211.1	34 113.0
	29 251.2	
	29 294.1	

The ground vibrational state lines for J 4–5, 5–6, and 6–7 were assigned as 24, 311.5, 29 173.5, and 34 033.7 Mc, respectively. This assignment was based on the somewhat greater intensity of these lines, and on their detectable enhancement at the expense of the other lines on cooling to −20°C. This assignment leads to a B_0 of 2 431.4 Mc.

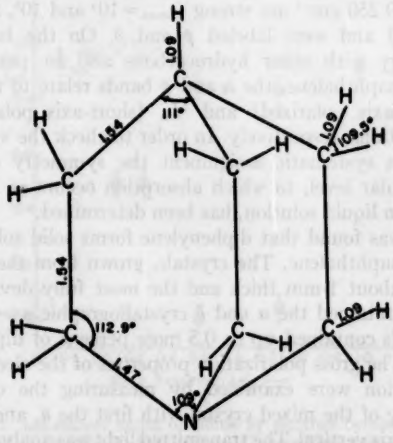

FIG. 1. Assumed structure of quinuclidine.

D_J was calculated to be 4±2 kc. Only an upper limit of 15 kc could be placed on D_{JK}, because of the unresolved hyperfine structure arising from quadrupole coupling of the nitrogen nucleus. One might reasonably expect that eqQ would be close to the value of −5.47 Mc, which Lide and Mann[1] report for trimethylamine.

The value of I_B obtained from the observed B_0 is 207.7 amu A². If one assumes the structure shown in Fig. 1, one obtains a calculated I_B of 201.6 amu A². In the assumed structure the carbon-nitrogen distances and angles are those of trimethylamine.[1]

[1] D. R. Lide and D. E. Mann, J. Chem. Phys. **28**, 572 (1959).
* Present address: Union Carbide Chemicals Company, Seadrift, Texas.

Electronic Absorption Spectrum of Diphenylene in Substitutional Solid-Solid Solution*

ROBIN M. HOCHSTRASSER

Chemistry Department, University of British Columbia, Vancouver, B. C. 8, Canada

(Received January 21, 1960)

DIPHENYLENE has the planar structure

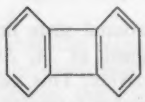

The absorption spectrum in liquid solution exhibits three main bands in the quartz ultraviolet.[1] The lowest energy band at 25 530 cm^{-1} is extremely weak (ϵ_{max}= 250) and was labeled α by Clar. The two remaining regions of absorption, which commence at 27 910 cm^{-1} and 40 250 cm^{-1} are strong ($\epsilon_{max}=10^4$ and 10^5, respectively) and were labeled p and β. On the basis of analogy with other hydrocarbons and in particular with naphthalene, the α and p bands relate to the ^1L_b (long-axis polarized) and ^1L_a (short-axis polarized) excitations, respectively. In order to check the validity of this systematic assignment the symmetry of the molecular level, to which absorption occurs at 27 910 cm^{-1} in liquid solution, has been determined.

It was found that diphenylene forms solid solutions with naphthalene. The crystals, grown from the melt, were about 1-mm thick and the most fully developed face contained the a and b crystallographic axes. The crystals contained up to 0.5 mole percent of diphenylene. The gross polarization properties of the electronic transition were examined by measuring the optical density of the mixed crystal with first the a, and then the b axis vertical. The transmitted light was analyzed by a Wollaston prism and the vertically polarized light

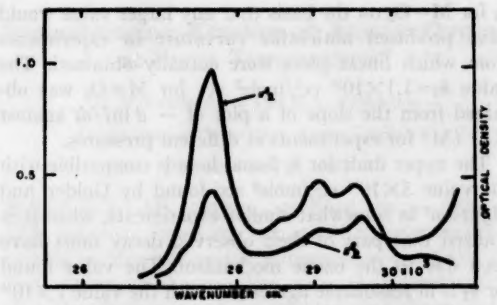

FIG. 1. The polarized absorption spectrum of diphenylene in a single crystal of naphthalene at room temperature. a—Crystal a vertical; b—crystal b axis vertical.

spot was focused on the spectrograph slit. A typical derived spectrum is shown on Fig. 1.

The properties of this crystal under the polarizing microscope indicated that it was a single crystal. The observed polarization properties obtained with different crystals indicated that the molecules were in true substitutional solid solution. It was then to be expected that the guest and host molecules would be similarly oriented in the lattice, that is, long axis to long axis, and with planes parallel. The direction cosines of the long and short molecular axes with respect to the a and b crystallographic axes of naphthalene[2] were used to calculate the expected polarization ratios I_b/I_a for long and short axis molecular transitions, on the basis of oriented gas model. These were 0.26:1 and 7.4:1, respectively. The ratio I_b/I_a at the 27 690 cm^{-1} peak was found experimentally to be 0.44:1 thus strongly indicating that the absorption in this region was due to excitation to a long-axis polarized molecular level. It was not possible to examine the weak system at 25 530 cm^{-1} owing to difficulties in obtaining crystals which were thick enough.

In each polarization there were three well-defined bands at 27 690 cm^{-1}, 29 083 cm^{-1}, and 29 620 cm^{-1} and at each peak the polarization ratio was approximately the same. The strongly b-polarized edge of the naphthalene absorption[3] is also shown in Fig. 1. This commenced at 29 600 cm^{-1} as evidenced by the sudden change in the polarization ratio in this region. The red shift between liquid and solid solution was 220 cm^{-1} which was expected on the basis of similar shifts for naphthalene,[4] anthracene,[5] and pyrene.[6]

Diphenylene was assumed to belong to the point group D_{2h} and the allowed transitions are to B_{2u} and B_{3u} levels which give rise to dipole moments directed along the long and short molecular axes, respectively. Thus the 27 690 cm^{-1} system of diphenylene may be assigned as $^1B_{2u}MA_{1g}$ or as $^1LiM^1A$ in the Platt notation. It is clear that the order of the states in diphenylene is not the same as in naphthalene[7] but rather they parallel the anthracene levels. This result is at variance with the systematic assignment which was made by Clar, as

the p band, by analogy with naphthalene and anthracene, would be polarized along the short molecular axis.

Calculations on the diphenylene molecule have indicated that the lowest transition is symmetry forbidden ($B_{2g} \leftarrow A_{1g}$). Conventional methods predict the symmetry of the second level to be $^1B_{2u}$ as has been found in this work. Clearly, the unusual hybridization of the carbon atoms in the cyclobutadiene ring will necessitate the the use of theoretical parameters which are not included in normal polyacene calculations.

Preliminary examinations of the vapor spectrum of diphenylene have shown that the O—O band of the lowest energy transition (25 810 cm^{-1} in the vapor) is present only when the temperature is relatively high (160°C). This supports the theoretical prediction of a forbidden transition.[8]

The author would like to thank Dr. J. R. Rowlands for a gift of the purified sample of diphenylene and for some interesting discussions.

* This research was supported by a grant from the National Research Council of Canada.

[1] E. Clar, *Aromatische Kohlenwasserstoffe* (Springer-Verlag, Berlin, Germany, 1952), p. 279.
[2] S. C. Abrahams, J. M. Robertson, and J. G. White, Acta Cryst. **2**, 233 (1949).
[3] A. Prikhotjko, Akad. Nauk S.S.S.R. Ser. Fiz. **12**, 499 (1948).
[4] D. S. McClure and O. Schnepp, J. Chem. Phys. **23**, 1575 (1955).
[5] J. W. Sidman, J. Chem. Phys. **25**, 115 (1956).
[6] Robin M. Hochstrasser (to be published).
[7] N. S. Ham and K. Ruedenberg, J. Chem. Phys. **25**, 13 (1956).
[8] Robin M. Hochstrasser, unpublished research.

Mass Spectra of Vapors in the Al-AlF_3 and Al-LiF-AlF_3 Systems*

RICHARD F. PORTER†

Department of Chemistry, Cornell University, Ithaca, New York

(Received June 10, 1960)

ENHANCEMENT of the volatility of AlF_3 in the presence of Al metal has been ascribed[1] to the reaction

$$AlF_3(s) + 2\,Al(s) \rightarrow 3\,AlF(g).$$

The experimental data indicate that the vapor in equilibrium with Al–AlF_3 mixtures is mostly $AlF(g)$ at vapor pressures suitable for measurement with the Knudsen effusion technique. In the present experiments, finely powdered samples of Al–AlF_3 mixtures were heated in graphite or molybdenum cells and were mass-spectrometrically analyzed as described previously.[2] For 100-v ionizing electrons, the major ions observed were AlF^+, Al^+, and AlF_2^+. The AlF^+ ion was the highest in intensity and had a low appearance potential, between 9 and 10 v. These observations are consistent with previous indications that $AlF(g)$ is the primary vaporization product. No evidence was found to suggest that AlF is appreciably associated as polymers. In one experiment where the molar Al/AlF_3 ratio in the condensed phase was small, AlF^+ eventually disappeared, while AlF_2^+ remained essentially constant as Al was distilled from the sample. This indicated that AlF_2^+ was not formed primarily by simple ionization of AlF_2 (g). The AlF_2^+ current is thus attributed to a fragmentation process involving $AlF_3(g)$.[2] The Al^+/AlF^+ ratio was usually about 0.15, and Al^+ is assumed to be formed by fragmentation of $AlF(g)$ under these conditions, since the ion current of Al^+ formed from $AlF_3(g)$[2] or $Al(g)$[3] is very small.

Ions characteristic of the Al–AlF_3 system were also observed in the mass spectra of vapors from Al–LiF–AlF mixtures. In the latter system, a high intensity of Li^+ was also observed. For condensed-phase mixtures with excess AlF_3, the Li^+ ion has been interpreted to originate almost exclusively by fragmentation of $LiF \cdot AlF_3(g)$.[2] It was noted that for molar compositions of $LiF:AlF_3 \leq 1$ the AlF^+/AlF_2^+ ratio did not vary appreciably from that observed with Al–AlF_3 mixtures. At high mole fractions of LiF, this ratio increased as is indicated in Fig. 1. This effect is assumed to result from lowering of the thermodynamic activity of AlF_3 in the LiF-rich region of the system. With the assumption

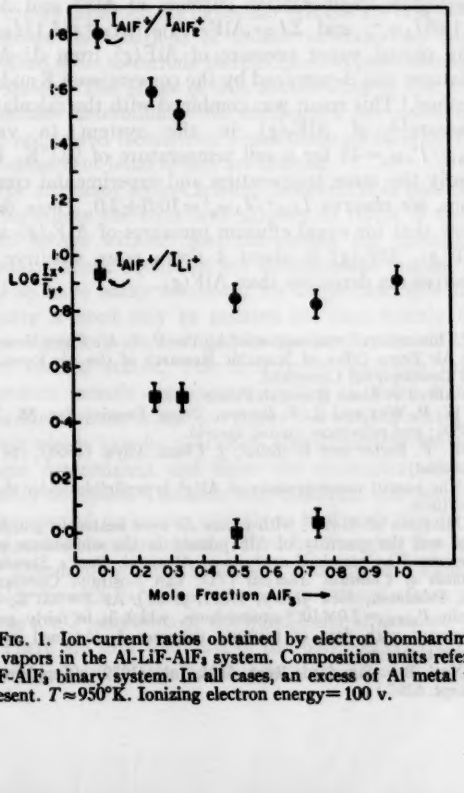

FIG. 1. Ion-current ratios obtained by electron bombardment of vapors in the Al-LiF-AlF_3 system. Composition units refer to LiF-AlF_3 binary system. In all cases, an excess of Al metal was present. $T \approx 950$°K. Ionizing electron energy = 100 v.

of unit activity of Al metal, the activity of AlF_3 may be expressed:

$$a_{AlF_3}=\{(P_{AlF_3}/P_{AlF})/(P_{AlF_3}/P_{AlF})_0\}^{\frac{1}{4}}$$

$$=\{(I_{AlF_2^+}/I_{AlF^+})/(I_{AlF_2^+}/I_{AlF^+})_0\}^{\frac{1}{4}},$$

where the terms with subscripts refer to arbitrary standard-state conditions. The above relationship may be derived, since geometrical factors, ionization cross section, detection efficiency and instrument sensitivity factors cancel. A marked change in the activity of AlF_3 was thus not apparent from the data (Fig. 1) for molar compositions of $LiF:AlF_3 \leq 1$. Activity effects were clearly obvious, however, for compositions of $LiF:AlF_3 \geq 2$. These latter effects may be associated with solid-compound formation. As shown in Fig. 1, variations in I_{AlF^+}/I_{Li^+} show a parallel relationship to that found for $I_{AlF^+}/I_{AlF_2^+}$.

For the Al–AlF_3 system we may write for constant temperature,

$$P_{AlF_3}/P_{AlF}=C\{\Sigma I_{(X^+)AlF_3}/\Sigma I_{(X^+)AlF}\}$$

where C is a temperature-insensitive constant which incorporates relative ionization cross section and detection-efficiency terms. Geometrical factors in C cancel if ion-current observations are made simultaneously. In this expression, $\Sigma I_{(X^+)}AlF_3=I_{AlF_2^+}+I_{AlF_3^+}+$ [negligible fragmentation currents of AlF^+ and Al^+] $\approx 1.05 I_{AlF_2^+}$, and $\Sigma I_{(X^+)}AlF=I_{AlF^+}+I_{Al^+}\approx 1.15 I_{AlF^+}$. The partial vapor pressure of $AlF(g)$ from Al–AlF_3 mixtures was determined by the conventional Knudsen method.[4] This result was combined with the calculated pressure[1,5] of $AlF_3(g)$ in the system to yield $P_{AlF}/P_{AlF_3}=45$ for a cell temperature of 933°K. For nearly the same temperature and experimental conditions, we observe $I_{AlF^+}/I_{AlF_2^+}=10.0\pm 2.0$. These data show that for equal effusion pressures of $AlF_3(g)$ and $AlF(g)$, $AlF_3(g)$ is about 4 times more sensitive to positive ion detection than $AlF(g)$.

* This research was supported by the U. S. Air Force through the Air Force Office of Scientific Research of the Air Research and Development Command.

† Alfred P. Sloan Research Fellow.

[1] W. P. Witt and R. F. Barrow, Trans. Faraday Soc. **55**, 730 (1959); and references quoted therein.

[2] R. F. Porter and E. Zeller, J. Chem. Phys. (1960), (to be published).

[3] The partial vapor pressure of $Al(g)$ is negligible under these conditions.

[4] Mixtures of Al-AlF_3 with excess Al were heated in graphite cells, and the quantity of AlF present in the condensate was determined by standard analysis of Al metal. *Scott's Standard Methods of Chemical Analysis* [(D. Van Nostrand Company, Inc., Princeton, New Jersey, 1939), p. 51]. At $T=933$°K, we obtain $P_{AlF(g)}=2.0\times 10^{-6}$ atmospheres, which is in fairly good agreement with data of footnote reference 1, obtained by a torsion technique.

[5] Natl. Bur. Standards Rept. 6484, July (1959). (Supplement to Rept. 6297.)

Effect of Oxygen on Semiconductivities of Mesonaphthodianthrene and Mesonaphthodianthrone*

H. Kuroda† and E. A. Flood

Division of Pure Chemistry, National Research Council, Ottawa, Canada

(Received April 15, 1960)

THE electron-spin resonance absorptions of mesonaphthodianthrene, I, and mesonaphthodianthrone, II, have been studied recently by Matsunaga.[1] In vacuum, both compounds exhibited broad absorption consisting of at least seven peaks separated by 4.4 oe. When I in powder form was exposed to air, the central peak of the ESR absorption grew slowly and reached a maximum intensity after a few days. However, when II was exposed to air, no oxygen effect was detected. The purpose of this note is to report the effect of oxygen on the semiconductivities[2] of I and II since these effects have a bearing on the interpretation of Matsunaga's results.

(I)

(II)

Compounds[3] I and II, respectively, in powder form, were out-gassed in high vacuum (10^{-6} mm Hg) and evaporated on glass plates carrying two platinum electrodes. The evaporated films were transparent and of the order of a few microns in thickness. The conductance was measured using a DC method.

When exposed to oxygen at 24°C, the conductivity of the film of I increased slowly dependent upon the oxygen pressure. At lower oxygen pressures (<5 mm Hg) the conductivity increased linearly with time, the rate of increase being nearly proportional to the pressure. At higher oxygen pressures, conductivities slowly approached saturation values; they took a few days to reach their maxima even at oxygen pressures greater than 100 mm Hg. Conductivity changes resulting from oxygen exposures were largely reversible. However, at temperatures below 50°C the rate of decrease of conductivity as the oxygen was pumped off was very slow.

Nitrogen was found to have no effect on the semiconductivity. The temperature dependencies of the semiconductivities of an oxygen-free film and that previously exposed to oxygen (10 cm Hg) were measured over the temperature range 0° to 230°C in a nitrogen atmosphere (70 cm Hg). The activation energy of the oxygen-free film is 0.74 ev throughout the temperature range, while after exposure to oxygen it is 0.74 ev in the higher temperature region and 0.40 ev in the lower temperature region. The temperature dependency of the semiconductivities were measured also in oxygen of various pressures over the temperature range, −30° to 50°C. The experimental results can be described by the equation

$$\sigma(T, P_{O_2}) = \sigma_1^0 \exp(-E_1/kT) + \sigma_2^0(P_{O_2}) \exp(-E_2/kT) \cdots, \quad (1)$$

where $E_1 = 0.74$ ev, $E_2 = 0.40$ ev. Only $\sigma_2^0(P_{O_2})$ is affected by oxygen. After being kept in air for a week, σ_2^0/σ_1^0 became constant at 10^{-3}. Evidently the semiconductivity of I is controlled by at least two different mechanisms; one is markedly dependent on the ambient oxygen pressure, while the other one is not. Probably the latter is due to a bulk conductivity and the former to a conduction mechanism associated with the surface states. The oxygen molecule seems to create a new source of charge carrier.

The effect of oxygen on the semiconductivity of mesonaphodianthrone, II, is in marked contrast to that described above. It has been found that a freshly evaporated film of II in vacuum has an activation energy of 0.73 ev at higher temperatures (>150°C) and of 0.43 ev at lower temperatures. When it is exposed to oxygen the conductivity associated with 0.43 ev decreases rather rapidly, the other remaining unchanged. This change is also largely reversible. The semiconductivity of II can be described again by Eq. (1) using 0.73 ev and 0.43 ev as E_1 and E_2, respectively. The value σ_2^0/σ_1^0 is, however, a maximum for a fresh film in vacuum where it is 10^{-6} and decreases in oxygen. Thus, in the case of II, oxygen does not create a new conduction mechanism. It, rather, seems to reduce the concentration of the charge carrier due to the surface of II.

It is known that the photoconductivity of anthracene increases on exposure to oxygen.[4-6] In this case, however, no change has been observed in the threshold frequency of the spectral response of the photoconductivity. Therefore the change was attributed to the reduction of the recombination rate of the charge carrier, which was due to the formation of peroxide on the surface.

There is a marked parallelism between the oxygen effect on ESR absorption reported by Matsunaga and the oxygen effect on the semiconductivity described above. This suggests a close correlation between the spin center responsible for the sharp increase of the central peak of ESR absorption and the source of the charge carrier created in I by exposure to oxygen. It would seem that an oxygen molecule adsorbed on the surface of I forms a molecular complex with the hydrocarbon molecule; this molecular complex has an unpaired electron which is responsible for the sharp central peak and contributes to the production of charge carriers.

The authors are indebted to Dr. Y. Matsunaga for his kind suggestion for this work.

* N.R.C. Contribution No. 5789.
† National Research Council Postdoctorate Fellow.
[1] Y. Matsunaga, Can. J. Chem. **38**, 323 (1960).
[2] H. Inokuchi, Bull. Chem. Soc. Japan **24**, 222 (1951).
[3] The materials were kindly supplied by Dr. Matsunaga.
[4] A. G. Chynoweth, J. Chem. Phys. **22**, 1029 (1954).
[5] A. Bree, D. J. Carswell, and L. E. Lyons, J. Chem. Soc. (London) **1955**, 1728.
[6] T. C. Waddington and W. G. Schneider, Can. J. Chem. **37**, 789 (1958).

Ambiguity in the Determination of Self-Consistent Bond Orders

G. G. Hall

Department of Mathematics, Imperial College, London, S.W. 7, England

(Received March 28, 1960)

In recent years the approximate molecular-orbital theory, in which the molecular orbitals are expressed as linear combinations of atomic orbitals, has been modified so as to include the electronic repulsions more accurately. The effect of this modification is that the equations determining the coefficients are nonlinear and are solved iteratively. From these coefficients the self-consistent bond orders are defined.

For alternant hydrocarbons, however, it is possible[1] to formulate the equations directly in terms of these bond orders without first calculating the molecular orbitals. These equations are simultaneous quadratics and so have many solutions. To understand this ambiguity it need only be pointed out that exactly the same equations are obtained for the bond orders of certain excited states. The alternative solutions must therefore include ones corresponding to these states. The form of the equations limits the excited states to those which can be described approximately using a single determinant and have the molecular orbitals doubly occupied. The alternate condition also restricts the occupied molecular orbitals so that each has its associated molecular orbital (found by changing the signs of alternate atomic orbitals) unoccupied. Thus a molecule with $2n$ carbon atoms has 2^n such states and there are 2^n solutions of the bond-order equations.

There are four solutions to the bond-order equation for butadiene. If the bond orders are denoted by the

unitary matrix

$$\begin{pmatrix} p_{12} & p_{14} \\ p_{23} & p_{34} \end{pmatrix} = \begin{pmatrix} \sin\alpha & -\cos\alpha \\ \cos\alpha & \sin\alpha \end{pmatrix},$$

then α is determined by

$$\beta_{23}\tan\alpha = 2\beta_{12} - \tfrac{1}{2}(2\gamma_{12} - \gamma_{23} - \gamma_{14})\sin\alpha,$$

where γ_{rs} is the Coulomb integral between atomic orbitals on atoms r and s. This equation has two distinct solutions for α. The remaining solutions are obtained by putting

$$\begin{pmatrix} p_{12} & p_{14} \\ p_{23} & p_{34} \end{pmatrix} = \begin{pmatrix} \sin\alpha & \cos\alpha \\ -\cos\alpha & \sin\alpha \end{pmatrix},$$

which leads to

$$\beta_{23}\tan\alpha = -2\beta_{12} + \tfrac{1}{2}(2\gamma_{12} - \gamma_{23} - \gamma_{14})\sin\alpha.$$

When β_{12}, β_{23}, γ_{rs} have the values suggested by Pariser and Parr[2] the solutions are given in Table I. The molecular orbitals have been numbered in the order of their nodes but are slightly different in each state.

TABLE I. Bond orders for trans-butadiene.

State	$1^2 2^2$	$1^2 3^2$	$2^2 4^2$	$3^2 4^2$
$P_{12} = P_{34}$	0.9771	0.9771	−0.9239	−0.9239
P_{23}	0.2127	−0.2127	0.3811	−0.3811
P_{14}	−0.2127	0.2127	−0.3811	0.3811

The single determinant is probably an inadequate approximation to an excited state wave function, particularly since it is not necessarily orthogonal to

TABLE II. Bond orders for benzene.

State	$1^2 2^2 3^2$	$1^2 4^2 5^2$	$2^2 3^2 6^2$	$4^2 5^2 6^2$
p	$\frac{2}{3}$	0	0	$-\frac{2}{3}$
r	$-\frac{1}{3}$	1	−1	$\frac{1}{3}$

the determinant representing the ground state. Nevertheless, it may be a useful tool in a more elaborate treatment. There is also a further difficulty which is illustrated by the benzene molecule. To conform to the sixfold symmetry, the bond orders are

$$\begin{pmatrix} p_{12} & p_{32} & p_{52} \\ p_{14} & p_{34} & p_{54} \\ p_{16} & p_{36} & p_{56} \end{pmatrix} = \begin{pmatrix} p & p & r \\ r & p & p \\ p & r & p \end{pmatrix}.$$

The conditions that this matrix should be unitary are that

$$2p^2 + r^2 = 1, \qquad p(p + 2r) = 0,$$

and these have the four solutions given in Table II. There are two further solutions but these correspond to determinants, such as $1^2 2^2 5^2$, which do not have sixfold symmetry and are not by themselves acceptable as approximate wavefunctions because of the degeneracy both of orbitals and determinants.

The multiplicity of solutions noted here is not confined to alternate hydrocarbons. Indeed the removal of the restriction to alternants, the inclusion of several atomic orbitals for each atom and the use of the equations for the coefficients instead of the bond-order equations will all increase the number of solutions.

These results raise the question of the stability of a molecule when some of its bonds have negative bond orders and also the mathematical question of the identity of the apparently unique solutions found by many iterative methods of calculation.

[1] G. G. Hall, Proc. Roy. Soc. (London) **A229**, 251 (1955).
[2] R. Pariser and R. G. Parr, J. Chem. Phys. **21**, 767 (1953).

Absorption Spectra of Anodic Niobium Oxide Films*

W. M. GRAVEN, R. E. SALOMON, AND G. B. ADAMS, JR.†
Department of Chemistry, University of Oregon, Eugene, Oregon

(Received May 23, 1960)

FOR continuation of an investigation of photoeffects with oxide-coated metallic electrodes it has become necessary to obtain the absorption spectra of anodically formed oxide films on niobium metal. A recently reported method[1] whereby thin transparent films of oxide, which had been anodically formed on the surface of metal foils, were isolated from the supporting metal has been utilized to obtain free films of niobium oxide suitable for absorption measurements.

Niobium foil, 0.5 mil thick, having a minimum purity of 99.7% was obtained from Fansteel Metallurgical Corporation. A sodium phosphate-phosphoric acid solution, buffered at pH 9, was used as electrolyte for anodizing most of the foils, although the use of a sodium borate-boric acid solution, also buffered at pH 9, resulted in films which showed equivalent spectra.

After cleaning with benzene and alcohol a 4-in.×4-in. sheet of foil was placed in an aluminum holder which exposed only one surface of the foil to the electrolyte used in the anodization. The applied voltage from a Heathkit power supply was gradually raised to the desired value and maintained there from three to ten hours. After washing a section of the anodized foil was transferred to the previously described Lucite mount.[1] A dilute solution of HNO_3 and HF, which was used to

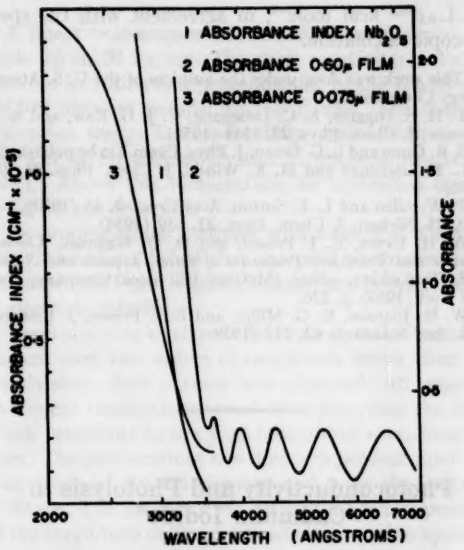

FIG. 1. Absorption spectra of thin niobium oxide films.

remove the exposed metal, was allowed to remain in contact with the unanodized surface until the film became transparent. This solution attacked the oxide, as well as the metal, but at a sufficiently slower rate so that complete removal of metal was possible for all except the thinnest films.

Absorbance measurements for eighteen films with formation voltages ranging from 25 to 250 v were obtained with a Cary model 11, recording spectrophotometer. Thicker films could not be produced since sparking occurred at higher formation voltages.

The transparent oxide films exhibited characteristic interference colors when viewed at an oblique angle. Interference patterns of alternating maximum and minimum absorption were observed with each of the films. The absolute thickness was obtained from the slope of the plot of the wave numbers of successive maxima and minima vs their respective ordinal numbers using a reported value of 2.3 for the index of refraction of Nb_2O_5.[2]

A direct proportionality between film thickness and formation voltage was demonstrated with the data, from which a thickness-voltage relation of 30 A/v has been computed for anodic films of Nb_2O_5. This value appears to be in agreement with kinetic data for anodic oxide formation on niobium.[3]

Absorption spectra of two typical films, obtained with 25-v and 200-v formation voltages, are shown in Fig. 1. By extrapolation the long wavelength limit of absorption is found to be about 3500 A, in agreement with a previously reported value of 3400 A.[2] The approximately constant "apparent" absorbances at longer wavelengths, attributed to reflection losses, have been subtracted from the observed absorbances in order to test the applicability of Lambert's law. Plots of corrected absorbance, at wavelengths between 3450 and 2750 A, vs film thickness were linear for films ranging in thickness from 0.075 to 0.75 μ. Absorbance indices obtained from the slopes of these lines are also shown in Fig. 1. Absorption of Nb_2O_5 commences at a longer wavelength than that of ZrO_2,[1] although the magnitudes of the absorbance indices are comparable.

* This work was carried out under the U. S. Atomic Energy Commission.

† Present address: Lockheed Aircraft Corporation, Missiles and Space Division, Sunnyvale, California.

[1] R. E. Salomon, W. M. Graven, and G. B. Adams, Jr., J. Chem. Phys. **32**, 310 (1960).

[2] O. A. Motovilov and V. N. Rozhdestvenskiĭ, Optiko-Mekh. Prom. **25**, 42 (1958); Chem. Abstracts **53**, 6773 (1959).

[3] L. Young, Trans. Faraday Soc. **52**, 502 (1956).

The Heats of Formation of BF_2Cl and $BFCl_2$*

STUART R. GUNN AND RUSSELL H. SANBORN

Lawrence Radiation Laboratory, University of California, Livermore, California

(Received April 7, 1960)

HIGGINS, Leisegang, Row, and Rossouw[1] have reported a value of 0.53 ± 0.04 for the equilibrium constant at 27−29°C of the reaction

$$BF_3+BCl_3=BF_2Cl+BFCl_2. \quad (1)$$

Current work on the determination of the heat of formation of B_2F_4 by measurement of its heat of chlorination[2] engendered an interest in the heats of formation of the mixed halides. While determination of the heat of reaction (1) does not permit calculation of the separate heats of formation of the two mixed species, it can give some idea of the magnitude of the perturbation of the thermochemical bond energies in these species.

Using the fundamental frequencies given by Lindeman and Wilson,[3] a B–F distance[4,5] of 1.295 A and a B–Cl distance[4] of 1.73 A, and assuming the bond distances and angles in the mixed species to be unchanged from those in the pure species, we have calculated the following standard entropies at 25°C: BF_3, 60.71; BF_2Cl, 65.67; $BFCl_2$, 68.72; BCl_3, 69.32 eu. Thus for reaction (1), ΔS is +4.36 eu. It may be noted that this is exactly equal to that ($2R\ln 3$) calculated from statistical considerations of the greater probability of mixed halogen atom distribution. From the equilibrium constant, the standard free-energy change of reaction (1) is calculated to be +0.38 kcal mole^{-1}; thus the heat of reaction is +1.68 kcal mole^{-1}.

Higgins *et al.* considered only the equilibrium of reaction (1) in the BF_3–BCl_3 system. However, two

other equilibria must exist, and their kinetics should be comparable with (1)

$$2BF_3Cl = BF_3 + BFCl_2 \quad (2)$$

$$2BFCl_2 = BF_2Cl + BCl_3. \quad (3)$$

A value of 0.53 for K_1 together with the statement of Higgins *et al.* that in an initially equimolar mixture of BF_3 and BCl_3 the mixed species at equilibrium comprise 42% of the total implies that K_2 and K_3 both have the value of 1.38, the three constants being related by the expression

$$K_1K_2K_3 = 1.$$

Higgins *et al.* measured only the initial amounts of reactants and the final concentration of BCl_3; from this it is not possible to determine all the constants. Three possible equilibrium mixtures formed from 0.5 mole each of BF_3 and BCl_3 are listed in Table I. It may be

TABLE I. Examples of possible BF_3—BCl_3 equilibria.

BF_3	BF_2Cl	$BFCl_2$	BCl_3	K_1	K_2	K_3
0.23	0.33	0.15	0.29	0.74	0.31	4.25
0.29	0.21	0.21	0.29	0.53	1.38	1.38
0.32	0.15	0.24	0.29	0.39	3.41	0.76

noted here that K_2 and K_3 (and consequently ΔF_2 and ΔF_3) are quite sensitive to small changes in K_1. Using -270.0 for ΔH_f^0 (BF_3)[6] and -97.11 for ΔH_f^0 (BCl_3)[7] and arbitrarily assigning the bond energy deficiency (ΔH_1, $+1.68$) equally to the two mixed species, we may calculate for ΔH_f^0 (BF_2Cl), -211.53; ΔH_f^0 $(BFCl_2)$, -153.90; ΔH_2, -0.84; ΔH_3, -0.84; ΔS_2, -1.91; ΔS_3, -2.45; ΔF_2, -0.27; ΔF_3, -0.11; K_2, 1.58; K_3, 1.20. Hence it appears probable that K_2 and K_3 are not greatly unequal and that K_1 is not greatly in error.

It is also possible to determine the heat of reaction (1) by measurement of the equilibrium constant as a function of temperature. Equal amounts of BF_3 and BCl_3 were mixed at a total pressure of 8 mm in a 10-cm water-jacketed cell with NaCl windows. Three pairs of spectra at 15° and 45° were recorded using a Perkin-Elmer model 21 spectrophotometer. Thirty to ninety minutes were allowed after a change of temperature for attainment of equilibrium. Several peaks due to the pure and mixed species were measured. In all cases the changes in absorption corresponded to a shift to the right in the equilibrium of reaction (1) with increasing temperature. The equilibrium constants calculated from the various peaks differed considerably within and between pairs of spectra; however, assuming an equilibrium constant of 0.53 at 28°, values of about 0.48 at 15° and 0.58 at 45° are obtained. Application of the van't Hoff equation yields a heat of reaction of $+1.1_{-0.5}^{+0.8}$ kcal mole^{-1}, in agreement with the spectroscopic calculation.

* This work was done under the auspices of the U. S. Atomic Energy Commission.

[1] T. H. S. Higgins, E. C. Leisegang, C. J. G. Raw, and A. J. Rossouw, J. Chem. Phys. **23**, 1544 (1955).
[2] S. R. Gunn and L. G. Green, J. Phys. Chem. (to be published).
[3] L. P. Lindeman and M. K. Wilson, J. Chem. Phys. **24**, 242 (1956).
[4] P. W. Allen and L. E. Sutton, Acta Cryst. **3**, 46 (1950).
[5] A. H. Nielsen, J. Chem. Phys. **22**, 659 (1954).
[6] W. H. Evans, E. J. Prosen, and D. D. Wagman, *Thermodynamic and Transport Properties of Gases, Liquids and Solids*, Y. S. Touloukian, editor (McGraw-Hill Book Company, Inc., New York, 1959), p. 226.
[7] W. H. Johnson, R. G. Miller, and E. J. Prosen, J. Research Natl. Bur. Standards **62**, 213 (1959).

Photoconductivity and Photolysis in Cadmium Iodide*

RICHARD A. FOTLAND
Horizons Incorporated, Cleveland 4, Ohio

(Received June 6, 1960)

THE fluorescence of cadmium iodide activated with either lead or manganese is well known. A survey by Putseiko and Terenin[1] indicates that photocurrents may be observed in cadmium iodide powders. Other investigators[2] have observed a darkening of the prism faces of cadmium iodide crystals under intense ultraviolet and in the presence of water vapor. The investigation summarized in this note was performed in order to study these effects in more detail.

Crystals were prepared from reagent-grade cadmium iodide both from aqueous solution and from the melt. After five regrowths in a sealed crucible, using the Bridgeman technique, transparent crystals as large as 2 in. × 4 in. were obtained. The solution-growth crystals were obtained after two recrystallizations. No significant difference in the electrical properties was observed between these two types of crystals. Total metallic impurities in these crystals were less than 180 ppm and consisted principally of calcium, lead, and iron. The electrodes were formed of either an air-drying silver paste or a transparent, evaporated gold film.

The optical absorption curve is flat out to the limit of measurement in the infrared (25 μ) but rises steeply at the absorption edge which occurs at 3.2 ev (0.39 μ). At 3.4 ev, the absorption coefficient is over 10^3 cm^{-1}. The refractive index for visible illumination propagated along the C direction is 2.5 ± 0.1. The absorption-edge shift with temperature exhibits a coefficient of -2×10^{-3} ev/°C. Photocurrents were observed for irradiation in the energy region of 3.0 to 3.3 ev. A peak quantum efficiency of approximately 1% was obtained at fields on the order of 1 kv/cm.

A linear volt-ampere relationship was observed for fields up to 20 kv/cm. The dark resistivity is 3×10^{7} ohm-cm in a direction perpendicular to the C axis and 4×10^{11} ohm-cm parallel to the C axis. The thermal activation energy for conductivity varied between 0.8 and 1 A ev for various crystals at temperatures below 270°C. Above this temperature, an activation energy of 3.0 ev was observed.

By probing across a sample with a beam of illumination, it was established that the peak photosensitivity occurs within 1 mm of each electrode and is independent of electrode polarity.

Upon applying an electric field to a crystal, a transient current over two orders of magnitude larger than the steady-state dark current was observed. An opposite and equal transient occurred upon removing the field. These transients have a time constant of approximately 5 sec. The photocurrent rise time is dependent upon the magnitude of the illumination and is on the order of 1–30 sec. The photocurrent decay time is independent of the magnitude of illumination and is equal to approximately 30 sec.

Although a Faraday law verification was not obtained because of the low conductivity of these crystals, it is probable that the room temperature dark current is ionic in nature, and that an ionic space charge is present under conditions of an applied electric field.

The photocurrent-illumination intensity relationship is linear up to illumination levels such that the optical excitation rate was 3×10^{13} quanta/cm³/sec. Beyond this level, the photocurrent varied as the $\frac{1}{2}$ power of the illuminating intensity. This relationship and breakoff point was observed for several different irradiating wavelengths and is indicative of a change from a monomolecular recombination process involving trapping at low light levels to a bimolecular process at higher light levels in which direct recombination occurs.

A filter paper was treated by first dipping the paper into a concentrated CdI_2 solution and then allowing the paper to dry in air. Exposure for 15 sec directly under a 100-w mercury arc lamp turned the paper dark brown. A gray-black color was obtained with longer exposures. Exposures with a calibrated monochromator established that an exposure of 10^{16} quanta/cm² at 3800 A would produce a barely detectable image. It was also established that the spectral response for forming an image was identical with the photoconductive spectral response. After a period of several days, the image fades somewhat. Since an image is observed with such a small exposure, the process probably occurs with a near-unity quantum efficiency.

Sensitive films were also prepared by precipitating CdI_2 in a gelatin and spreading the suspension on a glass plate. After a heavy exposure, the film was dissolved in boiling water, and an insoluble precipitate of cadmium metal was recovered.

Exposures of over 10^{20} quanta/cm² incident upon either CdI_2 powders or crystals produced no visible darkening. Evidently, necessary conditions for high sensitivity are that the powders be submicroscopic in size and adjacent to small amounts of moisture. Under these conditions, the free halogen is readily accepted by the water before it has a chance to recombine with the cadmium.

The author wishes to acknowledge the helpful suggestions of Alvin M. Goodman.

* From a thesis submitted to Case Institute of Technology in partial fulfillment of the requirements for the degree of Master of Science.

[1] E. K. Putseiko and A. N. Terenin, Doklady Akad. Nauk S.S.S.R. **90**, 1005 (1953).
[2] G. Cohn and J. A. Hedvall, J. Chem. Phys. **46**, 603 (1943).

Energy Transfer in Liquid Hydrocarbons Excited by γ Rays*

G. R. Freeman

Department of Chemistry, University of Alberta, Edmonton, Alberta

(Received May 10, 1960)

It is well established that when a solution of benzene B in cyclohexane C is irradiated with γ-rays, the reactions

$$C\text{—}\vee\vee\vee\rightarrow C'' \quad (1)$$

$$C''\rightarrow H_2+\text{products} \quad (2)$$

$$C''+B\rightarrow C+B^* \quad (3)$$

occur, among others; C'' and B^* represent excited species of cyclohexane and benzene, respectively. Reaction (2) represents an over-all process that might comprise several steps. The identity of C'' and the precise mechanism of reaction (3) are not known. If C'' is a positive ion, reaction (3) corresponds to the transfer of an electron from B to C''. If C'' is an electronically excited molecule, then reaction (3) represents the transfer of the excitation energy from C'' to B. Several mechanisms have been proposed for the latter type of process.[1,2]

Reaction (3) occurs so rapidly that it is evidently not controlled by molecular diffusion.[3] Reactions similar to 3 that occur in scintillator solutions have also been observed to have rate constants that are larger than would be allowed by molecular diffusion.[4,5]

Several of the theories of excitation transfer indicate that the transfer would be facilitated by an increase in the degree of order (relative orientation) among the molecules in the liquid.[1,6] Förster's theory, for example, assumes random orientation of the molecules and transfer times that are long enough to allow the nuclear motions in the excited molecules to reach thermal equilibrium ($>10^{-13}$ sec). The interactions that lead to energy transfer are increased in strength both by an

increase in order among the molecules and an increase in their concentration. Förster[6] stated that for very strong interactions his theory would be invalid and that the exciton theory[7,8] would be more applicable. The exciton theory also implies that there would be a strong dependence of the rate of exciton migration on the degree of order in the liquid.

The melting points of cyclohexane (+6.5°C) and of methylcyclohexane (−126.4°C) indicate that, at room temperature, there is a much higher degree of order in liquid cyclohexane than in liquid methylcyclohexane. The value of the ratio k_3/k_2 was 0.78±0.11 *l*/mole for the cyclohexane-benzene system.[3] Since the value of k_2 should be very similar in the methylcyclohexane and cyclohexane systems, a determination of the value of the ratio k_3/k_2 in the methylcyclohexane-benzene system might throw some light on the mechanism of reaction (3). From recent experiments in this laboratory, the value of this ratio has been found to be 0.64±0.10. Thus, the values of k_3 are very similar in the two systems. This seems to imply that the above-mentioned theories do not apply in these systems. It has previously been shown that the Förster theory yields too small a value for the corresponding k_3 in benzene-scintillator solutions.[4]

Extension of the electron transfer theory of Marcus[9] to the present systems indicates that the time required to transfer an electron from a C molecule to an adjacent C^+ ion, in liquid C, would be of the order of 10^{-15} sec. Here, C represents either cyclohexane or methylcyclohexane. It was previously shown that a value of $k_3/k_2 \approx 1$ l/mole can correspond to an energy (excitation or charge) transfer time of 10^{-14} to 10^{-15} sec.[3] Thus, the charge transfer picture is not inconsistent with the experimental observations.

Assuming that C'' is the positive ion C^+, the large rate of charge transfer would not permit the nuclear motions in the ion to reach thermal equilibrium. There would not be an individual entity that would be directly comparable to an isolated C^+ ion. The positive charge would belong to a "domain" in the liquid. When the rapidly moving charge interacted with a molecule that possessed a lower ionization potential, the charge could be "trapped" by that molecule.

Nosworthy, Magee and Burton[5] have postulated the existence of such domains to explain the luminescence minimum that is observed in certain scintillator solutions. They suggested that domains exist in the "better solvent" (e.g., benzene) when it is present above a certain low concentration. Further evidence that such domains can exist in benzene, even when this substance is present at relatively low concentrations in other liquids, may be drawn from recent results of Hisatsune and Jayadevappa.[10] The persistence of these domains (interactions between benzene molecules) is more pronounced when the "common solvent" is nonpolar, and it is even more pronounced in cyclohexane than in iso-octane.[10]

The author would like to express his appreciation to Prof. M. Burton for sending him a preprint of the paper by Nosworthy, Magee and Burton.

* This research was supported by the National Research Council of Canada, and the Trans-Mountain Oil Pipeline Company.

[1] J. B. Birks, *Scintillation Counters* (McGraw-Hill Book Company, Inc., New York, 1953).
[2] S. C. Curran, *Luminescence and the Scintillation Counter* (Butterworths Scientific Publications, Ltd., London, 1953).
[3] G. R. Freeman, J. Chem. Phys. (to be published).
[4] S. Lipsky and M. Burton, J. Chem. Phys. **31**, 1221 (1959).
[5] J. M. Nosworthy, J. L. Magee, and M. Burton, J. Chem. Phys. (to be published).
[6] T. Förster, Ann. Physik **2**, 55 (1948).
[7] J. Frenkel, Phys. Rev. **37**, 17, 1276 (1931).
[8] J. Franck and E. Teller, J. Chem. Phys. **6**, 861 (1938).
[9] R. A. Marcus, J. Chem. Phys. **24**, 966 (1956).
[10] I. C. Hisatsune and E. S. Jayadevappa, J. Chem. Phys. **32**, 565 (1960).